Consejo Superior de Investigaciones Científicas
Museo Nacional de Ciencias Naturales
Departamento de Paleobiología
Grupo de Paleoantropología

Universidad Autónoma de Madrid
Facultad de Ciencias
Departamento de Biología

CONTRIBUCIONES AL ESTUDIO DE LA VARIABILIDAD MORFOLÓGICA, FUNCIONAL Y EVOLUTIVA DEL ESQUELETO TORÁCICO HUMANO

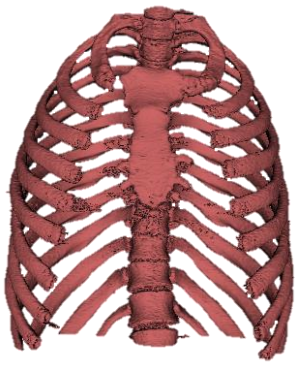

TESIS DOCTORAL

MEMORIA PRESENTADA PARA OPTAR AL GRADO DE DOCTOR EN BIOLOGÍA

POR

DANIEL GARCÍA MARTÍNEZ

V° B° DIRECTOR: DR. MARKUS BASTIR

(MUSEO NACIONAL DE CIENCIAS NATURALES; CSIC)

V° B° TUTOR: DR. ARMANDO GONZÁLEZ MARTÍN

(UNIVERSIDAD AUTÓNOMA DE MADRID)

MADRID, 2017

CONTRIBUTIONS TO THE STUDY OF THE MORPHOLOGICAL, FUNCTIONAL AND EVOLUTIONARY VARIABILITY OF THE HUMAN THORACIC SKELETON

TESIS DOCTORAL

MEMORIA PRESENTADA PARA OPTAR AL GRADO DE DOCTOR EN BIOLOGÍA

POR

DANIEL GARCÍA MARTÍNEZ

Tribunal titular:

Dr. José Luis Sanz García – Universidad Autónoma de Madrid (Madrid, España).

Dr. Antonio Rosas González – Museo Nacional de Ciencias Naturales (Madrid, España).

Dr. Scott Alan Williams – New York University (New York City, EE.UU.).

Dra. Eugenia Maria Guedes Pinto Antunes da Cunha – Universidade de Coimbra (Coimbra, Portugal).

Dr. José María Bermúdez de Castro y Risueño – Centro Nacional de Investigación sobre Evolución Humana (Burgos, España)

Tribunal suplente:

Dra. Almudena Estalrrich Albo – Senckenberg Museum (Frankfurt, Alemania).

Dr. Óscar Cambra Moo – Universidad Autónoma de Madrid (Madrid, Spain).

MADRID, 2017

A los que se han ido.

A los que se han quedado.

A los que algún día llegarán.

A todas las personas que han hecho de la ilusión el motor de sus vidas.

Desde el Pleistoceno hasta el día de hoy.

Al mundo.

“La vida es un arbusto de abundante ramificación, continuamente podado por el inexorable ángel de la muerte de la extinción, no una predecible escalera de progreso”

Stephen Jay Gould: Wonderful Life (1989), 35.

“Nada en la Biología tiene sentido excepto a la luz de la Evolución”.

Theodosius Dobzhansky: The American Biology Teacher (1973), 129.

La especie humana constituye el mayor y más interesante problema para un naturalista.

Carta de Darwin a Wallace (22 de Diciembre de 1857)

Contenido

Agradecimientos

Durante estos últimos años, he podido observar que el hecho de hacer una tesis doctoral, además de ser sumamente apasionante y motivador, supone un gran aprendizaje vital y un esfuerzo considerable. Además, ya que podido conocer sitios increíbles que nunca hubiera podido visitar si no llega a ser por la tesis doctoral. Por lo tanto, no puedo dejar de agradecer enormemente las personas, hechos y lugares que han de algún modo han contribuido a ese aprendizaje, dejando una huella maravillosa en mi vida.

En primer lugar, quiero plasmar mi agradecimiento al Dr. Markus Bastir, director de esta tesis y gran mentor, el haberme dado la oportunidad de dedicarme al mundo de la Evolución Humana y el haber demostrado confianza en mí desde el primer día. Agradezco enormemente no sólo el haberme apoyado a través de la contratación como técnico asociado a su proyecto de investigación (que en estos momentos de crisis considero crucial), sino el haberme apoyado a nivel científico en todos los problemas, dudas e incertidumbres que han ido surgiendo todos estos años. También agradezco el hecho de haber incentivado mi motivación y mi interés con enriquecedores comentarios, y el haberme permitido desarrollar mi potencial profesional y haber recibido positivamente mis comentarios y sugerencias acerca de nuestros proyectos de investigación. Finalmente, no puedo dejar de gradecer también el haber sido un referente en motivación personal y vital, habiendo demostrado que la perseverancia en el trabajo (a pesar del sudor de clavícula), acaba siempre produciendo unos muy buenos frutos.

También quiero agradecer a mi tutor, el Dr. Armando González Martín, el haber realizado una excelente tarea de tutor desde el PFC hasta el día de hoy y sobre todo el haberme dado el "empujón" y la motivación inicial en su asignatura "Origen y Evolución del Hombre". Agradezco también enormemente el hecho de que, cuando sólo era un estudiante 4º de

Biología, me atendiese y me recomendase que "escribiese al Dr. Markus Bastir, para ver si me podría ofrecer algún PFC". Sin este comentario y consejo, es probable que yo no estuviera escribiendo esta tesis hoy.

No puedo dejar de agradecer también al grupo de Paleoantropología del MNCN el haberme acogido durante los años de mi formación predoctoral y el haber hecho que creciera profesionalmente, en el seno de un gran grupo de investigación tanto a nivel científico como humano. Especialmente me gustaría agradecer al Profesor Antonio Rosas, no sólo el haberme dado el honor de tener acceso al material torácico del yacimiento de El Sidrón (del cual he sido "fan" desde que era alumno de Biología), sino también el haberme recibido tan positivamente en su grupo y el haber contribuido a mi formación Paleoantropológica con importantes discusiones científicas. También le agradezco el haberme permitido participar en el yacimiento de la Sierra de Quibas (Murcia), donde he podido ser nuevamente un "biólogo de campo". También necesito especialmente agradecer el apoyo incondicional, científico y personal, de personas que cuando entré en el grupo, eran compañeros de trabajo, pero que han acabado siendo amigos y referentes personales. A la Dr. Rosa Huguet, por haberme siempre apoyado y ayudado desde que estuve excavando en la Sima del Elefante (Atapuerca, Burgos), bajo su dirección, y por aportar siempre risas y comentarios agradables al grupo en todo momento. Aunque parezca un pequeño detalle, esto es muy importante para el día a día. También agradecer a Antonio García Tabernero (Tonchu) el haber tenido siempre la paciencia para ayudarme en todo lo que he necesitado siempre como compañero de despacho y por contribuir con su colaboración (y grapas) a mi formación. A la Dra. Estallrich (o Estalrrich, como ella prefiere escribirlo) también le quiero gradecer el haberse convertido en una hermana laboral, contribuyendo con su apoyo y motivación en todo momento y ayudando a que los días de investigación de 9 de la mañana a 21 de la noche, se hicieran más llevaderos. Tengo seguridad de que además de una gran compañera de trabajo, me llevo una amiga de por vida. A Francisco

Javier Rodríguez-Pérez (Fran) quiero agradecerle también que desde el Máster haya sido un compañero ideal y haya acabado convirtiéndose en un amigo, el cual estoy seguro que durará toda la vida. Su apoyo, consejos y "camaradería" han sido vitales para mí durante los años de tesis doctoral… Por no hablar de la maravillosa experiencia de Croacia (Doverdan te lo digo). A Laura le agradezco el haber compartido conmigo dudas y preocupaciones predoctorales, y a Nicole deseo todo lo mejor en su etapa predoctoral, que estoy seguro que disfrutará enormemente. Al resto de compañeros, tanto los que aún están en el MNCN (Bea, Laura, Nicole, Estefi, Alberto, Pedro, Carlos, Lucia, David, Daniel) como los que han decidido buscar su rumbo en otro lugar (Marta Menacho, Noelia-Lijas, Helena-Jellema, Susana, Nacho) les agradezco también todos los momentos compartidos, y el haber hecho del día a día una cosa más liviana. También desde aquí quiero agradecer a las recientes incorporaciones (Sonia, Sofía, Marta, Alba e Isa) el mantener la llama de la Paleoantropología de este museo viva, y les motivo a que sigan en ello, ya que tienen un gran futuro por delante.

También tengo que agradecer al resto de personas de la UAM, tanto profesores (Óscar Cambra, Jesús Marugán, Consuelo Prado, Margarita Carmente, Paula Acevedo, Pilar Montero) como estudiantes de Doctorado (Elena, Carlitos, Dani Vidal, Alejandro, Kristin, Laura, Tony, Orosia, Manolo, Josefina) por haber contribuido en mi formación académica y personal. Especialmente quiero agradecer a la Dra. Margarita Carmenate su ayuda constante como Secretaria del Programa de Doctorado en Biología y al Dr. Óscar Cambra por la ayuda prestada durante los últimos años de mi carrera profesional, así como por las interesantes discusiones científicas que hemos tenido.

Agradecer también a los profesores y estudiantes de la Universidade de Coimbra (Prof. Eugenia Cunha, Prof. Ana Luisa Santos, Lucy Shaw, Edilson Vicente, Inês Leandro, Richard Marques, Ricardo Melo) que me regalaron un semestre fructífero, tanto personal como académicamente, durante mi ERASMUS en Coimbra. Esta es una ciudad maravillosa, con

personas maravillosas, da que tenho muitas saudades e espero voltar algum dia. Específicamente, tengo que agradecer a la Prof. Eugenia Cunha y a los investigadores de DRYAS (Miguel Almeida, Maria Teresa Ferreira, Maria João Neves) el haberme permitido acceder a la colección de individuos identificados de Santarém, sin el cual gran parte de esta tesis no habría sido posible. También a mis compañeros de residencia (Juan, Fátima, Nacho, Raquel, Inma, Irene, Mariángeles, Macarena, Gustavo, Martin, Issobella, Alessandro, Chiara), los que hicieron de la estancia mucho más llevadera aportando alegría en los (muitos) días lluviosos de Coimbra.

I would like also to acknowledge the wonderful people (and scientists) that I meet during my stay in South Africa. First of all, I want to acknowledge Prof. Lee Roger Berger for giving me the opportunity to participate in the *Homo naledi* project. It probably was one of the most incredible experiences (from both professional and personal point of view) of my life and I am really thankful for that. I also want to acknowledge other senior researchers that helped me and inspired me during my stay in Witwatersrand University (Dr. John Hawks, Dr. Steven Churchill, Dr. Trenton Holliday and Dr. Peter Schmid) as well as the torso working team (Dr. Scott Williams, Dr. Caroline Van Sickle and Dr. Shahed Nalla) and specially to Dr. Scott Williams (team leader), whose tremendous knowledge on the evolution of the axial skeleton, inspired me and gave me motivation for my research. Additionally, since the Rising Star workshop was made up by more than 30 scientists, it is going to be difficult to mention here all of them… but I will try: therefore, I acknowledge Lucas Delezene (roommate), Tracy Kivell, Heather Garvin, Matthew Skinner, Charles Musiba, Will Harcourt-Smith, Rebecca Ackermann, Debi Bolter, Juliet Brophy, Zach Cofran, Kimberly Congdon, Andrew Deane, Mana Dembo, Marina Elliott, Elen Feuerriegel, David Green, Alia Gurtov, Joel Irish, Ashley Kruger, Myra Laird, Damiano Marchi and Davorka-Seki Radovcic (the other 2 European guys), Marc Meyer Lauren Schroeder, Jill Scott, Zachary Throckmorton,

Christopher Walker, Pianpian Wei and Bernhard Zipfel. I really thank their friendship, help and support while I was in South Africa. I would like to give some additional special thanks to Dr. Scott Williams. He and his family (Milena, Imara and Oliver) helped me a lot when I went to NYC (AMNH) and he made me feel like at home. Hopefully I will see you again there, and I will try to improve my "Hops" drawings for Imara :)

No puedo olvidar aquí a las personas que, tanto en mi desarrollo académico en la carrera de Biología (Kantala, Edu, Ángel, Carlitos, Gloria, Sonia, Juan, Geles, Rober, Belén rubia, Belén morena, Nacho, así como un largo etcétera) como en el máster de Antropología Física (Fran, Nuria, Mercedes, Miriam, Nerea, Antonio, Isa, Guille, Edu, Axel), fueron una maravillosa influencia para mí e hicieron de la vida académica mucho más llevadera (acordaos de aquellos 100 meses).

Entrando en el plano personal, no quiero olvidarme tampoco de mis "camaradas" preferidos, que ayudaban a olvidar los problemas laborales y que siempre estaban (y han estado) dispuestos a conseguir unas sonrisas (Álvaro, Miguel, Jaby).

También creo que este, es el sitio adecuado para agradecer al colegio P.P. Escolapios que contribuyesen a mi educación en un momento ontogenético tan crucial como es la adolescencia. Gracias tanto a los profesores (Asunción, Meñaca, Verde, Casillas, Miguel Ángel, Marco Antonio) como a los alumnos. Dentro de estos últimos, me gustaría dedicar unos agradecimientos especiales para Diego, Sara, María y Alberto, con los cuales ha sido un placer re-encontrarme recientemente.

Agradecer también tanto a otras personas que han estado ahí desde años (Paula, Maleni, José Ramón, Charo) como a aquellas que aunque se hayan incorporado recientemente (María José). Gracias por aportar siempre un granito de felicidad, apoyo y ayuda. También agradecer a David su reciente ayuda, sin la cual no habría sido posible culminar esta tesis tan airosamente.

Para acabar, aunque es obvio que tenían que haber estado en la parte superior de la lista de agradecimientos… a mi familia de siempre (Marisa-mamá, Jacinto-Tin, Javier, Miguel, Luna, Maripili, Paca, etc.), así como a las nuevas adquisiciones (Yoli y Alba). Por su confianza, apoyo y cariño, no sólo durante los años de vida académica, sino durante los 28 años de mi existencia. Es obvio que sin ellos mi vida no habría sido como es hoy en día, ya que de ellos ha dependido en gran parte, que sea lo que soy hoy. También a mi familia política (Conchi, Fran, Marina, Goyito, Alvarito, Gabriel, etc.) el haberme acogido siempre y el haberme apoyado con mi profesión. Me gustaría dedicar una mención especial a mi madre, la cual no sólo me ha educado, ayudado y criado en los momentos difíciles por los que hemos pasado, sino que se ha convertido en una gran referencia y modelo para mí… ¡Gracias madre!

And, last but not least… María. No sólo tengo que agradecerte la ayuda en estos últimos días, como las lecturas críticas intentando corregir mi Spanglish o los 5500 folios comprados… No hay palabras para expresar la eterna gratitud que te tengo, por tener sonrisas maravillosas para mí y estar cargada de energía todos y cada uno de los días, no solo durante el doctorado, sino durante 12 años (casi 13). Por confiar en mí, cuando ni yo lo hacía. Por palabras de apoyo y cariño cuando más falta hacían. Por querer compartir conmigo esta increíble aventura, que es nuestra vida. Por querer acompañarme al fin del mundo si es necesario. No hay palabras que expresen mi gratitud hacia ti; sé que no es difícil ser la pareja de alguien que se dedica a este mundo, más aún siendo tan peculiar como soy a veces. Por esto y por mucho más: te admiro enormemente, estoy tremendamente orgulloso de estar a tu lado y te quiero mucho más… Así que: ¡Thank you very much sweetheart!

NOTA: Aunque esta tesis doctoral no ha sido financiada como tal debido a factores externos, agradezco de nuevo a Markus la confianza en mí financiando esta investigación, como técnico a cargo de los proyectos CGL2015-63648P y CGL-20129-37279 (MINECO). También agradezco enormemente la financiación externa recibida para la toma de datos y la confianza depositada en mí, por parte de: marco ERASMUS (UAM-UC), South African Government and University of Witwatersrand, the Leakey Foundation, the Synthesys Project, the ESHE Society, the Paleoanthropology Society and the American Museum of Natural History.

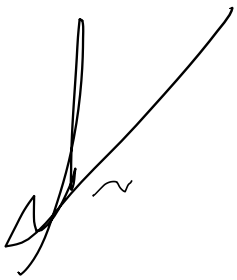

Fdo. Daniel García Martínez

Listado de publicaciones.

Publicación nº 1: Bastir, M., **García Martínez, D.**, Recheis, W., Barash, A., Coquerelle, M., Ríos, L., Peña-Melián, Á., García Río, F., O'Higgins, P., 2013. Differential growth and development of the upper and lower human thorax. PLoS One 8, e75128.

DOI: http://dx.doi.org/10.1371/journal.pone.0075128

Publicación nº 2: García-Martínez, D., Recheis, W., Bastir, M., 2016. Ontogeny of 3D rib curvature and its importance for the understanding of human thorax development. American Journal of Physical Anthropology 159, 423-431.

DOI: 10.1002/ajpa.22893

Publicación nº 3: Bastir, M., Higuero, A., Ríos, L., **García-Martínez, D.**, 2014. Three- dimensional analysis of sexual dimorphism in human thoracic vertebrae: Implications for the respiratory system and spine morphology. American Journal of Physical Anthropology 155, 513-521.

DOI: 10.1002/ajpa.22604

Publicación nº 4: García-Martínez, D., Torres-Tamayo, N., Torres-Sánchez, I., García-Río, F., Bastir, M., 2016. Morphological and functional implications of sexual dimorphism in the human skeletal thorax. American Journal of Physical Anthropology 161, 467-477.

DOI: 10.1002/ajpa.23051

Publicación nº 5: Bastir, M., **García-Martínez, D.**, Torres-Tamayo, N., Sanchís-Gimeno, J. A., O'Higgins, P., Utrilla, C., Torres-Sánchez, I., García-Río, F., 2017. In Vivo 3D Analysis of Thoracic Kinematics: Changes in size and shape during breathing and their implications for respiratory function in recent humans and fossil hominins. Anatomical Record 300, 255-264.

DOI: 10.1002/ar.23503

Publicación nº 6: Bastir, M., **García-Martínez, D.**, Williams, S.A., Recheis, W., Torres-Sánchez, I., García-Río, F., Oishi, M., Ogihara, N., en revisión. 3D geometric morphometrics of thorax variation in *Hominoidea*. Journal of Human Evolution.

Publicación nº 7: Tawane, G., **García-Martínez, D.**, Eyre, J., Bastir, M., Berger, L., Nalla, S., Williams, S.A., 2016. A hominin first rib discovered at the Sterkfontein Caves, South Africa. South African Journal of Sciences 112, 1-7.

DOI: http://dx.doi.org/10.17159/sajs.2016/20150278

Publicación nº 8: Williams, S.A., **García-Martínez, D.**, Bastir, M., Meyer, M.R., Nalla, S., Hawks, J., Schmid, P., Churchill, S.E., Berger, L.R., 2017. The vertebrae and ribs of *Homo naledi*. Journal of Human Evolution 104, 136-154.

DOI: http://dx.doi.org/10.1016/j.jhevol.2016.11.003

Publicación nº 9: García-Martínez, D., Barash, A., Recheis, W., Utrilla, C., Torres-Sánchez, I., García-Río, F., 2014. On the chest size of Kebara 2. Journal of Human Evolution 70, 69-72.

DOI: 10.1016/j.jhevol.2014.02.003

Publicación nº 10: Bastir, M., **García-Martínez, D.**, Estalrrich, A., García-Tabernero, A., Huguet, R., Ríos, L., Barash, A., Recheis, W., de la Rasilla, M., Rosas, A., 2015. The relevance of the first ribs of the El Sidrón site (Asturias, Spain) for the understanding of the Neanderthal thorax. Journal of Human Evolution 80, 64-73.

DOI: 10.1016/j.jhevol.2014.10.008

Publicación nº 11: Bastir, M., **García-Martínez, D.**, Ríos, L., Higuero, A., Barash, A., Martelli, S., García-Tabernero, A., Estalrrich, A., Huguet, R., de la Rasilla, M., Rosas, A., en prensa. 3D morphometrics of thoracic vertebrae in Neandertals: fossil evidence from El Sidrón (Asturias, Northern Spain). Journal of Human Evolution.

Publicación nº 12: García-Martínez, D., Bastir, M., Huguet, R., Estalrrich, A., García-Tabernero, A., Ríos, L., Cunha, E., de la Rasilla, M., Rosas, A., aceptado. The costal remains of the El Sidrón Neandertal site (Asturias, northern Spain) and its importance for understanding the Neandertal thorax morphology. Journal of Human Evolution.

ÍNDICE DE FIGURAS Y TABLAS

Figura 9: Proceso de *sliding* de *semilandmarks* de curva a lo largo de las rectas tangentes, donde se muestra a) *semilandmarks* en su posición original; b) *semilandmarks* después del *sliding*; c) *semilandmarks* proyectados de nuevo en la superficie. Modificado de Gunz y Mitteroecker (2013).

Figura 10: Cambio morfológico observado en la ontogenia de la caja torácica completa (parte superior) y de las costillas individuales (parte inferior). En la imagen inferior se observa que el cambio morfológico que ocurre en las costillas superiores (cuadro naranja) es diferente del que ocurre en las inferiores (cuadro verde).

Figura 11: Dimorfismo sexual observado en la caja torácica (parte superior) e ilustración de cómo el cambio morfológico en las *partes* (orientación de los procesos transversos de las vértebras torácicas) puede influir en la forma del *todo* al que pertenece (tórax).

Figura 12: Forma media de las cajas torácicas de las especies del clado *Hominoidea* (según los resultados de Bastir et al., en revisión). Como se observa, hay diferencias considerables en morfología de las hipotéticas cajas torácicas "funnel-shaped" y "barrel-shaped".

Figura 13: Esquema filogenético del clado de la Subtribu *Hominini* basado en Dembo et al. (2016), donde se representan géneros o especies de homininos, así como su hipotética morfología torácica según los resultados obtenidos en la presente tesis doctoral. Nótese que únicamente se representan aquellos de los que se tiene conocimiento de su tórax y *Homo georgicus* se excluye debido a la falta de resultados concluyentes sobre sus restos costales. La caja torácica representada como "*early Homo*" está basada en la especie *Homo naledi*. Aunque no se tiene cronología para esta especie, estudios realizados con análisis bayesianos han mostrado que se podría encontrar en la base de *Homo ergaster* y *Homo antecessor*. El símbolo ✞ significa que son géneros o especies extintas.

Tabla 1: Objetivos, capítulos donde esos objetivos son alcanzados, así como las publicaciones que contiene cada capítulo y el número de paginación que tienen dichos artículos en la presente tesis.

Resumen

Esta es una tesis sobre Antropología Física, con interés especial en el área de la Paleoantropología. En ella, se estudia la variabilidad morfológica torácica en diferentes vertientes de la biología humana, como la ontogenia, el dimorfismo sexual, la anatomía funcional, la anatomía comparada y la anatomía evolutiva. Aunque diferentes trabajos habían explorado previamente estos aspectos desde un punto de vista bidimensional, gran parte de los aspectos detallados de la morfología tridimensional aún no se conocían. Parte de esta limitación, se debía a que la metodología empleada para la cuantificación de la morfología torácica y costal (básicamente compuesta de curvas) no recogía la realidad tridimensional asociada a la biología de los organismos. Por lo tanto, al no cuantificar las tres dimensiones del tórax, las conclusiones obtenidas eran parcialmente sesgadas. Aunque este hecho es evidente observando la variabilidad humana reciente, se hace más evidente cuando se trata del estudio del registro fósil, ya que, en el caso del esqueleto torácico, este suele aparecer muy fragmentado. Para resolver el problema de la cuantificación metodológica, en esta tesis se ha desarrollado todo un protocolo que va desde la obtención de modelos tridimensionales hasta su medición detallada en un entorno virtual a través de la *morfometría geométrica* (MG) 3D de *sliding semilandmarks*. Para la obtención de datos, se han usado técnicas de imagen médica para la obtención de muestra de cajas torácicas de *Homo sapiens* y de otros primates hominoideos no humanos, así como técnicas de escaneo de superficie a fin de obtener modelos 3D de elementos torácicos aislados (costillas y vértebras) tanto de especies actuales como de especies extintas. Para su cuantificación, se han desarrollado protocolos de landmarks y semilandmarks, tanto para la caja torácica en su conjunto, como para sus elementos (costillas y vértebras) y se ha utilizado el método de *sliding semilandmarks* a través de la *bending energy* para convertir los *semilandmarks* en puntos matemáticamente homólogos, ya que, sin este proceso, los *semilandmarks* no cumplirían el principio de homología.

Los resultados obtenidos han mostrado que la variabilidad torácica (tanto actual como fósil) es bastante más complicada de lo propuesto hasta la fecha. De este modo, las diferencias observadas en la ontogenia y el dimorfismo sexual, podrían estar relacionadas con los patrones de respiración, la postura corporal o incluso con el tamaño del aparato digestivo y reproductivo. En cuanto a la anatomía comparada, se observa que la realidad morfológica 3D torácica de *Hominoidea*, no responde a las clasificaciones de tórax en forma de barril (*Homo* e *Hylobates*) y tórax en forma de embudo (*Pongo*, *Pan*, *Gorilla*) propuestas clásicamente en la literatura, sino que *Pongo* está morfológicamente más próximo a *Homo* e *Hylobates* que al resto de grandes simios. Respecto a la anatomía evolutiva de la caja torácica, los resultados aquí presentados apuntan a que la morfología del tórax superior expandido (característica de *Homo sapiens*) probablemente apareció antes que la morfología moderna del tórax inferior (proporcionalmente más estrecha). De este modo, la caja torácica de *Australopithecus* y de los primeros *Homo*, podría estar caracterizada por una parte inferior amplia (hipotéticamente arcaica), posiblemente heredada de homínidos del Mioceno como *Pierolapithecus*, y por una parte superior expandida (hipotéticamente derivada), similar a *Homo sapiens*. Este patrón de cajas torácicas inferiormente amplias podría estar presente incluso en Neandertales, aunque debido al mayor tamaño torácico de estos con respecto a especies previas, algunas ligeras diferencias debidas a factores alométricos o isométricos también serían esperables. Futuros trabajos deberían de ir encaminados a la cuantificación detallada no solo de los elementos aislados de la caja torácica de especies fósiles, sino también al estudio de como la interacción entre las *partes* (costillas y vértebras), tienen relevancia para entender los cambios del *todo* al que pertenecen (tórax). Adicionalmente, otros campos que no son recogidos en la presente tesis, como la ontogenia torácica de especie fósiles, la variabilidad o la anatomía comparada de primates con la inclusión de fósiles de primeros Hominoideos (como *Pierolapithecus*) también deberán ser estudiados en el futuro.

Abstract

This is a PhD dissertation in Physical Anthropology. Here, the morphological variability of the rib cage in topics such as ontogeny, sexual dimorphism, functional anatomy, comparative anatomy and evolutionary anatomy is addressed. Even though this variation has been previously explored from studies using two-dimensional measurements, detailed aspects of its three-dimensional morphology were poorly known. Part of this limitation was due to the fact that traditional measurements do not fully quantify the thorax or its parts because of their curved nature. Therefore, since three dimensions of the rib cage were not quantified by these works, their conclusions were partially biased. Even though this fact is observed in studies that addressed current thoracic variability, it is even more pronounced in studies about the rib cage of fossil species, where the record is extremely rare and fragmentary. In order to solve this problem, a complete protocol that ranges from the virtual data acquisition to the 3D detailed measurement of the bone has been developed in this dissertation. This has been carried out through techniques of virtual anthropology and 3D geometric morphometrics of sliding semilandmarks. Medical imaging techniques were used to acquire the sample of rib cages from current modern humans as well as from non-human hominoids. Additionally, 3D surface scanning was used to get virtual models of individual thoracic elements (ribs and vertebrae), both from extant and extinct species. For the quantification of those models, a protocol of landmarks and semilandmarks was developed, which were slid in such a wat that bending energy was minimized in order to mathematically homologize the semilandmarks.

This dissertation has shown that the thoracic variability, both extant and extinct, is more complicated than previously thought. Differences observed in ontogeny and sexual dimorphism could be related to breathing patterns, body posture or even with the size of the digestive and reproductive systems. Regarding comparative anatomy, it has been observed that the current 3D morphology of the rib cage in *Hominoidea* does not correspond with the

classification of barrel-shaped (*Homo* and *Hylobates*) and funnel-shaped thorax traditionally proposed in the literature. This is because *Pongo* thorax is morphologically closer to *Homo* and *Hylobates* than it is to *Pan* and *Gorilla*. Regarding the evolutionary anatomy of the rib cage, the results presented here suggest that the modern morphology of the upper thorax, expanded as in *Homo sapiens*, would have appeared in human evolution earlier than the morphology of the relatively narrow lower thorax. Therefore, the thorax morphology of Australopithecus and early *Homo* could have been characterized by a wide lower rib cage, possibly inherited from Miocene apes such as *Pierolapithecus*, and an expanded upper rib cage similar to *Homo sapiens*. This morphology of wide rib cages at the caudal part could have been presented even in Neanderthals, according to our results. However, morphological differences due to allometric or isometric factors may also occur in the Neanderthal rib cage because of its large size when compared to *Australopithecus* or early *Homo*. Future studies should address not only the morphology of the individual thoracic bones (ribs and vertebrae), but also the thoracic shape caused by the interaction of these elements. Additionally, future research on other topics not covered in this dissertation, such as the thoracic ontogeny of fossil species, or the thoracic anatomy of Primates but also including fossils from the first *Hominoidea* (such as *Pierolapithecus*, for instance), could contribute to our understanding of important issues in thorax evolution.

CAPÍTULO I – INTRODUCCIÓN

Capítulo 1.1 Introducción a la anatomía torácica, costal y vertebral humana.

La caja torácica (o tórax) es un compuesto esquelético multi-articular que se sitúa en la parte superior del tronco y se compone, en el ser humano, de 37 huesos (24 costillas, 12 vértebras y el esternón, si se considera este último como un solo hueso). A nivel esquelético, el tórax se encuentra comprendido anatómicamente entre la columna cervical en su parte craneal y la columna lumbar en su parte caudal (Gray, 1918; Spalteholz, 1970; Aiello y Dean 1990). Desde un punto de vista sistémico, la caja torácica pertenece a lo que se denomina el esqueleto axial, el cual está conectado con los miembros superiores e inferiores (esqueleto apendicular) a través de la cintura escapular y la cintura pélvica, respectivamente (Jellema et al., 1993; Bastir, 2008; Schmid et al., 2013; Bastir et al., 2014a). En el interior del tórax se hallan importantes órganos vitales como los pulmones o el corazón, así como vasos sanguíneos principales tales como la aorta o la vena cava inferior, por lo que una de sus principales funciones es la de proteger estos órganos y vasos que alberga de posibles daños mecánicos (Gray, 1918; Spalteholz, 1970). Sin embargo, a pesar de la rigidez necesaria para la protección de estos tejidos blandos, también es necesaria cierta movilidad a fin de lograr la cinemática respiratoria (ciclos de inspiración-espiración). Por lo tanto, la caja torácica podría ser señalada como una estructura rígida y elástica al mismo tiempo, ya que combina ambas características para lograr protección y actividad cinemática.

La caja torácica es una estructura metamérica que, en Primates, se compone típicamente de entre 12 y 14 segmentos dependiendo del género. De este modo, el número de segmentos oscila entre N=12 en géneros como *Homo*, *Pongo*, *Cercopithecus* y *Macaca* hasta N=14 en géneros tales como *Aluatta*, *Cebus* o *Ateles*, pasando por N=13 en los géneros de grandes simios africanos, *Pan* y *Gorilla* (Schultz, 1961; Aiello y Dean, 1990; Williams, 2012; Williams et al., 2016). Aunque en humanos el estándar es de 12 segmentos, se ha observado variación en este número, oscilando entre 11 y 13 (Foley y Whitehouse, 1969).

Cada segmento, se compone de dos costillas que se disponen lateralmente a cada lado del plano sagital mediante la articulación con una vértebra torácica que se sitúa en ese plano. Embriológicamente, costillas y vértebras se forman a partir de la capa central de las tres hojas embrionarias, el mesodermo (concretamente del mesodermo paraxial), alrededor de la cuarta semana de gestación (Carlson, 1994). A esta edad, el mesodermo paraxial se divide en estructuras secuenciales denominadas somitas, cuyo desarrollo está regulado por la expresión de genes Hox (Gómez et al., 2008; Mallo et al., 2010). Las somitas se diferenciarán posteriormente en diferentes tipos de tejido llamados esclerotoma, dermatoma y miotoma. El esclerotoma dará lugar a las costillas, vértebras y cartílagos costales, mientras que el miotoma dará lugar a los músculos de la caja torácica (entre otros) y el dermatoma dará lugar a la dermis de la piel dorsal (Pourquié y Tam, 2001). Las costillas, desde un punto de vista embriológico, crecen desde las apófisis costales de las vértebras torácicas rudimentarias, mientras que el esternón se forma de manera independiente a partir del mesodermo lateral-ventral (Carlson, 1994).

Aunque las costillas se forman únicamente a partir de las apófisis costales de las vértebras torácicas rudimentarias, debido a ciertas modificaciones en la regulación de la expresión de los genes Hox, en ocasiones es posible encontrar costillas en articulación con las últimas vértebras cervicales, con las primeras vértebras lumbares o incluso con las vértebras

sacro-coccígeas (Bateson, 1894; Ankel, 1967; Basmajian, 1975; Pais et al., 1978; Heligman et al., 1987; Aiello y Dean, 1990; Bots et al., 2011). Cuando aparecen estas costillas, son llamadas supernumerarias y sólo conllevan problemas de salud para el individuo cuando aparecen presentes en las vértebras cervicales (Bots et al., 2011), ya que no han sido observados problemas para el individuo cuando aparecen costillas lumbares (Pais et al., 1978; experiencia personal).

La anatomía general de cada costilla se compone de cabeza, cuello y cuerpo costal, pudiéndose diferenciar las siguientes partes (Spalteholz, 1970; Fig. 1):

- Tubérculo articular: situado entre el cuello y el cuerpo costal, en la parte externa del eje de la costilla. Su función es la articulación de la costilla con la apófisis transversa de la vértebra de su segmento.
- Tubérculo no articular (o ligamentoso): se encuentra situado a continuación del tubérculo articular en dirección distal y su función es dar estabilidad a la articulación costo-vertebral a través del ligamento costo-transverso del tubérculo.
- Ángulo costal (*angulus costæ*): se halla situado entre el tubérculo costal y el extremo distal, estando localizado más próximo al tubérculo articular en las costillas superiores, y más alejado de este cuanto más inferior es la costilla. Se reconoce como marca oblicua en dirección al eje de la costilla que se produce como resultado de la inserción del músculo *iliocostalis*. Aunque la primera costilla también posee inserción del músculo *iliocostalis*, ésta carece de un ángulo costal claramente discernible.
- Surco costal (*sulcus costæ*): surco que recorre la parte inferior del eje la costilla, por la parte interna del eje, desde la región del tubérculo articular hasta

difuminarse en la parte medio-distal (no llegando a alcanzar el extremo esternal de la costilla). En este surco se alberga la rama anterior de los nervios espinales (*nervi spinales*) torácicos, así como las venas y arterias intercostales, además de servir para la inserción de los músculos intercostales.

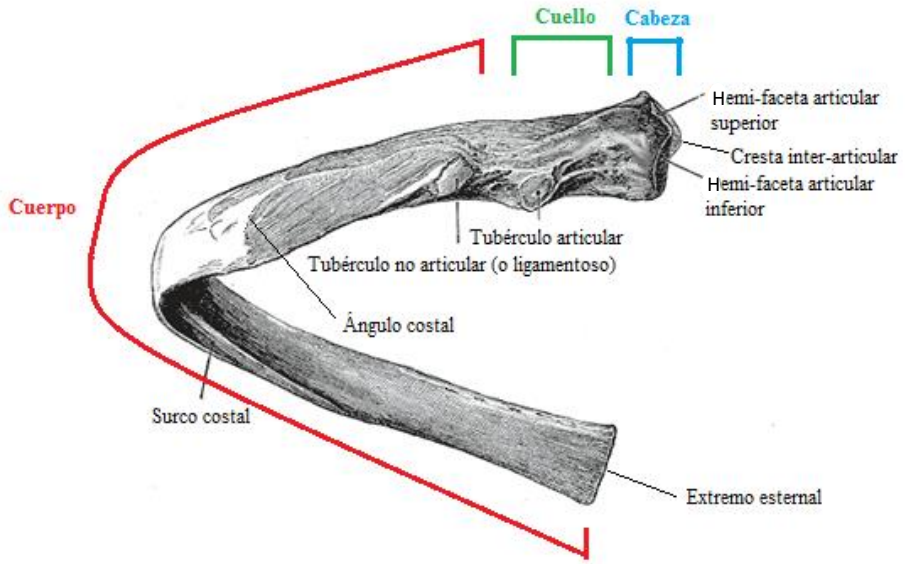

Figura 1: Anatomía costal detallada. Modificada de Spalteholz, 1970.

Cada vértebra, por su parte, se compone de un cuerpo vertebral (*corpus vertebræ*), también llamado pilar anterior, de forma más o menos cilíndrica cuyas bases se disponen supero-inferiormente, y del arco vertebral, también llamado pilar posterior. El cuerpo vertebral se encuentra conectado con el arco vertebral mediante unos pequeños puentes óseos denominados pedículos vertebrales (*radices arci vertebræ*). El arco a su vez se compone de la apófisis espinosa (*processus spinosus*) dispuesta en el plano medio-sagital en dirección caudal, de las apófisis transversas (*processus transversi*) que se disponen medio-lateralmente a cada lado de la vértebra y de las láminas (l*aminæ*). Estas láminas son dos placas óseas dirigidas en dirección cráneo-caudal que emergen de los pedículos y se unen en su parte medial. En el extremo de cada apófisis transversa, en la parte interna, se dispone una faceta articular para la articulación con el tubérculo articular del par de costillas correspondientes a su segmento. A ambos lados del cuerpo vertebral, en dirección dorsal, se encuentran situadas dos hemifacetas

para la articulación con la hemifaceta de la cabeza costal de la costilla de su segmento. Adicionalmente, dos facetas (llamadas inter-articulares o zigapófisis) en dirección craneal y dos en dirección caudal, emergen de la parte donde conecta el arco vertebral con los pedículos para la articulación con las vértebras adyacentes. El espacio ovalado o redondo que se encuentra entre el cuerpo y el arco vertebral es denominado canal neural (Spalteholz, 1970; Campillo y Subirá, 2004; Fig. 2).

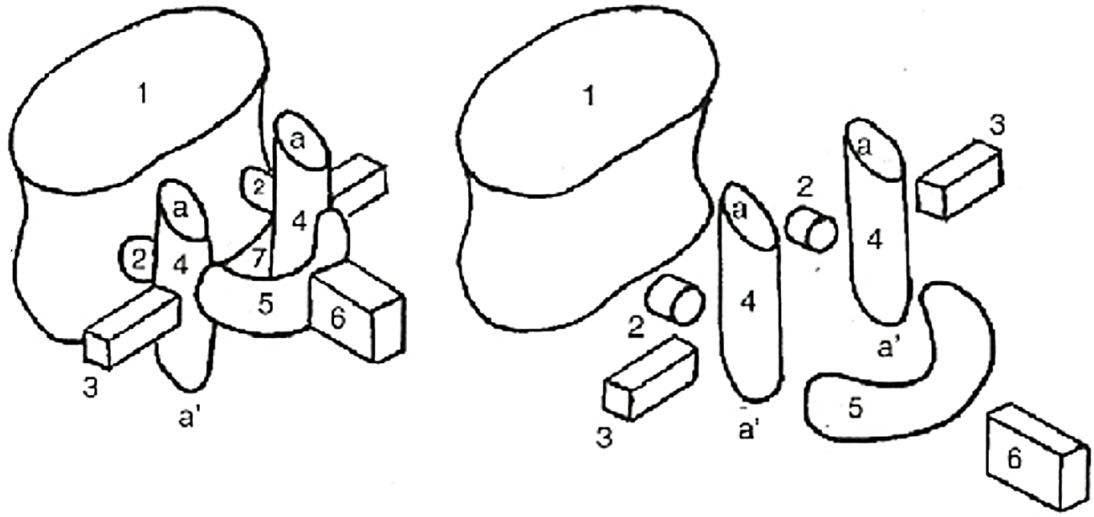

Figura 2: Anatomía vertebral de una vértebra idealizada, donde se muestra de manera esquemática 1 – cuerpo vertebral, 2 – pedículos, 3 – procesos transversos, 4 y 5 – lámina, 6 – proceso espinoso, a y a' – facetas interarticulares. Modificado de Campillo y Subirá, 2004.

La articulación costo-vertebral (costilla con vértebra) se produce en la parte proximal de las costillas. Consta de dos articulaciones, ambas de tipo sinovial con cápsula articular: cabeza costal - cuerpo vertebral (articulación costo-vertebral) y tubérculo articular costal - apófisis transversa vertebral (articulación costo-transversa) (Gray, 1918).

La articulación costo-vertebral es doble, ya que la cabeza costal está dividida en dos hemifacetas articulares ovaladas, divididas por una cresta inter-articular (Fig. 1). La hemifaceta superior articula con la correspondiente situada en la parte inferior del cuerpo vertebral de la vértebra de su segmento y la hemifaceta inferior articula con aquella situada en la parte superior del cuerpo de la vértebra del segmento inferior. Excepciones a esto son las facetas articulares de la cabeza de las costillas 1, 11 y 12, las cuales son simples y articulan únicamente con el

cuerpo de la vértebra de su correspondiente segmento, aunque en ocasiones la costilla 10 también posee una única faceta articular en la cabeza (Gómez-Olivencia et al., 2009; García-Martínez et al., aceptado). Esta articulación se encuentra reforzada por el denominado ligamento radiado de la cabeza costal (*ligamentum capituli costæ radiatum*) (Gray, 1918), el cual se compone de tres *fasciculi* que conectan la parte anterior de la cabeza de cada costilla con los cuerpos vertebrales de las vértebras adyacentes (*fasciculus* superior e inferior) y con el disco intervertebral (*fasciculus* central). En el caso de las costillas que articulan únicamente con una vértebra (costillas 1, 11 y 12), aunque el ligamento no se compone de tres *fasciculi*, sus fibras conectan igualmente la parte anterior de la cabeza costal con la vértebra de su segmento, así como con la vértebra del segmento inmediatamente superior. Adicionalmente, otro ligamento denominado interarticular o *ligamentum capituli costæ interarticulare*, se sitúa en el interior de la cápsula sinovial para reforzar la articulación (Gray, 1918).

La articulación costo-transversa es simple y está ausente en las costillas 11 y 12 (y ocasionalmente en la 10ª), ya que estas no presentan tubérculo articular costal. Esta articulación también se encuentra reforzada por ligamentos (Gray, 1918), denominados costo-transversos o *ligamentum costotrasversarius*, diferenciados en ligamento anterior (*ligamentum costotransversarium anterius*), ligamento posterior (*ligamentum costotransversarium posterius*), ligamento del cuello (*ligamentum colli costæ costotransverse*) y ligamento del tubérculo o lateral (*ligamentum tuberculi costæ posterior*) (Fig. 3). El ligamento anterior o superior, une el borde superior del cuello de la costilla con el borde inferior del proceso transverso de la vértebra inmediatamente superior. El ligamento posterior, une la parte inferior del cuello de la costilla con el borde lateral del proceso articular inferior de la vértebra inmediatamente superior. El ligamento del cuello, conecta la parte posterior del cuello de la costilla con la parte anterior del proceso transverso adyacente. Finalmente, el ligamento del tubérculo, une el tubérculo no articular de la costilla con la parte superior del proceso articular

de la vértebra de su segmento. En las costillas que no presentan tubérculo, este tipo de refuerzo ligamentoso no se observa.

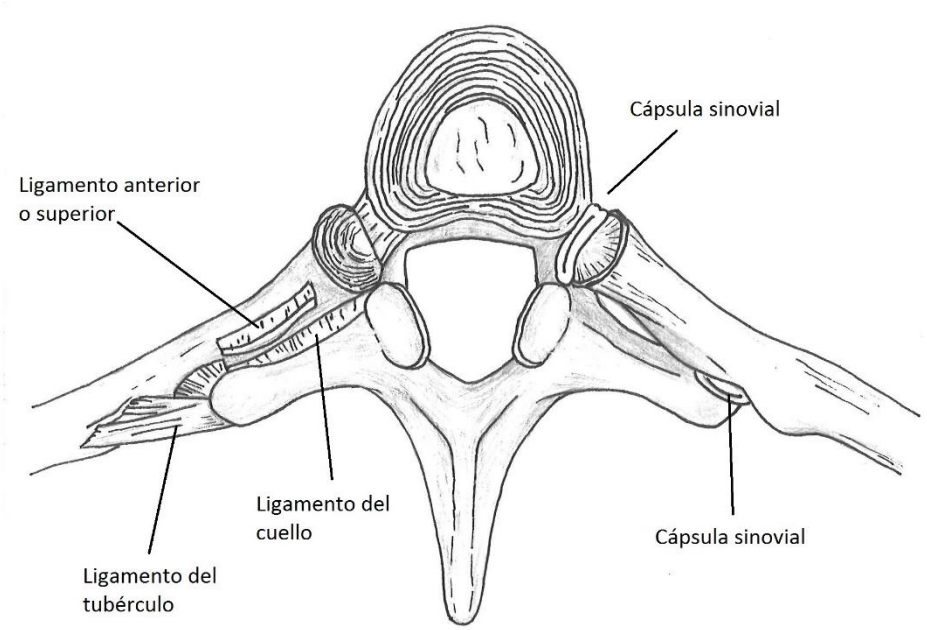

Figura 3: Anatomía detallada de la articulación costo-vertebral y sus ligamentos. Imagen cortesía de Anabel Ferrando. Basado en Gray (1918).

La articulación costo-esternal (costilla con esternón) se produce en la parte distal de las costillas. Esta puede darse de tres maneras diferentes, lo cual permite la clasificación de las costillas en 3 tipos (Gray, 1918; Spalteholz, 1970; Waldeyer y Mayer, 1987; White et al., 2011):

- Costillas verdaderas: costillas que se encuentran articuladas con su correspondiente vértebra en la parte proximal y que articulan con el esternón en su parte distal a través de una barra de cartílago hialino (típicamente son las costillas 1-7, aunque en ocasiones también es la costilla 8).
- Costillas falsas: costillas que articulan con su correspondiente vértebra en la parte proximal y con el esternón en su parte distal, pero que, a diferencia de las costillas verdaderas, la barra de cartílago conecta con el esternón a través de una conexión con el cartílago de la costilla precedente (típicamente son las costillas 8-10).

- Costillas flotantes: costillas que se encuentran articuladas con su correspondiente vértebra en la parte posterior, pero que no articulan con el esternón en su parte distal, terminando en la pared del abdomen (típicamente son las costillas 11 y 12).

Debido a la complejidad de las articulaciones anteriormente mencionadas y viendo el tórax como un *todo* anatómico compuesto por numerosas *partes* (costillas y vértebras torácicas), se hace evidente que cualquier variación en tamaño y/o forma de esas *partes* o en el modo en que ellas articulan va a tener claras repercusiones para la forma (y probablemente la función) del *todo* (como se verá en el **capítulo 8**). En referencia al registro fósil, que es en gran parte el foco de esta tesis, es crucial señalar que todas las *partes* posibles, así como el modo en que estas articulan, habrán de ser tenidas en cuenta para comprender la morfología del *todo* torácico. Cuando por motivos tafonómicos (de preservación o de conservación de los restos) no sea posible el estudio de todos los elementos que componen el tórax, hemos de tener en cuenta que las inferencias que estaremos haciendo sobre la caja torácica del individuo o la especie en cuestión van a ser parcialmente sesgadas y habremos de tener la debida prudencia en la interpretación de los resultados obtenidos.

Capítulo 1.2 Anatomía funcional de la caja torácica.

Una de las principales funciones de la caja torácica es la de soportar la mecánica respiratoria de los ciclos de inspiración-espiración, permitiendo de este modo el intercambio gaseoso necesario para los procesos básicos metabólicos del organismo humano (Silverthorn, 2009). La movilidad de las costillas en las articulaciones costo-vertebrales y costo-esternales hace posible que la cinemática respiratoria se efectúe eficazmente (De Troyer et al., 2005).

Durante la inspiración, el aire cargado de oxígeno entra en el organismo desde el exterior a través de las vías aéreas superiores (cavidad nasal, faringe, laringe y tráquea) hasta llegar a los pulmones, produciendo su expansión. El intercambio gaseoso (hematosis), que se

basa en la recepción de O_2 y la expulsión de CO_2 por parte del organismo, se produce cuando el oxígeno alcanza los alveolos pulmonares. La expansión pulmonar va acompasada por el movimiento expansivo de la parte esquelética de la caja torácica, el cual es producido de la siguiente manera (De Troyer et al., 2005): los músculos intercostales, cuyo origen es el borde inferior de las costillas y cuya inserción es el borde superior de la costilla inmediatamente inferior, elevan las costillas en el plano sagital desde un estado declinado (o de reposo) hasta un estado horizontal. Adicionalmente, se produce una contracción del diafragma, que es un músculo con forma de bóveda e inserción en las costillas 7-12, lo cual también produce una expansión medio-lateral de la caja torácica inferior. Aunque la inspiración es causada fundamentalmente por la acción de estos dos grupos musculares (músculos intercostales y diafragma), otros músculos como los serratos, los escalenos o los *levatores costarum* también están implicados en la cinemática inspiratoria (Gray, 1918). La espiración por su parte, es el proceso opuesto a la inspiración, ya que a través de esta se produce la salida del aire del organismo y, por lo tanto, del dióxido de carbono como producto de los procesos metabólicos. A diferencia de la inspiración, que es un proceso activo de contracción muscular, la espiración normal (no forzada) es un proceso pasivo mediante la cual los músculos se relajan y la caja torácica vuelve a su adquirir su morfología previa de reposo (De Troyer et al., 2005).

Algunos estudios detallados sobre la biomecánica del tórax, han descrito dos patrones de movimiento diferentes dentro de la caja torácica: el descrito como *pump handle-like* en las costillas superiores, cuyo movimiento fundamentalmente es en dirección cráneo-caudal y es producido por la acción de los músculos intercostales, y el descrito como *bucket handle-like* en las costillas inferiores, con una dirección del movimiento más medio-lateral y producido por la acción del diafragma (Williams y Warwick, 1980; Shipman et al., 1985; Aiello y Dean, 1990; Franciscus y Churchill, 2002; West, 2012; Beyer et al., 2014). Sin embargo, es probable que estos movimientos no ocurran de manera exclusiva a diferentes niveles torácicos. De hecho, es

probable que la cinemática del tórax superior sea predominantemente tipo *pump handle-like* complementada por un pequeño porcentaje de *bucket handle-like* y viceversa para el tórax inferior (Franciscus y Churchill, 2002) (Fig. 4). Adicionalmente, ha sido señalado un movimiento denominado como *spreading-caliper* (compás de espesor) para las costillas flotantes (Franciscus y Churchill, 2002; Chila, 2012) o incluso para las cinco últimas costillas (Magee, 2014).

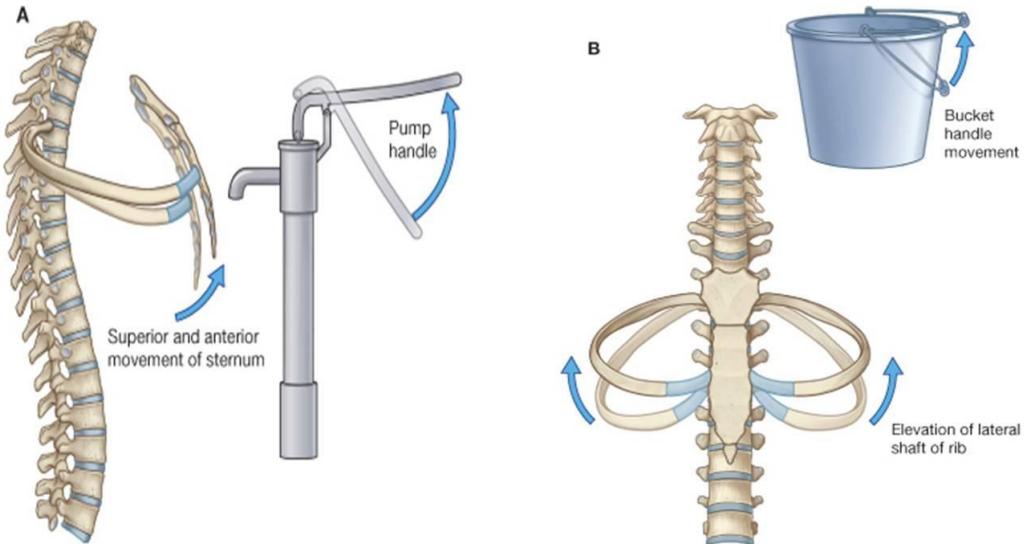

Figura 4: Ilustración gráfica de los movimientos de *pump-handle* and *bucket-handle like*. Modificado de Drake, et al. (2009).

La posibilidad de que dos tipos diferentes de movimiento ocurran en la parte superior e inferior del tórax, tiene también soporte desde el punto de vista de la mecánica de la pared torácica, ya que algunos autores también han propuesto dos tipos diferentes de respiración (Goldman et al., 1978; Grassino et al., 1978; Pinet, 2004): la respiración torácica, producida por la acción de los músculos intercostales en el tórax superior, y la respiración abdominal, producida por la acción del diafragma en el tórax inferior. Además, ha sido observado que las diferencias en la configuración de la pared torácico-abdominal, tienen repercusiones en la función de los músculos respiratorios (Goldman et al., 1978; Grassino et al., 1978; Pinet, 2004).

Finalmente, la separación superior-inferior observada en la biomecánica del esqueleto y de la pared torácica también tiene soporte desde un punto de vista estrictamente músculo-esquelético. Esto es así, ya que la caja torácica podría ser dividida en caja torácica pulmonar (costillas 1-6) y diafragmática (costillas 7-12), atendiendo a las inserciones de los músculos intercostales y del diafragma observadas en las diferentes costillas (Ward et al., 1992; Kenyon et al., 1997).

Si bien estos patrones de movimiento anteriormente explicados, son genéricos para las diferentes partes de la caja torácica, se ha propuesto que las posibles variaciones en la morfología costal y vertebral podrían influir en los patrones de movimiento torácicos. Esto se debe a que las variaciones en forma o tamaño en las *partes* (a través de factores como la torsión costal, la curvatura en vista craneal de la costilla o la orientación en el plano axial de los procesos transversos vertebrales) pueden modificar la morfología del *todo* torácico, de tal manera que la acción de los músculos del tórax también se puede ver modificada (Franciscus y Churchill, 2002; Gómez-Olivencia et al., 2009; véase **capítulo 8**).

Específicamente, ha sido observado en *Homo sapiens*, que las variaciones en la morfología torácica observadas en referencia a factores como el dimorfismo sexual (Bellemare et al., 2003, 2006; véase **capítulo 5**) o la ontogenia torácica (Openshaw et al., 1984; véase **capítulo 4**), tienen repercusión en la mecánica respiratoria y en el modo de respiración. Respecto al dimorfismo sexual, los individuos masculinos presentan, de manera general, una orientación de las costillas más horizontal y una caja torácica inferior más medio-lateralmente expandida que los individuos femeninos (Bellemare et al., 2003; Shi et al., 2014; Weaver et al., 2014; véase **capítulo 5**) Esta morfología se debe, al menos en parte, a que los individuos masculinos presentan los procesos transversos de las vértebras torácicas más posteriormente orientados, hecho que es más visible en el tórax inferior (véase **capítulo 5**). Estos factores de variabilidad, han sido también observados en la ontogenia, ya que individuos infantiles

presentan costillas más horizontalmente dispuestas (vista lateral) y cajas torácicas inferiores más medio-lateralmente expandidas que los individuos adultos (Openshaw et al., 1984; véase **capítulo 4**). Respecto al cambio en la orientación de los procesos transversos a lo largo del desarrollo ontogenético, hay un conocimiento muy escaso acerca de la ontogenia temprana de este factor. Sin embargo, ha sido observado que individuos juveniles presentan los procesos transversos más posteriormente orientados que los adultos *Homo sapiens* (Jellema et al., 1993; Latimer and Ward, 1993).

En ambos casos, tanto en dimorfismo como en ontogenia, la morfología torácica medio-lateralmente expandida en la parte inferior ha sido ligada a una potente actividad diafragmática. Esto es debido a que cuando las costillas están relativamente menos declinadas (como en infantiles respecto a adultos y en adultos masculinos respecto a femeninos), la elevación de estas es menos eficiente mediante la acción de los músculos intercostales y es el diafragma el encargado de llevar a cabo gran parte de la actividad respiratoria (De Troyer et al., 2005). Por lo tanto, la mecánica respiratoria podría tener un mayor componente de *bucket handle-like* en adultos masculinos que en el caso de los femeninos. Desde el punto de vista de la ontogenia, este mayor componente *bucket handle-like* se observaría en individuos infantiles frente a individuos adultos.

Las diferencias funcionales debidas a diferentes grados de actividad diafragmática e intercostal, han sido descritas no solo en variabilidad torácica actual (dimorfismo y ontogenia), sino que también han sido propuestas como un factor observable en anatomía comparada y evolutiva (Schmid, 1983; Schmid, 1991; Jellema et al., 1993; Franciscus y Churchill, 2002; Latimer et al., 2016; véanse **capítulos 7 y 8**). De este modo, en anatomía comparada de primates, ha sido hipotetizado que las cajas torácicas de los grandes simios también se caracterizan por una disposición horizontal de las costillas en el plano sagital o por una amplitud medio-lateral del tórax inferior, lo que también ha sido atribuido a una posible acción

diafragmática más intensa en los grandes simios que en *Homo sapiens* (Latimer et al., 2016). Sin embargo, investigaciones previas hipotetizaban que las diferencias morfológicas en el tórax de los grandes simios, no alterarían probablemente su mecánica respiratoria (Jellema et al., 1993). Sin embargo, respecto a la orientación de los procesos transversos, los grandes simios muestran unos procesos transversos menos posteriorizados que en *Homo sapiens*, por lo que la amplitud medio-lateral de la caja torácica que se observa en estos, ha de ser alcanzada de un modo diferente que lo observado en relación con el dimorfismo sexual o en la ontogenia. Es probable que la falta de declinación de las costillas junto con la elevada longitud de las mismas, sean los factores que provocan la expansión medio-lateral del tórax inferior (Jellema et al., 2013; Kagaya et al., 2008; véase **capítulo 7**).

Además de estos factores de variabilidad morfológica que repercuten en la función torácica, otro factor de variabilidad morfológica costal en especies actuales que ha sido observado por autores previos, es la forma de la sección costal en la parte central del eje (Jenkins, 1970; Jellema et al., 1993; Latimer et al., 2016). De este modo, ha sido observado en costillas de *Pan*, que estas presentan una morfología de la sección transversal redondeada, en claro contraste con la morfología más estrecha medio-lateralmente observada en la sección de costillas *Homo sapiens*. Por lo tanto, ha sido hipotetizado que esa morfología podría estar ligada no solo a una alta actividad diafragmática, sino también a una forma torácica ancha en la parte inferior y a una configuración también ancha de la cintura pélvica (Latimer et al., 2016). Contrastar la existencia de este factor de variabilidad en otros casos donde las diferencias en el modo de respiración ya han sido observadas, como en ontogenia y dimorfismo sexual, sería crucial para contrastar esta hipótesis.

Este razonamiento de correlación *forma-función* del tórax utilizado en anatomía comparada de primates actuales, también ha sido tradicionalmente extendido a la anatomía evolutiva de la caja torácica humana (Schmid, 1983; Schmid, 1991; Jellema et al., 1993;

Franciscus y Churchill, 2002; Gómez-Olivencia et al., 2009; **capítulo 8**). De este modo, una caja torácica inferior medio-lateralmente expandida, con costillas de sección redondeada y con poca declinación, ha sido propuesta por algunos autores como característica de homínidos del género *Australopithecus*, ligado a una actividad diafragmática hipotéticamente alta (Latimer et al., 2016). En lo que hace referencia a la orientación de los procesos transversos como generador de variabilidad torácica (como observado se ha observado en dimorfismo, ontogenia y anatomía comparada), no se han encontrado diferencias en la orientación de los mismos entre *Australopithecus*, *Homo erectus* y *Homo sapiens* (Jellema et al., 1993; Ward et al., 2012), por lo que este factor no contribuiría a generar variabilidad morfológica ni funcional.

Un trabajo recientemente publicado como parte de esta tesis doctoral (Williams et al., 2017) también propone una caja torácica ancha en la parte inferior para la especie de cronología incierta *Homo naledi* (Berger et al., 2015), que también podría estar relacionado con una actividad diafragmática elevada. Otros autores que han estudiado restos torácicos fósiles de homínidos del Pleistoceno Inferior como *Homo ergaster* u *Homo antecessor* (Jellema et al., 1993; Gómez-Olivencia et al., 2010) no han encontrado diferencias en lo que se refiere a estos aspectos, aunque esto es actualmente cuestionado y puede ser debido a limitaciones metodológicas en la cuantificación morfológica costal (véase **capítulo 8**). En un contexto de evolución humana más reciente, concretamente en el caso de los Neandertales, algunos autores también han propuesto una elevada capacidad diafragmática para esta especie en comparación con *Homo sapiens* (Franciscus y Churchill, 2002; Gómez-Olivencia et al., 2009; Gómez-Olivencia, 2015). Estas conclusiones se habrían alcanzado debido al gran tamaño de las costillas de la parte media-inferior del tórax, a la falta de torsión de las mismas, así como a la morfología también redondeada de la parte central del eje costal (Franciscus y Churchill, 2002). Una orientación más dorsal de los procesos transversos de las vértebras torácicas también podría contribuir a la mencionada expansión. Todos los aspectos relacionados con los cambios

morfológicos evolutivos de la caja torácica, así como sus implicaciones funcionales, serán tratados en detalle en el **capítulo 8**.

Capítulo 1.3 Anatomía comparada de la caja torácica en Primates.

Aunque la función de la caja torácica es la misma en todos los Primates actuales y extintos, y su condición metamérica se mantiene a lo largo del Orden, se observan variaciones considerables tanto en el número de segmentos que la componen (Schultz, 1961; Aiello y Dean, 1990; Williams, 2012; Williams et al., 2016) como en la morfología del conjunto torácico (Schultz, 1930, 1961; Jellema et al., 1993; Kagaya et al., 2008; Latimer et al., 2016).

Los trabajos de Schultz (1930, 1961) establecieron el conocimiento basal de lo que es la variabilidad morfológica torácica de los primates actuales. En sus trabajos, él encontró que los individuos que denominaba *apes and humans* [(Superfamilia *Hominoidea* según la nomenclatura actual de Goodman et al. (1998)], exhibían una caja torácica medio-lateralmente más expandida y antero-posteriormente menos profunda que los individuos que denominaba *monkeys* [(clasificados actualmente de manera parafilética como los miembros de la Superfamilia *Cercopitecoidea* junto a los miembros del Parvorden *Platyrrhini* o "monos del nuevo mundo", según la nomenclatura actual de Goodman et al. (1998)] (Fig. 5). Es importante resaltar en este punto, que las variaciones en la morfología torácica observadas en las diferentes especies primates, no fueron atribuidas a una re-estructuración sistémica del tronco (cintura escapular, caja torácica y cintura pélvica) debido las diferencias en la postura corporal y en los patrones de locomoción (braquiación, cuadrupedalismo arbóreo o terrestre, nudilleo –o *knuckle-walking* –, suspensión y bipedestación, entre otros) observadas en los diferentes grupos de primates (Schultz, 1961; Hunt et al., 1996; Schmid et al., 2013).

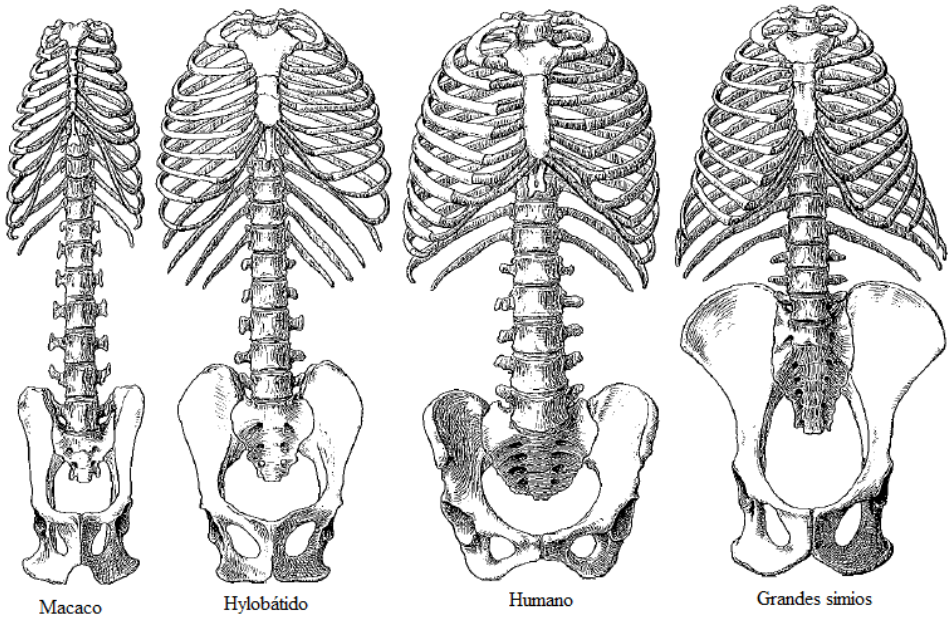

Figura 5: Representación de la morfología del tronco en diferentes primates. Véase no solo la diferencia en la morfología torácica y pélvica, sino también en la diferencia en el número de vertebras torácicas y lumbares. Modificado de Schultz (1961).

Centrándonos en el grupo *Hominoidea*, al cual pertenece el ser humano, tradicionalmente se ha propuesto que los géneros de "grandes simios", *Gorilla*, *Pan* y *Pongo*, presentaban una caja torácica en forma de embudo (o *funnel-shaped*), con una parte craneal proporcionalmente estrecha en dirección medio-lateral en comparación con la parte inferior que sería muy medio-lateralmente ancha, proporcionalmente (Figs. 4 y 5). Este patrón contrastaría con la morfología torácica propuesta para *Homo sapiens*, en forma de barril (o *barrel-shaped*), caracterizada por una morfología del tórax superior en forma de bóveda en la y una parte inferior medio-lateralmente más estrecha, proporcionalmente, que en las cajas torácicas *funnel-shaped* (Figs. 4 y 5). Los gibones y siamangs, pertenecientes al grupo de los Hilobátidos, han sido igualmente caracterizados por tener una caja torácica en forma de barril (Schultz, 1961; Kagaya et al., 2008; Holliday, 2012), lo cual ha sido atribuido a una posible convergencia evolutiva con *Homo sapiens* debido a que ambos tienen un modo de desplazamiento en posición ortógrada, bien por bipedestación en *Homo* o bien por braquiación en Hilobátidos.

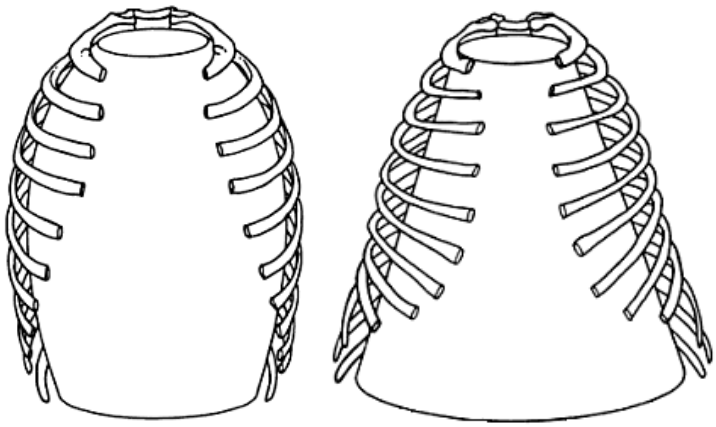

Figura 6: Detalle de la diferencia morfológica entre el patrón en forma de barril (izquierda) que caracteriza a los humanos y el patrón en forma de embudo (derecha) que caracteriza a los grandes simios. Modificado de Jellema et al. (1993).

La forma de torácica de embudo en grandes simios o de barril en *Homo* o *Hylobates*, según las hipótesis clásicas, podría ser una consecuencia de la restructuración sistémica del tronco (cintura escapular, pélvica y tórax) principalmente debida a diferencias posturales y en patrones de locomoción (Schultz, 1961; Jellema et al., 1993; Kagaya et al., 2008; Latimer et al., 2016). Sin embargo, otros factores como el tipo de dieta también han de ser tenidos en cuenta ya que la morfología de la caja torácica inferior, por su cercanía anatómica con la parte abdominal del tronco, podría verse condicionada por determinados requerimientos adaptativos de los órganos que el vientre alberga, como el hígado o el intestino (Aiello y Wheeler, 1995; Antón y Snodgrass, 2012; Ben-Dor et al., 2016).

En cajas torácicas en forma de embudo, la morfología superior medio-lateralmente estrecha proporcionalmente está vinculada según ciertos autores con una posición alta de los hombros, una posición dorsal de la escápula y a clavículas proporcionalmente cortas (Larson, 2007, 2015; Rosas et al., 2015, 2016; Feuerriegel et al., 2016; Rodríguez-Pérez et al., en revisión). Por su parte, una morfología de tórax inferior proporcionalmente amplia en dirección medio-lateral, estaría vinculada a una columna lumbar corta y poco flexible y a crestas ilíacas supero-inferiormente altas y medio-lateralmente amplias (Schultz, 1961; Jellema et al., 1993; Lovejoy, 2005; Latimer, 2016). Esta configuración anatómica del tórax (y el tronco) permitiría

un mayor rango de movimientos del miembro superior, la acomodación de un gran aparato digestivo ligado al amplio consumo de recursos vegetales, así como, posiblemente, una gran capacidad respiratoria diafragmática (Latimer et al., 2016).

En individuos que poseen tórax en forma de embudo, como hipotéticamente los grandes simios), la disposición anatómica de la columna lumbar junto con su reducido tamaño relativo, ayudaría a proteger la zona lumbar de posibles daños mecánicos durante los movimientos asociados a la locomoción suspensoria (Lovejoy y McCollum, 2010; Latimer et al., 2016; Williams et al., 2016). En individuos con cajas torácicas en forma de barril, como las que presentan los humanos modernos, la morfología superior en forma de bóveda estaría vinculada a una posición más baja de los hombros, con escápulas más lateralmente orientadas y clavículas proporcionalmente más elongadas (Larson, 2007, 2015; Rosas et al., 2015; Feuerriegel et al., 2017; Rodríguez-Pérez, en revisión). El tórax inferior, proporcionalmente estrecho en dirección medio-lateral, estaría vinculado en este caso a una columna lumbar relativamente elongada y flexible y una pelvis más corta supero-inferiormente y más estrecha medio-lateralmente (Schultz, 1961, Jellema et al., 1993, Lovejoy, 2005, García-Martínez et al., 2013a; Latimer et al., 2016). Dicha morfología torácica estaría vinculada a una cintura escapular adaptada al balanceo del miembro superior durante la locomoción bípeda, aunque otros factores como la manipulación o lanzamiento preciso de objetos también han sido propuestos como potenciales presiones selectivas detrás de esta morfología del miembro superior, según algunos autores (Roach y Richmond, 2015; Feuerriegel et al., 2017). A su vez, la parte inferior del tórax en forma de barril, en conexión con una columna lumbar elongada y una pelvis estrecha, habría facilitado la locomoción bípeda mediante marcha o carrera (*bipedal walking or running*) y podría haber sido el reflejo de un cambio de dieta orientada hacia un mayor aprovechamiento de recursos cárnicos (Aiello y Wheeler, 1995).

Capítulo 1.3 Anatomía evolutiva de la caja torácica humana.

La anatomía evolutiva de la caja torácica ha sido tradicionalmente menos estudiada con respecto a otras partes esqueléticas como el cráneo, los miembros superiores e inferiores o la cintura pélvica y escapular (Gómez-Olivencia et al., 2009), debido fundamentalmente a tres factores:

- La fragilidad de los elementos que componen el esqueleto torácico: debido a este factor, que se observa fácilmente en costillas, aunque también en vertebras torácicas, el registro fósil de esta parte anatómica tiende a ser extremadamente escaso, además de que los restos torácicos suelen presentar deformaciones o fragmentación debido a procesos tafonómicos. Adicionalmente, es importante señalar que, debido a la fragilidad de estos elementos, el proceso de excavación de restos fósiles torácicos no resulta una tarea fácil, por lo que es normal que los fósiles presenten lo que se denominan "fracturas recientes" o "de excavación". La preservación de los restos también depende en gran medida de si estos fueron expuestos al medio en el momento de la muerte del individuo, o si fueron intencionalmente protegidos (por motivos rituales, etc.). Por ejemplo, en el registro fósil de Neandertales que han sido propuestos como enterramientos intencionados (Kebara 2, Shanidar 3, La Chapelle-aux-Saints, entre otros), la preservación de los elementos del esqueleto torácico es mucho mejor que en individuos donde no se practicaba el tratamiento funerario de los individuos (como en el yacimiento de El Sidrón). Adicionalmente, la preservación de las vértebras suele ser mejor que la de las costillas de un mismo individuo, pero es importante señalar el caso del Neandertal Shanidar 3, donde la preservación de las costillas es mejor que el de las vértebras torácicas (Trinkaus, 1983). También hay que señalar, que no todas las partes de las costillas y las vértebras se preservan del mismo modo. De hecho, los

extremos proximales y distales no suelen preservarse en las costillas, mientras que las partes que se preservan con menor frecuencia en las vértebras torácicas son los procesos transversos y el proceso espinoso.

- La condición metamérica de la caja torácica: este hecho, hace que usualmente en el registro fósil nos encontremos únicamente algunas *partes* (costillas y vértebras) de la secuencia completa, lo que hace que resulte extremadamente complicada la estimación de la morfología del todo (*tórax*) del individuo. También se observa una preservación diferencial en algunos niveles costales específicos. De este modo, la primera costilla, por su morfología más compacta y su tamaño más reducido, suele preservarse mejor en el registro fósil que otras costillas con una morfología más elongada o con mayor torsión costal (Gorjanović-Kramberger, 1906; Schmid et al., 2013; véase **capítulo 8**). Esto se debe a que las fuerzas de presión que pueden sufrir los fósiles durante el proceso de fosildiagénesis, hacen más posible la fractura de las mismas.
- La complicada morfología tridimensional que presentan los elementos costales y vertebrales: esto hace que, tradicionalmente, haya sido complicado realizar una rigurosa cuantificación morfológica de los mismos utilizando morfometría tradicional (arcos, cuerdas y ángulos). Específicamente, la morfología costal ha sido más difícilmente cuantificable que la vertebral debido a que factores como la torsión costal (giro en espiral del eje de la costilla en torno a un eje imaginario) han sido complicados de medir mediante técnicas de morfometría tradicional. Esto, junto con la mejor preservación de las vértebras en el registro fósil, ha producido que, dentro del estudio de la caja torácica, se haya profundizado más en el estudio de la columna torácica que en el del esqueleto costal. En este trabajo de tesis doctoral, se pretende resolver este problema abordando el estudio de la caja torácica y de los elementos

que la componen desde un estudio tridimensional detallado, a través de técnicas cuantificación de curvas y superficies mediante *sliding semilandmarks* y MG 3D (Gunz et al., 2005, 2009).

Teniendo en cuenta todas estas limitaciones respecto al estudio de la evolución de la caja torácica, los primeros hominoideos en términos cronológicos y evolutivos del linaje de los hominoideos (grupo al que pertenecen los grandes simios, gibones, humanos y sus antecesores), que presentan material torácico, son los de la especie *Proconsul nyanzae* (Kenia, 18 millones de años; Ward, 1993). Ha sido sugerido que esta especie poseía una caja torácica estrecha medio-lateralmente y profunda antero-posteriormente, similar a lo que se observa en lo que Schultz (1961) llamaba *monkeys*, lo que sería debido a una adaptación locomotora al cuadrupedalismo pronógrado (Ward, 1993). De hecho, estos autores proponen que muchos aspectos de la morfología post-craneal de *Proconsul nyanzae* representan probablemente el patrón ancestral de la Superfamilia *Hominoidea* e incluso del infraorden *Catarrhini* (Fig. 7).

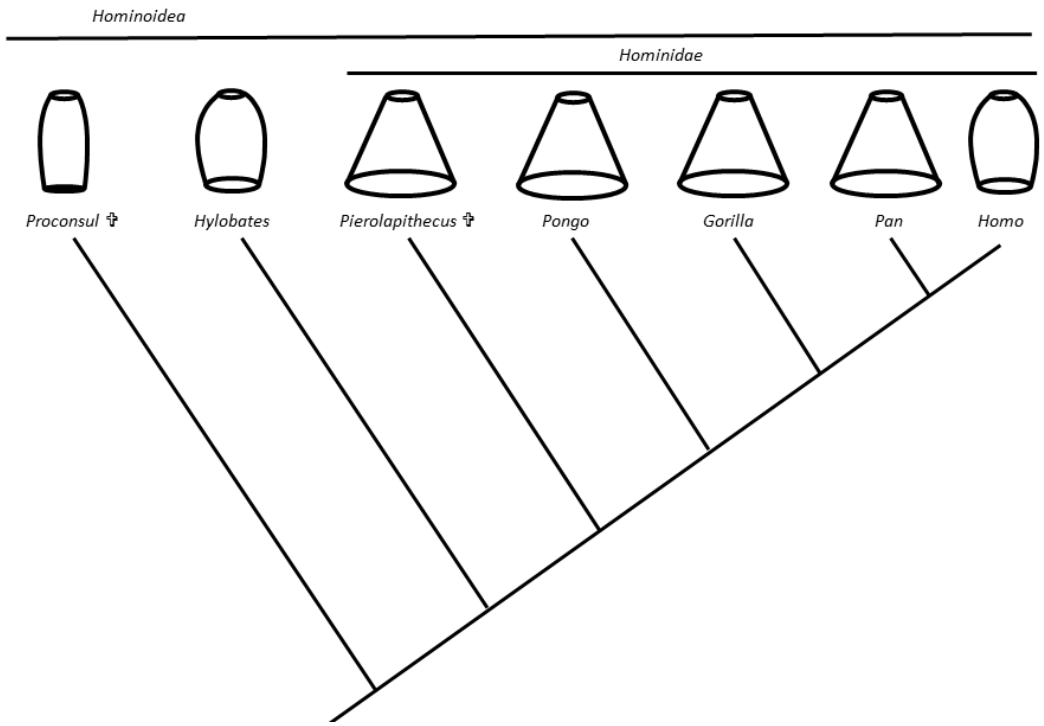

Figura 7: Esquema filogenético del clado *Hominoidea* basado en Alba et al. (2010), donde se representan los géneros de primates, así como su hipotética morfología torácica hipotética basada en Schultz (1930; 1961). Nótese que únicamente se representan aquellos fósiles de los que se tiene conocimiento de su tórax. El símbolo ✞ significa que son géneros extintos.

Estudios posteriores, basados en los fósiles españoles de *Pierolapithecus* (12 millones de años, según Moyà-Solà et al., 2004) e italianos de *Oreopithecus* (8,5 millones de años, según Azzaroli et al., 1986) han sugerido que estos especímenes ya poseían un tórax del tipo de los hominoideos actuales (medio-lateralmente ancho y poco profundo) en función a una adaptación a cambios hacia una locomoción y una postura más ortógrada (Moyà-Solà et al., 2004), representando probablemente el patrón torácico ancestral de la Superfamilia *Hominoidea* (Fig. 7).

Debido a la escasez de registro de fósiles homínidos durante el final del Mioceno y principio del Plioceno (periodo Mesiniense), las siguientes evidencias fósiles que pueden arrojar luz sobre la evolución de la caja torácica humana aparecen ya a finales de este último periodo, concretamente con el género *Australopithecus*. Respecto a la especie más antigua de la que se conocen restos torácicos fósiles, *Australopithecus afarensis* (África del Este; en torno a 3,7-2,9 millones de años; según Kimbel y Delezene, 2009), dos individuos fundamentalmente proporcionan datos acerca de su morfología torácica: A.L.288-1 y KSD-VP-1/1. El primero de ellos, A.L.288-1 también conocido como "Lucy", es un individuo supuestamente femenino y de tamaño corporal reducido datado en 3,2 millones de años y encontrado en Etiopia (Johanson et al., 1982). Aunque los autores de Johanson et al. (1982) únicamente describieron en detalle una primera costilla (A.L.288-1 ax), reconstrucciones posteriores de su caja torácica (Schmid, 1983) asumieron que la morfología torácica de este individuo era similar a la que podemos encontrar actualmente en grandes simios, es decir, en forma de embudo (Fig. 8). Esto estaría relacionado con una cintura pélvica ancha y con las crestas ilíacas dispuestas más coronalmente que en *Homo sapiens*, aunque no tan coronales como los chimpancés (Schmid, 1983). Debido a la fragmentación de los fósiles, es importante reconocer que en esa reconstrucción se tomó una cierta licencia artística (Dr. Peter Schmid, comunicación personal).

Teniendo esta reconstrucción como base, el conocimiento de la morfología torácica de *Australopithecus afarensis* (y probablemente de *Australopithecus* de forma general) permaneció inmutable como *funnel-shaped* hasta que, en 2010, fue hallado el individuo KSD-VP-1/1, también en Etiopia. Este espécimen, un individuo de mayor tamaño que A.L.288-1 aparentemente masculino, datado en torno a 3,6 millones de años (Haile-Selassie et al., 2010), preservaba suficientes restos costales como para hacer inferencias acerca de su caja torácica.

Recientes trabajos el individuo KSD-VP-1/1 (Latimer et al., 2016) apuntan a que su caja torácica inferior era medio-lateralmente expandida, similar a lo observado en grandes simios, y de acuerdo a lo propuesto según Schmid (1991) para A.L.288-1. Sin embargo, su caja torácica superior sería de tipo abovedado, similar a lo observado para *Homo sapiens* y en contra de lo propuesto por Schmid (1991). Esta morfología del tórax, hipotéticamente arcaica en la parte inferior y moderna en la superior (tomando como arcaico el patrón morfológico de los primates del Mioceno anteriormente citados), ha sido descrita por Latimer et al. (2016) como en forma de campana o *bell-shaped*. En este punto, es importante señalar que el término de tórax en forma de campana no fue acuñado primeramente para *Australopithecus*, sino que fue propuesto previamente para Neandertales (Sawyer y Maley, 2005), en un contexto evolutivo diferente. Este tema se tratará más ampliamente al final de la introducción.

Con respecto a las diferencias morfológicas entre los *Australopithecus afarensis* A.L.288-1 y KSD-VP-1/1, y dado que las diferencias de tamaño corporal son también llamativas, es posible que algunos factores alométricos pueden estar detrás del cambio desde la forma de embudo hacia la forma de campana. Sin embargo, dado que las técnicas bidimensionales empleadas por los citados trabajos no recogen de manera completa la morfología tridimensional costal, es probable que una rigurosa cuantificación tridimensional de la morfología costal de estos individuos contribuyera a aclarar esta discusión.

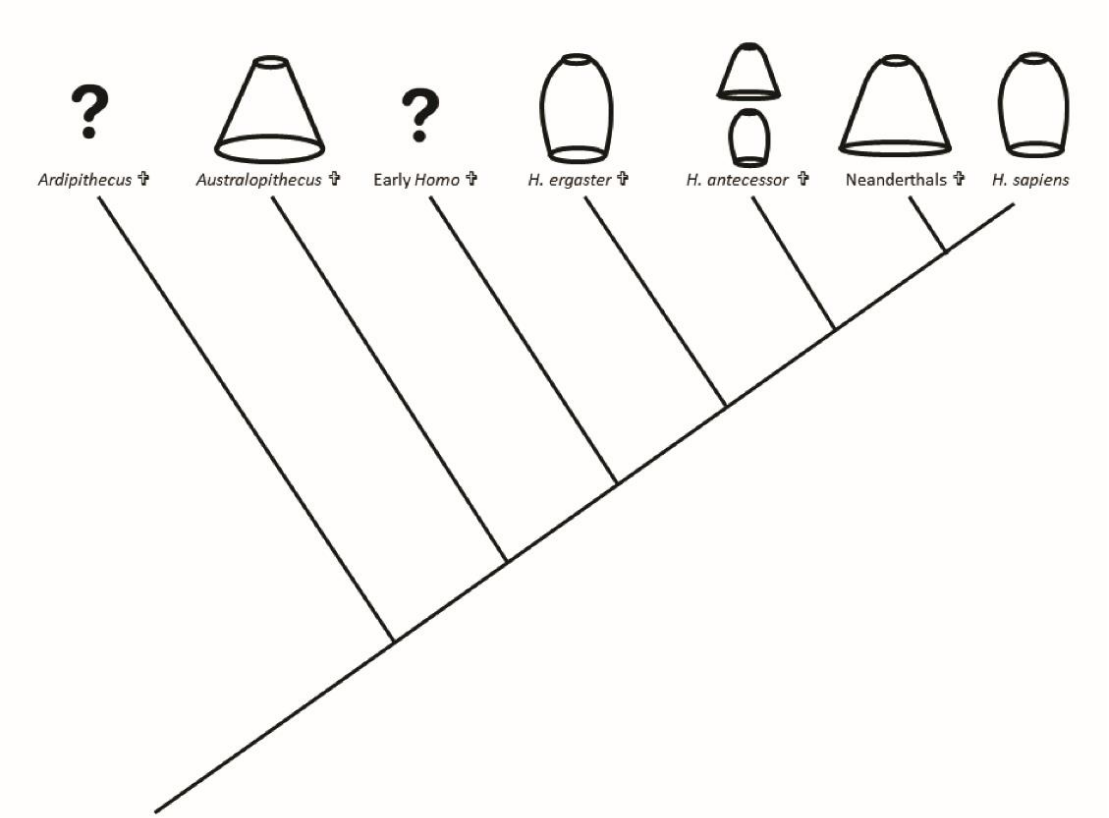

Figura 8: Esquema filogenético del clado de la Subtribu *Hominini* basado en Dembo et al. (2016), donde se representan géneros o especies de homininos, así como su hipotética morfología torácica según las hipótesis establecidas antes de la presente tesis doctoral. Nótese que únicamente se representan aquellos de los que se tiene conocimiento de su tórax y *Homo georgicus* se excluye debido a la falta de resultados concluyentes sobre sus restos costales. El símbolo ✞ significa que son géneros o especies extintas.

La siguiente especie, en términos cronológicos, de *Australopithecus* que presenta restos torácicos susceptibles de estudio es la especie *Australopithecus africanus*, hallada en África del Sur y con un rango cronológico que va desde 3 a 1,9 millones de años (Herries et al., 2013), aunque es posible que haya fósiles incluso más antiguos de esta especie (Partridge et al., 2003). El fósil que presenta una mejor preservación del esqueleto torácico es el conocido como Sts-14, que conserva una secuencia casi completa de las vértebras torácicas y algunas costillas aisladas del tórax medio e inferior (Robinson, 1972; Haeusler et al., 2002; Nalla, 2013). Sobre este individuo, hallado en las cuevas de Sterkfontein (Sudáfrica; datado en unos 2,6-2,4), se ha hipotetizado que, a pesar de su tamaño corporal reducido, podría tener una morfología torácica en forma de barril similar a la de *Homo sapiens* (Robinson, 1972), aunque esas conclusiones fueron alcanzadas únicamente a partir apreciaciones morfológicas y, hasta la fecha, no se han

realizado análisis detallados de su morfología costal tridimensional. Stw-431, un individuo de la especie *Australopithecus africanus* hallado también en las cuevas de Sterkfontein (Sudáfrica), de mayor tamaño corporal que Sts-14 y datado en 2,8-1,5 millones de años, presenta únicamente un fragmento proximal de una costilla derecha (Toussaint et al., 2003). Este fragmento, aunque poco informativo acerca de la morfología torácica, ha sido propuesto como una costilla 3 que, mayormente, presenta una morfología similar a la de los chimpancés (Nalla, 2013). Finalmente, un fragmento proximal de una primera costilla de *Australopithecus africanus* (StW-670), el cual puede proporcionar datos sobre la posible morfología del tórax superior de *Australopithecus*, ha sido recientemente publicado. Esta publicación forma parte de la presente tesis doctoral, por lo que será propiamente mostrado y discutido en el **capítulo 8a.** Finalmente, aunque algunos indicios apuntan hacia similitudes con *Homo sapiens* en la caja torácica de *Australopithecus africanus* (Robinson, 1972; Haeusler, 2002), un análisis más detallado tridimensional sobre los restos torácicos de los individuos anteriormente mencionados es imprescindible para contrastar la hipótesis de similitud entre el tórax de ambas especies.

La especie de *Australopithecus* más tardía que presenta restos torácicos bien preservados es la especie *Australopithecus sediba* (Berger et al., 2010), hallada en Sudáfrica y datada en torno a 1,95-1,78 millones de años (Dirks et al., 2010). Dos individuos de este yacimiento, MH1 (inmaduro masculino) y MH2 (adulto femenino), preservan material torácico en buen estado. Schmid et al. (2013), en el estudio de este material, hipotetizaron que esta especie poseía una caja torácica superior probablemente estrecha (similar a lo observado en tórax *funnel-shaped*) y un tórax inferior probablemente más estrecho proporcionalmente que los grandes simios (similar a lo observado en tórax *barrel-shaped*). Hay que señalar que la asignación de esta última característica anatómica no fue basada en medidas costales, sino que fue predicha en base a la reconstrucción de su morfología pélvica, hipotéticamente moderna

(Schmid et al., 2013; Kibii et al., 2011), y del nexo morfológico entre tórax inferior y cintura pélvica (Jellema et al., 1993; Bastir et al., 2014a). Por lo tanto, al haber sido encontrados en el tórax superior e inferior diferentes patrones morfológicos, los autores propusieron una evolución en mosaico para la caja torácica, donde sus diferentes partes habrían evolucionado en diferentes momentos a lo largo de la evolución humana. Sin embargo, hay que resaltar que recientes investigaciones, las cuales han cuantificado la morfología tridimensional tanto pélvica como torácica, están cuestionando estas hipótesis (Haeusler et al., 2016; **capítulo 8b**).

Teniendo en cuenta los estudios realizados hasta la fecha, es difícil especificar cuál sería el patrón morfológico de la caja torácica de *Australopithecus* o cuáles son los factores específicos que configuran su morfología, ya que la morfología propuesta por Latimer et al. (2016) y por Schmid et al. (2013) son, básicamente, opuestas. Por lo tanto, tomar la morfología torácica de *Australopithecus* como forma arcaica (o plesiomórfica) de cara a observar posibles plesiomorfías o apomorfías en el tórax de especies evolutivamente más tardías, puede presentar problemas debido a la incertidumbre mencionada.

Los siguientes representantes del linaje hominino son ya individuos del género *Homo*, el cual es hipotéticamente descendiente del género *Australopithecus* (Berger at al., 2010, 2015; Dembo et al., 2015, 2016; Wood y Boyle, 2016). Estos últimos, tienen sus últimos representantes hace unos 1,9 millones de años (*Australopithecus sediba*, específicamente). Aunque el primer representante del género *Homo* es hipotéticamente *Homo habilis* (2,6-1,6 millones de años; revisado por Wood y Boyle, 2016), los primeros individuos que presentan material torácico bien preservado de este género pertenecen a las especies *Homo ergaster* (1,8-1,4 millones de años; según McDougal et al., 2012) y *Homo georgicus* (1,8-1,7 millones de años; según Ferring et al., 2011). Específicamente, los restos del individuo KNM-WT 15000 o "niño de Nariokotome" (Walker y Leakey, 1993) y del yacimiento de Dmanisi (Lordkipanidze et al., 2007) son cruciales para la interpretación de la evolución de la caja torácica humana.

Ha sido aceptado tradicionalmente que la morfología torácica en forma de barril que se observa en *Homo sapiens*, pudo aparecer con la especie *Homo ergaster* (Jellema et al., 1993; Fig. 8). Desafortunadamente, las inferencias acerca de la caja torácica de esta especie se han hecho fundamentalmente basadas únicamente en KNM-WT 15000 debido a la escasez de material fósil de estas cronologías. Este individuo, encontrado en Kenia (cerca del Lago Turkana) y datado aproximadamente en 1,47 millones de años (McDougall et al., 2012), presenta una de las cajas torácica mejor preservadas de todo el registro fósil, dato muy llamativo para ser de una cronología tan antigua. Jellema et al. (1993) concluyeron que la evolución de la caja torácica humana hacia una morfología en forma de barril, presente en el fósil del niño de Nariokotome y persistente en la humanidad actual, habría conllevado tres cambios básicos con respecto a lo observado en el género *Australopithecus* (Jellema et al., 1993):

1. Expansión relativa de la zona superior del tórax (forma de bóveda) y estrechamiento medio-lateral relativo del tórax inferior.
2. Declinación de la porción esternal o anterior del eje de la costilla.
3. Invaginación de la columna vertebral torácica hacia la porción anterior del cuerpo.

Algunas de las características morfológicas propuestas para *Australopithecus*, y por lo tanto plesiomórficas, como la morfología redondeada de la sección transversal en la parte central del eje de la costilla o la amplitud medio-lateral de la parte central del tórax no se observan en este espécimen según Jellema et al. (1993). Sin embargo, la orientación de los procesos transversos en Nariokotome es similar tanto a *Australopithecus* como a *Homo sapiens* (Jellema et al., 1993; Latimer y Ward, 1993; Ward et al., 2012), por lo que este carácter en humanos podría ser considerado plesiomórfico. Adicionalmente, debido a un hipotético nexo morfológico entre la caja torácica inferior y la cintura pélvica (Jellema et al., 1993), Ruff y Walker (1993) propusieron para KNM-WT 15000 una morfología pélvica estrecha (similar

también a *Homo sapiens*) que sería coherente con la morfología torácica inferior estrecha en forma de barril (Jellema et al., 1993). Sin embargo, recientes investigaciones acerca de la morfología pélvica (Arsuaga et al., 1999; Holliday, 2012; Haeusler et al., 2016) o de la morfología costal (García-Martínez, 2013b) cuestionan la completa modernidad morfológica de este individuo, ya que es posible que tanto la cintura pélvica como el tórax inferior tengan amplitudes medio-laterales más elevadas que lo propuesto inicialmente. Esto será discutido en el **capítulo 8b**.

Otros fósiles de cronología similar (1,8 millones de años; según Ferring et al., 2011) provenientes del yacimiento georgiano de Dmanisi (Gabunia et al., 2000), también conservan costillas y vertebras bien preservadas, aunque éstas no han sido publicadas aún con suficiente detalle como para hacer inferencias sobre posibles plesio/apomorfías en su caja torácica (Lordkipanitze et al., 2007).

Finalmente, los restos del esqueleto axial de la recientemente descrita especie Sudafricana *Homo naledi* (Berger et al., 2015), han permitido concluir que la caja torácica de este individuo era probablemente ancha en la parte inferior (Williams et al., 2017). Estos datos apoyarían la hipótesis de una caja torácica amplia en la parte inferior, similar a lo propuesto en *Australopithecus* por Latimer et al. (2016). También se ha observado que presentaba la columna vertebral toraco-lumbar probablemente invaginada en función a una adaptación a la locomoción bípeda (Williams et al., 2017). Esto también será ampliamente discutido en el **capítulo 8b**.

Con respecto a la especie *Homo naledi* (Berger et al., 2015), puede ser problemático hacer inferencias filogenéticas o evolutivas de su caja torácica debido a su cronología incierta (Dirks et al., 2015). Aunque se asocia con *Homo erectus* u *Homo georgicus* por su morfología craneal (Laird et al., 2017; Schroeder et al., 2017), no hay que descartar que pueda ser una

relicto evolutivo que haya perdurado hasta hace relativamente poco tiempo, como ha ocurrido según algunos autores con la especie *Homo floresiensis* (Berger et al., 2008).

Otros miembros más tardíos del género *Homo*, hipotéticamente descendientes de *Homo ergaster* y ancestros de *Homo sapiens* y Neandertales, son los fósiles de la especie *Homo antecessor* (Bermúdez de Castro et al., 1997; Carbonell et al., 2005; Dembo et al., 2016). Desgraciadamente, la preservación de los restos vertebrales torácicos de esta especie no permite hacer inferencias acerca de su morfología torácica (Carretero et al., 1999) y las evidencias en base a estudios con medidas tradicionales del esqueleto costal realizadas hasta la fecha (Gómez-Olivencia et al., 2010) no permiten encontrar diferencias entre el tórax de *Homo antecessor* y el de *Homo sapiens* (Fig. 8). Aunque es posible que estas evidencias efectivamente no existan, estudios preliminares tridimensionales, los cuales son presentados en el **capítulo 8b,** apuntan a una mayor anchura en el tórax inferior en *Homo antecessor* que en el caso de *Homo sapiens* (Fig. 8).

Finalmente, con respecto a la caja torácica Neandertal (King, 1864), se conocen datos más detallados acerca de su caja torácica debido al mayor número de restos fósiles torácicos existentes y a la mayor cantidad de trabajos publicados hasta la fecha (Fuhlrott, 1859; Gorjanović-Kramberger, 1906; Boule, 1911-1913; McCown y Keith, 1939; Heim, 1976; Arensburg et al., 1991; Franciscus y Churchill, 2002; Weinstein, 2008; Gómez-Olivencia, 2015; Gómez-Olivencia et al., 2009; véase **capítulo 8c**). Los primeros estudios acerca de la caja torácica de estos homínidos, endémicos de Eurasia con cronologías que van desde los 200.000 hasta los 40.000 años (Higham, 2014), fueron llevados a cabo desde finales del siglo XIX hasta mediados del siglo XX. Entre ellos se encuentran los estudios de los restos costales fósiles del yacimiento de Feldhofer Grotte en Alemania (Fuhlrott, 1859), del yacimiento de Krapina en Croacia (Gorjanović-Kramberger, 1906), del yacimiento de Tabun en Israel

(McCown y Keith, 1939) y de los yacimientos franceses de La Chapelle-aux-Saints (Boule, 1911-1913) y la Ferrassie (Heim, 1976).

Hasta la fecha, lo más aceptado es que la caja torácica Neandertal estaría caracterizada por una gran capacidad torácica con respecto a lo observado en *Homo sapiens* (Franciscus y Churchill, 2002; Weinstein, 2008; Gómez-Olivencia et al., 2009; véase **capítulo 8c**). Sin embargo, no se conoce si esa mayor capacidad torácica viene definida por una expansión de la caja torácica en dirección antero-posterior, medio-lateral o ambas (Gómez-Olivencia et al., 2009). Aunque en términos funcionales, esta expansión torácica podría responder a los altos requerimientos energéticos hipotetizados para los individuos de esta especie, otros factores como la adaptación a climas fríos no puede ser completamente descartada (Franciscus and Churchill, 2002; Weinstein, 2008; Gómez-Olivencia et al., 2009). En términos evolutivos, se ha hipotetizado también que esta morfología, especialmente ancha en la parte inferior y con secciones transversales redondeadas podría ser un carácter heredado de homínidos del Pleistoceno Inferior (Franciscus y Churchill, 2002; Gómez-Olivencia et al., 2009; Gómez-Olivencia et al., 2010; véase **capítulo 8c**). De hecho, algunos autores han usado el término acampanado (*bell-shaped*) para definir el tórax Neandertal debido a su morfología superior en forma de bóveda (*dome-shaped* según McCown y Keith, 1939) y a su parte inferior ancha (Sawyer y Maley, 2005), término que recordemos ha sido también usado para definir el tórax del *Australopithecus* KSD-VP-1/1 (Latimer et al., 2016). Es importante señalar que se requiere cierta cautela en la interpretación de estos términos ya que *bell-shaped* en el contexto *Australopithecus* viene definido por "una porción superior similar a la humana pero que se expande de algún modo en su porción inferior" (Latimer et al., 2016: 147), pero que en el contexto Neandertal ha sido definido por una caja torácica superior en forma de bóveda, diferente a humanos modernos, y un tórax inferior expandido (Sawyer y Maley, 2005: 29). Por lo tanto, aunque en ambos contextos el término *bell-shaped* hace referencia a una expansión

del tórax inferior, el tórax superior *bell-shaped* sería similar a *Homo sapiens* para Latimer et al. (2016) pero diferente de *Homo sapiens* para Sawyer y Maley (2005). Esto hace evidente que la utilización de términos como *bell-*, *barrel-*, *dome-* o *funnel-shaped* para definir la compleja morfología tridimensional torácica, aunque es útil para tener una imagen general de su forma, simplifican excesivamente la realidad tridimensional del conjunto torácico y han de ser usados con mucha cautela. El hecho de que la caja torácica de *Homo sapiens* haya sido tradicionalmente clasificada como *barrel-shaped*, también es un ejemplo de esta excesiva simplificación, ya que variaciones que alejan la caja torácica del *barrel-shaped* han sido encontradas en factores como ontogenia y dimorfismo, como se ve en los **capítulos 4 y 5**. Una discusión más extensa de los problemas con la terminología torácica se podrá encontrar también en el **capítulo 7**, sobre la variabilidad en la morfología torácica del clado *Hominoidea*.

CAPÍTULO II – OBJETIVOS DE LA TESIS

La variabilidad morfológica de la caja torácica (tanto del *todo* torácico, como sus *partes* individuales) ha sido tradicionalmente poco estudiada en comparación con otros elementos esqueléticos (Gómez-Olivencia et al., 2009; véase **capítulo 8**). Esto aplica a todos los diferentes campos de conocimiento, desde la variabilidad intra-específica (dimorfismo sexual, ontogenia, anatomía funcional) hasta la variabilidad inter-específica (anatomía comparada y anatomía evolutiva). Los antecedentes indican por tanto una clara necesidad de un estudio exhaustivo cuantitativo del tamaño y la configuración tridimensional del tórax y sus variaciones en los citados campos.

El objetivo de la presente tesis doctoral es, por tanto, llenar ese vacío de conocimiento, teniendo como base un objetivo general que es **contribuir al conocimiento de la variabilidad morfológica de la caja torácica humana, así como sus implicaciones funcionales y evolutivas**.

Este, será desglosado en diferentes objetivos específicos dependiendo del área del conocimiento a investigar, los cuales son:

1. **Objetivo 1: contribuciones al conocimiento del desarrollo ontogenético de la caja torácica humana (véase capítulo 4: publicaciones nº 1 y 2)**. Trabajos previos han descrito cambios en la caja torácica durante la ontogenia, tanto en las dimensiones del conjunto torácico (anchura, altura) como en la disposición y forma de los elementos que la componen (Openshaw et al., 1984). Sin embargo, algunos autores han hipotetizado que las partes superior e inferior de la caja torácica están

morfológicamente integradas con el miembro superior en inferior respectivamente, a través de las cinturas pélvica y escapular (Jellema et al., 1993; Bastir, 2008; Schmid et al., 2013; Bastir et al., 2014a). Por lo tanto, se plantea la hipótesis de que la caja torácica pueda tener un desarrollo modular y que tórax superior e inferior tengan trayectorias ontogenéticas divergentes en cierto grado en función de esta integración diferencial. El principal objetivo de este punto será hacer un análisis morfológico detallado del desarrollo ontogenético de la caja torácica desde el nacimiento hasta la edad adulta, contrastando la hipótesis de la posible naturaleza modular del tórax humano (superior vs. inferior).

2. **Objetivo 2: contribuciones al conocimiento del dimorfismo sexual en la caja torácica humana (véase capítulo 5: publicaciones nº 3 y 4).** El dimorfismo sexual es un potencial generador de variabilidad que ha sido observado en el esqueleto humano tanto a nivel craneal como post-craneal (Rosas y Bastir, 2002; Bulygina et al., 2006; Reno et al., 2003; Carlson et al., 2007; Kranioti et al., 2009). Respecto a la caja torácica, trabajos previos han propuesto la existencia de ciertos patrones morfológicos diferenciales en hombres y mujeres a través del uso de medidas tradicionales (Bellemare et al., 2003, 2006). Sin embargo, dado que la caja torácica en una estructura tridimensional compleja y a que las medidas tradicionales no recogen completamente la variabilidad en aspectos como la profundidad, la anchura o la altura relativa, el objetivo de este punto es realizar un estudio detallado del posible dimorfismo sexual de la caja torácica en su configuración tridimensional, contrastando dichas diferencias y profundizando en las posibles implicaciones funcionales de las mismas.

3. **Objetivo 3: contribuciones al conocimiento de la anatomía funcional de la caja torácica humana (véase capítulo 6: publicación nº 5)**. Una de las principales funciones de la caja torácica es dar soporte a la mecánica respiratoria, la cual es producida por la interacción de las costillas, las vértebras y los músculos respiratorios (De Troyer, 2005). Ha sido previamente observado por otros autores, que la variación en estos factores puede producir diferencias en la mecánica respiratoria del tórax, tanto superior como inferior (Franciscus y Churchill, 2002; West, 2012; Beyer et al., 2014). Sin embargo, el impacto de esta variación morfológica no ha sido totalmente estudiado hasta la fecha, por lo que en esta tesis se contrastará la hipótesis de la diferencia en la cinemática en el tórax superior e inferior.

4. **Objetivo 4: contribuciones al conocimiento de la anatomía comparada reciente de la caja torácica humana (véase capítulo 7: publicación nº 6)**. Desde los estudios basales de Adolf Schultz, se ha establecido una tipología dicotómica de morfología torácica en primates hominoideos (Schultz, 1960, 1963). De este modo, el término de caja torácica *funnel-shaped* ha sido usado para los géneros *Pan*, *Gorilla* y *Pongo*, mientras que el término de caja torácica *barrel-shaped* ha sido usado para los géneros *Homo* e *Hylobates*. Sin embargo, estudios preliminares (García-Martínez et al., 2013a) han observado que, aunque estos términos permiten obtener una idea global de la forma del tórax, sobre-simplifican la complejidad de la morfología torácica. Por lo tanto, el objetivo de este punto será hacer un análisis detallado de la morfología torácica en los géneros de hominoideos previamente mencionados, contrastando la hipótesis de la dicotomía morfológica *funnel-* vs.

barrel-shaped y observando a qué nivel torácico se hacen más notables las diferencias.

5. **Objetivo 5: contribuciones al conocimiento de la anatomía evolutiva de la caja torácica humana (véase capítulo 8: publicaciones nº 7 a 13 y resúmenes de congreso nº 1 y 2)**. Debido a la frágil naturaleza de los restos torácicos, el registro fósil es escaso y fragmentado, lo cual ha hecho más complicado estudiar la anatomía evolutiva de la caja torácica. Como en esta tesis se estudia la anatomía evolutiva a través de diferentes especies de homínidos, este objetivo será descompuesto en diferentes apartados.

    Objetivo 5a: contribuciones al conocimiento de la anatomía evolutiva en el género *Australopithecus* (publicación nº 7 y resumen en congreso nº 1). Aunque inicialmente fue propuesto que la caja torácica de *Australopithecus*, hipotéticos antecesores del género *Homo*, era caracterizada por una forma *funnel-shaped* (Schmid, 1983, 1991), recientes estudios cuestionan estos resultados (Latimer et al., 2016). De este modo, en esta tesis doctoral se hace la presentación de un resto de primera costilla de *Australopithecus africanus* hallada en las cuevas de Sterkfontein, Sudáfrica (publicación nº 7), y se contrastan, de manera preliminar, diferencias en el tórax superior e inferior en *Australopithecus* en un marco de anatomía comparada (resumen en congreso nº 1).

    Objetivo 5b: contribuciones al conocimiento de la caja torácica de homínidos del Pleistoceno Inferior (*Homo ergaster* y *Homo antecessor*), así como de la especie *Homo naledi* (publicación nº 8 y resumen de

congreso nº 2). La especie *Homo ergaster* fue inicialmente descrita con una forma corporal similar a *Homo sapiens*, lo que conllevaba una caja torácica en forma de barril o *barrel-shaped* (Jellema et al., 1993). Sin embargo, recientes trabajos preliminares sobre la caja torácica de este individuo ponen en duda esta teoría (García-Martínez et al., 2013b), lo que es reforzado por la morfología de otro homínido del Pleistoceno Inferior, *Homo antecessor* (resumen de congreso nº2). Otra especie, morfológicamente afín a *Homo ergaster y erectus*, de cronología incierta, también podría arrojar luz sobre la morfología evolutiva de la caja torácica. En este punto se hace la descripción y análisis de los restos torácicos de *Homo naledi* (publicación nº 8) y se lleva a cabo un estudio detallado de la morfología costal de homínidos del Pleistoceno Inferior, *Homo ergaster* y *Homo antecessor*, contrastando diferencias en el tórax superior e inferior (resumen de congreso 2).

Objetivo 5c: contribuciones al conocimiento de la caja torácica Neandertal y sus implicaciones funcionales y evolutivas (publicaciones nº 9-12). Es aceptado que la caja torácica Neandertal era más voluminosa que la de humanos modernos (Franciscus y Churchill, 2002; Weinstein, 2008; Gómez-Olivencia et al., 2009), lo que podría ser debido a un patrón morfológico arcaico, a una adaptación a altos requerimientos energéticos, a una adaptación a climas fríos o a varios de estos factores en combinación. En este punto, en esta tesis se presenta el material torácico (tanto vertebral como costal) del yacimiento asturiano de El Sidrón (Asturias, España;

49,000 años de antigüedad), y se contrasta la hipótesis de diferencias en tamaño y forma de la caja torácica entre Neandertales y humanos modernos.

Ya que estos objetivos específicos se alcanzan a través de un compendio de publicaciones, para un seguimiento más fácil se ha recogido en la Tabla 1, información de los capítulos que corresponden a cada objetivo, así como las publicaciones que contiene cada capítulo.

	Capítulo	**Publicaciones**	**Paginación en la tesis**
Objetivo 1	Capítulo 4	Publicaciones nº 1 y 2	64-96
Objetivo 2	Capítulo 5	Publicaciones nº 3 y 4	98-124
Objetivo 3	Capítulo 6	Publicación nº 5	126-135
Objetivo 4	Capítulo 7	Publicación nº 6	137-186
Objetivo 5a	Capítulo 8	Publicación nº 7 y resumen congreso nº 1	188-195
Objetivo 5b	Capítulo 8	Publicación nº 8 y resumen congreso nº 2	197-223
Objetivo 5c	Capítulo 8	Publicaciones nº 9, 10, 11 y 12	225-339

Tabla 1: objetivos, capítulos donde esos objetivos son alcanzados, así como las publicaciones que contiene cada capítulo y el número de paginación que tienen dichos artículos en la presente tesis.

CAPÍTULO III – MATERIAL Y MÉTODOS

Capítulo 3.1 Material.

El material empleado para la elaboración de la presente tesis doctoral, comprende tanto cajas torácicas en conexión anatómica como costillas y vértebras individuales. Aunque en este capítulo se explica la muestra utilizada para llevar a cabo cada objetivo, dada la variedad de la muestra utilizada para el desarrollo de la presente tesis doctoral, dentro de cada publicación se detallará información más concreta. Es importante señalar que, cuando los datos fueron extraídos de pacientes hospitalarios, estos fueron anonimizados para cumplir con la Declaración de Helsinki (Goodyear et al., 2007).

Para alcanzar el objetivo 1 (**Contribuciones al conocimiento del desarrollo ontogenético de la caja torácica humana; capítulo 4: publicaciones nº 1 y 2**), se emplearon modelos 3D de cajas torácicas de sujetos hospitalarios, cuyo rango de edad comprende desde neonatos hasta adultos, obtenidos a través de tomografía axial computarizada (TAC). A la hora de hacer el estudio, se tuvo en cuenta que el motivo del escaneo de los individuos no fuese ninguna afección asociada al sistema respiratorio, descartando de este modo cualquier variación de la morfología torácica debida a factores patológicos. Todos los pacientes fueron escaneados en posición supina en el Hospital Universitario de Innsbruck (Austria), excepto tres individuos neonatos que fueron escaneados en el Hospital Universitario de Burdeos (Francia), dos de ellos por trauma y un tercero para la realización de una autopsia virtual.

Para alcanzar el objetivo 2 (**Contribuciones al conocimiento del dimorfismo sexual en la caja torácica humana; capítulo 5: publicaciones nº 3 y 4**), se emplearon dos muestras diferentes. La primera de ellas, empleada para la publicación nº 3, consta de 239 vértebras torácicas individuales pertenecientes a 24 individuos adultos no patológicos de sexo conocido (12 individuos masculinos y 12 femeninos), cuyas edades variaban entre los 20 y 42 años de edad. Estos restos se encuentran depositados en la Escuela de Medicina Legal de la Universidad Complutense de Madrid (Madrid, España). Para este estudio, únicamente se seleccionaron vértebras T1-T10 debido a que las vértebras T11 y T12 carecen de algunas estructuras como las facetas articulares de los procesos transversos, por lo que sus *landmarks* no son estrictamente homologables a los de las vértebras T1-T10. Para la publicación nº 4, se usaron modelos 3D obtenidos a partir de datos de TAC de cajas torácicas de 42 individuos adultos (18 individuos masculinos y 24 femeninos) cuya edad variaba entre los 40 y los 67 años de edad. Los individuos fueron escaneados en el Hospital Universitario de La Paz (Madrid, España), previamente a esta tesis doctoral, como grupo control (sano) para la comparación con individuos con afecciones respiratorias. Por lo tanto, patologías que pudiesen afectar a la morfología torácica estaban totalmente descartadas.

Para el desarrollo del objetivo 3 (**Contribuciones al conocimiento de la anatomía funcional de la caja torácica humana; capítulo 6: publicación nº 5)**", se usaron modelos 3D obtenidos a partir de datos de TAC de cajas torácicas de 20 individuos adultos (16 masculinos y 4 femeninos) escaneados tanto en inspiración máxima como en espiración máxima, cuya edad oscilaba entre los 40 y 67 años de edad.

Para llevar a cabo el objetivo4 de esta tesis doctoral (**Contribuciones al conocimiento de la anatomía comparada reciente de la caja torácica humana; capítulo 7: publicación nº 6**), se emplearon modelos 3D obtenidos a partir de TAC de cajas torácicas de diferentes primates adultos de la Superfamilia *Hominoidea*, los cuales fueron escaneados en posición

supina. Concretamente, fueron empleados 10 *Homo sapiens*, 5 *Gorilla gorilla*, 10 *Pan troglodytes*, 4 *Pongo pygmaeus* y 4 hilobátidos (2 *Hylobates lar*, 1 *Hylobates agilis*, 1 *Symphalangus syndactylus*). Los datos de imagen médica procedentes de hominoideos no humanos están disponibles online en Kyoto University Primate Research Institute (Kupri; http://dmm.pri.kyoto-u.ac.jp), mientras que los datos de *Homo sapiens* utilizados en el presente capítulo provienen tanto del Hospital Universitario de La Paz (Madrid, España) como del Hospital Universitario de Innsbruck (Innsbruck, Austria).

Finalmente, con respecto a la muestra empleada para llevar a cabo el objetivo 5 de la presente tesis doctoral (**Contribuciones al conocimiento de la anatomía evolutiva de la caja torácica humana; capítulo 8: publicaciones nº 7 a 13 y resúmenes de congreso 1 y 2**), se utilizó una muestra diferente para los objetivos específicos 5a, 5b y 5c.

Para llevar a cabo el objetivo 5a (**Contribuciones al conocimiento de la anatomía evolutiva en el género *Australopithecus*; publicación nº 7 y resumen en congreso nº 1**), se utilizaron costillas individuales de primates hominoideos no humanos (*Pongo*, *Pan*, *Gorilla* e hilobátidos), así como de humanos de poblaciones europeas y africanas. Respecto a la muestra fósil, para la publicación nº 7 se empleó un fragmento de primera costilla de *Australopithecus africanus*, Stw-670, el cual es presentado y estudiado en un marco comparado en esta tesis doctoral, así como modelos 3D de las primeras costillas de los fósiles A.L.288-1 (*Australopithecus afarensis*), MH1 y MH2 (*Australopithecus sediba*) y KNM-WT 15000 (*Homo ergaster*). Para el resumen en congreso nº 1 se utilizó el material costal completo de *Australopithecus sediba* presentado por Schmid et al. (2013).

Para llevar a cabo el objetivo 5b (**Contribuciones al conocimiento de la caja torácica de homínidos del Pleistoceno Inferior, así como de la especie *Homo naledi*; publicación nº 8 y resumen en congreso nº 2**), se utilizó un marco comparado de *Homo sapiens* tanto europeos como africanos y de *Pan troglodytes*, cuyas edades comprenden desde el estado juvenil hasta el estado adulto. Respecto al material fósil, para la publicación nº 8 se empleó todo el material axial de la especie *Homo naledi*, que es presentado en esta tesis doctoral, así como los fósiles de *Australopithecus africanus* (Sts-14), *Australopithecus afarensis* (A.L.288-1) y *Homo ergaster* (KNM-WT 15000). Con respecto a los fósiles empleados en el resumen en congreso nº 2, se utilizaron moldes de alta calidad del esqueleto costal de *Homo antecessor*, así como modelos 3D obtenidos de TAC de las costillas originales del *Homo ergaster* KNM-WT 15000.

Finalmente, para el desarrollo del objetivo 5c, "**Contribuciones al conocimiento de la caja torácica Neandertal y sus implicaciones funcionales y evolutivas (publicaciones nº 9-12)**", se emplearon diferentes muestras comparativas de *Homo sapiens* europeos. Respecto a la muestra de fósiles, se emplearon modelos 3D del material costal y vertebral de diferentes individuos Neandertales como La Chapelle-aux-Saints 1, Kebara 2, Shanidar 3, Tabun 1, La Ferrassie 1 y 6, así como el material original del yacimiento asturiano de El Sidrón, el cual es presentado en los artículos nº 10-12 de la presente tesis doctoral.

Capítulo 3.2 Métodos.

Capítulo 3.2.1 Antropología virtual

La Antropología virtual (*virtual anthropology*) es el análisis tridimensional de objetos antropológicos dentro de un entorno virtual, como un computador (Weber et al., 1998). Más concretamente, se conoce con este nombre al enfoque multidisciplinar del estudio de la morfología de los seres humanos, sus ancestros y sus parientes cercanos en 3 o 4 dimensiones, espacio o espacio-tiempo (Weber, 2015). El término multidisciplinar hace referencia a que la Antropología virtual hace uso herramientas que provienen de diferentes disciplinas como la Antropología, la Paleontología, la Primatología, la Medicina, las Matemáticas, la Estadística y la Ciencia Computacional.

El término Antropología virtual fue acuñado a mitad de los años 90, pero no fue hasta 1998 cuando este término fue por primera vez publicado desde una perspectiva de Antropología física (Weber et al., 1998). Aunque otros términos como "Paleoantropología asistida por computador" (*computer-assisted paleoanthropology*) también se han utilizado para referirse a la misma herramienta (Zollikofer et al., 1998), ha sido más extendido el término Antropología virtual, por lo que en la presente tesis doctoral será el término utilizado (bajo la abreviatura de AV, de aquí en adelante).

Con respecto al uso de estas técnicas, el pionero en la aplicación de métodos radiológicos en homínidos fósiles (aunque no en un contexto tridimensional) fue Gorjanović-Kramberger (1902), quién publicó la anatomía interna de los fósiles del yacimiento Neandertal de Krapina (Croacia) sólo 7 años después del descubrimiento de los rayos X (Röntgen, 1895). Fleagle y Simons (1982) fueron los primeros en utilizar tecnología de TAC para estudiar la sección transversal del húmero de *Aegyptopithecus* (35-38 millones de años; según Kay et al., 1981). A raíz de este trabajo, otra serie de artículos se fueron sucediendo a lo largo de los años

80 y 90 empleando técnicas de obtención de datos cada vez más avanzadas (Conroy y Vannier, 1984; Wind, 1984; Seidler et al., 1992; Spoor et al., 1994; Zollikofer et al., 1995) hasta llegar a la actualidad, donde las técnicas de AV se aprecian en alguna vertiente de gran parte de los estudios paleoantropológicos que se realizan (Weber y Bookstein, 2011).

La principal diferencia entre la AV y la Antropología clásica, es que en la AV se trabaja fundamentalmente con objetos virtuales, derivados de la obtención de modelos 3D a través de TAC o escáner de superficie (ver detalles más adelante), en vez de con objetos físicos. Aunque el estudio del objeto en cuestión en un entorno virtual (3D) no reemplaza en absoluto el estudio del objeto físico (observación personal), este conlleva una serie de ventajas relevantes, que Weber (2015) describe como cinco, pero que pueden resumirse en las siguientes tres.

1. En los casos de utilización del TAC, al tener acceso a las partes internas (no visibles) del objeto, nos va a permitir acceder (tras un procesado de imágenes virtual) a estructuras ocultas como los senos, el esmalte de los dientes o las cavidades medulares de los huesos. En pacientes vivos, el TAC nos va a permitir acceder y obtener modelos virtuales de huesos y órganos internos como los pulmones, el corazón o el cerebro.
2. Se puede disponer de una copia virtual permanente (accesible desde cualquier lugar a través de memorias extraíbles o servidores online) de los modelos 3D de los datos a utilizar. Por lo tanto, la dependencia obligada de un lugar físico y permanente de trabajo queda parcialmente anulada.
3. La posibilidad de obtener gran cantidad de medidas (tanto lineales como tridimensionales) de la geometría del objeto sin la necesidad de ningún instrumento físico, así como la posibilidad de visualizar de manera muy intuitiva los resultados obtenidos a través de deformaciones de modelos 3D.

Recientes trabajos han propuesto una división de la AV en 6 áreas operacionales (Weber y Bookstein, 2011; Weber, 2015): digitalizar, descubrir/desvelar, comparar, reconstruir, materializar y compartir, las cuales se resumen brevemente a continuación:

1. Digitalizar.

La digitalización es el primer paso, pero también el más importante ya que da pie al resto de ellos. Consiste en la transferencia de un objeto físico al mundo virtual. Los modelos virtuales se obtienen fundamentalmente a través de dos mecanismos: escáneres de superficie, cuando únicamente estamos interesados en obtener un modelo que recoja la forma (y en ocasiones también el color) del objeto que nos interesa; TAC, micro-TAC o Sincrotrón, cuando estamos interesados en obtener también información de la estructura interna del objeto. En ocasiones, el interés en recoger o no la parte interna del objeto no es el único factor a tener en cuenta a la hora de elegir entre TAC o escáner 3D, sino que otros factores como el coste, el tamaño del objeto, la resolución que queremos obtener, la disponibilidad de los aparatos, etc., son factores de relevancia.

Los modelos 3D de superficie, como los utilizados para las publicaciones nº 7-8 y nº 10-13 de la presente tesis doctoral, se basan en la creación de modelos 3D a partir de nubes de puntos en un entorno virtual obtenidos a partir de la superficie del objeto físico. Aunque hay diferentes tipos de escáneres, los más usados en Paleoantropología (ya que son máquinas relativamente ligeras, portables y que permiten obtener modelos 3D de gran calidad) son los escáneres ópticos y láser. El escáner óptico, o de luz estructurada, proyecta un patrón de luz en el objeto y analiza la deformación del patrón para generar la geometría del objeto en cuestión mediante algoritmos matemáticos complejos. El patrón de deformación suele ser una cuadrícula bidimensional o un modelo de líneas y tiene la ventaja de que son escáneres relativamente rápidos, comparados con los escáneres láser. El escáner láser, proyecta un haz

de luz láser sobre el objeto y usa una cámara para captar la ubicación de dicho punto al rebotar en el objeto escaneado, de modo que va reconociendo puntos en la superficie del mismo. Posteriormente, los puntos son unidos mediante triangulación, y la suma de los triángulos generados va creando la malla tridimensional del objeto en el entorno virtual.

Los modelos 3D obtenidos a través de TAC, como los utilizados en las publicaciones nº 1-6 y nº 9 de la presente tesis doctoral, se basan en el uso de imágenes médicas. Concretamente, los métodos tomográficos se basan en la combinación de un grupo de imágenes 2D, denominadas porciones o *slices*, que pueden dar lugar a un modelo 3D. Los TAC están basados en el uso de la tecnología de rayos X, donde se emite radicación a un objeto a través de un tubo de rayos X, los cuales penetran el objeto en diferente grado dependiendo de la densidad del mismo, y los restantes son absorbidos por una placa que se localiza detrás del objeto, donde son recogidas (Brant y Helms, 2012; Bushberg et al., 2012; Weber, 2015). Dado que los diferentes materiales absorben en diferente grado los rayos X, esto va a ser reflejado directamente en la imagen 2D generada en la producción de diferentes escalas de grises acorde al diferente grado de absorción de los diferentes materiales (Bushberg et al., 2012). Las láminas 2D, que en combinación darán lugar al objeto 3D, están compuestas (como si de un mapa de bits se tratase) de pequeñas porciones con diferentes valores tonales, que reciben el nombre de *voxels*. La diferencia entre un pixel y *voxel* es que estos últimos contienen información volumétrica, ya que los *voxels* tienen un grosor determinado (proporcionado por la máquina que realiza el TAC). A lo largo del grupo de imágenes 2D, utilizando diferentes softwares de procesado de imagen médica, podremos seleccionar los *voxels* de cada imagen que tienen la misma densidad de modo que, al ser extraídos a lo largo del grupo de imágenes, podremos obtener un modelo 3D del objeto que tiene la densidad seleccionada.

En los escáneres médicos, como los usados para obtener los datos de las publicaciones anteriormente mencionadas, el objeto (paciente en este caso) se mantiene inmóvil sobre una placa y es el sistema tubo-detector el que rota en torno al mismo. Estos escáneres tienen una resolución de entre 1 y 0,5 milímetros (Brant y Helms, 2012). Una mayor resolución se puede obtener a través de la tecnología del micro-TAC y del Sincrotrón, pudiendo alcanzar resoluciones hasta de 1 micra para el micro-TAC y de 0,7 micras para el Sincrotrón (Ritman, 2004; Burghardt et al., 2011; Sánchez et al., 2012). En estas últimas, a diferencia del TAC médico, es el objeto es el que rota dentro de la máquina y el sistema tubo-detector se mantiene fijo. Como limitación, hay que señalar que las tecnologías del micro-TAC y el Sincrotrón han sido diseñadas para el escaneo de objetos de tamaño reducido y el tiempo de escaneo es mucho mayor que en el caso de los escáneres médicos.

Otro tipo de tecnología proveniente del campo de la imagen médica que es usado en Paleoantropología, es la tomografía por resonancia magnética (RM). Como limitación clara cabe señalar que la RM está diseñada para la observación de datos de tejidos blandos, por lo que su uso con fósiles o material esquelético es nulo. Sin embargo, sirve como método para obtener modelos de tejidos blandos de pacientes vivos, como los pulmones, el corazón o el cerebro. La gran ventaja es que, al no trabajar con rayos X, no es perjudicial para el sujeto escaneado, como sí lo es la tecnología de TAC. Al no ser usado este tipo de tecnología en la presente tesis doctoral, no se profundizará más en ella, pero se puede encontrar información más detallada en Edelman y Warach (1993).

2. Descubrir/desvelar.

Como se ha comentado, las técnicas tomográficas permiten el estudio de partes internas que no pueden ser recogidas mediante escáneres de superficie, teniendo la gran ventaja de que, al trabajar en el espacio virtual, el objeto original ni se modifica ni se destruye para acceder a

sus partes internas. Por ejemplo, se han usado técnicas de segmentación para obtener estructuras internas como los canales semicirculares del oído interno (Spoor et al., 1994), la dentina de los dientes (Skinner et al., 2008) o incluso para realizar una disección virtual de momias con el fin de evitar alterar el objeto original (Lynnerup, 2003).

Otra variante es la preparación electrónica de fósiles, donde el objetivo es extraer, de manera virtual mediante técnicas de segmentación, el elemento deseado de una matriz en la que se encuentra embebido (Zollikofer y Ponce de León, 2005; Benazzi et al., 2011a; Bolliger et al., 2012). De nuevo, la gran ventaja es que el fósil original permanece intacto durante todo el proceso de segmentación virtual. El inconveniente es que, en ocasiones, cuando la densidad del fósil y de la matriz son muy similares, la segmentación mediante la diferenciación de escalas de grises se vuelve una tarea de gran dificultad.

3. Comparar.

Una vez que han sido obtenidos los modelos 3D, suele recurrirse normalmente al uso de técnicas comparativas para poder estudiarlos y contrastar hipótesis científicas. Sin embargo, las técnicas de comparación de especímenes varían enormemente en función de las preguntas de investigación a resolver, aunque como común denominador comparten la necesidad de cuantificación de la forma de los objetos bajo estudio. Las técnicas de cuantificación y análisis varían desde el uso de medidas tradicionales o de matrices de distancias euclídeas (Lele y Richtsmeier, 1991), hasta métodos de cuantificación complejos como los análisis de Fourier (Kuhl y Giardina, 1982) o las técnicas de MG 3D, las cuales están basadas en el uso de estadística multivariante y de coordenadas geométricas tridimensionales, son las empleadas fundamentalmente para el desarrollo de la presente tesis doctoral. Dichas técnicas serán más profundamente explicadas en el siguiente apartado de este capítulo, así como en la sección "material y métodos" de cada uno de los artículos que componen la sección de resultados.

4. Reconstruir.

Dado que en AV, y concretamente en Paleoantropología, se precisa del uso de fósiles para realizar los estudios, es importante señalar que algunos fósiles en ocasiones se encuentran deformados, fragmentados o alterados de otro modo, generalmente debido a los procesos de fosilización o a los procesos de excavación o manipulación. Por lo tanto, en muchas ocasiones es necesaria la reconstrucción del fósil antes te poder medir y analizarlos. Según Weber (2015) existen 4 tipos de alteraciones que se pueden observar en los fósiles:

- Alteración tipo 1: cuando un objeto se encuentra fragmentado, pero todos (o casi todos) sus fragmentos están presentes y bien preservados, por lo que se puede restaurar nuevamente usando adhesivos específicos para esa tarea.
- Alteración tipo 2: cuando hay una parte de un objeto ausente, pero la parte preservada se encuentra en buen estado (como por ejemplo una costilla a la que le falta la cabeza costal).
- Alteración tipo 3: cuando un objeto no está fragmentado, pero presenta una deformación que altera su morfología original, lo cual suele ser debido a las presiones geológicas durante los procesos postdeposicionales.
- Alteración tipo 4: cuando un objeto se encuentra bien preservado, pero no es accesible debido a que se encuentra embebido en algún tipo de matriz que lo oculta parcial o completamente.

Aunque estas alteraciones pueden aparecer aisladas, lo más frecuente es que puedan darse varias al mismo tiempo, siendo más fiables las reconstrucciones cuando se dan alteraciones del tipo 1 y 4 /Weber, 2015). Cuando se dan alteraciones del tipo 2 y 3 habremos de recurrir a la estimación, por lo que siempre habrá que asumir cierto margen de error, ya que este tipo de estimaciones incluyen asunciones de similitud morfológica tomando datos

comparativos. Por lo tanto, en las reconstrucciones virtuales, más marcadamente en los casos de alteraciones tipo 2 y 3, siempre tendremos estimas de reconstrucción con un parecido determinado al objeto original, pero nunca podremos tener completa confianza de que la reconstrucción sea completamente fiel al original (Weber, 2015; Gunz et al., 2009).

A pesar de esta limitación, la reconstrucción virtual tiene una ventaja frente a la reconstrucción física. Esta última está basada en la experiencia anatómica del restaurador, la cual (aunque pueda ser amplia) siempre estará condicionada por la subjetividad del mismo. Sin embargo, se pueden utilizar otras técnicas cuando se usan métodos de reconstrucción virtual, como por ejemplo la reconstrucción geométrica (Weber et al., 2003; Neubauer et al., 2004; Gunz et al., 2009). En este caso, se llevaría a cabo una reconstrucción estadística del fósil utilizando la información morfológica de un individuo de referencia, el cual puede ser un individuo del que sepamos que tiene afinidad morfológica con el fósil a estudiar o, idealmente, la media de una población que tenga afinidad morfológica con el mismo. Para estimar las partes perdidas del individuo objetivo, se utilizarían algoritmos de deformación (como el de minimización de la *bending energy*; véanse detalles más adelante) utilizando la información de las partes preservadas del mismo, en función de la localización de los *landmarks* del individuo referencia. También se pueden realizar otros tipos de reconstrucción a partir de regresiones multivariantes, utilizando la información de *landmarks* de individuos de una muestra completa (usada como referencia) para estimar *landmarks* del individuo objetivo.

5. Materializar.

La tecnología de prototipado rápido para la impresión de modelos 3D proviene de la tecnología industrial de los años 80. Esta tecnología, aplicada a la AV permite la creación de réplicas físicas de fósiles o elementos esqueléticos a través de la impresión física de modelos tridimensionales previamente adquiridos mediante las técnicas anteriormente mencionadas.

Para la impresión de los modelos 3D, se suele recurrir a lo que se denomina estereolitografía, la cual se basa en la construcción de un objeto 3D mediante la adición de finas capas de un material de impresión (plástico, resina, etc.), que varía en función de la impresora y del objeto a imprimir. De este modo, la suma de las capas va a ir generando el objeto 3D. El primer trabajo que utilizó esta tecnología con fines antropológicos fue el de Seidler et al. (1992) sobre el cráneo del individuo de la Edad del Cobre conocido como "Ötzi". Según Weber (2015), las principales ventajas de los métodos de prototipado rápido en AV son los siguientes:

- No se necesita molde físico del objeto del que se quiere hacer el molde.
- No es una técnica invasiva en ningún momento del proceso, por lo que no se precisa de contacto con el objeto original.
- Los modelos pueden ser impresos a cualquier escala, permitiendo la impresión de objetos de gran tamaño en escala reducida, y viceversa.

6. Compartir.

La generación masiva de modelos 3D de fósiles humanos que se está produciendo en la actualidad está permitiendo que compartir bases de datos y modelos 3D sea una práctica extendida entre la comunidad científica. Esta práctica resta dependencia al investigador de acudir al lugar físico donde se hallan los fósiles, lo cual puede ser costoso en algunos casos (observación personal). De tal manera se está incrementando el hecho de compartir este tipo de datos 3D, hasta el punto de que en la actualidad existen servidores web donde se pueden encontrar y descargar modelos 3D de fósiles o primates actuales con fines educativos o científicos. Algunos ejemplos de bases de datos de modelos 3D serían KUPRI[1], NESPOS[2], African fossils[3] o Morphosource[4], donde recientemente se han hecho disponibles gratuitamente los modelos 3D de los fósiles de *Homo naledi* y *Australopithecus sediba*, donde el autor de la presente tesis doctoral ha contribuido junto con su director. Dentro de este punto, es importante resaltar que el hecho de poner accesible para toda la comunidad científica modelos 3D de

1 www.dmm.pri.kyoto-u.ac.jp; 2 www.nespos.org; 3 www.africanfossils.org; 4 www.morphosource.org)

fósiles, es una práctica que no es aceptada por toda la comunidad científica, y que está actualmente en debate. Esto se debe a que, algunos investigadores opinan que todo el esfuerzo económico y de tiempo invertido en conseguir esos modelos 3D puede verse devaluado al poner un acceso libre y gratuito para estos fósiles.

Capítulo 3.2.2. Morfometría geométrica 3D y el uso de *sliding semilandmarks*.

La morfometría geométrica (MG) 3D se basa en la cuantificación de la forma de una estructura, la cual es capturada mediante coordenadas cartesianas de puntos anatómicos concretos (hitos o *landmarks*) en un espacio bidimensional o tridimensional (Bookstein, 1991), los cuales habrán de ser homólogos en todos los individuos de la muestra. Una de las grandes ventajas de este método es que permite un análisis estadístico del tamaño y la forma por separado, ya que, en MG, la morfología de un objeto se descompone en tamaño (*size*) y forma (*shape*). Según la definición tradicional de Kendall (1977), forma es "toda la información geométrica que resulta de eliminar los efectos de la posición, escalado y rotación de un objeto", de tal manera que las posiciones relativas entre los *landmarks* no varían, pero la posición absoluta sí lo hace, permitiéndonos de este modo estudiar la forma "pura" de un objeto (Kendall, 1977). A este proceso se le denomina superposición de Procrustes (Zelditch, 2012). Respecto al tamaño, en MG es empleado el llamado tamaño del centroide (*centroid size*), que se define por la raíz cuadrada de la suma de las distancias al cuadrado desde un grupo de *landmarks* al centroide que definen (Zelditch et al., 2004). Este centroide es resultante de la media de las coordenadas de todos los *landmarks* en X, Y, Z.

Respecto a los *landmarks*, tradicionalmente se han definido tres diferentes tipos de *landmarks* según su localización espacial (tipos I, II y III), sumados a los llamados *pseudolandmarks* y *semilandmarks* (Zelditch et al., 2004). Aunque este enfoque ha sido el clásicamente usado para discernir tipos de *landmarks*, recientes estudios evitan el empleo de

esa tipología y utilizan únicamente los términos *landmark*, para puntos claramente discernibles y homologables geométrica y biológicamente, y *semilandmark*, para el resto de puntos donde la homología es deficiente o cuestionable, en diferente grado (Gunz y Mitteroecker, 2013).

Para solucionar el problema de la deficiente homología biológica entre los *semilandmarks* que supuestamente deberían ser homólogos, se ha desarrollado la metodología del *sliding semilandmark* durante las últimas décadas (Bookstein, 1991, 1997; Gunz et al., 2005, 2009; Gunz y Mitteroecker, 2013; Mitteroecker y Gunz, 2009), la cual consigue la homología entre *semilandmarks* mediante algoritmos matemáticos. Para ello, han sido desarrollados dos métodos diferentes (Pérez et al., 2006; Gunz y Mitteroecker, 2013): el *sliding* para de alcanzar la mínima energía de deformación o *bending energy* respecto a una referencia (Bookstein, 1991, 1997; Green, 1996; Bookstein et al. 2002) y el *sliding* para alcanzar la mínima distancia Procrustes respecto a una referencia (Sampson et al. 1996; Bookstein et al. 2002; Sheets et al. 2004). La primera está basada en el *sliding* mediante deformación de *thin-plate-spline* (Bookstein, 1991) mientras que la segunda está basada en la superposición Procrustes (Rohlf y Slice, 1990).

El *thin-plate-spline* (TPS) es un algoritmo de interpolación que sirve para visualizar diferencias en forma entre dos especímenes, de modo que se mide la cantidad de deformación necesaria para deformar un set de coordenadas tomado como objetivo en otro conjunto de coordenadas tomado como referencia. Esto se cuantifica como energía de deformación (*bending energy*) necesaria para conseguir esta tarea, mediante el uso de modelos matemáticos que provienen de la Ingeniería Industrial (Bookstein, 1991). La ventaja del TPS es que permite visualizar las deformaciones de la forma, no sólo en deformaciones del set de coordenadas, sino de mallas 3D asociadas a las coordenadas, lo cual hace la comprensión y la visualización de los resultados muy intuitiva.

La distancia Procrustes entre dos especímenes es una medida que cuantifica diferencias en forma entre dos objetos mediante la superposición Procrustes y el cálculo de la raíz cuadrada de la suma de las distancias entre sus *landmarks* homólogos al cuadrado. Una mayor distancia Procrustes entre dos formas vendrá definida por una mayor distancia entre *landmarks* homólogos de esos conjuntos de coordenadas y, por lo tanto, significará una mayor diferencia morfológica. El método de *sliding* seguido en la presente tesis doctoral ha sido el de minimizar la *bending energy* entre los individuos *target* y la referencia.

La principal diferencia entre ambos enfoques es que la *bending energy* tiene en cuenta todos los *landmarks* y *semilandmarks* para calcular la energía de deformación como un todo o conjunto, y el *sliding* de cada semilandmark está influenciado por el *sliding* de los *landmarks* y *semilandmarks* adyacentes. Sin embargo, mediante el enfoque de la reducción de la distancia Procrustes, cada semilandmark hace el *sliding* separadamente y no está influenciado por la posición de los *landmarks* y *semilandmarks* adyacentes. Por lo tanto, potencialmente, al hacer el *sliding* mediante este enfoque, puede llegar incluso a darse el caso de que un semilandmark rebase un *landmark*, lo que, mediante el enfoque de la *bending energy*, sería imposible.

Sea cual sea el proceso utilizado, para que el *sliding* sea posible en términos matemáticos, los *semilandmarks* de curva deben deslizarse a lo largo de líneas tangentes a su curva, mientras que los *semilandmarks* de superficie se deslizan a lo largo de planos tangentes a su superficie (Gunz y Mitteroecker, 2013). Después de cada proceso de *sliding*, los *semilandmarks* han de proyectarse en la superficie para evitar que durante el proceso de *sliding* a lo largo de las curvas o planos tangentes, estos hayan quedado fuera de la superficie (Fig. 9).

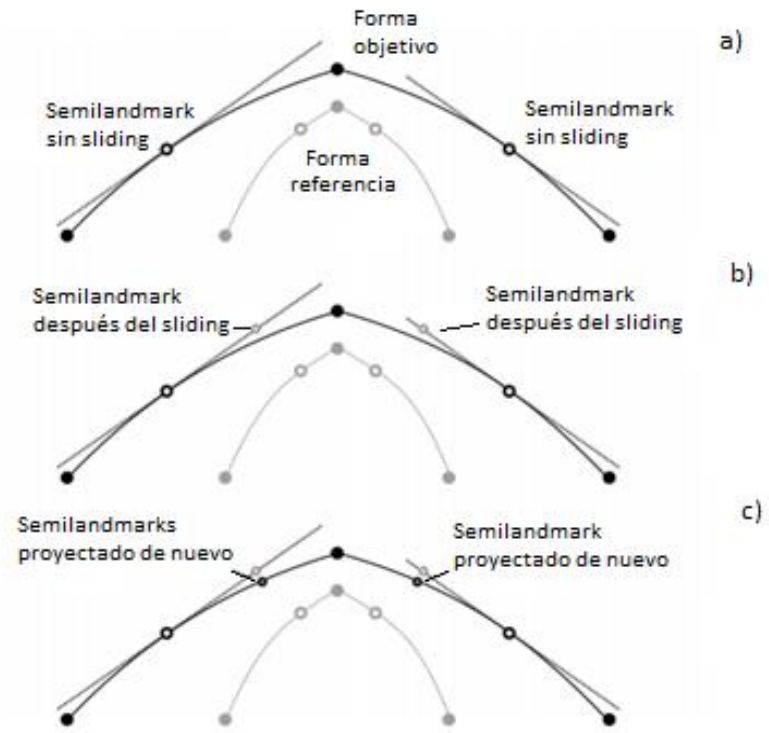

Figura 9: Proceso de *sliding* de *semilandmarks* de curva a lo largo de las rectas tangentes, donde se muestra a) *semilandmarks* en su posición original; b) *semilandmarks* después del *sliding*; c) *semilandmarks* proyectados de nuevo en la superficie. Modificado de Gunz y Mitteroecker (2013).

Es recomendable repetir del proceso del *sliding* dos veces para optimizar al máximo la posición de los puntos: en primer lugar, tomando como referencia cualquier individuo de la muestra a digitalizar (arbitrariamente) y, en segundo lugar, un segundo *sliding* debe ser realizado tomando como referencia la forma del individuo medio de la muestra (Gunz et al., 2009; Gunz y Mitteroecker, 2013). Después de todo este proceso, se conseguirá una homología que no es como la tradicional homología punto-punto, sino que este criterio puede ser extendido a una homología curva-curva o incluso superficie-superficie.

Finalmente, hay que señalar que una de las principales aplicaciones del uso de *sliding semilandmarks* es la de la estimación de puntos perdidos o *missing data*. Cuando estamos ante estructuras simétricas, en algunos casos se puede recurrir al uso de la simetría bilateral y la imagen especular para realizar la reconstrucción del espécimen (Zollikofer et al., 2005; Ponce de León et al., 2008; Gunz et al., 2009; Weber y Bookstein, 2011; O'Higgins et al., 2011). Sin

embargo, cuando las partes están ausentes en ambos laterales o estamos ante una estructura que no es simétrica, se puede recurrir a la estimación mediante el uso de *sliding semilandmarks* (Gunz, 2009).

Es importante señalar, en relación con estos aspectos, que el proceso normal del *sliding* ya se puede considerar como una estimación de datos perdidos *per se*, ya que en los *semilandmarks* de curva se estima la posición de una coordenada (a lo largo de la recta tangente) y en los de superficie se estiman 2 coordenadas (a lo largo del plano tangente). En el caso de la estimación de casos perdidos anteriormente mencionado, se pretenden estimar las 3 coordenadas (Gunz, 2009).

Es este caso el enfoque más recurrente ha sido el de la estimación a través de TPS. Según este, las coordenadas del individuo de referencia, donde todos los *landmarks* y *semilandmarks* están presentes, es utilizado a través de una función de interpolación para calcular los datos faltantes del espécimen objetivo utilizando la información de la referencia, de modo que la energía de deformación se minimice al máximo (Gunz et al., 2009).

A la hora de saber cómo de precisa es una estimación de datos perdidos, es importante tener en cuenta la información de los *landmarks* de la referencia para calcular los *landmarks* faltantes en la estructura en cuestión. Por lo tanto, cuantos más *landmarks* se tengan en torno a la estructura faltante, más información morfológica se tendrá y más precisión tendrá la estimación de estructuras perdidas (Gunz et al., 2009; Gunz y Mitteroecker, 2013). Otro método para ganar exactitud en la estima de datos perdidos es la creación de diferentes estimas utilizando diferentes individuos posibles como referencia. De este modo, tendremos diferentes estimas de la misma estructura y podremos tener cubierta de cierta manera la incertidumbre en torno al individuo que elegir como referencia (Gunz et al., 2009).

CAPÍTULO IV – RESULTADOS: VARIABILIDAD ONTOGENÉTICA DE LA CAJA TORÁCICA HUMANA

Los resultados obtenidos en referencia al **objetivo 1,** "**Contribuciones al conocimiento del desarrollo ontogenético de la caja torácica humana",** han sido íntegramente publicados en los siguientes artículos:

Bastir, M., **García Martínez, D.**, Recheis, W., Barash, A., Coquerelle, M., Ríos, L., Peña-Melián, Á., García Río, F., O'Higgins, P., 2013. Differential growth and development of the upper and lower human thorax. PLoS One 8, e75128.

DOI: http://dx.doi.org/10.1371/journal.pone.0075128

García-Martínez, D., Recheis, W., Bastir, M., 2016. Ontogeny of 3D rib curvature and its importance for the understanding of human thorax development. American Journal of Physical Anthropology 159, 423-431.

DOI: 10.1002/ajpa.22893

OPEN ACCESS Freely available online

PLOS ONE

Differential Growth and Development of the Upper and Lower Human Thorax

Markus Bastir[1*], Daniel García Martínez[1,2], Wolfgang Recheis[3], Alon Barash[4,5], Michael Coquerelle[1], Luis Rios[2,6], Ángel Peña-Melián[7], Francisco García Río[8], Paul O'Higgins[9]

1 Paleoanthropology Group, Museo Nacional de Ciencias Naturales (CSIC), Madrid, Spain, **2** Facultad de Ciencias, Universidad Autónoma de Madrid, Madrid, Spain, **3** Department of Radiology, Medizinische Universität Innsbruck, Innsbruck, Austria, **4** Faculty of Medicine, Galilee Bar Ilan University, Zefat, Israel, **5** Department of Anatomy and Anthropology, Sackler Faculty of Medicine, Tel Aviv, Israel, **6** Fundación Aranzadi, San Sebastián, Spain, **7** Departamento de Anatomía y Embriología, Universidad Complutense Madrid, Madrid, Spain, **8** Hospital Universitario La Paz, Biomedical Research Institute (IdiPAZ), Madrid, Spain, **9** Hull York Medical School (HYMS), University of York, York, United Kingdom

Abstract

The difficulties in quantifying the 3D form and spatial relationships of the skeletal components of the ribcage present a barrier to studies of the growth of the thoracic skeleton. Thus, most studies to date have relied on traditional measurements such as distances and indices from single or few ribs. It is currently known that adult-like thoracic shape is achieved early, by the end of the second postnatal year, with the circular cross-section of the newborn thorax transforming into the ovoid shape of adults; and that the ribs become inclined such that their anterior borders come to lie inferior to their posterior. Here we present a study that revisits growth changes using geometric morphometrics applied to extensive landmark data taken from the ribcage. We digitized 402 (semi) landmarks on 3D reconstructions to assess growth changes in 27 computed tomography-scanned modern humans representing newborns to adults of both sexes. Our analyses show a curved ontogenetic trajectory, resulting from different ontogenetic growth allometries of upper and lower thoracic units. Adult thoracic morphology is achieved later than predicted, by diverse modifications in different anatomical regions during different ontogenetic stages. Besides a marked increase in antero-posterior dimensions, there is an increase in medio-lateral dimensions of the upper thorax, relative to the lower thorax. This transforms the pyramidal infant thorax into the barrel-shaped one of adults. Rib descent is produced by complex changes in 3D curvature. Developmental differences between upper and lower thoracic regions relate to differential timings and rates of maturation of the respiratory and digestive systems, the spine and the locomotor system. Our findings are relevant to understanding how changes in the relative rates of growth of these systems and structures impacted on the development and evolution of modern human body shape.

Citation: Bastir M, García Martínez D, Recheis W, Barash A, Coquerelle M, et al. (2013) Differential Growth and Development of the Upper and Lower Human Thorax. PLoS ONE 8(9): e75128. doi:10.1371/journal.pone.0075128

Editor: Luca Bondioli, Museo Nazionale Preistorico Etnografico 'L. Pigorini', Italy

Received June 21, 2013; **Accepted** August 8, 2013; **Published** September 20, 2013

Funding: CGL2012-37279 (Spanish Ministry for Economy and Competition) Fyssen-foundation (http://www.fondationfyssen.fr). The funders had no role in study design, data collection and analysis, decision to publish, or preparation of the manuscript

Competing interests: The authors have declared that no competing interests exist.

* E-mail: mbastir@mncn.csic.es

Introduction

The thoracic skeleton is an osteo-cartilaginous framework that surrounds and protects the thoracic viscera and supports the mechanical function of ventilation. To fulfill its role in ventilation the thoracic skeleton offers a large surface area for muscle attachment (intercostal muscles, diaphragm, and accessory respiratory muscles) [1,2]. The muscles act to raise the ribs, which increases thoracic dimensions as a consequence of their angulation, form and joints. This leads to reduced intra thoracic pressure and so, to inspiration [1,2]. Expiration, as the ribs return to their original positions, is more passive. Thus, chest wall dynamics depend on rib morphology [1]. In consequence, how morphology changes postnatally is relevant clinically as well as to physiological modelling, and functional and evolutionary morphology [2-19].

We as yet have a poor understanding of how the thorax grows in size and develops in form throughout life. Although the advent of 3D imaging means that CT scans of the thoracic wall and contents are readily available [20-22], a major problem has inhibited the characterization of thoracic ontogeny: the difficulty in quantifying the detail of the 3D-features of thoracic wall and rib-curvature and the spatial relations of the ribs, sternum and spine. Despite these difficulties, one 3D geometric morphometric analysis has examined changes with old age in adult male ribcage morphology [11], demonstrating widening in

the lower thorax but providing no information on variations in rib curvature. Kagaya and colleagues [23] assessed rib curvature and thoracic shape in anthropoids using Bezier curves fitted to alternate ribs. Their data discriminated between the barrel-shaped thorax of *Hylobates* and the funnel-shaped thoraces of other hominoids (but see 24 and Discussion)

No 3D geometric morphometric analysis has yet addressed ontogenetic variation in humans. To date, ontogenetic studies of the human thorax have used linear distances and indices computed from them to describe the principal dimensions of the thorax or of a few ribs [25,26]. One such study [25] concluded, from analysis of indices of averaged linear measurements in horizontal cross sections at the manubrio-sternal junction, the diaphragmatic dome and midway between these reference levels, that adult-like thoracic shape is achieved early, by the end of the second postnatal year. In achieving this transformation from the circular cross-section of the newborn into the ovoid section of adults, the ribs become inclined such that their anterior borders are inferior to their posterior ones.

A key aim of the present study is to revisit the ontogeny of thoracic form to obtain a fuller picture of how it changes throughout life. This is because there are good reasons to expect a more complex picture of human thoracic ontogeny than that described above. Specifically, different ontogenetic changes can be expected with regard to upper (ribs 1-5) and lower (ribs 6-10) thoracic morphology (see Methods) since these regions are related to different organ and body systems that mature differentially during ontogeny. Thus, the upper thoracic region is related to the pulmonary part of the respiratory system and the upper limbs [27] while the lower thorax is anatomically related to the diaphragmatic part of the respiratory system, and also more closely to the abdominal cavity and locomotor apparatus [5,16]. Additionally, continuous descent of the anterior parts of the ribs is part of the aging process, related to a decline in lung function and vital capacity [11]. Finally, secondary ossification centres appear close to the articular tubercles around puberty [28,29] suggesting that new features of ontogenetic shape change may appear during later ontogeny.

Openshaw et al. [25] focused on the mid-thorax and as such, our knowledge of the ontogeny of ribcage form above and below this level is limited. No study has yet examined the detail of whole ribcage postnatal ontogeny and its spatial and temporal associations with the growth and maturation of related body systems. A useful analogy might be drawn with the craniofacial skeleton, which comprises modules that show a degree of independent growth that is reflected in curved ontogenetic trajectories of shape change [30-32]. Likewise, in this study we test the hypothesis that upper and lower thorax behave as modules with a degree of independence in ontogenetic trajectories.

To these ends we apply geometric morphometric methods to extensive 3D landmark configurations to assess how thoracic form and the form and spatial relationships of the ribs and sternum covary with ontogeny and the extent to which upper and lower regions of the thoracic covary throughout postnatal ontogeny. Particularly, we test the hypothesis that directions of shape change differ in the upper and lower parts of the thorax. This represents the first such study in humans.

Methods

Computed tomography (CT) data were obtained from subjects that were scanned previously for medical reasons unrelated to this study. All patients were scanned in supine position in maximum inspiration (Austria) except three newborns scanned in France, where two subjects were scanned for trauma in unknown respiratory status and one subject was scanned for virtual autopsy post mortem. However, in none of the cases any obvious pathologies affected skeletal thoracic form. The age and sex composition of the sample is detailed in Table 1 (N=27). Because the subjects were scanned previously for medical reasons unrelated to this study (retrospective), it is lawful and not necessary to obtain consent from the next of kin, caretakers, or guardians on the behalf of minors/children participants of this study. Consequently such consent was not required by the local ethic committees following local laws. The approval to use these pre-existing Ct scans for our research was obtained in writing from the *Comite consulitatif pour la protection des personnes dans la recherche biomédicale Bordeaux A* and from the Ethikkommission der Medizinischen Universität Innsbruck (AN5025, 323/4.24) (copies of approvals of both ethics committees have been submitted to manuscript central). Prior to analysis all CT-data were anonymized to comply with the Helsinki declaration [33].

Sliding semilandmarks

Landmarks and semilandmarks for sliding [34] were located on skeletal elements in-situ within 3D CT based reconstructions of the thorax. As such, landmark subsets describe the form of individual skeletal elements while the full landmark configuration describes the form of these elements, their relations to each other and the overall form of the thorax. On the ribs, landmarks were placed at the most superior, anterior and inferior points of the head, the most lateral point of the articular tubercle, the most inferior point at the angle at the lower rib border, (where the angle is most doubtlessly recognizable) and the most superior and inferior sternal extremes. Additionally 15 equidistant semilandmarks were sited along the lower costal border between the articular tubercle and the inferior sternal extreme. Each rib was thus described by twenty 3D landmarks. At the sternum two landmarks were sited in the midline, one in the manubrial notch and the other on the inferior border. The full data comprise 402 landmarks and semilandmarks (Figure 1).

The surface of the bony structures of the rib cage was segmented with threshold based techniques following the "full width half maximum" approach [35] thus allowing for reproducible results. We used this protocol in Amira 4 software (www.vsg3d.com) and obtained reasonably well represented 3D models of bony structures, which were further post-processed (cleaning, smoothing, mesh hole-filling, standardized positioning) by Artec Studio software (www.Artec3D.com) [36-39]. Final 3D models were then imported into Viewbox4 software (www.dhal.com) to position

Table 1. CT-data sets, sex and ages (age group definitions in Material and Methods).

Id	Age (years)	sex	age group
TX001	1	female	group1
TX002	3	female	group2
TX003	6	female	group2
TX004	11	female	group2
TX005	14	female	group2
TX006	40	male	group3
TX007	60	male	group3
TX008	50	male	group3
TX010	62	female	group3
TX011	27	female	group3
TX012	59	male	group3
TX013	0.08	male	group1
TX014	0.25	female	group1
TX015	0.4	male	group1
TX022	0.11	male	group1
TX024	18	male	group3
TX025	6	male	group2
TX026	7	male	group2
TX027	8	male	group2
TX028	10	male	group2
TX029	0.06	male	group1
TX030	0.6	male	group1
TX031	1.8	male	group1
TX032	4	male	group2
TX041	15.6	female	group2
TX045	5	male	group2
TX046	10.5	female	group2

doi: 10.1371/journal.pone.0075128.t001

3D landmarks and semilandmarks along the inferior curves of ribs 1-10. Because of uncertainty in terms of their locations along the ribs, semilandmarks were then slid along their corresponding curves with respect to the fixed landmarks so as to minimize bending energy, first during landmarking between each specimen and the template (first specimen) and after that, a second time against the sample average configuration [30,34]. This procedure adjusts their relative locations along the curve. After sliding the semilandmarks on the lower border of each rib represent the shape of the lower border. The semilandmark set for each curve should be interpreted as a whole, i.e. as a single curve, rather than as discrete points. We also used a TPS approach with the semilandmarks to estimate missing data, which in a few cases was necessary for the landmarks at the sternal extremes of ribs 9 and 10 [37,38,40]. Finally, the resulting 32562 3D-measurements (x,y,z-coordinates) were analyzed statistically.

Age groups, statistical analyses and visualization

In order to address Openshaw et al.'s [25] hypothesis, that adult-like thoracic shape is achieved by the end of the second postnatal year the data were divided into three groups. Group 1 contained individuals ranging from newborns to two years following Openshaw et al.'s [25] hypothesis. Group 3 was composed of adults (above 18 years [30]). Group 2 contained all subjects between from three to eighteen years. Despite its large range of ages, group 2 is potentially interesting due a considerable lack of knowledge about respiratory apparatus ontogeny in these stages [41,42].

Shape data were symmetrized in MorphoJ-software [43] using reflected relabelling and principal components analysis (PCA) of Procrustes shape coordinates was carried out to visualise ontogenetic shape trajectories in PC1-2 and PC1-3 projection. We also used these PCA projections to assess how many non-adult individuals plot within the 95% confidence intervals of adult thoracic shape configurations. To optimally investigate full thoracic growth allometry we also performed a PCA in Procrustes form space [40,44,45].

In addition to the PCA analyses in shape and form spaces we used the age groups to compare mean shapes and mean sizes (centroid size) to further evaluate the hypotheses. Mean shapes were compared by permutation tests of group membership (N=10000) [40,46]. Centroid size followed a normal distribution (KS d=0.135, p=n.s) so ANOVA and Bonferroni post-hoc comparisons were used for group mean size comparisons [47].

Our data come from anonymized clinical hospital CT scans and visual inspection did not reveal signs of skeletal morphological alterations due to pathology. However, to validate quantitatively our visual assessment of normal skeletal morphology, a control group of CT data of four healthy adults related to different (and not yet published) research was compared with the six adults of the present study. Our validation analysis showed a complete overlap in principal components space of the known-healthy adults and the adults in this study. Also, mean shape comparisons did not produce statistically significant results. Consequently, normal skeletal morphology is assumed for the full sample.

Upper versus lower thorax ontogeny

To test the hypothesis that the upper and lower thorax follow different ontogenetic trajectories [48-50], the landmark data were divided into an upper (ribs 1-5) and lower part (ribs 6-10). Such a division reflects the fact that the upper part is more related to respiration, upper limb articulation and movement, while the lower part is more related to diaphragmatic respiration, posture, and subthoracic viscera (e.g. intestines, liver, reproductive systems) [1,2,5,6]. Many of these systems grow with different ontogenetic maturation patterns.

Because both parts share the same number of landmarks a common superimposition was possible, placing them into the same shape space. Therefore, to compare their ontogenetic allometries multivariate regressions of shape on centroid size were computed for each and the angle between these regression lines was calculated. Small angles indicate similar, and large angles different relationships between shape and centroid size [49,51]. Statistical assessment of the resulting angles is often done by comparison of true angles to those between randomly permuted groups in the multivariate space of interest [48,50]. Random vectors are drawn from a uniform distribution on a hypersphere with the appropriate

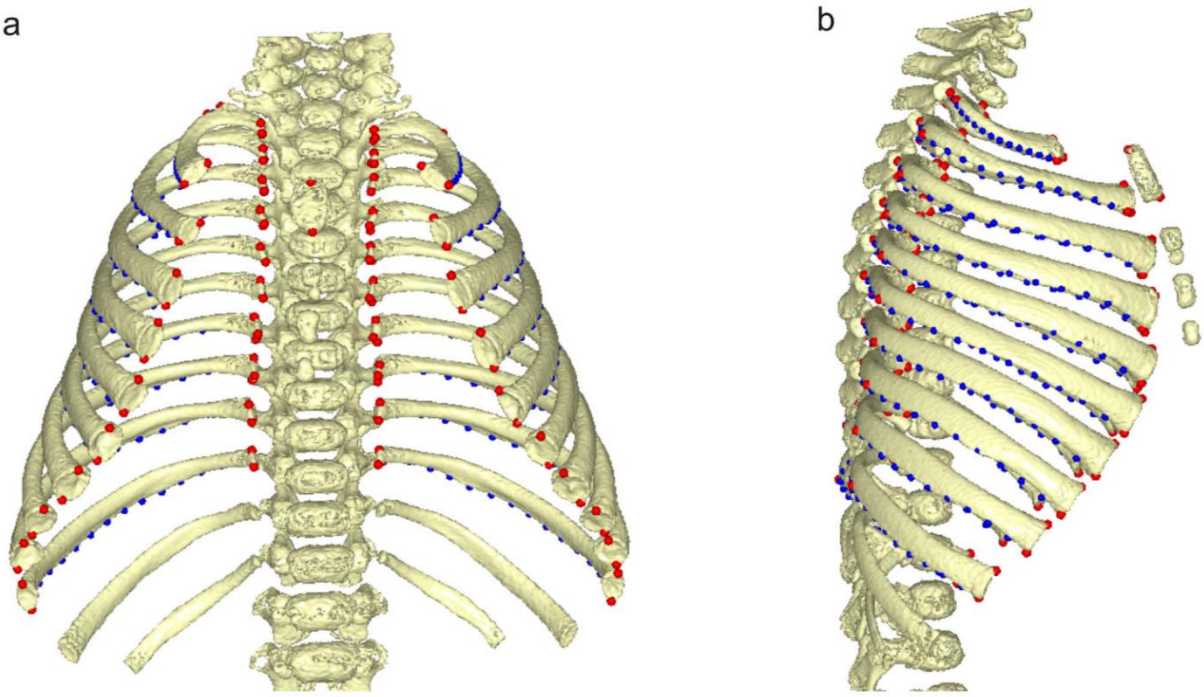

Figure 1, Bastir et al.

Figure 1. 3D landmarks. Landmarks (red) and sliding semilandmarks (blue) used to describe the thoracic skeleton; newborn subject in frontal (a) and lateral (b) view.
doi: 10.1371/journal.pone.0075128.g001

dimensionality. These comparisons have usually been done by randomisation, but a closed-form formula for the probability has recently been published [52] which allows rapid computation of significance levels [51]. The angles were computed and assessed statistically using MorphoJ software [43].

Hypothesis testing

Openshaw et al's[25]. hypothesis would be supported if all individuals older than 2 years (groups 2 and 3) plot within the 95% range of the adults. Additionally, the hypothesis predicts significantly different mean shapes between group 1 and group 2, group 1 and group 3 and (less to) no difference between group 2 and group 3.

The hypothesis of modular growth of the upper and lower thorax is assessed by computing the angle and its significance between the multivariate regressions of shape on centroid size for these regions. Non-significant angles indicate a lack of evidence for significant differences, small but significant angles indicate similarities, and large significant angles indicate differences.

In addition to the angle comparisons, visual inspection of 3D warped thoracic surfaces along the first principal component of form space, which reflects the majority of growth allometry [44,45], allowed appraisal of ontogenetic differences in the upper and lower thorax. The surface warps are based on thin-plate splines and thus contain measured information at the landmarks and semilandmarks and interpolated information (not directly measured) at the remaining parts of the surface meshes.

Results

Size analysis

Growth is characterized by a high rate of increase in centroid size in the early years, tailing off slowly until a marked deceleration occurs at around 10-11 years. Figure 2 suggests that adult thoracic size is achieved in adolescence around 14-15 years. ANOVA revealed highly significantly different group means ($F(2, 25)=115.89$; $p=0.0001$;CS of group 1: 1072.5; CS of group 2: 1951.4; and CS of group 3: 2761. Bonferroni post-hoc corrections identified highly significant differences in all pairwise comparisons (between MS=4928; df=25; $p=0.001$).

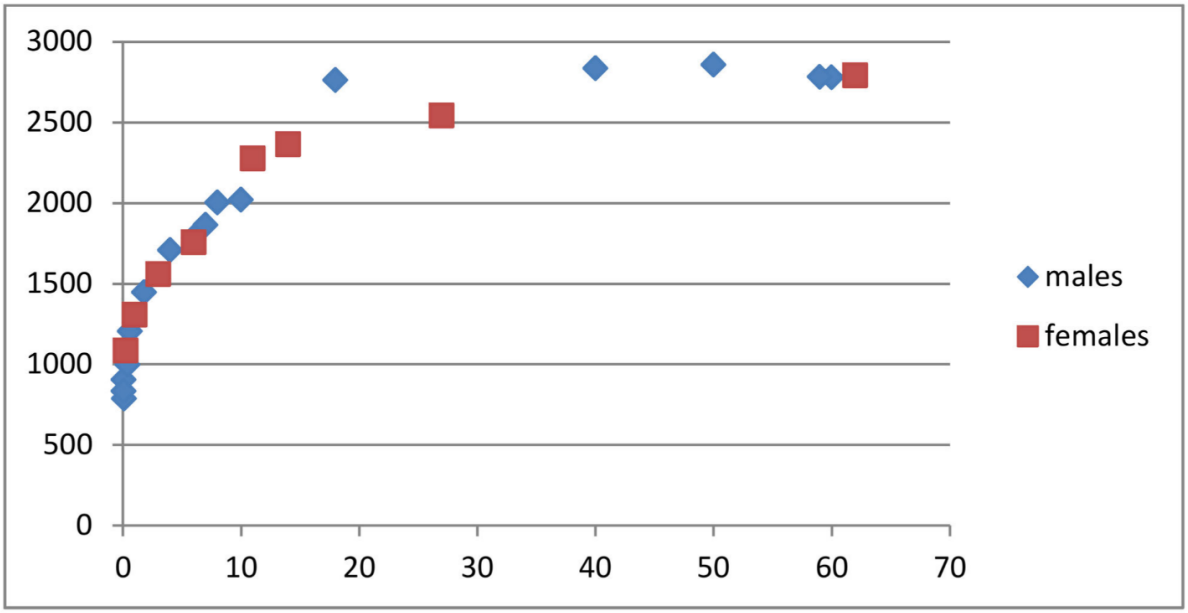

Figure 2, Bastir et al

Figure 2. Ontogenetic increase of thoracic size. Changes in centroid size in males and females. X-axis shows age in years, y-axis shows centroid size.

doi: 10.1371/journal.pone.0075128.g002

Shape analysis

The 95% confidence intervals (CI) in the PCA of shape space (Figure 3) suggest that the hypothesis of Openshaw et al [25] is not fully supported in terms of shape. However, this depends to some degree on the projection. In the PC1-2 subspace of shape (PC1: 52.34% of total variance, PC2: 13.67% tot. var.) the 95% CI includes only half of the individuals of group 2 leaving out six individuals aged older than 2 years. All individuals of group 1 are outside the adult 95% range. However, in the PC1-PC3 subspace (PC3: 10.23% tot. var.), all but two subjects of group 2 and two members of group 1 are included within the adult range. Taking both plots together adult shape appears to be the result of both early and later ontogenetic modifications.

Procrustes form space analysis

PCA suggests a very tight association between size and shape and also shows the age groups are well-ordered along PC1 (95.9% of total variance, PC2: 1.3% and PC3: 0.7%). A plot of PCs1, 2 and 3 (98% of total variance) suggests a gently curved allometric growth trajectory (Figure 4). Between group 2 and group 3 the orientation of the trajectory changes with particularly with changes along PC3 adding to the general growth changes along PC1.

The warps associated with PC1 in form space (Figure 4C-I, Movie S1) show that the newborn thorax is pyramidal, with a narrow upper and a wider lower medio-lateral diameter (Figure 4C). The ribs of the upper thorax in newborns are mostly horizontal, whereas the ribs of the lower thorax are downwardly inclined (Figure 4D). After growth, all ribs show a sternal elongation, and a downward curve at the sternal ends (Figure 4H), but, in addition to the rib elongation, the sternal ends of the lower thorax also become shifted anteriorly due to increased lumbar curvature of the spine (Figure 4H).

The growth expansion of the upper thorax (Figure 4G) is produced by a complex curvature change in which the mid-third of the rib shaft not only expands medio-laterally but also curves upwards, relative to its costo-vertebral attachments and the sternal extremes. Figure 4H shows a lowering of the rib orientation. A top view shows a considerably “invagination” of the spine (Figure 4I). As a consequence of that process in the smallest and youngest the posterior-most structures of the thorax are the spinous processes of the thoracic vertebrae in the midline, while in adults themost posterior structures are parts of the rib cage located lateral to the *angulus costae* (compare posterior thorax outline in Figure 4E and 4I).

As a consequence of all these changes the upper thorax starts off in newborns with a circular and ends up, in adults, with an ovoid cross section, which fits with the prediction of Openshaw et al. [25]. However, the lower thorax starts with an ovoid cross section and ends up with a circular one in adults,

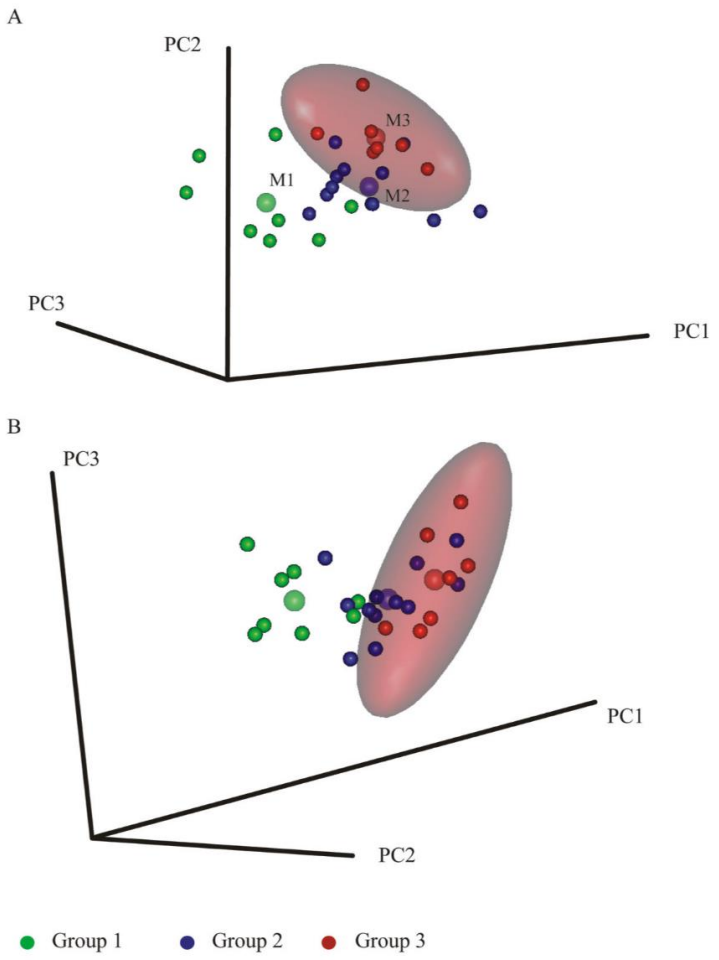

Figure 3, Bastir et al

Figure 3. Principal components analysis in shape space. 3D Scatterplots of principal components of shape with 95% confidence intervals of the adults (red ellipses) (a) PC1 versus PC2, (b) PC1 versus PC3. Note that 95% of the adult range in (a) excludes not only all group 1 subjects but also almost half of group 2. (b) The adult range includes most of group 2 and excludes most of group 1. Group mean markers are slightly enlarged and semitransparent.

doi: 10.1371/journal.pone.0075128.g003

which is contrary to the prediction (see mean shape comparisons below).

Statistical comparisons of the three age group means (Table 2) show clear differences between group1 and group 2 and between group 1 and group 3, which differ at $p<0.0001$ with 10000 permutations. The significance of mean shape differences between group 2 and group 3 varied between between $p<0.04$ and $p<0.08$ during different randomization analyses.

Quantified morphological features of mean shapes

Mean shapes for each age group are shown in Figure 5, and are superimposed for comparison in Figure 6. The first phase of growth between age groups 1 and 2 (Figure 6; a, d, g, j) results in an increase of the upper thorax (Figure 6a, d, g, j) relative to the lower thorax which becomes narrower (Figure 6a, j, compare also with PC1 warps in Figure 4c, g, and Movie S1). This produces a more barrel shaped frontal outline (Figure 5a vs. 5b). Relatively more posterior positioning of the angles of the upper ribs (Figure 6d) deepens the posterior parasagittal guttering of the rib cage. The physiological kyphosis of the

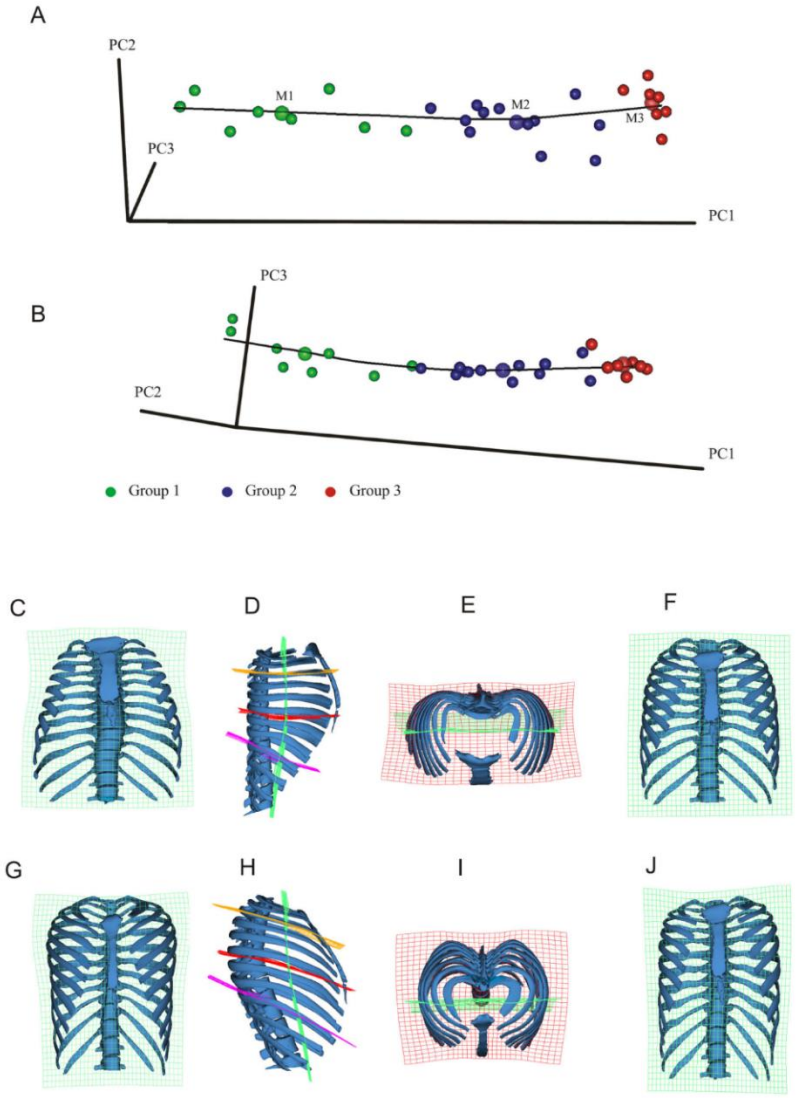

Fig 4, Bastir et al

Figure 4. Principal components analysis in Procrustes form space. Form space ontogenetic shape trajectory. The growth allometry is curved in form space. A line between the enlarged semitransparent dots representing the means of the three age groups illustrates this change of orientation in growth allometry. Different projections of the ontogenetic shape trajectory show (A) PC1-PC2 and (B) PC1-PC3. The warped ribcage models show frontal views of the smallest (youngest) specimen (C) and the largest individual (G). The green transformation grid (x-y plane) shows relative upper thoracic expansion and lower thorax contraction during growth from C to G. The lateral views show shape changes from the smallest (D) to the largest individual (H) and demonstrate the complex changes in rib orientation, axial and lateral curvature. These ae more pronounced in the upper thorax (orange and red TPS grid) than in the lower (violet TPS grid) during growth. Note how the lower thoracic spine and the relative elongation of the lower ribs both contribute the lower thoracic shape changes. Superior views show the realtively strongly medio-laterally expanded thorax of the smallest (E) and the realtivley deeper chest in the largest (I). This view also shows that the posterior-most structure in the smallest individuals is the spine while in the largest it is the bilateral posterior projection of the ribcage lateral to the *angulus costae* (invagination of the vertebral spine). The frontal views in F) and J) illustrate the changes in thoracic shape represented by PC3 which are a considerable component of the differences between the means of group 2 (blue) and group 3 (red). These changes likely reflect growth of stature during later ontogeny.

doi: 10.1371/journal.pone.0075128.g004

Table 2. Mean shape comparisons (Procrustes distance, p-levels).

	Group 1	Group 2
Group 2	0.111 (p<0.0001)	
Group 3	0.1375 (p<0.0001)	0.0564 (p<0.045-0.081)

doi: 10.1371/journal.pone.0075128.t002

thoracic vertebral column (Figure 5d, vs. 5e) also increases. Further, the lateral (Figure 5d, e, Figure 6d, e) and axial views (Figure 5g, h; Figure 6g, h) show that the antero-posterior dimensions decrease relative to lateral ones in the midline (Figure 5h, j) while the sternal portions of the ribs expand anteriorly (Figure 6d,g). As a consequence, the upper part of the sternum shifts posteriorly and becomes lowered in age group 2 when compared to age group 1 (Figure 6d). This is accompanied by a relative decrease in thoracic antero-posterior diameter (Figure 6g, j) despite relative anterior lengthening of the upper ribs. Increased antero-posterior angulation of the upper ribs (attaching to the sternum; Figure 6a, d) relative to the spine accompanies and likely contributes to the descent of the sternum and the consequent relative decrease in upper thoracic antero-posterior diameter. The posterior part of the upper thorax becomes elevated relative to the anterior due to lateral elevation (Figure 6d). At the same time, the rib angles project more posteriorly, which increases lateral antero-posterior thoracic diameters relative to the midline (Figure 6g, h). In consequence, in group 1 the maximal antero-posterior dimension of the thorax is at the mid-sagittal plane (Figure 5g), while in group 2 the largest a-p diameters are found bilaterally, off the midline, easily appreciated in axial view (Figure 5h) (see also Figure 4e, i). This is also related to the development of the physiological lordosis in the thoracic part of the vertebral column which is relatively straight in group 1 and develops later (Figure 5, d,e).

Between age groups 2 and 3, in the second growth phase (compare Figure 4f, j) changes in thoracic shape are less pronounced (Figure 5; Figure 6, b, e, h, k) and in contrast to the transformation between age groups 1 and 2 they are concentrated in the mid- and lower thorax. This change results in more subtle differences that lead to a small relative increase in upper thoracic height (Figure 6e, see also Figure 4f,j) and in lower anterior thoracic width (Figure 6b,h,k). The upper thorax slightly increases in a-p diameter and this is (Figure 6e), accompanied by a relative forward shift of the sternum (Figure 6e,h, k).

Upper and lower thoracic growth vectors

Multivariate regressions of shape on size of the upper thorax explained 36.4% (p<0.001), and of the lower thorax 42.9% (P<0.001) of the total variance in thoracic shape. The angle between regression lines was highly statistically significant (p<0.0001) at 36.4 degrees. This result supports the hypothesis of different growth allometries for the upper and lower thorax.

Taking together the ontogeny of centroid size and the shape and form space trajectories, our findings suggest the existence of significant changes in form between the three age groups.

Discussion

This study has examined how the thorax changes in shape, and size over time and has tested the hypothesis that adult thoracic shape is achieved early, by the age of two [25]. Beyond this, it has been possible to compare the growth allometries of the upper and lower thorax and so to consider, below, how these integrate respiratory function with the demands of locomotion (posture) and the relative size of the abdominal contents, principally the digestive system.

The analyses of this study indicate that postnatal ontogenetic shape changes in the thorax are complex and show a shift between early and later phases of ontogeny. Consistent with the hypothesis [25], the early growth phase comprises relatively marked changes in thoracic shape between birth and the third year of postnatal life, particularly in the transverse diameter of the upper thorax relative to the lower [25,53]. Thus, Figure 6 shows that by the third year of life the pyramidal neonatal thorax is transformed into the more barrel shaped thorax typical of adults. Our analyses also demonstrate that further, but smaller ontogenetic changes in shape and particularly size later fully establish the typical adult rib cage configuration.

Our results show that widening in the coronal plane is particularly a feature of upper thoracic ontogeny (3rd to 5th rib) (Figure 5). This is likely integrated with the growth of the lungs, which show a major increase in volume during the first two years [54]. In contrast, the lower thorax of the newborn is relatively wider than that of adults. This contrasts with Openshaw et al.'s [25] findings (from midsternal transverse sections) and likely relates to relative growth differences between respiratory and digestive (including the liver) systems as well as relative vertical lengthening of the abdomen, such that the abdominal contents can be accommodated by a relatively narrower abdomen. Thus, the transformation from a pyramidal to a barrel shaped thorax is reminiscent of the difference between great apes and modern humans, where the former have a pyramidal thorax, at least in part to accommodate the relatively greater volume of the abdominal organs. In this case the differences in shape are driven by dietary differences [55] whereas in human ontogeny they are driven by differences in developmental trajectories between thoracic and sub-thoracic organs and spines. Thus, very different anatomical factors can lead to pyramidal thoracic shapes with narrower upper and wider lower openings. This has recently been indicated by García-Martínez et al. [24]. These authors demonstrated overall morphological similarity in different non-human primate thoraces on the one hand, but with clearly recognizable differences in 3D details of rib curvatures on the other. It has thus been suggested [24] that describing pyramidal versus barrel shaped thorax morphologies in considerations of human and primate evolution leads to oversimplification.

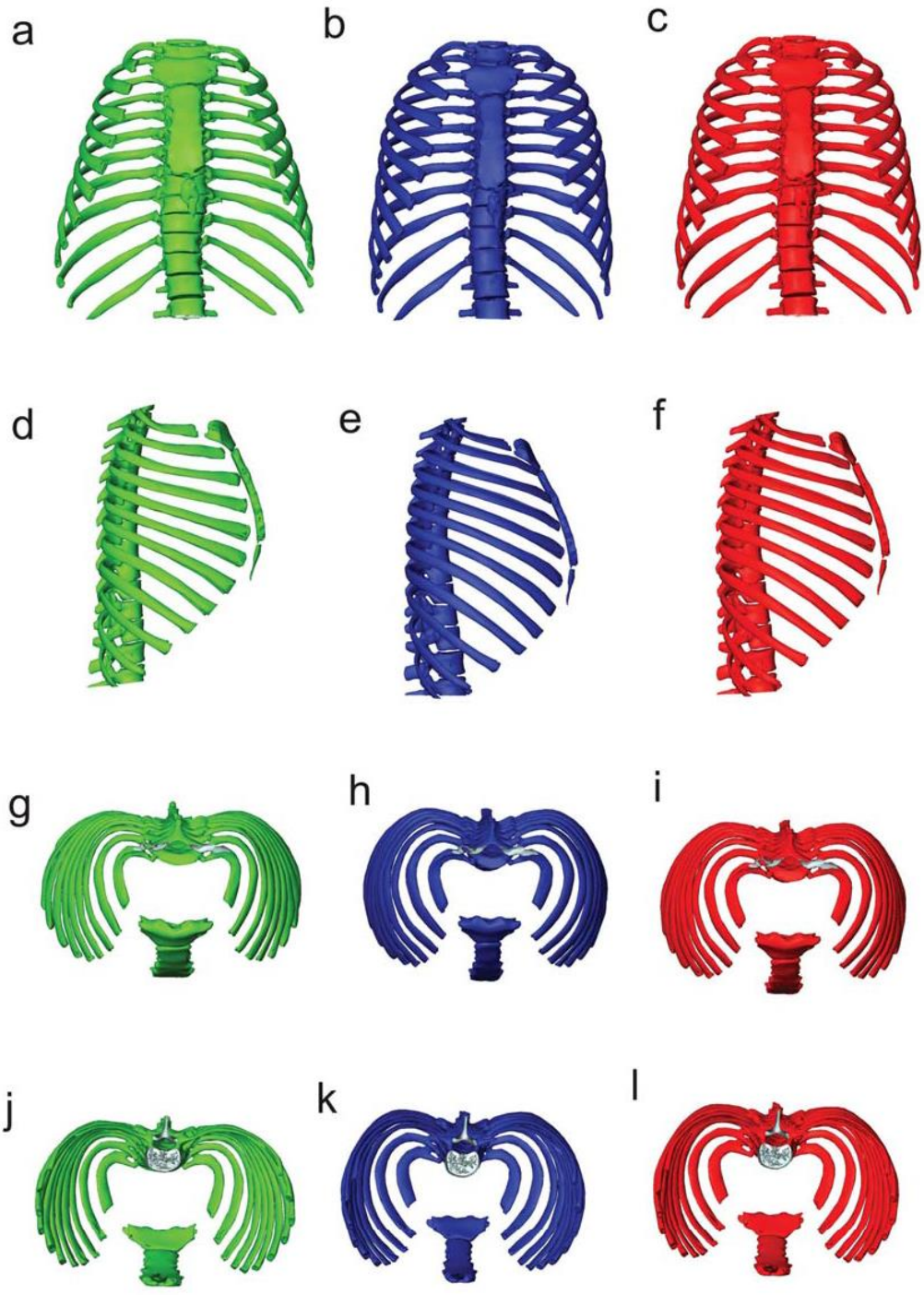

Figure 5, Bastir et al

Figure 5. Mean shapes of age groups. Group 1 (green), 2 (blue) and 3 (red) in frontal (a-b), left lateral (d–f), superior (g-i) and inferior (j-l) views.

doi: 10.1371/journal.pone.0075128.g005

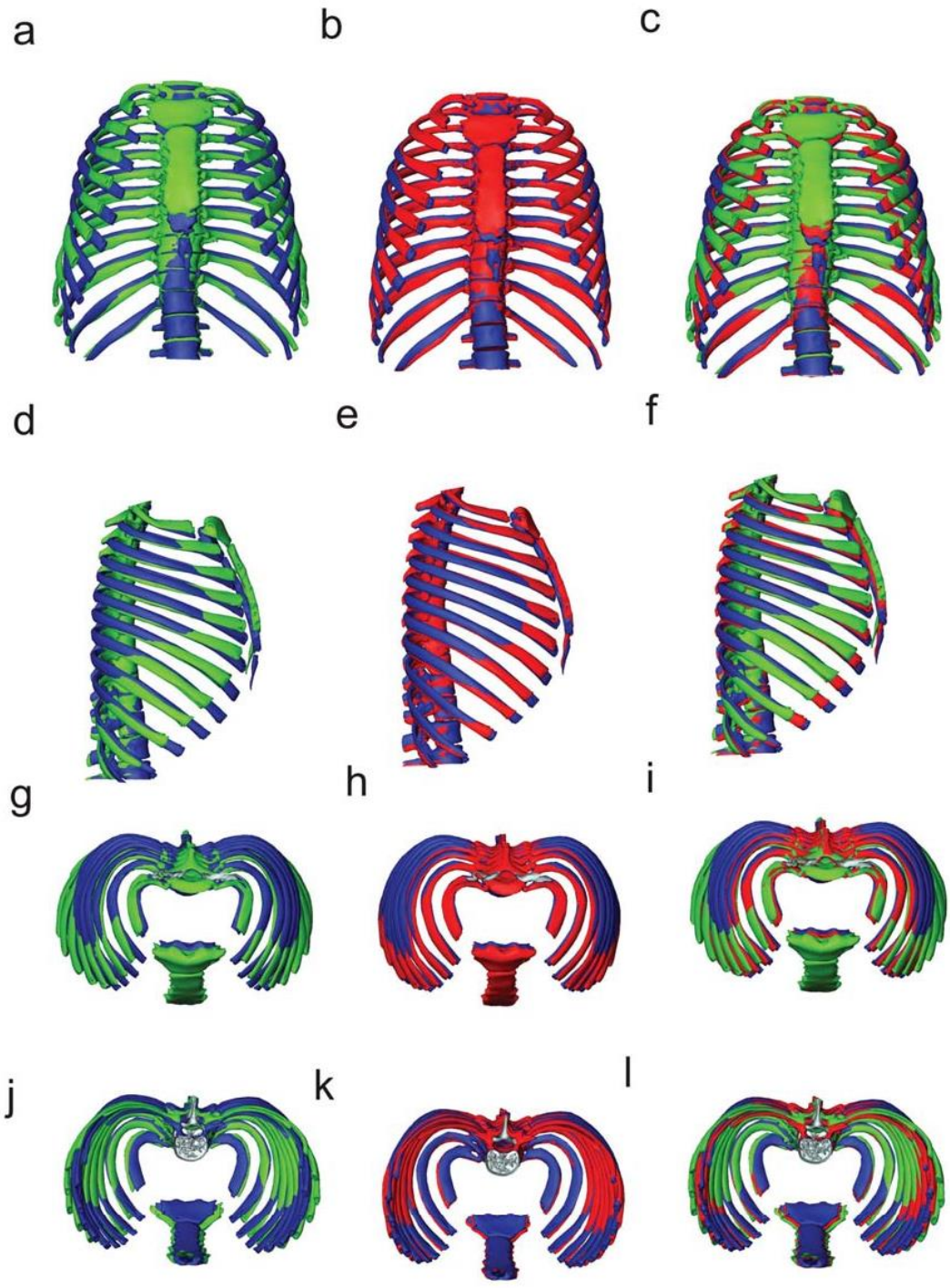

Figure 6. Procrustes registered means of age groups. Group 1 (green) and 2 (blue) (a,d,g,j), age groups 2 (blue) and 3 (red) (b,e,h,k), and of all three age groups in frontal (a-b), left lateral (d–f), superior (g-i) and inferior (j-l) views.
doi: 10.1371/journal.pone.0075128.g006

In addition to widening of the upper thorax, the lower sternum becomes relatively elongated and the anterior ends of ribs 2-10 come to lie relatively more medially and posteriorly. Sternal rib orientation is also altered, with the anterior ends coming to lie relatively more inferiorly as the sternum comes to lie relatively more inferiorly. This is due in part to lengthening of the ribs, but the change in orientation of the ribs is also accompanied by increased antero-posterior angulation of the upper ribs and elevation of the posterior third of the rib shaft close to the angle. As a result a complex axial and lateral 3D curvature develops in the upper ribs [56]. This reconfiguration of rib-curvature and orientation is functionally important as it underlies changes in respiratory mode in the first few years of life [57,58]. Breathing in the newborn child is essentially diaphragmatic, and because the ribs are more horizontal than in adults, the respiratory muscles cannot raise them effectively [1]. However, with changing rib-orientation during the first three years, biomechanically more efficient thoracic breathing becomes possible [1,2].

The female adult sternum is located at the level of the third thoracic vertebra while the male is located higher [29,59]. Bellemare et al [60] have linked the lower female sternal position and greater rib inclination to functional adaptations to pregnancy and the female's capacity to achieve relatively greater volume expansions. Our analyses are unable to determine if lowering of the anterior part of the thorax relative to the posterior (Figure 6d) occurs differentially in males and females or if differences are already present at birth. Larger, sexed, developmental series are necessary to address this.

The development of the thoracic kyphosis contributes to further anterior extension of the sternal rib extremes of the lower sternal ribs (Figure 6) [53,61]. An important interaction between posture, ribcage configuration and respiratory physiology has also recently been identified by a kinematic study [16]. These authors show that malformations of the spine cause inefficient positioning and orientation of the ribs, which precludes the respiratory muscles from coordinated and efficient kinematics [16].

During later childhood and adolescence further, smaller, but important modifications in thoracic shape occur. Centroid size increases steeply (Figure 2) until adult size is reached around adolescence. Little is known about later ontogenetic growth but form space analysis clearly points to an increase in vertical thoracic height (Figure 4f, j), likely in relation to increase in stature [62]. Clearly, group 2 covers a wide ontogenetic range and ideally should be divided into later childhood and adolescence [62] in order to better detail skeletal morphological changes. However, in terms of shape there is a degree of overlap between younger and older members of group2. Larger samples are necessary to investigate size and shape changes in more detail.

A relative increase in middle to lower thoracic width and depth (Figure 6e,k) could reflect previous findings [11] of deepening and an increase in posterior width in males between the ages of 20 and 65. Our data show that this is particularly so in the mid to lower ribcage and suggest that this not related to modifications of rib-shape itself but rather to modifications of sub-thoracic organs and modifications of the lower spine. Also, age-related shortening of pre-lumbar vertebral bodies and intervertebral discs could contribute to these changes.

One important critical aspect is that our data come from CT data sets produced in the supine position. As confirmed by a recent study variation in posture can affect functional performance [63]. To what extent changes in performance are related to posture-related changes in skeletal ribcage morphology should be addressed in future research.

Our results have shown that adult thoracic shape is the result of a shape trajectory that changes over time, it is curved. This reflects a modular growth pattern; the upper and lower parts of the thorax grow differentially because of differing relative influences of the developing lungs, abdominal viscera and the locomotor apparatus. Different kinematic factors are also likely important. For example, Ward et al [64] have suggested that muscle insertions divide the thorax into an upper compartment related to the insertions of the parasternal and scalenus muscle insertions (ribs 1-6) and a lower compartment related to the insertion of the diaphragm (ribs 7-12). This differential effect of muscles may reflect and point to the mechanisms underlying the mosaic evolution of upper and lower parts of the australopithecine thorax [19]. The differential growth of upper and lower thorax, quantified here, may be also be important in relation to understanding how childhood respiratory disease impacts on the development of adult thoracic shape and so function. However, better understanding of variations in thoracic form among recent and fossil humans as well as how these impact on function requires more extensive data and will be the subject of future studies.

Supporting Information

Movie S1. Ontogenetic allometry. The movie shows the shape changes of the skeletal thorax represented by Principal Component 1 of Form space which reflects the major part of ontogenetic allometry. Note the different patterns of shape change in the upper and lower thorax units.
(AVI)

Acknowledgements

We thank Demetrios Halazonetis for constant support with Viewbox4 software and as well as Peter Schmid and Charles Oxnard for helpful discussions, Maribel Torres (IdiPAZ, Madrid) for assistance with CT data and one anonymous reviewer for helpful comments on a previous version of this manuscript.

Author Contributions

Conceived and designed the experiments: MB. Performed the experiments: MB DGM MC. Analyzed the data: MB DGM MC. Contributed reagents/materials/analysis tools: MB DGM MC WR. Wrote the manuscript: MB PO WR AB LR FGR APM.

References

1. De Troyer A, Kirkwood PA, Wilson TA (2005) Respiratory Action of the Intercostal Muscles. Physiol Rev 85: 717-756. doi:10.1152/physrev.00007.2004. PubMed: 15788709.
2. Ward J (2005) Physiology of breathingl. Surgery 23: 419-424.
3. Jordanoglou J (1954) Rib movement in health, kyphoscoliosis, and ankylosing spondylitis. Thorax 24: 407-414. PubMed: 5795643.
4. Wilson TA, Rehder K, Krayer S (1987) Geometry and respiratory displacement of human ribs. J Appl Physiol 62: 1872-1877. PubMed: 3597261.
5. Jellema LM, Latimer B, Walker A (1993) The rib cage. The Nariokotome Homo Erectus Skeleton. Cambridge. Harvard University Press. pp. 294-325.
6. Yoganandan N, Pintar FA (1998) Biomechanics of human thoracic ribs. J Biomech Eng 120: 100-104. doi:10.1115/1.2834288. PubMed: 9675687.
7. Goldfield EC, Schmidt RC, Fitzpatrick P (1999) Coordination Dynamics of Abdomen and Chest during Infant Breathing: A Comparison of Full-Term and Preterm Infants at 38 Weeks Postconceptional Age. Ecol Psychol 11: 209-232. doi:10.1207/s15326969eco1103_2.
8. Glass RBJ, Norton KI, Mitre SA, Kang E (2002) Pediatric Ribs: A Spectrum of Abnormalities 1. RadioGraphics 22: 87-104. PubMed: 11796901.
9. Gea J (2007) The Evolution of the Human Species: A Long Journey for the Respiratory System. Acta Bronconeum 44: 263-270.
10. Mohr M, Abrams E, Engel C, Long WB, Bottlang M (2007) Geometry of human ribs pertinent to orthopedic chest-wall reconstruction. J Biomech 40: 1310-1317. doi:10.1016/j.jbiomech.2006.05.017. PubMed: 16831441.
11. Gayzik FS, Yu MM, Danelson KA, Slice DE, Stitzel JD (2008) Quantification of age-related shape change of the human rib cage through geometric morphometrics. J Biomech 41: 1545-1554. doi: 10.1016/j.jbiomech.2008.02.006. PubMed: 18384793.
12. Gómez-Olivencia A, Eaves-Johnson KL, Franciscus RG, Carretero JM, Arsuaga JL (2009) Kebara 2: new insights regarding the most complete Neandertal thorax. J Hum Evol 57: 75-90. doi:10.1016/j.jhevol.2009.02.009. PubMed: 19540563.
13. Pham TMT, Yuill M, Dakin C, Schibler A (2011) Regional ventilation distribution in the first 6 months of life. Eur Respir J 37: 919-924. doi: 10.1183/09031936.00034310. PubMed: 20650987.
14. Bastir M, García-Martínez D, Coquerelle M, Barash A, Recheis W (2012) Systems-approaches to skeletal variation in paleoanthropology: the human thorax. In: PESHE. 2012 21, and 22.09.2012. Bordeaux. 35.
15. García-Martínez D, Recheis W, Bastir M (2012) The whole and its parts: 3D geometric morphometrics of human thorax evolution. Valencia.
16. LoMauro A, Pochintesta S, Romei M, D'Angelo MG, Pedotti A et al. (2012) Rib Cage Deformities Alter Respiratory Muscle Action and Chest Wall Function in Patients with Severe Osteogenesis Imperfecta. PLOS ONE 7: e35965. doi:10.1371/journal.pone.0035965. PubMed: 22558284.
17. Redding GJ, Kuo W, Swanson JO, Phillips GS, Emerson J et al. (2012) Upper thoracic shape in children with pectus excavatum: Impact on lung function. Pediat Pulmonol.
18. Tsai A, Coats B, Kleinman PK (2012) Stress profile of infant rib in the setting of child abuse: A finite element parametric study. J Biomech 45: 1861-1868. doi:10.1016/j.jbiomech.2012.05.049. PubMed: 22727522.
19. Schmid P, Churchill SE, Nalla S, Weissen E, Carlson KJ et al. (2013) Mosaic Morphology in the Thorax of Australopithecus sediba. Science 340: 1234598. PubMed: 23580537.
20. Ferretti GR, Bricault I, Coulomb M (2001) Virtual tools for imaging of the thorax. Eur Respir J 18: 381-392. doi: 10.1183/09031936.01.00217701. PubMed: 11529300.
21. Ravenel JG, McAdams HP (2003) Multiplanar and three-dimensional imaging of the thorax. Radiol Clin North Am 41: 475-489. doi:10.1016/S0033-8389(03)00032-0. PubMed: 12797601.
22. Dworzak J, Lamecker H, Berg J, Klinder T, Lorenz C et al. (2010) 3D reconstruction of the human rib cage from 2D projection images using a statistical shape model. Int J Comp Assist Radiol Surg 5: 111-124. doi: 10.1007/s11548-009-0390-2. PubMed: 20033504.
23. Kagaya M, Ogihara N, Nakatsukasa M (2008) Morphological study of the anthropoid thoracic cage: scaling of thoracic width and an analysis of rib curvature. Primates 49: 89-99. doi:10.1007/s10329-007-0064-z. PubMed: 17902025.
24. García-Martínez D, Bastir M, Recheis W, Barash A (2013) Two different barrels for two different primates: 3D geometric morphometrics of sliding semilandmarks of the Hominoidea superfamily thorax. Bilbao. pp. in press.
25. Openshaw P, Edwards S, Helms P (1984) Changes in rib cage geometry during childhood. Thorax 39: 624–627. doi:10.1136/thx.39.8.624. PubMed: 6474391.
26. Weitz CA, Garruto RM, Chin CT, Liu JC (2004) Morphological growth and thorax dimensions among Tibetan compared to Han children, adolescents and young adults born and raised at high altitude. Ann Hum Biol 31: 292-310. doi:10.1080/03014460420000196316. PubMed: 15204346.
27. Bastir M (2008) A systems-model for the morphological analysis of integration and modularity in human craniofacial evolution. Anthropol Sci 86: 37-58. PubMed: 19934468.
28. Ríos L, Cardoso HFV (2009) Age estimation from stages of union of the vertebral epiphyses of the ribs. Am J Phys Anthropol 140: 265-274. doi: 10.1002/ajpa.21065. PubMed: 19358290.
29. Scheuer L, Black S (2000) Developmental Juvenile Osteology. Academic Press.
30. Bastir M, Rosas A, O'Higgins P (2006) Craniofacial levels and the morphological maturation of the human skull. J Anat 209: 637-654. doi: 10.1111/j.1469-7580.2006.00644.x. PubMed: 17062021.
31. O'Higgins P, Bastir M, Kupczik K (2006) Shaping the human face. Int Con Ser 1296: 55-73. doi:10.1016/j.ics.2006.03.036.
32. Bastir M, Rosas A (2009) Mosaic evolution of the basicranium in *Homo* and its relation to modular development. Evol Biol 36: 57-70. doi: 10.1007/s11692-008-9037-4.
33. Goodyear MDE, Krleza-Jeric K, Lemmens T (2007) The Declaration of Helsinki. BMJ 335: 624-625. doi:10.1136/bmj.39339.610000.BE. PubMed: 17901471.
34. Gunz P, Mitteroecker P, Bookstein FL (2005) Semilandmarks in three dimensions. In: D Slice. Modern Morphometrics in Physical Anthropology. New York. pp. 73-98.
35. Spoor CF, Zonneveld FW, Macho GA (1993) Linear measurements of cortical bone and dental enamel by computed tomography: applications and problems. Am J Phys Anthropol 91: 469-484. doi:10.1002/ajpa.1330910405. PubMed: 8372936.
36. Bastir M, Rosas A, Lieberman DE, O'Higgins P (2008) Middle cranial fossa anatomy and the origins of modern humans. Anat Rec 291: 130-140. doi:10.1002/ar.20636.
37. Bastir M, Rosas A, Gunz P, Peña-Melian A, Manzi G et al. (2011) Evolution of the base of the brain in highly encephalized human species. Nat Commun 2: 588. doi:10.1038/ncomms1593. PubMed: 22158443.
38. Gunz P, Mitteroecker P, Neubauer S, Weber GW, Bookstein FL (2009) Principles for the virtual reconstruction of hominin crania. J Hum Evol 57: 48-62. doi:10.1016/j.jhevol.2009.04.004. PubMed: 19482335.
39. O'Higgins P, Cobb SN, Fitton LC, Gröning F, Phillips R et al. (2011) Combining geometric morphometrics and functional simulation: an emerging toolkit for virtual functional analyses. J Anat 218: 3-15. doi: 10.1111/j.1469-7580.2010.01301.x. PubMed: 20880075.
40. Mitteroecker P, Gunz P (2009) Advances in Geometric Morphometrics. Evol Biol 36: 235-247. doi:10.1007/s11692-009-9055-x.
41. Hibbert M, Lannigan A, Raven J, Landau L, Phelan P (1995) Gender differences in lung growth. Pediat Pulmonoly 19: 129-134. doi:10.1002/ppul.1950190208. PubMed: 7659468.
42. Nysom K, Ulrich CS, Hesse B, Dirksen A (1997) Published models and local data can bridge the gap between reference values of lung function for children and adults. Eur Respir J 10: 1591-1598. doi: 10.1183/09031936.97.10071591. PubMed: 9230253.
43. Klingenberg CP (2011) MorphoJ: an integrated software package for geometric morphometrics. Mol Ecol Resour 11: 353-357. doi:10.1111/j.1755-0998.2010.02924.x. PubMed: 21429143.
44. Mitteroecker P, Gunz P, Bernhard M, Schaefer K, Bookstein FL (2004) Comparison of cranial ontogenetic trajectories among great apes and humans. J Hum Evol 46: 679-698. doi:10.1016/j.jhevol.2004.03.006. PubMed: 15183670.
45. Bastir M, O'Higgins P, Rosas A (2007) Facial ontogeny in Neanderthals and modern humans. Proc R Soc Lond B 274: 1125-1132. doi:10.1098/rspb.2006.0448. PubMed: 17311777.
46. Zelditch ML, Swiderski DL, Sheets HD, Fink WL (2004) Geometric Morphometrics for Biologists: A Primer. San Diego: Elsevier Academic Press. 443pp.
47. Sokal RR, Rohlf FJ (1998) Biometry. New York: W. H. Freeman and Company. 850pp.
48. O'Higgins P (2000) The study of morphological variation in the hominid fossil record: biology, landmarks and geometry. J Anat 197: 103-120. doi:10.1046/j.1469-7580.2000.19710103.x. PubMed: 10999273.
49. Bastir M, Rosas A (2004) Facial heights: Evolutionary relevance of postnatal ontogeny for facial orientation and skull morphology in

humans and chimpanzees. J Hum Evol 47: 359-381. doi:10.1016/j.jhevol.2004.08.009. PubMed: 15530353.
50. Cobb S, O'Higgins P (2004) Hominins do not share a common postnatal facial ontogenetic shape trajectory. J Exp Zool Mol Dev Evol 302B: 302-321. doi:10.1002/jez.b.21005.
51. Klingenberg CP, Marugán-Lobón J (2013) Evolutionary Covariation in Geometric Morphometric Data: Analyzing Integration, Modularity and Allometry in a Phylogenetic Context. Syst Biol.
52. Li S (2011) Concise formulas for the area and volume of a hyperspherical cap. Asian J Math Statist: 66-70.
53. Berry M, Standring S, Bannister L (1995) Gray's Anatomy; C Livingstone. London: Harcourt Publishing House Brace and Company Limited.
54. Thurlbeck WM (1982) Postnatal human lung growth. Thorax 37: 564-571. doi:10.1136/thx.37.8.564. PubMed: 7179184.
55. Aiello LC (1997) Brains and guts in human evolution: The Expensive Tissue Hypothesis. Braz J Genet 20.
56. Mann RW (1993) A Method for Siding and Sequencing Human Ribs. J Forens Sci 38: 151-155.
57. Moriette G, Van Reempts P, Moore M, Cates D, Rigatto H (1985) The effect of rebreathing CO2 on ventilation and diaphragmatic electromyography in newborn infants. Respir Physiol 62: 387-397. doi:10.1016/0034-5687(85)90093-3. PubMed: 3937194.
58. Reis F, Cates D, Landriault L, Rigatto H (1994) Diaphragmatic activity and ventilation in preterm infants. II. The effects of inhalation of 3% CO2 and abdominal loading. Biol Neonate 65: 69-76..
59. Aiello L, Dean C (1990) An introduction to human evolutionary anatomy. London: Academic Press Harcourt Brace & Company.
60. Bellemare F, Fuamba T, Bourgeault A (2006) Sexual dimorphism of human ribs. Respir Physiol Neurobiol 150: 233-239. doi:10.1016/j.resp.2005.04.002. PubMed: 16476656.
61. Wagner H, Liebetrau A, Schinowski D, Wulf T, de Lussanet MH (2012) Spinal lordosis optimizes the requirements for a stable erect posture. Theoret Biol Med Mod 9: 13. doi:10.1186/1742-4682-9-13. PubMed: 22507595.
62. Baume RM, Buschang PH, Weinstein S (1983) Stature, head height, and growth of the vertical face. Am J Orthod 83: 477-484. doi:10.1016/0002-9416(83)90246-4. PubMed: 6574704.
63. Romei M, Mauro AL, D'Angelo MG, Turconi AC, Bresolin N et al. (2010) Effects of gender and posture on thoraco-abdominal kinematics during quiet breathing in healthy adults. Respir Physiol Neurobiol 172: 184-191. doi:10.1016/j.resp.2010.05.018. PubMed: 20510388.
64. Ward ME, Ward JW, Macklem PT (1992) Analysis of human chest wall motion using a two-compartment rib cage model. J Appl Physiol 72: 1338-1347. PubMed: 1592724.

Ontogeny of 3D Rib Curvature and Its Importance for the Understanding of Human Thorax Development

Daniel García-Martínez,[1,2]* Wolfgang Recheis,[3] and Markus Bastir[1]

[1]*Paleoanthropology Group, Paleobiology Department, Museo Nacional de Ciencias Naturales (MNCN-CSIC), JG. Abascal 2, Madrid 28006, Spain*
[2]*Biology Department, Faculty of Sciences, Universidad Autónoma De Madrid. Darwin 2, Madrid 28049, Spain*
[3]*Department of Radiology, Medizinische Universität Innsbruck, 6020, Austria*

KEY WORDS rib cage; geometric morphometrics; development; geometric morphometrics; development; individual ribs; ontogeny

Objectives: Sagittal and axial rib orientation relative to the spine are two factors that modify rib cage morphology during ontogeny. Some studies suggest that these factors do not operate in the same way at the upper (ribs 1–5) and lower thorax (ribs 6–10) during postnatal growth, but it is unknown if the ontogenetic thoracic changes are produced by morphological changes of the ribs (intrinsic rib factors) or by external factors related to costal joints (extrinsic rib factors).
Material and methods: To clarify these questions, we applied 3D geometric morphometrics of landmarks and sliding semilandmarks ($N = 20$/rib) to 280 individual ribs (1–10) of *Homo sapiens* comprising the entire human ontogeny and growth simulations were carried out.
Results: PCA shows that intrinsic rib factors (rib torsion and axial rib curvature) are ontogenetic factors of variability that contribute to configuring the adult thorax shape. Moreover, growth simulations and regression slopes suggest that the upper thorax unit is comprised by ribs 1–7 and the lower unit at least by ribs 8–10.
Discussion: These results suggest anatomical constraints for ontogenetic rib variation, since ribs 1–7 (true ribs) are directly linked to the sternum. Moreover, these results are supported by functional anatomy because pulmonary kinematics would influence the upper unit and diaphragmatic kinematics would influence the lower one. Our findings are relevant not only to understanding how changes at individual ribs contribute to the adult thorax morphology, but also to the development and evolution of the modern human rib cage. Am J Phys Anthropol 159:423–431, 2016.

INTRODUCTION

The understanding of the 3D morphological changes that occur in the rib cage during the ontogeny (from newborns to adults) of *H. sapiens* has changed little since the early 80's (Openshaw, 1984). Nevertheless, in recent years it has received special attention in different fields of study such as biomechanics or evolutionary biology (Gayzik et al., 2008; Bastir et al., 2013a,b; Shi et al., 2014; Weaver et al., 2014). This is in part due to methodological advances and improvements in morphometric quantification due to the use of semilandmark methods (Bastir et al., 2013a,b, 2015; García-Martínez, 2013; García-Martínez et al., 2013, 2014a; Shi et al., 2014; Weaver et al., 2014). However, it should be noted that this research has mainly focused on the variability of thorax morphology in anatomical connection.

Some authors have addressed ribcage ontogeny considering it as a whole (Openshaw, 1984; Gayzik et al., 2008; Shi et al., 2014; Weaver et al., 2014) but there is evidence that morphological growth changes at the upper rib cage could be different from those at the lower (Bastir et al., 2013a,b). Different morphometric patterns of the upper and lower thorax have been observed not only during human ontogeny but also in the sexual dimorphism of the thoracic vertebrae or even throughout the evolution of the thorax shape in different hominin lineages (Bastir et al., 2013b, 2014a, 2015; Schmid et al., 2013; García-Martínez et al., 2014a,2014b; García-Martínez and Bastir, 2015).

Ontogenetic implications

Specifically, some authors (Openshaw et al., 1984; Bastir et al., 2013a, b; Weaver et al., 2014) have found that from newborns to young adults (not the elderly), lowering of the ribs relative to the spine into the sagittal plane and medio-lateral expansion of the ribcage in the axial plane are the main factors which configure the shape of the adult rib cage. However, Bastir et al.

Additional Supporting Information may be found in the online version of this article.

Grant sponsor: CGL2012-37279 Project (Ministry of Science and Competitivity, Spain); Grant sponsor: Leakey Foundation.

*Correspondence to: Daniel García-Martínez, Paleoanthropology group, Museo Nacional de Ciencias Naturales, 28006 Madrid, Spain. E-mail: dan.garcia@mncn.csic.es

Received 12 June 2015; revised 26 October 2015; accepted 29 October 2015

DOI: 10.1002/ajpa.22893
Published online 17 November 2015 in Wiley Online Library (wileyonlinelibrary.com).

(2013b) have suggested that these factors do not occur in the same way at the upper and lower thorax, suggesting modular growth. According to these last authors, there is an increase in the relative medio-lateral dimensions of the upper thorax compared with a relative narrowing of the lower thorax throughout ontogeny, which transforms the pyramidal infant thorax into the barrel-shaped thorax of adults. These authors related this transition to morpho-functional interactions with the shoulder or pelvic girdle as well as insertions of the diaphragm in ribs 7–12 (Spaltzeholtz, 1970; De Troyer et al., 2005).

Intrinsic and extrinsic rib factors modulating thorax development

Because the ribcage is an anatomical composite structure, the adult thorax shape is configured not only by the ontogenetic development of the ribs, but also by the ontogenetic development of their costal joints at the sternal and vertebral ends. Therefore, to study the factors that contribute to variability in the construction of the adult rib cage, it is important to separate the intrinsic rib factors (change of the proper rib morphology) from the extrinsic ones (change at the costal joints without change of rib morphology).

As an example, lowering of the ribs has been identified as an important factor of variability during human ontogeny. Such lowering, which has been observed previously (Openshaw, 1984; Bastir et al., 2013a,b; Weaver et al., 2014), could be a mechanical rotation at the costovertebral joint (extrinsic rib factor). In fact, a classic text book on human anatomy (Gray, 1918) suggests that this lowering is caused by rotation of the ribs because of gravitational effects related to posture. However, other authors have observed that rib torsion in adults (understood as the three-dimensional spiraling of the rib shaft independent of the costal joints, and therefore an intrinsic rib factor) is an important factor of variability, which could contribute to lowering of the ribs relative to the sagittal plane (Schmid, 1991; Dudar, 1993; Mann, 1993; Bastir et al., 2015). However, since there is a lack of knowledge about the individual rib ontogeny, we do not have information about the possibility of rib torsion contributing to the lowering of the ribs observed in the human ontogenetic process. If lowering is produced only by declination (an extrinsic rib factor), we should expect that postnatal ontogeny does not alter the degree of rib torsion (an intrinsic rib factor). It is also possible that both intrinsic and extrinsic factors interplay together to produce morphological variation in rib plane orientation relative to the sagittal plane during ontogeny.

Regarding medio-lateral expansion of the thorax, some authors (Openshaw et al., 1984; Bastir et al., 2013a,b) have argued that this feature is produced by changes in axial rib curvature (an intrinsic factor) throughout ontogeny. However, extrinsic factors, such as the orientation of the transverse processes of the thoracic vertebrae, could also contribute to medio-lateral expansion of the thorax at least in adults (Bastir et al., 2014a), and there is evidence for ontogenetic changes in this orientation (Latimer and Ward, 1993). Because no 3D rib growth study is currently available, it is not clear how the axial rib curvature contributes (intrinsically) to medio-lateral expansion of the thorax.

If medio-lateral expansion of the thorax is caused by the orientation of the transverse processes (an extrinsic rib factor), we should expect no changes in axial rib curvature during ontogeny (an intrinsic rib factor). It is also possible that both intrinsic and extrinsic factors interact to produce morphological variation in the medio-lateral expansion of the thorax during ontogeny.

Functional implications of morphological costal changes

Morphological changes in rib orientation linked to kinematic function have been reported in several studies. However, lowering of the ribs observed from newborns to young adults makes elevation by intercostal muscle action possible (De Troyer et al., 2005; Ratnovsky et al., 2008). However, it is still unknown whether this lowering is caused by a rotation of the ribs at the costal joints (an extrinsic rib factor) or by an increase of rib torsion (an intrinsic rib factor).

However, medio-lateral expansion of the lower thorax makes diaphragmatic action possible (De Troyer et al., 2005; Ratnovsky et al., 2008; García-Martínez et al., 2014a,b). However, it is still unknown whether mediolateral expansion of the thorax is caused by a different orientation of the transverse processes (an extrinsic rib factor) or by differences in the axial rib curvature (intrinsic rib factor).

Breathing in new-borns is essentially diaphragmatic because the ribs are more horizontal than in adults, so the respiratory muscles cannot raise them effectively. Since the lower thorax is mediolaterally expanded, the diaphragm will also be broader and will allow for more efficient diaphragmatic functioning. However, because of changes in the 3D configuration of the ribcage caused by changes in rib-orientation during the first three years, the intercostal muscles are able to raise the ribs more efficiently and thoracic breathing also becomes more effective (De Troyer et al., 2005; Bastir et al., 2013a,b).

Thorax modularity

Openshaw et al. (1984) hypothesized that mediolateral expansion of the thorax occurs in the whole thorax during postnatal ontogeny. However, Bastir et al. (2013b) were more specific, suggesting that this mediolateral expansion is more pronounced in the upper than the lower thorax. Thus, if mediolateral widening of the rib cage is observable at the individual costal level, we should expect a different growth pattern in ribs belonging to the upper (ribs 1–5) and lower thorax (ribs 6–10).

Hypotheses that explain the modularity of the thorax include association with the sternum, kinematics of respiration, and integration with adjacent anatomical regions. First of all, this fact could be attributed to thorax anatomy, since the ribs belonging to the upper unit (true ribs) have the anatomical constraint of the direct link to the sternum, while the lower ribs (mainly false and floating ribs) do not (Spalteholtz, 1970). Secondly, functional anatomy also supports this separation since the development of the upper thorax could be influenced mainly by pulmonary kinematics while the growth of the lower thorax could be influenced by diaphragmatic kinematics (De Troyer et al., 2005; Bastir et al., 2013b; García-Martínez et al., 2014a,b). Finally, anatomical integration could also account for this separation (Bastir, 2008). This is because upper thorax development could be influenced by that of the shoulder girdle (Schmid et al., 2013; Roach and Richmond, 2015) whereas lower thorax development would be influenced by spine lordosis related to posture (Slijper, 1942; Bastir et al., 2013b,

TABLE 1. Percentage of variance explained by PC1-PC3 of the principal component analysis (PCA) in form space of each subset of ribs

	PC1 (%)	PC2 (%)	PC3 (%)	PC1-PC3 (%)
1st rib PCA	95.91	1.73	0.90	98.54
2nd rib PCA	97.95	0.92	0.43	99.30
3rd rib PCA	98.03	0.95	0.40	99.38
4th rib PCA	97.92	1.20	0.41	99.53
5th rib PCA	98.43	0.79	0.41	99.63
6th rib PCA	98.49	0.81	0.30	99.60
7th rib PCA	98.48	0.83	0.29	99.60
8th rib PCA	98.48	0.83	0.30	99.61
9th rib PCA	98.69	0.65	0.31	99.65
10th rib PCA	98.46	0.76	0.32	99.54

To analyze this, we calculated 10 allometric growth vectors in form space (one for each rib subset) taking the mean infant form as a starting point of the vectors and the mean adult form as the vectors' target. Then, we applied each vector (10 vectors in total) to grow the mean infant of the remaining rib subsets, thus creating nine simulations and one control specimen (the mean infant rib growth with its proper ontogenetic vector) for each rib subset.

To observe whether simulations fall inside the range of the true adult ribs of each subset and since the ontogenetic trajectory of each rib subset is mainly linear, we have computed 10 regressions of Procrustes shape coordinates on size (one for each rib subset) in MorphoJ 1.05f (Klingenberg, 2011). Then, we traced a 95% confidence ellipse around the true adult sample and observed whether the nine adult simulations for each mean infant rib fall inside of the true adult range.

Elements that do not share common growth trajectories show different slopes in theirs growth curves (Cobb and O'Higgins, 2004; Bastir and Rosas, 2004, Mitteroecker et al., 2005). Therefore, to reinforce our results, we have calculated the slope of each regression with the 95% confidence interval, observing whether the slopes of upper ribs fall inside of the interval of lower ribs. These analyses were carried out in PAST software (Hammer et al., 2001).

RESULTS

Form spaces

Ten PCA analyses in form space showing PC1, PC2, and PC3 projection suggest a very close link between size and shape (Fig. S1, Supporting Information) thus reflecting a mainly ontogenetic change and explaining a reasonable amount of variance for each rib subset (Table 1). The linearity of each plot suggests linear growth during ontogeny (at least using this set of landmarks).

The warps associated with PC1 in form space of each rib subset can be observed in Figures 1 and 2. Different growth patterns at the upper and lower ribs occur in regard to axial rib curvature but not in rib torsion. Regarding rib torsion, in newborns the upper and lower ribs have less torsion than those of the central thorax. After growth, all adult ribs show an increase in torsion compared to that observed in newborns, but the pattern of torsion along the rib sequence in adults is still very similar to that of newborns: ribs of the central thorax have more torsion than those of the upper and lower thorax. Due to this increase in torsion during ontogeny, nonadult ribs are generally less helicoidal than their adult counterparts.

As for axial rib curvature, we can observe that infant ribs are straighter (less curved) in the axial view than their adult counterparts (Fig. 2). A different growth pattern can be observed in the upper and lower ribs. After growth, all adult ribs are more curved than those belonging to infants, but the upper ribs present their point of maximum curvature at the mid-shaft while in the lower ribs this point is observed more dorsally, closer to the *angulus costae*.

The warps associated with PC1 in form space (Figs. 1 and 2) show that ribs undergo several complex changes in their 3D curvature throughout ontogeny due to intrinsic rib factors. All ribs of the sequence undergo an increase in rib torsion (sagittal curve) and we observe changes in axial curvature of the ribs, which is different in the upper and lower ribs. These results suggest that hypothesis 1 (we should expect that postnatal ontogeny will not alter the degree of rib torsion) and hypothesis 2 (we should expect no changes in axial rib curvature throughout the ontogeny) should be rejected and hypothesis 3 (we should not expect the same growth pattern in ribs belonging to the upper and lower thorax) should be accepted.

Ontogenetic growth vectors and regression analysis

Figure 2a–j from Supporting Information show a close link between size and shape, which explains a reasonable amount of the variance for each rib subset (at least >7.13%; at least $P < 0.05$; Table 2). Moreover, it is important to note that a larger amount of variance is collected in the central rib subsets compared with upper and lower rib subsets (Table 2).

Growth trajectories of ribs 8–10 are not useful for simulating the true adult morphologies of the rest of the ribs (ribs 1–7) because when these vectors are used for simulation, the predictions fall outside the 95% confidence ellipse of the true adults (this is because the point of maximum curvature is more dorsal than it really is in true ribs; Figure 2a–g from Supporting Information). However, when we predict ribs 8–10, we observe that any trajectory can be used to predict a true adult rib since all the predictions fall inside the 95% confidence ellipse of real adults (Fig. 2h–j from Supporting Information).

This suggests that adult ribs 8–10 have a more variable morphology than ribs in the remaining thorax since they are more widely spread out along the ordinate axis of the regression. This fact is also reflected by the low percentage of variance explained by the lower rib regressions. Finally, Table 3 shows regression slopes of each rib subset regression with 95% confidence interval. The slopes of ribs 1–7 are outside of the interval of ribs 8–10 and vice versa.

DISCUSSION

This study has examined how intrinsic rib factors, such as rib torsion and axial rib curvature, are important to understanding rib growth during postnatal ontogeny. In addition, we tested whether ontogenetic modularity observed at the thorax level could also be recognized in individual ribs, or whether thorax modularity is an emergent phenomenon (novelty) of an

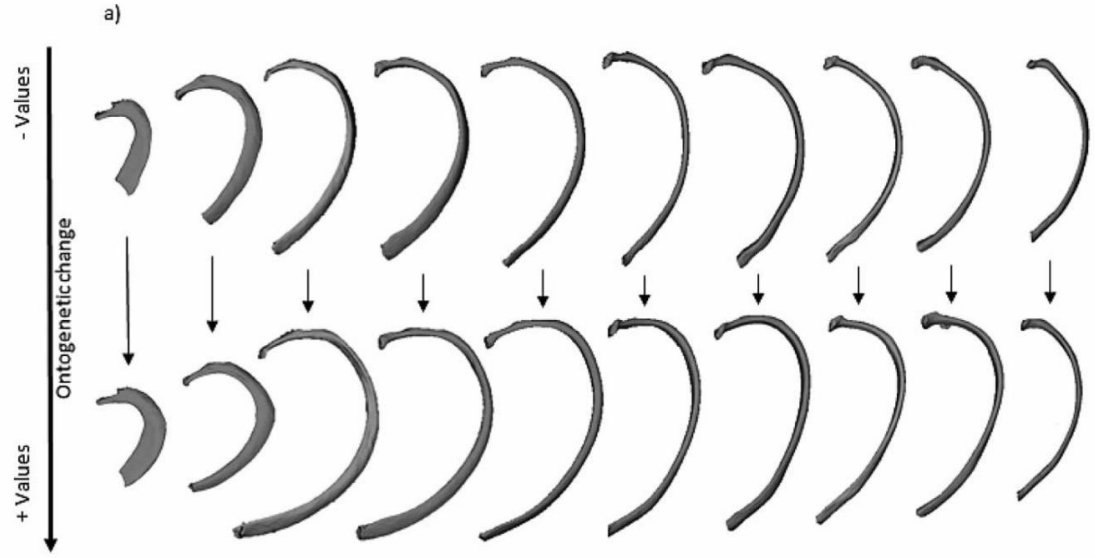

Fig. 1. 3D warps showing morphological changes undergone along the ontogeny at every rib level observed in the axial view. The ribs are displayed in anatomical sequence 1–10 from the left to the right side of the figure. The arrow shows the direction of the ontogenetic change.

anatomical composite structure, a phenomenon imposed by mutual anatomical constraints of vertebrae and ribs.

Implications of the ontogenetic variability of the ribs during human ontogeny

This study indicates that postnatal ontogenetic shape changes observed in rib features such as sagittal or axial curvatures are more complex than previously thought. Our data show that the lowering of the ribs within the thorax is caused by an increase in rib torsion during ontogeny, a phenomenon observed to occur in a similar way at every rib level. This result does not contradict the possibility that extrinsic rib factors at the costal joints (rib declination) could also be involved in the lowering of the ribs. Nonetheless, our results demonstrate that rib torsion is an important intrinsic rib factor during postnatal ontogeny.

In accordance with our results, we can reject hypothesis 1 (we should expect that postnatal ontogeny will not alter the degree of rib torsion) because we observe changes in the torsion pattern of ribs (an intrinsic rib factor) during ontogeny. Instead, we believe that rib declination and rib torsion are two related phenomena that occur together and modify the thoracic configuration throughout ontogeny. However, it is important to note that extrinsic rib factors (rib declination) become apparent only when looking at the thorax in anatomical connection; intrinsic rib factors (rib torsion), on the other hand, become more evident when we look at individual ribs.

Regarding medio-lateral expansion, our results show that axial rib curvature is an important intrinsic rib factor that causes adult ribs to be more axially curved than their non-adult counterparts. Therefore, we can also reject hypothesis 2 (we should expect no changes in axial rib curvature throughout the ontogeny). Instead, we believe that axial rib curvature and transverse processes orientation could be two related phenomena that modify the mediolateral dimension of the thorax during ontogeny. However, the ontogeny of the transverse processes is not addressed in this study, and should be investigated in future research to know how vertebral ontogeny contributes to the mediolateral expansion of the rib cage.

The information provided in this study could be important not only for understanding the generation of variation among adult *Homo sapiens*, for example, in sexual dimorphism (Bellemare et al., 2003, 2006) or in specific climatic adaptation (Weinstein, 2007), and also in the generation of different thorax morphologies proposed for other hominin species such as Neanderthals (Franciscus and Churchill, 2002; Weinstein, 2008; Gómez-Olivencia et al., 2009; García-Martínez et al., 2014a,b; Bastir et al., 2015). In addition, the understanding of rib ontogeny could help us to understand the thorax morphology of important sub-adult fossil specimens such as the *Homo ergaster* KNM-WT 15000 (Jellema et al., 1993; Roach and Richmond, 2015) or the *Australopithecus sediba* MH1 (Schmid et al., 2013).

Functional implications of rib changes for understanding thorax ontogeny

Anatomy textbooks (e.g., Gray, 1918) show newborns' ribs to be more horizontal than those of adults, and show that they become more caudally oriented during early ontogeny because of mechanical rotation (declination) due to gravitational processes caused by bipedal posture. This phenomenon has also been found in several recent studies (Openshaw et al., 1984; Bastir et al., 2013b; Shi et al., 2014; Weaver et al., 2014). However, since all of these works studied the thorax in anatomical connection, it was not clear if this rib lowering was caused solely by declination, or if intrinsic rib factors were also involved.

Our regression results demonstrate for the first time that this lowering of the ribs, accounting for important functional changes from diaphragmatic breathing to intercostal muscle breathing, could be caused by changes

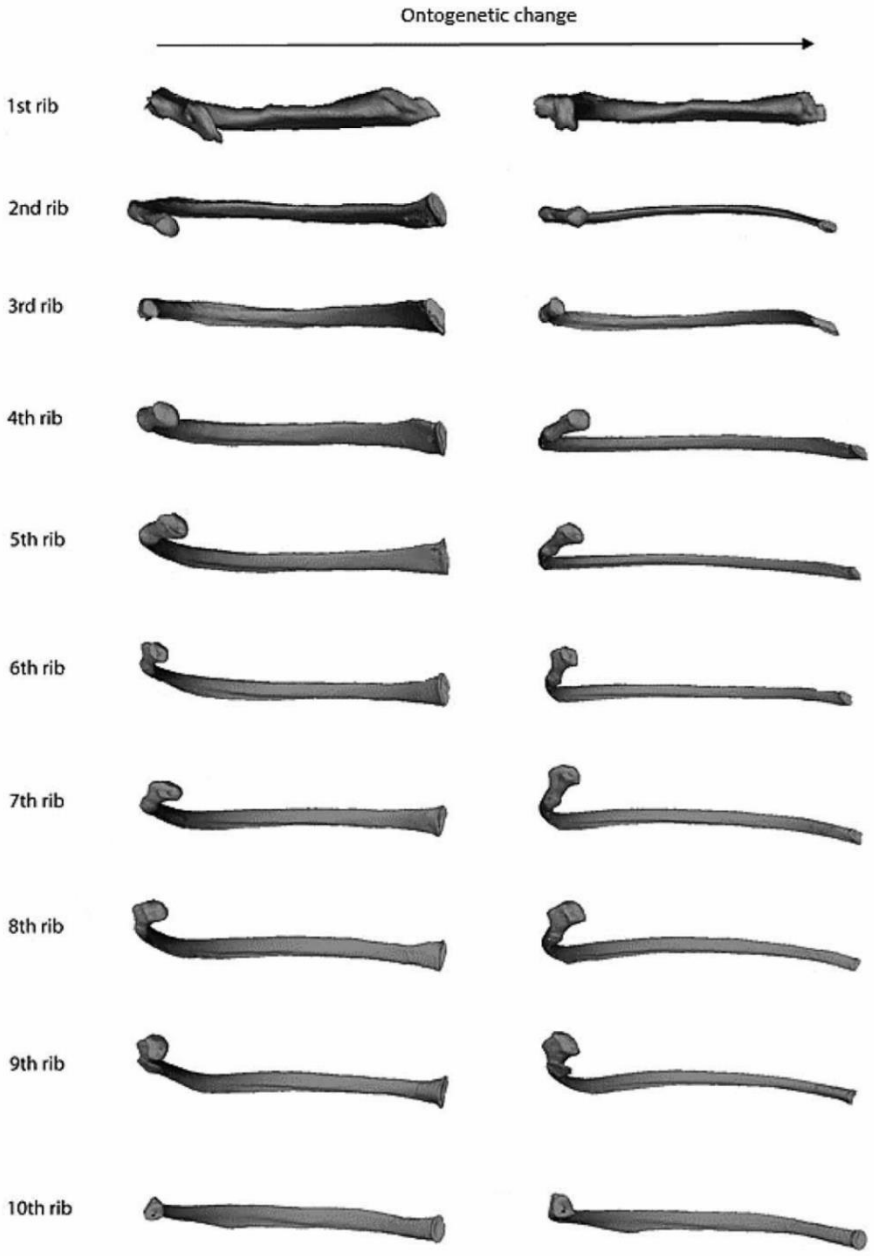

Fig. 2. 3D warps showing morphological changes undergone along the ontogeny at every rib level observed in interior lateral view. The ribs are displayed in anatomical sequence 1–10 from the top to the bottom of the figure. The arrow shows the direction of the ontogenetic change.

of rib torsion. This is an intrinsic rib factor that cannot be easily determined by looking at the thorax in anatomical connection, and thus requires exclusive analysis of individual ribs. Our results do not exclude some degree of rib declination (an extrinsic rib factor) as a factor that contributes to rib lowering.

Biomechanical action of intercostal muscles elevates ribs from a declined state that cause thoracic inspiration (De Troyer et al., 2005). When ribs are more horizontal (in newborns, for instance) the respiratory muscles cannot raise the ribs effectively. This breathing mode becomes insufficient for respiration and must be compensated by diaphragmatic breathing. However, the increase in rib torsion observed during ontogeny makes thoracic breathing more efficient, because when ribs are more declined, the intercostal muscles can raise them more effectively (De Troyer et al., 2005; Bastir et al., 2013a, b). This is important for understanding functional changes of the rib cage during ontogeny, but is also important for understanding human evolution, since some studies have observed that changes in rib torsion could affect the functional anatomy of respiratory system

TABLE 2. Percentage of variance explained for each regression analyses of the Procrustes coordinates on size of each subset of ribs employed in the study as well as their statistic P-value

	% of variance	*P*-value
1st rib regression	10.86	0.01
2nd rib regression	22.55	<0.01
3rd rib regression	21.18	<0.01
4th rib regression	19.09	<0.01
5th rib regression	19.91	<0.01
6th rib regression	20.08	<0.01
7th rib regression	17.75	<0.01
8th rib regression	8.54	0.02
9th rib regression	8.03	0.04
10th rib regression	7.13	0.04

TABLE 3. Slope (a) of the multivariate regression analysis of each subset of ribs, as well as their 95% confidence intervals in parentheses.

	Slope (CI)
1st rib slope (a)	8.52 (6.80–10.11)
2nd rib slope (a)	7.97 (6.00–9.62)
3rd rib slope (a)	7.93 (5.72–9.54)
4th rib slope (a)	7.68 (5.55–9.46)
5th rib slope (a)	8.49 (6.41–10.30)
6th rib slope (a)	8.20 (6.19–10.00)
7th rib slope (a)	8.19 (5.90–9.98)
8th rib slope (a)	12.36 (8.56–15.23)
9th rib slope (a)	14.66 (10.26–18.21)
10th rib slope (a)	14.97 (9.16–19.03)

in other hominin species such as *Australopithecus* or Neanderthals (Schmid, 1991; Bastir et al., 2015).

It should be noted that since there is some percentage of variance not covered (see Table 2) by our regressions, our landmark protocol does not collect all morphological variance. Future research is needed to address this question and cover a larger amount of the variance.

Implications of the ontogenetic variability of ribs for understanding thoracic units

Our results show that different changes in axial rib curvature (but not in rib torsion) are observed in the growth of upper and lower thorax units. After growth, the upper ribs present the point of maximum curvature at the mid-shaft while in the lower ribs this point is observed more dorsally, closer to the *angulus costae*. This different growth seen in lower ribs could be related to the invagination of the spine (thoraco-lumbar lordosis) that has been observed in the ontogenetic process by different authors (Gayzik et al., 2008; Bastir et al., 2013b; Shi et al., 2014; Weaver et al., 2014). This phenomenon, together with the previously observed increase in rib torsion, would cause lower rib cages in adults to be narrower than those of nonadults. For that reason, our results support hypothesis 3 (we should not expect the same growth pattern in ribs belonging to the upper and lower thorax) since we observe that the modular pattern of the thorax is also observable at costal level.

However, this hypothesis can only be partially accepted. Our results allow us to be more specific in establishing this separation than previously (Bastir et al., 2013a,b) since the upper unit is comprised of true ribs (ribs 1–7) while the lower thorax is comprised (at least) of ribs 8–10. This modular pattern is observable at the confidence intervals of the regression slopes (Table 3) because the lower rib slopes (ribs 8–10) are outside the interval of that of the upper ribs. However, it is important to note that this is not as clear when observing predicted adult individuals through the use of growth trajectories. This is because upper ribs predicted by lower rib growth vectors fall outside the modern human adult range, while the lower ones predicted with the upper rib vectors fall inside the confidence range of true adult individuals (Fig. 2a–j from Supporting Information). The confidence ellipses for adult lower ribs are wider than those of upper ribs because adult ribs are more spread out along the ordinate axis (shape). This observation suggests that adult lower rib morphology is more variable than morphology of adult upper ribs, a fact also observable because lower rib regressions are less explanatory than regressions of upper ribs.

It is interesting to note that the morphological architecture of the first rib is very different from that of the rest of the ribs, and that its muscle attachments are very specific (Spaltzeholtz, 1970). Anatomical and functional integration could support specific integration of the first ribs with the neck or shoulder girdle not observed in other ribs (Schmid et al., 2013; Roach and Richmond, 2015). However, our results (see Table 3) show that the first rib regression slope (shape on size) falls between the confidence interval of ribs 1–7 but is outside of the interval of the rest of the ribs. Finally, regarding floating ribs, here we hypothesize that the eleventh and twelfth ribs share a common growth pattern with ribs 8–10. However, this issue should be addressed in future studies because in the present study we have not quantified them because of the lack of homology in the landmarks of the rib head.

The modular model proposed in this work (upper unit – ribs 1–7; lower unit – at least ribs 8–10) is coherent with thorax anatomy. This is because development of ribs belonging to the upper unit (so-called true ribs), are the only ones which have the anatomical constraint of a direct link to the sternum, while ribs belonging to the lower unit (at least false and probably floating ribs, as well) do not present this constraint (Spaltzeholtz, 1970). Functional anatomy also supports this separation since the development of the upper unit could be influenced by pulmonary kinematics while lower unit growth could be influenced by diaphragmatic kinematics (De Troyer et al., 2005; Bastir et al., 2013b; García-Martínez et al., 2014a,b).

Finally, anatomical integration (Bastir, 2008) could also account for this separation. This is because upper thorax development may be influenced by the shoulder girdle (Schmid et al., 2013; Roach and Richmond, 2015) and lower thorax development may be influenced by spine lordosis related to posture (Slijper, 1942; Bastir et al., 2013b, 2014a), thoraco-pelvic integration (Jellema et al., 1993; Bastir et al., 2014b) or even by sub-thoracic systems such as guts (Aiello, 1997). This is also reinforced by the mosaic features found in the thorax of fossil species like *Australopithecus sediba* (Schmid et al., 2013), since the upper thorax shows archaic features (probably related to an adaptation to arboreal locomotion of the scapular girdle, or a retention of primitive characters) whereas the lower thorax presents a more modern-like morphology, probably also linked to a more modern-like pelvis.

LIMITATIONS OF THE STUDY

Although this article greatly expands our knowledge of individual rib ontogeny, more research is needed in order to clarify some questions, for example, the growth trajectories of floating ribs. Methodological improvements in the landmark quantification protocol or a larger sample of ontogenetic data could also help us confirm the results presented here.

CONCLUSIONS OF THE STUDY

This study has shown for the first time that intrinsic rib factors, such as rib torsion and axial rib curvature, are important factors during postnatal ontogeny, which contribute to establishing the 3D configuration of the adult thorax. However, our results do not exclude the possibility that ontogeny of extrinsic rib factors, such as rib declination or the orientation of transverse processes, are also involved in configuring the morphology of the adult thorax. These problems should be addressed in future research.

Our results make evident the difference between rib torsion and rib declination, and, because extrinsic rib factors such as rib declination are not observable at costal level, suggest that rib torsion should be focused on in studies on individual ribs. In addition, this study has allowed us to be more specific in the assessment of thoracic units. Growth simulations and individual rib ontogenetic trajectories suggest an upper thoracic unit comprised of ribs 1–7 and a lower unit comprised of ribs 8–10 (at least), a result that is consistent with aspects of functional and anatomical integration.

Our findings are relevant to understanding how intrinsic rib factors cause changes in individual ribs that contribute to configuring the 3D morphology of the adult thorax. This information could also be important for understanding the development and evolution of the modern human rib cage and the thoracic morphology of other hominin species.

ACKNOWLEDGMENTS

The authors acknowledge Michael Coquerelle for data contribution (Bordeaux Hospital) and the Paleoanthropology group from the Museo Nacional de Ciencias Naturales (MNCN-CSIC, Madrid) for support and discussions related to this article. They acknowledge reviewers for detailed suggestions which helped to improve the manuscript, specifically reviewer 1 for an intensive revision about grammar and uses of English. They also thank copy editor Zach Tobias (zstobias@gmail.com) for proofread and correct the manuscript for proper English grammar.

AUTHOR CONTRIBUTION

Conceived and designed the experiments: DGM, MB. Performed the experiments: DGM MB. Analyzed the data: DGM MB. Contributed reagents/materials/analysis tools: DGM MB WR. Wrote the manuscript: DGM MB.

LITERATURE CITED

Aiello LC. 1997. Brains and guts in human evolution: the expensive tissue hypothesis. Braz J Genet 20:141–148.

Bastir M. 2008. A systems-model for the morphological analysis of integration and modularity in human craniofacial evolution. J Anthropol Sci 86:37–58.

Bastir M, García-Martínez D, Barash A, Been E, Torres I, García-Río F. 2014. Thorax kinematics and the reconstruction of body models in hominin evolution. In: Proceedings of ESHE, editor. Florence. p 35.

Bastir M, García-Martínez D, Estalrrich A, García-Tabernero A, Huguet R, Ríos L, Barash A, Recheis W, de la Rasilla M, Rosas A. 2015. The relevance of the first ribs of the El Sidrón site (Asturias, Spain) for the understanding of the Neanderthal thorax. J Hum Evol 80:64–73.

Bastir M, García-Martínez D, Recheis W, Barash A, Coquerelle M, Rios L, Peña A, O'Higgins P. 2013a. 3D analysis of human ribcage ontogeny. American Journal of Physical Anthropology. S56:75-

Bastir M, García-Martínez D, Recheis W, Barash A, Coquerelle M, Rios L, Peña-Melián A, García-Río F, O'Higgins P. 2013b. Differential Growth and Development of the Upper and Lower Human Thorax. PloS One 8:e75128-

Bastir M, Higuero A, Ríos L, García-Martínez D. 2014a. Three-dimensional analysis of sexual dimorphism in human thoracic vertebrae: implications for the respiratory system and spine morphology. Am J Phys Anthropol 155:513–521.

Bastir M, Rosas A. 2004. Facial heights: evolutionary relevance of postnatal ontogeny for facial orientation and skull morphology in humans and chimpanzees. J Hum Evol 47:359–381.

Bastir M, Rosas A, O'Higgins P. 2006. Craniofacial levels and the morphological maturation of the human skull. J Anat 209:637–654.

Bellemare F, Fuamba T, Bourgeault A. 2006. Sexual dimorphism of human ribs. Respir Physiol Neurobiol 150:233–239.

Bellemare F, Jeanneret A, Couture J. 2003. Sex differences in thoracic dimensions and configuration. Am J Respir Crit Care Med 168:305–312.

Cobb S, O'Higgins P. 2004. Hominins do not share a common postnatal facial ontogenetic shape trajectory. J Exp Zool B Mol Dev Evol 302B:302–321.

De Troyer A, Kirkwood PA, Wilson TA. 2005. Respiratory action of the intercostal muscles. Physiol Rev 85:717–756.

Dryden IL, Mardia KV. 1998. Statistical shape analysis, Vol. 4. New York: Wiley.

Dudar JC. 1993. Identification of rib number and assessment of intercostal variation at the sternal rib end. J Forensic Sci 38: 788–797.

Esteve-Altava B, Marugán -Lobón J, Botella H, Bastir M Rasskin -Gutman D. 2013. Grist for Riedl's mill: a network model perspective on the integration and modularity of the human skull. J Exp Zool B Mol Dev Evol 320: 489–500.

Franciscus RG, Churchill SE. 2002. The costal skeleton of Shanidar 3 and a reappraisal of Neandertal thoracic morphology. J Hum Evol 42:303–356.

García-Martínez D. 2013. 3D geometric morphometrics of the rib cage of the Homo ergaster KNM-WT 15000 and their possible evolutionary implications: an application of sliding semilandmarks on virtual anthropology to the morphology of the ribs, Universidad Autónoma de Madrid-Museo Nacional de Ciencias Naturales CSIC.

García-Martinez D, Bastir M, Recheis W, Barash A. 2013. Dos barriles diferentes para dos primates diferentes: Morfometría geométrica 3D de Sliding semilandmarks del tórax de la superfamilia Hominoidea. En libro de resúmenes del XVIII Congreso de la Sociedad Española de Antropología Física. p 39.

García-Martínez D, Barash A, Recheis W, Utrilla C, Torres SI, García-Río F, Bastir M. 2014a. On the chest size of Kebara 2. J Hum Evol 70:69–72.

García-Martínez D, Bastir M. 2015. The modular nature of the Neanderthal Thorax: status quo. Proceedings of Bioanthropological Meeting. Coimbra. p 22.

García-Martínez D, Bastir M, Estalrrich A, García-Tabernero A, Huguet R, Cunha E, de la Rasilla M, Rosas A. 2014b. Preliminary study of the head-neck complex of Neanderthal ribs from the El Sidrón site (Asturias, Spain). Proceeding of ESHE. Florence. p 76.

Gayzik FS, Yu MM, Danelson KA, Slice DE, Stitzel JD. 2008. Quantification of age-related shape change of the human rib

cage through geometric morphometrics. J Biomech 41:1545–1554.
Gómez-Olivencia A, Eaves-Johnson KL, Franciscus RG, Carretero JM, Arsuaga JL. 2009. Kebara 2: new insights regarding the most complete Neandertal thorax. J Hum Evol 57:75–90.
Goodyear MD, Krleza-Jeric K, Lemmens T. 2007. The declaration of Helsinki. BMJ 335:624.
Gray H. 1918. Anatomy of the human body. Philadelphia: Lea & Febiger.
Gunz P, Mitteroecker P, Bookstein FL. 2004. Semilandmarks in three dimensions. In: Slice DE, editor. Modern morphometrics in physical anthropology. New York: Kluwer Press. p 73–98.
Hammer Ø, Harper DAT, Ryan PD. 2001. Past: Paleontological Statistics Software Package for education and data analysis. Paleontol Electrón 4:1–9.
Jellema LM, Latimer B, Walker A. 1993. The rib cage. The Nariokotome Homo erectus skeleton. Cambridge, MA: Harvard University Press. p 294–325.
Klingenberg CP. 2011. MorphoJ: an integrated software package for geometric morphometrics. Mol Ecol Resour 11:353–357.
Latimer B, Ward CV. 1993. The thoracic and lumbar vertebrae. The Nariokotome Homo erectus skeleton. Cambridge, MA: Harvard University Press. 266–293.
Mann RW. 1993. A method for siding and sequencing human ribs. J Forensic Sci 38:151–155.
McNulty KP, Frost SR, Strait DS. 2006. Examining affinities of the Taung child by developmental simulation. J Hum Evol 51:274–296.
Mitteroecker P, Gunz P, Bernhard M, Schaefer K, Bookstein FL. 2004. Comparison of cranial ontogenetic trajectories among great apes and humans. J Hum Evol 46:679–698.
Mitteroecker P, Gunz P, Bookstein F. 2005. Heterochrony and geometric morphometrics: a comparison of cranial growth in *Pan paniscus* versus *Pan troglodytes*. Evol Dev 7:244–258.
Neubauer S, Gunz P, Hublin JJ. 2010. Endocranial shape changes during growth in chimpanzees and humans: A morphometric analysis of unique and shared aspects. J Hum Evol 59:555–566.
Openshaw P, Edwards S, Helms P. 1984. Changes in rib cage geometry during childhood. Thorax 39:624–627.
Ratnovsky A, Elad D, Halpern P. 2008. Mechanics of respiratory muscles. Respiratory physiology & neurobiology 163:82–89.
Rosas A, Bastir M. 2004. Geometric morphometric analysis of allometric variation in the mandibular morphology of the hominids of Atapuerca, Sima de los Huesos site. The Anatomical Record Part A: Discoveries in Molecular, Cellular, and Evolutionary Biology 278:551–560.
Roach NT, Richmond BG. 2015. Clavicle length, throwing performance and the reconstruction of the *Homo erectus* shoulder. J Hum Evol 80:107–113.
Schmid P. 1991. The trunk of the australopithecines. Origine (s) de la Bipédie chez les Hominidés. Presses du CNRS, Paris, 225–234.
Schmid P, Churchill SE, Nalla S, Weissen E, Carlson KJ, de Ruiter DJ, Berger LR. 2013. Mosaic Morphology in the thorax of *Australopithecus sediba*. Science 340:1234598-
Shi X, Cao L, Reed MP, Rupp JD, Hoff CN, Hu J. 2014. A statistical human rib cage geometry model accounting for variations by age, sex, stature and body mass index. J Biomech 47: 2277–2285.
Slijper EJ. 1942. Biologic-anatomical investigations on the bipedal gait and upright posture in mammals, with special reference to a little goat, born without forelegs. Proc K Ned Akad Wet 45:288–295.
Spalteholtz W. 1970. Atlas de Anatomía Humana, 5th ed. Barcelona: Labor, S.A.
Spoor CF, Zonneveld FW, Macho GA. 1993. Linear measurements of cortical bone and dental enamel by computed tomography: applications and problems. Am J Phys Anthropol 91: 469–484.
Weaver AA, Schoell SL, Stitzel JD. 2014. Morphometric analysis of variation in the ribs with age and sex. J Anat 225:246–261.
Weinstein KJ. 2007. Thoracic skeletal morphology and high-altitude hypoxia in Andean prehistory. Am J Phys Anthropol 134:36–49.
Weinstein KJ. 2008. Thoracic morphology in Near Eastern Neandertals and early modern humans compared with recent modern humans from high and low altitudes. J Hum Evol 54: 287–295.

Supplementary Information

Table 1. Id name, chronological age, sex and age group (following Bastir et al., 2013) of each individual studied.

Id	Age (years)	sex	Age group
TX001	1	female	1
TX013	0.08	male	1
TX014	0.25	female	1
TX015	0.4	male	1
TX022	0.11	male	1
TX029	0.06	male	1
TX030	0.6	male	1
TX031	1.8	male	1
TX032	4	male	2
TX041	15.6	female	2
TX045	5	male	2
TX046	10.5	female	2
TX002	3	female	2
TX003	6	female	2
TX004	11	female	2
TX005	14	female	2
TX025	6	male	2
TX026	7	male	2
TX027	8	male	2
TX028	10	male	2
TX006	40	male	3
TX007	60	male	3
TX008	50	male	3
TX010	62	female	3
TX011	27	female	3
TX012	59	male	3
TX023	29	female	3
TX024	18	male	3

Figure 1: Principal component analyses (PCA) of each rib subset in form space showing the morphological variance along the ontogeny at each rib level.

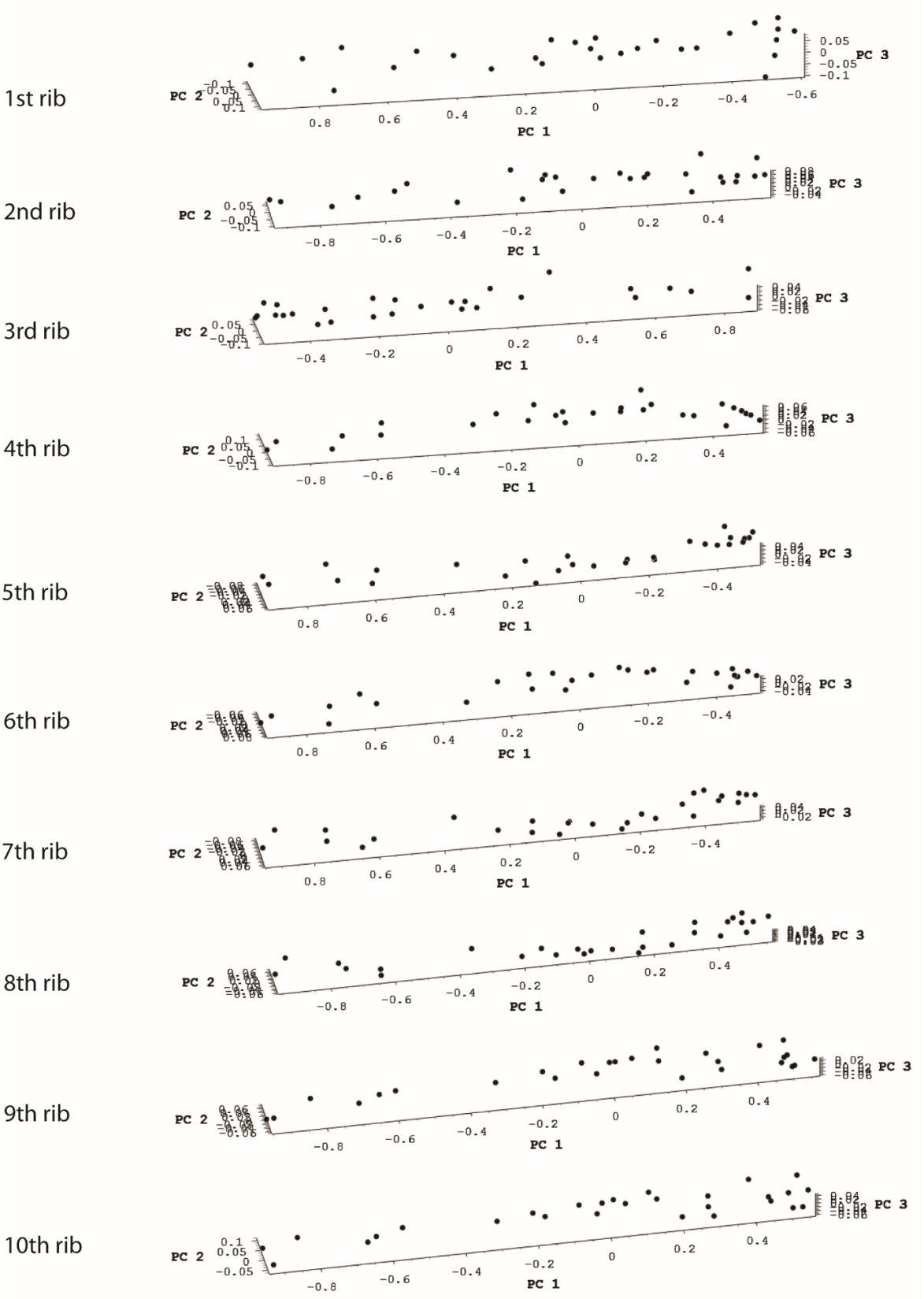

Figure 2a: regression analysis of Procrustes coordinates on size of the 1st ribs subset collecting the morphological change of the costal outer curvature along the ontogeny. The non-adult individuals are shown as blue dots, the true adult individuals as green dots and the simulated adults as red dots. A 95% confidence ellipse is traced around the true individuals. The labels of the simulated individual mean the ontogenetic vector that we employed to simulate this individual, so "simulation v1st" means that this simulated individual has been growth throughout a first rib ontogenetic vector, and so on.

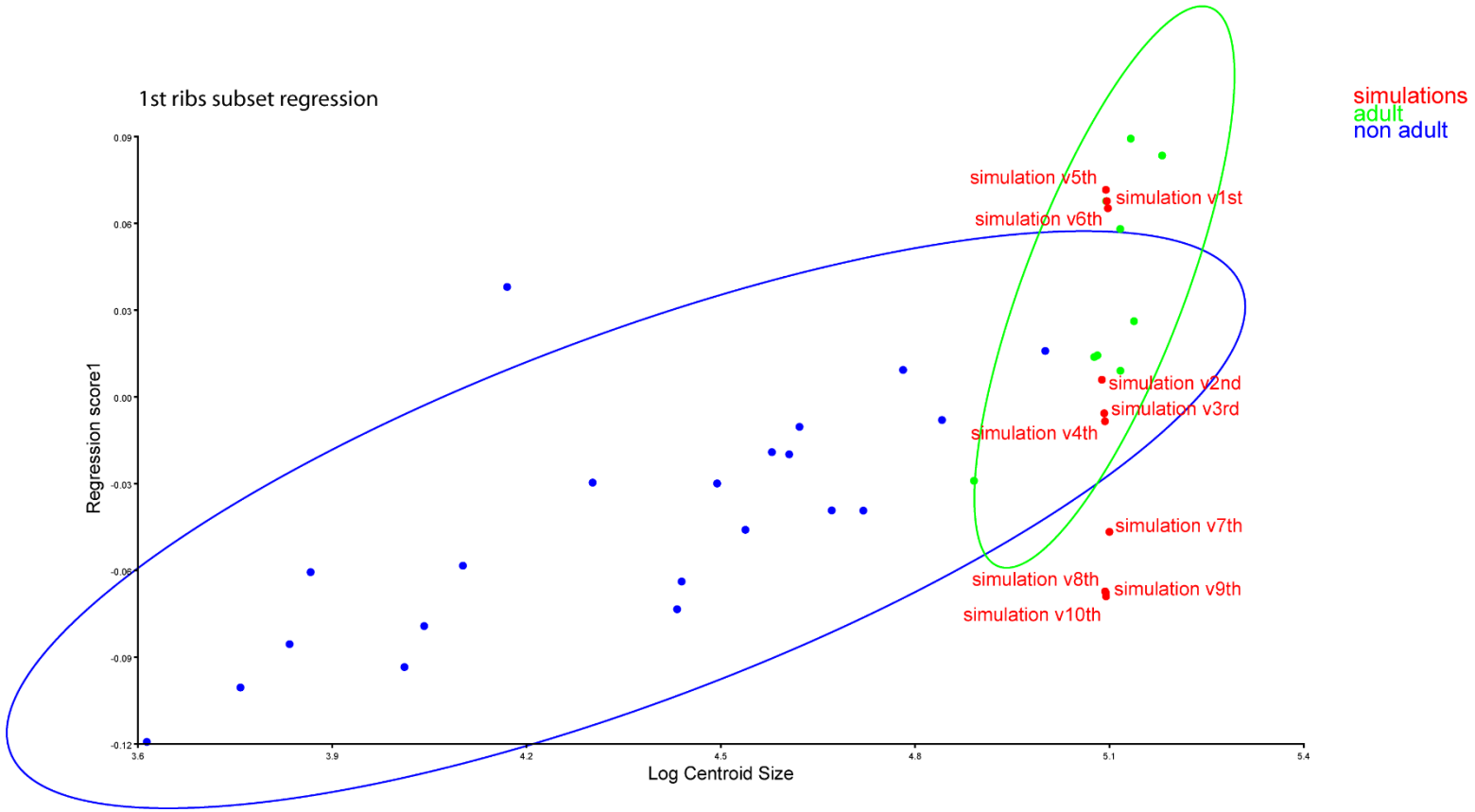

Figure 2b: regression analysis of Procrustes coordinates on size of the 2nd ribs subset collecting the morphological change of the costal outer curvature along the ontogeny. The non-adult individuals are shown as blue dots, the true adult individuals as green dots and the simulated adults as red dots. A 95% confidence ellipse is traced around the true individuals. The labels of the simulated individual mean the ontogenetic vector that we employed to simulate this individual, so "simulation v1st" means that this simulated individual has been growth throughout a first rib ontogenetic vector, and so on.

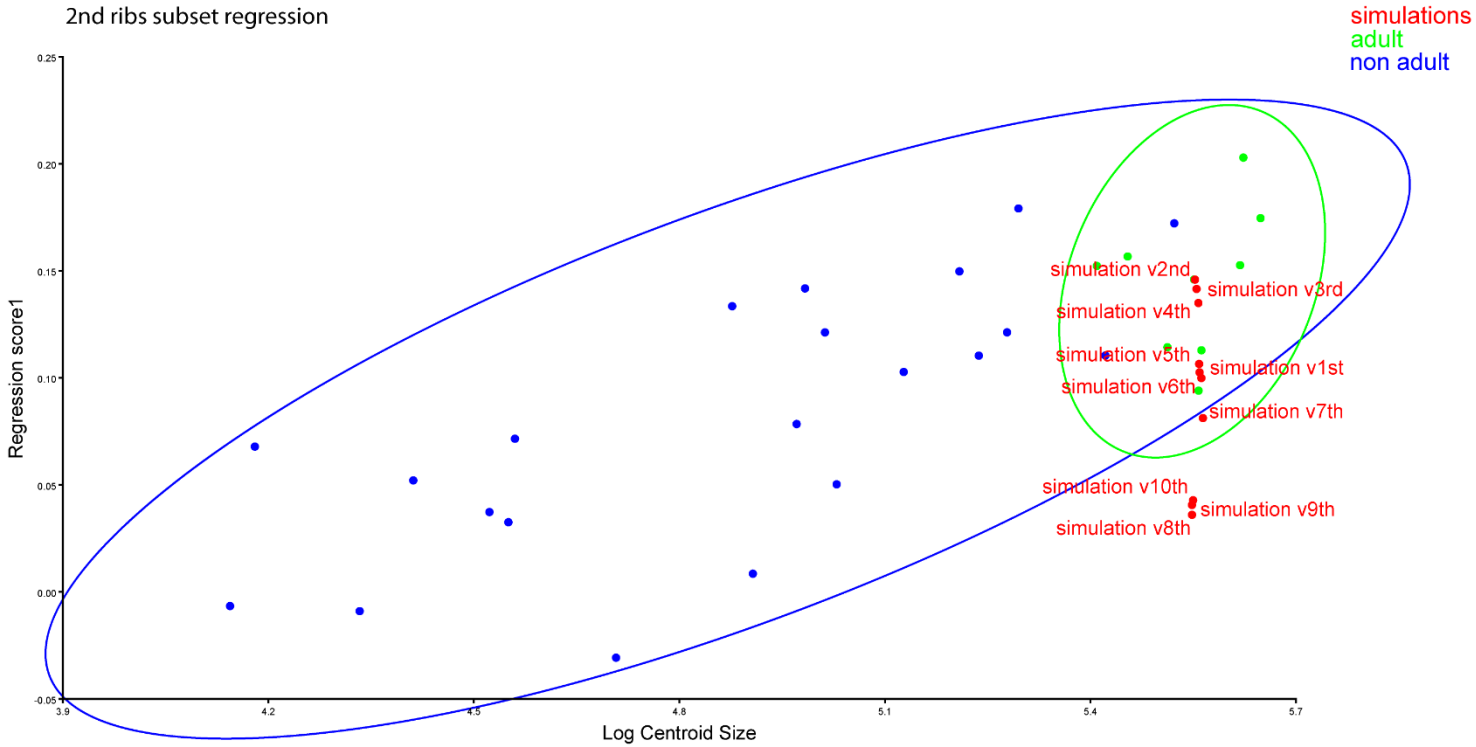

Figure 2c: regression analysis of Procrustes coordinates on size of the 3rd ribs subset collecting the morphological change of the costal outer curvature along the ontogeny. The non-adult individuals are shown as blue dots, the true adult individuals as green dots and the simulated adults as red dots. A 95% confidence ellipse is traced around the true individuals. The labels of the simulated individual mean the ontogenetic vector that we employed to simulate this individual, so "simulation v1st" means that this simulated individual has been growth throughout a first rib ontogenetic vector, and so on.

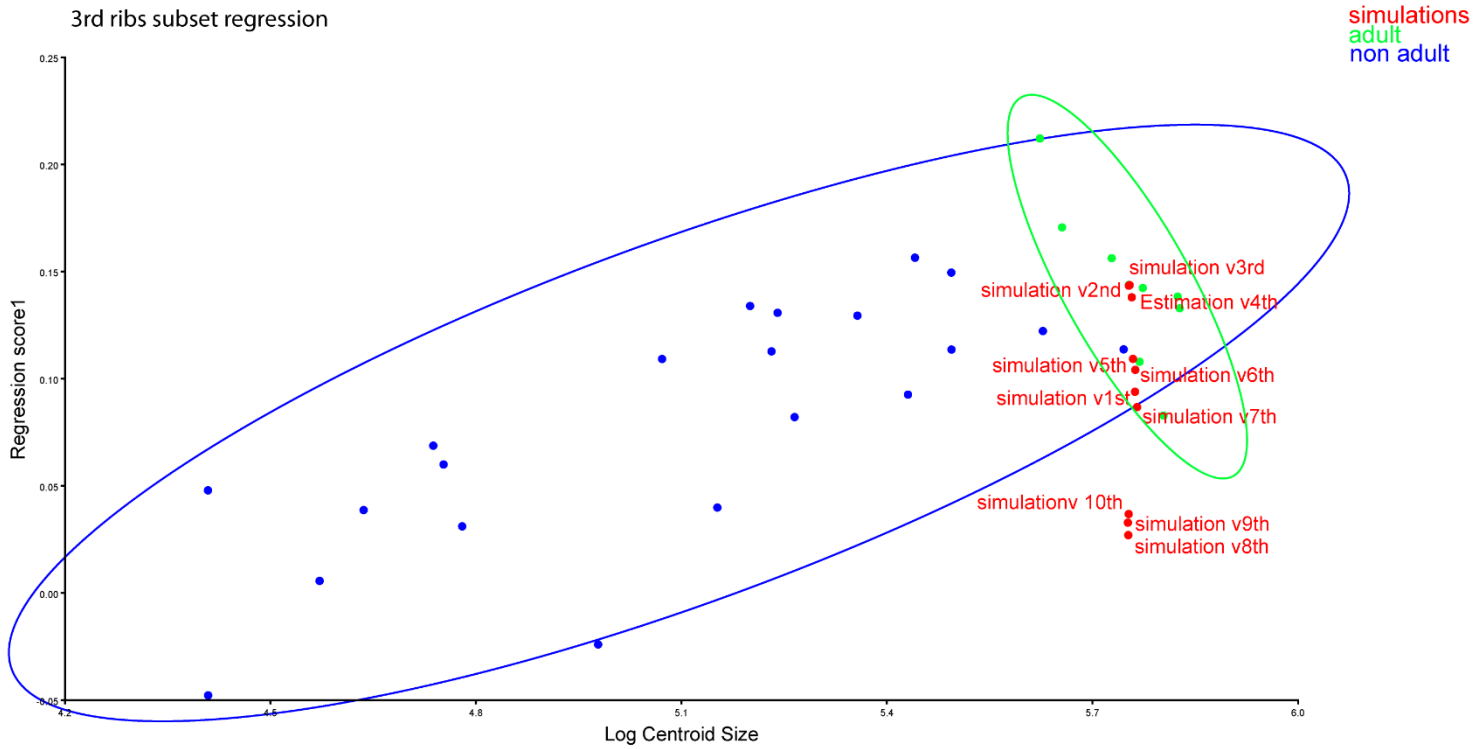

Figure 2d: regression analysis of Procrustes coordinates on size of the 4th ribs subset collecting the morphological change of the costal outer curvature along the ontogeny. The non-adult individuals are shown as blue dots, the true adult individuals as green dots and the simulated adults as red dots. A 95% confidence ellipse is traced around the true individuals. The labels of the simulated individual mean the ontogenetic vector that we employed to simulate this individual, so "simulation v1st" means that this simulated individual has been growth throughout a first rib ontogenetic vector, and so on.

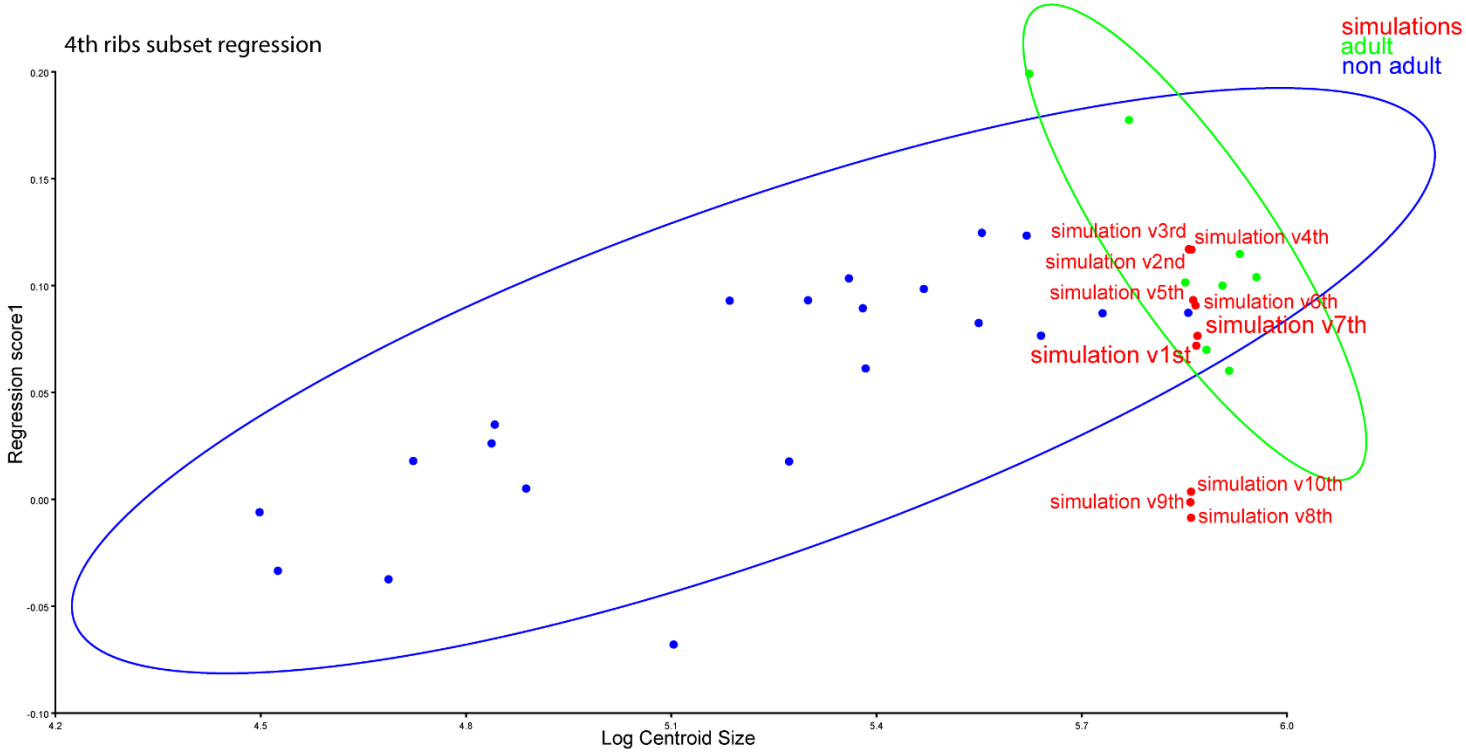

Figure 2e: regression analysis of Procrustes coordinates on size of the 5th ribs subset collecting the morphological change of the costal outer curvature along the ontogeny. The non-adult individuals are shown as blue dots, the true adult individuals as green dots and the simulated adults as red dots. A 95% confidence ellipse is traced around the true individuals. The labels of the simulated individual mean the ontogenetic vector that we employed to simulate this individual, so "simulation v1st" means that this simulated individual has been growth throughout a first rib ontogenetic vector, and so on.

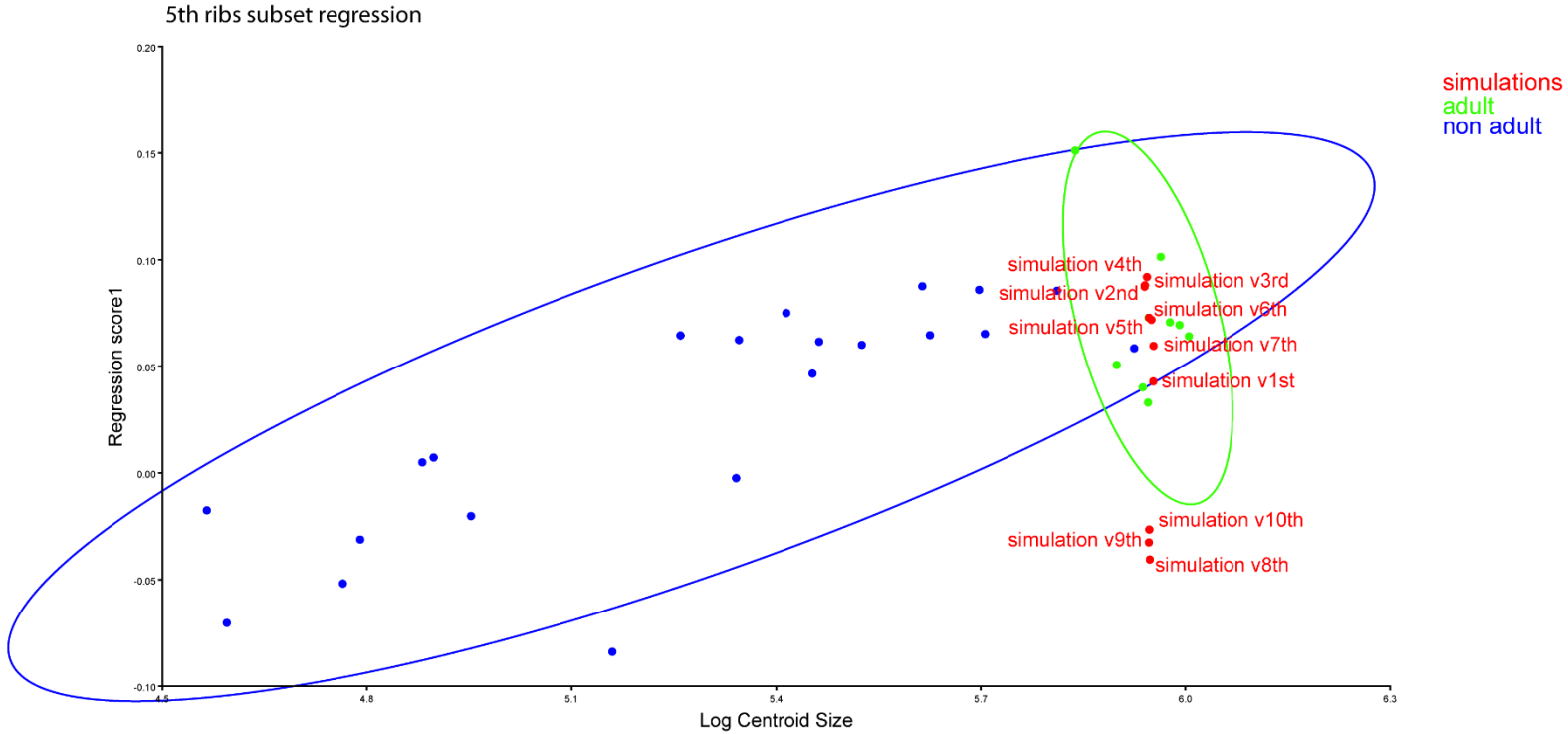

Figure 2f: regression analysis of Procrustes coordinates on size of the 6th ribs subset collecting the morphological change of the costal outer curvature along the ontogeny. The non-adult individuals are shown as blue dots, the true adult individuals as green dots and the simulated adults as red dots. A 95% confidence ellipse is traced around the true individuals. The labels of the simulated individual mean the ontogenetic vector that we employed to simulate this individual, so "simulation v1st" means that this simulated individual has been growth throughout a first rib ontogenetic vector, and so on.

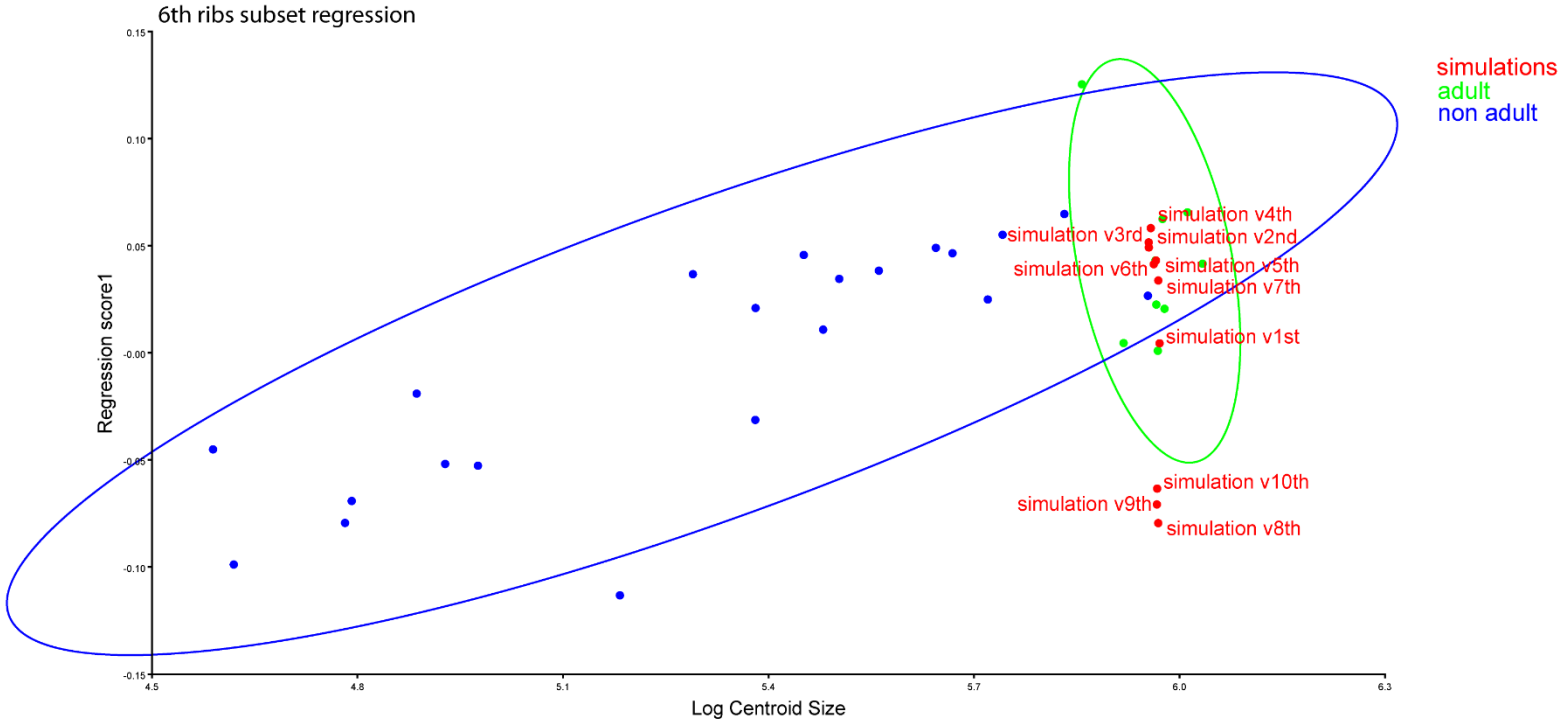

Figure 2g: regression analysis of Procrustes coordinates on size of the 7th ribs subset collecting the morphological change of the costal outer curvature along the ontogeny. The non-adult individuals are shown as blue dots, the true adult individuals as green dots and the simulated adults as red dots. A 95% confidence ellipse is traced around the true individuals. The labels of the simulated individual mean the ontogenetic vector that we employed to simulate this individual, so "simulation v1st" means that this simulated individual has been growth throughout a first rib ontogenetic vector, and so on.

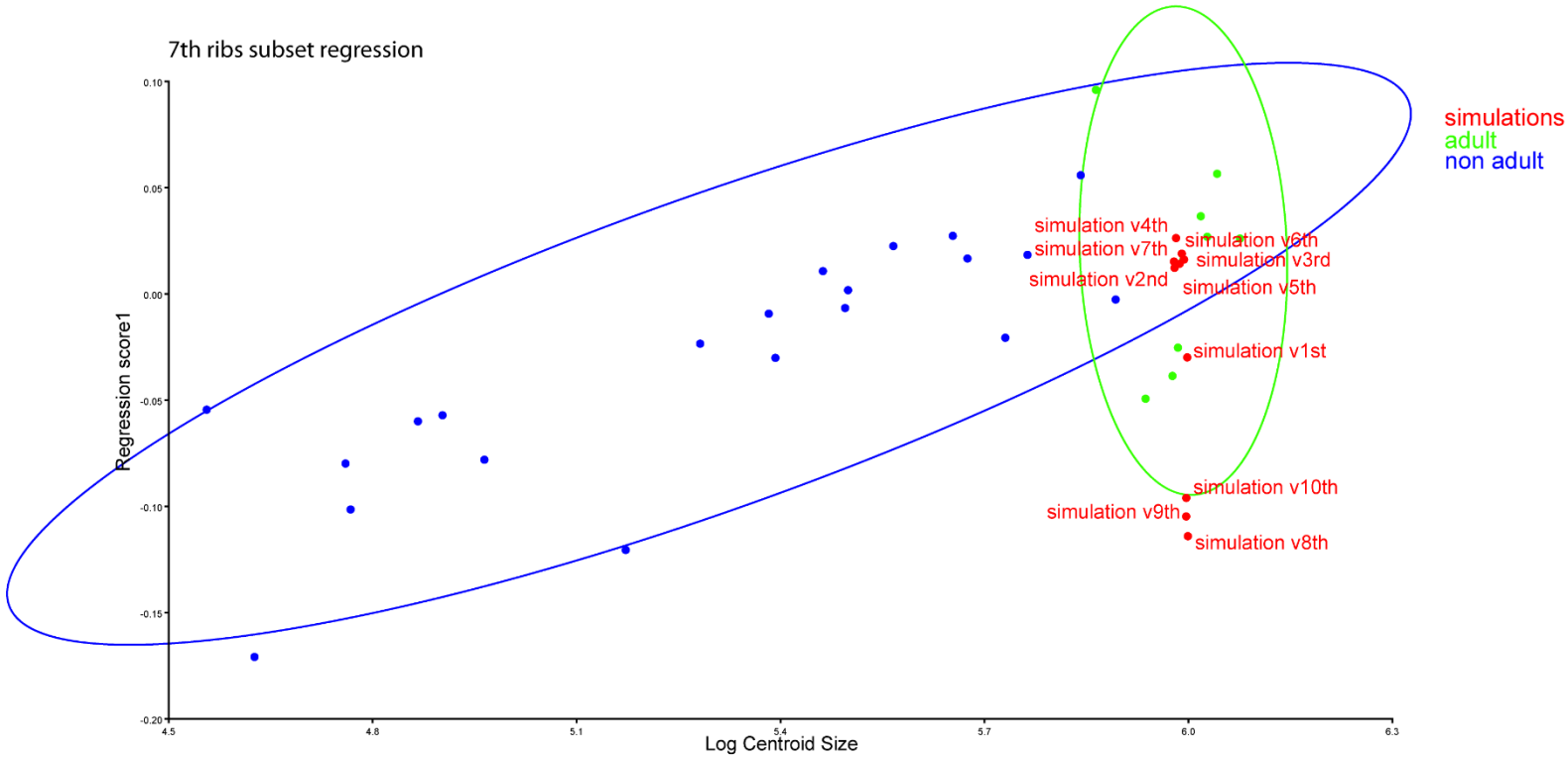

Figure 2h: regression analysis of Procrustes coordinates on size of the 8th ribs subset collecting the morphological change of the costal outer curvature along the ontogeny. The non-adult individuals are shown as blue dots, the true adult individuals as green dots and the simulated adults as red dots. A 95% confidence ellipse is traced around the true individuals. The labels of the simulated individual mean the ontogenetic vector that we employed to simulate this individual, so "simulation v1st" means that this simulated individual has been growth throughout a first rib ontogenetic vector, and so on.

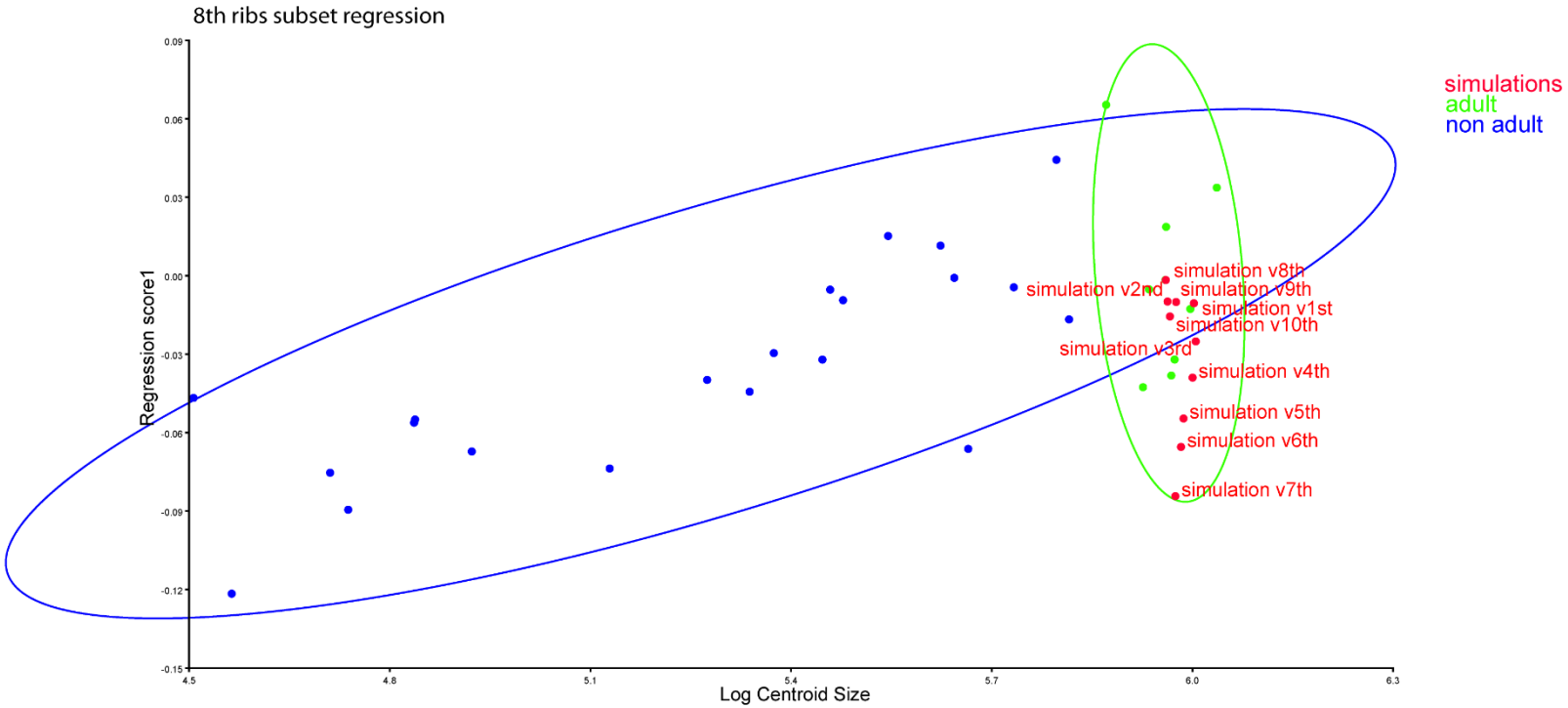

Figure 2i: regression analysis of Procrustes coordinates on size of the 9th ribs subset collecting the morphological change of the costal outer curvature along the ontogeny. The non-adult individuals are shown as blue dots, the true adult individuals as green dots and the simulated adults as red dots. A 95% confidence ellipse is traced around the true individuals. The labels of the simulated individual mean the ontogenetic vector that we employed to simulate this individual, so "simulation v1st" means that this simulated individual has been growth throughout a first rib ontogenetic vector, and so on.

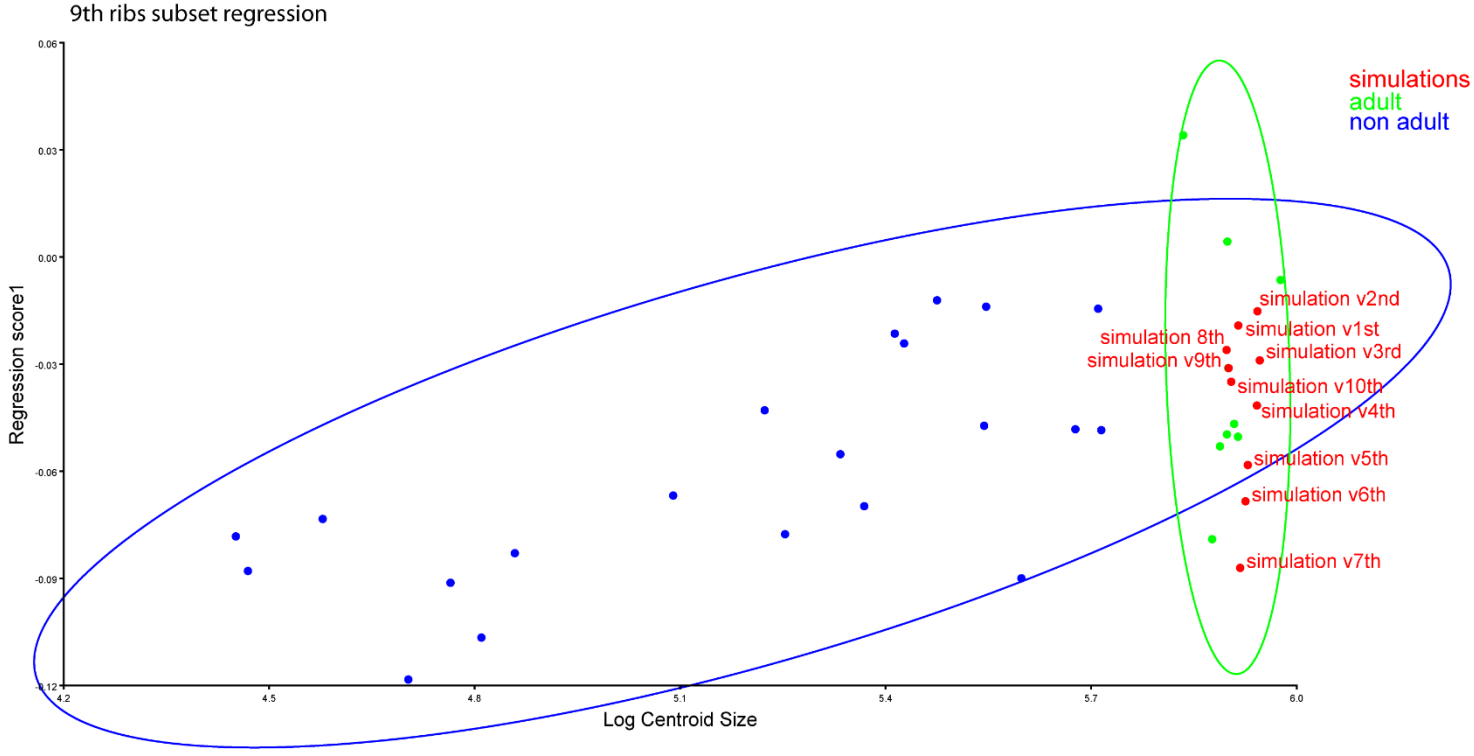

Figure 2j: regression analysis of Procrustes coordinates on size of the 10th ribs subset collecting the morphological change of the costal outer curvature along the ontogeny. The non-adult individuals are shown as blue dots, the true adult individuals as green dots and the simulated adults as red dots. A 95% confidence ellipse is traced around the true individuals. The labels of the simulated individual mean the ontogenetic vector that we employed to simulate this individual, so "simulation v1st" means that this simulated individual has been growth throughout a first rib ontogenetic vector, and so on.

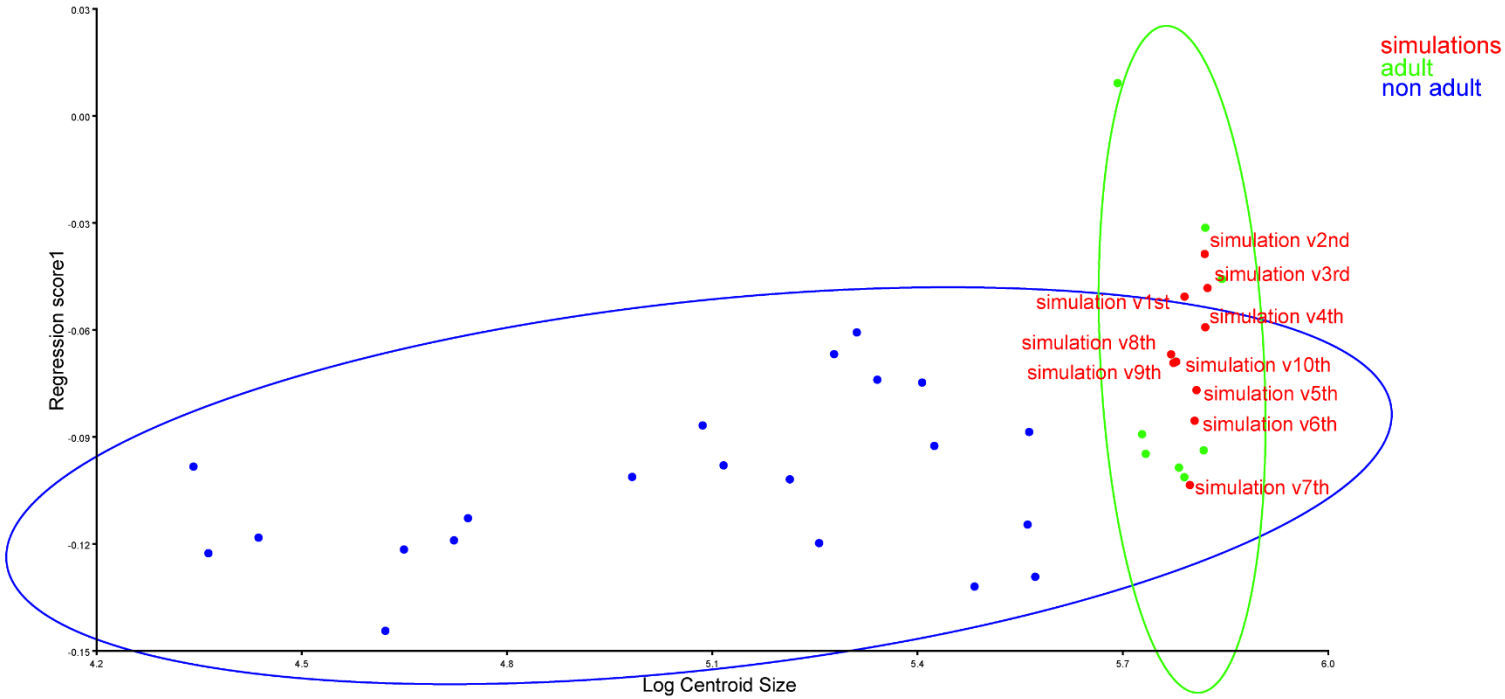

CAPÍTULO V – RESULTADOS: DIMORFISMO SEXUAL EN LA CAJA TORÁCICA HUMANA

Los resultados obtenidos en referencia al **objetivo 2 "Contribuciones al conocimiento del dimorfismo sexual en la caja torácica humana"** han sido íntegramente publicados en los siguientes artículos:

Bastir, M., Higuero, A., Ríos, L., **García-Martínez, D.**, 2014. Three-dimensional analysis of sexual dimorphism in human thoracic vertebrae: Implications for the respiratory system and spine morphology. American Journal of Physical Anthropology 155(4), 513-521.

DOI: 10.1002/ajpa.22604

García-Martínez, D., Torres-Tamayo, N., Torres-Sánchez, I., García-Río, F., Bastir, M., 2016. Morphological and functional implications of sexual dimorphism in the human skeletal thorax. American Journal of Physical Anthropology 161, 467-477.

DOI: 10.1002/ajpa.23051

Three-Dimensional Analysis of Sexual Dimorphism in Human Thoracic Vertebrae: Implications for the Respiratory System and Spine Morphology

Markus Bastir,[1]* Antonio Higuero,[2] Luís Ríos,[1,3] and Daniel García Martínez[1]

[1]*Paleoanthropology Group, Museo Nacional de Ciencias Naturales, CSIC. J. G. Abascal 2, 28006, Madrid, Spain*
[2]*MSc-Program of Human Osteology and Palaeopathology, University of Bradford, Bradford, United Kingdom*
[3]*Department of Physical Anthropology, Aranzadi Zientzia Elkartea, Zorroagagaina 11, 20014, Donostia, Basque Country, Spain*

KEY WORDS vertebral column; thorax; respiratory system; geometric morphometrics

ABSTRACT Sexual dimorphism is important for intraspecific variation and well studied in the human skeleton. In the thoracic part of the spine sexual dimorphism is expected for differences in the respiratory system related to body mass, lung capacity, and energetics, and in the reproductive system for adaptations to pregnancy (lower spine lordosis, posture). However, little is known about sexual dimorphism in this anatomical region. We use three-dimensional (3D)-geometric morphometrics to test hypotheses on sexual dimorphism in the first 10 thoracic vertebrae (T1–T10). Forty-six 3D-landmarks were measured on vertebrae of 24 adult females and males of known age and sex. Results confirm that male vertebrae are consistently larger than female ones. Males show more dorsally oriented transverse processes and relatively larger vertebral bodies in upper *and* lower thoracic vertebrae. Sexual dimorphism in lower thoracic vertebrae affects the orientation of the spinous processes, which is more horizontal in females but more caudal in males. Such regional pattering of sexual dimorphism emerges also from principal component analyses reflecting a complex interaction between the effects of sex and serial position on shape variation. Greater dorsal orientation of male transverse processes reorients the ribs and could lead to greater radial thorax diameters. This fits with greater male respiratory capacities, but may indicate also greater invagination of the male spine within the thorax. Horizontal orientation of the spinous processes in females could allow for a greater thoraco-lumbar lordosis during pregnancy, but more comparative research is necessary to test these hypotheses. Am J Phys Anthropol 155:513–521, 2014.

Sexual dimorphism is an important factor of intra- and interspecific variation in primates (Frayer and Wolpoff, 1985). It has been widely addressed in craniodental and postcranial skeletal morphology of nonhuman primates (e.g., Wood, 1976; Leutenegger and Cheverud, 1985; Plavcan and van Schaik, 1994) and fossil hominins (e.g., Trinkaus, 1980; Frayer and Wolpoff, 1985; McHenry, 1991; Rehg and Leigh, 1999; Rosas et al., 2002). Also in recent modern humans sexual dimorphism has been investigated both at the level of the postcranium (e.g., Bellemare et al., 2006; Carlson et al., 2007; Kranioti et al., 2009) and the craniofacial system (e.g., Rosas and Bastir, 2002; Bulygina et al., 2006; Bastir et al., 2011a).

These latter studies indicate that human craniofacial dimorphism is related to the respiratory system (Enlow, 1990, Rosas and Bastir, 2002; Bastir et al., 2011a). Higher energy consuming males have both absolutely and relatively larger cranial airways than females, a fact that provides males with a greater respiratory capacity than females (Enlow, 1990; Rosas and Bastir, 2002; Hall, 2005; Bastir et al., 2006, 2011a; Bastir and Rosas, 2013; Holton et al., 2013).

However, because the respiratory system consists of cranial *and* postcranial components (Bastir, 2008) also the ribcage and its constituent elements, i.e., the thoracic vertebrae, the ribs and the sternal complex (García-Martínez et al., 2012; Bastir et al., 2013) should reveal features related to greater respiratory capacities in males. In fact, males, once corrected for differences in body size, still have larger respiratory capacities than females (Silbernagl and Despopoulos, 1991), which is reflected by greater radial diameters of the male thorax relative to stature (Bellemare et al., 2003). As a consequence, the male rib-cage volume is approximately 10–12% larger than in females of the same age and stature (Bellemare et al., 2003).

Sexual dimorphism of thoracic vertebrae is important in this context because the spatial position of the transverse (costal) processes influences the spatial position of the ribs, as they develop, grow and vary jointly (Bardeen, 1905; Aoyama et al., 2005). Thus, a rib of any given size and shape will give rise to a greater radial

Additional Supporting Information may be found in the online version of this article

Grant sponsor: The Leakey Foundation; Grant number: CGL2012-37279 (MINECO; Spain).

*Correspondence to: Dr. Markus Bastir. E-mail: mbastir@mncn.csic.es

Received 17 January 2014; accepted 15 August 2014

DOI: 10.1002/ajpa.22604
Published online 28 August 2014 in Wiley Online Library (wileyonlinelibrary.com).

diameter of the thorax when its articulation site at the transverse process is oriented more dorsally.

The morphology of the thoracic vertebrae could also account for another feature of sexual dimorphism in the rib cage. Bellemare et al. (2003) reported a greater inferior (caudal) inclination of the sixth rib in females, which differed from males by approximately 4°. Greater caudal orientation can be caused by an elevation of the transverse process relative to the vertebral body. If the facet of the rib tubercle at the transverse process of the thoracic vertebra in females is located more superiorly than the facet for the rib head, the entire rib will be rotated into a more caudal position, with the sternal end more inferiorly than the vertebral end. Caudal rib orientations were suggested a possible female adaptation to sub-thoracic space expansion during pregnancy (Bellemare et al., 2003).

Adaptation to pregnancy has also been suggested for lower thoracic vertebrae from an evolutionary point of view. Because of bipedalism, increased body mass in pregnant females, caused by the growing foetus, can lead to changes in posture due to an anterior shift of the gravitation center of the trunk (Whitcome et al., 2007; Masharawi et al., 2010). This shift of the trunk gravitation center would be compensated by a specific increase in the lumbar lordosis affecting the lumbar, but possibly also lower thoracic vertebrae in females (Vialle et al., 2005; Whitcome et al., 2007; Masharawi et al., 2010). However, other studies did not detect evidence of sexual dimorphism in the lumbar lordosis (Been et al., 2010; Kalichman et al., 2011) and thus a better knowledge of the three-dimensional (3D) geometry of the thoracic vertebrae can contribute to this discussion.

Thus, upper and lower thoracic vertebrae likely show different patterns of sexual dimorphism. A distinction between upper and lower parts of the thorax has been further established on developmental and evolutionary factors (Bastir et al., 2013; Schmid et al., 2013; Williams et al., 2013). But also functional anatomical features suggest such a regional distinction. In the upper part of the thorax, ventilatory movement is produced mainly by the external intercostal muscles (De Troyer, 2005; West, 2012). Kinetics of the lower rib cage is also related to the activity of the diaphragm (Saadé et al., 2010; West, 2012). Reduction of sub-thoracic space during pregnancy may alter diaphragmatic activity in females (Bellemare et al., 2003) and interactions between reproductive and respiratory systems in lower regions of the thorax can be expected.

The question of sexual dimorphism in human vertebrae has been addressed by several authors with the main goal of sex estimation in forensic and archaeological contexts, and have focused on the first, second, and seventh cervical vertebrae (Marino, 1995; Wescott, 2000; Marlow and Pastor, 2011; Bethard and Seet, 2013; Amores et al., 2013), and the twelfth thoracic and first lumbar vertebrae (MacLaughlin and Oldale, 1992; Yu et al., 2008; Zheng et al., 2012; Hou et al., 2012, Amores et al., 2013), as they are relatively easy to identify in anatomical isolation. All these authors concur in that male vertebrae are larger than female vertebrae, and that such sex-differences are a direct function of differences in body size, likely related to either higher overall body growth rates and/or longer growth duration in males (Baume et al., 1983; O'Higgins and Jones, 1998; Bogin, 1999; Bulygina et al., 2006; Bastir et al., 2012, 2013).

The present study aims to test four different hypotheses. H1: Thoracic vertebrae are larger in males than in females. H2: The angulation of the costo-vertebral joint relative to the vertebral body differs with greater dorsal orientation of the transverse processes in males than in females. H3: The costo-vertebral joints in females are more vertically oriented, that is, the articular facet for the rib tubercle at transverse processes in females is located in a more cranial position relative to the facet for the rib head at the vertebral body than in males. H4: Sexual dimorphism in upper thoracic vertebrae differs from that of lower thoracic vertebrae.

MATERIAL AND METHODS

We measured 239 vertebrae from nonpathological vertebral columns of 24 individuals of known age and sex (12 males and 12 females) that ranged in age from 20 to 42 years and belong to the identified skeletal collection curated at the School of Legal Medicine, Complutense University, Madrid. From 24 complete columns only one female lacked one vertebra (T3). Missing data due to bone conservation state were few (7%), and were estimated using multivariate regressions (Bastir et al., 2014). Also, only the first 10 thoracic vertebrae were selected for the present study in order to collect the same landmarks in all vertebrae including the facets for the rib tubercles located at the transverse processes, which are variable and sometimes absent at T11 and T12.

A Microscribe G2 digitizer was used to digitize 46 3D landmarks (Supporting Information Table S1) in each vertebra. We used standard geometric morphometric procedures to obtain centroid size and shape data (O'Higgins, 2000).

The size and shape data of this study comes from serial anatomical objects that belong to individuals, i.e., 10 vertebrae per thoracic spine (or individual). Thus, statistically, the landmark data of vertebrae pertaining to one individual are not independent from each other. Consequently, when analysing all data together either a correction for degrees of freedom for standard parametric statistics or a specific analytical protocol that accounts for such nonindependence is required.

First, we conducted 10 independent generalized Procrustes analyses on each class of vertebrae comparing size and shape (full shape space). Due to the lower individual sample sizes normality could not be assumed and Mann–Whitney U tests were performed to test for size differences (H1; Sokal and Rohlf, 1998). Permutation tests (N = 10.000) and 3D-visualizations of warped surface models were used to assess mean shape differences measured in Procrustes distances (Klingenberg, 2011), relevant to H2 and H3.

Second, in addition to the individual shape analyses, a male and a female vector of shape change was calculated for the vertebrae of the upper and lower parts of the thoracic spine in common shape space (common Procrustes registration). These regressions quantify vectors of vertebral shape change along their serial positions (T1, T2, T3, T4, and T5, for the upper spine, and T6, T7, T8, T9, and T10 for the lower spine) and were carried out on pooled within-groups (individuals) covariance matrices. The pooled within-group design removes the effect of belonging to the same individual by subtracting the individual mean from each vertebra, thus controlling for pseudoreplication of this factor in the serial data. These

TABLE 1. Sexual dimorphism in separate classes of vertebrae

Vertebra	Female (CS)	Male (CS)	Size difference	*P* (*U* test)	Procrustes distance	*P*	PC 1 (*P*)	PC 2 (*P*)	PC 3 (*P*)
T1	146.49	160.76	14.27	**<0.001**	0.05	*0.060*	0.119	**<0.001**	**0.033**
T2	140.58	155.5	14.92	**<0.001**	0.04	0.230	0.686	**<0.001**	0.106
T3	135.74	150.97	15.23	**<0.001**	0.04	0.180	0.424	**<0.001**	**0.012**
T4	136.53	150.35	13.82	**<0.001**	0.04	0.210	0.525	**<0.001**	0.106
T5	138.58	153.04	14.46	**<0.001**	0.39	0.230	*0.094*	**<0.001**	**0.043**
T6	142.43	157.49	15.06	**<0.001**	0.43	*0.060*	0.133	**<0.001**	**0.003**
T7	143.85	159.51	15.66	**<0.001**	0.04	*0.070*	0.204	**<0.001**	**0.011**
T8	145.14	161.22	16.08	**<0.001**	0.05	**0.016**	0.184	**<0.001**	**0.002**
T9	146.12	162.32	16.2	**<0.001**	0.05	**0.046**	**0.033**	**<0.001**	**0.021**
T10	150.15	165.34	15.19	*0.06*	0.05	0.300	**0.002**	**0.002**	**0.028**

Comparisons of mean size (Mann–Whitney *U* tests) and shape (Procrustes distance in full shape space, permutations) from individual Procrustes registrations and of mean shapes in PC1–PC3 subspace (60.5% of total variance) in common Procrustes registration (bold: $P < 0.05$; italics: $0.05 < P < 0.09$).

vectors were calculated in common shape space for vertebrae belonging to the upper and lower spine as well as for females and males. Therefore, angles between male and female vectors of vertebral shape change along serial anatomical position can be calculated within the upper and lower parts of the spine that can be used as a further assessment of sexual dimorphism with specific relevance to H4.

Finally, a principal components analysis (PCA) was carried out in Procrustes Form space (Mitteroecker and Gunz, 2009; Bastir et al., 2011b). The scores of the first three principal components were further used as shape data for male and female mean comparisons of Procrustes distances in this sub-space, and also carried out by Mann–Whitney *U* tests (Sokal and Rohlf, 1998).

The assessment of the hypotheses was based on statistical analyses and on the corresponding visualizations of the surface models that are directly and quantitatively driven by the landmark data underlying the statistical analyses (O'Higgins, 2000; Mitteroecker and Gunz, 2009). All analyses were carried out in the 3D Morphometrics Lab of the Museo Nacional de Ciencias Naturales using Statistica (StatSoft, 1999), MorphoJ-software (Klingenberg, 2011), and ET-software (EVAN-Society, 2010).

RESULTS

All analyses revealed significant evidence for sexual dimorphism in male and female thoracic vertebrae in size (CS) and shape, including full shape space, the first three components of Form space PCA, and the regression analyses. The quantitative results are shown in Table 1 (mean comparisons) and Table 2 (regression analyses). Males show consistently significantly larger vertebrae compared with females, which supports H1. Table 1 also shows that sexual dimorphism in vertebra shape reflects a regional patterning. Some features are dimorphic in all vertebrae, while specific features are dimorphic only in specific regions. Table 1 indicates that significant shape differences were obtained for T1, T5, T6, T7, T8, and T9 at variable significance levels in full shape space.

The morphological details of these differences are depicted in Figure 1. Sexual dimorphism at T1 demonstrates clear differences in the orientation of the transverse processes. In females these adopt a more ventral and caudal position, while in males they are oriented more cranially and dorsally. The male T1 spinal process is slightly relatively longer. The superior and inferior

TABLE 2. Vector comparisons between upper (T1–T5) and lower (T6–T10) thoracic spine

Units of thoracic spine	% expl var.	*P*
Upper female serial position vector	63.7	<0.0001
Upper male serial position vector	65.6	<0.0001
Lower female serial position vector	37	<0.0001
Lower male serial position vector	38.6	<0.0001

Vectors describe sex-specific shape change along serial positions.

intervertebral joints (laminae) are more vertically oriented in males than in females, where they are much more horizontally aligned. As a consequence, in lateral view the angle between the spinal process and the laminae tends to form a right angle in males so that the caudal intervertebral facets are relatively closer to the posterior border of the vertebral body than in females. Due to the enlarged structures of the neural arch in males, the relative size difference at the vertebral body of T1 is not as clearly evident as in lower vertebrae.

In the lower thoracic vertebrae (Fig. 1) the female vertebral foramen is rounded while the male is more oval. The transverse processes in males are consistently more elongated and, as in upper vertebrae (T1), oriented more dorsally and cranially than in females. The relative size of the costal facets for articulation with the rib heads is consistently larger in males, particularly in lower vertebrae. Zygapophyseal joints, however, are more variable in relative size and sometimes relatively smaller in males than in females (such as evident by comparing the correspondingly colored structures in T1 of the interactive Supporting Information Fig. S1, but also T8 in Supporting Information Fig. S2). However, most importantly, in lower vertebrae the spinous process orientation is more horizontal in females but more caudal in males. This is thus an important dimorphic feature of the lower thoracic region which is not observed in upper thoracic vertebrae, e.g., T1.

The dorsal flexion and elongation of the male transverse processes, clearly evident in axial views in Figure 1, support H2. However, the fact that in females the transverse processes are more inferiorly located than in males does not support H3 (lateral views in Fig. 1). There is no cranio-caudal orientation of the costovertebral articulation in females. The lateral view shows that in females the costal tubercle facet at the transverse process is always below the level of the cranial plate of the vertebral body, while in males (except in T6) it is located more superiorly.

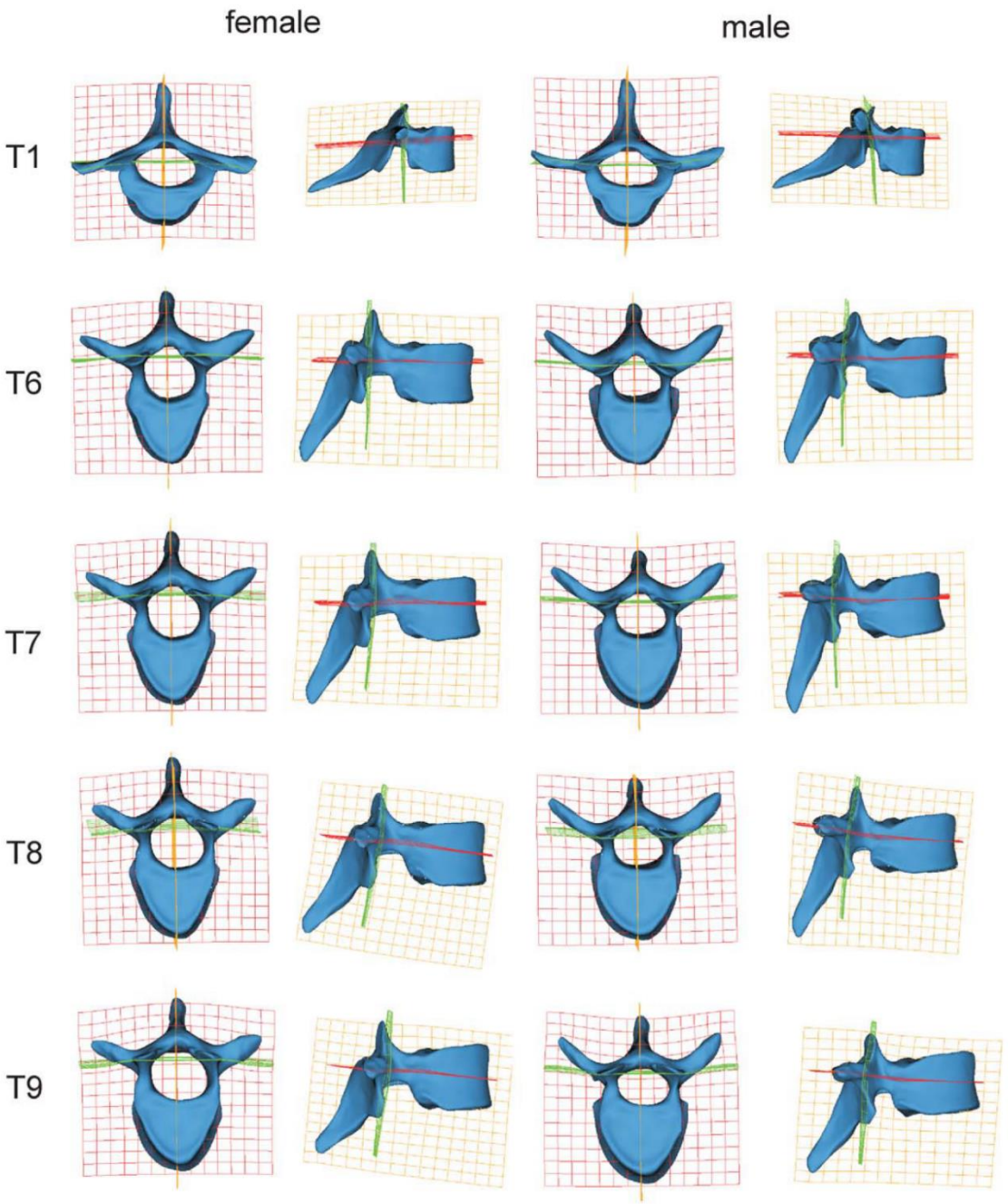

Fig. 1. Axial and right-lateral views of thoracic vertebrae T1, T6–T9 of female (left), and male (right) mean shapes. Thin-plate spline transformations visualize the differences between the Procrustes average into female (left) and male (right) configurations. Axial views show sexual dimorphism of the orientation of the transverse processes. The lateral views also indicate the orientation of the spinous processes. In T1 there is no difference in the orientation of the spinous processes. In lower vertebrae the spinous process in males systematically projects more caudally while in females this process is oriented horizontally. The lateral views show relatively larger sizes of the facets for the rib head in males. Lateral views also clearly indicate that the facets located at the transverse processes in males are consistently more superiorly (cranially) located relative to the cranial plates of the vertebral body. This is particularly clear at T1, T7, and T8. In females, the transverse processes are at the same level or below the level of the cranial plates of the vertebral bodies. At T9 tangents to the cranial and caudal plates of the vertebral body suggests a slight posterior wedging (relatively smaller vertebral body height posteriorly than anteriorly). [Color figure can be viewed in the online issue, which is available at wileyonlinelibrary.com.]

H4 is supported because the orientation of the spinous process in T1 does not differ between males and females while in lower vertebrae (e.g., T8) in males the spinous process is oriented caudally and in females horizontally (Fig. 1). This indicates different patterns of sexual dimorphism in upper and lower vertebrae [supporting

H4; see also the interactive 3D models in the Supporting Information Figs. S1 (T1) and S2 (T8)].

Regression analyses of shape on serial position indicate that the vectors of vertebral shape change explain a fairly high amount of variance which is almost twice in the upper part of the spine than in the lower part (Table 2). The angle between male and female vectors indicates a highly significant but low divergence in the upper part (10.9°; $P < 0.0001$) and a twice as large divergence in the lower part (19.6°; $P < 0.0001$). This is further quantitative evidence for differences in shape dimorphism in the upper and lower thoracic vertebrae. It is also reflected in Figure 1 showing the comparisons between T1 vs. T6–T9. These results support altogether H4.

The form space PCA (Fig. 2) shows curved serial shape trajectories of males and females and Figure 3 illustrates shape variation along PC1 to PC3 scores. PC1 (35.3% of total variance) orders the vertebrae of the upper spine according to their anatomical position but not those inferior to T5 (Figs. 2 and 3). Instead PC1 scores emit a signal of sexual dimorphism in the lowest vertebrae (T9, T10; Table 1). In males, serial ordination along PC1–PC2 is continuous while in females the PC1 scores of T1 plot well apart from the remaining upper vertebrae, indicating a discontinuous morphology (see previous descriptions of sexual dimorphism of T1). Variation along PC2 (17.5% of total variance) reflects a general pattern of sexual dimorphism (Figs. 2 and 3). Females tend to plot at lower PC2 scores than males (Table 1) in all vertebral categories. Figure 3 shows that shape variation associated to PC2 polarizes vertebrae that are expanded mediolaterally at positive scores (males, wide vertebrae) and anteroposteriorly toward negative scores (females, long vertebrae). PC2 in lower vertebrae also carries a signal of serial shape change. Variation along PC3 shows a signal of sexual dimorphism in T1 and all lower vertebrae from T5 to T10. All this supports regional patterning of sexual dimorphism across vertebrae of the upper and lower parts of the thoracic spine (H4).

DISCUSSION

Several studies have addressed sexual dimorphism in human vertebrae, most of them developed with the purpose of sex estimation in forensic and archaeological settings (MacLaughlin and Oldale, 1992; Marino, 1995; Wescott, 2000; Yu et al., 2008; Marlow and Pastor, 2011; Zheng et al., 2012; Amores et al., 2013; Bethard and Seet, 2013; Hou et al., 2013), and a few others focused on the appearance of dimorphism during growth in basic vertebral dimensions with more clinically oriented objectives (Hinck et al., 1962; Taylor and Twomey, 1984).

In a broader evolutionary context, sexual dimorphism of the thoracic vertebrae is important in the light of the physiology of the respiratory system and also in light of obstetric adaptations (Rosas and Bastir, 2002; Bellemare et al., 2003; Whitcome et al., 2007; Bastir, 2008; Masharawi et al., 2010; Bastir et al., 2011a). Such questions are all related to the *spatial* configuration of the vertebrae and are better addressed through 3D geometric morphometric analysis. With the exception of the study of Manfreda et al. (2006), who focused on the first cervical vertebra and modes of locomotion in primates, this is the first study that uses 3D geometric morphometrics to address questions of sexual dimorphism in thoracic vertebrae.

Our study identified factors of size and shape dimorphism that can be observed in all thoracic vertebrae (general factors) and others, that are only evident in the lower part of the spine (regional factors).

General factors of thoracic vertebral dimorphism

Our results show that for T1–T10, male vertebrae are consistently larger than female ones (Table 1), an observation that concurs with the aforementioned studies on vertebral dimorphism (MacLaughlin and Oldale, 1992; Marino, 1995; Wescott, 2000; Yu et al., 2008; Marlow and Pastor, 2011; Zheng et al., 2012; Amores et al., 2013; Bethard and Seet, 2013; Hou et al., 2012), and with most studies of sexual dimorphism of the human skeleton, which reported greater sizes in males than females (Clutton-Brock, 1985; Frayer and Wolpoff, 1985; Leutenegger and Cheverud, 1985; Plavcan and Schaik, 1994; Spradley and Jantz, 2011).

General factors include also some shape features, that is, the dorso-ventral and cranio-caudal orientation of the transverse processes, and the shape of the neural canal. Figure 1 shows that the transverse processes in males are dorsally oriented in the upper (T1) and lower vertebrae (T5–T9) and ventrally in females. The differences very likely have important spatial "knock-on" effects for the lower thorax morphology that can be discussed in the light of thorax capacities. Because the ribs are articulated with the facets on the transverse process and the body of the vertebra, any posterior flexion of the transverse process will reorientate entirely a rib of a given shape into a more posterior position. This leads then to a (bilateral) divergence of anterior (sternal) rib extremes and will thus increase the medio-lateral width of the enclosed space of the thorax in this area. This is likely to be the case in male thoracic vertebrae, because Bellemare et al. (2006) did not find sex specific differences in the absolute lengths of the third, sixth, and ninth ribs. Differences in their costal process orientation (Fig. 1) could thus be interpreted as a "vertebral" contribution to greater relative thorax diameters in males (Bellemare et al., 2003) and the associated increased respiratory capacity in males (Silbernagl and Despopoulos, 1991, Bellemare et al., 2003, 2006).

This may not only be relevant to human sexual dimorphism, but also to human evolution. Recent research on fossil ribs of the Kebara 2 Neandertal (García-Martínez et al., 2014) demonstrates that the lower thorax in some Neandertals could have been larger than in modern humans (Franciscus and Churchill, 2002; Gómez-Olivencia et al., 2009). The present findings suggest that thorax size could be produced by differences both in rib size *and* in the orientation of the transverse processes. 3D morphometric analysis of thoracic vertebrae in Neandertals should be carried out in this respect.

In an evolutionary sense, the orientation of the transverse processes has also been related to the position of the spine within the ribcage (invagination) and is important to the evolution of bipedal posture (Jellema et al., 1993). Being a factor of modern human sexual dimorphism could indicate a greater invagination of the male spine within the rib cage than in females. This hypothesis requires analyses of ribcages in anatomical connection.

Bellemare et al. (2003) reported a greater inferior (cranio-caudal) inclination of the ribs in females, yet the sites for the attachment of the ribs to the thoracic

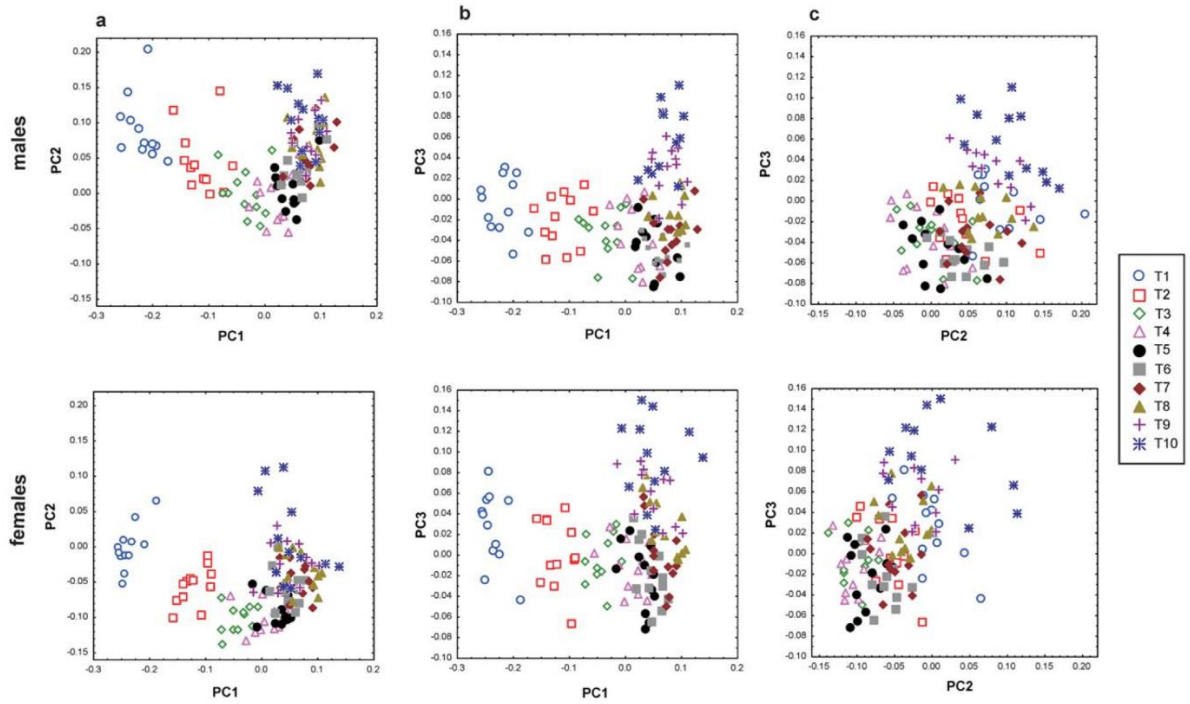

Fig. 2. Principal components analysis in form space. (**a**) Sequential shape trajectory along PC1–PC2, (**b**) sequential shape trajectory along PC1–PC3, and (**c**) PC2–PC3; upper row shows males, the lower row shows females. Males and females are plotted within the same range along the axes so that sexual dimorphism can be observed comparing the corresponding scatter plots. PC1 orders shapes along serial position in T1–T5 and shows sexual dimorphism in T9 and T10. PC2 carries a general signal of sexual dimorphism but orders also along serial position. PC3 orders lower vertebrae (T5–T10) according to serial position and shows sexual dimorphism in T1 and T5–T10. All projections show thus an interaction between serial position and sexual dimorphism in different classes of vertebrae along the thoracic spine. [Color figure can be viewed in the online issue, which is available at wileyonlinelibrary.com.]

vertebrae in our data show opposite orientations (Fig. 1). Mean shapes (Fig. 1) and PC2 demonstrates visually (Fig. 3) by the elevated facets for the rib tubercle and the relatively lower facet for the rib head and quantitatively (Table 1) that the cranio-caudal inclination of the rib attachment sites is a male feature of sexual dimorphism and common to all vertebrae.

It follows that the greater cranio-caudal inclination observed in female ribs should be either a consequence of sexual dimorphism of rib curvature in females (Bellemare et al., 2006), or the consequence of a different position of the rib within its costo-vertebral joints. The fact that the facets for articulation in the rib-tubercles are slightly more superiorly oriented in females compared to males (Fig. 3, PC2, PC3 in lateral views) could indicate such different position within the articulation. Future research should focus on these possibilities particularly addressing the spatial relations between vertebral *and* costal articulation facets.

Also the configuration of the neural canal is dimorphic at all vertebral levels (Figs. 1–3; Table 1, PC2) although the dorso-ventral expansion in females is clearer at the lower parts than in the upper parts (Fig. 1). Amores et al. (2013) reported already a "surprisingly" strong dimorphic signal in this structure and related it to sexual dimorphism of spinal cord weight. Although our data cannot support such causal relationships between neural and bony structures, they do provide evidence for a relatively larger and more circular neural canal in females and a relatively smaller and more oval vertebral foramen shape in males, findings that are also compatible with a recent study reporting dynamic shape variation of the neural arch (Masharawi and Salame, 2011).

Regional factors of thoracic vertebral dimorphism

Some features of shape dimorphism are only observed at the lower thoracic vertebrae. These include the relative sizes of the rib head facets, and the orientation of the spinous processes.

In lower thoracic vertebrae the orientation of the spinous process is more horizontal (superior) in females (Figs. 1 and 3). This orientation gives rise to the increased antero-posterior length of a typical female thoracic vertebra. In addition, a horizontal spinous process, such as observed here, allows spatially for a greater lordosis in the thoraco-lumbar spine and fits with proposed obstetric adaptations suggested by Whitcome et al. (2007) and Masharawi et al. (2010). The former authors observed that human females present adaptations in the lumbar vertebrae (wedging pattern, relative zygapophyseal surface area, prezygapophyseal joint surfaces orientation), allowing for a greater lordosis and reinforcement of the spine during pregnancy. In turn, these changes compensate the displacement of the center of mass above the hips associated to the fetal load. The results of Masharawi et al. (2010) supported these findings, and these authors found that for the segment T9-L4, female vertebrae presented less kyphotic wedging, relatively

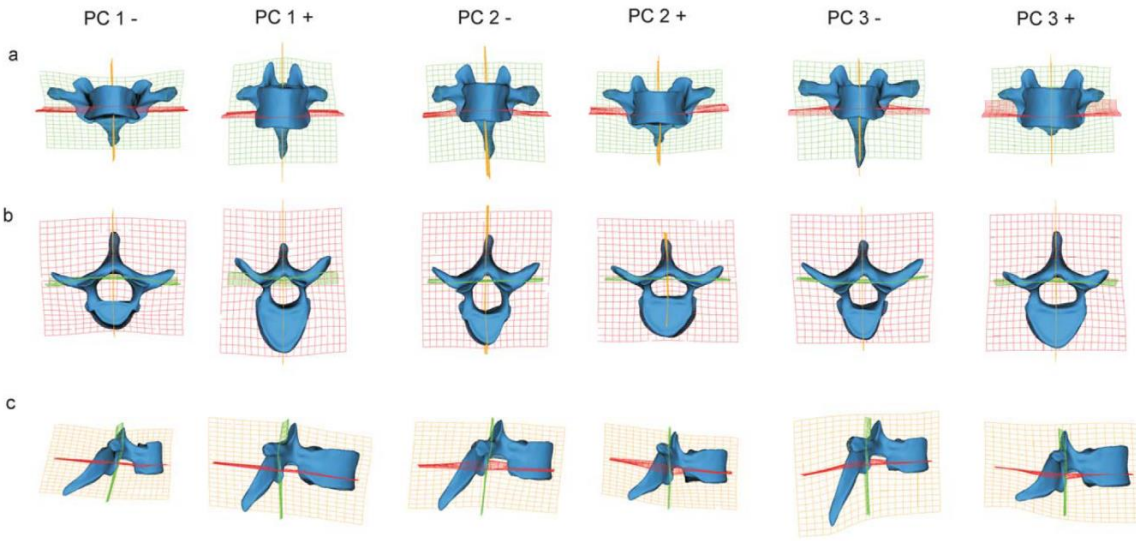

Fig. 3. Shape variation associated to scores of Form space PC1–PC3 in frontal, axial and left-lateral view. PC1 orders upper vertebrae along serial position and correspondingly polarizes mediolaterally wide and vertically short vertebrae, with anteriorly oriented transverse processes and relatively smaller bodies toward negative PC1 scores and narrow, vertically high vertebrae, with posteriorly oriented transverse processes and relatively larger bodies toward positive scores. The latter describe sexual dimorphism at T9 and T10. Shape variation along PC2 describes robustness and width of vertebral bodies, superiorly elevated transverse processes, horizontal orientation of the spinous process and oval vertebral foramen shape toward positive scores (males) and the opposite shape trends toward negative scores (females). There is some ordination of inferior vertebrae according to seriality. Variation along PC3 describes bilateral relative elongation of the transverse processes and a strong vertical orientation of the spinous process. It reflects sexual dimorphism particularly at the lower vertebrae, supporting H4, but also ordination according to serial position in lower vertebrae (T6–T10). [Color figure can be viewed in the online issue, which is available at wileyonlinelibrary.com.]

thinner lumbar spinous processes, and relatively wider superior interfacet distances.

However, other studies have not found evidence for sexual dimorphism in the lumbar lordosis (Kalichman et al., 2011; Been et al., 2012). The horizontal spinous process orientation and the more posterior orientation of the zygapophysis (Fig. 1) in lower female thoracic vertebrae would *allow*, in principle, for a greater development of thoraco-lumbar lordosis. Whether this is expressed or not may be determined by additional factors, for example, in relation to how vertebrae are finally connected via intervertebral discs to give rise to a final spine curvature. The anticipation of morphological characteristics in thoracic vertebrae that allow for lumbar lordosis may reflect effects of serial development along the lower spine. This may be also foreshadowed by greater relative sizes of the intervertebral joints (at lower vertebrae, T8), in females and has been identified as sexual dimorphic feature in lumbar vertebrae (Whitcome et al., 2007). However, in our sample also intervertebral facets of some upper (T1) are relatively enlarged. Future study should focus on the biomechanical significance of these structures in more detail.

The particularly expanded lower part of the male vertebral bodies shown in Figures 1 and 3 fits with findings on linear measurements in these areas reported by others (Zheng et al., 2012; Amores et al., 2013). Figure 1 shows that lower widths of T6, T8, and T9 are markedly expanded due to enlarged rib head facets, thus reflecting increased overall size and robustness of male ribs. Figure 3 shows a simultaneous expansion of the relative rib head facet size and transverse process length (Fig. 3B, negative PC3 scores) likely in relation to developmental coordination of the transverse processes with the rib head and neck (Aoyama et al., 2005).

Development may also be important for the observation that sexual dimorphism is particularly clear at T1 and T6–T10 by showing significant difference in full shape space (Table 1). This could reflect both genetic and functional factors. Genetic factors could be involved as ontogenetic maturation in the spine occurs bidirectionally from the extremes toward the center (Scheuer and Black, 2000; Cardoso and Ríos, 2009; Cardoso and Ríos, 2011). Genetic factors could also be expressed through differences in the timing of fusion of the epiphyses of the vertebrae associated to the sexual difference in the onset and duration of the adolescent stage, when several epiphyses of the skeleton start to fuse (Bogin, 1999; Cardoso and Ríos, 2009; Cardoso and Ríos, 2011). This variation could be potentially translated into differences in growth and orientation of the transverse processes. Clearly, our data cannot test that hypothesis, which would require an ontogenetic study, but the fact that sexual dimorphism coincides with those structures that mature earlier during ontogeny, coupled to differences in timing of fusion between sexes, could point toward such genetic relations.

Our results demonstrate a solid signal of sexual dimorphism in size and regionally different patterns of sexual dimorphism in shape related to the respiratory system, the reproductive apparatus and posture. Principal components analysis show a complex pattern of shape variation related to interactions between sex and serial position. Further studies on larger samples should include the whole spine (cervical, thoracic, and lumbar vertebrae), and ribs of humans and other hominoids at

different ontogenetic stages, in order to advance our knowledge of the evolution, ontogeny and dimorphism of the human thorax and trunk.

ACKNOWLEDGMENTS

We thank Professor José Antonio Sánchez Sánchez and Technician Elena Gómez (Faculty of Medicine, Universidad Complutense de Madrid) for permission to study the collection and support during scanning process. We thank Ella Been (Tel Aviv University), Scott Williams (New York University), and one anonymous reviewer for helpful suggestions that greatly improved this article.

LITERATURE CITED

Amores A, Botella MC, Alemán I. 2013. Sexual dimorphism in the 7th cervical and 12th thoracic vertebrae from a Mediterranean population. J For Sci.

Aoyama H, Mizutani-Koseki S, Koseki H. 2005. Three developmental compartments involved in rib formation. Int J Dev Biol 49:325–333.

Bardeen CR. 1905. The development of the thoracic vertebræ in man. Am J Anat 4:163–174.

Bastir M. 2008. A systems-model for the morphological analysis of integration and modularity in human craniofacial evolution. J Anthropol Sci 86:37–58.

Bastir M, Böhme M, Sanchiz B. 2014. Middle Miocene remains of Alytes (Anura, Alytidae) as an example of the unrecognised value of fossil fragments for evolutionary morphology studies. J Vert Paleontol.

Bastir M, García-Martínez D, Coquerelle M, Barash A, Recheis W. 2012. In: PESHE, editor. Systems-approaches to skeletal variation in paleoanthropology: the human thorax. Bordeaux: ESHE, European Society for the Study of Human Evolution. p 14.

Bastir M, García Martínez D, Recheis W, Barash A, Coquerelle M, Rios L, Peña-Melián Á, García Río F, O'Higgins P. 2013. Differential growth and development of the upper and lower human thorax. PLoS ONE 8:e75128.

Bastir M, Godoy P, Rosas A. 2011a. Common features of sexual dimorphism in the cranial airways of different human populations. Am J Phys Anthropol 146:414–422.

Bastir M, Rosas A. 2013. Cranial airways and the integration between the inner and outer facial skeleton in humans. Am J Phys Anthropol 152:287–293.

Bastir M, Rosas A, Gunz P, Pena-Melian A, Manzi G, Harvati K, Kruszynski R, Stringer C, Hublin J-J. 2011b. Evolution of the base of the brain in highly encephalized human species. Nat Commun 2:588.

Bastir M, Rosas A, O'Higgins P. 2006. Craniofacial levels and the morphological maturation of the human skull. J Anat 209:637–654.

Baume R, Buschang P, Weinstein S. 1983. Stature, head height, and growth of the vertical face. Am J Orthod 83:477–484.

Been E, Barash A, Pessah H, Peleg S. 2010. A New Look at the Geometry of the Lumbar Spine. Spine 35:E1014–E1017. 1010.1097/BRS.1010b1013e3181ddd1433.

Been E, Gómez-Olivencia A, Kramer PA. 2012. Lumbar lordosis of extinct hominins. Am J Phys Anthropol 147:64–77.

Bellemare F, Fuamba T, Bourgeault A. 2006. Sexual dimorphism of human ribs. Resp Physiol Neurol 150:233–239.

Bellemare F, Jeanneret A, Couture J. 2003. Sex differences in thoracic dimensions and configuration. Am J Resp Crit Car Med 168:305–312.

Bethard JD, Seet BL. 2013. Sex determination from the second cervical vertebra: a test of Wescott's method on a modern American sample. J For Sci 58:101–103.

Bogin B. 1999. Patterns of human growth. Cambrige: Cambridge University Press.

Bulygina E, Mitteroecker P, Aiello L. 2006. Ontogeny of facial dimorphism and patterns of individual development within one human population. Am J Phys Anthropol 131:432–443.

Cardoso HFV, Ríos L. 2011. Age estimation from stages of epiphyseal union in the presacral vertebrae. Am J Phys Anthropol 144:238–247.

Carlson KJ, Grine FE, Pearson OM. 2007. Robusticity and sexual dimorphism in the postcranium of modern hunter-gatherers from Australia. Am J Phys Anthropology 134:9–23.

Clutton-Brock TH. 1985. Size, sexual dimorphism, and polygeny in primates.In: Jungers WL, editor. Size and scaling in primate biology. New York: Plenum Press. p 51–60.

De Troyer A, Kirkwood PA, Wilson TA. 2005. Respiratory action of the intercostal muscles. Physiol Rev 85:717–756.

Enlow DH. 1990. Facial growth. Philadelphia: W.B. Saunders Company.

EVAN-Society. 2010. ET, toolkit for geometric morphometric analysis.

Franciscus RG, Churchill SE. 2002. The costal skeleton of Shanidar 3 and a reappraisal of Neandertal thoracic morphology. J Hum Evol 42:303–356.

Frayer D, Wolpoff M. 1985. Sexual Dimorphism. Ann Rev Anthropol 14:429–473.

García-Martínez D, Recheis W, Bastir M. 2012. The whole and its parts: 3D geometric morphometrics of human thorax evolution. Encuentro de Jovenes Investigadores en Paleontología Valencia.

García-Martínez D, Barash A, Recheis W, Torres Sanchez I, Garcia Rio F, Bastir M. 2014. On the chest size of the Kebara 2 Neandertal. J Hum Evol 70:69–72.

Gómez-Olivencia A, Eaves-Johnson KL, Franciscus RG, Carretero JM, Arsuaga JL. 2009. Kebara 2: new insights regarding the most complete Neandertal thorax. J Hum Evol 57:75–90.

Hall RL. 2005. Energetics of nose and mouth breathing, body size, body composition, and nose volume in young adult males and females. Am J Hum Biol 17:321–330.

Hinck VC, Hopkins CE, Savara BS. 1962. The size of the atlantal spinal canal: a sex difference. Hum Biol 34: 197–205.

Higham T, Compton T, Stringer C, Jacobi R, Shapiro B, Trinkaus E, Chandler B, Gröning F, Collins C, Hillson S, O'Higgins P, FitzGerald C, Fagan M. 2011. The earliest evidence for anatomically modern humans in northwestern Europe. Nature 479:521–524.

Holton NE, Yokley TR, Froehle AW, Southard TE. 2013. Ontogenetic scaling of the human nose in a longitudinal sample: implications for genus Homo facial evolution. Am J Phys Anthropol.

Hou WB, Cheng KL, Tian SY, Lu YQ, Han YY, Lai Y, Li YQ. 2012. Metric method for sex determination based on the 12th thoracic vertebra in contemporary north-easterners in China. J For Leg Med 19:137–143.

Jellema LM, Latimer B, Walker A. 1993. The rib cage. The Nariokotome Homo Erectus Skeleton. Cambridge: Harvard University Press. p 294–325.

Kalichman L, Li L, Hunter DJ, Been E. 2011. Association between computed tomography–evaluated lumbar lordosis and features of spinal degeneration, evaluated in supine position. Spine J 11:308–315.

Klingenberg CP. 2011. MorphoJ: an integrated software package for geometric morphometrics. Mol Ecol Res 11:353–357.

Kranioti EF, Bastir M, Sánchez-Meseguer A, Rosas A. 2009. A geometric-morphometric study of the cretan humerus for sex identification. Forensic Science International 189:111.e111–111.e118.

Leutenegger W, Cheverud JM. 1985. Sexual dimorphism in primates.In: Jungers WL, editor. Size and scaling in primate biology. New York: Plenum Press. p 33–50.

MacLaughlin SM, Oldale KNM. 1992. Vertebral body diameters and sex prediction. Ann Hum Biol 19: 285–292.

Manfreda E, Mitteroecker P, Bookstein FL, Schaefer K. 2006. Functional morphology of the first cervical vertebra in humans and nonhuman primates. Anat Rec 289B:184–194.

Marino EA. 1995. Sex estimation using the first cervical vertebra. Am J Phys Anthropol 97:127–133.
Marlow EJ, Pastor RF. 2011. Sex determination using the second cervical vertebra—a test of the method. J For Sci 56:165–169.
Masharawi Y, Dar G, Peleg S, Steinberg N, Medlej B, May H, Abbas J, Hershkovitz I. 2010. A morphological adaptation of the thoracic and lumbar vertebrae to lumbar hyperlordosis in young and adult females. Eur Spine J 19:768–773.
Masharawi Y, Salame K. 2011. Shape variation of the neural arch in the thoracic and lumbar spine: characterization and relationship with the vertebral body shape. Clin Anat 24:858–867.
McHenry HM. 1991. Sexual Dimorphism in Australopithecus afarensis. J Hum Evol 20:21–32.
Mitteroecker P, Gunz P. 2009. Advances in geometric morphometrics. Evol Biol 36:235–247.
O'Higgins P. 2000. The study of morphological variation in the hominid fossil record: biology, landmarks and geometry. J Anat 197:103–120.
O'Higgins P, Jones N. 1998. Facial growth in Cercocebus torquatus: an application of three-dimensional geometric morphometric techniques to the study of morphological variation. J Anat 193:251—272.
Plavcan JM, van Schaik CP. 1994. Canine dimorphism. Evol Anthropol 2:208–214.
Rehg JA, Leigh SR. 1999. Estimating sexual dimorphism and size differences in the fossil record: a test of methods. Am J Phys Anthropol 110:95–104.
Ríos L, Cardoso HFV. 2009. Age estimation from stages of union of the vertebral epiphyses of the ribs. Am J Phys Anthropol 140:265–274.
Rosas A, Bastir M. 2002. Thin-plate spline analysis of allometry and sexual dimorphism in the human craniofacial complex. Am J Phys Anthropol 117:236–245.
Rosas A, Bastir M, Martínez Maza C, Bermúdez de Castro JM. 2002. Sexual dimorphism in the Atapuerca-SH hominids. The evidence from the mandibles. J Hum Evol 42:451–474.
Saadé J, Didier A-L, Villard P-F, Buttin R, Moreau J-M, Beuve M, Shariat B. 2010. A preliminary study for a biomechanical model of the respiratory system. In: International joint conference on computer vision, imaging and computer graphics theory and applications (VISAPP).
Scheuer L, Black S. 2000. Developmental juvenile osteology. San Diego: Academic Press.
Silbernagl S, Despopoulos A. 1991. Taschenatlas der Physiologie. Stuttgart, New York: Georg Thieme Deuscher Taschenbuch-Verlag.
Schmid P, Churchill SE, Nalla S, Weissen E, Carlson KJ, de Ruiter DJ, Berger LR. 2013. Mosaic morphology in the thorax of *Australopithecus sediba*. Science 340.
Sokal RR, Rohlf FJ, 1998. Biometry, 3 ed. W. H. Freeman and Company, New York.
Spradley MK, Jantz RL. 2011. Sex estimation in forensic anthropology: skull versus postcranial elements. J For Sci 56: 289–296.
StatSoft I. 1999. STATISTICA for windows, 99 ed. Tulsa, OK: StatSoft.
Taylor JR, Twomey LT. 1984. Sexual dimorphism in human vertebral body shape. J Anat 138:281–286.
Trinkaus E. 1980. Sexual differences in Neandertal limb bones. J Hum Evol 9:377–397.
Vialle R, Levassor N, Rillardon L, Templier A, Skalli W, Guigui P. 2005. Radiographic analysis of the sagittal alignment and balance of the spine in asymptomatic subjects. J Bone Joint Surg 87:260–267.
Wescott DJ. 2000. Sex variation in the second cervical vertebra. J For Sci 45:462–466.
West JB. 2012. Respiratory physiology the essentials. Philadelphia, Baltimore, New York, London, Buenos Aires, Hong Kong, Sydney, Tokyo: Wolters Kluwer, Lippincott Williams & Williams.
Whitcome KK, Shapiro LJ, Lieberman DE. 2007. Fetal load and the evolution of lumbar lordosis in bipedal hominins. Nature 450:1075–1078.
Williams SA, Ostrofsky KR, Frater N, Churchill SE, Schmid P, Berger LR. 2013. The vertebral column of *Australopithecus sediba*. Science 340.
Wood BA. 1976. The nature and basis of sexual dimorphism. J Zool Lond 180:15–34.
Yu S-B, Lee UY, Kwak D-S, Ahn Y-W, Jin C-Z, Zhao J, Sui H-J, Han S-H. 2008. Determination of sex for the 12th thoracic vertebra by morphometry of three-dimensional reconstructed vertebral models. J For Sci 53:620–625.
Zheng WX, Cheng FB, Cheng KL, Tian Y, Lai Y, Zhang WS, Zheng YJ, Li YQ. 2012. Sex assessment using measurements of the first lumbar vertebra. For Sci Int 219:285.e281–285.e285.

Supplementary Information

Table S1. 3D landmarks and definitions.

Landmarks (lm)	Name and definitions
lm1	anterosuperior edge of the vertebral body, the most anterior point in the medium sagittal plane.
lm2	posterosuperior edge of the vertebral body, the most posterior point in the medium sagittal plane.
lm3	right laterosuperior edge of the vertebral body, the most lateral point.
lm4	left laterosuperior edge of the vertebral body, the most lateral point.
lm5	right upper demi-facet, the most superoanterior point.
lm6	right upper demi-facet, the most superoposterior point.
lm7	right upper demi-facet, the most inferior point.
lm8	right superior articular process, the most superior point.
lm9	right superior articular process, the most inferior point.
lm10	right superior articular process, the most medial point.
lm11	right superior articular process, the most lateral point.
lm12	facet of the right transverse process, the most medial point.
lm13	facet of the right transverse process, the most lateral point.
lm14	facet of the right transverse process, the most inferior point.
lm15	facet of the right transverse process, the most superior point.
lm16	The most posterosuperior point vertebral foramen.

lm17	right lower demi-facet, the most inferoanterior point.
lm18	right lower demi-facet, the most inferoposterior point.
lm19	right lower demi-facet, the most superior point.
lm20	anteroinferior edge of the vertebral body, the most anterior point in the medium sagittal plane.
lm21	posteroinferior edge of the vertebral body, the most posterior point in the medium sagittal plane.
lm22	right lateroinferior edge of the vertebral body, the most lateral point.
lm23	left lateroinferior edge of the vertebral body, the most lateral point.
lm24	right inferior articular process, the most superior point.
lm25	right inferior articular process, the most inferior point.
lm26	right inferior articular process, the most medial point.
lm27	right inferior articular process, the most lateral point.
lm28	left inferior articular process, the most superior point.
lm29	left inferior articular process, the most inferior point.
lm30	left inferior articular process, the most lateral point.
lm31	left inferior articular process, the most medial point.
lm32	The most inferior point spinous process.
lm33	left lower demi-facet, the most inferoanterior point.
lm34	left lower demi-facet, the most inferoposterior point.
lm35	left lower demi-facet, the most superior point.

lm36	facet of the left transverse process, the most medial point.
lm37	facet of the left transverse process, the most lateral point.
lm38	facet of the left transverse process, the most inferior point.
lm39	facet of the left transverse process, the most superior point.
lm40	left superior articular process, the most superior point.
lm41	left superior articular process, the most inferior point.
lm42	left superior articular process, the most lateral point.
lm43	left superior articular process, the most medial point.
lm44	left upper demi-facet, the most superoanterior point.
lm45	left upper demi-facet, the most superoposterior point.
lm46	left upper demi-facet, the most inferior point.

Received: 13 January 2016 | Revised: 20 May 2016 | Accepted: 1 July 2016

DOI 10.1002/ajpa.23051

RESEARCH ARTICLE

WILEY American Journal of PHYSICAL ANTHROPOLOGY

Morphological and functional implications of sexual dimorphism in the human skeletal thorax

Daniel García-Martínez[1,2] | Nicole Torres-Tamayo[1] | Isabel Torres-Sanchez[3] | Francisco García-Río[3] | Markus Bastir[1]

[1]Paleoanthropology Group, Paleobiology Department, Museo Nacional de Ciencias Naturales (MNCN-CSIC), Madrid, Spain

[2]Biology Department, Faculty of Sciences, Universidad Autónoma De Madrid, Madrid, Spain

[3]Hospital Universitario La Paz, Biomedical Research Institute (IdiPAZ), Madrid, Spain

Correspondence
Daniel García-Martínez, Paleoanthropology group, Museo Nacional de Ciencias Naturales, 28006 Madrid, Spain.
Email: dan.garcia@mncn.csic.es

Abstract

Objectives: The human respiratory apparatus is characterized by sexual dimorphism, the cranial airways of males being larger (both absolutely and relatively) than those of females. These differences have been linked to sex-specific differences in body composition, bioenergetics, and respiratory function. However, whether morpho-functional variation in the thorax is also related to these features is less clear. We apply 3D geometric morphometrics to study these issues and their implications for respiratory function.

Material and methods: Four hundred two landmarks and semilandmarks were measured in CT-reconstructions of rib cages from adult healthy subjects ($N_{male} = 18$; $N_{female} = 24$) in maximal inspiration (MI) and maximal expiration (ME). After Procrustes registration, size and shape data were analyzed by mean comparisons and regression analysis. Respiratory function was quantified through functional size, which is defined as the difference of rib cage size between MI and ME.

Results: Males showed significantly larger thorax size ($p < .01$) and functional size ($p < .05$) than females. In addition, the 3D-shape differed significantly between sexes ($p < .01$). Male rib cages were wider (particularly caudally) and shorter, with more horizontally oriented ribs when compared to females. While thorax widening and rib orientation were unrelated to allometry, thorax shortening showed a slight allometric signal.

Conclusions: Our findings are in line with previous research on sexual dimorphism of the respiratory system. However, we add that thorax shortening observed previously in males is the only feature caused by allometry. The more horizontally oriented ribs and the wider thorax of males may indicate a greater diaphragmatic contribution to rib cage kinematics than in females, and differences in functional size fit with the need for greater oxygen intake in males.

KEYWORDS
geometric morphometrics, rib cage, sex differences

1 | INTRODUCTION

Sexual dimorphism has been observed as an important source of intraspecific variation in living and fossil hominins (Frayer & Wolpoff, 1985). In current day human populations, it has been addressed both at craniofacial (Bastir, Godoy, & Rosas, 2011; Bulygina, Mitteroecker, & Aiello, 2006; Hall, 2005; Lam, Pearson, & Smith, 1996; Loth & Henneberg, 1996; Rosas & Bastir, 2002; Rosas et al., 2002; Steyn & Işcan, 1998; Wood, Li, & Willoughby, 1991) and postcranial levels (Arsuaga & Carretero, 1994; Bastir, Higuero, Ríos, & García Martínez, 2014; Carlson, Grine, & Pearson, 2007; Gama, Navega, & Cunha, 2015; Işcan & Shihai, 1995; Kranioti & Michalodimitrakis, 2009; Navega, Vicente, Vieira, Ross, & Cunha, 2015; Reno, Meindl, McCollum, & Lovejoy, 2003; Richmond & Jungers, 1995; Rodriguez-Perez, 2014; Rosas et al., 2015; Rosas et al., 2016; Ruff, 1987) with size and shape differences between males and females. It is important to note that some of these shape changes could be explained by allometry (shape differences explained by differences in size), since males are generally larger than females.

1.1 | Sexual dimorphism in the respiratory apparatus

With reference to the respiratory apparatus, geometric morphometric studies of cranial airways (Bastir et al., 2011; Holton, Yokley, Froehle, & Southard, 2014; Rosas & Bastir, 2002) showed that sexual dimorphism in the human skull influences the morphology of the upper airways. This is because males present consistently larger nasal cavities and relatively longer, narrower, and higher nasal floors than females of the same body size. These differences have been linked to sex-specific differences of the musculo-skeletal system, body composition, and basal metabolic rate (BMR) associated with greater energy expenditure and oxygen consumption in males than in females (Bastir et al., 2011; Bitar, Fellmann, Vernet, Coudert, & Vermorel, 1999; Froehle & Churchill, 2009; Hall, 2005; Wells, 2007). This higher oxygen intake is necessary because adult males have larger total lean mass and smaller fat mass than females (Wells, 2007).

Sexual dimorphism of the rib cage has been studied less than that of cranial airways. It was not until the beginning of 21st century that the first detailed two-dimensional approaches began to emerge in order to study sexual dimorphism of the rib cage in anatomical connection (Bellemare, Jeanneret, & Couture, 2003). Bellemare et al. (2003) quantified radiographic pulmonary images through the use of traditional measurements such as lengths and diameters. The authors suggested that adult female thoraces are around 10–12% smaller than those of males. These size differences can be expected since Stahl (1967) proposed that total lung capacity (and thus lungs) scales isometrically with overall body size in static allometry across taxa. So, since males present a larger body size than females (Ruff, 2002), a larger lung size is also expected for them. Regarding shape, Bellemare et al. (2003) observed that female thoraces were characterized by a smaller medio-lateral dimension in relation to height (so a shorter diaphragm length), a greater declination of ribs and a higher position of the sternum compared to males.

Recently, methodological advances in morphometric quantification of rib curvature through the use of semilandmark methods (Bastir et al., 2013, 2015; García-Martínez et al., 2014; García-Martínez, Recheis, & Bastir, 2016; Shi et al., 2014; Weaver, Schoell, & Stitzel, 2014) have allowed for a more accurate quantification of the 3D structure of the rib cage. Specifically, Shi et al. (2014) and Weaver et al. (2014) developed thoracic models that could be used to study thoracic injury patterns due to motor vehicle crashes or falls. These authors addressed thorax shape variation related to several factors from a 3D point of view, including sexual dimorphism (body mass index, stature, etc.). Shi et al. (2014) measured the left side of rib cages of individuals of both sexes through the use of semilandmark methods, quantifying rib orientation relative to the axial and sagittal planes. These authors concluded that male ribs were more horizontally oriented than those of females and that the rib cages of males were deeper than those of females of the same stature, which they linked to a greater rib cage volume in males. Weaver et al. (2014) quantified age- and sex-related changes of the 3D rib cage morphology through a semilandmark approach, pointing out the higher degree of rib declination that females of different ages showed compared to males. Importantly, these studies did not specify in which kinematic state (inspiration or expiration) the thorax anatomy was quantified; therefore, controlling for respiratory movements might be required in order to attain a clearer idea of sexual dimorphism in a neutral kinematic state. This problem could potentially be solved by averaging inspiratory and expiratory thorax form. In addition, it is unclear to what degree overall size and static allometry contribute to the shape differences observed by previous studies.

1.2 | Functional anatomy related to sexual dimorphism

Bellemare et al. (2003) hypothesized that declination of ribs in females should allow for greater inspiratory muscle contribution during resting breathing than in males. This is mainly caused by intercostal muscle action (De Troyer, Kirkwood, & Wilson, 2005; Spalteholz, 1970). On the other hand, because of a higher oxygen intake in males than in females via the cranial airways (Bastir et al., 2011; Rosas & Bastir, 2002), a greater inspiratory volume is expected in the male thorax. This greater volume in males is supported by Jammes, Auran, Gouvernet, Delpierre, and Grimaud (1979), Harms et al. (1998), and Demet et al. (2011) who suggested ventilatory advantages and a greater thoracic expansion in males relative to females during breathing. Following this evidence, if more efficient intercostal muscle action has been observed in females (Bellemare et al., 2003) but a greater thoracic expansion during inspiration has been observed in males (Harms et al., 1998; Jammes et al., 1979; Demet et al., 2011) it is possible that the lower efficiency of intercostal muscles in males is compensated by their greater diaphragmatic efficiency (producing thus a greater thoracic expansion).

This is because differences in thoraco-abdominal configuration have been demonstrated to impact the function of the respiratory muscles (De Troyer et al., 2005; Goldman, Grassino, Mead, & Sears, 1978; Grassino, Goldman, Mead, & Sears, 1978; Pinet, 2004). Regarding sexual dimorphism, dimorphic features have been found between thoracic and abdominal breathing (by intercostal muscles and diaphragm, respectively): the breathing mode for males and females was proposed as abdominal during quiet breathing but the abdominal movements were significantly stronger in males than in females during deep breathing or vital capacity manoeuvers (Ragnarsdóttir & Kristinsdóttir, 2006; Kaneko & Horie, 2012; Verschakelen & Demedts, 1995). Because abdominal breathing is related to diaphragmatic action, a greater diaphragmatic contribution could be expected in males, at least in specific situations.

This possibility is reinforced by recent studies of 3D thoracic vertebrae morphology (Bastir et al., 2014), where authors found statistical differences in transverse process orientation between sexes. They showed that the transverse processes of thoracic vertebrae are more posteriorly oriented at the lower thorax in males, which could allow for greater medio-lateral expansion at the caudal part of the rib cage and thus a stronger diaphragmatic contribution.

1.3 | Aims of this study

Sexual dimorphism of the thoracic respiratory system has received little attention compared to the cranio-facial respiratory system. Previous

studies have showed sex-related differences in size and shape, but the potential association between these factors and their link to functional anatomy are still unclear. In order to clarify these issues, the present study aims to detail size and shape differences through a 3D approach and test the following hypotheses:

According to Bellemare et al. (2003), males have greater thoracic volume than females, but this has been never quantified through 3D approaches. As a result, we expect the same size differences observed previously in 2D. Therefore, we test *Hypothesis 1*, which predicts that males have larger thoraces than females (*H1*).

Since previous studies found shape differences between females and males (Bellemare et al., 2003; Shi et al., 2014; Weaver et al., 2014) we test *Hypothesis 2*, which predicts that shape differences are presented between both groups (*H2*). In addition, we provide a detailed explanation of 3D differences.

Moreover, since possible differences observed in shape are perhaps caused by size differences (allometry) and this issue remains unresolved, we aim to test *Hypothesis 3*, which predicts that sex-related shape differences are caused by allometric factors (*H3*).

Finally, since higher oxygen intake at the cranial airways has been proposed in males, we also expect them to show a greater size increase during inspiration in order to process this oxygen. Therefore, we test *Hypothesis 4*, which predicts that males have a greater increase in thorax size during inspiration than do females (*H4*).

2 | MATERIAL AND METHODS

2.1 | Materials

In order to test the hypotheses, we have used computed tomography (CT) reconstructions of the rib cages of 42 adult individuals (18 males and 24 females). The age range studied was from 40 to 67 years old (with an average of 50.9). Each individual was CT-scanned both in maximum inspiration and maximum expiration, so 84 scans of rib cages were ultimately studied. The data were obtained from hospital subjects who had been previously scanned as a healthy control group and compared with pathological individuals belonging to a different research project at the Hospital Universitario La Paz (Madrid, Spain). In none of the cases could any pathologies affecting skeletal thorax form be detected. The ID and sex composition are detailed in Supporting Information Table 1. Consent was given to use these CT-data for research purposes and prior to analysis all CT-data were anonymized to comply with the Helsinki declaration (Goodyear, Krleza-Jeric, & Lemmens, 2007).

2.2 | Methods

Each thorax was segmented through a semi-automatic segmentation protocol of DICOM images using the Mimics 8.0 (http://biomedical.materialise.com/mimics) software program. The post-processing of the 3D surface models of skeletal elements (cleaning, smoothing, and mesh hole-filling) was carried out with Artec Studio software (www.Artec3D.com) and the final 3D thorax models were imported into Viewbox4 software (www.dhal.com). Then, landmarks and semilandmarks for sliding (Gunz, Mitteroecker, & Bookstein, 2005) were located on thorax models following the protocol by Bastir et al. (2013). The thorax morphology is described thus by 20 homologous 3D landmarks and sliding semilandmarks on each rib (1–10) and two additional landmarks at the sternum (402 landmarks and sliding semilandmarks in each thorax). The breathing ribcage is a mobile structure with different possible morphologies. In order to best focus on static overall shape differences of the thorax, we calculated the mean shape of each individual between inspiration and expiration. In this way we finally studied 42 individuals (18 males and 24 females) in a neutral kinematic state (average).

Because of uncertainty of their location along the ribs, semilandmarks were slid along their corresponding curves with respect to the fixed landmarks in order to minimize bending energy (BE) following standardized procedures for semilandmark analyses (Gunz et al., 2005; Gunz & Mitteroecker, 2013). First, semilandmarks were slid so as to minimize BE between each specimen of the sample and the template specimen (the first thorax digitized). Then, once the average shape of the total sample was calculated, the semilandmarks were slid so as to minimize BE between each specimen of the sample and the template specimen

First, semilandmarks were slid so as to minimize BE between each specimen of the sample and the template specimen (the first thorax digitized), and a second time, once the average shape of the total sample was calculated, between each specimen and the sample average form.

Size and shape data were obtained by Generalized Procrustes Analysis (GPA) of this landmark data set (Zelditch, Swiderski, Sheets, & Fink, 2004). Thorax size was quantified as centroid size, which is defined by the square root of the sum of squared distances of a set of landmarks from their centroid (Mitteroecker & Gunz, 2009; O'Higgins, 2000). First, we studied centroid size distribution between groups in a neutral kinematic state (average between inspiration and expiration of each individual) in order to test *H1*. Then, we studied the difference in centroid size between inspiration and expiration (functional size onwards) of each individual as a proxy to test *H4*. Patterns of shape variation along the distribution were studied throughout Principal Component Analysis (PCA) in Procrustes shape space (Zelditch et al., 2004) of the thorax in a neutral kinematic state in order to explore changes in thoracic shape possibly attributed to sexual dimorphism (H2). Ordinations were calculated and shape differences of the surface associated with variations along the PC axes were visualized using EVAN Toolkit (version 1.71; http://www.evan-society.org/). In addition, in order to confirm differences in shape between males and females (also *H2*), a mean shape analysis was carried out in MorphoJ software (Klingenberg, 2011). Differences were assessed through Procrustes distance between means and a permutation test for testing equal group means. Group means were also warped and showed using EVAN Toolkit. Finally, in order to test *H3* and explore the degree to which allometry causes morphological differences, we first carried out a regression of shape (Procrustes coordinates) on size (centroid size) and analyzed the residuals of this regression model for potential sex-specific differences,

TABLE 1 Student's *t*-test results of PC1-PC3 comparisons between males and females

Centroid Size	Mean Male (CI)	Mean Female (CI)	*t*-value	*p*-value
	2834.1 (2789.2–2879.1)	2521.4 (2489.5–2553.2)	−12.22	<.01
Functional size	Mean Male (CI)	Mean Female (CI)	*t*-value	*p*-value
	41.66 (32.15–51.17)	31.26 (25.61–36.91)	−2.09	.04

Mean values with 95% confidence intervals (CI) between parentheses are shown, as well as the statistics.

similar to a MANCOVA approach (Bastir et al., 2011; Rosas & Bastir, 2002).

3 | RESULTS

Analyses revealed significant evidence for sexual dimorphism between male and female thorax in size (both in neutral kinematic state and in functional size) and shape, including the PC scores of the first component of shape space PCA, the mean shapes comparison based on Procrustes coordinates, as well as the mean shape comparison based on regression residuals.

3.1 | Size differences

Table 1 shows 95% confidence intervals which reveal statistical size differences between females and males in centroid size (CS) of the thorax in neutral kinematic status as well as in their functional size. Males are larger in neutral kinematic state than females (Mean Fem. CS = 2,521.40; Mean Male CS = 2,864.10; $t = -12.22$; $p < .01$) and they also present a larger functional size (Mean Fem. = 31.26; Mean Male = 41.67; $t = -2.09$; $p < 0.05$). These results allow us to accept *H1* and *H4*.

3.2 | Shape differences

The first three main components of the PCA explain 65.3% of the variance (see Supporting Information Table 2 for more details). Figure 1 shows variation along PC1–PC2–PC3, and polarization between groups occurs mainly along PC1. PC1 shows statistical differences between distributions of both groups (Table 2), since males are more polarized toward negative values than are females. Morphological variation along PC1 (35.4% of the variance) is related to height and width

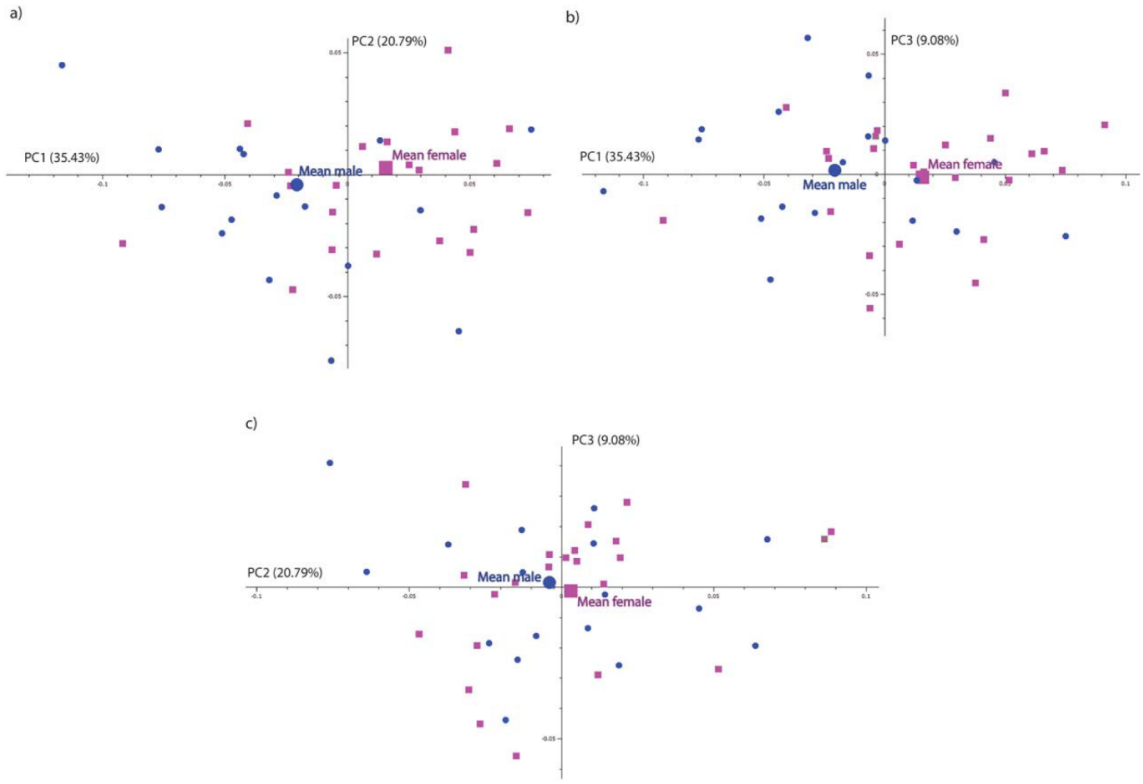

FIGURE 1 PC1-PC2 (a), PC1-PC3 (b), and PC2-PC3 (c) projections of the principal component analysis (PCA) of Procrustes coordinates. Variance explained by each PC is showed between parentheses close to each axis. Male individuals are represented by blue squares and female ones are represented by purple dots. Mean individual of each group is displayed double-sized

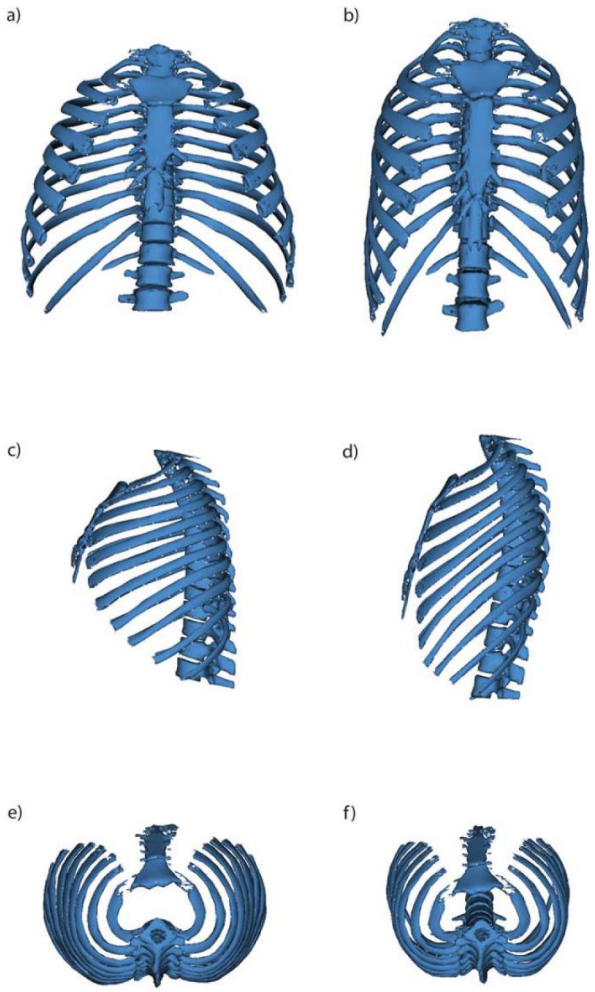

FIGURE 2 Surface warps associated to PC1 scores in frontal (a, b), lateral (c, d), and axial view (e, f). Negative values of PC1 are represented in left hand side images (a, c, d) and positive values are represented in right hand side images (b, d, f)

of the rib cage as well as to rib orientation relative to sagittal plane (rib torsion and rib declination) and sternum position (Figure 2). Morphological variation in PC2 (20.8% of the variance) is associated with thorax depth and the sagittal orientation of the distal end of the ribs of the cranial third, which is related to a volumetric expansion of this part of the rib cage (Supporting Information Figure 1). Finally, morphological variation related to PC3 (9.1% of the variance) is associated with sagittal orientation of the midshaft of the ribs, which is also related to volumetric expansion of the cranial third of the rib cage (Supporting Information Figure 2).

Morphological differences associated with PC1 are the ones linked to sexual dimorphism, whereas the ones associated with PC2 and PC3 reflect other factors of intra-specific variation. Anatomical details explained by PC1 are shown in Figure 2 and anatomical details explained by PC2 and PC3 are shown in of Supporting Information Figures 1 and 2, respectively.

Mean shape comparison of Procrustes coordinates ($d = 0.04$; $p < .01$) showed statistical differences between sexes of thoraces in neutral kinematic status. Surface warps associated with mean shapes based on Procrustes coordinates (Figure 3 and Supporting Information Figure 3; differences magnified two times in order to observe them clearly) show that thoraces in males are wider (more evident at the lower thorax) and present the ribs in a more horizontal position than females. Moreover, male thoraces are shorter craniocaudally and present the sternum in a lower position than females. Therefore, these results allow us to accept *H2*, providing a detailed explanation of differences in three-dimensional configurations.

3.3 | Size and shape covariation

Although the regression of shape on size presented statistically significant results, it is important to note that only a low percentage of total variance was predicted ($r^2 = 0.07$; $p = .03$). Moreover, as we can see in Figure 4, it is interesting to note the lack of overlap between the distributions of the sexes; this could indicate different ontogenetic trajectories for each sex. When we remove the allometric component and carry out mean comparison of regression residuals between groups, we still observe statistical shape differences between them (Proc. Dist. = 0.009; $p < .01$). We observe in the associated warps (Figure 5 and Supporting Information Figure 4; differences magnified ten times in order to observe them clearly) that the relative shortening of the thorax in males disappears when removing the allometric component. However, other features are retained, for example, the more horizontal disposition of ribs, the lower position of the sternum, and the wider thorax which is more pronounced at the lower part in males. Finally, an emergent feature is observed when removing the allometric component, since then we can observe a very different curvature of the distal part of ribs belonging to the upper thorax, which shift caudally in males and cranially in females.

TABLE 2 t-Student results of PC1–PC3 comparisons between males and females

PC1 scores	Mean Male (CI)	Mean Female (CI)	*t*-value	*p*-value
	−0.021 (−0.04 to 0.002)	0.016 (−0.002 to 0.03)	2.65	.01
PC2 scores	Mean Male (CI)	Mean Female (CI)	*t*-value	*p*-value
	−0.004 (−0.02 to 0.01)	0.003 (−0.01 to 0.02)	0.63	.53
PC3 scores	Mean Male (CI)	Mean Female (CI)	*t*-value	*p*-value
	−0.001 (−0.01 to 0.01)	0.001 (−0.01 to 0.008)	−0.37	.71

Mean values with 95% confidence intervals (CI) between parentheses are shown, as well as the statistics.

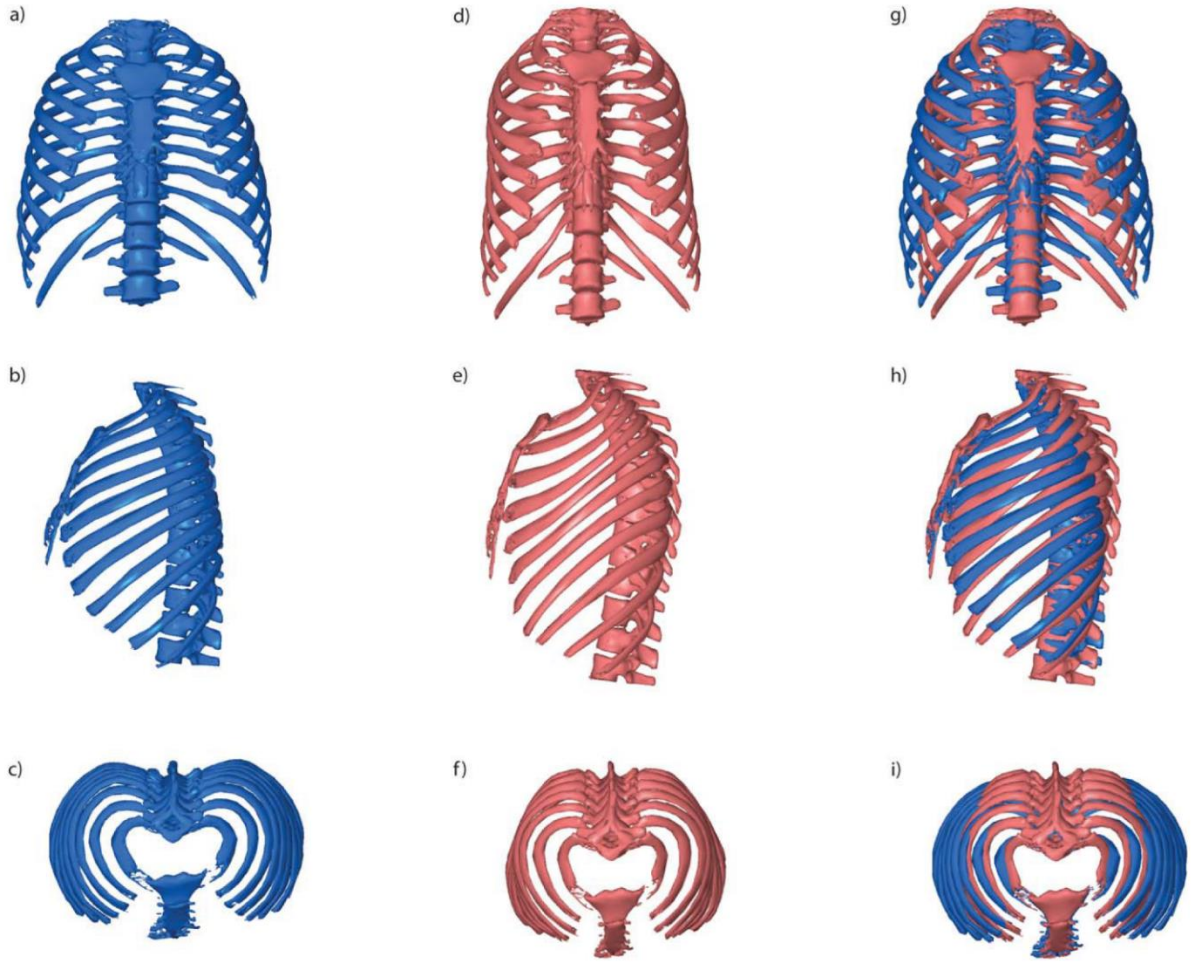

FIGURE 3 Surface warps associated to mean shapes based on Procrustes coordinates in frontal (a, d, g), lateral (b, e, h), and axial view (c, f, i). Males are displayed in blue color (left hand side images) and females are displayed in red color (central images). Warps of group means are displayed in Procrustes superimposition in the right hand side images

4 | DISCUSSION

Sexual dimorphism in the thoracic respiratory system has received less attention than that of the cranio-facial respiratory system. A few studies were carried out on this topic through 2D and 3D approaches (Bellemare et al., 2003; Bellemare, Fuamba, & Bourgeault, 2006; Shi et al., 2014; Weaver et al., 2014). These studies expanded the knowledge of sex-related differences in the human rib cage, revealing differences in both size and shape. However, detailed knowledge on the full 3D configuration (in frontal, lateral, and axial views), the possible allometric component of these differences well as the functional implications of sexual dimorphism are not well known. Additionally, some studies have looked at sexual dimorphism of the respiratory system from a functional point of view (Kaneko & Horie, 2012; Ragnarsdóttir & Kristinsdóttir, 2006; Verschakelen & Demedts, 1995), but detailed knowledge of these differences in full 3D configuration is also still missing. This study addresses sexual dimorphism of the 3D configuration of the rib cage by testing hypotheses about size and shape differences as well as sex-specific differences not related to allometry.

Larger size in males relative to females has been found in many parts of both the cranial and postcranial skeleton (Arsuaga & Carretero, 1994; Bastir et al., 2011, 2014; Bulygina et al., 2006; Carlson et al., 2007; Frayer & Wolpoff, 1985; Gama et al., 2015; Hall, 2005; Işcan & Shihai, 1995; Kranioti & Michalodimitrakis, 2009; Lam et al., 1996; Loth & Henneberg, 1996; Navega et al., 2015; Reno et al., 2003; Richmond & Jungers, 1995; Rodriguez-Perez, 2014; Rosas & Bastir, 2002; Rosas et al., 2002; Rosas et al., 2015; Rosas et al., 2016; Ruff, 1987; Steyn & Işcan, 1998; Wood et al., 1991). Regarding the respiratory apparatus, absolutely and relatively larger cranial airways have been attributed to males both in the soft and hard tissues (Bastir et al., 2011; Bulygina et al., 2006; Hall, 2005; Holton et al., 2014; Rosas & Bastir, 2002); this has been linked to body composition and bioenergetics (Bitar et al., 1999; Froehle & Churchill, 2009; Hall, 2005; Wells, 2007) since males have a greater demand for oxygen than do females due to males' larger lean mass and lower fat mass percentage.

Because of the functional link between the cranio-facial (nasal cavity) and post-cranial (thorax) respiratory systems (Bastir, 2008), greater oxygen intake through the nasal cavities should also be reflected in the

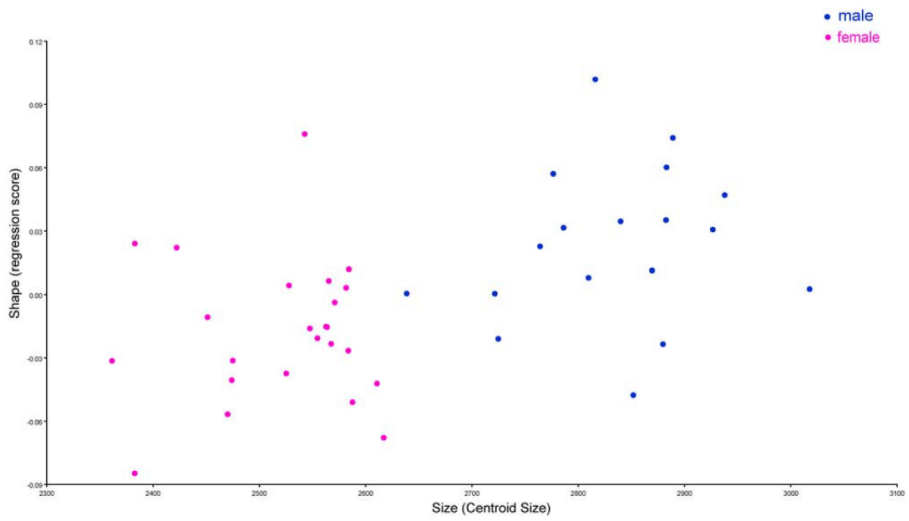

FIGURE 4 Regression analysis of Procrustes coordinates (shape) on centroid size (size). Males are displayed as blue dots and females are represented by purple dots

thoracic skeleton. Moreover, since human males generally present a larger body size than females, and since lung size scales isometrically with body size in static allometry, differences in thorax size could also be expected in humans.

4.1 | Size differences

We evaluated differences in thorax size through a centroid size (CS) approach. Our results show statistical differences between males and females. Males show 12.4% larger thoraces than females in a neutral kinematic state (Table 1). This supports previous findings made by Bellemare et al. (2003) in lung size and as well as our *H1* (which predicts that males have larger thoraces than females). Regarding thoracic expansion during inspiration, we studied this variation in thorax size through the approach of functional size, observing that males present a statistically larger size increase during inspiration than females (33.3% larger; taking female functional size mean as the 100% reference; see Table 1). This is consistent with the larger cranial airways in males proposed by previous authors both in the skeleton (Bastir et al., 2011; Rosas & Bastir, 2002) and in the soft tissue (Hall, 2005; Holton et al., 2014) and allows us to accept our *H3* (which predicts that sex-related shape differences are caused by allometric factors).

It is interesting to note that the 12.4% absolute size difference does not correspond to the 33% difference in functional size. We believe that this is due to geometric features that influence the capacity of thoracic expansion. Barrel-shaped inferior expansions appear to produce less volumetric difference than pyramidal-shaped expansion, at least at the pulmonary level (Torres-Tamayo et al., 2016). The larger volumetric expansion of the male thorax compared to the female thorax could allow for the greater oxygen intake needed to sustain males' higher BMR, which has been observed across different populations (Froehle & Churchill, 2009).

4.2 | Shape differences

Mean shape comparisons and PC1 scores based on 3D Procrustes shape coordinates showed statistical differences between both sexes. In accordance with previous findings (Bellemare et al., 2003; Shi et al., 2014; Weaver et al., 2014), we confirm that male thoraces are relatively broader and shorter than those of females. In addition, our findings demonstrate that this feature is more evident at the lower thorax (Figure 3), which was not specified by Bellemare et al. (2003). The relatively larger craniocaudal length of females compared to that of males (as observed in Figure 3) could be related to the scaling process during the Procrustes superimposition with wider male rib cages. However, female thoraces have been hypothesized to be adapted to accommodate volumetric expansion during pregnancy (Bellemare et al., 2003). Similarly, the relatively larger cranio-caudal length observed in females (Figure 3) could be involved in housing the internal reproductive organs as well as the accommodation of a potential fetus during pregnancy. This does not exclude that other factors, such as the muscles arising from the upper limbs or pelvis, could also be involved in the differences observed in the upper and lower thorax. We confirm that female ribs are more declined than those of males and that the sternum is located in a higher position in females (Figure 3). However, our results do not allow us to support the hypothesis that males have a deeper thorax in males than females (as proposed by Shi et al., 2014), since differences in thorax depth between sexes are not observed in the surface warps associated with mean comparison nor in the ones associated with PC1 scores (Figures 2 and 3). However, although PC2 clearly reflects variation in thorax depth, our results show that this is unrelated to sexual dimorphism and could reflect intra-specific variation.

4.3 | Allometric implications

Regression analysis of shape on size showed a statistically significant correlation between both factors ($p = .03$). However, the percentage of

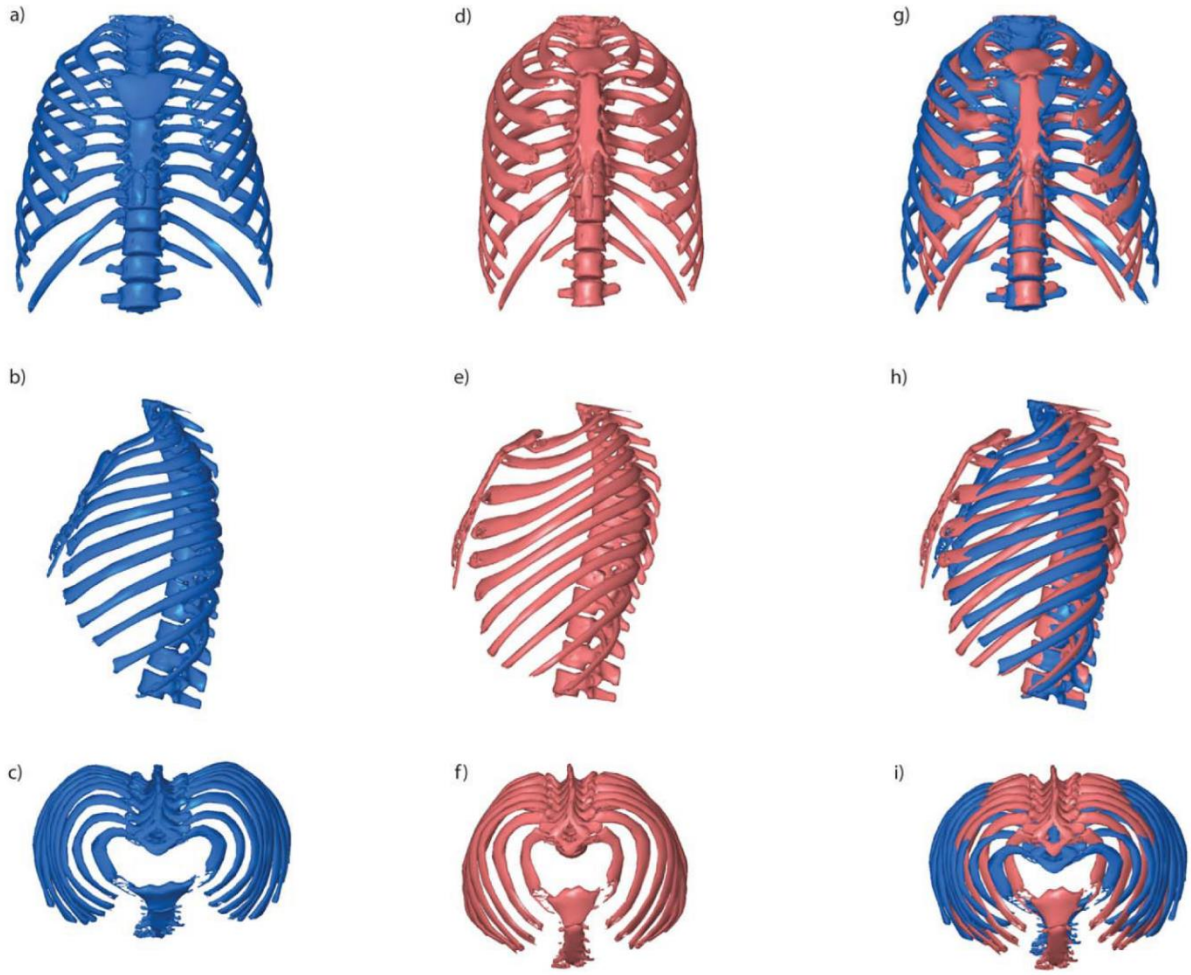

FIGURE 5 Surface warps associated to mean shapes based on regression residuals in frontal (a, d, g), lateral (b, e, h), and axial view (c, f, i). Males are displayed in blue color (left hand side images) and females are displayed in red color (central images). Warps of group means are displayed in Procrustes superimposition in the right hand side images

total variation explained was low ($r^2 = 0.0722$). More interestingly, because of the lack of overlap between the distributions of the sexes (Figure 4), we hypothesize different ontogenetic trajectories for each sex. Furthermore, when we carried out mean comparisons of regression residuals, we still observed statistical shape differences between males and females ($d = 0.009$; $p < .01$). This supports the view that the male thorax is not an allometrically scaled version of a female thorax and that shape differences may be caused by different ontogenetic trajectories.

Different trajectories during postnatal ontogeny in the respiratory system between sexes have been observed in human lung volumes or alveolar surface areas (Becklake & Kauffman, 1999; Thurlbeck, 1982). Specifically, Thurlbeck (1982) showed that boys have larger lungs than girls at the same age and body size, a difference that becomes significant at the age of two or at a height of 110 cm. Ontogenetic differences between sexes have also been observed in the cranio-facial respiratory system, for example, in the human face (Bulygina et al., 2006) or nose (Holton et al., 2014).

As for shape, when removing the allometric component the shorter thorax in males is not detected, but other features, such as males' broader thorax (more evident at the lower part), or a higher sternum in females, are observed in the same way as before removing the allometric component. However, other features, such as the declination of the ribs, seem to be combined with an emergent phenomenon not fully observed previously: rib torsion. Males and females seem to differ in the torsion pattern of the distal part of the rib at the upper thorax (Figure 4): in males they shift cranially, while in females they shift caudally. It is important to note that while this feature is observed while looking at the thorax in anatomical connection, a recent study (García-Martínez et al., 2016) showed that rib torsion is a morphological pattern more easily observed when looking at individual ribs.

Regarding sexual dimorphism of individual ribs, some studies have addressed this question from a forensic point of view. Specifically, the width and height of the sternal end of the human fourth rib were proposed as dimorphic in the mid-80s (Işcan, 1985), a fact that was later confirmed in different populations (Koçak, Aktas, Ertürk, Aktas, &

Yemisçigil, 2003—Turkish population; Macaluso, Rico, Santos, & Lucena, 2012—Spanish population; Meena, Mittal, Chouksey, & Rani, 2015 —Indian population; Wiredu, Kumoji, Seshadri, & Biritwum, 1999—Ghana population). Meanwhile, Bellemare et al. (2006) quantified the rib length of the third, sixth, and ninth ribs of a Canadian population and found no statistical differences in this measurement between both sexes. Later, Cirillo & Henneberg (2012) quantified sexual dimorphism in human ribs through seven traditional measurements both at the proximal and distal end, concluding that although males were larger in some dimensions, a low level of sexual dimorphism was detected in the population they studied.

Although these studies expanded our knowledge of dimorphic features observed in human ribs, rib architecture is defined by complex 3D curves and two-dimensional measurements that are difficult to quantify for the entire rib form, thus complicating the study of sexual dimorphism in ribs. Future studies should address sexual dimorphism of individual ribs from a 3D point of view in order to confirm previous findings.

4.4 | Functional implications

Biomechanical action of intercostal muscles elevates ribs from a declined state to a horizontal state; this process produces thoracic inspiration (De Troyer et al., 2005). When ribs are more declined (as found in females), the intercostal muscles could raise ribs efficiently producing thoracic breathing. However, when ribs are less declined (as found in males) the intercostal muscles cannot raise the ribs effectively and abdominal breathing has to compensate the lack of intercostal muscle efficiency throughout the diaphragmatic action.

Following this principle, Bellemare et al. (2003) proposed a mechanical advantage of the inspiratory muscles in females over those of males due to the greater declination of females' ribs. Despite the hypothetical lower efficiency of inspiratory muscles in males, we observed that they present a 33% larger functional size than females, which is consistent with the higher oxygen intake proposed in the upper airways (Rosas & Bastir, 2002). To explain this, differences in the thoraco-abdominal configuration have been observed to impact the function of the respiratory muscles (De Troyer et al., 2005; Goldman et al., 1978; Grassino et al., 1978; Pinet, 2004). Since abdominal breathing (related to diaphragmatic action) has been observed to be stronger in males, at least in some situations (Kaneko & Horie, 2012; Ragnarsdóttir & Kristinsdóttir, 2006; Verschakelen & Demedts, 1995), we can deduce that the aforementioned male thorax morphology (wider at the caudal part) leads their functional size to be greater than that of females. This difference is probably linked to the stronger diaphragmatic action found in males. It is important to note that if this hypothesis is accepted and a different diaphragmatic contribution is accepted for males, we should expect different breathing patterns between groups, which should be tested in future studies.

Additionally, it is important to note that a stronger diaphragmatic action supported by the horizontal orientation of male ribs and medio-lateral expansion of the lower thorax mentioned above could imply an advantage for physical activity of high intensity or endurance. This is because the diaphragm has traditionally been observed to be more resistant to fatigue than the intercostal muscles during breathing (Derenne, Macklem, & Roussos, 1978; Gallagher, Hof, & Younes, 1985; Roussos, 1985). It could also be essential for understanding the evolution of the thorax in different hominin species. For example, Neanderthals have been shown to present a medio-lateral expansion of the lower thorax compared to modern humans (Bastir et al., 2015; Franciscus & Churchill, 2002; García-Martínez et al., 2014; Gómez-Olivencia, Eaves-Johnson, Franciscus, Carretero, & Arsuaga, 2009) and also a greater energetic expenditure than modern humans related to the greater oxygen demand associated with high levels of activity (Churchill, 2006).

4.5 | Limitations of the study

This study addressed sexual dimorphism of the rib cage in anatomical connection by collecting information of ribs 1–10. Ribs 11 and 12 could not be digitized because no CT-data from this area were available. Therefore, future studies must address this issue. This study is based on a Spanish population, so the results presented here should also be tested in other populations. Finally, here we addressed the size differences between inspiration and expiration through a centroid size approach, but future studies should combine these measurements with physiological or volumetric values in order to confirm our results.

4.6 | Conclusions of the study

For the first time, this study tests for sex-related differences both in size and shape of the rib cage in a European population through the use of a 3D approach that accounts for allometric and non-allometric factors with functional implications. Our findings allow us to confirm results observed in 2D by previous authors of a larger thorax size in males than in females. However, we add that males also showed a larger functional size than females due to males' greater inspiratory size increase. We confirm sex-related differences in shape pointed out by previous authors, but we also provide a detailed explanation of these differences in frontal, superior, and lateral views: we observed that male rib cages are wider than females ones, a fact that is more evident at the caudal part, and that the sternum is in a higher position in females. We also observed that male ribs are more horizontally oriented than those of females and we did not find differences in thorax depth between sexes. Additionally, we conclude that features like the thorax shortening observed in males are only caused by size differences (allometric factors), whereas other differences, such as the thorax widening observed in males or a higher position of the sternum in females, are not caused by allometric factors. We also hypothesize that differences observed in shape between groups are not caused by allometric scaling; rather, they may be caused by different ontogenetic trajectories for each sex.

ACKNOWLEDGEMENTS

This research is funded by CGL2012-37279 Project from Ministerio de Economía y Competitividad (MINECO, Spain) and the Leakey

Foundation. The authors acknowledge the Paleoanthropology group of Museo Nacional de Ciencias Naturales for support, specially FJRP, LPC and AIFE for discussion. They also thank copy editor Zach Tobias (zstobias@gmail.com) for proofread and correct the manuscript for proper English grammar.

AUTHOR CONTRIBUTIONS

Conceived and designed the experiments: DGM, MB. Performed the experiments: DGM MB. Analyzed the data: DGM MB. Contributed discussion/materials/analysis tools: DGM MB NTT FGR ITS. Wrote the manuscript: DGM.

REFERENCES

Arsuaga, J. L., & Carretero, J. M. (1994). Multivariate analysis of the sexual dimorphism of the hip bone in a modern human population and in early hominids. *American Journal of Physical Anthropology*, *93*, 241–257.

Bastir, M. (2008). A systems-model for the morphological analysis of integration and modularity in human craniofacial evolution. *Journal of Anthropological Science*, *86*, 37–58.

Bastir, M., García-Martínez, D., Estalrrich, A., García-Tabernero, A., Huguet, R., Ríos, L., … Rosas, A. (2015). The relevance of the first ribs of the el sidrón site (Asturias, Spain) for the understanding of the neandertal thorax. *Journal of Human Evolution*, *80*, 64–73.

Bastir, M., García Martínez, D., Recheis, W., Barash, A., Coquerelle, M., Rios, L., … O'higgins, P. (2013). Differential growth and development of the upper and lower human thorax. *PLoS One*, *8*, e75128.

Bastir, M., Godoy, P., & Rosas, A. (2011). Common features of sexual dimorphism in the cranial airways of different human populations. *American Journal of Physical Anthropology*, *146*, 414–422.

Bastir, M., Higuero, A., Ríos, L., & García Martínez, D. (2014). Three-dimensional analysis of sexual dimorphism in human thoracic vertebrae: Implications for the respiratory system and spine morphology. *American Journal of Physical Anthropology*, *155*, 513–521.

Becklake, M. R., & Kauffmann, F. (1999). Gender differences in airway behaviour over the human life span. *Thorax*, *54*, 1119–1138.

Bellemare, F., Fuamba, T., & Bourgeault, A. (2006). Sexual dimorphism of human ribs. *Respiratory Physiology & Neurobiology*, *150*, 233–239.

Bellemare, F., Jeanneret, A., & Couture, J. (2003). Sex differences in thoracic dimensions and configuration. *American Journal of Respiratory and Critical Care Medicine*, *168*, 305–312.

Bitar, A., Fellmann, N., Vernet, J., Coudert, J., & Vermorel, M. (1999). Variations and determinants of energy expenditure as measured by whole-body indirect calorimetry during puberty and adolescence. *The American Journal of Clinical Nutrition*, *69*, 1209–1216.

Bulygina, E., Mitteroecker, P., & Aiello, L. (2006). Ontogeny of facial dimorphism and patterns of individual development within one human population. *American Journal of Physical Anthropology*, *131*, 432–443.

Carlson, K. J., Grine, F. E., & Pearson, O. M. (2007). Robusticity and sexual dimorphism in the postcranium of modern hunter-gatherers from Australia. *American Journal of Physical Anthropology*, *134*, 9–23.

Churchill, S. E. (2006). Bioenergetic perspectives on Neanderthal thermoregulatory and activity budgets. In: Harvati, K,Harrison, T, editors. Neanderthals revisited: New approaches and perspectives (pp. 113–133). New York: Springer.

Cirillo, J., & Henneberg, M. (2012). Sequencing human ribs into anatomical order by quantitative multivariate methods. *HOMO—Journal of Comparative Human Biology*, *63*, 182–201.

De Troyer, A., Kirkwood, P. A., & Wilson, T. A. (2005). Respiratory action of the intercostal muscles. *Physiological Reviews*, *85*, 717–756.

Demet, G. V., Gutierrez, C. V., Valenza, M. C., Lorenzo, C. M., & Peinado, F. M. O. (2011). Movilidad torácica ya bdominal en adultos jóvenes de ambos sexos sin patología conocida. *Scientia: Revista Multidisciplinar De Ciencias De La Salud*, *16*, 85–94.

Derenne, J. P., Macklem, P., & Roussos, C. (1978). The respiratory muscles: Mechanics, control, and pathophysiology. III. *American Review of Respiratory Disease*, *118*, 581–601.

Frayer, D. W., & Wolpoff, M. H. (1985). Sexual dimorphism. *Annu Rev Anthropol*, *14*, 429–473.

Franciscus, R. G., & Churchill, S. E. (2002). The costal skeleton of Shanidar 3 and a reappraisal of Neandertal thoracic morphology. *Journal of Human Evolution*, *42*, 303–356.

Froehle, A. W., & Churchill, S. E. (2009). Energetic competition between Neandertals and anatomically modern humans. *PaleoAnthropology*, *2009*, 96–116.

Gallagher, C., Hof, V. I., & Younes, M. (1985). Effect of inspiratory muscle fatigue on breathing pattern. *Journal of Applied Physiology*, *59*, 1152–1158.

Gama, I., Navega, D., & Cunha, E. (2015). Sex estimation using the second cervical vertebra: A morphometric analysis in a documented Portuguese skeletal sample. *International Journal of Legal Medicine*, *129*, 365–372.

García-Martínez, D., Barash, A., Recheis, W., Utrilla, C., Torres Sánchez, I., García Río, F., & Bastir, M. (2014). On the chest size of Kebara 2. *Journal of Human Evolution*, *70*, 69–72.

García-Martínez, D., Recheis, W., & Bastir, M. (2016). Ontogeny of 3D rib curvature and its importance for the understanding of human thorax development. *American Journal of Physical Anthropology*, *159*, 423–431.

Goldman, M. D., Grassino, A., Mead, J., & Sears, T. A. (1978). Mechanics of the human diaphragm during voluntary contraction: Dynamics. *Journal of Applied Physiology*, *44*, 840–848.

Gómez-Olivencia, A., Eaves-Johnson, K. L., Franciscus, R. G., Carretero, J. M., & Arsuaga, J. L. (2009). Kebara 2: New insights regarding the most complete Neandertal thorax. *Journal of Human Evolution*, *57*, 75–90.

Goodyear, M. D. E., Krleza-Jeric, K., & Lemmens, T. (2007). The declaration of Helsinki. *BMJ: British Medical Journal*, *335*, 624–625.

Grassino, A., Goldman, M. D., Mead, J., & Sears, T. A. (1978). Mechanics of the human diaphragm during voluntary contraction: Statics. *Journal of Applied Physiology*, *44*, 829–839.

Gunz, P., Mitteroecker, P., & Bookstein, F. L. (2005). *Semilandmarks in three dimensions. Modern morphometrics in physical anthropology* (pp. 73–98). New York: Kluwer Press.

Hall, R. L. (2005). Energetics of nose and mouth breathing, body size, body composition, and nose volume in young adult males and females. *American Journal of Human Biology*, *17*, 321–330.

Harms, C. A., McClaran, S. R., Nickele, G. A., Pegelow, D. F., Nelson, W. B., & Dempsey, J. A. (1998). Exercise-induced arterial hypoxaemia in healthy young women. *The Journal of Physiology*, *507*, 619–628.

Holton, N. E., Yokley, T. R., Froehle, A. W., & Southard, T. E. (2014). Ontogenetic scaling of the human nose in a longitudinal sample: Implications for genus homo facial evolution. *American Journal of Physical Anthropology*, *153*, 52–60.

Işcan, M. (1985). Osteometric analysis of sexual dimorphism in the sternal end of the rib. *Journal of Forensic Sciences*, *30*, 1090–1099.

Işcan, M. Y., & Shihai, D. (1995). Sexual dimorphism in the Chinese femur. *Forensic Science international*, *74*, 79–87.

Jammes, Y., Auran, Y., Gouvernet, J., Delpierre, S., & Grimaud, C. (1979). Ventilatory pattern of conscious man according to age and morphology. *Bulletin Europeen de Physiopathologie Respiratoire-Clinical Respiratory Physiology*, *15*, 527–540.

Kaneko, H., & Horie, J. (2012). Breathing movements of the chest and abdominal wall in healthy subjects. *Respiratory Care*, *57*, 1442–1451.

Klingenberg, C. P. (2011). MorphoJ: An integrated software package for geometric morphometrics. *Molecular Ecology Resources*, *11*, 353–357.

Koçak, A., Aktas, E., Ertürk, S., Aktas, S., & Yemisçigil, A. (2003). Sex determination from the sternal end of the rib by osteometric analysis. *Legal Medicine*, *5*, 100–104.

Kranioti, E. F., & Michalodimitrakis, M. (2009). Sexual dimorphism of the humerus in contemporary cretans—A population-specific study and a review of the literature. *Journal of Forensic Sciences*, *54*, 996–1000.

Lam, Y. M., Pearson, O. M., & Smith, C. M. (1996). Chin morphology and sexual dimorphism in the fossil hominid mandible sample from Klasies river Mouth. *American Journal of Physical Anthropology*, *100*, 545–557.

Loth, S. R., & Henneberg, M. (1996). Mandibular ramus flexure: A new morphologic indicator of sexual dimorphism in the human skeleton. *American Journal of Physical Anthropology*, *99*, 473–485.

Macaluso, P. J., Rico, A., Santos, M., & Lucena, J. (2012). Osteometric sex discrimination from the sternal extremity of the fourth rib in a recent forensic sample from southwestern Spain. *Forensic Science International*, *223*, 1–375. e371–e375.

Meena, M. C., Mittal, S., Chouksey, V. K., & Rani, Y. (2015). Sex determination from fourth rib by osteometric analysis. *International Journal of Forensic Science & Pathology*, *3*, 148–151.

Mitteroecker, P., & Gunz, P. (2009). Advances in geometric morphometrics. *Evolutionary Biology*, *36*, 235–247.

Navega, D., Vicente, R., Vieira, D. N., Ross, A. H., & Cunha, E. (2015). Sex estimation from the tarsal bones in a portuguese sample: A machine learning approach. *International Journal of Legal Medicine*, *129*, 651–659.

O'Higgins, P. (2000). The study of morphological variation in the hominid fossil record: Biology, landmarks and geometry. *Journal of Anatomy*, *197*, 103–120.

Pinet, C. (2004). Propriétés mécaniques et fonctionnelles de la cage thoracique. *Revue Des Maladies Respiratoires*, *21*, 652–655.

Ragnarsdóttir, M., & Kristinsdóttir, E. K. (2006). Breathing movements and breathing patterns among healthy men and women 20–69 years of Age. *Respiration*, *73*, 48–54.

Richmond, B. G., & Jungers, W. L. (1995). Size variation and sexual dimorphism in australopithecus afarensis and living hominoids. *Journal of Human Evolution*, *29*, 229–245.

Reno, P. L., Meindl, R. S., McCollum, M. A., & Lovejoy, C. O. (2003). Sexual dimorphism in australopithecus afarensis was similar to that of modern humans. *Proceedings of the National Academy of Sciences United States of America*, *100*, 9404–9409.

Rodriguez-Perez, F. J. (2014). Alometría y dimorfismo sexual de la clavícula de Homo sapiens y su comparación con la de neandertal (M.Sc. Dissertation). Autonomous University of Madrid (Spain).

Rosas, A., & Bastir, M. (2002). Thin-plate spline analysis of allometry and sexual dimorphism in the human craniofacial complex. *American Journal of Physical Anthropology*, *117*, 236–245.

Rosas, A., Bastir, M., Martínez-Maza, C., & Bermúdez de Castro, J. M. (2002). Sexual dimorphism in the Atapuerca-SH hominids: The evidence from the mandibles. *Journal of Human Evolution*, *42*, 451–474.

Rosas, A., Pérez-Criado, L., Bastir, M., Estalrrich, A., Huguet, R., García-Tabernero, A., … De la Rasilla, M. (2015). A geometric morphometrics comparative analysis of Neandertal humeri (epiphyses-fused) from the El Sidrón cave site (Asturias, Spain). *Journal of Human Evolution*, *82*, 51–66.

Rosas, A., Rodriguez-Perez, F. J., Bastir, M., Estalrrich, A., Huguet, R., García-Tabernero, A., Pastor, J. F., & de la Rasilla, M. (2016). Adult Neandertal clavicles from the El Sidrón site (Asturias, Spain) in the context of Homo pectoral girdle evolution. *Journal of Human Evolution*, *95*, 55–67.

Roussos, C. (1985). Function and fatigue of respiratory muscles. *CHEST Journal*, *88*, 124S–132S.

Ruff, C. B. (1987). Sexual dimorphism in human lower limb bone structure: Relationship to subsistence strategy and sexual division of labor. *Journal of Human Evolution*, *16*, 391–416.

Ruff, C. (2002). Variation in human body size and shape. *Annual Review of Anthropology*, *31*, 211–232.

Shi, X., Cao, L., Reed, M. P., Rupp, J. D., Hoff, C. N., & Hu, J. (2014). A statistical human rib cage geometry model accounting for variations by age, sex, stature and body mass index. *Journal of Biomechanics*, *47*, 2277–2285.

Stahl, W. R. (1967). Scaling of respiratory variables in mammals. *Journal of Applied Physiology*, *22*, 453–460.

Steyn, M I., & Işcan, M. Y., (1998). Sexual dimorphism in the crania and mandibles of South African whites. *Forensic Science International*, *98*, 9–16.

Spalteholz, W. (1970). *Atlas de anatomía humana* (5a ed). Barcelona: Ed. Labor, S. A.

Torres-Tamayo, S. N., García-Martínez, D., Utrilla, C., Torres, I., García-Río, F., & Bastir, M. (2016). Geometric morphometrics of sexual dimorphism and pulmonary kinematics in Homo Sapiens. *American Journal of Physical Anthropology*, *159*, 316.

Thurlbeck, W. M. (1982). Postnatal human lung growth. *Thorax*, *37*, 564–571.

Verschakelen, J. A., & Demedts, M. G. (1995). Normal thoracoabdominal motions. Influence of sex, age, posture, and breath size. *American Journal of Respiratory and Critical Care Medicine*, *151*, 399–405.

Weaver, A. A., Schoell, S. L., & Stitzel, J. D. (2014). Morphometric analysis of variation in the ribs with age and sex. *Journal of Anatomy*, *225*, 246–261.

Wells, J. C. K. (2007). Sexual dimorphism of body composition. *Best Practice & Research Clinical Endocrinology & Metabolism*, *21*, 415–430.

Wiredu, E. K., Kumoji, R., Seshadri, R., & Biritwum, R. B. (1999). Osteometric analysis of sexual dimorphism in the sternal end of the rib in a West African population. *Journal of Forensic Sciences*, *44*, 921–925.

Wood, B., Li, Y., & Willoughby, C. (1991). Intraspecific variation and sexual dimorphism in cranial and dental variables among higher primates and their bearing on the hominid fossil record. *Journal of Anatomy*, *174*, 185.

Zelditch, M. L., Swiderski, D. L., Sheets, H. D., & Fink, W. L. (2004). *Geometric morphometrics for biologists: A primer*. San Diego: Elsevier.

SUPPORTING INFORMATION

Additional Supporting Information may be found in the online version of this article.

Supporting information

Table S1: Id and sex of each individual in the sample.

Id	Sex
IdiPAZ780419	Female
IdiPAZ2001326	Female
IdiPAZ1098479	Female
IdiPAZ1376099	Female
IdiPAZ1638379	Female
IdiPAZ1687535	Female
IdiPAZ611461	Female
IdiPAZ616945	Female
IdiPAZ627267	Female
IdiPaz2147359	Female
IdiPAZ2508332	Female
IdiPAZ675169	Female
IdiPAZ677093	Female
IdiPAZ1392762	Female
IdiPAZ717040	Female
IdiPAZ780418	Female
IdiPAZ796821	Female
IdiPAZ853292	Female
IdiPAZ1933028	Female
IdiPAZ2664993	Female
IdiPAZ1937532	Female
IdiPAZ2688253	Female
IdiPAZ1199748	Female
IdiPAZ1231084	Female
IdiPAZ1497971	Male
IdiPAZ152534	Male
IdiPAZ158324	Male
IdiPAZ1784006	Male
IdiPAZ1989386	Male
IdiPAZ2134971	Male
IdiPAZ2318866	Male
IdiPAZ2466803	Male
IdiPAZ2587539	Male
IdiPAZ2657162	Male
IdiPAZ2666564	Male
IdiPAZ2699703	Male
IdiPAZ2715683	Male
IdiPAZ2723458	Male
IdiPAZ2749218	Male
IdiPAZ2783237	Male
IdiPAZ674564	Male
IdiPAZ683814	Male

Table S2: Percentage of variance and cumulative variance explained by each component of the PCA.

	Variance (%)	Cumulative Variance
PC 1	35.4275	35.4275
PC 2	20.7918	56.2193
PC 3	9.0799	65.2992
PC 4	7.65085	72.9501
PC 5	4.62057	77.5706
PC 6	3.34386	80.9145
PC 7	2.45385	83.3683
PC 8	1.92105	85.2894
PC 9	1.64918	86.9386
PC 10	1.37357	88.3121
PC 11	1.17023	89.4824
PC 12	1.07428	90.5567
PC 13	0.917942	91.4746
PC 14	0.800181	92.2748
PC 15	0.720702	92.9955
PC 16	0.661153	93.6566
PC 17	0.577313	94.2339
PC 18	0.558289	94.7922
PC 19	0.490577	95.2828
PC 20	0.45855	95.7414
PC 21	0.437241	96.1786
PC 22	0.407192	96.5858
PC 23	0.331207	96.917
PC 24	0.317937	97.2349
PC 25	0.281888	97.5168
PC 26	0.260039	97.7769
PC 27	0.241682	98.0186
PC 28	0.227991	98.2465
PC 29	0.205411	98.452
PC 30	0.196895	98.6488
PC 31	0.190344	98.8392
PC 32	0.174768	99.014
PC 33	0.163181	99.1771
PC 34	0.147807	99.3249
PC 35	0.133039	99.458
PC 36	0.118608	99.5766
PC 37	0.11203	99.6886
PC 38	0.104742	99.7934
PC 39	0.0857527	99.8791

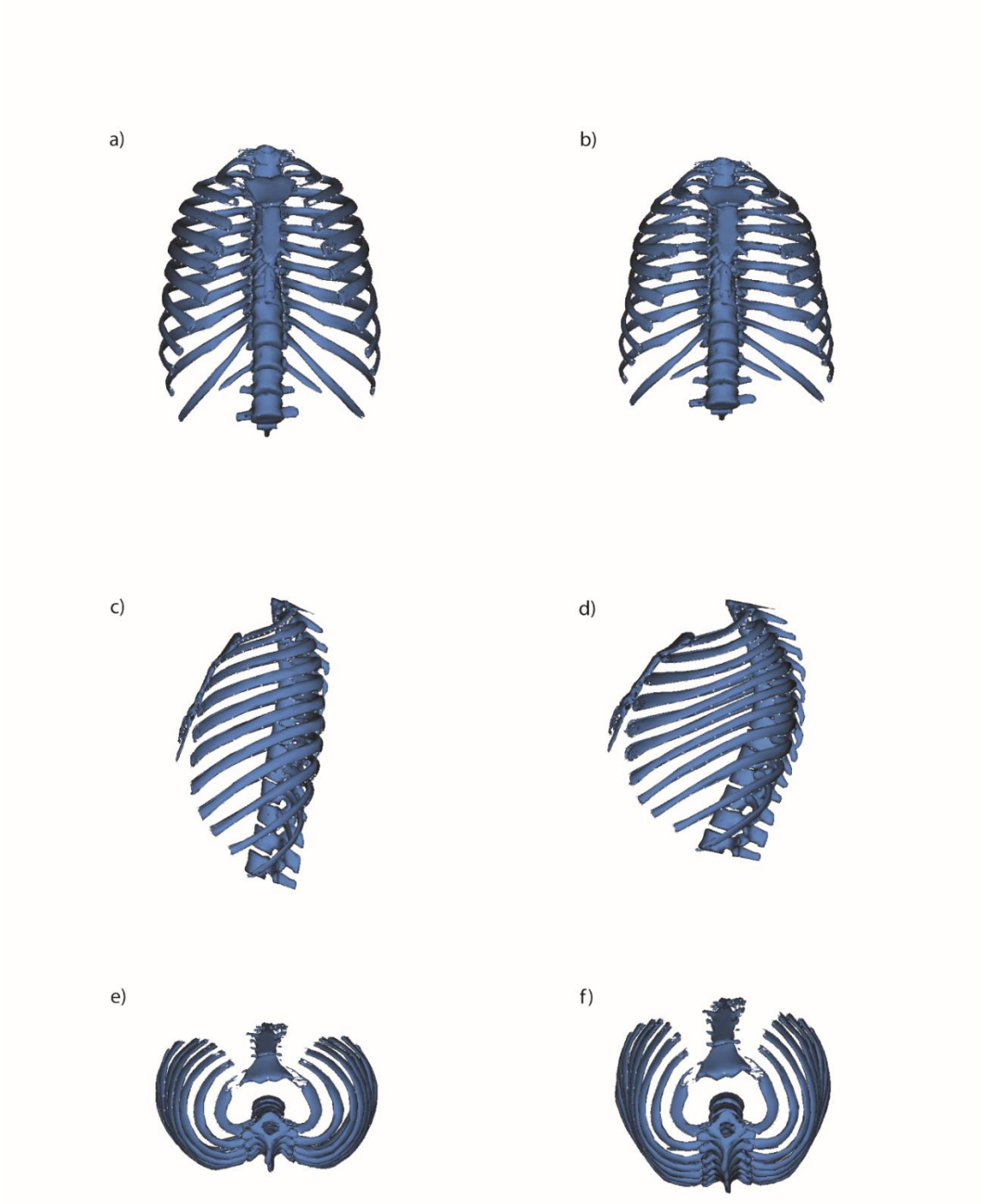

Figure S1: surface warps associated to PC2 scores in frontal (a, b), lateral (c, d) and axial view (e, f). Negative values of PC1 a represented in left hand side images (a, c, d) and positive values are represented in right hand side images (b, d, f).

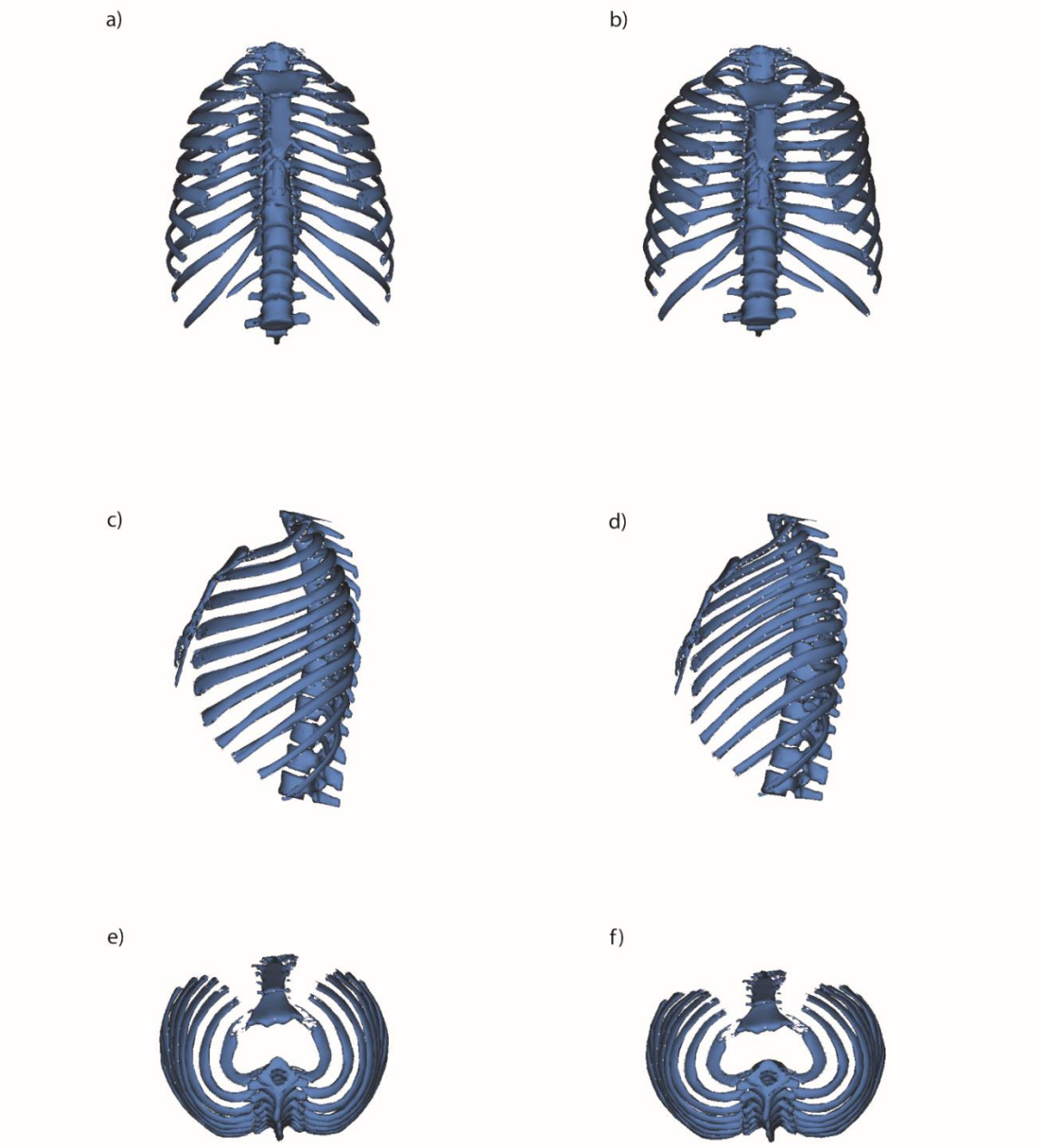

Figure S2: surface warps associated to PC3 scores in frontal (a, b), lateral (c, d) and axial view (e, f). Negative values of PC1 a represented in left hand side images (a, c, d) and positive values are represented in right hand side images (b, d, f).

CAPÍTULO VI – RESULTADOS: ANATOMÍA FUNCIONAL DE LA CAJA TORÁCICA HUMANA

Los resultados obtenidos en referencia al **objetivo 3 "Contribuciones al conocimiento de la anatomía funcional de la caja torácica humana"** han sido íntegramente publicados en el siguiente artículo:

Bastir, M., **García-Martínez, D**., Torres-Tamayo, N., Sanchís-Gimeno, J. A., O'Higgins, P., Utrilla, C., Torres-Sánchez, I., García-Río, F., 2017. In Vivo 3D Analysis of Thoracic Kinematics: Changes in size and shape during breathing and their implications for respiratory function in recent humans and fossil hominins. Anatomical Record 300, 255-264.

DOI: 10.1002/ar.23503

In Vivo 3D Analysis of Thoracic Kinematics: Changes in Size and Shape During Breathing and Their Implications for Respiratory Function in Recent Humans and Fossil Hominins

MARKUS BASTIR,[1]* DANIEL GARCÍA-MARTÍNEZ,[1,2] NICOLE TORRES-TAMAYO,[1] JUAN ALBERTO SANCHIS-GIMENO,[3] PAUL O'HIGGINS,[4] CRISTINA UTRILLA,[5] ISABEL TORRES SÁNCHEZ,[5] AND FRANCISCO GARCÍA RÍO[5]

[1]Department of Paleobiology, Paleoanthropology Group, Museo Nacional de Ciencias Naturales, CSIC, Madrid, Spain
[2]Department of Biology, Science Faculty, Autónoma University of Madrid, Madrid, Spain
[3]Department of Anatomy and Human Embryology Faculty of Medicine, University of Valencia, Valencia, Spain
[4]Department of Archaeology and Hull York Medical School, The University of York, York, United Kingdom
[5]Hospital Universitario La Paz Biomedical Research Institute (Idipaz), Madrid, Spain

ABSTRACT

The human ribcage expands and contracts during respiration as a result of the interaction between the morphology of the ribs, the costovertebral articulations and respiratory muscles. Variations in these factors are said to produce differences in the kinematics of the upper thorax and the lower thorax, but the extent and nature of any such differences and their functional implications have not yet been quantified. Applying geometric morphometrics we measured 402 three-dimensional (3D) landmarks and semilandmarks of 3D models built from computed tomographic scans of thoraces of 20 healthy adult subjects in maximal forced inspiration (FI) and expiration (FE). We addressed the hypothesis that upper and lower parts of the ribcage differ in kinematics and compared different models of functional compartmentalization. During inspiration the thorax superior to the level of the sixth ribs undergoes anteroposterior expansion that differs significantly from the medio-lateral expansion characteristic of the thorax below this level. This supports previous suggestions for dividing the thorax into a pulmonary and diaphragmatic part. While both compartments differed significantly in mean size and shape during FE and FI the size changes in the lower compartment were significantly larger. Additionally, for the same degree of kinematic shape change, the pulmonary thorax changes less in size than the

This article includes AR WOW Videos. Video 1 can be viewed at http://bcove.me/3imgemwk.

Grant sponsor: Spanish Ministry of Economy and Competitiveness; Grant numbers: CGL2012-37279, CGL2015-63648-P; MINECO; Grant sponsor: Ministry of Health, Spain (Fondo de Investigación Sanitaria); Grant number: PI10/02089; Grant sponsor: Leakey Foundation.

*Correspondence to: Dr. Markus Bastir. Museo Nacional de Ciencias Naturales, CSIC, Calle JG Abascal 2, 28006 Madrid, Spain. Tel.: +34-91-566-8976, Fax: 34-915668960; E-mail: mbastir@mncn.csic.es

Received 13 January 2016; Revised 16 June 2016; Accepted 18 July 2016.

DOI 10.1002/ar.23503

Published online 19 October 2016 in Wiley Online Library (wileyonlinelibrary.com).

diaphragmatic thorax. Therefore, variations in the form and function of the diaphragmatic thorax will have a strong impact on respiratory function. This has important implications for interpreting differences in thorax shape in terms of respiratory functional differences within and among recent humans and fossil hominins. Anat Rec, 300:255–264, 2017. © 2016 Wiley Periodicals, Inc.

Key words: thorax; rib cage; kinematics; breathing

INTRODUCTION

The human ribcage expands and contracts during breathing as a result of rib motion and the interaction between the curved ribs, their sternal connections, the anatomy and actions of the respiratory muscles and the ranges of movement at the costo-vertebral joints (Ratnovsky et al., 2008; Beyer et al., 2014). Two different patterns of ventilatory rib motion are commonly described, a "pump handle-like" movement of the upper ribs, and a "bucket handle-like" movement of the lower ribs (Franciscus and Churchill, 2002; West, 2012; Beyer et al., 2014). Additionally, a "caliper-like" motion has been ascribed to the lowest two (Chila, 2010) or lowest five ribs (Magee, 2014). However, the impact of these movements on functional changes of the size and shape of the skeletal thorax during respiration are unclear.

So far, functional studies of thoracic breathing kinematics have focused mainly on external chest wall movements. These studies found that the diaphragm and the lower thorax contribute considerably more to changes in thoracic volume during breathing than the upper thorax (Romei et al., 2010; LoMauro et al., 2012; Silvattia et al., 2012).

A recent *in vivo* 3D kinematic analysis of rib motion in the skeletal thorax suggested that the traditional dichotomy of "bucket handle" and "pump handle" rib rotations applies simultaneously to all levels (Beyer et al., 2014). But how do rib rotations contribute to differences in 3D size and shape changes of the entire thorax during breathing? What are the functional implications of kinematic shape changes of the thorax?

A given rib rotation will have a different effect on thoracic movement when carried out by flatter and straighter ribs than by more curved ribs with greater torsion. Consequently, because curvature and torsion differ among ribs of the upper and lower regions of the thorax (García Martínez et al., 2016a), during inspiration the kinematic transformations experienced by these regions should also differ. This is not only important for breathing function in recent humans, but also in fossil hominins. Recent research and discoveries increasingly demonstrate the enormous 3D variation in curvature, torsion and size of fossil hominin ribs (Gómez-Olivencia et al., 2009; Berger, 2013; Schmid et al., 2013; García-Martínez et al., 2014; Bastir et al., 2015; Berger et al., 2015; Tawane et al., 2016).

Consequently, there is a need to better understand the 3D kinematic changes in thoracic size and shape that occur during breathing in healthy subjects, and the functional significance of such variations. Such knowledge will be of use in relation to interpreting evolutionary transformations in rib size and shape in our own lineage and has the potential to be applicable in clinical contexts, e.g., lung disease, ribcage pathologies etc.

From a skeletal point of view, the ribs are conventionally classified into true ribs (1–7), false ribs (8–10), and floating ribs (11, 12) (Waldeyer and Mayet, 1987; Drake et al., 2010; White et al., 2011). Comparative ontogenetic study has also shown that growth trajectories of true ribs (1–7) are similar to each other, and differ from those of lower ribs (García-Martínez et al., 2016a). However, recent studies (Bastir et al., 2013) within the nonfloating ribs (ribs 1–10) have divided the thorax into an upper (ribs 1–5), and a lower unit (ribs 6–10). Additionally, it has been suggested that the first five thoracic vertebrae (T1–T5) and their costo-vertebral joints show a different pattern of serial morphological shape changes than the lower ones (T6–T10) (Bastir et al., 2014).

From a musculo-skeletal point of view, the thorax has been divided into a pulmonary ribcage (ribs 1–6) and diaphragmatic ribcage (ribs 7–12) (Ward et al., 1992; Kenyon et al., 1997). This is based on the apposition of the inner surface of the first six ribs to the lungs, and the attachment of the diaphragm to the lower six ribs (Ward et al., 1992). Muscle insertions further suggest such a compartimentalization: the scalenes, parasternal intercostals and the sternocleidomastoid muscles insert onto ribs 1-6, and the diaphragm arises from ribs 7–12 (Kenyon et al., 1997; De Troyer et al., 2005). Thus, the direct actions of the major extrinsic respiratory muscles are almost exclusively on the pulmonary rib cage which differs regarding its movements from the diaphragmatic and abdominal part of the ribcage (Ward et al., 1992).

In this study we quantify in 3D, the kinematic changes among the parts of the thorax bounded by the first 10 ribs in healthy nonsmoker subjects during breathing. We first explore the geometric shape changes during breathing kinematics in the full thorax and their relation to classical descriptions in terms of pump and bucket handle and caliper-like movements. We then examine the extent to which different modes and magnitudes of size and shape change exist among and within different regions of the upper and lower thorax during breathing.

METHODS

Subjects

Thoracic computed tomography (CT) scans of 20 adult subjects (16 males, 4 females) in maximal forced inspiration (FI) and maximal forced expiration (FE) during the CT study were obtained from healthy non-smoker volunteers. Consistent with the Helsinki protocol (Goodyear

et al., 2007) and in compliance with the stipulations of the local ethical committee, written consent was obtained to use these data for research purposes. Ages ranged from 40 to 67 years (average 50.9 years). Subjects presented an average total lung volume of 6.8l (sd. 1.19) and their average residual volume was 2.1l (sd. 0.45).

3D-Data

All CT examinations were performed with a 16-MDCT scanner (Somatom Sensation 16, Siemens Medical Solutions, Erlangen, Germany). Scanning voltage was 120 kV and current was 160 mA. CT of the thorax was performed from the lung apex to the level of the diaphragm in forced inspiration (FI) followed by forced expiration (FE). All imaging was performed with a collimation of 16 $\times$ 0.75 mm^2, table feed of 30 mm/rotation, and rotation time of 0.6 s/360° tube rotation with a standard reconstruction algorithm. CT capture lasted less than one minute. All subjects were previously instructed how to correctly carry out FI and FE in order to minimize inter-individual variation in depth of breathing and so, size and shape changes in the thorax.

The 3D-surface meshes of upper and lower rib cages were extracted by MIMICS software (http://biomedical.materialise.com/mimics) from the CT data and a total of 402 landmarks and semilandmarks (Bastir et al., 2013) were placed using ViewBox 4 (www.dhal.com) software on these models: one landmark at the uppermost, one at the lowermost part of the articular surface of the rib head, and one at the anterior-most point on the intra-articular crest, two landmarks at the inferior and superior limits of the sternal extremity, one at the most lateral articular tubercle, and one at the inferior part of the costal angle. In addition, we measured 13 evenly spaced semilandmarks along the shaft of each rib and two landmarks at the manubrium (Fig. 1). Because CT-scanning was carried out to include the skeletal thorax to the level of the diaphragm, in many cases the 11th and 12th rib were not available for measurement. In consequence, we only took landmark coordinates on the non-floating ribs (1–10).

While landmarks characterize homologous anatomical structures as points (Oxnard and ÓHiggins, 2009), curve semilandmarks respect homology at a different level. Rather than the (semi)landmark itself, the curve in total (i.e., the rib shaft) is considered biologically comparable (Gunz and Mitteroecker, 2013). Semilandmarks were slid twice, the first time to the template specimen (the first specimen in the sample) and after that all specimens were slid again to the overall mean, so as to minimize the bending energy between each ribcage and this mean (Gunz and Mitteroecker, 2013). This sliding manoeuvre minimizes variation due to error in siting of semilandmarks along the curve.

Geometric Morphometric Analyses

The 3D coordinates were subjected to a Generalized Procrustes analysis (GPA) that applies translation, scaling and rotation to the landmark coordinates to produce Procrustes shape coordinates (O'Higgins, 2000). Shape differences are quantified by Procrustes distance (*Pd*, the summed, squared interlandmark distances between

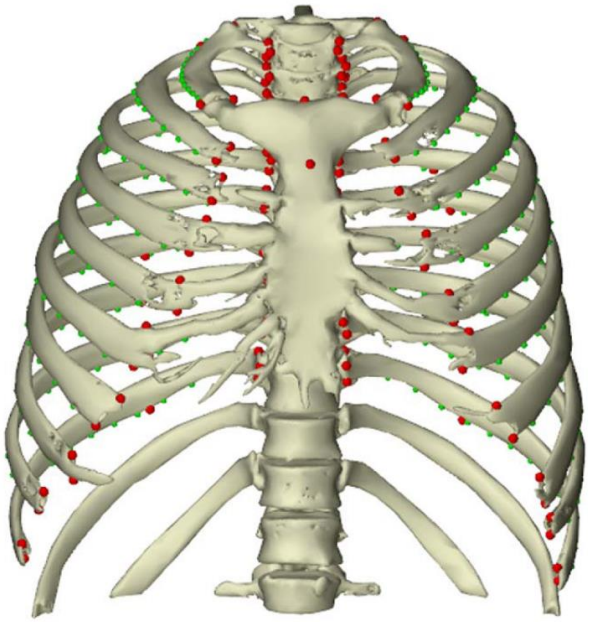

Fig. 1. 3D reconstruction of an adult thorax in forced inspiration (FI). The red dots mark anatomical landmarks, the green dots semilandmarks which characterize the 3D curvature of the ribs.

corresponding landmarks) (O'Higgins, 2000; Gunz and Mitteroecker, 2013). Size is measured as Centroid size (CS), the summed squared distances between each landmark and the center of the full landmark configuration. Centroid size is extracted as a scaling factor that emerges during GPA when all landmark configurations are standardised to unit size (O'Higgins, 2000; Gunz and Mitteroecker, 2013). Shape data were corrected for sexual dimorphism by multivariate regression of shape on sex-dummy variables because of unbalanced sex sampling similar to a MANCOVA approach (Rosas and Bastir, 2002). Asymmetries were removed by computing the mean of each thoracic landmark configuration and its reflection after GPA (Bastir et al., 2013).

Kinematic differences in ribcage shape were assessed by regression of shape on kinematic status (forced expiration/forced inspiration) and by mean shape comparisons. A permutation test ($N = 10000$) with permuted kinematic status was used to estimate the statistical significance of the observed shape difference (Klingenberg, 2011). The differences between mean inspiratory and expiratory ribcage shapes were visualized using transformation grids calculated using a triplet of thin plate splines (TPS). TPS-grids were positioned in the coronal and sagittal plane (red grids) and in two transverse planes, one within the upper (green grid), and the other within the lower thorax (orange grid). Warpings of the grids were computed between the overall mean shape (reference) and the mean shapes at FI and FE.

To identify differences in rib kinematics among regions of the thorax we assessed the significance of apparent differences among adjacent pairs of ribs. Thus, we compared shape changes occurring in the portion of the thorax bounded by rib pairs 1–2 with that bounded

by rib pairs 2–3. This was repeated for ribs 3–4 vs. 4–5, and so on until rib pair 9–10. Because each pair is represented by an equivalent set of landmarks we were able to directly perform GPA and subsequent statistical analyses. These comparisons allowed us to assess the validity in terms of function of subdivision of the thorax into two regions. The regions enclosed by ribs 1–5 and 6–10 have previously employed by us based on vertebral geometry and for convenience (equivalent sets of landmarks) of morphometric analysis (Bastir et al., 2013, 2014), whilst the regions enclosed by ribs 1–6 and 7–10 have also been proposed to reflect the functional split between pulmonary and diaphragmatic divisions (Ward et al., 1992, Kenyon et al., 1997). Regions enclosed by ribs 1–7 and 8–10 have been differentiated by other workers based on skeletal anatomical criteria distinguishing between true and false ribs and on the basis of their ontogenetic trajectories (Waldeyer and Mayet, 1987; White et al., 2011; García Martínez et al., 2016a).

Regression of the shapes of each partial thoracic region (rib pair) on kinematic status (forced inspiration, forced expiration) produced one kinematic vector connecting mean inspiratory and mean expiratory shape for each region of the thorax (or rib pair) and provided information on the magnitude of shape change due to breathing in the upper and lower thorax region (or rib pair). To compare these vectors among successive pairs of ribs, the angle between them was calculated. Its significance was estimated using a closed-form formula (Li, 2011) implemented in Morpho-J (Klingenberg, 2011; Klingenberg and Marugán-Lobón, 2013). Small angles indicate roughly parallel kinematic vectors (similar shape change during breathing), while greater angles indicate divergent vectors (different breathing kinematics).

Functional size, that is, the differences in centroid size (CS) between the inspiratory and expiratory configurations of upper and lower thoracic regions was used to test the hypothesis of different kinematic size changes of the upper and lower thoracic compartments during breathing. Functional shape is defined as the shape difference, measured as Procrustes distance, between thorax shape at FI and FE and was used to test the hypothesis of different kinematic shape changes of the upper and lower thoracic compartments during breathing. Mean size and shape differences between inspiration and expiration, and between upper and lower compartments, were compared using a paired t-test, with normality of the differences in CS and the Procrustes shape distances having been confirmed beforehand by the Kolmogorov Smirnov test (Sokal and Rohlf, 1998). Reduced major axis regressions were used to compare scaling relationships of kinematic differences in CS (functional size) and shape (Pd, functional shape) in the upper and lower thorax (Sokal and Rohlf, 1998).

RESULTS

Mean Shape Comparisons of Full Rib Cage

Permutation tests (1000 permutations) indicated significant differences in mean shapes ($Pd = 0.055$; $P < 0.004$) between whole ribcages in inspiration and expiration. The associated TPS-transformation grids of Figure 2 are shown in frontal, left lateral and cranial axial views. Frontal views show that the lateral (midshaft) part of the ribs becomes elevated relative to the spine throughout the entire ribcage. While the upper thorax expands antero-posteriorly the lower thorax expands medio-laterally from the 6th and 7th ribs onwards. There is no mediolateral expansion at the upper part of the thorax. The arrows drawn at the sternal ends of the fourth and eight ribs show this differential medio-lateral expansion. In addition, cranial, axial views illustrate that during inspiration the upper thorax increases in relative antero-posterior dimensions (green TPS grid), while the lower thorax shows a small increase in relative width (orange TPS grid). Thus, upper and lower parts of the thorax appear to deform differently during breathing.

Kinematic Vector Angle between Adjacent Rib Pairs

Table 1 presents the associated regression results and tabulates the angles. The angles at rib level 2 and rib level 6 are slightly larger than at other levels indicating kinematic changes. This suggests that, from a functional point of view, the thorax can be divided into the thoracic aperture (1st and 2nd rib level), a region superior to the 6th rib and a region inferior to the 6th rib. These latter results are compatible with a division of the ribcage according to kinematics into a pulmonary and a diaphragmatic part following musculo-skeletal criteria (Ward et al., 1992, Kenyon et al., 1997). The slight increase in angle at the level 5 may indicate the action of the rectus abdominis muscle.

Pulmonary and Diaphragmatic Ribcage Compartments

When the results of the previous analyses (Table 1) are taken as a basis for a division of the ribcage into an upper and lower part, kinematic vector comparisons of the pulmonary and diaphragmatic thoracic regions lend quantitative support to apparent visual differences (Fig. 2). Mean shapes at FI and FE were different both in the pulmonary ($Pd = 0.046$; $P < 0.001$) and the diaphragmatic thorax ($Pd = 0.035$; $P < 0.05$). Mean centroid sizes (CS) at FE ($CS = 1517.2$) and at FI ($CS = 1529.8$) within the pulmonary ribcage also differed significantly ($t = -7.892$, $P < 0.0001$). Within the diaphragmatic ribcage mean centroid sizes at FE ($CS = 1628$) and at FI ($CS = 1662.5$) differed also significantly ($t = -7.596$, $P < 0.0001$). The angle between the pulmonary and diaphragmatic kinematic vectors was 36.6 degrees ($P < 0.0001$) indicating different breathing kinematics.

Magnitudes of Kinematic Size and Shape Differences

Differences in CS between expiration and inspiration (functional size) were significantly greater in the diaphragmatic thorax (34.47) than the pulmonary thorax (12.62). Normality was not rejected by the Kolmogorov–Smirnov test ($d = 0.1$; ns) and the paired t test found a statistical difference ($t = -4.54$, $P < 0.01$).

For the pulmonary thorax the Procrustes distance between mean inspiratory and expiratory shapes (functional shape) was 0.053, and for the diaphragmatic, 0.046. Normality was not rejected by the Kolmogorov–Smirnov test ($d = 0.20$; n.s.) and a paired t test indicated

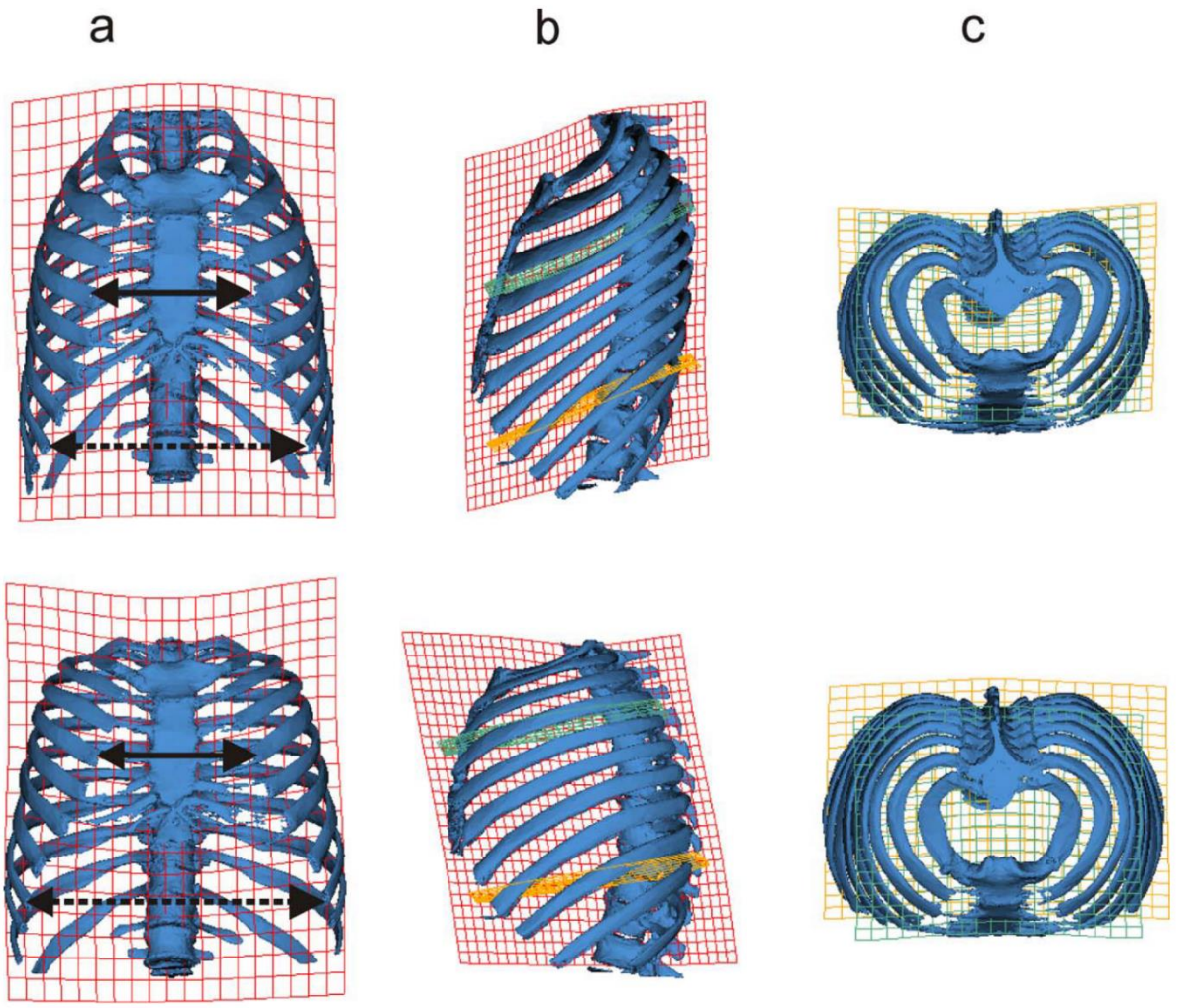

Fig. 2. How the thorax changes shape during breathing. Upper row: forced expiration; lower row: forced inspiration; a, anterior; b, left lateral; c, superior axial views.Grids are warped from the overall mean shape to the mean shapes at forced inspiration and forced expiration. In frontal view the red transformation grids are drawn through the center of the ribcage, in lateral view the grids are drawn through the mid-sagittal plane. In axial view grids are drawn in the transverse plane at the level of the mid upper thorax (green grid) and mid lower thorax (orange grid). (a) shows the relatively lower position of the lateral parts of the ribs which become elevated during inspiration. In addition, the lower thorax becomes mediolaterally wider relative to the upper, also shown by transformation grids in (c). The solid line and arrows show no change in width in the upper part of the thorax. The dashed line and arrows show medio-lateral expansion in the lower thorax during inspiration. Left lateral views (b) show a considerably more marked antero-posterior expansion of the upper than of the lower thorax. The cranial axial views also illustrate that the upper thorax in expiration (c) is shallower in the antero-posterior direction relative to the lower thorax, becoming relatively deeper during inspiration. Thus, the green transformation grid in the upper thorax is relatively shorter in FE than in FI, while the orange grid changes in its medio-lateral width, but not in its anteroposterior depth.

no differences in Procrustes distances ($t = 1.07$, n.s) (Table 2).

Thus, the pulmonary thorax produced less size difference during inspiration than the diaphragmatic part of the ribcage with similar amounts of deformation in shape. This is also seen in the regression analyses (Fig. 3, Table 3). The slope of the regression of functional size on functional shape or the pulmonary thorax is significantly smaller than that for the diaphragmatic, indicating that it needs to deform significantly more than the diaphragmatic thorax to produce the same size difference. Additionally, the functional size of the pulmonary thorax is only weakly related to functional size of the diaphragmatic thorax, while functional shapes of both thorax compartments are very highly correlated (Table 3).

DISCUSSION

This study explored the geometric shape changes during breathing in the full thorax in adult healthy non-smoker subjects. We addressed the relationship of these

TABLE 1. Regression of rib-pair shape on kinematic status and kinematic angles between rib pairs

Rib pairs	% of explained variance	*P* value	Angle (degrees)	*P* value
Pair 1–2	13.14	0.001		
Pair 2–3	14.73	0.001	18.91	0.0000
Pair 3–4	12.64	0.001	12.87	0.0000
Pair 4–5	9.12	0.006	11.31	0.0000
Pair 5–6	6.95	0.036	13.72	0.0000
Pair 6–7	5.88	0.061	14.57	0.0000
Pair 7–8	5.06	0.114	12.25	0.0000
Pair 8–9	4.71	0.128	11.88	0.0001
Pair 9–10	4.62	0.137	13.51	0.0001

Each angle is calculated between the kinematic trajectory of the pair of ribs in whose row the value is indicated and those in the row above.

TABLE 2. Kinematic differences in centroid size (mm) and shape (Procrustes distance, Pd) between forced inspiration and forced expiration in the pulmonary thorax and the diaphragmatic thorax

Units	Pulmonary thorax	Diaphragmatic thorax	*t*	*P*
Centroid size	12.62	34.47	−4.54	<0.0001
Procrustes distance	0.053	0.046	1.07	ns

ns: not significant.

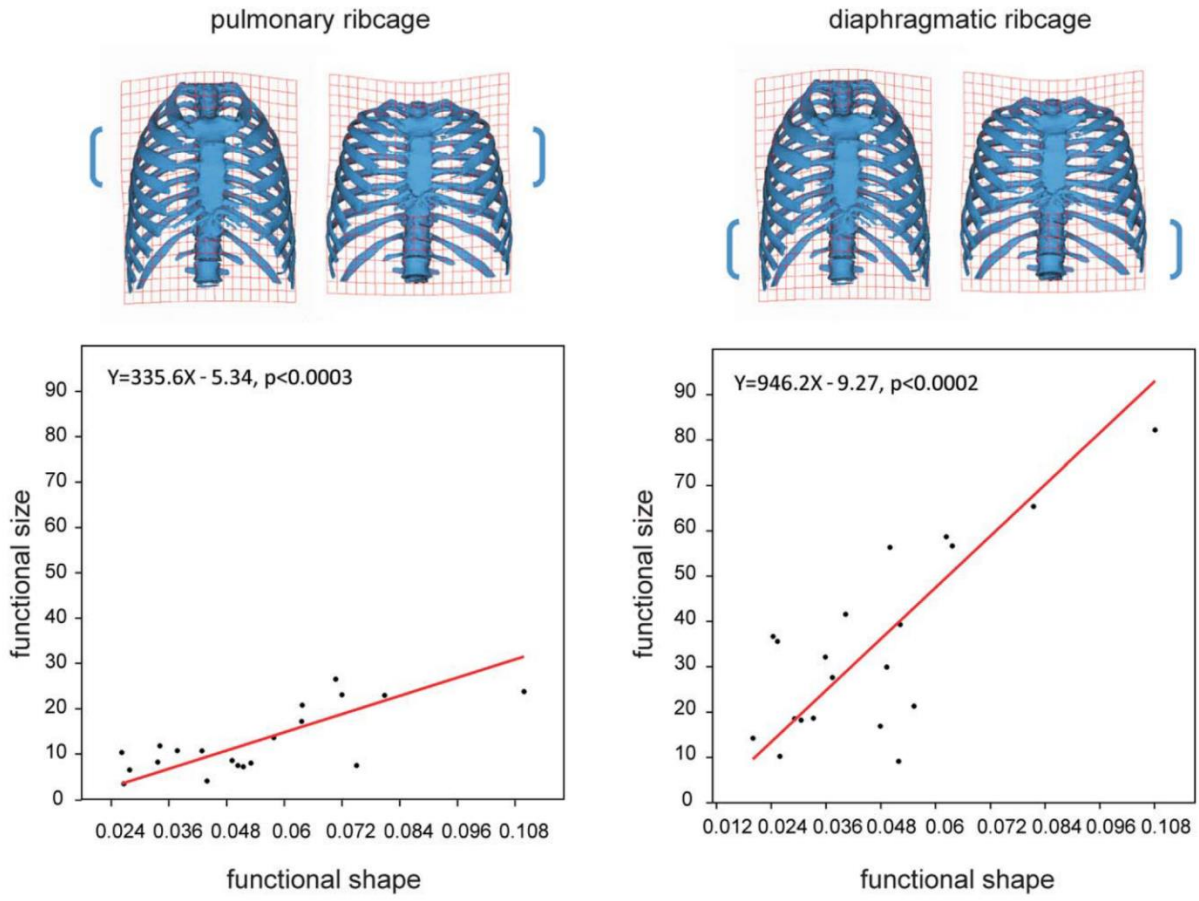

Fig. 3. Functional size and shape changes of the pulmonary and diaphragmatic ribcage. The slope of the pulmonary ribcage is considerably smaller than that of the diaphragmatic ribcage. Therefore, within the lower thorax, less shape change is necessary to produce the same degree of size difference as in the upper thorax.

TABLE 3. Relationships between functional size (f_s) and functional shape (f_{sh}) of the pulmonary thorax (PT) and diaphragmatic thorax (DT)

Units	Slope (95% C.I.)	Intercept	*r*	*P*
Functional size: PT vs. DT	0.35 (0.21–1.13)	0.47 (−25.19–4.52)	0.41	0.07
Functional shape: PT vs. DT	0.99 (0.75–1.09)	0.007 (0.001–0.016)	0.95	0.0001
PT *fs* vs. PT *fsh*	335.6 (191.8–422.9)	−5.34 (−20.03–6.385)	0.73	0.0002
DT *fs* vs. PT *fsh*	946.22 (609.7–1097)	−9.27 (−20.03–6.385)	0.77	0.0002

Reduced major axis regression analyses (slopes, 95% confidence intervals), intercept, correlation coefficient, and *P* value.

shape changes to classical descriptions of rib motion in terms of pump and bucket handle and caliper-like movements (Ratnovsky et al., 2008; West, 2012; Beyer et al., 2014). We also investigated the basic functional implications of kinematic size and shape changes of the upper and lower thoracic compartments and assess our findings in an evolutionary morphological and clinical context.

Kinematic Deformations, Rib Rotations and Morpho-Functional Divisions

In recent humans and fossil hominins there is substantial variation in the size and shape of the upper and lower thorax (Schmid et al., 2013; García Martínez et al., 2014; Bastir et al., 2015) with potential implications for breathing. In fact, upper and lower parts of the ribcage have been proposed to evolve (Schmid et al., 2013) and develop (Bastir et al., 2013, García Martínez et al., 2016a) relatively independently. Various propositions as to how to divide the ribcage into an upper and lower compartment have been made following statistical, musculo-skeletal and purely skeletal criteria (Ward et al., 1992; White et al., 2011; Bastir et al., 2013, 2014, García Martínez et al., 2016a). Our results suggest from a kinematic point of view a musculo-skeletal division of the thorax into a pulmonary part (ribs 3–6) and a diaphragmatic or abdominal part (ribs 7–10) according to Ward et al. (1992) and Kenyon et al. (1997) who proposed such divisions on the basis of muscle insertions and contact between the ribs and lungs.

Table 1 also provides evidence for specific kinematic changes at the upper thoracic aperture (ribs 1 and 2). This has not previously been observed and may indicate the action of the accessory respiratory muscles—scalene muscles—necessary in forced inspiration. The flatness of ribs 1 and 2 compared to the torsion of mid-thoracic and lower ones (Mann, 1993; Dudar, 1993; García Martínez et al., 2016a) and the supine posture in the CT-scanner (Romei et al., 2010) may well reflect the specific kinematics of this region as indicated by the higher angle (Table 1).

The significant and large angle (36.6 degrees, $P < 0.0001$) between pulmonary and diaphragmatic kinematic vectors together with the differences in transformation grid deformations between upper and lower thoracic regions (Fig. 2) provide clear evidence for different modes of deformation of the upper and lower parts of the breathing thorax.

The shape changes observed in the thorax do not completely reflect the oversimplification that "pump handle like" motions of the ribs characterize the upper thorax, and "bucket handle like" motions, the lower (Chila, 2010; Magee, 2014; West, 2012). In part this is because these terms are ill defined and so, are difficult to relate to a quantitative analysis of 3D motion, and in part because both motions are evident to some degree throughout the thorax (Beyer et al., 2014). This may account for the limited variation in kinematic angles among rib pairs (Table 1). Also a third motion, caliper-like spreading apart of the anterior ends of the lower ribs (Chila, 2010; Magee, 2014) is observed in Figure 2. Rib shape and costosternal joints likely constrain these motions leading to pump-handle and caliper like motion in these lower parts increasing the distance between the anterior ends of the ribs of the diaphragmatic thorax. This caliper-like motion is not, as is commonly stated (Chila, 2010), restricted to the last two 'floating ribs' but affects all lower ribs to some degree, supporting Magee (2014). This caliper-like motion may also reflect active muscle force during forced expiration because of the abdominal muscle insertions.

Respiratory movements of the thoracic cage are produced by the cumulative effects of small movements of the ribs at each costovertebral joint (Ward and Macklem, 1985). The axes of movement are complex and, particularly, those of the lower ribs are not well understood (Beyer et al., 2014). Moreover, these axes change cranio-caudally as the transverse processes become increasingly posteriorly orientated (Latimer and Ward, 1993; Bastir et al., 2014) with kinematic consequences for thoracic shape changes during breathing. Regional differences in kinematic patterns shown in Figure 2 may reflect the successive changes in the articular surfaces, rib axes, and attachments. The upper ribs hinge about an axis running along their neck, their convex tubercle rotating within the concavity of the costo-transverse joint. The ribs become more horizontal during inspiration. Their anterior end moves forwards and upwards, but only slightly laterally due to costosternal constraints. This results in anteroposterior expansion of the thoracic cavity and elevates the thoracic cage anteriorly (Fig. 2) (Agostini and Dángelo, 1985).

Because of the increasingly posteriorward sweep of the transverse processes, and so, of the axes of the necks of the ribs (Bastir et al., 2014), their anterior ends become progressively more laterally orientated in inspiration (Agostini and Dángelo, 1985), as is observed in Figure 2. Because the ribs increase cranio-caudally in length and curvature, upward rotation during inspiration shifts the ribs around the thorax at any given horizontal plane (Agostini and Dángelo, 1985; Mead et al., 1985). Moreover, the movement of the lower ribs includes a slight degree of eversion, which elevates the most lateral part of the rib shaft relative to a plane passing through its head posteriorly and the anterior end of its costal cartilage, anteriorly (Agostini and Dángelo, 1985).

In the lower thorax the shape and inclination of the costotransverse articular facets also allows for a gliding component (Ward and Macklem, 1985). In deep inspiration, the rib tubercles glide posteriorly, superiorly, and medially, swinging the anterior ends of the ribs horizontally laterally, away from each other (Agostini and Dángelo, 1985; Mead et al., 1985; Ward and Macklem, 1985). This further contributes to transverse expansion of the lower chest (Fig. 2).

Functional and Evolutionary Anatomy

The breathing kinematics of the upper thorax produced a smaller functional size difference than in the lower thorax (Table 2, Fig. 3). There is also evidence that size changes in the upper and lower thorax are weakly correlated (Table 3). This weak correlation may reflect variation among subjects in breathing preferences with some being predominantly thoracic breathers and others, diaphragmatic breathers. This requires further investigation; however, recent work on sexual dimorphism suggests that the form of the lungs (Torres Tamayo et al., 2016) and that of the ribcage (Bellemare et al., 2003, 2006; García Martínez et al., accepted) correlate with differences in respiratory function. Thus, females, who tend to show more prismatic (barrel shaped) thoraces also show reduced expansion capacities when compared to more pyramidal (funnel) shaped males (Bellemare et al., 2003; Romei et al., 2010; Layton et al., 2011). Variations related to skeletal aging might also contribute to the weak relationship between the functional sizes of the upper and lower parts of the thorax because aging leads to increased ossification in the costo-sternal cartilages and this, in turn, limits upper thoracic mobility (Oskvig, 1999; Gayzik et al., 2008).

The finding of a greater overall contribution to functional thorax size changes of the lower thorax is consistent with studies on external chest wall kinematics that have shown greater volumetric differences in the lower part of the chest than in the (upper) thoracic part (Romei et al., 2010; LoMauro et al., 2012; Silvattia et al., 2012). Because the diaphragm and its movements are not considered in our study, it is likely that changes in size of the upper skeletal thorax with breathing more directly reflect lung volumetric changes than those of the lower skeletal thorax, although the latter are functionally more relevant than the former.

Frontal and lateral views in Figure 2 (and See Video 1: http://bcove.me/3imgemwk) show that the rib rotations described by Beyer et al. (2014) lead to different costosternal motions in the upper thorax than in the lower. Costosternal joints of the upper ribs deform less than those of the lower, possibly as a consequence of differences in the lengths and orientations of the costosternal cartilages (Fig. 2). Thus, short and horizontally aligned cartilages are likely to permit smaller changes in thoracic width than longer and more caudally oriented costosternal cartilages. This costosternal constraint may also be reflected in the results of the regression analyses (Table 3), where the smaller slope in the pulmonary thorax indicates that for the same amount of size change, the upper thorax needs to change shape much more than the lower during breathing (Fig. 3). The reduced curvature and torsion of the upper ribs also contributes to smaller volumetric differences. Thus, greater curvature, torsion and lateral extension of the midshaft in shallow rib cages produce greater size differences between inspiration and expiration than in deep rib cages with less curved upper ribs. We have shown elsewhere that this mode of rib shape variation is a feature of normal variation, rather than being pathological (Bastir et al., 2015, García Martínez et al., 2016a).

The larger lower ribs enhance the degree of expansion of the lower rib cage during breathing (Table 2). As noted above, a recent study on modern human sexual dimorphism demonstrates a larger and relatively wider lower thorax in males combined with a significantly greater expansion capacity when compared to females (García Martínez et al., 2016b). The present findings with respect to how kinematic size and shape changes of upper and lower thoraces relate to rib and thorax shape are consistent with this, in that a wider thorax is expected to show greater volumetric changes during breathing. Furthermore, the larger sizes of the mid- and lower thoracic ribs relative to the upper ribs in fossil hominins, such as Neandertals (García-Martínez et al., 2014; Bastir et al., 2015) and *Australopithecus* (Schmid et al., 2013, Tawane et al., 2016) can be expected to have important implications for breathing kinematics in these hominins, and so potentially contribute to better understanding of the energy demands and behaviours of our fossil relatives. This is a topic to be explored in future work.

Clinical Implications

This study has focused on healthy subjects but the findings are of relevance to future research in pathological subjects. Thus, Chronic Obstructive Pulmonary Disease (COPD) results in pulmonary hyperinflation and respiratory muscle dysfunction (Bellemare et al., 2001; O'Donnell, 2001). Muscle dysfunction is characterized by changes in mechanical advantages and alterations of muscle fiber lengths, and intrinsic muscle structure (Marchand and Decramer, 2000). The diaphragm shows a flatter dome configuration, and loses its capacity to further expand the lower thorax (Marini, 1998). In consequence, the intercostal muscles become critical for inspiratory flow generation in these patients.

Such changes in respiratory muscles likely directly affect the kinematics of the upper and lower ribcage and these are further impacted by changes in the diaphragm that result in decreased lower chest expansion. Changes in ribcage kinematics in COPD impact lung expansion with consequences for the ventilation/perfusion ratio. Indeed, recent work shows that lung morphology and kinematics differ between COPD patients and healthy controls (Torres-Tamayo et al., 2015). The regional kinematic differences shown here (Figs. 2 and 3; Table 2) are likely important in the light of mismatching between ventilation and flow, the commonest cause of hypoxemia in lung diseases (Kent et al., 2011). As such, it will be of interest to apply the methods used in the present study to a comparison of the breathing kinematics of upper and lower thoracic compartments among COPD patients and healthy subjects.

Alveolar recruitment, that is, opening of alveoli that remain closed during breathing at low lung volumes, can be a compensatory mechanism to minimize the consequences of gas exchange imbalance (Rodríguez-Roisin

and Wagner, 1990; West, 1990; Engel and Paiva, 1981). The lateral displacement of the lower thorax observed in this study (Fig. 2a,c) likely favors increased lung expansion during inspiration and, consequently, may be a key mechanism underlying alveolar recruitment, with significant clinical implications in asthma and chronic bronchitis (Palmer and Diament, 1967).

Age is another factor that impacts breathing kinematics as alveolar recruitment will decrease with aging and its associated clinical problems (Oskvig, 1999). This is because as we age the ribs come to lie more horizontally. This is illustrated for the lower ribs by Weaver et al. (2014). Further with increasing age comes increasing thoracic kyphosis (Gayzik et al., 2008). This further impacts rib orientation, which reduces respiratory muscle strength, one of the most important physiological changes in the respiratory system associated with aging (Janssens et al., 1999). With age, joints become stiffer and less flexible and ribcage calcification extends from the costochondral junctions to the sternocostal junctions (Ontell et al., 1997). The resulting stiffening of ribcages in older subjects compromises their respiratory biomechanics, leading to "hyperinflation," with possible clinical effects similar to those of COPD patients. The approaches we have applied in the present study may well have application in future clinical assessment of these age changes.

Other potential applications include assessment of the progress and effects of thoracic and spinal skeletal dysplasias and of progressive thoracic skeletal deformities such as occur in *Osteogenesis imperfecta*. In fact, in a recent study of chest wall motion in Type III *Osteogenesis imperfecta* patients, asynchronies between upper and lower thorax kinematics were reported (LoMauro et al., 2012). These authors related these asynchronies to the presence of more horizontally aligned ribs. Figure 2 shows clearly that inspiratory expansion of the upper thorax occurs in the antero-posterior direction facilitated by kinematic elevation of upper ribs. Therefore, disease leading to more horizontal upper ribs, will also likely lead to clinical problems related to ventilation.

In this study we assessed the size and shape changes that occur in the upper and lower skeletal thorax during breathing by means of CT. This provided different insights into breathing mechanics than those that arise from the more usual studies of the diaphragm and intercostal muscle function (Romei et al., 2010; LoMauro et al., 2012; Silvattia et al., 2012) because breathing also involves the actions of the serratus, scalene, pectoral and abdominal wall muscles (Thibodeau and Patton, 2008; Drake et al., 2010; White et al., 2011). While CT studies cannot reveal respiratory muscle morphology and functioning during breathing they can potentially reveal the changes in function that arise as a consequence of muscular changes. Future research examining breathing kinematics using could be complemented by magnetic resonance imaging and electromyography to allow integration of data on muscle functioning with data on thorax motion.

CONCLUSIONS

Our study shows that the pulmonary and diaphragmatic parts of the thorax differ in terms of breathing kinematics, particularly in their modes of shape change during breathing while the degree of shape change is similar in both compartments. In contrast, the diaphragmatic part undergoes greater changes in size than the pulmonary part. In consequence a greater degree of deformation of the upper thorax is required to produce a similar degree of size change to that of the lower thorax. This has important implications with regard to the functional impact of variations in rib cage form among living and fossil hominins. The approaches employed in this study have potential clinical applications in assessing the impact and progress of the effects of disease and aging on breathing kinematics.

ACKNOWLEDGEMENTS

The authors thank Nick Milne for discussions.

LITERATURE CITED

Agostini E. Dángelo E. 1985. Statics of the chest wall. In: Roussos CJ, Macklem PT, editors. The Thorax. New York: Marcel Dekker Inc. p 259–295.

Bastir M, García-Martínez D, Estalrrich A, Tabernero AG, Huguet R, Ríos L, Barash A, Recheis W, Rasilla MDI, Rosas A. 2015. The relevance of the first ribs of the El Sidrón site (Asturias, Spain) for the understanding of the Neanderthal thorax. J Hum Evol 80: 64–73.

Bastir M, García-Martínez D, Recheis W, Barash A, Coquerelle M, Rios L, Peña-Melián Á, García Río F, O'Higgins P. 2013. Differential growth and development of the upper and lower human thorax. PLoS One 8:e75128.

Bastir M, Higuero A, Ríos L, García-Martínez D. 2014. Three-dimensional analysis of sexual dimorphism in human thoracic vertebrae: Implications for the respiratory system and spine morphology. Am J Phys Anthropol 155:513–521.

Berger LR. 2013. The mosaic nature of *Australopithecus sediba*. Science 340:163–165.

Berger LR, Hawks J, de Ruiter DJ, Churchill SE, Schmid P, Delezene LK, Kivell TL, Garvin HM, Williams SA, DeSilva JM, et al. 2015. *Homo naledi*, a new species of the genus Homo from the Dinaledi Chamber, South Africa. eLife 4.

Bellemare J-F, Cordeau M-P, Leblanc P, Bellemare F. 2001. Thoracic dimensions at maximum lung inflation in normal subjects and in patients with obstructive and restrictive lung diseases. Chest 119: 376–386.

Bellemare F, Fuamba T, Bourgeault A. 2006. Sexual dimorphism of human ribs. Respir Physiol Neurobiol 150:233–239.

Bellemare F, Jeanneret A, Couture J. 2003. Sex differences in thoracic dimensions and configuration. Am J Respir Crit Care Med 168:305–312.

Beyer B, Sholukha V, Dugailly PM, Rooze M, Moiseev F, Feipel V, Van Sint Jan S. 2014. In vivo thorax 3D modelling from costovertebral joint complex kinematics. Clin Biomech 29:434–438.

Chila A. 2010. Foundations of osteopathic medicine, 3 ed. Philadelphia: Lippincott Williams & Wilkins.

De Troyer A, Kirkwood PA, Wilson TA. 2005. Respiratory action of the intercostal muscles. Physiol Rev 85:717–756.

Drake RL, Wayne-Vogel A, Mitchell AWM, editors. 2010. Gray's anatomy, 2nd ed. Barcelona: Elsevier. p 124–158.

Dudar CJ. 1993. Identification of rib number and assessment of intercostal variation at the sternal rib end. J Sci 38:788–797.

Engel LA, Paiva M. 1981. Analysis of the sequential filling and emptying of the lung. Respir Physiol 45:309–321.

Franciscus RG, Churchill SE. 2002. The costal skeleton of Shanidar 3 and a reappraisal of Neandertal thoracic morphology. J Hum Evol 42:303–356.

García-Martínez D, Barash A, Recheis W, Utrilla C, Torres Sánchez I, García Río F, Bastir M. 2014. On the chest size of Kebara 2. J Hum Evol 70:69–72.

García Martínez D, Recheis W, Bastir M. 2016a. The 3D variation of human rib curvature along ontogeny and its importance for the understanding of the thorax development. Am J Phys Anthropol 159:423–431.

García-Martínez D, Torres-Tamayo N, Torres-Sanchez I, García-Río F, Bastir M, 2016b. Morphological and functional implications of sexual dimorphism in the human skeletal thorax. American Journal of Physical Anthropology 161(3):467–477.

Gayzik FS, Yu MM, Danelson KA, Slice DE, Stitzel JD. 2008. Quantification of age-related shape change of the human ribcage through geometric morphometrics. J Biomech 41:1545–1554.

Gómez-Olivencia A, Eaves-Johnson KL, Franciscus RG, Carretero JM, Arsuaga JL. 2009. Kebara 2: New insights regarding the most complete Neandertal thorax. J Hum Evol 57:75–90.

Goodyear MDE, Krleza-Jeric K, Lemmens T. 2007. The declaration of Helsinki. BMJ 335:624–625.

Gunz P, Mitteroecker P. 2013. Semilandmarks: A method for quantifying curves and surfaces. Hystrix 24:103–109.

Janssens JP, Pache JC, Nicod LP. 1999. Physiological changes in respiratory function associated with aging. Eur Respir J 13:197–205.

Jellema LM, Latimer, B, Walker A. 1993. The rib cage, the nariokotome Homo erectus skeleton. Cambridge: Harvard University Press. p 294–325.

Kent BD, Mitchell PD, McNicholas WT. 2011. Hypoxemia in patients with COPD: Cause, effects, and disease progression. Int J Chron Obstruct Pulmon Dis 6:199–208.

Kenyon CM, Cala SJ, Yan S, Aliverti A, Scano G, Duranti R, Pedotti A, Macklem PT. 1997. Rib cage mechanics during quiet breathing and exercise in humans. J Appl Physiol 83:1242–1255.

Klingenberg CP. 2011. MorphoJ: An integrated software package for geometric morphometrics. Mol Ecol Res 11:353–357.

Klingenberg CP, Marugán-Lobón J. 2013. Evolutionary covariation in geometric morphometric data: Analyzing integration, modularity and allometry in a phylogenetic context. Syst Biol 62:591–610.

Latimer B, Ward CV. 1993. The thoracic and lumbar vertebrae: The nariokotome Homo erectus skeleton. Cambridge: Harvard University Press. p 266–293.

Layton AM, Garber CE, Thomashow BM, Gerardo RE, Emmert-Aronson BO, Armstrong HF, Basner RC, Jellen P, Bartels MN. 2011. Exercise ventilatory kinematics in endurance trained and untrained men and women. Respir Physiol Neurol 178:223–229.

Li S. 2011. Concise formulas for the area and volume of a hyperspherical cap. Asian J Math Stat 4:66–70.

LoMauro A, Pochintesta S, Romei M, D'Angelo MG, Pedotti A, Turconi AC, Aliverti A. 2012. Ribcage deformities alter respiratory muscle action and chest wall function in patients with severe osteogenesis imperfecta. PLoS One 7:e35965.

Magee DJ. 2014. Orthopedic physical assessment, 6th ed. Saunders, Elsevier, St. Lois, Missouri.

Mann RW. 1993. A method for siding and sequencing human ribs. J Sci 38:151–155.

Marchand E, Decramer M. 2000. Respiratory muscle function and drive in chronic obstructive pulmonary disease. Clin Chest Med 21:679–692.

Marini JJ. 1998. Dynamic hyperinflation. In: Marini KK, Alutsky AS, editors. Physiological basis of ventilatory support. New York: Marcel Dekker. p 453–490.

Mead J, Smith JC, Loring SJ. 1985. Volume displacements of the chest wall and their mechanical significance. In: Roussos CJ, Macklem PT, editors. The thorax. New York: Marcel Dekker Inc. p 369–392.

O'Donnell DE. 2001. Assessment of bronchodilator efficacy in symptomatic COPD: Is spirometry useful? Chest 117:42S–47S.

O'Higgins P. 2000. The study of morphological variation in the hominid fossil record: Biology, landmarks and geometry. J Anat 197: 103–120.

Ontell FK, Moore EH, Shepard JA, Shelton DK. 1997. The costal-cartilage in health and disease. RadioGraphics 17:571–577.

Oskvig RM. 1999. Special problems in the elderly. Chest J 115: 158S–164S.

Oxnard C, O'Higgins P. 2009. Biology clearly needs morphometrics. Does morphometrics need biology? Biol Theory 4:84–97.

Palmer KN, Diament ML. 1967. Spirometry and blood-gas tensions in bronchial asthma and chronic bronchitis. Lancet 2:383–384.

Ratnovsky A, Elad D, Halpern P. 2008. Mechanics of respiratory muscles. Respir Physiol Neurol 163:82–89.

Rodríguez-Roisin R, Wagner PD. 1990. Clinical relevance of ventilation-perfusion inequality determined by inert gas elimination. Eur Respir J 3:469–482.

Romei M, Mauro AL, D'Angelo MG, Turconi AC, Bresolin N, Pedotti A, Aliverti A. 2010. Effects of gender and posture on thoracoabdominal kinematics during quiet breathing in healthy adults. Respir Physiol Neurol 172:184–191.

Rosas A, and Bastir M. 2002. Thin-Plate Spline Analysis of Allometry and Sexual Dimorphism in the Human Craniofacial Complex. Am J Phys Anthropol 117:236–245.

Schmid P, Churchill SE, Nalla S, Weissen E, Carlson KJ, de Ruiter DJ, Berger LR. 2013. Mosaic morphology in the thorax of *Australopithecus sediba*. Science 340(6129).

Silvattia AP, Sarrob KJ, Cerveric P, Baronic G, Barrosa RML. 2012. A 3D kinematic analysis of breathing patterns in competitive swimmers. J Sport Sci 30:1551–1560.

Sokal RR, Rohlf FJ. 1998. Biometry, 3 ed. New York: W. H. Freeman and Company.

Tawane G, García-Martínez D, Eyre J, Bastir M, Berger L, Nalla S, Williams SA. 2016. A hominin first rib discovered at the Sterkfontein Caves, South Africa. South Afr J Sci 112.

Thibodeau GA, Patton KT. 2008. Structure and function of the body, 13th ed. Barcelona: Elsevier.

Torres-Tamayo SN, García-Martínez D, Bastir M, Utrilla C, Torres Sánchez I, García Río F. 2015. Estudio de la morfología pulmonar en pacientes con EPOC, y su influencia en el patrón de movimiento respiratorio. X Jornadas Complutenses, IX Congreso Nacional Investigación Alumnos Pregraduados en CC. De la Salud y XIV Congreso CC. Veterinarias y Biomédicas. Madrid, España. Universidad Complutense de Madrid.

Waldeyer A, Mayet A. 1987. Anatomie des Menschen. de Gruyter, Berlin, New York, 493 p.

Ward ME, Macklem PT. 1985. Kinematics of the chest wall. In: Roussos CJ, Macklem PT, editors. The thorax. New York: Marcel Dekker. p 515–533.

Ward ME, Ward JW, Macklem PT. 1992. Analysis of human chest wall motion using a two-compartment rib cage model. J Appl Physiol 72:1338–1347.

Weaver AA, Schoell SL, Stitzel JD. 2014. Morphometric analysis of variation in the ribs with age and sex. J Anat 225:246–261.

West JB. 1990. Respiratory physiology: the essentials, 4th ed. Baltimore: Williams & Wilkins.

West JB. 2012. Respiratory physiology, the essentials, 9th ed. Philadelphia: Wolters Kluwer.

White TD, Black MT, Folkens TA, editors. 2011. Human osteology, 3rd ed. Oxford: Academic Press.

CAPÍTULO VII – RESULTADOS: ANATOMÍA DE LA CAJA TORÁCICA EN LA SUPERFAMILIA *HOMINOIDEA*

Los resultados obtenidos en referencia al **objetivo 4 "Contribuciones al conocimiento de la anatomía comparada reciente de la caja torácica humana"** serán íntegramente publicados en el siguiente artículo, el cual está en fase de revisión:

Bastir, M., **García-Martínez, D.**, Williams, S.A., Recheis, W., Torres-Sánchez, I., García-Río, F., Oishi, M., Ogihara, N., en revisión. 3D geometric morphometrics of thorax variation in *Hominoidea*. Journal of Human Evolution.

Elsevier Editorial System(tm) for Journal of Human Evolution

Manuscript Draft

Manuscript Number: HUMEV-E-15-00323R2

Title: 3D geometric morphometrics of thorax variation in Hominoidea

Article Type: Full Length Article

Keywords: ribcage, geometric morphometrics, barrel-shaped, funnel-shaped

Corresponding Author: Dr. Markus Bastir, Ph.D.

Corresponding Author's Institution: MNCN-CSIC

First Author: Markus Bastir, Ph.D.

Order of Authors: Markus Bastir, Ph.D.; Daniel García-Martínez, Phd; Scott A Williams, Phd; Wolfgang Recheis, Phd; Isabel Isabel Torres Sánchez, MD; Francisco García Río , MD; Motoharu Oishi , Phd; Naomichi Ogihara , Phd

Abstract: Thorax morphology is an important character in primate and human evolution. Since the seminal papers of Adolph Schultz, the morphology of hominoid primate ribcages has been described as either "funnel-"or "barrel-shaped". Following this dichotomic typology it is currently held that H. sapiens and hylobatids (gibbons and siamangs) share a barrel-shaped ribcage and that they are more similar to each other than to funnel shaped thoraces of African great apes (Gorilla, Pan) and orangutans (Pongo). We address this hypothesis by 3D morphometrics of thoraces in anatomical connection obtained by computed tomography scans of 23 hominoid cadavers and 10 humans. We examined thorax compartments composed of 7 ribs (upper thorax) and of 11 ribs (extended thorax). Upper thorax results do not reflect a funnel-barrel shape dichotomy and show that gorillas, humans, and orangutans are relatively wider and more similar to each other than to chimpanzees and hylobatids. Human upper thoraces are further flat due to torsion close to the vertebral rib ends. In extended thorax analyses the barrel-shaped humans contrast with funnel-shaped African great apes. Orangutans and hylobatids are closer to humans because of a wider upper thorax, which in African great apes is particularly narrow, relative to the lower thorax. However, these analyses are affected by problems related to serial homology. Hominoid thorax variation shows complex interactions between allometry, rib curves, torsion, and declination, and the morphology of the costo-vertebral joint and the thoracic vertebral column. Functional specializations are overlaid on phylogenetic relationship, which are not well covered by "Schultzian" terminology.

3D geometric morphometrics of thorax variation in *Hominoidea*

Markus Bastir [a]*, Daniel García-Martínez [a], Scott A. Williams[b, c], Wolfgang Recheis [d], Isabel Torres [e], Francisco García Río [e], Motoharu Oishi [f], Naomichi Ogihara [g]

[a] Paleoanthropology Group. Museo Nacional de Ciencias Naturales (CSIC), J. G. Abascal 2, 28006, Madrid, Spain

[b] Center for the Study of Human Origins, Department of Anthropology, New York University, 25 Waverly Place, New York, NY 10003

[c] New York Consortium for Evolutionary Primatology, New York, NY 10024

[d] Medizinische Universität Innsbruck, Innrain 52, Christoph-Probst-Platz, 6020 Innsbruck, Austria

[e] Hospital Universitario La Paz, Biomedical Research institute (Idipaz), Madrid, Spain

[f] Laboratory of Anatomy 1, School of Veterinary Medicine, Azabu University, 1-17-71 Fuchinobe, Chuo-ku, Sagamihara-shi, Kanagawa 252-5201 Japan

[g] Department of Mechanical Engineering, Faculty of Science and Technology, Keio University, Yokohama 223-8522, Japan

*****corresponding author: Dr. Markus Bastir, e-mail: mbastir@mncn.csic.es, Museo Nacional de Ciencias Naturales (CSIC), J. G. Abascal 2, 28006, Madrid, Spain. Tel +34 91 566 8976

Abstract

Thorax morphology is an important character in primate and human evolution. Since the seminal papers of Adolph Schultz, the morphology of hominoid primate ribcages has been described as either "funnel-" or "barrel-shaped". Following this dichotomic typology it is currently held that *Homo sapiens* and hylobatids (gibbons and siamangs) share a barrel-shaped ribcage and that they are more similar to each other than to funnel shaped thoraces of African great apes (*Gorilla*, *Pan*) and orangutans (*Pongo*). We address this hypothesis by 3D morphometrics of thoraces in anatomical connection obtained by computed tomography scans of 23 hominoid cadavers and 10 humans. We examined thorax compartments composed of 7 ribs (upper thorax) and of 11 ribs (extended thorax). Upper thorax results do not reflect a funnel-barrel shape dichotomy and show that gorillas, humans, and orangutans are relatively wider and more similar to each other than to chimpanzees and hylobatids. Human upper thoraces are further flat due to torsion close to the vertebral rib ends. In extended thorax analyses the barrel-shaped humans contrast with funnel-shaped African great apes. Orangutans and hylobatids are closer to humans because of a wider upper thorax, which in African great apes is particularly narrow, relative to the lower thorax. However, these analyses are affected by problems related to serial homology. Hominoid thorax variation shows complex interactions between allometry, rib curves, torsion, and declination, and the morphology of the costo-vertebral joint and the thoracic vertebral column. Functional specializations are overlaid on phylogenetic relationship, which are not well covered by "Schultzian" terminology.

Introduction

The evolution of modern human thorax morphology and its differences to non-human primates have long attracted the interest of the scientific community (Schultz, 1961; Schmid, 1983, 1991; Jellema et al., 1993; Ward, 1993; Kagaya et al., 2008; Haile-Selassie et al., 2010; Ward et al., 2012; Schmid et al., 2013; García-Martínez et al., 2013; Latimer et al., 2016). In his seminal review, Schultz (1961) established a typological scheme for the description and dichotomic classification of thorax morphology of different primate species, which is still employed today (Schultz, 1961; Schmid, 1983, 1991; Jellema et al., 1993; Franciscus and Churchill, 2002; Sawyer and Maley, 2005; Barker and Ward, 2008; Gómez-Olivencia et al., 2009, 2010; Ward et al., 2012; Schmid et al., 2013; García-Martínez et al., 2013, 2014; Bastir et al., 2015; Latimer et al., 2016).

On the one hand, Schultz (1961) used the term "barrel-shaped" to describe ribcage morphology of *Homo sapiens* and hylobatids (gibbons and siamangs), which are characterized by a cylindrical thorax with a wider thoracic cupola (upper thoracic region) and roughly parallel lateral thoracic walls. On the other hand, he described the cranially converging (conical) ribcage morphology of great apes (*Pan*, *Gorilla* and *Pongo*) as "funnel-shaped" with a narrow cupola and caudally diverging lateral thoracic walls. Schultz (1961) suggested that funnel-shaped morphologies emerge due to more gradual size increase in the upper ribs, while in the barrel-shaped thorax rib size increase is more abruptly, "particularly in the second ribs. The last few ribs are more curved in man than in the great apes […]" (Schultz, 1961:53). This suggests that the upper and lower regions of the thorax are both informative regarding rib cage geometry.

Later studies have supported these ideas. In recent anthropoids, Kagaya et al. (2008) used Bezier curves to analyze the curvature of ribs, which they articulated manually to their corresponding vertebrae to approximate thorax morphology at specific

levels. Their findings support wider thoraces in hominoids as compared to anthropoids, also partly as a result of allometric scaling. Moreover, their results also support Schultz' (1961) observations on barrel-shape thorax anatomy in hylobatids. Barke and Ward (2008) analyzed the first six ribs in hominoids. They reported similarly broader upper thorax morphologies in hylobatids and humans that differed from *Pan*, *Gorilla*, and *Pongo*, which also corroborates Schultz's (1961) observations. Holliday (2012) suggested convergence of hylobatids and modern humans towards a cylindrical (barrel-shaped) corporal model (cf. Ruff, 1991) in relation to upright locomotor behavior. Long distance travel and wide ranging behavior, fully upright body posture and associated respiratory physiology are features in which hylobatids are comparable with modern humans (Holliday, 2012; pers comm.). Importantly, most of these studies investigated isolated elements (ribs) of the thorax. However, one recent but preliminary 3D shape analysis of thoraces in anatomical connection provided evidence that morphological details between modern humans and hylobatids may be considerably different (García-Martínez et al., 2013). Clarifying these details and understanding 3D factors of hominoid thorax shape is therefore important for better understanding primate and hominin evolution, and for interpreting fossil material.

Fossil rib fragments in *Proconsul* suggest a narrow and deep (monkey-like) thorax morphology as the primitive hominoid condition (Ward, 1993), while evidence for a shallow and broad (ape-like) ribcage emerges with the later Miocene hominoids *Pierolapithecus* and *Oreopithecus* (Moyá-Solá et al., 2004). Changing thorax geometries document evolutionary changes in the postural and locomotor behavior as they are informative about scapula position and thus upper limb mobility potential (Ward, 1993; Moyá-Solá et al., 2004; Lovejoy, 2005; Williams and Russo, 2015).

Funnel- and barrel-shaped ribcages have also gained considerable importance in paleoanthropology, where these terms are used as general morphological characters that describe thoracic remains of fossil hominins, their potential phylogenetic relations and functional anatomy (Schmid, 1983; 1991; Jellema et al., 1993; Franciscus and Churchill, 2002; Sawyer and Maley, 2005; Haile-Selassie et al., 2010; García-Martínez, 2013; Schmid et al., 2013; García-Martínez et al., 2014; Schmid et al., 2013; Bastir et al., 2015; Tawane et al., 2016).

It has long been thought that the basic bauplan of a modern human barrel-shaped thorax appeared with *Homo ergaster* (African *Homo erectus*), as evident in the rib morphology of the Nariokotome partial skeleton (Jellema et al., 1993). In australopiths it has been argued that the ribcage was funnel-shaped, similar to great apes (Schmid, 1991; Schmid et al., 2013). More recently, however, the hypothesis of funnel-shaped thoraces in australopiths has been challenged based on upper thoracic ribs in large-bodied *A. afarensis* remains (Haile-Selassie et al., 2010). These authors detected evidence for upper thoracic expansion and suggested that thorax morphology of KSD-VP-1/1 ribs was "fundamentally *Homo*-like" (Haile-Selassie et al., 2010:12122). Despite some overlap with Gorilla the upper thoracic KSD-VP-1/1 ribs were shown to be clearly different from those of funnel-shaped thoraces of African apes and described as "bell-shaped" (Sawyer and Maley, 2005; Latimer et al., 2016).

Classifications of fossil hominin thorax shape are mostly based on assessments of isolated rib morphology and often on simplified quantitative assessments such as indices, areas or lengths of actually very complex 3D curved morphologies. As mentioned before, this also applies to many studies of comparative anatomy of recent primates. No study has yet assessed thorax geometry measuring the 3D configuration of thoraces with their

ribs in anatomical connection such as obtained when CT scanning entire ape cadavers by 3D landmarks and semilandmarks (Bastir et al., 2013).

These distinctions between different thorax shapes are important in the context of hominin paleobiology and locomotor patterns. In the funnel-shaped ribcages, the narrow cupola is thought to indicate biomechanical adaptations to climbing, suspension or knuckle walking (Schmid, 1983; 1991; Preuschoft, 2004; Thorpe et al., 2007; Schmid and Krause, 2011; Schmid et al., 2013; Latimer et al., 2016). Also, their broad lower thorax fits with broad iliac blades and a stiff lumbar column, which stabilizes the lower back in heavy animals with forelimb-dominated locomotor behaviors (Jungers, 1984; Ward, 1993; Schmid, 1991; Lovejoy, 2005). In the barrel-shaped human thorax the upper part is considerably expanded mediolaterally and the lower thorax is narrowed and more rounded in cross section, a configuration that favors lower trunk torque in bipedal endurance walking or running and arm swinging to balance this torque (Schmid, 1991; Lovejoy, 2005; Schmid et al., 2013). The torsion of the ribs in humans causes a declined (oblique) orientation when viewed laterally (García-Martínez et al., 2016a). This contributes further to a barrel-shaped human ribcage and also facilitates thoracic (intercostal) breathing kinematics based on the elevation of inferiorly declined ribs during inspiration (de Troyer et al., 2005; Daley et al., 2013; Bastir et al., 2013; García-Martínez et al., 2016b; Bastir et al., 2016).

For these reasons, it is important to improve our understanding of how 3D morphological features of the hominoid ribcage relate to standard morphological categories described traditionally by barrel- and funnel-shaped thoraces (Schultz, 1961). The aim of this study therefore is to explore variation in ribcage morphology in hominoids. Specifically, we use 3D morphometrics to test whether the morphological

distance between “barrel-shaped” modern humans and hylobatids is smaller than between the “funnel-shaped” great apes (*Pongo*, *Pan*, *Gorilla*) (Schultz, 1961).

Material and Methods

We used 3D geometric morphometrics of virtual 3D thorax models obtained from computed tomography (CT) scans of living humans (*Homo sapiens*, N=10) and 23 cadavers of hominoid primates [*Gorilla gorilla*, N=5; Hylobatids, N=4 (2 *Hylobates lar*, 1 *Hylobates agilis*, 1 *Symphalangus syndactylus*); *Pongo pygmaeus*, N=4; *Pan troglodytes*, N=10] (Table 1). (Supplementary Table S1). The sex proportions of the species samples are only balanced in humans and chimpanzees, but not in the remaining groups. This affects statistical estimates of their size and shape means.

Because the thorax is a metameric structure, composed of serial elements that vary numerically in hominoids (Schultz, 1961; Pilbeam, 2004; Williams, 2012a; Williams et al., 2016), we carried out two analyses. The first analysis focuses on the ribcage as composed of the true ribs (ribs 1-7, upper thorax), while the second analysis focuses on a more complete thorax, composed of ribs 1-11 (extended thorax). We decided to exclude the 12th rib pair, which is the last set in *Homo* and also most often in *Pongo*, and prone to considerable variation in length due to relatively common homeotic morphologies at the thoraco-lumbar border (Ogilvie et al., 1998; Haeusler et al., 2002; Williams et al., 2016). In most hylobatids and African great apes the last rib pair is located at the 13th thoracic level (Schultz, 1961; Pilbeam, 2004; Williams, 2012a). Therefore, in the comparisons of the extended thorax *Homo* and *Pongo* are represented by 91.7% of their thorax geometry, while hylobatids and African Apes by only 84.6%. The comparability of extended thorax analysis is thus slightly limited.

CT-scanning

Each non-human thorax was scanned using a helical computed tomography scanner. Cross-sectional images were reconstructed with a pixel size of 0.623 - 0.781 mm and slice interval of 0.5 - 1.0 mm, depending on the size of specimen. A triangular mesh model of the 3D surface of the thorax was then generated by the marching-cube algorithm using commercial software (Analyze 9.0, Mayo Clinic, Rochester, MN, USA). For some large specimens, CT-scanning was performed multiple times to cover the entire thorax, and the surface models were registered to each other using commercial software (Rapidform 2004, INUS Technology, Seoul, Korea) to obtain the entire surface of the thorax. Human thorax CT data were obtained in supine position from clinical scans and described elsewhere (Bastir et al., 2013; García-Martínez et al., 2014).

The ape cadavers were kept frozen in supine position. Frozen conservation avoids any deformation due to fixation. Prior to CT scanning, the frozen specimens were thawed at room temperature. Then skins, muscles and internal organs were removed to avoid possible deformation of the rib cage due to gravity. No ethic statements were necessary because the cadavers used in this study were brought to research institutions from zoos after the animals died naturally and were not sacrificed for this or other research.

3D-Measurements

A total of 524 3D landmarks and semilandmarks were measured (Fig. 1). We located twenty landmarks on the ribs 1-10 (most superior and inferior points of the rib head, most lateral point of the articular tubercle, the most inferior point at the angulus costae and most superior and inferior points of sternal extremes) (Bastir et al., 2013; 2015, García-Martínez et al., 2016a) and nineteen landmarks on the 11th ribs. Equidistant semilandmarks were placed along the lower costal border between the articular tubercle

and the inferior sternal extreme. Additionally, four landmarks at each of the twelve thoracic vertebrae (most antero-superior and antero-inferior points on the vertebral body at the midline and the most superior and inferior points at the lower part of the spinous processes) were measured so as to quantify the main features of thoracic morphology at the ribs and thoracic vertebral column. Semilandmarks were slid twice, a first time to the template during digitizing (ViewBox 4 software; www.dhal.com) and a second time to the sample average following standard sliding protocol (Mitteroecker and Gunz, 2009; Bastir et al., 2013).

Statistical analyses

Differences in mean centroid size were analysed by ANOVA. Shape data were produced using Generalized Procrustes Analysis (Zelditch et al., 2012), and analyzed by principal component analyses (PCA) in shape space to assess the 3D variation in light of funnel- and barrel-shape thorax configurations. These were performed for landmark data of the upper and extended thoraces. Allometry was also analyzed by Procrustes Form space analysis (Mitteroecker et al., 2004) of data from the upper thorax. Mean shape comparisons were carried out using permutation tests (N=1000) of Procrustes distances (Klingenberg, 2011). Neighbour joining trees were calcuated based on Procrustes distances of all individuals of the sample to enquire whether hylobatids and modern humans were closer to each other and different from the great apes. All visualizations were carried using EVAN-toolkit (EVAN-Society, 2010).

Results

Upper thorax analyses

Centroid size of the upper thorax was normally distributed and ANOVA found significant differences between the group means [($F(4, 28) = 55.045$, $p<0.001$) (Table 1)].

The PCA of the upper thorax is shown in Figure 2. PC1 (31.3% of total variance) polarizes Gorilla and *Pongo* on the one extreme of PC1, while *Pan* and hylobatids plot on the other extreme. Humans are intermediate, slightly closer to *Gorilla* and *Pongo*. Figure 3 shows shape variations along PC1 indicating that towards negative PC1 scores ribcages are caudally more divergent, wider and relatively flatter than towards positive PC1 scores. Thoracic vertebral columns are slightly invaginated (axial views) towards negative PC1 scores. Variation in mid-thoracic width is also reflected in frontal view by distances between the sternal ends of corresponding rib pairs. These intersternal distances are relatively longer in wider thoraces (negative PC1 scores) where they also increase more markedly in caudal direction. Positive PC1 scores show in lateral view that the sternal ends of the upper ribs are curved cranially; the frontal view shows that this is related to coronal declination at the vertebral rib end. These connect almost orthogonally to the thoracic column towards negative scores (wider, flatter thoraces), while towards positive PC1 scores the angle between the column and the vertebral rib end decreases, leading to narrower ribcages (declined proximal ribs). PC1 carries an allometric signal because larger Gorilla, humans and *Pongo* plot together as opposed to smaller *Pan* and especially hylobatids.

PC2 (26.6% of total variance) polarizes humans and apes. Both lateral and frontal views show that humans are particularly shallow in thoracic depth (antero-posteriorly).

This is caused by rib torsion close to the rib head producing rib declination in coronal and sagittal planes (oblique orientation). Apes, all of which plott towards positive PC2 scores, have deeper thoraces caused by horizontally aligned ribs without any declination in the sagittal plane. The frontal view shows also that apes vertebral rib shafts are more horizontally oriented. In humans, vertebral rib shafts are declined inferiorly in the coronal plane (frontal view), but also in a sagittal plane (lateral view). As a consequence the sternal ends come to lie much lower than the vertebral ends. The frontal view illustrates this further because of the increasing declination of the vertebral rib shaft in the coronal plane, the anterior (sternal) extremes of ribs 4-7 are closer to each other. The angle between two lines produced by the right and left sternal ends of the ribs is much smaller in humans than in non-human hominoids. All this, together with increasing axial curvature at ribs 2, 3 (axial view, Fig. 3) and the associated pronounced invagination of the thoracic vertebral column that increases towards the mid-thorax, produces the characteristic human thorax configuration.

Procrustes form space PCA (Figs. 4, 5) directly addresses allometric features of thorax variation. PC1 (85.6% of total variance, Fig. 5) shows common allometric features indicating that larger ribcages are wider because of greater axial rib curvature and less declination of the vertebral rib shaft, with a slightly invaginated thoracic vertebral column, and shallower because of sternal rib ends that are more medially (axial view) and more caudally curved (sagittal view). Along PC3 (2.8 of total variance, Fig. 4) African apes plot towards the positive scores characterized by greater mid-thoracic depth. Humans, hylobatids and *Pongo* plot towards negative scores because of smaller mid-thoracic depth (not shown).

Mean shape comparisons reveal that all species are highly significantly different from each at $p < 0.01$ (Table 2). In terms of mean Procrustes distances, *Gorilla* and *Pongo*

are closest to humans while hylobatids are most distant from humans. The neighbour joining tree (Fig. 6) also reflects these relationships: most specimens of humans, Gorilla and *Pongo* form one cluster, while chimpanzees and hylobatids group together in a second cluster. The upper thorax analysis does not support a morphological classification of barrel-shaped thoraces in humans and hylobatids and funnel-shaped thoraces in great apes.

Extended thorax analyses

ANOVA shows that all groups differ significantly in centroid size [$F(4, 28)=65.896$, $p<0.001$]. Gorilla shows the largest ribcages and hylobatids the smallest. No differences were found between *Pan* and *Pongo*, both of which slightly smaller than humans (Table 3).

Principal components (PCs) 1-3 account for approximately 72.7% of the total variance of the sample (PC1: 35.1%; PC2: 25.1%; PC3: 12.5%). Scatterplots in Figure 7 show that along PC1 modern humans plot towards negative scores, African apes towards positive scores and Asian apes are intermediate. PC2 (Fig. 7a) polarizes hylobatids and *Pan* at negative scores from *Gorilla* and *Pongo* towards positive scores. PC3 (Fig. 7b) polarized *Gorilla* towards positive scores, away from the rest of the sample.

Morphologically, PC1 clearly contrasts barrel-shaped modern humans with funnel-shaped African apes (Fig. 8). The Asian apes are intermediate. The thorax of the African apes (positive PC1 scores) is characterized by a very narrow superior thoracic aperture, relative greater length of the mid-thoracic and lower ribs, and a reduced axial curvature at the proximal midshaft of the lower most ribs. In the barrel-shaped modern humans (negative PC1 scores), the superior thorax aperture is relatively wider compared to African apes and in relation to the lower thorax (Fig. 8, with upper ribs that are axially

more curved and the lower ribs relatively shorter. The greater axial curvature of the lower ribs and the strong coronal declination of the proximal rib shafts lead to a narrower lower thorax. Axial views in humans show that the thoracic vertebral column is also more strongly invaginated into the ribcage, in contrast with African apes, which show less invagination.

PC2 contrasts *Pan* and *Gorilla* within the African apes and hylobatids and *Pongo* within the Asian apes (Fig. 7). *Gorilla* and *Pongo* plot towards positive PC2 scores and hylobatids and *Pan* towards negative scores. Morphologically (Fig. 8), these contrasts are related to overall thorax width, and greater relative distances between sternal extremes of corresponding rib pairs. When these intersternal distances are increased they generate a wide and anteriorly open skeletal ribcage with ribs that are less curved axially (positive PC2 scores). These sterno-costal distances increase cranio-caudally, but more so towards positive than towards negative PC2 scores.

In lateral view, ribcages at positive PC2 scores show relatively shorter, more horizontally oriented ribs with an elevated sternum and a decreased kyphosis. These features describe *Gorilla* and *Pongo* and differentiate them from *Pan* and hylobatids at negative PC2 scores. In the latter, the ribs are relatively longer, a factor that lowers the sternum relative to the thoracic vertebral column, which is more kyphotic. The axial view shows clear differences in relative widths and depths (Fig. 8).

In PC3 *Gorilla* loads on the positive scores (Fig. 8). This is morphologically related to antero-posteriorly flat ribcages, a feature in which they are not too different from modern human thoraces (Fig. 7b) but clearly different from the antero-posteriorly deep overall chests of *Pan,* and *Pongo* and hylobatids that populate the negative PC3 scores. Lateral views suggest that thoracic flatness at positive PC3 scores is produced by

downward curved distal shafts of lower ribs. When these curves are absent (at negative PC3 scores), the thorax is antero-posteriorly deeper.

Plotting centroid size in the PC1-PC2 (Fig. S1b) subspace indicates a complex allometry pattern because both humans and gorillas are large but on opposite ends of PC1 due to different thorax shapes (Table 4). Along PC2, the smaller species, hylobatids and chimpanzees produce negative scores while the larger species, *Pongo* and *Gorilla*, plot in positive PC2 scores.

Mean shape differences were again highly statistically significant (Table 5). *Homo* was closest to *Pongo* and hylobatids, and *Pongo* was very different from *Pan* and *Gorilla*. The neighbor joining tree of the Procrustes distances of the extended thorax data reveals one cluster composed of humans and *Pongo* and another one of composed of *Gorilla*, *Pan* and hylobatids (Fig. 9). The PCA (Figs 7, 8) supports Schultz's dichotomy in terms of barrels and funnels; however, there are highly significant differences between the funnel-shaped thoraces of Asian and African apes, with the latter showing considerably narrower cupola than the Asian apes. Therefore these do not fall together in the way described by Schultz (1961).

Discussion

Schultz (1961) suggested two basic morphological patterns of thorax geometry in *Hominoidea*: funnel shapes in *Pongo*, *Gorilla*, and *Pan* and barrel shapes in hylobatids and anatomically modern humans. Similarities between barrel-shaped humans and hylobatids have also been observed by other researchers (Barker and Ward, 2008; Kagaya et al., 2008; Holliday, 2012). Here we used 3D morphometric analyses on thorax reconstructions of hominoid cadaver CT-scans to address the hypothesis that "barrel-shaped" modern humans and hylobatids are more similar to each other than to "funnel-

shaped" great apes (*Gorilla*, *Pan* and *Pongo*) (Schultz, 1961, Kagaya et al 2008; Barker and Ward, 2008; Holliday; 2012). Our analysis were divided into an analysis of the upper thorax, composed of the first 7 (true) ribs and vertebrae, and a second analysis of an extended thorax compartment, composed of the first 11 segments. This was necessary because of the metameric variation of ribcages of different species that consist of different numbers of serial thoracic segments (Schultz, 1961; Pilbeam, 2004; Williams, 2012a; Williams et al., 2016).

Upper thorax analyses

Schultz (1961) proposed that barrel and funnel thoracic geometries are the result of a more steady rib size increase in the upper thorax of funnel-shaped thoraces and a more abrupt rib size increase in the barrel shaped ribcages. This implies that barrel and funnel shape patterns could be recognized well in the upper thorax, a suggestion that is supported on the analyses of isolated ribs of the upper thorax (Jellema et al., 1993; Barker and Ward, 2008).

Our analyses of the upper thorax do not support this hypothesis. The principal components analysis illustrates clearly that all thoraces are much narrower cranially than caudally (Fig. 3). There is no evidence to divide them into barrel or funnel shaped geometries, nor are humans and hylobatids closer to each other than to the African apes and *Pongo*. Instead, the neighbor joining trees, calculated from the Procrustes distances in full shape space group humans, *Gorilla*, and *Pongo* together in one cluster and hylobatids and chimpanzees in a second one (Fig. 6). These groupings are also evident in the PCA results of Procrustes form space (Fig. 5) and suggest a considerable influence of size and scaling in this thoracic region: larger individuals show relatively wider and flatter upper ribcages than smaller specimens that are characterized by deeper and relatively narrower thoraces.

Allometric influence of thorax width has been proposed previously by Kagaya et al. (2008) although in manually remounted skeletons from osteological collections. Our results support their findings in ribcages in natural anatomical connections. Procrustes form space analysis (Fig. 5) shows more details of allometric variation: upper thoracic widening is produced by greater axial curvatures and accompanied by a slight invagination of the thoracic vertebral column. Smaller ribcages are less invaginated than larger ribcages. Thus, *Gorilla* shows a more strongly invaginated vertebral column than *Pan* (Kagaya et al., 2008) (Figs. 3, 5). This fits with Schultz's observation (1961) that thoracic vertebral column invagination is not strictly a *Homo*-like feature related to bipedalism. However, while PC1 (Fig. 3) shows invagination towards larger thoraces as a general allometric feature, PC2 (Fig. 3) illustrates that human thoracic columns are particularly invaginated (Schultz, 1961; Jellema et al., 1993). Figure 3 offers more details showing that the stronger invagination of the mid-thoracic vertebral column likely reflects greater human thoracic kyphosis as part of the full set of spinal curvatures necessary for bipedal locomotion (Preuschoft, 2004; Lovejoy, 2005; Latimer et al., 2016).

Allometry is also important regarding rib orientation. Larger ribcages show more horizontally aligned proximal (vertebral) rib ends (Fig. 5). This orientation contributes also to thorax width because more horizontally aligned vertebral rib shafts bring the lateral part of the rib in a more lateral position, thus increasing thorax width. These thorax features can be better identified in the anatomical complex than in isolated ribs (Jellema et al., 1993, Ward et al., 2012; Latimer et al., 2016; García-Martínez et al., 2016b). Differences between the morphologies of isolated ribs and anatomically connected thoraces could also explain the absence of barrel and funnel shapes in the upper part of the thorax (Barke and Ward, 2008) and the lack of morphological similarity between hylobatids and humans proposed previously (Schultz, 1961; Kagaya et al., 2008; Barke

and Ward, 2008; Holliday, 2012). The primate thorax – as an anatomical composite – is more than the shape of the ribs or vertebrae in isolation (Jellema et al., 1993, Latimer and Ward, 1993, Ward et al., 2012, Bastir et al., 2014b; 2015).

However, despite the absence of a barrel-funnel dichotomy in the upper thorax analysis, a clear human configuration is recognizable. Humans show greater upper thoracic width and an oblique orientation of ribs relative to the thoracic vertebral column (Figs. 2, 3). Oblique rib orientation is caused by declination and torsion of the vertebral rib end and twist along the rib shaft (Jellema et al,. 1993; Schmid et al,. 2013, García-Martínez et al., 2016a; Latimer et al., 2016). In lateral view the angle between the ribs and the thoracic vertebral column in the relatively deep thorax of apes is almost orthogonal due to a lack of human-like torsion, while in the shallow, broad chests of humans this torsion produces a markedly reduced angle (Fig. 3).

Extended thorax analyses

The extended thorax analysis supports Schultz's dichotomic patterns (Schultz, 1961; Kagaya et al., 2008; Barke and Ward, 2008; Holliday, 2012). This makes clear that data from both the upper and the lower thorax are necessary to assess overall thoracic geometry (Fig. 8). However, while in PC-space funnels and barrels are clearly recognizable and a major component of shape variation (Fig. 8), these patterns of variation do not reflect the affinities suggested by Schultz (1961) (Fig. 9), which challenge his typological propositions that great apes are united and fundamentally differently shaped than humans and hylobatids.

Asian apes are intermediate in PC space (Fig. 8) with *Pongo* clustering together with humans in full shape space (Fig.9). Whether this is related to the fact that African ape thoraces are less completely represented by 11 thoracic levels than the Asian apes is

difficult to assess here. Geometric morphometrics cannot process data sets consisting of different landmark numbers (Mitteroecker and Gunz, 2009). In humans and *Pongo*, the thorax is normally formed by twelve levels, while in African apes one additional level normally participates in the formation of the skeletal thorax (e.g., 12 thoracic vertebrae and associated ribs in *Pongo* and *H. sapiens* versus 13 in chimpanzees and gorillas; Schultz, 1961). However, hylobatids also show higher number of thoracic vertebral elements, comparable to that of African apes (Schultz, 1961; Pilbeam, 2004; Williams, 2012a; Williams et al., 2016), but have thoraces closer in shape to humans. This lends support not only to previous observations on similarities between humans and hylobatids (barrel shaped or not) (Barker and Ward, 2008; Kagaya et al., 2008; Holliday, 2012), but also argues against dissimilar numbers of thoracic segments causing an artificial statistical signal of morphological differences and thus leading to an erroneous rejection of Schultz's group of funnel-shaped hominioids consisting of *Pan, Gorilla,* and *Pongo*. A clear need for developing methodological alternatives for the 3D quantification of variable metameric anatomical structures by geometric morphometrics exists.

However, and importantly, our findings demonstrate that similar outlines of thorax geometry can be produced by the combination of different individual morphologies of ribs and their connections to thoracic vertebrae and columns. Actually, several shape features along PC2 and even PC3 (Fig. 8) could all be interpreted to some degree as funnel or barrel shapes. Yet, thoracic elements connect with each other in coronal, sagittal and transverse planes. Vertebral and rib morphological features, such as transverse process angles and curvatures and torsion of proximal ribs, or curvature of distal rib shafts all interact with each other within these anatomical planes, giving rise to a wide range of possible thorax morphologies (Latimer and Ward, 1993; Ward et al., 2012; Bastir et al., 2014b; Latimer et al., 2016). For example, reduction of thorax width

can be produced by any one of the following: a stronger proximal rib declination (Fig. 3) (in coronal plane) because of smaller size and allometry, because of simple declination (Fig. 5), by lesser rib curvature (in transverse plane), or by lesser dorsal orientation of the transverse process of the associated thoracic vertebrae (Jellema et al., 1993; Latimer and Ward, 1993; Bastir et al., 2016; García-Martínez et al., 2016b). Interactions of these different factors along the thoracic column produce the spectrum of frontal thoracic outlines shown in Figure 8. Here is another example: A broad shallow thorax can be caused by shorter midhafts of the ribs in sagittal plane, by proximal rib torsion leading to overall rib declination, or by torsion at the sternal (distal) end leading to downwards and/or medialwards curved ribs (Kagaya et al., 2008). Also allometrically-driven axial rib curvature reduces relative antero-posterior thorax proportions (depth). This illustrates how different factors give rise to overall similarities in thorax shape; however, such overall similarities may have different functional implications or adaptive explanations.

We suggest that morphological assessments of thoracic outline morphology need to be accompanied by assessments of morphological features of individual ribs and vertebrae (Franciscus and Churchill, 2002; Gómez-Olivencia et al., 2009; Tawane et al., 2016; Williams et al., in revision). For example, morphological characters closer to the costo-vertebral joints may carry a greater phylogenetic signal because of strong genetic-developmental factors (Aoyama et al., 2005; Tawane et al., 2016) than morphological features related to the mid-shaft and sternal parts of the ribcage. These latter could show more plasticity being affected by later growth and aging (Gayzik et al., 2008; Bastir et al., 2013; García-Martínez et al., 2016a).

Evolutionary morphology

The extreme funneling of the African ape thorax shown in Figure 8 deserves special attention. Jellema et al. (1993), and more recently Latimer et al. (2016), note that

the funnel-shaped thorax of *Pan* exists because of both extreme narrowing of the upper part of the thorax (cupola) and additional flaring (widening) beginning at ribs 9 and 10 to meet long and broad iliac blades. Figure 8 suggests this effect characterizes both *Pan* and *Gorilla*. A very narrow thoracic cupola may question the likelihood of its presence in a *Pan*-human last common ancestor (Lovejoy et al., 2009; Latimer et al., 2016).

Upper thorax remains of *Australopithecus* may be intermediate between African apes and humans (Haile-Selassie et al., 2010; Schmid et al., 2013). Latimer et al. (2016) suggest that the African ape ribcage is part of an integrated morpho-functional torso complex with shoulder and pelvic girdles suited for arboreality and, particularly, knuckle-walking. This is because in African apes the extremely narrow cupola ("frustum-shaped thorax"; Latimer et al., 2016:151), which permits the glenohumeral joints to align and face ventrally and inferiorly and so to oppose ground reaction forces caused by knuckle-walking. This locomotion type is accompanied by unique gait and muscle recruitment parameters involving adduction of the forelimb during hindlimb overstride (Larson and Stern, 1987). However, the biomechanics of knuckle-walking are not well understood, and more work in this area is needed to test the hypothesis that a narrow upper thorax, shared by African apes, is indeed advantageous in knuckle-walking. The wider lower thorax and shorter lumbar vertebral columns with lower lumbar vertebrae entrapped within vertically tall and coronalized iliac blades are thought to contribute to lower torso stiffening favorable in forelimb-dominated behaviour (Jungers, 1984; Schmid, 1991; Ward, 1993; Lovejoy, 2005; Latimer et al., 2016).

Theoretically, spine length, and in particular, thoraco-lumbar vertebral column length, is related to flexibility, both at the level of absolute length and when assessed by the number of elements (Schultz, 1961; Maurer, 1970; Schmid, 1991; Thorpe et al., 2007; Williams, 2012b; Williams et al., 2013). Our results show that at the first 11 levels,

African apes have slightly shorter thoracic vertebral columns but whether this difference would persist after adding the necessary remaining 12th element is not clear (although hylobatids would suggest otherwise as previously discussed).

Pongo, besides hylobatids, fall closer to humans due to the combination of a slightly wider upper thorax and a slightly narrower lower thorax (Fig. 8). It has been argued that human bipedalism might have evolved from a somewhat generalized locomotor behavior retained from a common great ape ancestor (Thorpe et al., 2007). In this perspective and in the light of the results in Figure 8, *Pongo* appears less specialized than the African apes. Similarities between orangutans and modern human ribcages are not restricted to thoracic shape. The average number of thoracic segments is very similar in humans (12.0) and orangutans (11.99) (Williams et al., 2016); However, orangutans clearly present reduced thoracolumbar and total vertebra numbers compared to other hominoids and are almost certainly derived in this regard (Schultz, 1961; Pilbeam, 2004; Williams, 2012a,b; Williams and Russo, 2015; Williams et al., 2016). Also, similarities between humans and hylobatids are considered homoplasy in relation to upright locomotor behavior (Holliday, 2012). However, additionally and importantly, our orang sample does not contain male specimens, and a larger *Pongo* sample including males may affect these results and interpretations. Nevertheless, female *Pongo* ribcages are closest in overall form to humans in our dataset, and their degree of cranial thoracic widening could be somehow similar to potential upper thorax widening in early hominins (Thorpe et al., 2007; Bastir et al., 2016; Latimer et al., 2016).

Paleoanthropological implications

Recent discoveries of ribs from different australopiths have fueled discussions on the evolution of early hominin thorax shape. On the basis of evidence on ribs (Johanson et al., 1982; Schmid, 1983; Haile-Selassie et., 2010; Latimer et al., 2016) and vertebrae

(Ward et al., 2012) of *A. afarensis* it was suggested that the thoraces of early hominins likely had less cranially constricted cupolae than African apes. Haile-Selassie et al. (2010) reported a *Homo*-like pattern (despite some overlap with *Gorilla*) of rib morphology in large KDS-VP1/1 upper thoracic ribs, which they quantified by a rib-shape index. This index quantifies the axial curvature of the rib head and neck relative to the proximal shaft.

Figure 2 shows that humans, *Gorilla* and *Pongo* all plot together because of wider upper thoraces (Fig. 3). However, Figure 2 illustrates also that the human-like pattern is not only the widening, related to allometry, but more particularly the torsion and declination of these upper ribs relative to a strongly invaginated thoracic column (Schmid, 1983, 1991; Jellema et al., 1993; Latimer and Ward, 1993; Haile-Selassie et al,. 2010, Schmid et al., 2013). These doubtlessly *Homo*-like features are not quantified well by the rib-shape index (Haile-Selassie et al., 2010) illustrating the difficulties in studies on hominin thorax evolution based on simplified measurements and isolated, fragmented ribs. Recently, Latimer et al., (2016) provided cross sectional morphology (rib flatness) to argue for possible torsion but the relation between torsion, cross-sectional morphology and rib flatness topology is not very unclear due to wide ranges of intraspecific variation (Franciscus and Churchill, 2002; and M.B., personal observations). Figure 2 suggests that lateral views of the KSD- VP-1/1 ribs would better illustrate a potential *Homo*-like pattern more effectively. Ideally, 3D semilandmark curves, similar to the present approach, should be used to analyze the morphology of KSD-VP-1/1 and other fossil hominin rib material.

However, axial views highlight allometric effects on upper thoracic widening which is congruent with large-bodied individual of *A. afarensis* [(Haile-Selassie et al., 2010 and supported by the present results (Fig. 2, S1)]. Preliminary analysis of first ribs of *A. sediba* points towards incipient widening of its cupola making evident that only

complete ribs, or at least rib-shafts fragments that preserve its heads and necks, could demonstrate these relations (Schmid et al., 2013; Bastir et al., 2016). As indicated previously, axial rib curvature related to allometry may have a different biological meaning than rib curvature related structurally to spinal curvatures and bipedalism and more work is necessary to disentangle this important problem.

However, allometry seems to establish a size-related overall integration pattern linking axial curvature of upper ribs, relative thorax width and thoracic vertebral column invagination also potentially important for understanding thorax and body shape evolution in Miocene apes. Their fossil record documents an evolutionary trend from smaller to larger body size and from narrow deep to shallower and wider ribcages (Ward, 1993; Moyá-Solá et al., 2004). Kagaya et al. (2008) suggested that scaling may be involved in this morphological change reflecting a possible evolutionary link between body size and locomotor behavior. Ribs of *Pierolapithecus catalaunicus* from the upper, mid and lower thorax all show a higher degree of curvature and increased angulation, providing further evidence for links between size and rib morphology (Moyá-Solá et al., 2004).

Thorax shape and functional anatomy

The morphology of the ribcage is important for respiratory and locomotor function (Thorpe et al., 2007; Jellema et al., 1993; Schmid et al., 2013; Latimer et al., 2016). Our study makes evident that the relation between respiratory function and thorax shape should be considered in two morphological aspects: the relationship of upper and lower thoracic size as a reflection of upper and lower lung volumes and the declination of the ribs as a reflection of respiratory kinematics. Declined ribs provide potential for elevation by intercostal muscle action (De Troyer et al., 2005). The size and shape of the lower ribs are important indicators for diaphragmatic muscle action (Schmid, 1991;

Ratnovsky et al., 2008; Bastir et al., 2016). Both features can be observed in the result of this study.

The ribs of the upper thorax in African apes are smaller and more horizontally orientated than in the rest of the sample (Fig. 8). Horizontal upper ribs cannot be elevated much further. This reduces intercostal muscle contribution to breathing and suggests a strong diaphragmatic respiratory action in African apes (Schmid, 1991; Bastir et al., 2016). Accordingly, the elongated and axially less curved lower ribs of African provide a solid attachment for large and powerful diaphragm for abdominal respiration (Schmid, 1991; Schmid et al., 2013). A large diaphragm may also compensate the reduced upper pulmonary capacity indicated by the small, narrow upper thorax.

The intermediate position of Asian apes along PC1 is caused by a slightly expanded upper thorax shape and could indicate an increased additional reliance on upper thoracic lung volumes shared with modern humans (De Troyer et al., 2005; Holliday, 2012; Bastir et al., 2016). However, it is important to note that this upper thoracic expansion (Fig. 3) is not accompanied by proximal rib torsion and declination which reduces the potential for intercostal breathing (De Troyer et al., 2005; Ratnovsky et al., 2008). Clearly, larger Asian ape samples, including male orangutans, are needed in this respect combined with the addition of kinematic research.

On the other hand, it is important to note that in hominin evolution both upper thorax expansion and upper rib declination should be investigated. The latter could be important in the context of long distance running because a combined effect of thoracic and abdominal breathing may optimize pulmonary ventilation and could be an important feature in human evolution (Bramble and Lieberman, 2004; Schmid et al., 2013). A ribcage optimal for pulmonary expansion would be one with declined ribs for intercostal

muscle action and considerable lower width for a powerful diaphragm (Bastir et al., 2016).

But thorax morphology is also important for primate locomotion. A narrow upper ribcage allows for enhanced mobility of the shoulder girdle and upper limbs for climbing and forelimb-dominated arboreal locomotor behaviors (Preuschoft, 2004; Lovejoy, 2005; Schmid and Krause, 2011). A specifically narrow upper thorax such as evident in Figure 8 has been associated directly with knuckle-walking (Latimer et al., 2016). Finally, an increased upper thorax width such as that observed in modern humans allows for arm sway in bipedal walking and running. This counteracts the torque between the lower thorax and the upper pelvis produced by the oblique abdominal muscles (Schmid, 1983, 1991; Jellema et al., 1993; Lovejoy, 2005; Schmid et al., 2013, Latimer et al., 2016).

In this sense, a narrow lower thorax morphology is highly correlated with the relatively narrow modern human upper pelvis shape (Schultz, 1961; Jellema et al., 1993; Lovejoy, 2005; Schmid et al., 2013; Bastir et al., 2014a) and a mobile, free lumbar vertebral column (Lovejoy, 2005; Williams et al., 2013, Latimer et al., 2016), which together contribute to the biomechanics of effective bipedalism. In turn, the wide, un-curved lower thorax seen in apes (Fig. 5a, b) does not allow for such kind of movements (but see Thompson et al., 2015).

Conclusions

The present study has shown that thorax morphology varies considerably among hominoid primates. Schultz's (1961) hypothesis that hylobatids and modern humans are morphologically closer to each other, sharing a barrel-shaped ribcage, and distinct from those of funnel-shaped great apes is not supported. Allometry is an important factor for understanding thorax morphology driving variation in thorax width relative to depth, and

partly thoracic column invagination. 3D analyses suggest that it is not possible to recognize funnel and barrel geometries in the upper part of the ribcage alone casting doubt on such classifications proposed on fossil hominin remains. Of all living apes, *Pongo* is most similar to modern humans in total thorax shape and size and both are markedly distinct from African apes. Our findings suggest that classifying ribcages into barrel and funnel shapes may only describe general outlines, whereas the functional anatomy of the ribcages can be better assessed at closer morphological details. The size of upper and lower ribs, the various 3D curvatures in axial and sagittal planes as well as spatial aspects of torsion either closer to the vertebral or sternal rib ends, and the way the ribs articulate with the vertebral column are biologically meaningful for respiratory and locomotor function. 3D assessment of thorax shape contributes to analyzing features that affect thorax morphology, which is difficult to understand and interpret when described only from a simplified outline point of view. This is particularly relevant in the paleoanthropological context, where often fragmentary and dissociated thoracic remains must be interpreted.

Acknowledgments

Research funding: Spanish Ministry of Economy and Competitivity MINEO CGL2012-37279 and CGL2015-63648-P; The Leakey Foundation, The Cooperation Research Program of the Primate Research Institute, Kyoto University, and the Grant-in-Aid for Scientific Research (25840171) from the Japan Society for the Promotion of Science. We thank Nakatsukasa M. (Kyoto Uni), Egi N. (KUPRI), Fujita M. (NVLU), and Hasegawa D. (NVLU) for CT scanning, Endo H. (Tokyo Uni), Kawada S. (NMNS), Une Y. (Aazabu Uni), Great Ape Information Network (GAIN) for access to the specimens.

References

Aoyama, H., Mizutani-Koseki, S., Koseki, H., 2005. Three developmental compartments involved in rib formation. Int. J. Dev. Biol. 49, 325-333.

Barker, K.B., Ward, C.V., 2008. Patterns of upper rib morphology in hominoids. Am. J. Phys. Anthropol. S46, 64.

Bastir, M., García-Martínez, D., Recheis, W., Barash, A., Coquerelle, M., Rios, L., Peña-Melián, Á., García Río, F., O'Higgins, P., 2013. Differential growth and development of the upper and lower human thorax. PLoS ONE 8, e75128.

Bastir, M., García-Martínez, D., Barash, A., Been, E., Torres, I., García Río, F., 2014a. Thorax kinematics and the reconstruction of body models in hominin evolution, European Society for the Study of Human Evolution, Florence, p. 35.

Bastir, M., Higuero, A., Ríos, L., García-Martínez, D., 2014b. Three-dimensional analysis of sexual dimorphism in human thoracic vertebrae: Implications for the respiratory system and spine morphology. Am. J. Phys. Anthropol. 155, 513-521.

Bastir M, Garcia-Martinez D, Estalrrich A, Garcia-Tabernero A, Huguet R, Rios L, Barash A, Recheis W, de la Rasilla M, Rosas A. 2015. The relevance of the first ribs of the El Sidron site (Asturias, Spain) for the understanding of the Neandertal thorax. J. Hum. Evol. 80, 64-73.

Bastir, M., García-Martínez, D., O'Higgins, P., Utrilla, C., Torres, M., García Río, F., 2016. In vivo 3D analysis of thoracic kinematics: changes in size and shape during breathing and their implications for respiratory function in recent humans and fossil hominins. Anat. Rec. (in press)

Bastir, M., Garcia-Martínez, D., Williams, S.A., Nallah, S., Eyre, J.E., Oishi, M., Ogihara, N., Churchill, S.E., Berger, L., Schmid, P., 2016. Preliminary findings of the 3D analysis of the costal remains of *Australopithecus sediba*, Paleoanthropology Society, Atlanta, A2-A3.

Bastir, M., Higuero, A., Ríos, L., García-Martínez, D., 2014. Three-dimensional analysis of sexual dimorphism in human thoracic vertebrae: Implications for the respiratory system and spine morphology. Am. J. Phys. Anthropol. 155, 513-521.

Bramble, D.M., Lieberman, D.E., 2004. Endurance running and the evolution of *Homo*. Nature 432, 345-352.

Churchill, S.E., Holliday, T.W., Carlson, K.J., Jashashvili, T., Macias, M.E., Mathews, S., Sparling, T.L., Schmid, P., de Ruiter, D.J., Berger, L.R., 2013. The Upper Limb of *Australopithecus sediba*. Science 340.

Daley MA, Bramble DM, Carrier DR. 2013. Impact Loading and Locomotor-Respiratory Coordination Significantly Influence Breathing Dynamics in Running Humans. PLoS ONE 8(8), e70752.

De Troyer, A., Kirkwood, P.A., Wilson, T.A., 2005. Respiratory Action of the Intercostal Muscles. Physiol. Rev. 85, 717-756.

EVAN-Society, 2010. ET, Toolkit for geometric morphometric analysis.

Franciscus, R.G., Churchill, S.E., 2002. The costal skeleton of Shanidar 3 and a reappraisal of Neandertal thoracic morphology. J. Hum. Evol. 42, 303-356.

García-Martínez, D., Barash, A., Recheis, W., Utrilla, C., Torres Sánchez, I., García Río, F., Bastir, M., 2014. On the chest size of Kebara 2. J. Hum. Evol. 70, 69-72.

García-Martínez, D., Bastir, M., Recheis, W., Barash, A., 2013. Two different barrels for two different primates: 3D geometric morphometrics of sliding semilandmarks of the *Hominoidea* superfamily thorax, Sociedad Española de Antropología Física, Bilbao, p. 39.

García-Martínez, D., 2013. 3D geometric morphometrics of the rib cage of the *Homo ergaster* KNM-WT 15000 and their possible evolutionary implications: an application of sliding semilandmarks on virtual anthropology to the morphology of the ribs. MSc thesis, Universidad Autónoma de Madrid-Museo Nacional de Ciencias Naturales CSIC, Madrid, p. 100.

García-Martínez D, Recheis W, Bastir M. 2016a. Ontogeny of 3D rib curvature and its importance for the understanding of human thorax development. Am. J. Phys. Anthropol. 159(3), 423-431.

García-Martínez, D., Torres-Tamayo, N., Torres-Sanchez, I., García-Río, F., Bastir, M., 2016b. Morphological and functional implications of sexual dimorphism in the human skeletal thorax. Am. J. Phys. Anthropol. 161, 467-477.

García-Martínez, D., Bastir, M., Estalrrich, A., García Tabernero, A., Huguet, R., Cunha, E., de la Rasilla, M., Rosas, A., 2014. Preliminary study of the head-neck complex of Neanderthal ribs from the El Sidrón site (Asturias, Spain), in: PESHE (Ed.). Society for the Study of Human Evolution, Florence, p. 76.

Gayzik, F.S., Yu, M.M., Danelson, K.A., Slice, D.E., Stitzel, J.D., 2008. Quantification of age-related shape change of the human rib cage through geometric morphometrics. J. Biomech. 41, 1545-1554.

Gómez-Olivencia, A., Eaves-Johnson, K.L., Franciscus, R.G., Carretero, J.M., Arsuaga, J.L., 2009. Kebara 2: new insights regarding the most complete Neandertal thorax. J. Hum. Evol. 57, 75-90.

Gómez-Olivencia A, Carretero JM, Lorenzo C, Arsuaga JL, Bermúdez de Castro JM, and Carbonell E. 2010. The costal skeleton of *Homo antecessor*: preliminary results. J. Hum. Evol. 59(6):620-640.

Haeusler, M., Martelli, S.A., Boeni, T., 2002. Vertebrae numbers of the early hominid lumbar spine. J. Hum. Evol. 43, 621-643.

Haile-Selassie, Y., Latimer, B.M., Alene, M., Deino, A.L., Gibert, L., Melillo, S.M., Saylor, B.Z., Scott, G.R., Lovejoy, C.O., 2010. An early *Australopithecus afarensis* postcranium from Woranso-Mille, Ethiopia. Proc. Natl. Acad. Sci. 107, 12121-12126.

Holliday, T.W., 2012. Locomotor Convergence and other Homoplasies: the *Homo* and *Hylobates* Example, in: PESHE (Ed.), ESHE, European Society for the study of human evolution, Bordeaux, p. 14.

Jellema, L.M., Latimer, B., Walker, A., 1993. The rib cage, in Walker, A., Leakey, R. (Eds.), The Nariokotome *Homo Erectus* Skeleton. Harvard University Press, Cambridge, pp. 294-325.

Johanson, D.C., Lovejoy, C.O., Kimbel, W.H., White, T.D., Ward, S.C., Bush, M.E., Latimer, B.M., Coppens, Y., 1982. Morphology of the Pliocene partial hominid skeleton (A.L. 288-1) from the Hadar formation, Ethiopia. Am. J. Phys. Anthropol. 57, 403-451.

Jungers, W.L., 1984. Scaling of the hominoid locomotor skeleton with special reference to lesser apes, in: Preuschoft, H., Chivers, D.J., Brockelman, W.Y. (Eds.), The

Lesser Apes: Evolutionary and Behavioral Biology. Edinburgh University Press, Edinburgh, pp. 146-169.

Kagaya, M., Ogihara, N., Nakatsukasa, M., 2008. Morphological study of the anthropoid thoracic cage: scaling of thoracic width and an analysis of rib curvature. Primates 49, 89-99.

Klingenberg, C.P., 2011. MorphoJ: an integrated software package for geometric morphometrics. Mol. Ecol. Res. 11, 353-357.

Larson, S.G., Stern, J.T., 1987. EMG of chimpanzee shoulder muscles during knuckle-walking: problems of terrestrial locomotion in a suspensory adapted primate. J. Zool. 212, 629-655.

Latimer, B., Ward, C.V., 1993. The thoracic and lumbar vertebrae, The Nariokotome Homo Erectus Skeleton. Harvard University Press, Cambridge, pp. 266-293.

Latimer, B., Lovejoy, C.O., Haile-Selassie, Y., 2016. The thoracic cage of KSD-VP-1/1, in Haile-Selassie, Y., Su, D.F. (Eds.), The Postcranial Anatomy of *Australopithecus afarensis*: New Insights KSD-VP-1/1. Springer, Dordrecht, Netherlands, pp. 143-153.

Lovejoy, C.O., 2005. The natural history of human gait and posture. Gait & Posture 21, 95-112.

Lovejoy, C.O., Suwa, G., Simpson, S.W., Matternes, J.H., White, T.D., 2009. The great divides: *Ardipithecus ramidus* reveals the postcrania of our last common ancestors with African apes. Science 326, 73, 100-106. Maurer, R., 1970. Skelettrumpflänge, Skelettproportionen und Allometrien, Institut fuer Anthropologie. Zuerich, p. 92.

Mitteroecker P, Gunz P, Bernhard M, Schaefer K, Bookstein FL. 2004. Comparison of cranial ontogenetic trajectories among great apes and humans. J. Hum. Evol. 46(6),679-698.

Mitteroecker, P., Gunz, P., 2009. Advances in Geometric Morphometrics Evolutionary Biology 36, 235-247.

Moyá-Solá, S., Kohler, M., Alba, D.M., Casanovas-Vilar, I., Galindo, J., 2004. *Pierolapithecus catalaunicus*, a new Middle Miocene great ape from Spain. Science 306, 1339-1344.

Ogilvie, M.D., Hilton, C.E., Ogilvie, C.D., 1998. Lumbar anomalies in the Shanidar 3 Neandertal. J. Hum. Evol. 35, 597-610.

Pilbeam, D., 2004. The anthropoid postcranial axial skeleton: comments on development, variation, and evolution. J. Exp. Zool. (Mol. Dev. Evol.) 302B, 241-267.

Preuschoft, H., 2004. Mechanisms for the acquisition of habitual bipedality: are there biomechanical reasons for the acquisition of upright bipedal posture? J. Anat. 204, 363-384.

Ratnovsky, A., Elad, D., Halpern, P., 2008. Mechanics of respiratory muscles. Resp. Physiol. Neurobiol. 163, 82-89.

Rohlf, 1997. NTSYS-pc: Numerical taxonomy and multivariate analysis system. Exeter Software, Setauket, New York.

Ruff, C.B., 1991. Climate and body shape in hominid evolution. J. Hum. Evol. 21, 81-105.

Sawyer, G.J., Maley, B., 2005. Neanderthal reconstructed. Anat. Rec. 283B, 23-31.

Schmid, P., 1983. Eine Rekonstruktion des Skelettes von A.L. 288-1 (Hadar) und deren Konsequenzen. Folia Primatol. (Basel) 40, 283-306.

Schmid, P., 1991. The trunk of the australopithecines, in: Coppens, Y., Senut, B. (Eds.), Origine(s) de la Bipédie chez les Hominidés. Anatole, France: Éditions du Centre National de la Recherche Scientifique, pp. 225-234.

Schmid, P., Churchill, S.E., Nalla, S., Weissen, E., Carlson, K.J., de Ruiter, D.J., Berger, L.R., 2013. Mosaic morphology in the thorax of *Australopithecus sediba*. Science 340.

Schmidt M, and Krause C. 2011. Scapula Movements and Their Contribution to Three-Dimensional Forelimb Excursions in Quadrupedal Primates. In: D'Août K, and Vereecke EE, editors. Primate Locomotion, Linking Field and Laboratory Research. New York Dordrecht Heidelberg London: Springer p83-108.

Schultz, A., 1961. Vertebral column and thorax, Primatología, Handbuch der Primatenkunde, pp. 1-66.

Schultz, A., 1961. Vertebral column and thorax, in: Hofer, H., Schultz, A.H., Starck, D. (Eds.), Primatologia, Handbuch der Primatenkunde. Karger, Basel (Schweiz), New York, pp. 1-66.

Tawane G, García-Martínez D, Eyre J, Bastir M, Berger L, Nalla S, and Williams S. 2016. A hominin first rib discovered at the Sterkfontein caves. S. Afr. J. Sci. (in press).

Thompson, N.E., Demes, B., O/'Neill, M.C., Holowka, N.B., Larson, S.G., 2015. Surprising trunk rotational capabilities in chimpanzees and implications for bipedal walking proficiency in early hominins. Nat Commun 6.

Thorpe, S.K.S., Holder, R.L., Crompton, R.H., 2007. Origin of human bipedalism as an adaptation for locomotion on flexible branches. Science 316, 1328-1331.

Ward, C.V., 1993. Torso morphology and locomotion in *Proconsul nyanzae*. Am. J. Phys. Anthropol. 92, 291-328.

Ward, C., Kimbel, W., Harmon, E., Johanson, D., 2012. New postcranial fossils of *Australopithecus afarensis* from Hadar, Ethiopia (1990–2007). J. Hum. Evol. 63, 1-51.

Williams, S.A., 2012a. Variation in anthropoid vertebral formulae: implications for homology and homoplasy in hominoid evolution. J. Exp. Zool. B (Mol. Dev. Evol.) 318, 134-147.

Williams, S.A., 2012b. Placement of the diaphragmatic vertebra in catarrhines: implications for the evolution of dorsostability in hominoids and bipedalism in hominins. Am. J. Phys. Anthropol. 148, 111-122.

Williams, S.A., Middleton, E.R., Villamil, C.I., Shattuck, M.R., 2016. Vertebral numbers and human evolution. Y. Phys. Anthropol. 159, S19-S36.

Williams, S.A., Ostrofsky, K.R., Frater, N., Churchill, S.E., Schmid, P., Berger, L.R., 2013. The vertebral column of *Australopithecus sediba*. Science 340, 1232996.

Williams, S.A., Russo, G.A., 2015. Evolution of the hominoid vertebral column: the long and the short of it. Evol. Anthropol. 24, 15-32.

Zelditch, M.L., Swiderski, D.L., Sheets, H.D., Fink, W.L., 2012. Geometric Morphometrics for Biologists: A Primer, 2nd edition ed. Elsevier Academic Press, San Diego.

Table 1. Mean centroid size comparisons of the upper thorax.

Group	**Mean CS**	**Std. error**	**-95%**	**+95%**
Homo	1994.13	46.15	1899.59	2088.67
Pan	1646.61	46.15	1552.07	1741.15
Gorilla	2401.15	65.27	2267.45	2534.85
Pongo	1656.25	72.97	1506.76	1805.73
Hylobatids	1060.27	72.97	910.79	1209.75

Table 2. Procrustes distances between upper thorax mean shapes (all at least significant at $p<0.01$).

	Gorilla	***Homo***	**Hylobatids**	***Pan***
Homo	0.112			
Hylobatids	0.163	0.134		
Pan	0.129	0.114	0.080	
Pongo	0.107	0.113	0.158	0.124

Table 3. Mean centroid size comparisons of the extended thorax.

Group	**Mean CS**	**Std. error**	**-95%**	**+95%**
Homo	2948.28	62.97	2819.31	3077.26
Pan	2509.14	62.97	2380.16	2638.12
Gorilla	3623.20	89.05	3440.79	3805.60
Pongo	2510.23	99.56	2306.30	2714.17
Hylobatids	1574.81	99.56	1370.87	1778.74

Table 4. Procrustes distances between extended thorax mean shapes (all at least significant at $p<0.01$).

	Gorilla	***Homo***	**Hylobatids**	***Pan***
Homo	0.166			
Hylobatids	0.158	0.135		
Pan	0.118	0.146	0.095	
Pongo	0.158	0.133	0.161	0.153

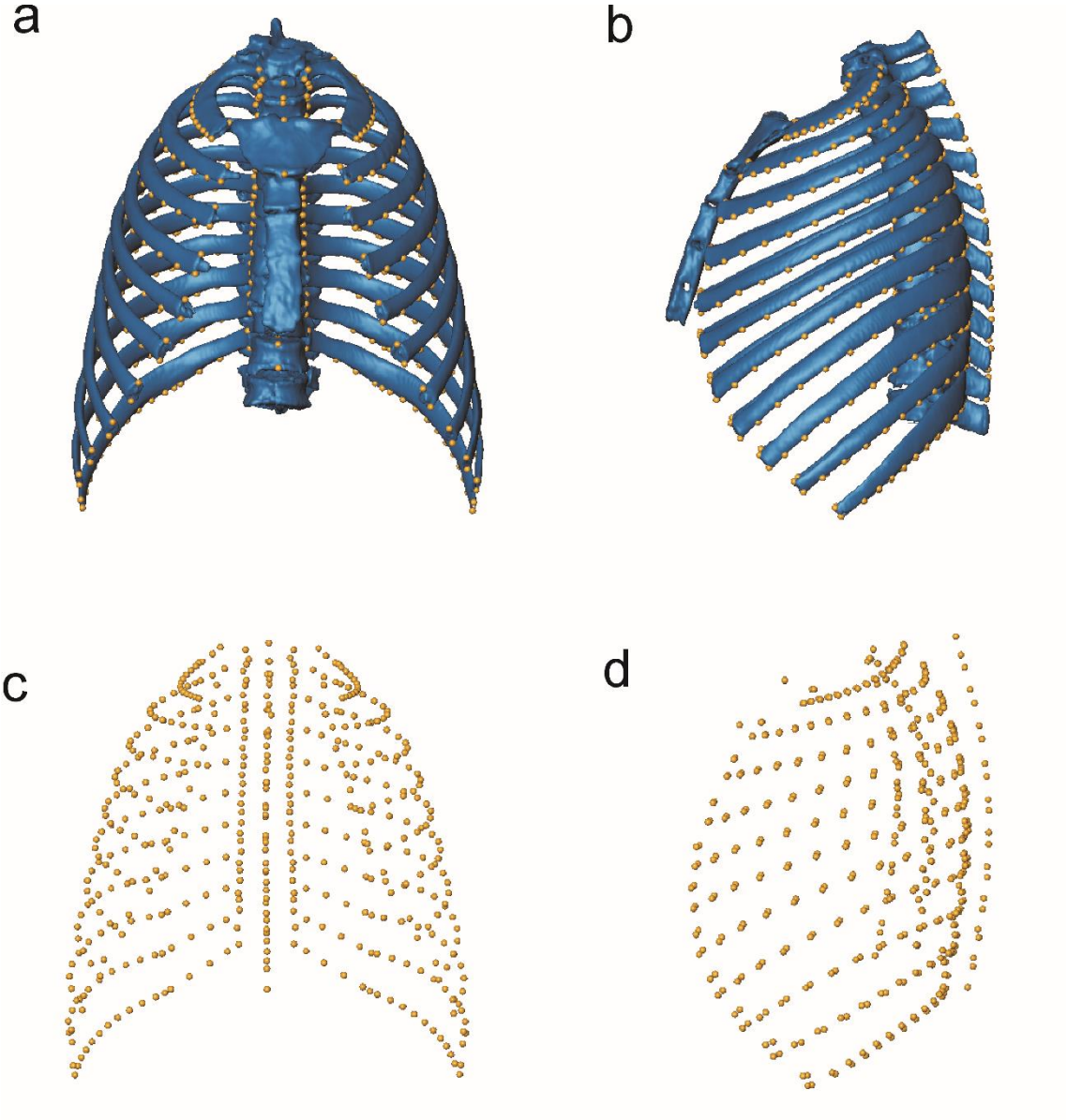

Figure 1. a) Frontal and b) lateral view of the 3D landmark configuration of the grand mean of 11 thoracic levels and the relation of the landmarks to rib and thorax morphology. c) 3D landmarks in frontal view and d) in left lateral view.

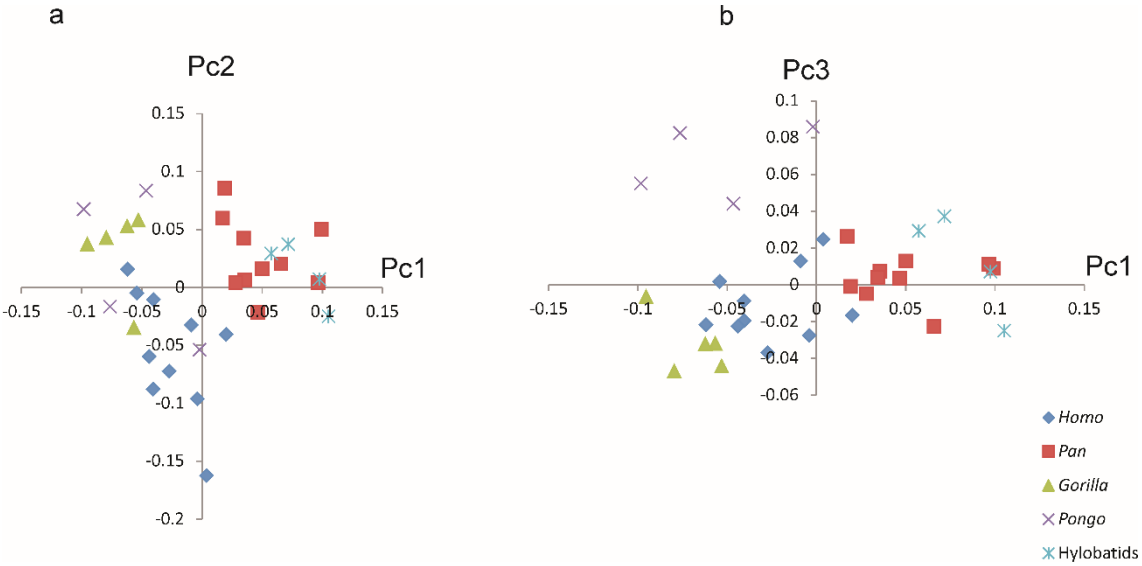

Figure 2. Scatterplots of principal component scores in shape space of the upper thorax data. (a) PC1 vs PC2 and (b) PC1 vs PC3. Note that *Gorilla*, humans and *Pongo* plot together towards positive PC1, *Pan* and hylobatids towards negative PC1. Humans plot towards negative PC2 scores while all hominoids plot towards positive PC2 scores. PC3 polarizes *Pongo* from the remaining species.

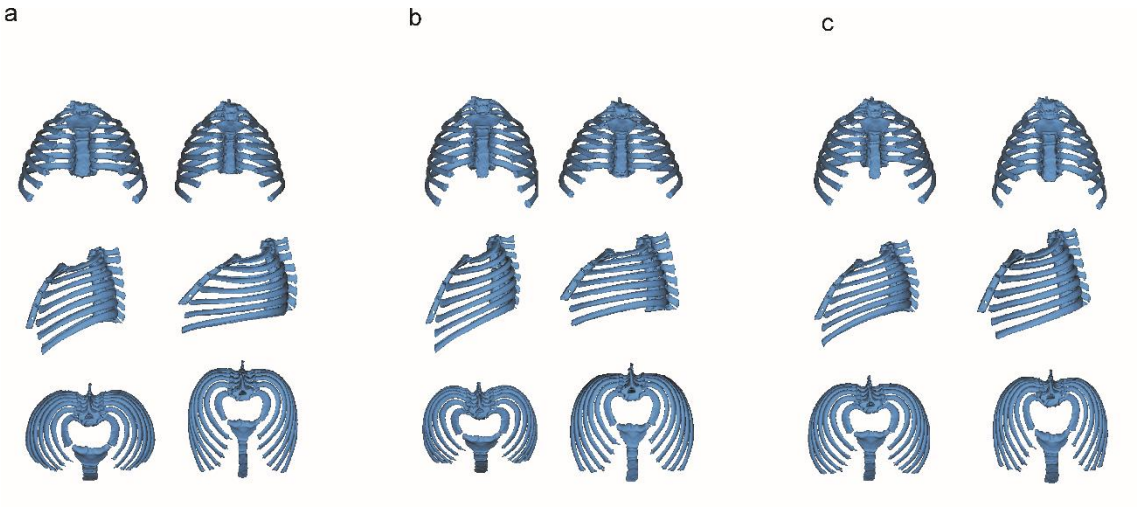

Figure 3. Shape variations associated to the principal component analysis of upper thorax data shown in frontal, left lateral and superior axial views. Left columns show negative loadings, right columns show positive loadings, both at maximal observed ranges; (a) PC1, (b) PC2, (c) PC3.

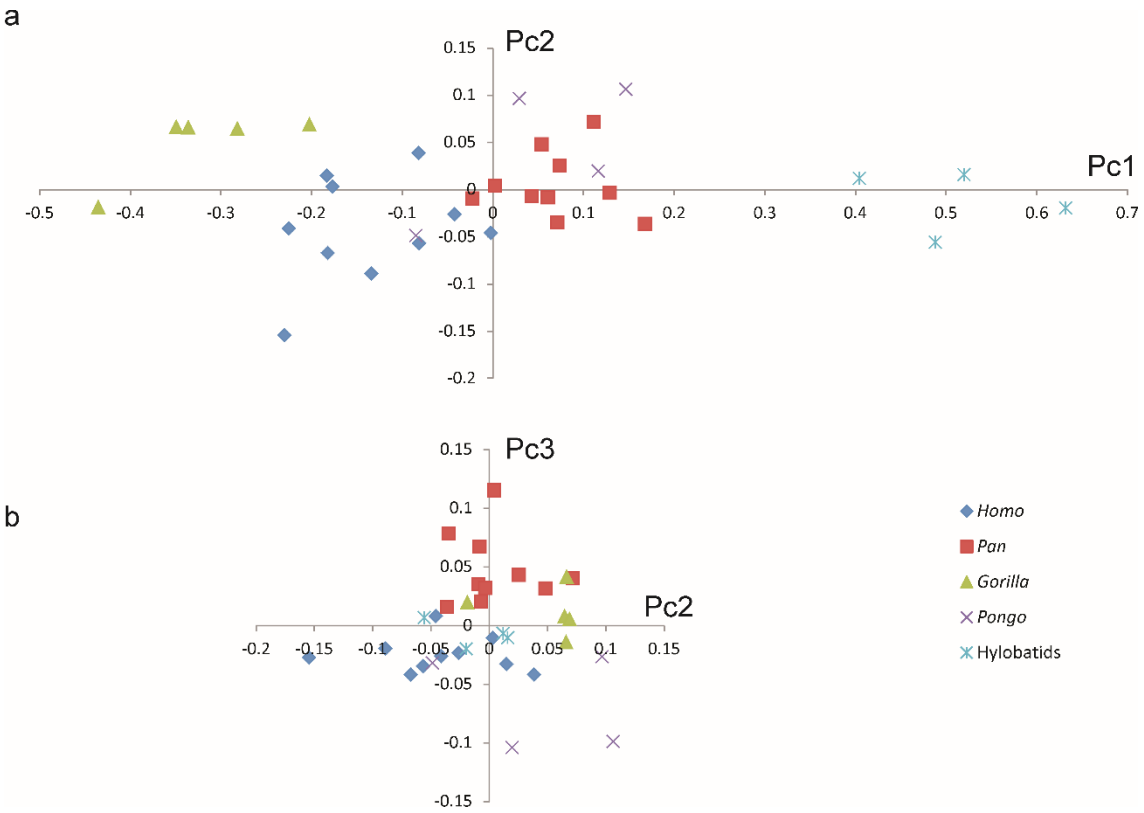

Figure 4. Scatterplots of principal component scores in Procrustes Form space of the upper thorax data. (a) PC1 vs PC2 and (b) PC2 vs PC3. Note that PC1-PC2 projections order the data according to size. PC3 polarizes African apes and the rest.

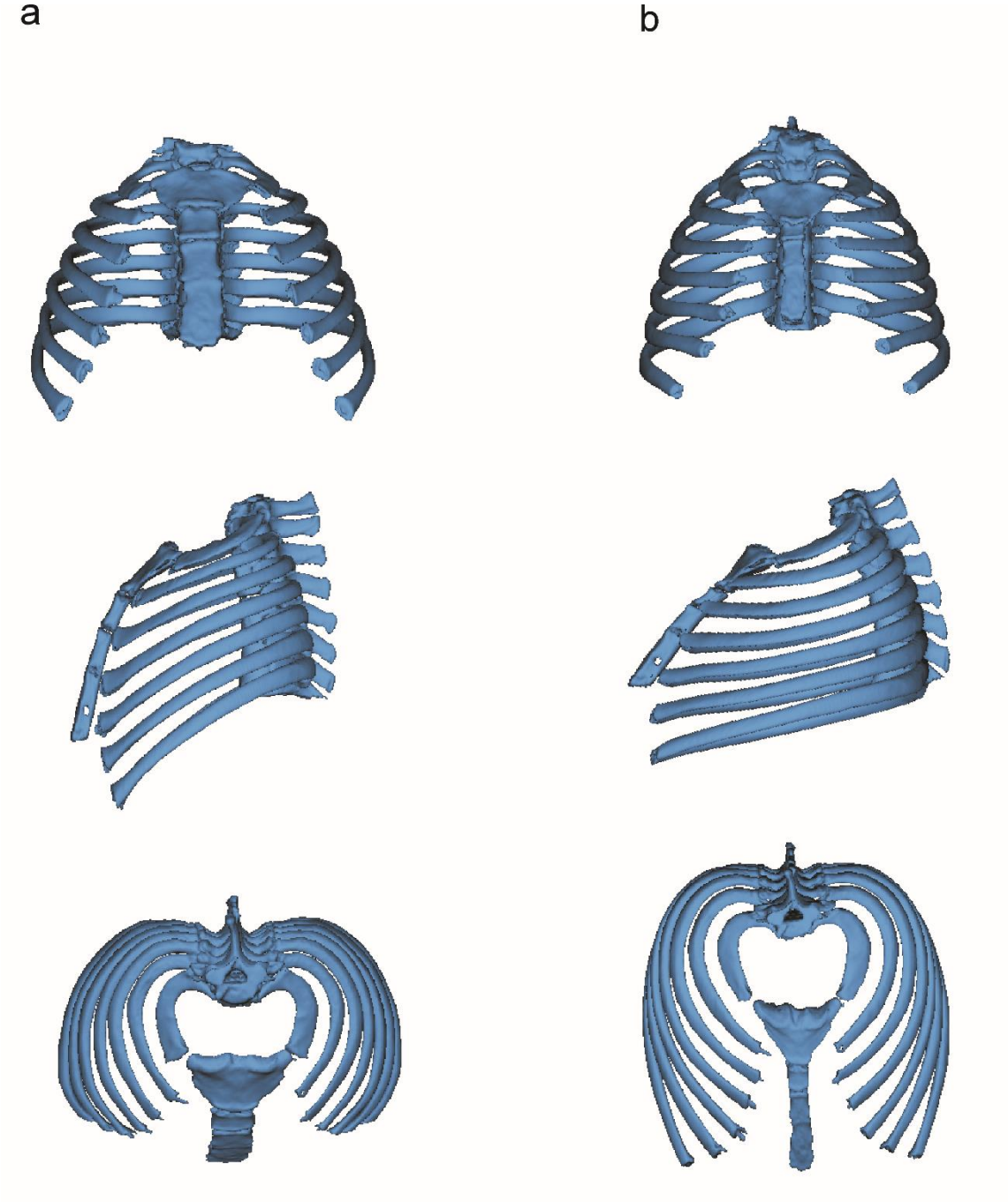

Figure 5. Shape variations associated the principal component analysis of Procrustes form space illustrate common features of allometric shape variation in frontal, left lateral and superior axial views. (a) Shapes with negative PC1 loadings (large specimens, (b) shapes with positive PC1 loadings (small specimens); both shapes are shown at maximal observed ranges.

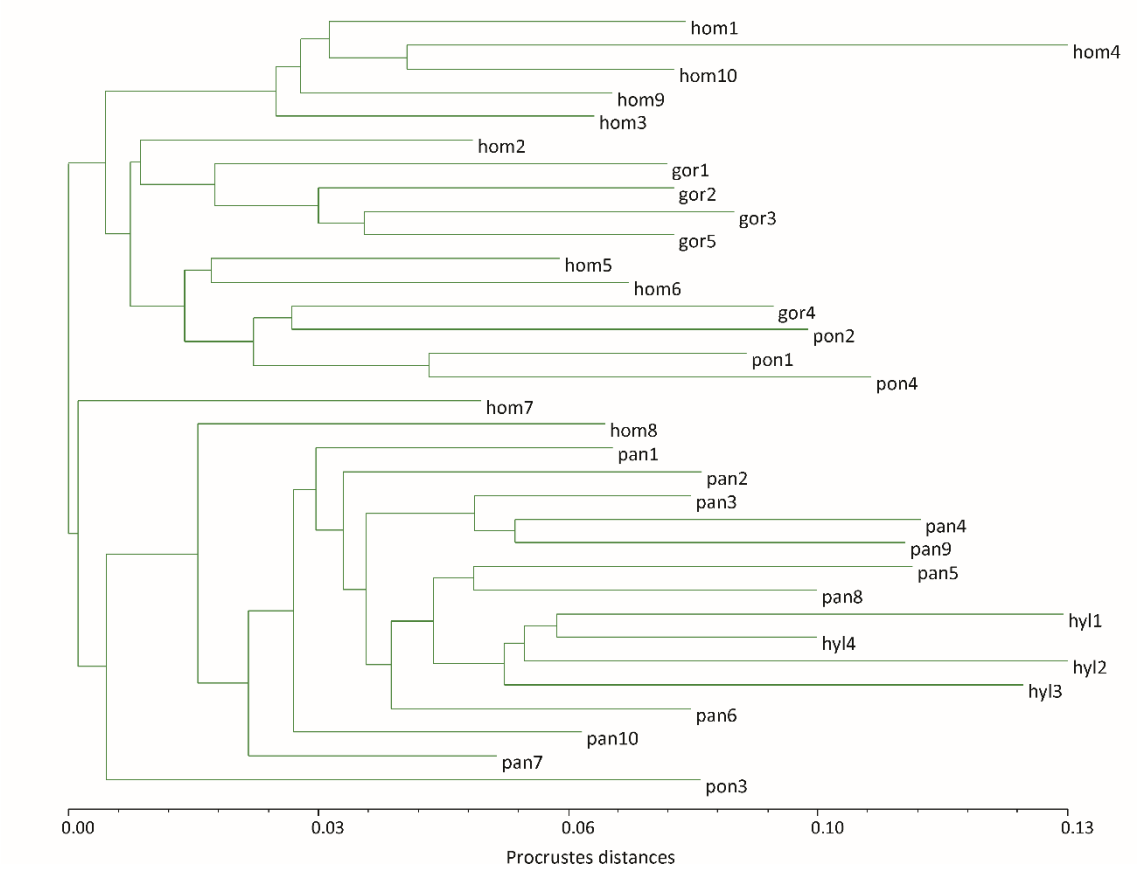

Figure 6. Neighbour joining tree based on Procrustes distances between all shapes of the upper thorax sample. Humans, *Gorilla* and *Pongo* cluster together and differ from the second cluster composed of *Pan* and hylobatids.

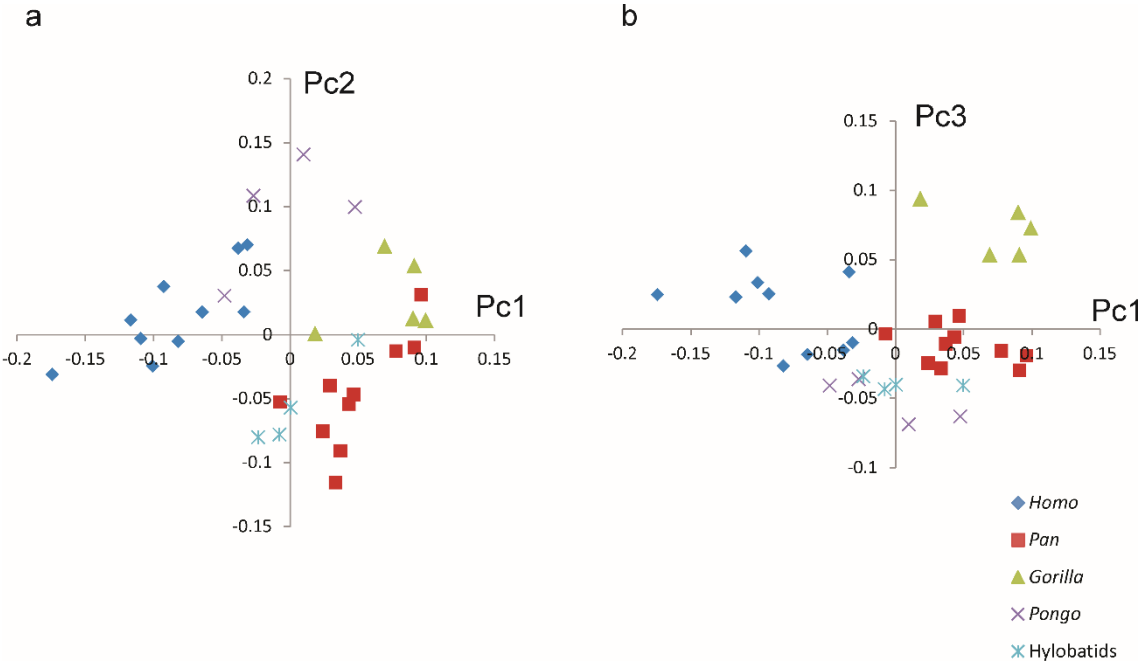

Figure 7. Scatterplots of principal component scores in shape space of the extended thorax data. (a) PC1 vs PC2 and (b) PC1 vs PC3. PC1 orders the data polarizing humans and African apes. PC2 orders larger versus smaller specimens within the apes. Note the relationships between humans and *Pongo* and the rest of the sample. PC3 polarizes *Pongo* from the remaining species.

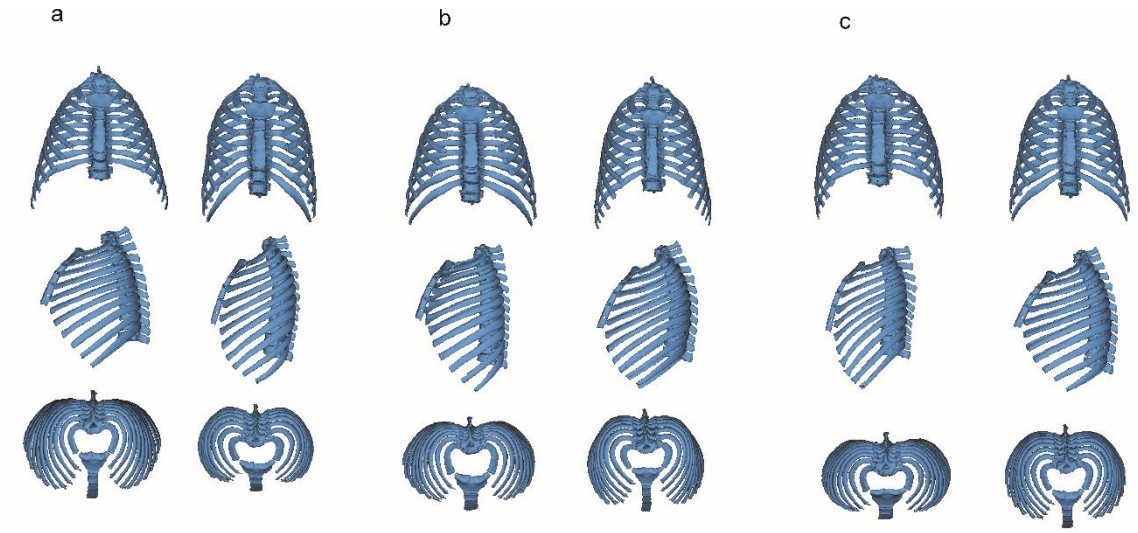

Figure 8. Shape variations associated the principal component analysis of extended thorax data shown in frontal, left lateral and superior axial views. Left columns show negative loadings, right columns show positive loadings, both at maximal observed ranges; (a) PC1, (b) PC2, (c) PC3.

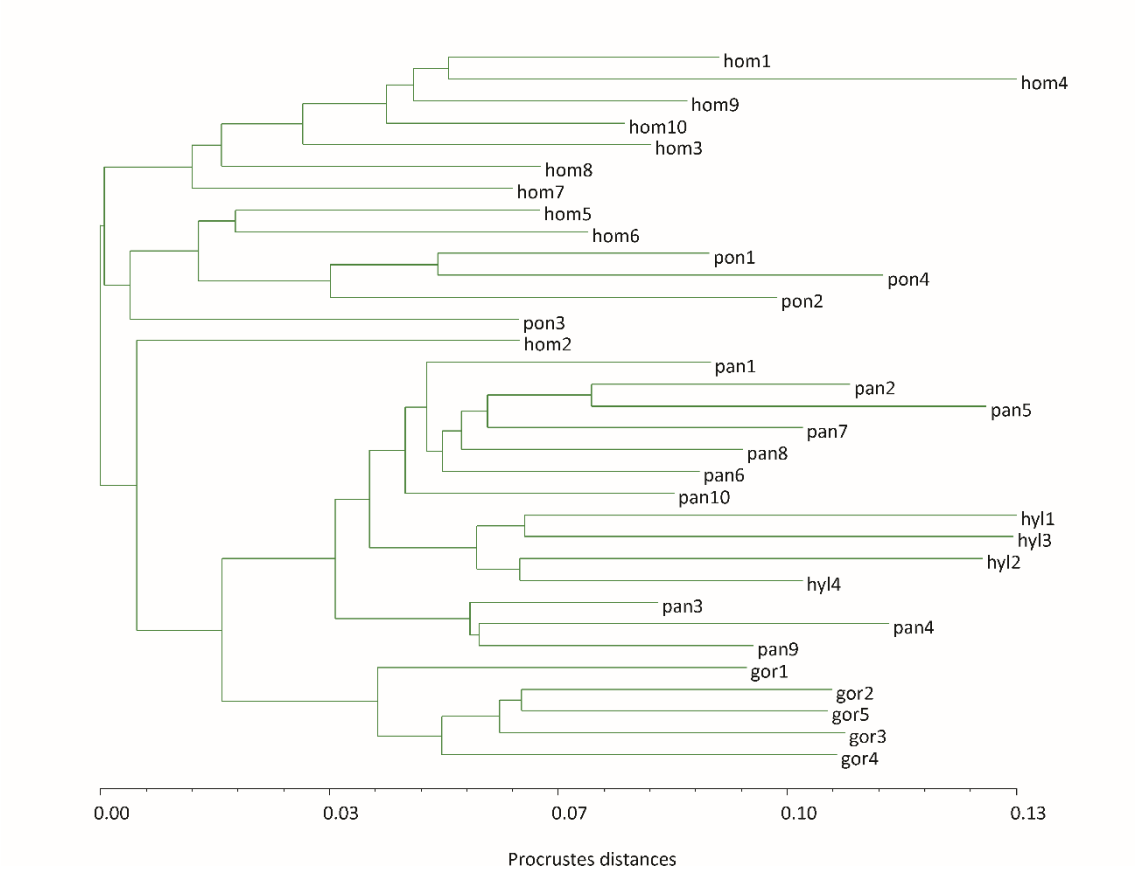

Figure 9. Neighbour joining tree based on Procrustes distances between all shapes of the extended thorax sample. Humans and *Pongo* cluster together and differ from the second cluster composed of the African great apes and hylobatids.

Supplementary Table S1. Data sets (species, sex, age and institution).

Name	Specie	Sex	Age (years)	Institution
HTX002	*Hylobates lar*	Female	32	Primate Research Institute, Kyoto
HTX003	*Hylobates agilis*	Male	30	Primate Research Institute, Kyoto
HTX008	*Hylobates lar*	Male	33	Primate Research Institute, Kyoto
HTX027	*Symphalangus syndactylus*	Male	Adult	National Museum of Nature and Science, Tokyo
HTX014	*Pongo pygmaeus*	Female	42	Primate Research Institute, Kyoto
HTX019	*Pongo pygmaeus*	Female	19	National Museum of Nature and Science, Tokyo
HTX031	*Pongo pygmaeus*	Male	13	Primate Research Institute, Kyoto
HTX004	*Gorilla gorilla*	Male	46	Primate Research Institute, Kyoto
HTX017	*Gorilla gorilla*	Female	40	National Museum of Nature and Science, Tokyo
HTX021	*Gorilla gorilla*	Male	38	Tokyo University
HTX025	*Gorilla gorilla*	Male	33	Primate Research Institute, Kyoto
HTX006	*Pan troglodytes*	Female	34	Primate Research Institute, Kyoto
HTX012	*Pan troglodytes*	Female	Adult	Primate Research Institute, Kyoto
HTX015	*Pan troglodytes*	Female	44	Primate Research Institute, Kyoto
HTX016	*Pan troglodytes*	Male	27	Primate Research Institute, Kyoto
HTX018	*Pan troglodytes*	Male	35	National Museum of Nature and Science, Tokyo
HTX020	*Pan troglodytes*	Female	45	National Museum of Nature and Science, Tokyo
HTX022	*Pan troglodytes*	Male	38	Primate Research Institute, Kyoto
HTX023	*Pan troglodytes*	Female	8	Azabu University
HTX024	*Pan troglodytes*	Male	34	Azabu University
HTX026	*Pan troglodytes*	Male	47	Azabu University
TX006	*Homo sapiens*	Male	40	University Hospital of Innsbruck
TX007	*Homo sapiens*	Male	60	University Hospital of Innsbruck
TX010	*Homo sapiens*	Female	62	University Hospital of Innsbruck
TX011	*Homo sapiens*	Female	27	University Hospital of Innsbruck
TX050	*Homo sapiens*	Female	57	University Hospital of La Paz, Madrid
TX052	*Homo sapiens*	Male	49	University Hospital of La Paz, Madrid
TX054	*Homo sapiens*	Male	67	University Hospital of La Paz, Madrid
TX060	*Homo sapiens*	Female	49	University Hospital of La Paz, Madrid
TX068	*Homo sapiens*	Female	61	University Hospital of La Paz, Madrid
TX070	*Homo sapiens*	Male	67	University Hospital of La Paz, Madrid

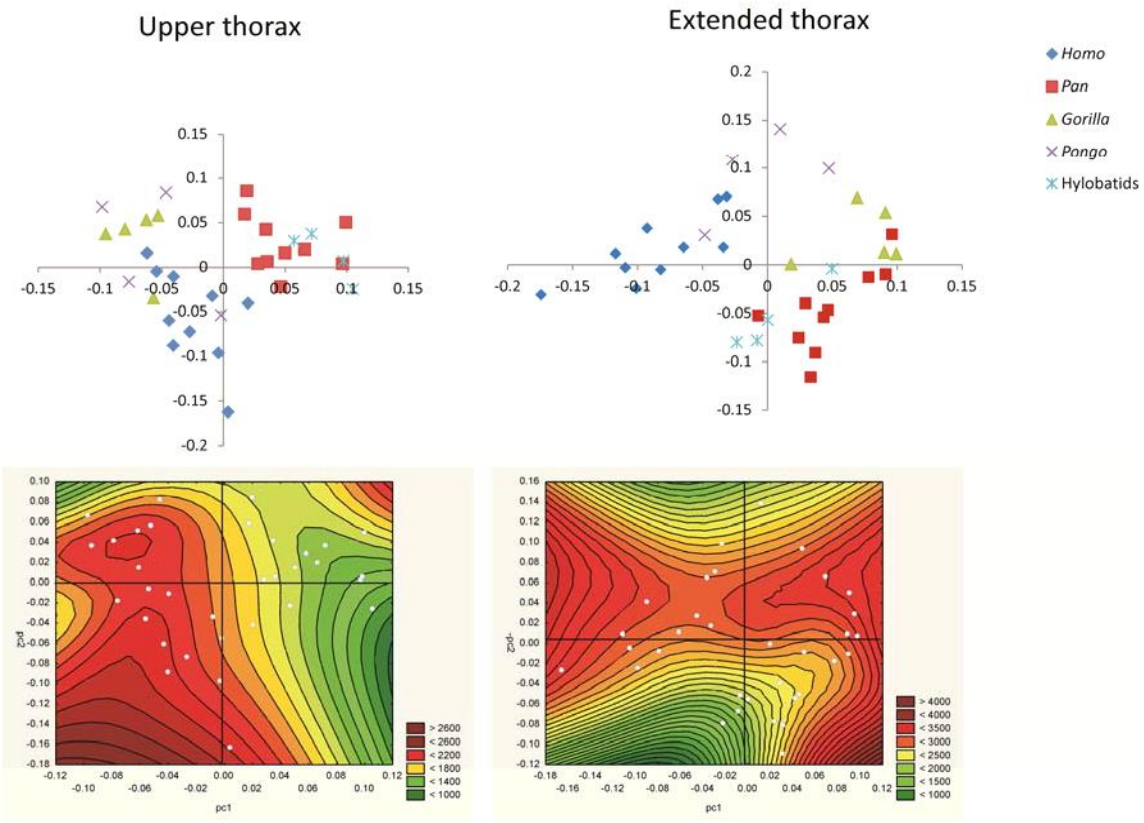

Figure S1. Size shape relations. Scatterplots of PC1 and PC2 scores of upper (left) and extended thorax (right) analysis. The lower row plots centroid size into this space. Note that in the upper thorax the size-shape relations are much clearer distributed along PC1 than in the extended thorax analysis.

CAPÍTULO VIII – RESULTADOS: ANATOMÍA EVOLUTIVA DE LA CAJA TORÁCICA

Los resultados obtenidos en referencia al **objetivo 5 "Contribuciones al conocimiento de la anatomía evolutiva de la caja torácica humana"** son mostrados por objetivos alcanzados.

Dentro del **objetivo 5a** "**Contribuciones al conocimiento de la anatomía evolutiva en el género *Australopithecus***" se ha publicado un artículo y un resumen en congreso:

Tawane, G., García-Martínez, D., Eyre, J., Bastir, M., Berger, L., Nalla, S., Williams, S.A., 2016. A hominin first rib discovered at the Sterkfontein Caves, South Africa. South African Journal of Sciences 112, 1-7.

DOI: http://dx.doi.org/10.17159/sajs.2016/20150278

Bastir, M., **García-Martínez, D.**, Williams, S. A., Nalla, S., Eyre, J., Oishi, M., Ogihara, N., Churchill, S.E., Hawks, J., Berger, L.R., Schmid, P., 2016. Preliminary findings of 3D analyses of the costal remains of *Australopithecus sediba*. Abstracts of the Paleoanthropology Society 2016 Meeting; PaleoAnthropology 2016: A3.

http://www.paleoanthro.org/media/journal/content/PAS2016A.pdf

A hominin first rib discovered at the Sterkfontein Caves, South Africa

AUTHORS:
Gaokgatlhe Tawane[1]
Daniel García-Martínez[1,2,3]
Jennifer Eyre[4,5]
Markus Bastir[1,2]
Lee Berger[1]
Peter Schmid[1,7]
Shahed Nalla[1,6]
Scott A. Williams[1,4,5]

AFFILIATIONS:
[1]Evolutionary Studies Institute and Centre for Excellence in Palaeosciences, University of the Witwatersrand, Johannesburg, South Africa
[2]Palaeoanthropology Group, National Museum of Natural Sciences (MNCN-CSIC), Madrid, Spain
[3]Biology Department, Faculty of Sciences, Autonomous University of Madrid, Madrid, Spain
[4]Center for the Study of Human Origins, Department of Anthropology, New York University, New York, New York, USA
[5]New York Consortium in Evolutionary Primatology, New York, New York, USA
[6]Department of Human Anatomy and Physiology, Faculty of Health Sciences, University of Johannesburg, Johannesburg, South Africa
[7]Anthropological Institute and Museum, University of Zurich, Zurich, Switzerland

CORRESPONDENCE TO:
Daniel García-Martínez

EMAIL:
dan.garcia@mncn.csic.es

POSTAL ADDRESS:
Palaeoanthropology Group, Museo Nacional de Ciencias Naturales (MNCN-CSIC) – Paleobiology, José Gutierrez Abascal 6, 28006 Madrid, Spain

DATES:
Received: 29 July 2015
Revised: 11 Dec. 2015
Accepted: 08 Jan. 2016

KEYWORDS:
upper thorax; rib cage; *Australopithecus africanus*; geometric morphometrics; Gauteng Province

HOW TO CITE:
Tawane G, García-Martínez D, Eyre J, Bastir M, Berger L, Nalla S, et al. A hominin first rib discovered at the Sterkfontein Caves, South Africa. S Afr J Sci. 2016;112(5/6), Art. #2015-0278, 7 pages. http://dx.doi.org/10.17159/sajs.2016/20150278

First ribs – the first or most superior ribs in the thorax – are rare in the hominin fossil record, and when found, have the potential to provide information regarding the upper thorax shape of extinct hominins. Here, we describe a partial first rib from Member 4 of the Sterkfontein Caves, South Africa. The rib shaft is broken away, so only the head and neck are preserved. The rib is small, falling closest to small-bodied *Australopithecus* first ribs (AL 288-1 and MH1). Given that it was recovered near the StW 318 femur excavation, which also represents a small individual, we suggest that the two may be associated. Three-dimensional geometric morphometric analyses were used to quantify the rib fragment morphology and compare it to extant hominoid and other fossil hominin ribs. While only the proximal end is preserved, our analyses show that South African *Australopithecus* share derived features of the proximal first rib more closely resembling *A. afarensis* and later hominins than great apes.

Introduction

Ribs are rare in the human fossil record because of their delicate structure; this scarcity is particularly pronounced in the early hominin fossil record. Moreover, those that have been discovered are usually fragmentary and distorted, and their interpretation is difficult because of the complicated morphological quantification of their 3D curvature.[1-5] In spite of the scarcity of these remains, it is important to note that, among ribs, the first rib is generally the best preserved in the fossil record as a result of its unique morphology relative to the rest of the ribs in the thorax.[6,7] The first rib is also important because it bears diagnostic features informative of upper thorax morphology.[7-9] For example, the modern human first rib usually has a univertebral articulation (with the T1 vertebra), as do those of early hominins, whereas the other great apes have a bivertebral articulation (with the C7 and T1 vertebrae).[10]

In early hominins, first ribs are known from *Australopithecus afarensis* (AL 288-1ax)[11], *Homo erectus* (KNM-WT 15000 AG and AY&AZ)[12], *A. sediba* (MH1, UW88-148; MH2, UW88-198 and UW88-187)[8] and *H. naledi* (UW101-83)[13]. *A. afarensis* AL 288-1 and *A. sediba* (MH1 and MH2) were hypothesised as presenting a narrow upper thorax, as extant apes do, and this thoracic shape is probably related to suspensory locomotor behaviour.[8,11,14,15] This narrow upper thorax has also been observed in the recently published small-bodied species *H. naledi.*[13] In contrast, other early hominin specimens, such as *H. erectus* (KNM-WT 15000) and the large-bodied *A. afarensis* (KSD-VP-1/1), have been proposed to have modern human-like, expanded upper thoraces.[12,16]

Sterkfontein Caves (located 40 km from Johannesburg) – one of the most important South African sites regarding the quantity and quality of the fossils discovered[17-20] – has yielded several costal remains, but a first rib has not been reported from this site to date. The *A. africanus* partial skeleton Sts 14, discovered at Sterkfontein in 1947, is associated with a number of ribs.[21] Robinson's analysis positioned the preserved ribs toward the lower thorax. According to Robinson[21], these ribs are smaller than those of modern *H. sapiens* but are characterised by a similar degree of curvature. The features observed on the ribs suggested a modern human-like lower thorax shape, but there is still some degree of uncertainty about the upper thorax shape of *A. africanus*.

In 1987, another partial skeleton, StW 431, this time of a larger-bodied, presumed male *A. africanus* was discovered at Sterkfontein in Bed B of Member 4.[22] StW 431 preserves a right rib with the head, neck and tubercle, which was assessed as a probable third rib.[22] However, the preservation of this fragment was not sufficient to discuss upper thorax morphology in *A. africanus* from an evolutionary point of view.

Here we report, present and discuss, in a comparative anatomical context, a well-preserved proximal part of a first rib previously recovered at Sterkfontein but neither identified nor published, as well as its provenance and its relation to the previously discovered remains from the Sterkfontein Caves.

Materials and methods

The new fossil, a proximal fragment of a first rib from the right side (StW 670; Figure 1) was discovered at Sterkfontein site (Cradle of Humankind, Gauteng, South Africa) in grid square V 46, at 21 feet 1 inches to 22 feet 4 inches (27'2–28'2), Member 4[23] (Figure 2). The date of the discovery of the rib is unknown. The collection from Sterkfontein Caves housed at the University of the Witwatersrand dates from 1966 to present excavations. Material collected from Sterkfontein prior to 1966 is housed at Ditsong Museum (formerly known as the Transvaal Museum).

Preservation, morphology and ontogenetic assessment of StW 670

A detailed description of the preservation status as well as the morphology was carried out on StW 670 based on the principal anatomical features of the first rib. Frequencies of single/double articular facet/s of rib head in the comparative sample were also studied (Supplementary table 1 of the supplementary material).

The maturation state of the first rib was evaluated based on the epiphyseal fusion of the articular tubercle of the rib and the articular facet of the rib head.[24] However, it should be noted that the maturation rate of *Australopithecus* epiphyseal fusion could differ from that of *H. sapiens*.

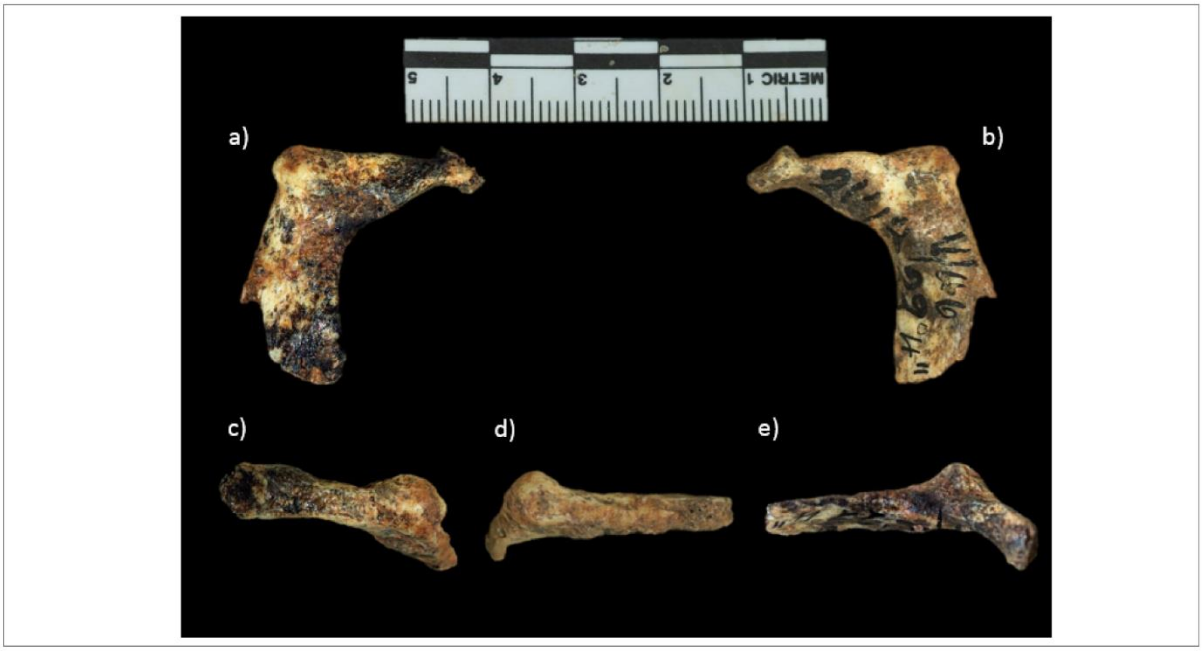

Figure 1: Rib StW 670 in different views: (a) superior, (b) inferior, (c) posterior, (d) exterior and (e) interior.

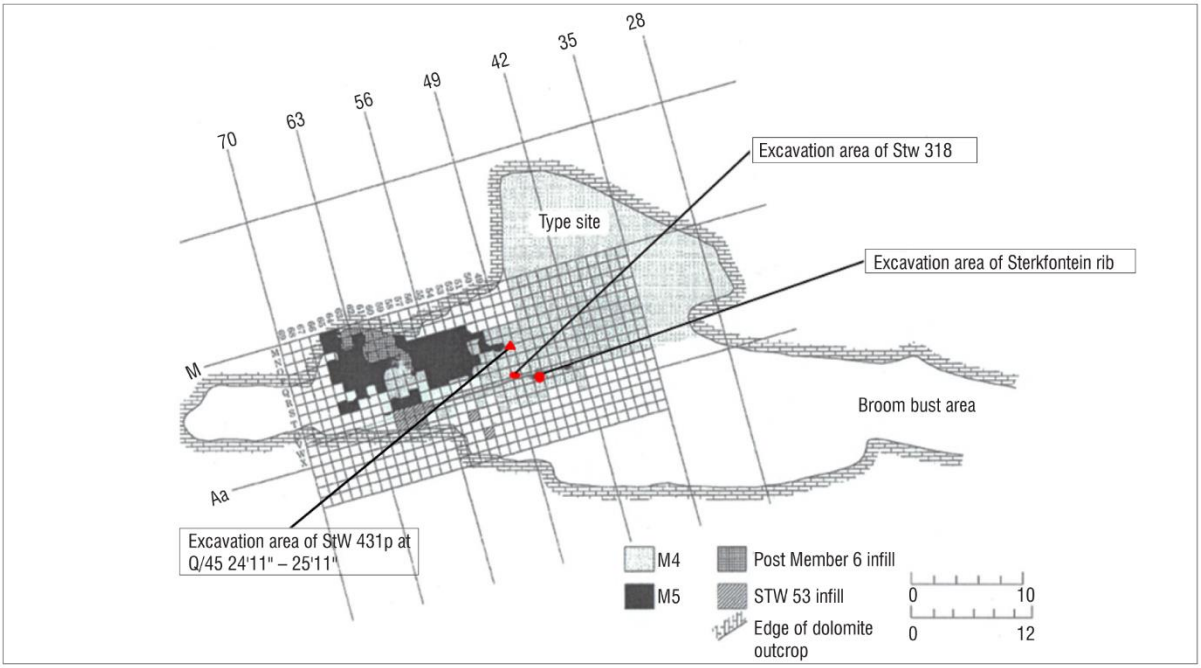

Figure 2: Stratigraphy of Sterkfontein Members 4 and 5, indicating the locality of excavation of StW 670 and StW 318.

Linear measurements

Linear measurements taken on StW 670 were carried out on the original remains. The linear measurements taken were: head height (superoinferior diameter of the rib head), head width (anteroposterior diameter of the rib head), neck length (distance from the medial-most point on the rib head to the medial-most point on the articular facet of the tubercle) and neck width (taken midway between the rib head and articular tubercle in anteroposterior dimension).[2,9,25] Each measurement was calculated from the average of three measurements in order to reduce intra-observer error.[1,2,25] The measurements are given in Table 1.

Table 1: Linear measurements taken on StW 670

	Head height (mm)	Head width (mm)	Neck length (mm)	Neck width (mm)
StW 670	6.4	6.7	18.8	5.5

Measurements on StW 670 were made with standard anthropometric instruments following the definitions used in previous studies.[2,9,25]

Geometric morphometric analyses

For 3D geometric morphometrics, 3D high-resolution laser scans of original fossils – StW 670, *A. sediba* MH1 (UW88-148) and MH2 (UW88-198) – and of a high-quality cast of AL 288-1ax *(A. afarensis)* were used. These scans were obtained using a NextEngine 3D laser scanner in 'wide mode' (with a resolution of 0.38 mm and an accuracy of 6 points per mm). Additionally, computerised tomography (CT) scans of the original remains of *H. erectus* KNM-WT 15000 (AG and AY&AZ) were employed for the analyses (Supplementary table 1).

For the 3D geometric morphometrics analyses, remains of 33 *H. sapiens* (20 Europeans, 10 sub-Saharan Africans, 1 small-bodied member of the San population and 2 small-bodied individuals from the Andaman Islands) were analysed (Supplementary table 1). These scans were also obtained through a NextEngine 3D laser scanner in 'wide mode' (with a resolution of 0.38 mm and an accuracy of 6 points per mm). Additionally, 8 ribs of *Pan troglodytes* (chimpanzee), 3 ribs of *Gorilla gorilla* (gorilla), 3 ribs of *Pongo* sp. (orangutan) and 3 ribs of *Hylobates* sp. (gibbon) from Kyoto University Primate Research Institute (www.pri.kyoto-u.ac.jp) were used to represent non-hominin morphological pattern (Supplementary table 1). Technical specifications of CT scanning can be obtained from www.pri.kyoto-u.ac.jp.

Six 3D type 1 landmarks were collected on each rib, quantifying morphological information of the rib head and the articular tubercle as well as the thickness of the rib neck (Figure 3). Landmarks were collected at the rib head on the most lateral, most medial, most caudal and most cranial points of the articular facet/s of the rib head and at the most lateral point of the articular tubercle. Additionally, one landmark was located at the point defined by the shortest distance from the most lateral point of the articular tubercle to the internal margin of the rib curvature ('d' distance in Figure 3). Because StW 670 is missing a large part of the body of the rib and the sternal end, no landmarks were taken on this area of the comparative sample.

Size was measured as centroid size.[26,27] The size relations between the Sterkfontein first rib and the rest of the individuals in our sample were explored using a box plot. These analyses were carried out in PAST software version 3.[28] In order to study the shape relations along the variability of the sample, we superimposed the landmark configurations using generalised Procrustes analysis.[26,27] The superimposed coordinates were then submitted to principal component analysis (PCA) in shape space in order to reduce the dimensionality of data and to visualise the main axes of variation.

Ordinations were computed into MorphoJ 1.05f software[29] and the shape differences of the surface associated with PC1 and PC2 axes were warped and visualised using the EVAN Toolkit software version 1.62 (www.evan-society.org/). A box plot of Procrustes distances was used to compare and explore shape relations from the individual under study (StW 670) to the different groups of the sample. These analyses were carried out in the Virtual Morphology Lab of the National Museum of Natural Sciences (Madrid, Spain).

Results

Preservation, morphology and ontogenetic assessment of StW 670

There is sufficient preservation of features in the first rib fragment (StW 670) to make description, comparison and analysis possible, even though the fossil is incomplete. The fragment has a well-preserved head, neck, tubercle and most of the proximal part of the body, although the rest of the body is lacking distally.

The rib fragment StW 670 was determined as a first rib from the right side. Siding was determined because the head is positioned at an angle caudal to the tubercle and shaft which produces a mediolateral slope of the neck. Moreover, as the caudal surface of the shaft is smoother than the cranial surface, this feature also confirms the side of the rib as a first rib from the right side.

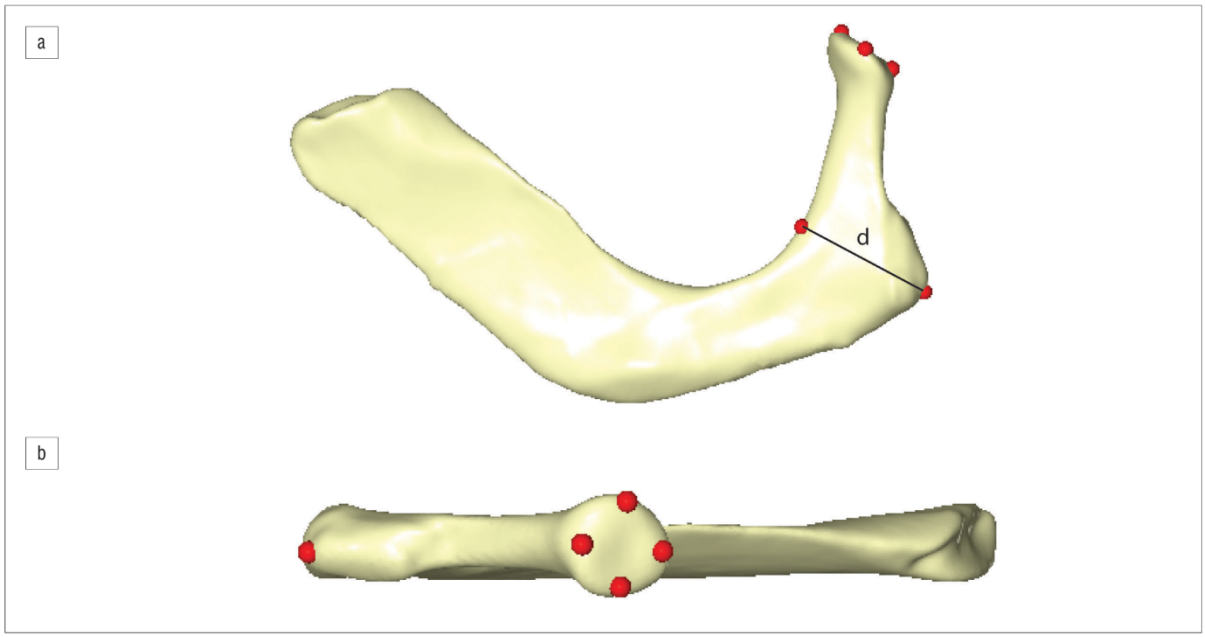

Figure 3: Anatomical location of the six landmarks type 1 taken on the sample. In (a), landmarks at the rib head on the most lateral, most medial and most cranial points of the articular facet/s of the rib head as well as at the most lateral point of the articular tubercle and the landmark defined by the distance 'd' are observed. In (b), the four landmarks at the rib head as well as the one at the tubercle are observed. Measurement 'd' is defined by the shortest distance from the most lateral point of the articular tubercle to the internal margin, which is important to calculate the landmark defined by this measurement.

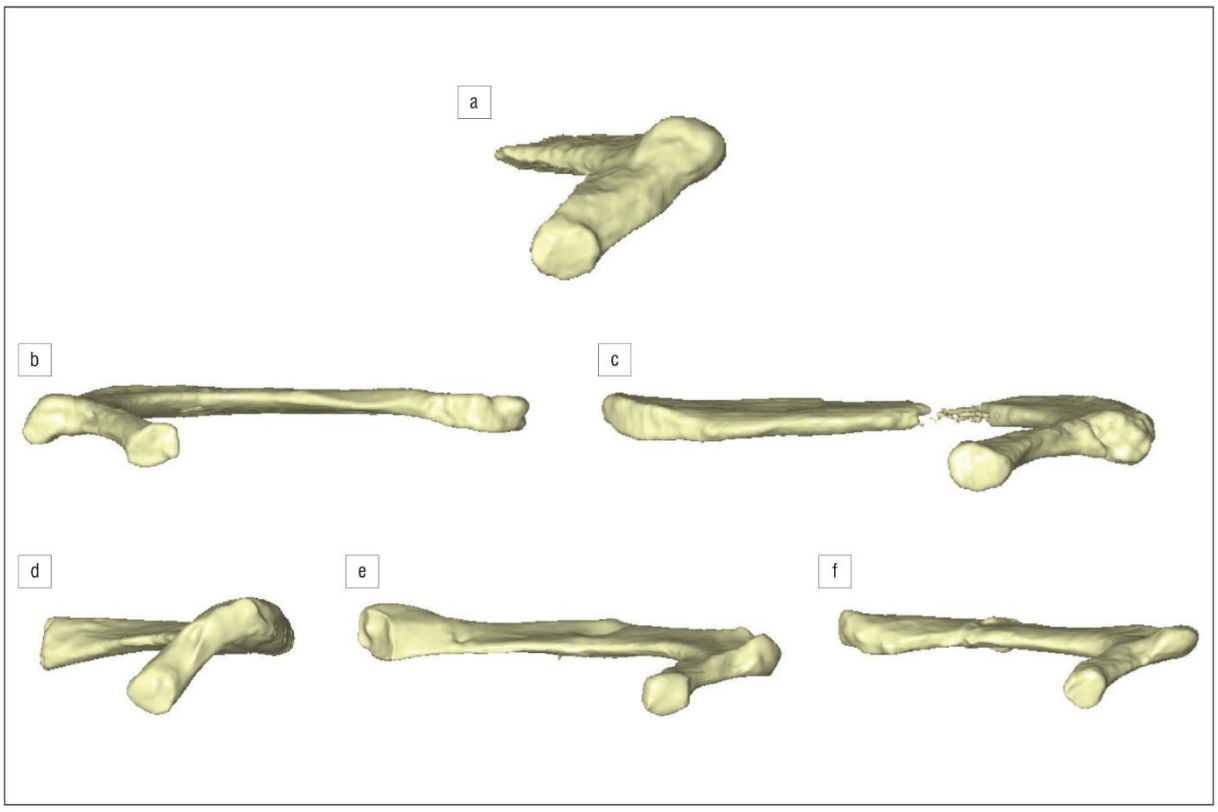

Figure 4: Detail of the single articular facet at the rib head of every fossil specimen studied in the sample: (a) StW 670, (b) KNM-WT 15000 left, (c) KNM-WT 15000 right, (d) AL 288-1, (e) MH1 and (f) MH2. As the goal of this image is to display the single facets, every specimen has been scaled to the same size.

The head has a rim that is thickened for the attachment of the costovertebral ligament. The angle and the tubercle coincide – a feature that is presented in extant and fossilised primate first ribs. The neck is narrow proximally and widens distally as the tubercle is approached. The neck is also rounded proximally and flattened distally. The tubercle is well developed and has a well-defined, smooth and rounded articular facet. The non-articular part of the tubercle for the attachment of the lateral costotransverse ligament is present.

The head has a single articular facet, which is rounded – a morphology that most closely resembles modern humans. The rest of the fossil specimens studied also presented a single articular facet (Figure 4). Regarding the comparative sample, 95% of the European modern humans presented a single articular facet at the rib head for articulation with T1, while 100% of the African modern humans presented this feature. In contrast, all of the non-hominin hominoids (*Pan*, *Gorilla*, *Pongo* and *Hylobates*) presented a double facet for articulation with C7 and T1.

The preservation of the fragment does not allow for the finer detail of anterior scalene and anterior serrate muscle insertions elevations, but it does allow us to study the scalene medium muscle insertion, which is only slightly marked in StW 670. The epiphysis at the articular tubercle and the rib head are well preserved and totally fused with the metaphysis, suggesting that the individual was adult at the time of death.[24]

Geometric morphometric analyses

Figure 5 shows a box plot of centroid size distribution of the different groups included in the sample. The centroid size of the StW 670 fossil is smaller than that of *H. erectus* (KNM-WT 15000, both antimeres), *A. sediba* (MH2), the great apes (*Pan, Gorilla* and *Pongo*) and *H. sapiens* (including the small-bodied individuals), and larger than that of *Hylobates*, and is located closest to the centroid size of *A. afarensis* AL 288-1 and *A. sediba* MH1.

Regarding shape, in Figure 6, we can observe that PC1 (44.3% of the total variation) polarises most of the non-hominin hominoids on the positive side of the axis, whereas the scatter of *H. sapiens* of different populations is located mostly towards the negative values of the PC1 axis. As it can be observed on the associated warps (Figure 6), the positive values of PC1 (associated with great apes) correspond to first ribs with a shorter relative distance between the head and the articular tubercle and a larger neck width at the articular tubercle. The negative values of PC1 (mainly associated with hominins) correspond to first ribs with a larger relative distance between the head and the articular tubercle and a shorter neck width at the articular tubercle. Moreover, PC1 polarisation differentiates between different rib head orientations. That is, in the positive values of PC1 (associated with non-hominin hominoids), the plane of the rib head is more oblique to the plane of the neck, while in the negative values of PC1 (mainly associated with modern humans and fossil specimens – so hominins), the plane of the rib head is more parallel to the plane of the neck.

As PC2 (16.7% of the total variation), which explains intraspecific variation, does not polarise between groups observed in PC1, as is observed in Figure 6, we will not discuss PC2. The rest of the principal components explain little of the variation so they also will not be discussed here.

Finally, looking at shape similarities according to the Procrustes distances, it is observed in the box plot (Figure 7) that the closest groups to StW 670 are *A. sediba* (mean distance=0.09), small-bodied Andaman *H. sapiens* (mean distance=0.09), European *H. sapiens* (mean distance=0.11), *H. erectus* (mean distance=0.11), small-bodied San *H. sapiens* (distance=0.12), *A. afarensis* (distance=0.12) and the sub-Saharan African *H. sapiens* (mean distance=0.13). The farthest groups are *P. troglodytes* (mean distance=0.16), *Hylobates* sp. (mean distance=0.21), *G. gorilla* (mean distance=0.22) and *Pongo* sp. (mean distance=0.28).

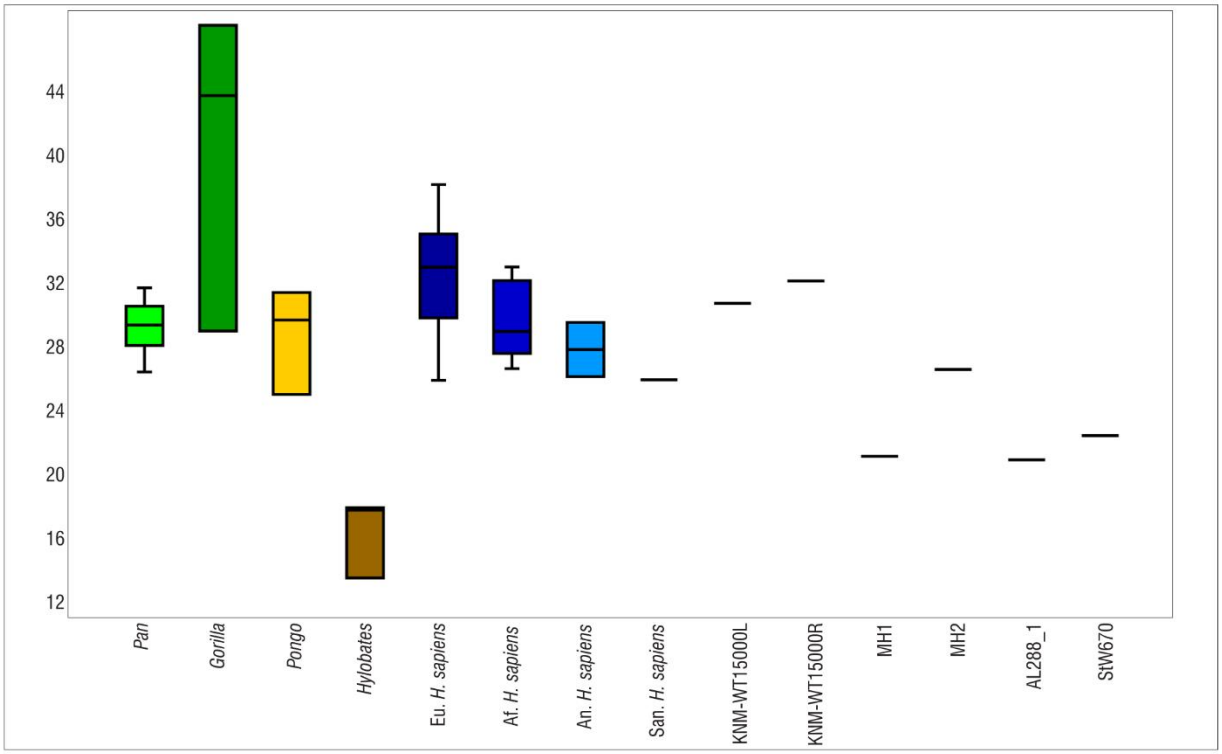

Eu, European; Af, African; An, Andaman

Figure 5: Centroid size distribution of StW 670 compared to first ribs in the comparative sample. StW 670 centroid size is smaller than that of *Homo erectus* (KNM-WT 15000, both antimeres), the great apes (*Pan, Pongo* and *Gorilla)* and *H. sapiens* (including small-bodied ones); bigger than that of *Hylobates;* and is located between the centroid sizes of the two *Australopithecus* species (*A. afarensis* AL 288-1 and *A. sediba* MH1). Comparative extant sample sizes are listed in Supplementary table 1.

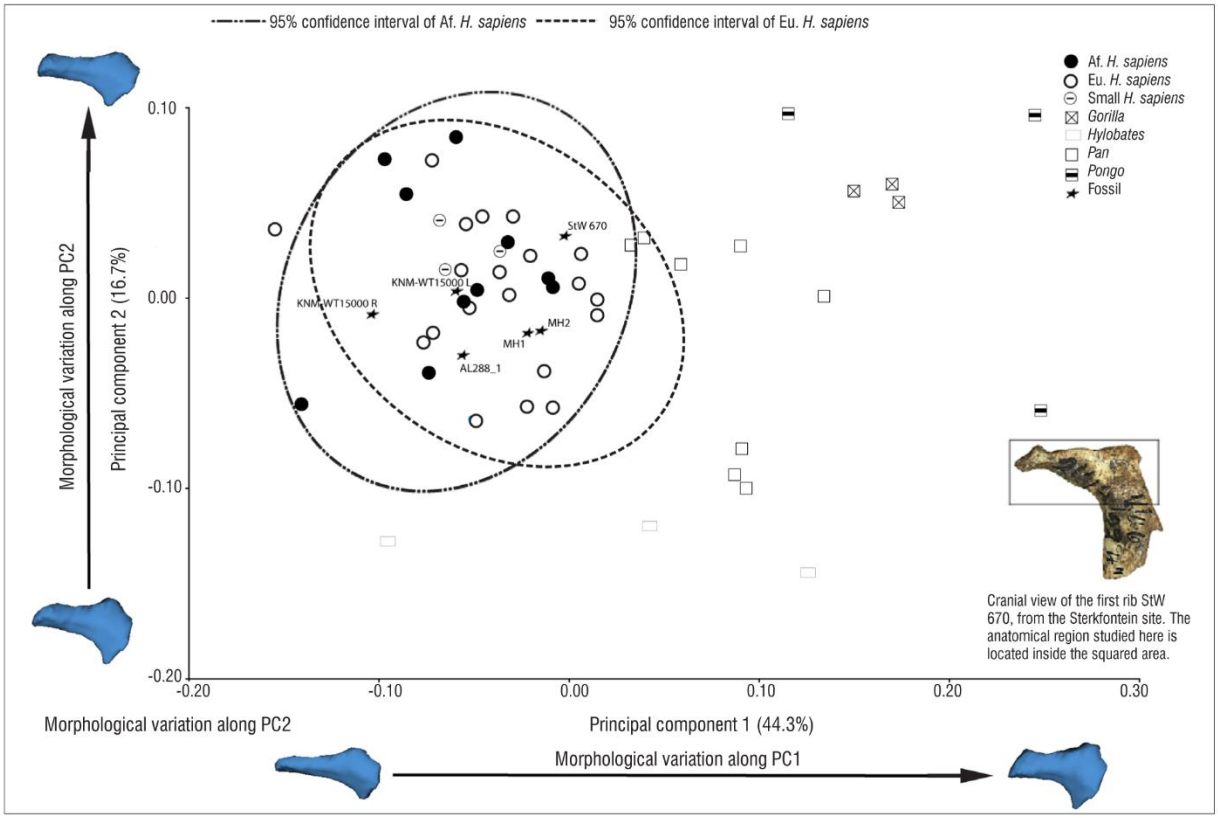

Figure 6: Principal component (PC)-shape analysis of first ribs of all specimens. Scatterplot of PC1 (44.3% of total variance) and PC2 (16.7% of total variance), and warped 3D models of proximal parts of first ribs in axial view. Note that fossil specimens (stars) are within the 95% confidence ellipse of European (Eu) and African (Af) *Homo sapiens.*

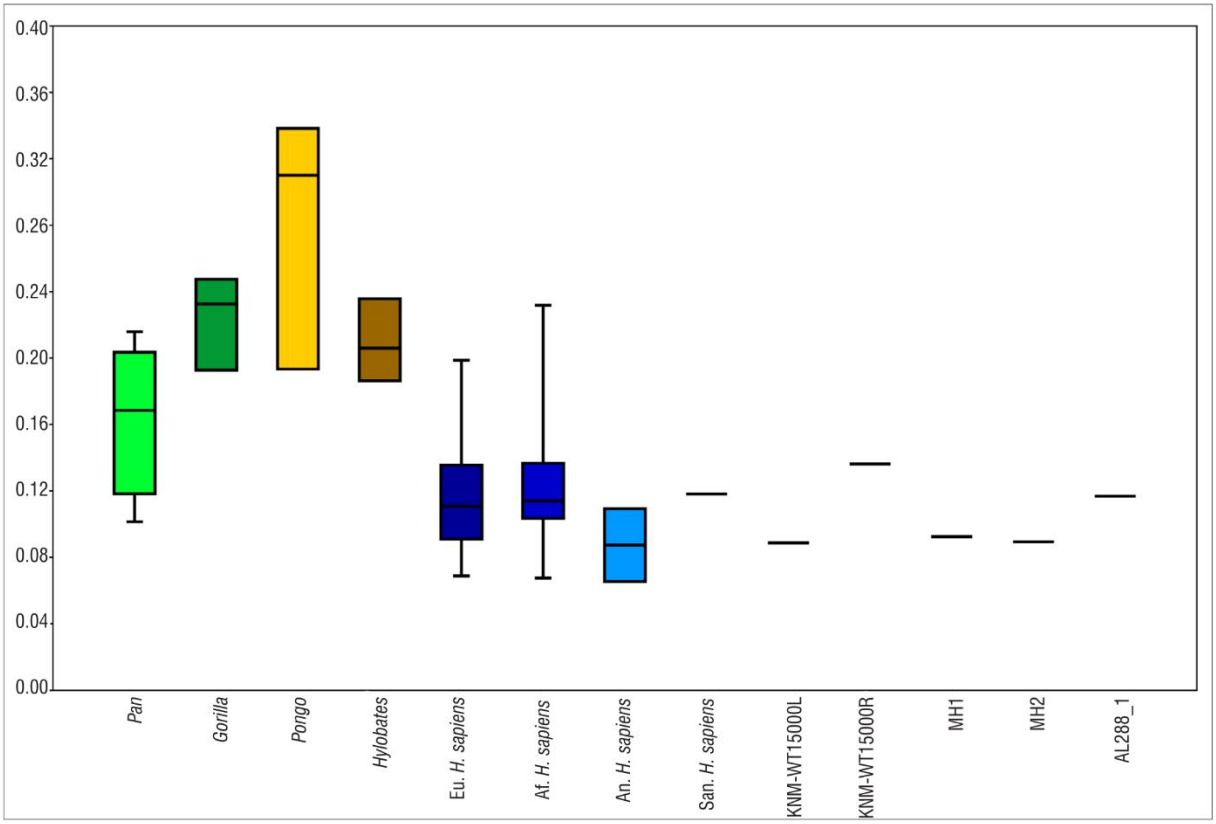

Figure 7: Box plot comparing the Procrustes distances between StW 670 (distance: 0.00) and the comparative sample. The closest groups to StW 670 are *Australopithecus sediba* (mean distance=0.09), small-bodied Andaman (An) *Homo sapiens* (mean distance=0.09), European (Eu) *H. sapiens* (mean distance=0.11), *H. erectus* (mean distance=0.11), small-bodied San *H. sapiens* (distance=0.12), *A. afarensis* (0.12) and sub-Saharan African (Af) *H. sapiens* (mean distance=0.13). The farthest groups are *Pan* (mean distance=0.16), *Hylobates* (mean distance=0.21), *Gorilla* (mean distance=0.22) and *Pongo* (mean distance=0.28).

Discussion and conclusion

Sterkfontein Member 4 has yielded quite a number of hominin remains, with Sts 14 and StW 431 (both *A. africanus*) among the best-known and well-studied hominins from this locality.[21,22] Four beds are recognised within Member 4 – labelled A, B, C and D.[23] StW 431 was excavated in Member 4 Bed B. The excavation beds of Sts 14 and StW 670 were apparently never recorded, so we do not know for certain from which bed StW 670 was excavated. However, StW 670 was excavated close to the excavation area of StW 318, a femur found at U/49 24'0"–25'0". Berger and McHenry[30] surmised the femur to be from an individual of small stature, weighing about 45–50 kg. The small size of the StW 670 rib may mean it is associated with this femur.

Three-dimensional geometrics morphometric analyses, which take into account the 3D spatial relationship between rib head and tubercle, show that the morphology of the preserved portion of StW 670 first rib is quite similar to *A. sediba* as it is close to this taxon in the box plot of the Procrustes distances. Regarding the morphological similarities with the rest of the groups, we can see that, besides *A. sediba*, the morphology of StW 670 is more similar to the *H. sapiens* groups, *H. erectus* and *A. afarensis* than it is to non-hominin hominoids (*Pan*, *Pongo, Gorilla* and *Hylobates).* In fact, in the PCA analyses, every fossil specimen (StW 670, MH1, MH2, AL 288-1 and KNM-WT 15000) falls inside the 95% confidence interval ellipse of *H. sapiens* (Figure 6).

Morphologically, the similarity of the fossils to modern humans observed in this PCA is because these groups are characterised by a larger relative distance between the head and the articular tubercle, and a shorter neck width at the articular tubercle, and because the plane of the rib head is more parallel to the plane of the neck in modern humans and the fossils than in the non-human hominoids. This latter feature observed at the rib head should probably be reflected in the orientation of the transverse processes of the T1 vertebrae, thus future studies should investigate this possibility.

Additionally, the presence of a single facet observed in every early hominin studied (*Australopithecus* and *H. erectus*) also supports the modern-like pattern of this fragment. This observation contrasts strongly with the pattern observed in the great apes (*Pan*, *Pongo*, *Gorilla* and *Hylobates*) as all of them present two articular facets at the rib head. Although we are conscious of the limitations of our sample size, we think that the observations made here are relevant to discuss the modernity of this character in StW 670. So, in the light of these observations, we conclude that the single facet of the rib head of the first rib is a feature unique to the hominin lineage, which emerged, at least, with the genus *Australopithecus.*[10] Moreover, aspects observed in the rib head should be reflected in the adjacent vertebrae as well, but because an associated vertebra does not exist and an assessment of vertebral morphology is not the goal of this work, it should be addressed in future studies.

The similarity of the proximal rib morphology observed in *Australopithecus* and *H. sapiens* first ribs is interesting because it has traditionally been thought that the upper thorax morphology of *Australopithecus* is characterised by a great ape-like form.[6,7] So, another hypothesis to be tested in future studies is that if we accept the derived morphology of the proximal part of the first rib in *Australopithecus* (*A. afarensis*, *A. sediba* and *A. africanus*), we can infer that the archaic pattern of the upper *Australopithecus* thorax should be found at the distal part of the ribs. This would suggest that the proximal part of the rib became derived in the direction of the *H. sapiens* morphology earlier than did the distal part of the first rib. This suggestion is consistent with the fact that the proximal and distal parts of the first rib belong to different morphogenetic modules in ontogeny,[31] which allows both units to evolve at different rates according to different requirements.

Great apes are often described as having a narrow upper thorax, while humans have a more expanded one.[32] It would be useful to be able to use fragmentary ribs in the hominin fossil record to determine when the transition between the two morphologies took place. The 2D analyses performed in previous studies do not make this goal look promising because of the complex morphology of ribs and the ribcage more broadly; however, the 3D analyses performed here show that the spatial configuration of the rib head and articular tubercle could be informative about the archaic or derived morphology, at least of the proximal part of the first rib. This fact, together with features such as the single facet of the rib head[10], could be informative in finding evolutionary traits in the upper thorax of early hominins. More research employing 3D techniques is needed on complete first ribs as well as the rest of the ribs in the costal sequence (from first to twelfth) in order to better quantify and understand *Australopithecus* rib morphology and the role of the thorax in hominin evolution more broadly.

Acknowledgements

We thank Bernhard Zipfel and the Access Committee of the Evolutionary Studies Institute, University of the Witwatersrand, as well as the South African National Centre of Excellence in Palaeosciences for hosting us whilst the materials were studied. D.G-M. and M.B. were funded through CGL2012-37279-MINECO (Spain) and a Leakey Research Grant to D.G-M. S.A.W. and J.E. were funded through the New York University Research Challenge Fund. We thank Emma Mbua, Fred Spoor and the National Museums of Kenya Earth Science Department for providing CT scans of the KNM WT-15000 axial skeleton. We also thank the reviewers for their comments which improved the previous version of the manuscript.

Authors' contributions

G.T. identified the rib fragment as hominin and described it. D.G-M. and J.E. analysed the 3D and linear data, respectively. G.T., D.G-M., J.E., S.N. and S.A.W. wrote the paper. M.B., P.S. and L.B. provided data and supervisory support, respectively.

References

1. Franciscus RG, Churchill SE. The costal skeleton of Shanidar 3 and a reappraisal of Neandertal thoracic morphology. J Hum Evol. 2002;42:303–356. http://dx.doi.org/10.1006/jhev.2001.0528
2. Gómez-Olivencia A, Eaves-Johnson KL, Franciscus RG, Carretero JM, Arsuaga JL. Kebara 2: New insights regarding the most complete Neandertal thorax. J Hum Evol. 2009;57:75–90. http://dx.doi.org/10.1016/j.jhevol.2009.02.009
3. Bastir M, García-Martínez D, Recheis W, Barash A, Coquerelle M, Rios L, et al. 3D analysis of human ribcage ontogeny. Am J Phys Anthropol. 2013;S56:75.
4. Garcia-Martinez D, Barash A, Recheis W, Utrilla C, Sanches T, Garcia Rio F, et al. On the chest size of Kebara 2. J Hum Evol. 2014;70:69–72. http://dx.doi.org/10.1016/j.jhevol.2014.02.003
5. García-Martínez D, Recheis W, Bastir M. Ontogeny of 3D rib curvature and its importance for the understanding of human thorax development. Am J Phys Anthropol. 2016;159(3):423–431. http://dx.doi.org/10.1002/ajpa.22893
6. Aiello L, Dean C. An Introduction to human evolutionary anatomy. London: Academic Press; 1990.
7. Nalla S. The morphology of the upper thorax of *Australopithecus sediba* within the context of the selected hominoids [PhD thesis]. Johannesburg: University of the Witwatersrand; 2013.
8. Schmid P, Churchill SE, Nalla S, Weissen E, Carlson KJ, De Ruiter DJ, et al. Mosaic morphology in the thorax of *Australopithecus sediba*. Science. 2013;340:163–165. http://dx.doi.org/10.1126/science.1234598
9. Bastir M, Garcia-Martinez D, Estalrrich A, García-Tabernero A, Huguet R, Ríos L, et al. The relevance of the first ribs of the El Sidron site (Asturias, Spain) for the understanding of the Neandertal thorax. J Hum Evol. 2015;80:64–73. http://dx.doi.org/10.1016/j.jhevol.2014.10.008
10. Ohman JC. The first rib of hominoids. Am J Phys Anthropol. 1986;70:209–229. http://dx.doi.org/10.1002/ajpa.1330700208
11. Johanson DC, Lovejoy CO, Kimbel WH, White TM, Ward SC, Bush ME, et al. Morphology of the Pliocene partial hominid skeleton (A.L. 288-1) from the Hadar Formation, Ethiopia. Am J Phys Anthropol. 1982;57:403–451. http://dx.doi.org/10.1002/ajpa.1330570403
12. Jellema L, Latimer B, Walker A. The rib cage. In: Leakey RE, Walker A, editors. The Nariokotome *Homo erectus* skeleton. Cambridge, MA: Harvard University Press; 1993. p. 294–325. http://dx.doi.org/10.1007/978-3-662-10382-1_13
13. Berger LR, Hawks J, De Ruiter DJ, Churchill SE, Schmid P, Delezene LK, et al. *Homo naledi*, a new species of the genus *Homo* from the Dinaledi Chamber, South Africa. eLife. 2015;4, e09560, 35 pages. http://dx.doi.org/10.7554/eLife.09560
14. Schmid P. The trunk of the australopithecines. Paris: Origine(s) de la Bipédie chez les Hominidés Presses du CNRS; 1991. p. 225–234.
15. Williams SA. Modern or distinct axial bauplan in early hominins? Comments on Haeusler et al. (2011). J Hum Evol. 2012;63:552–556. http://dx.doi.org/10.1016/j.jhevol.2012.01.007
16. Haile-Selassie Y, Latimer BM, Alene M, Deino AL, Gibert L, Melillo SM, et al. An early *Australopithecus afarensis* postcranium from Woranso-Mille, Ethiopia. Proc Natl Acad Sci USA. 2010;107(27):12121–12126. http://dx.doi.org/10.1073/pnas.1004527107
17. Broom RR, Robinson JT. Man contemporaneous with the Swartkrans ape-man. Am J Phys Anthropol. 1950;8:151–156. http://dx.doi.org/10.1002/ajpa.1330080211
18. Hughes AR, Tobias PV. A fossil skull probably of the genus *Homo* from Sterkfontein, Transvaal. Nature. 1977;265:310–312. http://dx.doi.org/10.1038/265310a0
19. Kuman K, Clarke RJ. Stratigraphy, artefact industries and hominid associations for Sterkfontein, Member 5. J Hum Evol. 2000;38:827–847. http://dx.doi.org/10.1006/jhev.1999.0392
20. Partridge TC, Granger DE, Caffee MW, Clarke RJ. Lower Pliocene hominid remains from Sterkfontein. Science. 2003;300:607–612. http://dx.doi.org/10.1126/science.1081651
21. Robinson JT. Early hominid posture and locomotion. Chicago: University of Chicago Press; 1972.
22. Toussaint M, Macho GA, Tobias PV, Partridge TC, Hughes AR. The third partial skeleton of a late Pliocene hominin (StW 431) from Sterkfontein, South Africa. S Afr J Sci. 2003;99:215–223.
23. Partridge TC, Watt IB. The stratigraphy of the Sterkfontein hominid deposit and its relationship to the underground cave system. Palaeontol Afr. 1991;28:35–40.
24. Rios L, Cardoso HFV. Age estimation from stages of union of the vertebral epiphyses of the ribs. Am J Phys Anthropol. 2009;140:265–274. http://dx.doi.org/10.1002/ajpa.21065
25. Gómez-Olivencia A, Carretero JM, Lorenzo C, Arsuaga JL, Bermúdez de Castro J-M, Carbonell E. The costal skeleton of Homo antecessor: preliminary results. J Hum Evol. 2010;59:620–640. http://dx.doi.org/10.1016/j.jhevol.2010.07.023
26. Zelditch ML, Swiderski DL, Sheets HD, Fink WL. Geometric morphometrics for biologists: A primer. London: Academic Press; 2004.
27. O'Higgins P. The study of morphological variation in the hominid fossil record: Biology, landmarks and geometry. J Anat. 2000;197:103–120. http://dx.doi.org/10.1046/j.1469-7580.2000.19710103.x
28. Hammer Ø, Harper D, Ryan P. PAST: Paleontological statistics software package for education and data analysis. Palaeontol Electron. 2001;4(1), Art. #4, 9 pages. http://palaeo-electronica.org/2001_1/past/issue1_01.htm
29. Klingenberg CP. MorphoJ: An integrated software package for geometric morphometrics. Mol Ecol Resour. 2011;11:353–357. http://dx.doi.org/10.1111/j.1755-0998.2010.02924.x
30. Berger LR, McHenry HM. Body proportions in *Australopithecus afarensis* and *A. africanus* and the origin of the genus *Homo*. J Hum Evol. 1998;35:1–22. http://dx.doi.org/10.1006/jhev.1997.0197
31. Aoyama H, Mizutani-Koseki S, Koseki H. Three developmental compartments involved in rib formation. Int J Dev Biol. 2005;49:325–333. http://dx.doi.org/10.1387/ijdb.041932ha
32. Schultz AH. Vertebral column and thorax. Primatologia. 1961;4:1–66.

Note: This article includes supplementary material

Bastir et al.

Preliminary Findings of 3D Analyses of the Costal Remains of *Australopithecus sediba*

The thorax of *Australopithecus sediba* is hypothesized to follow a mosaic evolutionary pattern showing a greater similarity with *Australopithecus afarensis* and great apes in the upper thorax and a greater similarity with humans at the lower thorax and waist (Berger et al. 2011; Schmid et al. 2013). This study presents first results of a comparative analysis of the *Australopithecus sediba* costal material using 3D geometric morphometrics. Twenty landmarks and semilandmarks were measured at the external outline of 3D rib reconstructions of computed tomography scans from ribcages of modern humans and extant apes and compared with costal remains and virtual reconstructions of MH1, MH2, and AL-288-1. Shape data were generated by generalized Procrustes superimposition and analyzed by Principal Components analyses. Our results point to ribs with an uncurved and un-torsioned overall shaft geometry, which is compatible with the hypothesis of a funnel shaped upper thorax in this species (Schmid et al. 2013). However, our analyses also suggest that shaft morphology alone may not be sufficient to comfortably predict overall rib cage morphology. This is because the morphology of the head-neck complex and the shaft, which are fully preserved in the first ribs of the *Australopithecus* sample, indicates a greater similarity between *Au. sediba*, AL-288-1, *Hylobates*, and humans than with great apes. These findings could indicate that hypotheses on early hominin thorax shape should consider also "emergent" morphological features when putting together elements of anatomical complexes such as ribs and vertebrae. Thus, in order to improve hypotheses on the rib cage morphology of *Au. sediba*, costal analyses should be combined with shape analyses of the vertebrae and the manubrium.

Dentro del **objetivo específico 5b** "**Contribuciones al conocimiento de la caja torácica de homínidos del Pleistoceno Inferior (*Homo ergaster* y *Homo antecessor*), así como de la especie de cronología incierta *Homo naledi***" se ha publicado un artículo y un resumen en congreso:

Williams, S.A., **García-Martínez, D.**, Bastir, M., Meyer, M.R., Nalla, S., Hawks, J., Schmid, P., Churchill, S.E., Berger, L.R., 2017. The vertebrae and ribs of *Homo naledi*. Journal of Human Evolution 104, 136-154.

DOI: http://dx.doi.org/10.1016/j.jhevol.2016.11.003

García-Martínez, D., Spoor, F., Bastir, M., 2016. 3D Assessment of rib curvatures in KNM-WT 15000. Abstracts of the Paleoanthropology Society 2016 Meeting; PaleoAnthropology 2016: A13.

http://www.paleoanthro.org/media/journal/content/PAS2016A.pdf

Journal of Human Evolution 104 (2017) 136–154

Contents lists available at ScienceDirect

Journal of Human Evolution

journal homepage: www.elsevier.com/locate/jhevol

The vertebrae and ribs of *Homo naledi*

Scott A. Williams [a, b, c, *, 1], Daniel García-Martínez [d, e, b, 1], Markus Bastir [d, b], Marc R. Meyer [f], Shahed Nalla [g, b], John Hawks [h, b], Peter Schmid [i, b], Steven E. Churchill [j, b], Lee R. Berger [b]

[a] Center for the Study of Human Origins, Department of Anthropology, New York University, 25 Waverly Place, New York, NY 10003, USA
[b] Evolutionary Studies Institute and Centre for Excellence in PalaeoSciences, University of the Witwatersrand, Private Bag 3, Wits 2050, South Africa
[c] New York Consortium in Evolutionary Primatology, New York, NY 10024, USA
[d] Paleoanthropology Group, Museo Nacional de Ciencias Naturales (MNCN-CSIC), J.G. Abascal 6, 28006 Madrid, Spain
[e] Faculty of Sciences, Biology Department, Universidad Autónoma de Madrid, 28049 Madrid, Spain
[f] Department of Anthropology, Chaffey College, Rancho Cucamonga, CA 91737, USA
[g] Department of Human Anatomy and Physiology, Faculty of Health Sciences, University of Johannesburg, PO Box 524, Auckland Park 2006, South Africa
[h] Department of Anthropology, University of Wisconsin-Madison, Madison, WI 53593, USA
[i] Anthropological Institute and Museum, University of Zurich, Winterthurerstr. 190, CH-8057 Zurich, Switzerland
[j] Department of Evolutionary Anthropology, Box 90383, Duke University, Durham, NC 27708, USA

ARTICLE INFO

Article history:
Received 28 September 2015
Accepted 17 November 2016
Available online 13 January 2017

Keywords:
Thorax
Vertebral column
Ribcage
Trunk
Australopithecus
Bipedalism

ABSTRACT

Hominin evolution featured shifts from a trunk shape suitable for climbing and housing a large gut to a trunk adapted to bipedalism and higher quality diets. Our knowledge regarding the tempo, mode, and context in which these derived traits evolved has been limited, based largely on a small-bodied *Australopithecus* partial skeleton (A.L. 288-1; "Lucy") and a juvenile *Homo erectus* skeleton (KNM-WT 15000; "Turkana Boy"). Two recent discoveries, of a large-bodied *Australopithecus afarensis* (KSD-VP-1/1) and two *Australopithecus sediba* partial skeletons (MH1 and MH2), have added to our understanding of thorax evolution; however, little is known about thorax morphology in early *Homo*. Here we describe hominin vertebrae, ribs, and sternal remains from the Dinaledi chamber of the Rising Star cave system attributed to *Homo naledi*. Although the remains are highly fragmented, the best-preserved specimens—two lower thoracic vertebrae and a lower rib—were found in association and belong to a small-bodied individual. A second lower rib may belong to this individual as well. All four of these individual elements are amongst the smallest known in the hominin fossil record. *H. naledi* is characterized by robust, relatively uncurved lower ribs and a relatively large spinal canal. We expect that the recovery of additional material from Rising Star Cave will clarify the nature of these traits and shed light on *H. naledi* functional morphology and phylogeny.

1. Introduction

The postcranial axial skeleton does not preserve well in the fossil record and is difficult to reconstruct due to the multitude of bones involved in this anatomical region. Consisting of the vertebral column and ribcage, the postcranial axial skeleton is evolved to allow spinal flexibility and mobility during ventilation, provides trunk stability, and serves to house and protect the spinal cord, lungs, and mediastinal structures. Much of what is known about the evolution of the hominin axial skeleton has been based on partial skeletons of small-bodied, female *Australopithecus africanus* (Sts 14; Robinson, 1972) and *Australopithecus afarensis* (A.L. 288-1; Johanson et al., 1982; Schmid, 1983). Vertebrae and ribs from larger-bodied, presumed male *A. africanus* (StW 8/41, StW 431, StW 670; Sanders, 1998; Toussaint et al., 2003; Tawane et al., 2016) and *A. afarensis* (A.L. 333, A.L. 444, KSD-VP-1/1; Lovejoy et al., 1982; Haile-Selassie et al., 2010; Ward et al., 2012; Latimer et al., 2016; Meyer, 2016) have also been described, as has axial skeletal material from two partial skeletons of *Australopithecus sediba* (Schmid et al., 2013; Williams et al., 2013). An early *Homo erectus* partial skeleton from Dmanisi preserves axial material (Meyer, 2005;

DOI of original article: http://dx.doi.org/10.1016/j.jhevol.2016.04.008.
* Corresponding author.
E-mail address: sawilliams@nyu.edu (S.A. Williams).
[1] These authors contributed equally to the manuscript.

http://dx.doi.org/10.1016/j.jhevol.2016.11.003
0047-2484/

Lordkipanidze et al., 2007; Meyer and Haeusler, 2015), as does the Nariokotome *H. erectus* skeleton (Jellema et al., 1993; Latimer and Ward, 1993; Haeusler et al., 2011), both of which belong to juveniles. Several Middle and Late Pleistocene partial skeletons also preserve axial material (Gorjanović-Kramberger, 1906; McCown and Keith, 1939; Trinkaus, 1983; Arensburg, 1991; Gómez-Olivencia et al., 2009, 2010, 2013a, b; Bonmatí et al., 2010; Gómez-Olivencia, 2013a, b; 2015; Arsuaga et al., 2015; Bastir et al., 2015a).

African great apes possess "funnel-shaped" thoraces with narrow upper ribcages and wide, "flaring" lower ribcages atop short lumbar columns entrapped within superoinferiorly tall iliac blades (Schultz, 1961; Lovejoy, 2005). This anatomical configuration allows for the accommodation of substantial gut size for a diet of plant resources and extensive upper limb mobility in climbing, while preventing bending and buckling of the lumbar vertebrae and protecting the integrity of the lower back during forelimb-dominated suspensory behavior (Cartmill and Milton, 1977; Jungers, 1984; Ward, 1993; Sanders and Bodenbender, 1994; Lovejoy and McCollum, 2010; Williams and Russo, 2015; Latimer et al., 2016). In contrast, modern humans have a more "barrel-shaped" thorax with a wide upper ribcage and a relatively narrow lower thorax to match the less flaring iliac blades of the pelvis (Schultz, 1961; Jellema et al., 1993; Lovejoy, 2005; García-Martínez et al., 2013; Latimer et al., 2016). Together with a relatively long lumbar column, a narrow lower thorax contributes to a long, narrow waist, facilitating extended bouts of bipedal walking and running (Jellema et al., 1993; Sanders, 1998; Bramble and Lieberman, 2004; Preuschoft, 2004; Schmid et al., 2013; Latimer et al., 2016). This derived morphology attributed to *H. erectus* has also been argued to reflect a reduction in the relative mass of gut tissue, reflective of a dietary shift toward higher energy animal foods or extracted plant foods (Aiello and Wheeler, 1995; Antón and Snodgrass, 2012; but see; Ben-Dor et al., 2016).

Robinson (1972:108) interpreted the fragmentary ribs associated with Sts 14 as similar in curvature to those of a small-bodied modern human at his disposal, which to him suggested "the same sort of thorax shape as that in *Homo sapiens* and the hominoids in general." Robinson did not attempt to differentiate the ribs amongst hominoids. Although preserving more rib material than Sts 14, the thorax of A.L. 288-1 ("Lucy") has long been the subject of debate. Initially interpreted by its discoverers as "of modern human form" and indicative of a committed terrestrial biped (Johanson et al., 1982:437), Schmid (1983:283) reconstructed the ribcage as "funnelshaped" [sic] and invoked a high degree of suspensory behavior. Based on rib material of a large-bodied *A. afarensis* individual, Haile-Selassie et al. (2010:12122) concluded that "there is little question that the upper thorax of KSD-VP-1/1 was fundamentally *Homo*-like." Latimer et al. (2016) revisited thorax shape in KSD-VP-1/1 and concluded that *A. afarensis* is characterized by a transversely broad upper thorax coupled with a relatively broad lower ribcage. They argue that this "bell-shaped" thorax is maintained throughout hominin evolution until the emergence of a "barrel-shaped" thorax in *H. sapiens* (see also Sawyer and Maley, 2005). Compared to small-bodied *A. afarensis* and *A. africanus*, *H. erectus* and *H. sapiens* are envisioned to share a body plan with elongated hindlimbs, larger mass and stature, larger brains, and a barrel-shaped thorax (Jellema et al., 1993; Aiello and Wheeler, 1995; Bramble and Lieberman, 2004).

Recently though, new discoveries and interpretations have called into question this dichotomy. New pelvic material from Gona (BSN49/P27) assigned to *H. erectus* (but see Ruff, 2010) demonstrates a very wide bi-iliac breadth (Simpson et al., 2008, 2014; Holliday, 2011), challenging notions of narrow lower thoracic form in *H. erectus* (see also Arsuaga et al., 1999). Previous reconstructions of thorax shape in *H. erectus* are based on a single subadult skeleton, KNM-WT 15000, initially reconstructed with a narrow pelvis and waist (Jellema et al., 1993) but possibly more primitive postcranially than previously thought (Franciscus and Churchill, 2002; Simpson et al., 2010; García-Martínez, 2013; García-Martínez et al., 2016a). Additionally, thorax and pelvic morphology of two *A. sediba* partial skeletons suggests a narrower, more human-like lower thorax (Kibii et al., 2011; Schmid et al., 2013; but see Haeusler et al., 2016 for a different assessment of its pelvic morphology). Recent three-dimensional (3D) geometric morphometric work on the 1st ribs of *A. sediba* suggests that the upper thorax may have been broader than previously thought (Bastir et al., 2016). These observations suggest that the upper and lower components of the ribcage can evolve independently of one another (i.e., are somewhat modular), allowing for the evolution of different thoracic capacities (Bastir et al., 2013, 2015b; García-Martínez et al., 2016b).

Here, we describe the postcranial axial material from the Dinaledi chamber of the Rising Star cave system in the Cradle of Humankind, South Africa. The Dinaledi hominin sample, attributed to the new species *Homo naledi* (Berger et al., 2015), includes a minimum number of 15 individuals, although presently it is of unknown geological age (Dirks et al., 2015). Cranio-dental morphology of *H. naledi* is most similar to early members of the genus *Homo* (*Homo habilis*, *Homo rudolfensis*, and early *H. erectus*), although the cranial and dental features in combination do not fit with the hypodigm of any single existing taxon. Some aspects of postcranial morphology are shared with *Australopithecus*, some with *Homo*, including both early *Homo* and later, Pleistocene hominins, and other traits are found in no known species (Berger et al., 2015; Kivell et al., 2015; Harcourt-Smith et al., 2015). Specifically, the shoulder is quite primitive (Feuerriegel et al., 2017), whereas aspects of the lower limb, foot, and hand are derived (Harcourt-Smith et al., 2015; Kivell et al., 2015; VanSickle et al., submitted) and the pelvis shows a mix of primitive and derived traits (VanSickle et al., submitted). As the central components of the postcranial skeleton, the vertebral column and ribcage act as bridges between the upper and lower limbs and the skull and pelvis. Therefore, the morphology of the postcranial axial skeleton is highly relevant to functional and evolutionary interpretations of *H. naledi*.

2. Materials and methods

2.1. Dinaledi postcranial axial skeletal material

The Dinaledi collection includes two nearly complete lower thoracic vertebrae and 30 additional discernable vertebral fragments (Figs. 1–3), seven diagnostic ribs (Fig. 4) and 45 additional rib fragments, and an isolated sternebral fragment (not figured). Remains from all vertebral regions are represented, ranging from the first cervical through to the sacro-coccygeal vertebrae (pelvic material, including sacral and coccygeal vertebrae, is included in the description of the pelvis; VanSickle et al., in review). Proximal fragments of the first and second ribs are preserved, as are two rib shafts from the central thorax and proximal ends of 11th and 12th ribs (Fig. 4). A complete list of specimens is included in Supplementary Online Material (SOM) Table S1. The Dinaledi collection is curated at the Evolutionary Studies Institute (ESI), University of the Witwatersrand, Johannesburg, South Africa.

Figure 1. Cervical and thoracic vertebrae from the Dinaledi Chamber. Each vertebra is shown in cranial (top), caudal (bottom), and right lateral, ventral, left lateral, and dorsal (middle row, from left to right) views. Two lower thoracic vertebrae are shown in a separate figure (Fig. 2). Major units of scale in cm.

2.2. Descriptive and metric methods

Qualitative observations and quantitative measurements were conducted on the original specimens in the Dinaledi hominin collection. A full morphological description of each specimen, standard measurements and other metrics, and comparisons with available comparative material are included. Our consideration of the specimens includes identification and seriation of vertebral and rib elements and assessment of developmental age where applicable. Diagnostic anatomical information and state of preservation for each fragment is provided. Fragments that lack diagnostic morphology are listed with approximate identification.

2.3. Comparative sample

We compared the Dinaledi vertebrae and ribs to those of extant taxa (see individual analyses below for species and sample sizes; Tables 1–4) and to relevant fossil hominin axial materials. Original fossils were studied in all cases except Neandertal vertebrae, where high-quality casts of Kebara 2 were studied and data were taken from the literature (see Tables 1–3), and in the case of the KSD-VP-1/1 ribs, where published images were used for comparative purposes. The core comparative sample of recent humans (*H. sapiens*, $N = 51$) and chimpanzees (*Pan troglodytes*, $N = 19$) for traditional metric analyses of vertebrae was collected at the American Museum of Natural History (New York, NY; AMNH) and the Cleveland Museum of Natural History (Cleveland, OH). Standard measurements described in Bräuer (1988) and additional linear measurements (all defined in Tables 1–3) were collected with digital calipers. Vertebral wedging was calculated as an angle using the method outlined in Digiovanni et al. (1989). Scaled photographs of the core sample were taken, and ImageJ was used to measure surface area of the vertebral body and cross-sectional area of the spinal canal. A small sample of siamangs (*Symphalangus syndactulus*, $N = 6$) was included in the lower thoracic vertebra geometric mean analysis for comparison with *H. naledi* lower thoracic vertebrae (see below), but photographs and surface area measurements were not taken on this taxon.

The comparative fossil hominin material for 3D analyses consisted of 3D laser scans of a high quality cast of the 11th rib of *A. afarensis* (A.L. 288-1), housed at the ESI, as well as a 3D reconstruction of original CT-scans of the 11th rib (KNM-WT 15000 AN following the designation in Jellema et al., 1993; KNM-WT 15000 BS following Haeusler et al., 2011) of KNM-WT 15000 (Nariokotome juvenile *H. erectus*) and of the left one from Kebara 2 Neandertal. These recent and fossil data were compared with U.W. 101-524, assessed as an 11th rib of the left side and one of the most complete of the *H. naledi* costal sample (see below). The recent comparative material consists of 3D surface models (generated using NextEngine and Artec Spider HD Optic laser scanners) of the penultimate ribs of extant primates. The 11th

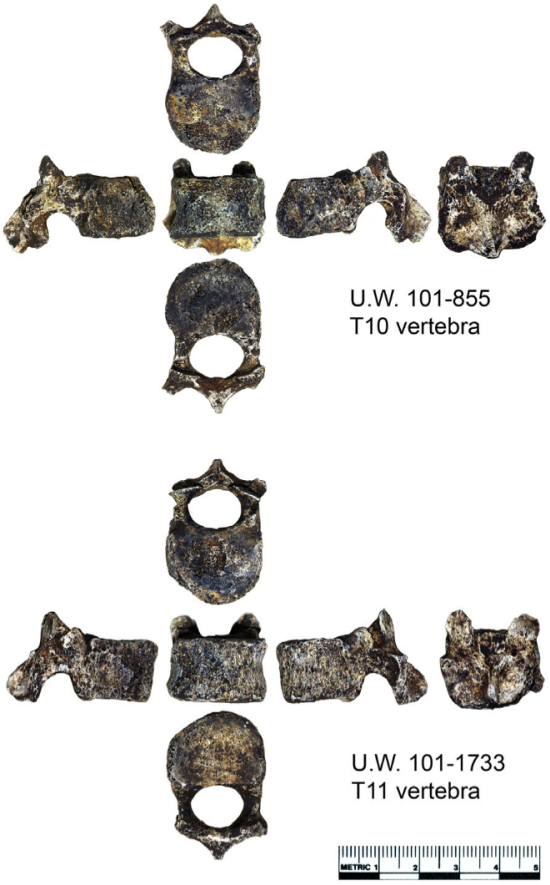

Figure 2. Lower thoracic vertebrae from the Dinaledi Chamber, U.W. 101-855 (T10) and U.W. 101-1733 (T11) found in near-articulation (Fig. 6, SOM Fig. S1). They are shown here in cranial (top), caudal (bottom), and in right lateral, ventral, left lateral, and dorsal (middle row, from left to right) views. Major units of scale in cm.

ribs of 30 adult humans (sex balanced sample; SOM Table S2) from two populations were scanned: a European population (21st century Identified Skeletal Collection, housed at the Laboratory of Forensic Anthropology, University Of Coimbra, Portugal; Ferreira et al., 2014) and a Sub-Saharan African population (Paseo de Anel Verde, DRYAS Octopetala, Coimbra, Portugal; $N = 10$; Martiniano et al., 2014; Wasterlain et al., 2016). Additionally, the 11th ribs of one small-bodied member of the San population and two small-bodied individuals from the Andaman Islands were scanned following the same protocol at the AMNH and at the Natural History Museum (London, U.K.). Three-dimensional models of penultimate ribs (usually 12th) of 30 bonobos and chimpanzees (*Pan paniscus* and *P. troglodytes*; balanced sexes) were scanned at the Royal Museum for Central Africa (RMCA, Tervuren, Belgium).

The lower rib of Sts 14, which we use in our comparative analyses, deserves particular attention here. Whereas Robinson (1972) treated the sixth presacral vertebra (Sts 14f) as the first lumbar vertebra for a number of reasons (see Haeusler et al., 2002; Williams, 2012a), Haeusler et al. (2002) associated a floating rib with Sts 14f (although it is accompanied on the left side by either a short, ankylosed rib or a lumbar transverse process; see Haeusler et al., 2002; Williams, 2012a). Because Sts 14f is highly asymmetrical, we compare the *H. naledi* lower ribs to the rib associated with Sts 14g, the 7th last pre-sacral vertebra identified as T11 by Haeusler et al. (2002). It presents a single facet at the rib head and the articular tubercle is not observed, features that are consistent with 11th or 12th rib anatomy. However, because it seems to be relatively short in length and presents a sigmoidal shape (features which are characteristic of human 12th ribs), we are of the opinion that this rib is a reasonable and better comparison for the last rib of *H. naledi* than the anomalous rib associated with Sts 14f.

2.4. Geometric morphometrics of individual ribs

In the rib sample (total $N = 68$), we measured 25 3D landmarks and semi-landmarks in Viewbox4 software (www.dhal.com) in order to quantify rib head and posterior angle morphology, 3D rib curvature, shaft height, and shaft thickness for geometric morphometric analyses (Fig. 5). Four landmarks were measured at the cranial-, caudal-, medial-, and lateral-most points of the rib head. Another four landmarks were placed at the posterior angle, two of them located in the craniocaudal dimension at the caudal- and cranial-most point at the maximum distance following the shaft maximum diameter at angle (SMXD; Franciscus and Churchill, 2002), and the other two located in the medio-lateral dimension at the medial- and lateral-most point at the maximum distance following the shaft minimum diameter at angle (Franciscus and Churchill, 2002). In order to quantify rib curvature and shaft height, five equidistant curve semi-landmarks were located along the upper costal border between the cranial-most point of the rib head and the cranial-most point of the posterior angle cross section, and another five equidistant curve semi-landmarks were located at the lower costal border between the caudal-most point of the rib head and the caudal-most point of the posterior angle cross section. Finally, in order to quantify rib thickness, three surface semi-landmarks were equidistantly located at the external surface of the rib shaft following its midline from the lateral-most point of the rib head to the lateral-most point of the posterior angle. Another three surface semi-landmarks were equidistantly located at the internal surface of the rib shaft following its midline from the medial-most point of the rib head to the medial-most point of the posterior angle.

Because of uncertainty in terms of their locations along a rib, semi-landmarks were slid along their corresponding curves relative to the fixed landmarks to minimize bending energy. First, this was done between each specimen and the template (first specimen) and after that, semi-landmarks were slid a second time along their curves to minimize bending energy between each specimen and the sample average (Mitteroecker and Gunz, 2009). This sliding procedure adjusts their relative locations along the curve. Because we measured only landmarks that are actually preserved in U.W. 101-524 (from rib head to posterior angle), no missing data estimation was necessary in the sample. Shape data of this dataset were obtained by Generalized Procrustes Analysis (GPA). Size was quantified as centroid size (i.e., the square root of the summed squared distances of each landmark to the centroid; O'Higgins, 2000; Mitteroecker and Gunz, 2009), and box plots used to compare and explore the size relations between U.W. 101-524 and the rest of the sample.

Shape data were subjected to Principal Components Analysis (PCA) to reduce the dimensionality of data and to visualize the main axes of variation (O'Higgins, 2000) using Morphologika v2.5 (O'Higgins and Jones, 1999). Shapes associated with variations along PC1 and PC2 axes were visualized as warps of the sample mean shape into shapes corresponding to the observed maximum and minimum ranges of PC1–PC3 scores. This was done using the EVAN Toolkit (ET-software) version 1.63 (http://www.evan-society.org/). A box plot of Procrustes distances was used to compare and explore shape relations between U.W. 101-524 and the different groups of the sample.

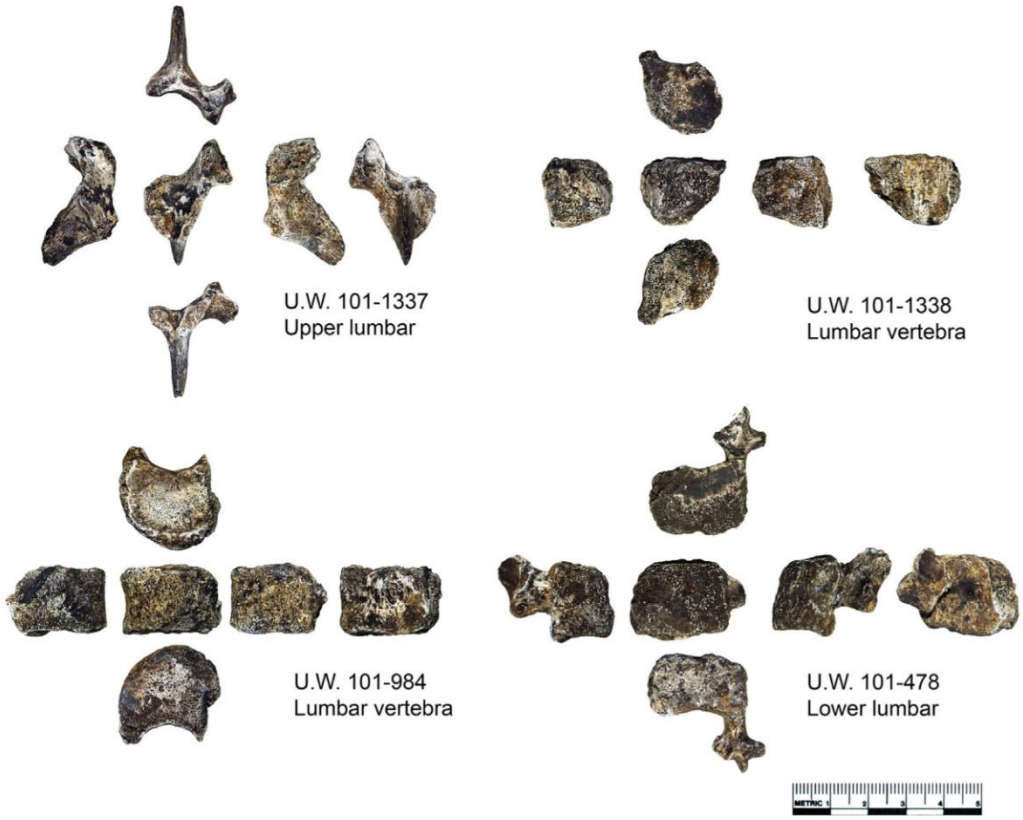

Figure 3. Lumbar vertebrae from the Dinaledi Chamber. These vertebrae lack costal facets or show other features diagnostic of lumbar vertebrae. They are shown in cranial (top), caudal (bottom), and in right lateral, ventral, left lateral, and dorsal (middle row, from left to right) views. Major units of scale in cm.

3. Results

3.1. Description of cervical vertebrae

3.1.1. U.W. 101-651 This is the partial neural arch of the right side of an atlas (C1). It preserves the superior articular facet (for articulation with the occipital condyle), the transverse foramen, and part of the lamina. The caudal aspect of the superior articular facet is abraded and exposes trabecular bone. The right superior articular facet is "kidney"-shaped. Measurements are shown in Table 1.

3.1.2. U.W. 101-331 This is the neural arch, including midline, of an atlas (C1) vertebra.

3.1.3. U.W. 101-1279 and U.W. 101-489 The body of an axis (C2) vertebra (U.W. 101-1279) and an associated odontoid process (U.W. 101-489) that do not refit directly but probably belong to the same vertebra (Fig. 1). Partial superior articular facets are all that is preserved otherwise. The odontoid process is broken from the body. The caudal portion of the body is abraded ventrally and the neural arch, which bears partial superior articular facets superiorly, is broken inferiorly and dorsally. Ring apophyses are present on the dorsal side of the caudal body, consistent with this vertebra belonging to an adult.

Measurements are listed in Table 1. The vertebral body is tall, and the odontoid process is separated from the body and unfortunately does not refit due to post-depositional damage. The odontoid process bears an ovoid articular surface ventrally for articulation with the dens notch on the atlas vertebra. Although the odontoid process is broken, its preserved morphology suggests it would have been oriented vertically, rather than slightly dorsally-angled as in African great apes.

3.1.4. U.W. 101-1692 This is an isolated odontoid process of the axis (C2) vertebra. The right and left sides of the dens are fused but retain a fusion line, and the base is not fused to the remainder of the vertebra. The apex has not yet fused and is not present. By human standards, therefore, this belongs to an immature individual aged approximately 2–3 years.

3.1.5. U.W. 101-732 This is an axis (C2) vertebra with a partial body present (the odontoid process is broken) and preserving the partial left neural arch. Articular facets are missing.

3.1.6. U.W. 101-174 This is the neural arch of a middle cervical vertebra. It preserves much of the left lamina, a small piece of the right lamina just lateral to the spinous process, and the base of the spinous process.

3.1.7. U.W. 101-081 This is the spinous process of a lower cervical or upper thoracic vertebra. It is broken distally and skews slightly to the right, as in U.W. 101-1054 and U.W. 101-1337.

3.1.8. U.W. 101-1673 This is a small neural arch of a cervical vertebra belonging to an immature individual. The superior and inferior articular facets from the right side are present.

3.2. Description of the thoracic vertebrae

3.2.1. U.W. 101-1614 This is the neural arch of an upper thoracic vertebra, preserving the left superior and inferior articular facets, base of the left transverse process, and spinous process, broken distally (Fig. 1). This vertebra possesses features diagnostic of upper thoracic levels: the superior articular facet leads caudally onto a

Figure 4. Ribs from the Dinaledi Chamber. Views are external, internal, cranial, and caudal (from top to bottom in each set except U.W. 101-83 and U.W. 101-351). For U.W. 101-83, views are cranial, internal, caudal, and external, and for U.W. 101-351, views are external, cranial, internal, and caudal. Major units of scale in cm.

Table 1
Available measurements (in mm) on the *H. naledi* atlas (C1), axis (C2), and comparative data.[a]

	H. naledi[g]	*A. afarensis* A.L. 333[h]	*P. robustus* SK854	*P. boisei*? KNM-ER 1825[i]	*H. erectus* Dmanisi	*H. antecessor* Gran Dolina[j]	Neandertals[k]	Modern humans	*Pan troglodytes*
C1 SAF dorsoventral diameter[b]	14.1	23.1	–	20.0	–	19.5	24.1 (2.3, $N = 6$)	21.7 (2.4, $N = 20$)	17.9 (1.4, $N = 7$)
C1 SAF transverse diameter[c]	7.9	10.8	–	10.0	–	13.5	11.3 (0.4, $N = 6$)	10.7 (1.2, $N = 19$)	8.8 (1.3, $N = 7$)
C2 Body inferior transverse diameter (M8)[d]	13.8	–	14.8	–	14.7	–	19.8 (1.6, $N = 5$)	18.2 (1.6, $N = 49$)	13.0 (1.7, $N = 18$)
C2 Body inferior dorsoventral diameter (M5)[e]	10.4	–	11.2	–	13.7	–	17.4 (1.6, $N = 4$)	15.1 (1.4, $N = 49$)	12.1 (1.1, $N = 18$)
C2 Maximum height (axis with dens) (M1a)[f]	27.1[l]	–	–	–	29.9	–	36.2 (1.4, $N = 5$)	35.2 (2.8, $N = 49$)	30.1 (2.0, $N = 18$)

[a] Taxa with more than one individual are shown as means, with standard deviation and sample size in parentheses. Original fossil specimens were studied except when indicated. M = Martin number.
[b] Superior articular facet (SAF) dorsoventral diameter: the dorsal-most point of the facet measured along its midline to the ventral-most point.
[c] Superior articular facet transverse diameter: measured at the maximum facet width orthogonal to the dorsoventral measurement.
[d] Defined in Bräuer (1988) as the inferior vertebral body transverse diameter at the most laterally projecting points.
[e] Defined in Bräuer (1988) as the inferior vertebral body dorsoventral diameter measured at the sagittal midline.
[f] Defined in Bräuer (1988) as the maximal height of the axis at the sagittal midline, including the odontoid process.
[g] U.W. 101-651 (C1) and U.W. 101-1279 (C2) are included.
[h] A.L. 333-83 (C1) and A.L. 333-101 (C2) are included.
[i] KNM-ER 1825 data from Leakey and Walker (1985).
[j] ATD6-90 data from Carretero et al. (1999).
[k] VC3 and VC7 (Sima de los Huesos) data from Gómez-Olivencia et al. (2007); Kebara 2, La Chapelle-aux-Saints, La Ferrassie, Regourdou, and Shanidar 2 data from Gómez-Olivencia et al. (2013a).
[l] This measurement is based on a slight reconstruction.

Table 2
Measurements (in mm) on antepenultimate thoracic vertebrae.[a]

	H. naledi 101–855	*A. afarensis* A.L. 288-1AD	*A. afarensis* A.L. 333X-12	*A. africanus* Sts 14	*A. sediba* MH1	*P. robustus* SKX-41692	*H. erectus* KNM-WT 15000	Neandertal Kebara 2	Modern humans	Modern humans (small-bodied)	*Pan troglodytes*
Body superior transverse diameter (M7)[b]	22.8	20.2	26.2	19.0	20.8	24.9	–	34.9	31.0 (3.0, $N = 46$)	28.1 (1.6, $N = 4$)	26.7 (1.6, $N = 19$)
Body superior dorsoventral diameter (M4)[c]	17.8	20.9	20.0	16.0	–	20.5	–	–	25.2 (3.1, $N = 46$)	23.4 (0.7, $N = 4$)	22.0 (1.9, $N = 19$)
Body inferior transverse diameter (M8)	23.9	21.0	27.9	22.3	26.8	24.1	–	34.4	34.5 (3.6, $N = 46$)	30.7 (1.9, $N = 4$)	30.1 (2.0, $N = 18$)
Body inferior dorsoventral diameter (M5)	19.0	16.0	20.1	–	15.1	20.3	–	30.9	25.3 (2.9, $N = 45$)	23.7 (1.0, $N = 4$)	22.5 (1.8, $N = 18$)
Body ventral height (M1)[d]	14.3	12.0	12.6	14.7	11.2	15.4	–	–	20.3 (1.9, $N = 46$)	19.4 (0.6, $N = 4$)	15.7 (1.5, $N = 19$)
Body dorsal height (M2)[e]	15.8	14.5	14.7	17.5	13.0	16.2	–	20.1	21.3 (1.9, $N = 46$)	20.1 (0.7, $N = 4$)	17.4 (1.1, $N = 18$)
Max. inter-SAF dist.[f]	21.2	23.1	23.2	21.2	21.6	22.6	27.4	36.1	31.9 (3.3, $N = 44$)	30.3 (3.4, $N = 4$)	27.9 (2.6, $N = 19$)
Min. inter-SAF dist.[g]	8.9	11.5	9.5	5.7	8.5	9.8	11.0	14.0	12.3 (1.8, $N = 41$)	11.5 (1.2, $N = 4$)	10.4 (1.3, $N = 19$)
Max. inter-IAF dist.[h]	23.7	27.2	25.9	23.7	24.2	23.0	31.5	34.0	33.6 (3.7, $N = 44$)	30.3 (1.3, $N = 4$)	30.4 (3.6, $N = 18$)
Min. inter-IAF dist.[i]	7.8	12.0	9.3	9.7	9.4	9.1	12.3	11.1	11.7 (1.7, $N = 41$)	11.1 (0.6, $N = 4$)	11.1 (1.5, $N = 18$)
Superoinferior inter-AF height[j]	23.3	23.6	27.3	25.0	25.9	24.5	27.1	35.7	36.1 (2.7, $N = 46$)	32.7 (3.1, $N = 4$)	30.0 (1.9, $N = 19$)
Canal dorsoventral diameter (M10)[k]	10.3	12.9	11.9	10.5	9.6	9.5	–	14.1	14.5 (1.4, $N = 46$)	12.7 (0.3, $N = 4$)	11.2 (1.3, $N = 19$)
Canal transverse diameter (M11)[l]	13.0	11.0	10.9	9.9	11.2	11.2	11.6	19.5	15.2 (1.3, $N = 46$)	14.7 (1.3, $N = 4$)	13.5 (1.3, $N = 19$)
SAF superoinferior diameter[m]	7.2	7.5	8.6	8.0	9.1	8.4	9.4	12.0	11.2 (1.7, $N = 41$)	9.5 (1.7, $N = 4$)	10.9 (1.4, $N = 19$)
SAF transverse diameter[n]	6.1	6.5	7.2	6.9	6.7	6.8	–	11.2	10.2 (1.2, $N = 41$)	9.7 (2.5, $N = 4$)	9.4 (1.1, $N = 18$)
IAF superoinferior diameter[o]	8.0	8.7	10.3	8.3	10.0	9.3	10.9	12.2	11.9 (1.5, $N = 41$)	9.6 (1.6, $N = 4$)	11.6 (1.7, $N = 18$)
IAF transverse diameter[p]	7.6	9.6	8.8	7.3	8.4	7.2	9.5	11.0	11.4 (1.4, $N = 41$)	9.4 (1.7, $N = 4$)	10.3 (1.5, $N = 18$)
Pedicle superoinferior height[q]	8.8	10.6	11.2	10.8	7.9	9.8	10.4	14.4	13.9 (1.3, $N = 44$)	11.9 (1.4, $N = 4$)	11.4 (1.2, $N = 19$)
Pedicle transverse breadth[r]	4.7	5.5	6.8	4.6	4.1	3.7	5.5	8.0	7.1 (1.2, $N = 44$)	5.9 (0.7, $N = 4$)	6.3 (1.1, $N = 19$)
Pedicle dorsoventral length[s]	6.2	8.8	6.5	4.6	4.7	4.7	–	10.3	8.3 (1.2, $N = 33$)	4.7 (0.5, $N = 4$)	6.6 (1.2, $N = 16$)
Lamina superoinferior height[t]	14.0	11.7	15.5	14.3	14.6	14.0	15.3	21.3	21.5 (1.9, $N = 40$)	17.6 (2.2, $N = 4$)	16.6 (1.0, $N = 19$)
Lamina transverse width[u]	22.7	28.1	26.4	22.7	24.8	23.1	30.7	35.3	33.5 (3.2, $N = 46$)	30.2 (2.4, $N = 4$)	30.8 (3.4, $N = 19$)

[a] Taxa with more than one individual are shown as means, with standard deviation and sample size in parentheses. M = Martin number.
[b] Defined in Bräuer (1988) as the superior vertebral body transverse diameter at the most laterally projecting points.
[c] Defined in Bräuer (1988) as the superior vertebral body dorsoventral diameter measured at the sagittal midline.
[d] Defined in Bräuer (1988) as ventral superoinferior height of the vertebral body at the sagittal midline.
[e] Defined in Bräuer (1988) as dorsal superoinferior height of the vertebral body at the sagittal midline.
[f] Maximum inter-superior articular facet distance: measured from the lateral aspect of one superior articular facet to the lateral aspect of the other.
[g] Minimum inter-superior articular facet distance: measured from the medial aspect of one superior articular facet to the medial aspect of the other.
[h] Maximum inter-inferior articular facet distance: measured from the lateral aspect of one inferior articular facet to the lateral aspect of the other.
[i] Minimum inter-inferior articular facet distance: measured from the medial aspect of one inferior articular facet to the medial aspect of the other.
[j] Superoinferior inter-articular facet height: measured from the most superior aspect of the superior articular facet to the most inferior aspect of the inferior articular facet on the same side. The right side is measured unless it is broken or pathological, in which case the left side is measured. If the two sides are asymmetrical and one is not pathological, the mean is recorded.
[k] Defined in Bräuer (1988) as dorsoventral spinal canal diameter measured at the sagittal midline.
[l] Defined in Bräuer (1988) as transverse spinal canal diameter measured at the roots of the vertebral arch.
[m] Superior articular facet superoinferior diameter: measured at the middle of the facet. The right side is measured unless it is broken or pathological, in which case the left side is measured. If the two sides are asymmetrical and one is not pathological, the mean is recorded.
[n] Superior articular facet transverse diameter: measured at the most lateral aspects of the articular surface. The right side is measured unless it is broken or pathological, in which case the left side is measured. If the two sides are asymmetrical and one is not pathological, the mean is recorded.
[o] Inferior articular facet superoinferior diameter: measured at the middle of the facet. The right side is measured unless it is broken or pathological, in which case the left side is measured. If the two sides are asymmetrical and one is not pathological, the mean is recorded.
[p] Inferior articular facet transverse diameter: measured from the most medial aspect to the most lateral aspect of the articular surface. The right side is measured unless it is broken or pathological, in which case the left side is measured. If the two sides are asymmetrical and one is not pathological, the mean is recorded.
[q] Superoinferior height of the pedicle: measured at its midpoint. The right side is measured unless it is broken or pathological, in which case the left side is measured. If the two sides are asymmetrical and one is not pathological, the mean is recorded.
[r] Transverse breadth of the pedicle: measured at its midpoint. The right side is measured unless it is broken or pathological, in which case the left side is measured. If the two sides are asymmetrical and one is not pathological, the mean is recorded.
[s] Dorsoventral length of the pedicle: measured anterior from its junction with the superior articular process to its junction with the dorsal edge of the vertebral body.
[t] Superoinferior height of the lamina: measured on one side between the spinous process and the superior articular facets and the inferior articular facets, respectively. The right side is measured unless it is broken or pathological, in which case the left side is measured. If the two sides are asymmetrical and one is not pathological, the mean is recorded.
[u] Transverse width of the lamina: measured from the lateral aspects between the superior and inferior articular facets.

Table 4
Rib shaft cross-section measurements/indices from Figure 14.

Taxon/Specimen[a]	Internal-external width (mm)	Cranial-caudal height (mm)	Shape index[b]
H. sapiens pen.	5.3	13.4	0.40
Kebara 2 pen.	7.1	13.6	0.52
KNM-WT 15000 BS (pen.)	5.6	9.3	0.60
Sts-14 pen.	5.8	8.4	0.69
A.L. 288-1 AW (pen.)	5.4	8.7	0.62
U.W. 101-524 (pen.)	4.2	6.5	0.64
P. troglodytes pen.	5.9	9.4	0.63
H. sapiens ult.	5.1	11.8	0.43
Kebara 2 ult.	8.1	9.1	0.89
KNM-WT 15000 AN (ult.)	6.0	9.5	0.63
Sts-14 ult.	4.4	7.0	0.63
U.W. 101-1119 (ult.)	5.4	5.0	0.93
P. troglodytes ult.	7.0	10.2	0.69

[a] Pen. = penultimate rib, ult. = ultimate (last) rib.
[b] Mid-shaft cross sectional shape index: calculated as (I–E width)/(Cr.–Ca. height).

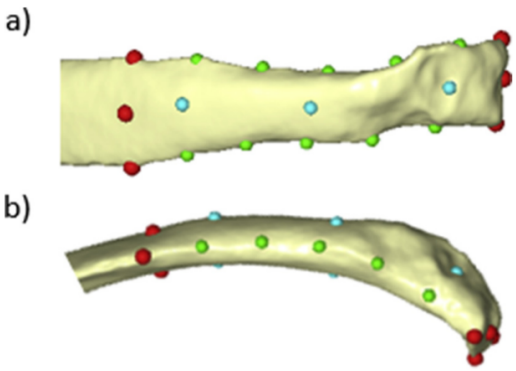

Figure 5. Three-dimensional landmarks taken on the preserved proximal portion of U.W. 101-524 and on specimens in the comparative sample. The rib model shown is a modern human 11th rib shown in external (top) and superior (bottom) views. True landmarks are depicted in red whereas curve- and surface semilandmarks are depicted in green and blue, respectively.

protostome burrowing). The ventral body measures 13.2 mm in craniocaudal height (M1); the dorsal body 14.5 mm (M2).

3.2.7. U.W. 101-855 (10th thoracic vertebra, T10) This is a mostly complete lower thoracic vertebra that preserves only the bases of transverse and spinous processes, which are broken distally (Fig. 2). The left transverse process base is preserved better than the right. The edges of the articular facets and the body are abraded and a portion of the ventrocranial centrum is broken. The left pedicle is eroded laterally and broken, but the left side is intact and bears a costal facet superiorly. Ring apophyses are presented both cranially and caudally, consistent with an adult.

A full set of measurements is listed in Table 2. The centrum is relatively wide and ovoid in shape. The ventral and dorsal heights of the body contribute to a ventrally wedged vertebra (with a wedging angle of 4.7°). There is a demifacet superiorly at the body-pedicle border, but not one inferiorly, as in human 9th thoracic vertebrae.

The right pedicle, which bears approximately half of a demifacet superiorly (the other half of the demifacet extends onto the dorsal side of the vertebral body), is 5.8 mm in dorsoventral length, measures 8.7 mm in craniocaudal height, and 4.1 mm in mediolateral width. The superior articular facets are dorsally and slightly laterally oriented and the inferior articular facets are ventrally and slightly medially oriented. The lamina measures 14.0 mm craniocaudally. The transverse and spinous processes are broken at their bases. U.W. 101-855 articulates with and is superjacent to U.W. 101-1733, which itself articulates with an 11th rib; therefore, U.W. 101-855 is a 10th thoracic vertebra.

3.2.8. U.W. 101-1733 (11th thoracic vertebra, T11) This is a nearly complete lower thoracic vertebra that was found in articulation with and subjacent to U.W. 101-855 (Fig. 1). This element is more complete in general than U.W. 101-855, but also lacks the distal ends of transverse and spinous processes. The body is abraded ventrolaterally and there is damage to the superior surface, perhaps caused by the intrusion of an intermingled long bone (see Fig. 6). The inferior articular facets are eroded, especially on the right side, such that the articular surface of the facet is entirely worn away. Ring apophyses are fused.

A full set of measurements is included in Table 3. The vertebral body is slightly ventrally wedged (2.9°). Costal facets are present at the body-pedicle border, fully preserved on the left side and slightly eroded on the right. The costal facets are superiorly placed and rise above the pedicles dorsally.

The spinal canal is large and ovoid in shape. The superior articular facets are dorsally and somewhat laterally oriented, and the inferior articular facets are flat and face directly ventrally. Therefore, the presumed penultimate thoracic vertebra is not the transitional vertebra (with flat, "thoracic-like" superior articular facets and sagittally-oriented, "lumbar-like" inferior articular facets; see Haeusler et al., 2002, 2011; Williams, 2012a, b).

The morphology of the bases of the transverse processes suggests thin, non-rib-bearing transverse processes characteristic of human T11 and T12 vertebrae. As with U.W. 101-855, the transverse and spinous processes are broken at their bases.

3.2.9. U.W. 101-581 This is an isolated spinous process of an upper thoracic vertebra. It is broken distally and skews slightly to the left. It is oriented in a dorso-caudal direction.

3.2.10. U.W. 101-1302 This is the left neural arch of a thoracic vertebra. The transverse process is broken at its base and the spinous process is missing entirely. The left pedicle, superior articular facet, and left lamina are preserved. The superior articular facet measures 6.4 mm craniocaudally and 6.3 mm mediolaterally.

3.2.11. U.W. 101-439 This is the dorsal aspect of the neural arch of a middle thoracic vertebra. The laminae, inferior articular facets, and base of the spinous process are preserved. Although the two halves of the neural arch are fused at the midline, given its diminutive size, it likely belongs to an immature individual.

3.2.12. U.W. 101-1493 This is the lamina of an upper thoracic vertebra that, due to its small size, likely belongs to an immature individual.

3.2.13. U.W. 101-1054 This is an isolated spinous process of a thoracolumbar vertebra that is relatively tall craniocaudally (13.2 mm) and narrow mediolaterally (3.9 mm). Although it is broken distally, it would be relatively short dorsoventrally (approximately 18 mm). The inferior surface of the spinous process appears to be skewed somewhat to the right side, as in U.W. 101-1337.

3.2.14. U.W. 101-581 This is an isolated spinous process from an upper thoracic vertebra. The spinous process is broken distally, precluding its measurement.

Figure 6. The *Homo naledi* lower thoracic vertebrae in situ (top) and in articulation (bottom). The vertebrae were discovered in close association and near articulation. U.W. 101-855 articulates with U.W. 101-1733, which in turn articulates with an 11th rib discovered alongside the vertebrae. The vertebrae are shown in articulation in right lateral, ventral, left lateral, and dorsal views (from left to right). The costal facet for the preserved 11th rib (U.W. 101-524) is visible in left lateral view of T11. Major units of scale in cm.

3.2.15. U.W. 101-1669 This is a spinous process belonging to a middle thoracic vertebra. It is oriented almost completely caudally and is broken distally.

3.2.16. U.W. 101-1124 This is an isolated spinous process belonging to a lower thoracic vertebra. It is fully preserved ventrally and broken cranially and distally, precluding its measurement.

3.2.17. U.W. 101-1599 This is the left part of the neural arch of a lower cervical or upper thoracic vertebra. The spinous process is absent and the transverse process is broken at its base. The articular facets are wider mediolaterally than tall craniocaudally, and the inferior articular facet is laterally-placed and flat in the coronal plane. Given these features, it most likely belongs to an upper thoracic vertebra.

3.2.18. U.W. 101-656 This is an isolated thoracic superior articular facet from the right side. Craniocaudal height of the facet is 6.6 mm; mediolateral width is 6.4 mm.

3.2.19. U.W. 101-1693 This thoracic fragment is represented by the superior articular facet, pedicle, and ventral portion of the vertebral body. The superior articular facet measures 8.5 mm craniocaudally and 5.3 mm mediolaterally.

3.3. Description of the lumbar vertebrae

3.3.1. U.W. 101-1337 This is a partial neural arch of an upper lumbar vertebra. It preserves both the laminae, the spinous process, and the left superior articular process, all of which are broken along their edges: the superior articular facet is abraded superiorly, the mammillary process is broken off dorsally, the left lumbar transverse process is broken distally, and the spinous process is abraded distally and superiorly (Fig. 3). The spinous process is long and oriented near-horizontally and slightly caudally. Although the spinous process is abraded distally, it is likely fairly complete and measures 23.3 mm in length. It appears to be somewhat asymmetrical, skewing slightly to the right. The spinous process bears a sharp crest caudally that forms distally from its base; the asymmetrical orientation of this crest confirms the right skew observed generally. The crest, which anchors the interspinous ligament is sharp rather than blunt and rounded as in modern humans, but it is not as extended as it is in chimpanzees. Caudally, the base of the spinous process leads ventrally into a wedge-shaped pit situated between the right and left inferior articular facets, a morphology typical of human and fossil hominin lower thoracic and upper lumbar vertebrae.

The laminae bear large, seemingly symmetrical pits superiorly and lateral to the base of the spinous process, again typical of lower thoracic and upper lumbar vertebrae. The superior articular facet is curved and its articular process is sagittally oriented relative to the midline as in lumbar vertebrae and occasionally the ultimate thoracic vertebra. The base of the transverse process is very small and slender like those in first lumbar vertebrae that occasionally lack or possess vestigial lumbar transverse processes. Since the lumbar transverse process, a costal homolog, is present, it is apparent that this vertebra did not anchor a rib via a costal facet. Therefore, it is likely that this neural arch represents an upper lumbar vertebra.

3.3.2. U.W. 101-1338 This is a fragmented vertebral body that preserves the side of the centrum and the base of the right pedicle (Fig. 3). Otherwise, the body is incomplete and broken. There does not appear to be a costal facet on the right side, suggesting this is a lumbar vertebra. The dorsal vertebral body height measures 18.9 mm craniocaudally (M2).

3.3.3. U.W. 101-984 This is a vertebral body with bases of the pedicles (Fig. 3). Approximately one-eighth of the right side of the body is broken craniocaudally from top to bottom. The cranial surface is mostly eroded away, especially at the dorsal body-pedicle border, and there is a wedge of bone broken ventro-

laterally on the right side. The caudal surface of the body is intact except on the broken lateral right side. Ring apophyses are fused on the caudal surface of the body and apparent on aspects of the cranial surface as well. U.W. 101-984 is a lumbar vertebra by definition as it lacks a costal facet for rib articulation on the preserved left side of the body-pedicle border.

3.3.4. U.W. 101-478 This is a lower lumbar vertebra that preserves the dorsal aspect of the body at midline (Fig. 3). It is eroded ventrally and laterally, so the body is not complete. There appears to be remnants of a ring apophysis on the caudal body dorsally. The left neural arch bears the superior articular facet, left superior portion of the pars interarticularis of the lamina, and the base of the lumbar transverse process. The left lower articular facet, spinous process, and entire right neural arch are missing.

The body measures 21.1 mm craniocaudally at the preserved dorsal body midline (M2). The body appears to slope caudally from the dorsal edge, but extensive erosion begins approximately 7 mm ventral to the dorsal edge of the body. Human lower lumbar vertebrae are often somewhat concave on the cranial articular surface of the body, a morphology that would present itself similarly to the preserved portion of U.W. 101-478. Alternatively, it is possible that the body is ventrally wedged; however, preserved morphology precludes this assessment. Therefore, there is no way to determine if its vertebral body is dorsally or ventrally wedged. A large basivertebral canal is situated in the craniocaudal and mediolateral middle of the dorsal side of the centrum.

The spinal canal, although not fully preserved, would be of an unusual shape for a lower lumbar vertebra. Its left side is preserved by the partial neural arch and suggests an ovoid, “kidney” shape rather than the triangular one commonly observed in human and panin lower lumbar vertebrae. The base of the transverse process is relatively thick dorsoventrally and angles relative to the sagittal midline at approximately 84°. The preserved left superior articular facet (which measures 9.5 mm craniocaudally and 9.0 mm mediolaterally) is situated low relative to the superior surface of the body as in lower lumbar vertebrae and is angled approximately 60° relative to the sagittal midline.

3.3.5. U.W. 101-765 This is the left lumbar transverse process and mammillary process of an upper to middle lumbar vertebra. The remaining parts of the pedicle and superior articular process, including the superior articular facet, are not present. The mammillary process is inferiorly and laterally placed relative to the superior articular facet, as in middle and particularly upper lumbar vertebrae. In middle and especially lower lumbar vertebrae, the mammillary process is more superiorly positioned on the lateral side of the superior articular facet or fully incorporated into it.

3.3.6. U.W. 101-538 This is the isolated superior articular facet of a lumbar vertebra or sacrum with the superior portion of the pedicle or ala preserved ventrally. The craniocaudal superior articular facet height measures 10.3 mm and 8.9 mm mediolaterally. The infero-medial portion of the articular facet bears a fissure, deepest inferiorly and shallowing superior-laterally, possibly of developmental or postdepositional taphonomic origin.

3.4. Description of the true and false ribs (1–10)

A table of diagnostic rib fragments is included in SOM Table S1.

3.4.1. U.W. 101-083 This is a 1st rib from the left side (Fig. 4). The rib head is not preserved in this fragment. The neck is flattened in its craniocaudal dimension. The internal margin of the neck is sharp and presents a groove at the junction between the neck and shaft. The external margin is thick and is eroded at its proximal part. The neck measures 7.2 mm (internally-externally [IE]) by 2.8 mm (craniocaudally [SI]) proximally, and measures 4.2 mm IE by 7.7 mm SI at the tubercle.

The tubercle and the posterior angle coincide. The facet of the articular tubercle is damaged post-mortem. The cranial surface exhibits an elevation, which indicates a point of ossification between the neck and shaft and the insertion of the serratus anterior muscle. The cranial surface of the shaft appears roughened when compared to the caudal surface. The insertion of m. scalenus medius is visible on this cranial surface. Only the proximal part of the inner margin of the rib shaft is undamaged. This aspect of the shaft measures 10.2 mm IE by 4.7 mm SI. The groove for the subclavian artery is shallow and indistinct and markings for the costoclavicular ligament are not evident. The caudal surface is smooth and featureless. The distal end of the shaft is missing.

3.4.2. U.W. 101-621 This is a left 1st rib fragment (Fig. 4). The tubercle and an immediately adjacent part of the proximal shaft is preserved. The rib head is not preserved in this fragment. The neck is flattened in its SI dimension and descends in vertebro-inferior direction. The neck appears oval in cross-section. The inner margin is rounded and the outer margin is not visible due to taphonomic damage. The tubercle exhibits an articular facet that is oval in shape, measuring 5.9 mm proximally-distally (PD) and 5.5 mm SI. There appear to be matrix filled pits on the tubercle. The tubercle-inner margin distance is 7.4 mm. The shaft is missing in its entirety and thus no features are observed nor any measurements taken.

3.4.3. U.W. 101-385 This is a right 2nd rib proximal fragment (Fig. 4). It represents part of the neck, the tubercle, and a proximal part of the shaft. The rib head is not preserved in this fragment. The neck is flattened in its craniocaudal dimension and descends in a vertebro-inferior direction. The neck presents a depression on the cranial surface that measures 8.2 mm PD by 3.6 mm IE. The internal margin of the neck is rounded. The external margin is also rounded. The neck measures 6.7 mm IE by 3.4 mm SI at the tubercle. The insertion of m. scalenus posterior is not visible on this element.

The tubercle and the posterior angle are coincident. The facet of the articular tubercle is visible and it is concave. It measures 4.1 mm SI by 5.5 mm PD. The non-articular part of the tubercle is visible and presents a ridge of bone projecting caudally and distally on to the proximal part of the shaft. There are some full-matrix pits on the upper part of the articular tubercle. The cranial and caudal surfaces of the shaft are smooth. The shaft appears oval in cross-section.

3.4.4. U.W. 101-1291 This is a left 2nd rib fragment (Fig. 4). It represents a medial part of a 2nd rib, which preserves the insertion of m. scalene posterior in the upper surface. The fragment is flattened in its craniocaudal dimension. The internal and external margins are rounded.

3.4.5. U.W. 101-979 and 1009 This is a right rib from the upper thorax (Fig. 4). It represents a medial part of a 3rd–6th rib. The costal groove is not very marked in the fragment preserved and the costal angle is not present in this fragment.

3.4.6. U.W. 101-351 This is a left rib fragment of the middle of the thorax (Fig. 4). It represents a medial part of a 6th–9th rib. The costal groove is marked in this fossil and the posterior angle is completely preserved.

3.5. Description of the floating ribs (11th–12th)

3.5.1. U.W. 101-524 This is a left 11th rib (Fig. 4) that was found in close association with the lower thoracic vertebrae (U.W. 101-855 and -1733). It does not present an articular tubercle for articulation with the transverse process of the vertebrae as non-floating ribs would. Instead, it presents a single facet at the rib head that articulates directly with the T11 vertebra (U.W. 101-1733). The fragment represents a part of the head and the proximal shaft reaching far from the angulus costae (posterior angle). The head is broken proximally on the internal aspect. The external part exhibits an articular facet that is rounded. The measurements of the facet are 8.1 mm SI by 6.4 mm PD. The IE width of the head is 4.4 mm. The shaft appears pinched IE immediately distal to the head and thickens as it progresses distally.

The cranial surface presents an expanded surface area for the attachment of the intercostal musculature of the 10th intercostal space and is smoother than the caudal surface. The shaft appears cuboidal in cross-section at the distal end break. The measurements of the shaft proximally are: 5.2 mm SI by 6.3 IE and distally are: 5.3 mm SI and 6.0 IE.

3.5.2. U.W. 101-1119 This is a left 12th rib (Fig. 4). The fragment represents a small part of the head and the proximal shaft. The head is absent except for a small part of the most caudal part. The shaft appears pinched IE immediately distal to the head and pinched SI along the rest of the preserved rib shaft.

The cranial surface presents an expanded surface area for the attachment of the intercostal musculature of the 11th intercostal space. The caudal surface is for the attachment of m. quadratus lumborum. The shaft appears cuboidal in cross-section proximally and appears more flattened IE distally. The measurements of the shaft proximally are 4.3 mm SI by 5.4 mm IE and distally are 6.3 mm SI and 4.4 IE. The distal shaft exhibits taphonomic damage and is absent.

3.6. Sternal material

3.6.1. U.W. 101-870 This is the ventral portion of the lamina of a middle sternal segment. It is cuboidal in shape and exhibits a complete cranial border and an inferior border that is taphonomically partially damaged. The ventral surface exhibits a slight concavity. The dorsal aspect of the fragment is composed to the inner cortical bone. The lateral borders exhibit partial facets at each angle of the cuboid fragment with the left caudal facet being damaged. The maximum cranial-caudal length of the fragment is 18.3 mm. The medio-lateral width of the cranial border is 19.9 mm. The mid-sternebra width between the two concavities is 15.1 mm. No measurement of the inferior border was taken due to it being incomplete.

3.7. Comparative summary of metric analyses

The Dinaledi collection includes rib and vertebral remains of two different-aged immature individuals and two adult left ribs, establishing a minimum number of individuals represented by the postcranial axial skeleton as four (SOM Table S2). Additionally, the collection includes two lower thoracic vertebrae that were found in partial articulation with each other (U.W. 101-855 and -1733, Figs. 2 and 6). These additionally articulate with the proximal 11th rib (U.W. 101-524, Fig. 4), which was found in close association with the vertebrae (SOM Fig. S1). The articulated lower thoracic vertebrae and 11th rib are among the smallest known in the hominin fossil record (Figs. 7–9), comparable in size to female *A. africanus* (Sts 14) and female *A. afarensis* (A.L. 288-1, 'Lucy'), which are among the smallest adult individuals known from their respective species.

The *H. naledi* lower thoracic vertebrae are small in overall size, falling between female chimpanzees and mixed male/female siamangs among extant hominoids, and larger only than the T10 vertebra of Sts 14 among fossil hominins; however, the *H. naledi* T10 and T11 vertebral body superior surface areas are larger than those of both Sts 14 and close in size to A.L. 288-1, even though the latter are substantially larger in overall size (Fig. 10).

The spinal canal area of *H. naledi* is absolutely larger than that of australopiths, similar in size to KNM-WT 15000 and the

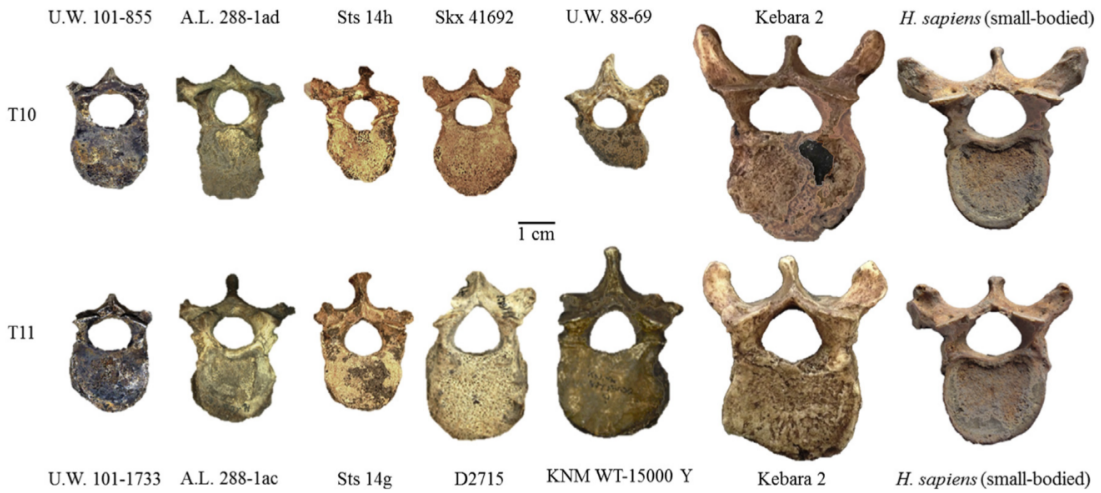

Figure 7. Tenth (T10; top row) and eleventh (T11; bottom row) vertebrae in comparative perspective. From left to right: *H. naledi* (top: U.W. 101-855; bottom: U.W. 101-1733), *A. afarensis* (top: A.L. 288-1ad; bottom: A.L. 288-1ac), *A. africanus* (top: Sts 14h; bottom: Sts 14g), *Paranthropus robustus* (top: SKX 41692) and Dmanisi *H. erectus* (bottom: D2715), *A. sediba* (top: U.W. 88-69 [MH1]) and Nariokotome *H. erectus* (bottom: KNM-WT 15000 Y), *Homo neanderthalensis* (top: Kebara 2 T10; bottom: Kebara 2 T11), and small-bodied modern *H. sapiens*. Note the small absolute size of the *H. naledi* vertebrae overall, but the relatively large size of the spinal canal.

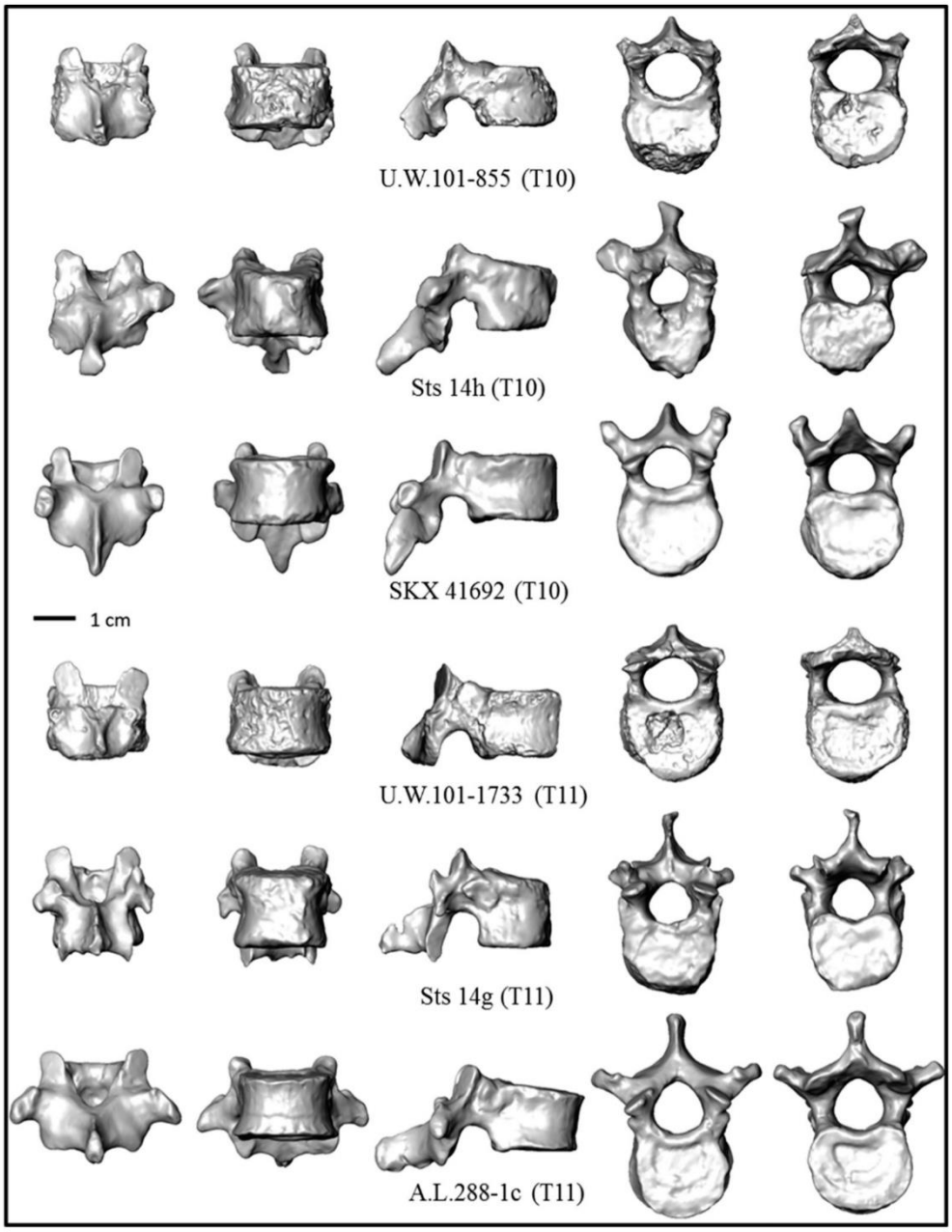

Figure 8. Lower thoracic vertebrae of *H. naledi* and other small-bodied hominins. 10th (above scale bar) and 11th (below scale) thoracic vertebrae in dorsal, ventral, lateral, cranial, and caudal views (from left to right). T10 vertebrae are (from top down) *H. naledi* (U.W.101-855), *A. africanus* (Sts 14h), and *P. robustus* (SKX 41692); T11 vertebrae are (from middle down), *H. naledi* (U.W.101-1733), *A. africanus* (Sts 14g), and A. afarensis (A.L.288-1c). A.L. 288-1d (T10) is not shown because its vertebral body is pathologically extended (see Fig. 4), as is A.L. 288-1c (shown), albeit to a lesser degree.

chimpanzee sample mean, both of which belong to much larger vertebrae than *H. naledi* (Fig. 10). When the spinal canal area is compared to the area of the superior vertebral body, *H. naledi* demonstrates a relatively large T10 canal compared to other early hominins (Fig. 11). Whether the relatively large size and ovoid shape of the *H. naledi* spinal canal reflects large lumbosacral nerve endowment to innervate and control relatively long hindlimbs, or whether it is instead a consequence of neural arch architecture uncorrelated with spinal cord size remains to be determined.

The proximal ends of two first ribs (U.W. 101-083 and U.W101-621) and a second rib (U.W. 101-385) lack of much of the shaft and sternal end, so it impedes estimation of their overall curvature. A middle shaft fragment from a 3rd–6th rib (U.W. 101-979/1009; Fig. 4) is relatively straight (uncurved). The 11th rib (U.W. 101-524) is straight in both axial and sagittal planes, presenting a lack of rib torsion (Figs. 4 and 9). It is most similar in overall morphology and size to (although is substantially smaller than) A.L. 288-1 (Figs. 9 and 12), likely contributing to a wide lower thorax that is comparable to that reconstructed for the small-bodied female *A. afarensis* (A.L. 288-1; Schmid, 1983). This feature is also observed in other fossil individuals like KNM-WT 15000 (AN and BS, following Jellema et al., 1993 and Haeusler et al., 2011; respectively), whereas Neandertal Kebara 2 and modern humans present a different

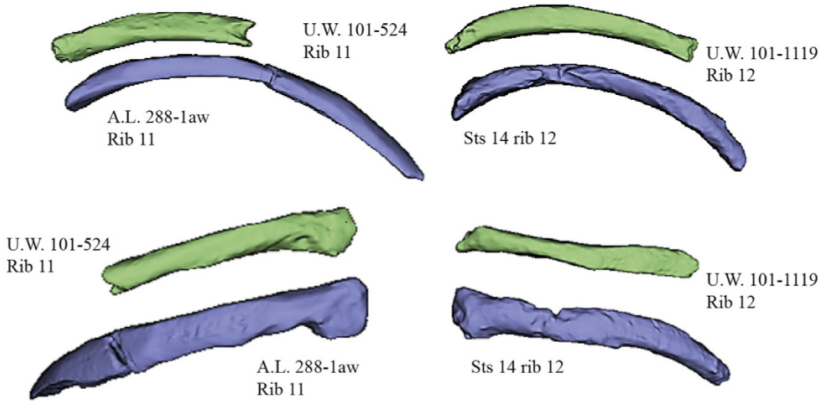

Figure 9. Comparisons of the *H. naledi* 11th and 12th ribs to *A. afarensis* (left) and *A. africanus* (right) 11th and 12th ribs, respectively. *Homo naledi* is shown in green; *Australopithecus* in blue. The Sts 14 12th left rib is mirror imaged to compare directly with U.W. 101-1119. Views are cranial (top images) and dorsal (bottom images). The shaft curvature of the *H. naledi* rib appears similar to that observed in the *A. afarensis* rib and less curved than of the corresponding *A. africanus* specimen.

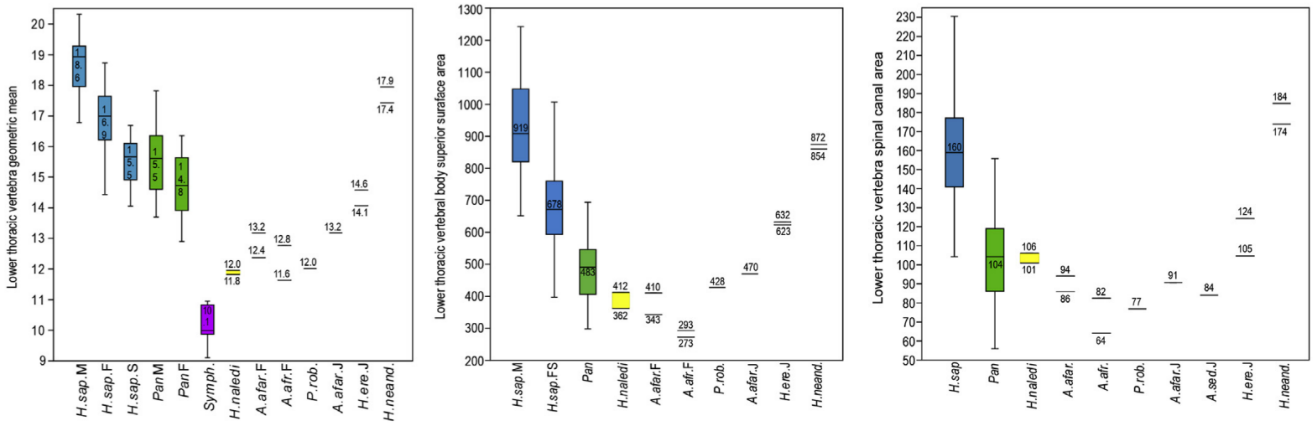

Figure 10. Three measurements of penultimate and antepenultimate thoracic vertebra size. Left: Vertebra geometric mean is used as a proxy for overall size (in the absence of association with commonly used proxies of body size); Middle: Vertebral body superior surface area (mm^2); Right: Spinal canal cross-sectional area (mm^2). Two data points are shown for fossil taxa when one individual preserves both T10 and T11 (as is the case in *H. naledi*, Sts 14, and A.L. 288-1), or in the case of *H. erectus*, where Dmanisi and Nariokotome are grouped together as juveniles (in all three plots, Dmanisi produces a larger value than Nariokotome). Body surface area (middle) and canal cross-sectional area (right) were measured on standardized photographs using ImageJ (imagej.nih.gov/ij/). In each plot, extant subgroups (e.g., males and females) are separated when statistically different from each other and pooled when not; T10 and T11 levels are not statistically different in any extant group, so they are pooled. Means are shown for each group; fossils are shown as individual data points. Sample sizes are as follows: *H. sapiens* (males $N = 36$; females $N = 50$; small-bodied mixed sex $N = 8$), *Pan troglodytes* (males $N = 17$; females $N = 18$), *S. syndactylus* (mixed sex $N = 6$). M = male; F = female; J = juvenile; S = small-bodied humans: Andaman Islander, Mbuti "pygmy," San "Bushman," and very small adults from other modern human groups; *H. sap.* = Homo *sapiens*; *Symph.* = *Symphylangus*; *A. afar.* = *Australopithecus afarensis*; *A. afr.* = *Australopithecus africanus*; P. rob. = *Paranthropus robustus*. *A. afarensis* is represented by adult female A.L. 288-1 (T10, below; T11 above) and subadult A.L. 333x-12 (T10), *A. africanus* by Sts 14 (T10, below; T11 above), *P. robustus* by SKX-41692 (T10), and *H. erectus* by KNM-WT 15000 from Nariokotome (T11, above) and D2713 from Dmanisi (T11, below). Measurements included in the geometric mean are body superior transverse diameter (M7), body inferior transverse diameter (M8), body superior dorsoventral diameter (M4), body inferior dorsoventral diameter (M5), body ventral height (M1), body dorsal height (M2), superior-inferior inter-articular facet height, superior articular facet superior-inferior diameter, superior articular facet transverse diameter, superior maximum inter-articular facet distance, superior minimum inter-articular facet distance, canal dorsoventral diameter (M10), canal transverse diameter (M11), pedicle superior-inferior height, pedicle transverse breadth, lamina superior-inferior height, and lamina transverse width (see Tables 1 and 2 for all measurement definitions).

morphological pattern, since rib torsion is clearly evident as increased curvature both in sagittal and transverse planes (Fig. 13). As observed in PC1–PC2 projection of the morphology of the proximal end of the 11th rib (Fig. 13), fossil specimens (except Neandertal Kebara 2) present the plane of the rib head more parallel to the shaft plane, whereas the ribs of the rest of the fossil sample present a more acute orientation between the head and the shaft planes. This feature may be the result of rib torsion. In the PC1–PC3 projection (Fig. 13), humans and chimpanzees are separated diagonally—humans produce negative values on PC1 and PC3, whereas chimpanzees produce the opposite pattern. U.W. 101-524 shows a very negative value on PC3 and a very positive one in PC1, falling out in a different part of the morphospace with a robust rib shaft and relatively uncurved rib head. PC1–PC3 projection (Fig. 13) reveals a feature not previously observed in the literature, which is the shaft height relative to shaft length (from the rib head to the posterior angle). The morphospace area close to the *H. naledi* rib is characterized by an increased rib shaft height relative to the head-angle length. Although this feature is observed in some fossils such as A.L. 288-1 or KNM-WT 15000 BS, it is much more pronounced in the *H. naledi* 11th rib.

The 12th rib (U.W. 101-1119, Fig. 4) preserves part of the shaft, which is straight and appears less curved than the 12th rib of Sts 14 (Fig. 9). The *H. naledi* 12th rib is also very broad and square-

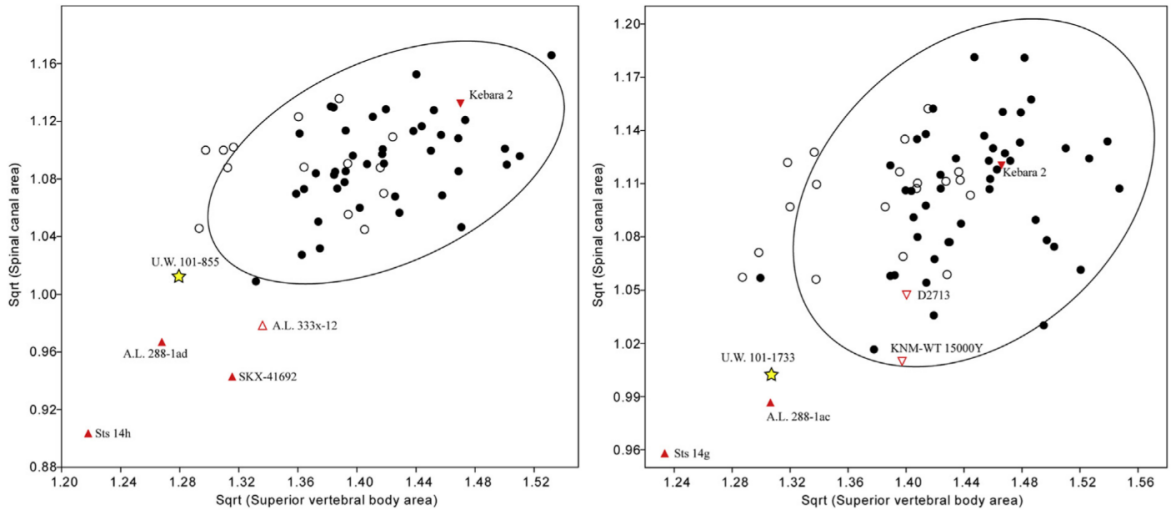

Figure 11. Square root of the vertebral body surface area (in mm) plotted against square root of the spinal canal cross-sectional area (in mm) in *H. naledi* T10 (left) and T11 (right) vertebrae and in fossil and extant hominins. The variables were logged and are significantly correlated but produce very low correlation coefficients (T10: $r^2 = 0.11$, $p = 0.01$; T11: $r^2 = 0.08$, $p = 0.02$). *Homo naledi* is shown with a yellow star in each plot, australopiths with triangles, fossil *Homo* with inverted triangles, and modern humans with circles. Adults are shown with filled symbols; subadults with open symbols. Sqrt = square root.

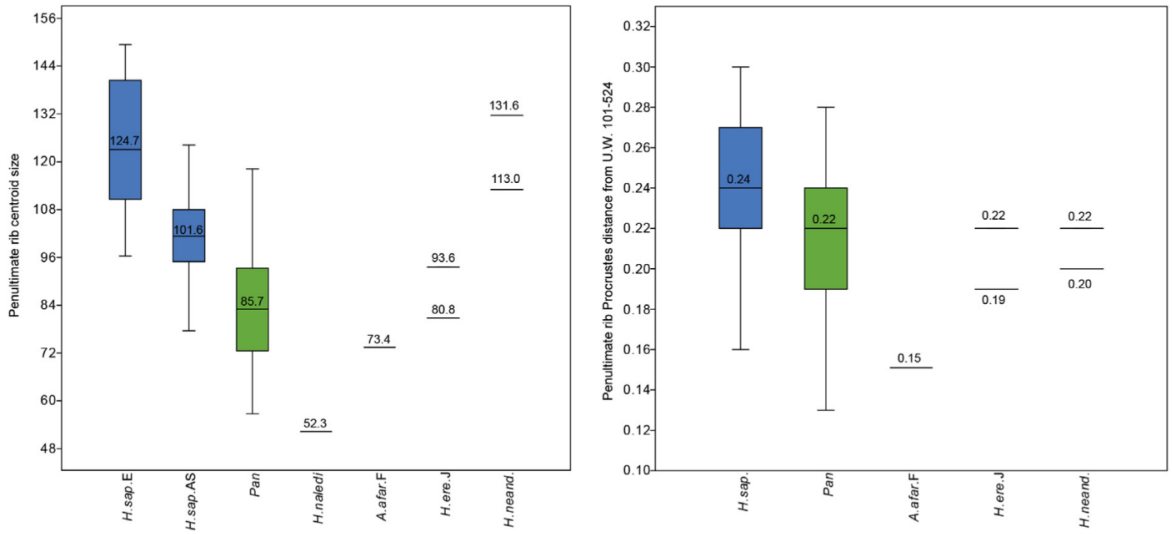

Figure 12. *Homo naledi* 11th rib centroid size in comparative context (left) and Procrustes distances of the comparative sample from it (right). Left: Centroid size of U.W. 101-524 is the smallest of the sample. Right: Procrustes distances between U.W. 101-524 (distance from itself = 0) and the comparative sample of penultimate ribs. *A. afarensis* is represented by A.L. 288-1, *H. erectus* by KNM-WT 15000, and Neandertals by both antimeres of Kebara 2. Sample sizes are as follows: *P. paniscus* (equal sexes $N = 10$), *P. troglodytes* (equal sexes $N = 20$), and *H. sapiens* (E = Europeans, N = 20; AS = sub-Saharan and small-bodied populations, $N = 13$). As in Figure 7, human subgroups are included, as well as bonobos and chimpanzees, but the latter are not statistically distinct from each other so are pooled and shown as "Pan." Species abbreviations follow Figure 10.

shaped in cross-section (Fig. 14). We speculate that the apparent lack of rib torsion in this hominin thus suggests a wide lower thorax morphology, perhaps coupled with a cranially convergent upper thorax that is dissimilar to that of modern humans and perhaps Neandertals and other members of the genus *Homo* (Figs. 12 and 13).

4. Discussion

The shape of the thorax and overall trunk morphology are among the most problematic anatomical areas to study in fossil hominins. Partial or composite skeletons rarely present enough diagnostic morphology to adequately document thorax shape, and the complex forms of vertebrae and ribs are difficult to quantify. These challenges have led to a long history of debate regarding thorax evolution in human evolution (Gorjanović-Kramberger, 1906; Boule, 1911–1913; Robinson, 1972; Johanson et al., 1982; Schmid, 1983; Ohman, 1986; Jellema et al., 1993; Franciscus and Churchill, 2002; Sawyer and Maley, 2005; Gómez-Olivencia et al., 2009; Haile-Selassie et al., 2010; Simpson et al., 2010; García-Martínez, 2013; Schmid et al., 2013; García-Martínez et al., 2014; Bastir et al., 2015b; Latimer et al., 2016; Tawane et al., 2016).

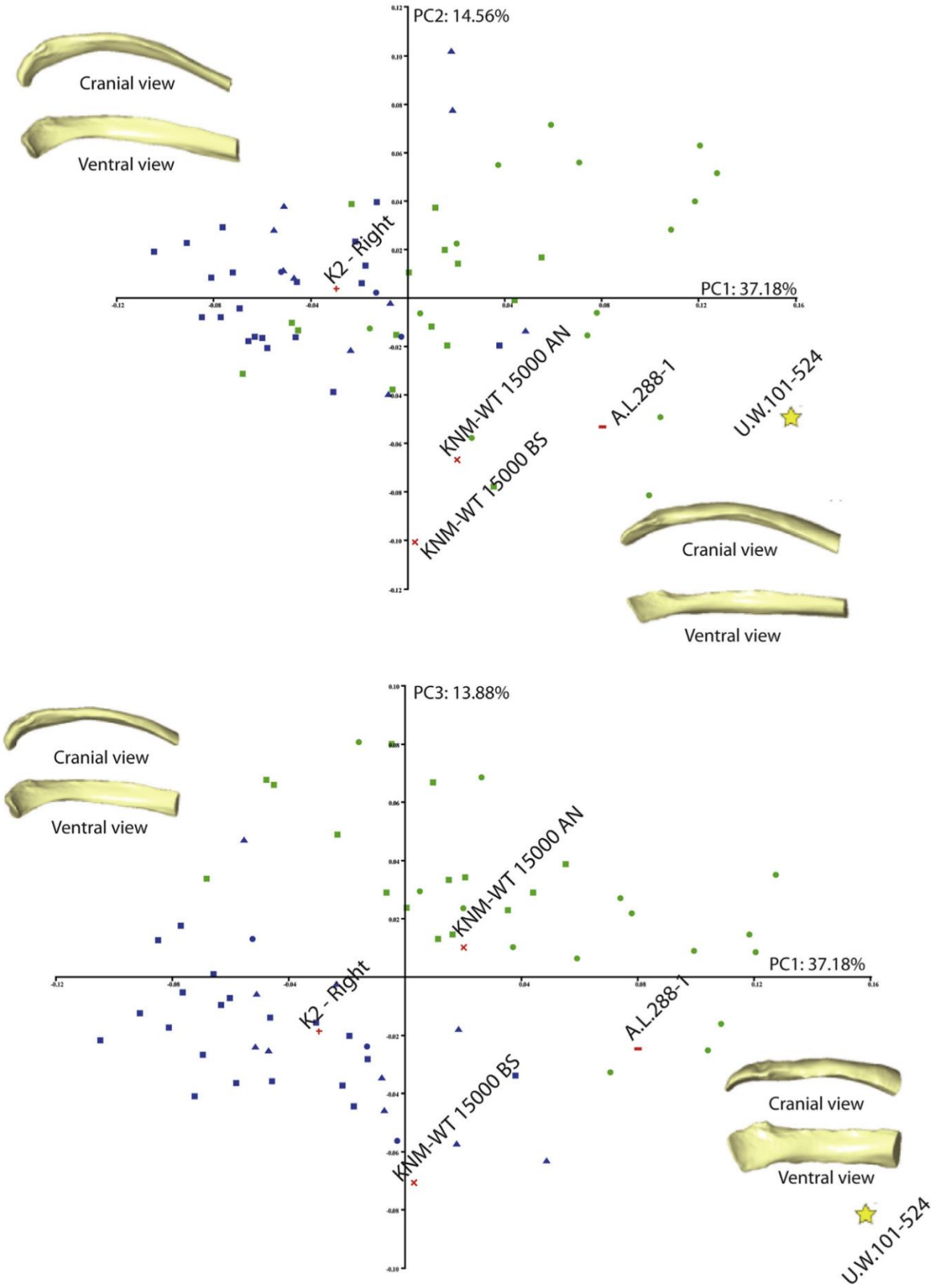

Figure 13. Proncipal component-shape analysis of the proximal part of penultimate ribs. Modern humans (in blue) include samples from Europeans, sub-Saharan Africans, and small-bodied (Andaman, Mbuti) populations. Both *P. paniscus* and *P. troglodytes* (green points) are also included. Top: Scatterplot of PC1 (37.18% of total variance) and PC2 (14.56% of total variance) and warped 3D models of proximal parts of the penultimate ribs in cranial and ventral views. Note that KNM-WT 15000, U.W. 101-524, and A.L. 288-1 11th ribs polarize towards the negative values in PC2 because their straight rib morphology and orientation of the rib head plane relative to the rib shaft plane. Bottom: PC 1 and PC 3 scatterplot (13.88% of total variance), along with warped 3D models of the penultimate ribs in cranial and ventral views. Positive values of PC1 combined with negative values of PC3 (where *H. naledi* 11th rib is observed) are characterized by an increased rib height relative to the length. Despite increased rib height relative to the length is observed in some fossils such as A.L. 288-1 or KNM-WT 15000 BS, this is much more pronounced in the *H. naledi* 11th rib. Neandertal Kebara 2 (K2) left rib plots close to the distribution of modern humans.

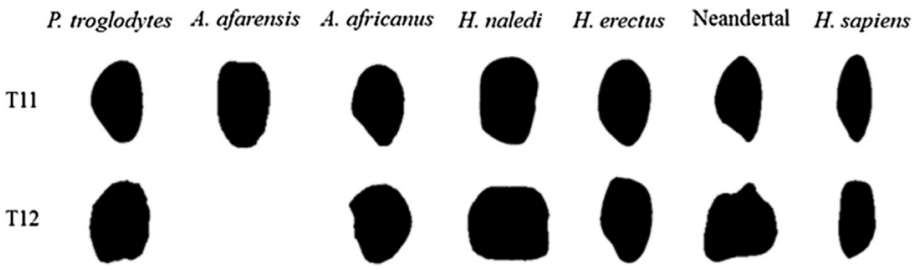

Figure 14. Cross-sectional anatomy of the midshaft of the penultimate and ultimate ribs of extant and fossil hominins. At the penultimate rib level (above), *H. naledi* exhibits a cross-section with a rounded cranial margin and a flattened caudal margin. A similar cross-sectional shape is observed in the 11th rib of *A. afarensis* (A.L. 288-1). The remaining cross-sections differ in exhibiting a narrower and sharper caudal margin, although the cranial margins also appear rounded. At the last rib level (below), the cranial and caudal margins of *H. naledi*, the Kebara 2 Neandertal, and chimpanzees (*P. troglodytes*) appear wider in cross-section, producing a cuboidal cross-sectional shape. The flattened and widened cranial and caudal margins provide an increased surface area for the attachment of the intercostal musculature and for the quadratus lumborum muscle, respectively. In contrast, *A. africanus* (Sts 14) and modern humans (*H. sapiens*) exhibit an oval cross-sectional shaft shape. *Homo erectus* penultimate and last ribs are represented by KNM-WT 15000 BS and KNM-WT 15000 AN, respectively (following Haeusler et al., 2011). Note that the images are scaled to the same height. Raw measurements of the rib cross-sections are included in Table 4.

The preserved parts of the *H. naledi* lower thorax appear primitive in morphology (Figs. 9, 12, and 13), an observation supported by evidence for wide iliac blades of the pelvis (Berger et al., 2015; VanSickle et al., submitted). Latimer et al. (2016) have recently argued that a "bell-shaped" thorax—one wide and human-like cranially and broad caudally—persisted throughout most of hominin evolution (contra Schmid, 1983; Schmid et al., 2013). The proximal upper rib ends in *H. naledi* are too incomplete to allow reconstruction of their curvature; however, a strongly cranially-oriented glenoid and an elevated clavicle and shoulder are suggestive of a narrow upper thorax (Berger et al., 2015; Feuerriegel et al., 2017). This morphology contrasts with evidence for long lower limbs and striding bipedalism (Berger et al., 2015; Harcourt-Smith et al., 2015) and other derived features of the hands and skull (Berger et al., 2015; Kivell et al., 2015; Schroeder et al., 2017). Despite derived lower limb morphology, the elevated shoulder and wide lower thorax of *H. naledi* suggests to us that this species was not adapted to efficient long-distance running (suggested as a key trait in *H. erectus*; Bramble and Lieberman, 2004; but see Thompson et al., 2015), while arboreal activities may have been important aspects of the behavioral repertoire of *H. naledi* (Berger et al., 2015; Kivell et al., 2015; Feuerriegel et al., 2017).

The *H. naledi* 11th rib demonstrates a combination of features—a lack of rib torsion and straightness of the proximal part of the rib shaft, the orientation of the rib head plane relative to the shaft, and an increased shaft height relative to shaft length—that are similarly observable in early hominins to the exclusion of Neandertals and *H. sapiens*. The broad 12th rib cross-sections in *H. naledi* (Fig. 14) seems to reflect a marked attachment for intercostal musculature superiorly and particularly for m. quadratus lumborum inferiorly. This morphology contrasts strongly with that observed in extant great apes, modern humans, and Pliocene and early Pleistocene hominins. The Kebara 2 Neandertal 12th rib, while similarly broad inferiorly, bears a strong crest superiorly for attachment of the diaphragm; in contrast, the *H. naledi* 12th rib bears a weak scar for diaphragm attachment (see Fig. 14).

The vertebrae of *H. naledi* are small in overall size and accordingly present absolutely small vertebral body surface areas and spinal canal dimensions; however, the latter are relatively large (Figs. 7, 8, and 10) in the best preserved specimens (U.W. 101-855 and -1733), especially at the T10 level (Fig. 11). The presumed penultimate thoracic vertebra is not the transitional vertebra, as is the case in all currently known early hominins (Haeusler et al., 2002, 2011; Williams, 2011, 2012b; Williams et al., 2013, 2016; Meyer et al., 2015). Whether this means that *H. naledi* is more similar to later members of the genus *Homo* in this regard or that the single individual from which lower thoracic vertebrae are currently known is atypical of the species will require the recovery and study of additional specimens.

The limited rib and vertebra material of *H. naledi* that has been recovered and studied thus far suggests that some members of the genus *Homo* were fairly small-bodied (cf. Brown et al., 2004; Grabowski et al., 2015) and additionally supports the paradigm shift (cf. Antón et al., 2014) that lineages previously thought to be committed terrestrial bipeds possessed decidedly non-modern body plans (Johanson et al., 1987; Leakey et al., 1989; Simpson et al., 2008, 2014; Graves et al., 2010; Holliday, 2011; Domínguez-Rodrigo et al., 2013). While little from the axial skeleton is currently known, future recovery and study of specimens from Rising Star Cave are likely to enhance our understanding of the postcranial morphology and locomotion of *H. naledi* and perhaps shed light on the increasingly ambiguous transition between *Australopithecus* and *Homo*.

Acknowledgments

The authors thank the Editor Sarah Elton, the AE, and reviewers who provided useful and encouraging feedback at this journal and on earlier versions of this manuscript. We thank the many funding agencies that supported this work, in particular the National Geographic Society, the National Research Foundation, the Lyda Hill Foundation, and the Lee R. Berger Foundation for Exploration for particularly significant funding of the discovery, recovery, and analysis of this material. We also thank the University of the Witwatersrand and the Evolutionary Studies Institute, as well as the South African National Centre of Excellence in PalaeoSciences and Bernhard Zipfel for curating the material and hosting the authors while studying the material. Erik Trinkaus made casts of Neandertal vertebrae available to SAW. DGM and MB were funded through CGL2012-37279, MINECO, Spain, and a Leakey Research Grant to DGM. A visit to the Royal Museum for Central Africa (RMCA; Tervuren, Belgium) by DGM was funded by the European Commission's Research Infrastructure Action via the Synthesys Project (BE-TAF-5639). We thank the following individuals for curating and providing access to comparative materials in their care: Stephany Potze and Lazarus Kgasi (Ditsong Museums); Yonas Yilma, Tomas Getachew, Jared Assefa, and Getachew Senishaw (National Museum of Ethiopia and Authority for Research and Conservation of Cultural

Heritage); Eugenia Cunha (Santarém collection); Miguel Almeida, Maria Teresa Ferreira, and Sofia Wasterlain (Paseo de Anel Verde Collection); Wim Wendelen and Emmanuel Gilissen (RMCA); Lyman Jellema and Yohannes Haile-Selassie (Cleveland Museum of Natural History); and Eileen Westwig, Eleanor Hoeger, Aja Marcato, and Neil Duncan (American Museum of Natural History). SAW was funded through the New York University Research Challenge Fund. Contributions to mapping the cave system from the Speleological Exploration Club, the Free cavers, and CROSA caving societies are acknowledged. We thank Emma Mbua, Fred Spoor, and the National Museums of Kenya Earth Science Department for providing CT scans of the KNM WT-15000 axial skeleton and Wolfgang Recheis (Medical University, Innsbruck) for modern human data. We thank the South African Heritage Resource Agency for the necessary permits to work on the Rising Star site; the Jacobs family and Lee R. Berger Foundation for Exploration for granting access; our exploration team consisting of Pedro Boshoff, Rick Hunter, and Steve Tucker; excavators K. Lindsay Eaves, Marina Elliot, Elen Feuerriegel, Alia Gurtov, Hannah Morris, and Becca Peixotto; and Wilma Lawrence, Bonita De Klerk, Natasha Barbolini, Merrill Vanderwalt, and Justin Mukanku for their assistance during all phases of the project.

Supplementary Online Material

Supplementary online material related to this article can be found at http://dx.doi.org/10.1016/j.jhevol.2016.11.003.

References

Aiello, A., Wheeler, P., 1995. The expensive tissue hypothesis: the brain and digestive system in human and primate evolution. Curr. Anthropol. 36, 199–221.
Antón, S., Potts, R., Aiello, L., 2014. Evolution of early *Homo*: an integrated biological perspective. Science 345, 1236828.
Antón, S.C., Snodgrass, J.J., 2012. Origins and evolution of genus *Homo*: new perspectives. Curr. Anthropol. 53, S479–S496.
Arensburg, B., 1991. The vertebral column, thoracic cage and hyoid bone. In: Bar Yosef, O., Vandermeersch, B. (Eds.), Le Squelette Mousterian de Kebara 2. Editions du C.N.R.S., Paris, pp. 113–146.
Arsuaga, J.-L., Lorenzo, C., Carretero, J.M., Gracia, A., Martínez, I., García, N., Bermúdez de Castro, J.-M., Carbonell, E., 1999. A complete human pelvis from the Middle Pleistocene of Spain. Nature 399, 255–258.
Arsuaga, J.L., Carretero, J.-M., Lorenzo, C., Gómez-Olivencia, A., Pablos, A., Rodríguez, L., García-González, R., Bonmatí, A., Quam, R.M., Pantoja-Pérez, A., Martínez, I., Aranburu, A., Gracia-Téllez, A., Poza-Rey, E., Sala, N., Garcia, N., Alcázar de Velasco, A., Cuenca-Bescós, G., Bermúdez de Castro, J.M., Carbonell, E., 2015. Postcranial morphology of the middle Pleistocene humans from Sima de los Huesos. Spain. Proc. Natl. Acad. Sci. USA 112, 11524–11529.
Bastir, M., García-Martínez, D., Recheis, W., Barash, A., Coquerelle, M., Rios, L., Peña-Melián, Á., García Río, F., O'Higgins, P., 2013. Differential growth and development of the upper and lower human thorax. PLoS One 8, e75128.
Bastir, M., García-Martínez, D., Estalrrich, A., García-Tabernero, A., Huguet, R., Ríos, A., Recheis, W., de la Rasilla, M., Rosas, A., 2015a. The relevance of the first ribs of the El Sidrón site (Asturias, Spain) for the understanding of the Neanderthal thorax. J. Hum. Evol. 80, 64–73.
Bastir, M., García-Martínez, D., Barash, A., 2015b. The 3D structure of thoracic vertebrae and their significance for size and shape of the ribcage in Neandertals, Proceedings of the European Society for the Study of Human Evolution, London.
Bastir, M., García-Martínez, D., Williams, S.A., Nalla, S., Eyre, J., Oishi, M., Ogihara, N., Churchill, S.E., Berger, L., Schmid, P., 2016. Preliminary findings of 3D analyses of the costal remains of *Australopithecus sediba*. PaleoAnthropology A2–A3.
Ben-Dor, M., Gopher, A., Barkai, R., 2016. Neandertals' large lower thorax morphology may represent adaptation to high protein diet. J. Hum. Evol. 160, 367–378.
Berger, L.R., Hawks, J., DeRuiter, D., Churchill, S.E., Schmid, P., Delezene, L., Kivell, T., Garvin, H.M., Williams, S.A., DeSilva, J.M., Skinner, M., Musiba, C.M., Cameron, N., Holliday, T.W., Harcourt-Smith, W., Ackermann, R.R., Bastir, M., Brophy, J., Cofran, Z.D., Congdon, K.A., Deane, A.S., Dembo, M., Elliot, M., Feuerriegel, E.M., García-Martínez, D., Green, D.J., Gurtov, A., Kruger, A., Laird, M.F., Marchi, D., Meyer, M.R., Nalla, S., Negash, E.W., Radovcic, D., Scott, J.E., Schroeder, L., Throckmorton, Z., VanSickle, C., Walker, C.S., Wei, P., Zipfel, B., 2015. *Homo naledi*, a new species of the genus *Homo* from the Dinaledi Chamber, South Africa. eLIFE 4, e09560.
Bonmatí, A., Gómez-Olivencia, A., Arsuaga, J.L., Carretero, J.M., Gracia, A., Martínez, I., Lorenzo, C., Bérmudez de Castro, J.M., Carbonell, E., 2010. Middle Pleistocene lower back and pelvis from an aged human individual from the Sima de los Huesos site. Spain. Proc. Natl. Acad. Sci. USA 107, 18386–18391.
Boule, M., 1911-1913. L'homme fossile de La Chapelle-aux-Saints. Ann. Paléontol. 6, 111-172; 7, 21-56, 85-192; 8, 1–70.
Bramble, D.M., Lieberman, D.E., 2004. Endurance running and the evolution of *Homo*. Nature 432, 345–352.
Brown, P., Sutikna, T., Morwood, M.J., Soejono, R.P., Jatmiko, Saptomo, E.W., Due, R.A., 2004. A new small-bodied hominin from the Late Pleistocene of Flores, Indonesia. Nature 431, 1055–1061.
Bräuer, G., 1988. Osteometrie. In: Knussmann, R. (Ed.), Anthropologie. Handbuch der vergleichenden Biologie des Menschen. Gustav Fischer, Stuttgart, pp. 160–232.
Carretero, J.M., Lorenzo, C., Arsuaga, J.L., 1999. Axial and appendicular skeleton of *Homo antecessor*. J. Hum. Evol. 37, 459–499.
Cartmill, M., Milton, K., 1977. The lorisiform wrist joint and the evolution of "brachiating" adaptations in Hominoidea. Am. J. Phys. Anthropol. 47, 249–272.
Digiovanni, B.F., Scoles, P.V., Latimer, B.M., 1989. Thoracic vertebral bodies in Scheuermann's kyphosis: an anatomic study. Spine 14, 712–716.
Dirks, P.H.G.M., Berger, L.R., Roberts, E.M., Kramers, J.D., Hawks, J.H., Randolph-Quinney, P.S., Elliott, M., Musiba, C.M., Churchill, S.E., de Ruiter, D.J., Schmid, P., Backwell, L.R., Belyanin, G.A., Boshoff, P., Hunter, K.L., Feuerriegel, E.M., Gurtov, A., Harrison, J.G., Hunter, R., Kruger, A., Morris, H., Makhubela, T.V., Peixotto, B., Tucker, S., 2015. Geological and taphonomic context for the new hominin species Homo naledi from the Dinaledi Chamber, South Africa. eLife 4, e09561.
Domínguez-Rodrigo, M., Pickering, T.R., Baquedano, E., Mabulla, A., Mark, D.F., Musiba, C., Bunn, H.T., Uribelarrea, D., Smith, V., Diez-Martin, F., Pérez-González, A., Sánchez, P., Santonja, M., Barboni, D., Gidna, A., Ashley, G., Yravedra, J., Heaton, J.L., Arriaza, M.C., 2013. First partial skeleton of a 1.34-million-year-old *Paranthropus boisei* from Bed II, Olduvai Gorge, Tanzania. PLoS One 8, e80347.
Ferreira, M.T., Vicente, R., Navega, D., Gonçalves, D., Curate, F., Cunha, E., 2014. A new forensic collection housed at the University of Coimbra, Portugal: The 21st century identified skeletal collection. For. Sci. Int. 245, 202-e1.
Feuerriegel, E.M., Green, D.J., Walker, C.S., Schmid, P., Hawks, J., Berger, L.R., Churchill, S.E., 2017. The upper limb of *Homo naledi*. J. Hum. Evol. 104, 155–173.
Franciscus, R.G., Churchill, S.E., 2002. The costal skeleton of Shanidar 3 and a reappraisal of Neandertal thoracic morphology. J. Hum. Evol. 42, 303–356.
García-Martínez, D., 2013. 3D geometric morphometrics of the rib cage of the *Homo ergaster* KNM-WT 15000 and their possible evolutionary implications: an application of sliding semi-landmarks on virtual anthropology to the morphology of the ribs. Master's Thesis, Universidad Autónoma de Madrid-Museo Nacional de Ciencias Naturales CSIC.
García-Martínez, D., Bastir, M., Recheis, W., Barash, A., 2013. Two different barrels for two different primates: 3D geometric morphometrics of sliding semi-landmarks of the Hominoidea superfamily thorax. Proceedings of Sociedad Española de Antropología Física, Bilbao (Spain), p. 39.
García-Martínez, D., Barash, A., Recheis, W., Utrilla, C., Torres Sánchez, I., García Río, F., Bastir, M., 2014. On the chest size of Kebara 2. J. Hum. Evol. 70, 69–72.
García-Martínez, D., Spoor, F., Bastir, M., 2016a. 3D assessment of rib curvatures in KNM-WT 15000. PaleoAnthropology 2016, A12. http://www.paleoanthro.org/media/journal/content/PAS2016A.pdf.
García-Martínez, D., Recheis, W., Bastir, M., 2016b. Ontogeny of 3D rib curvature and its importance for the understanding of human thorax development. Am. J. Phys. Anthropol. 159, 423–431.
Gómez-Olivencia, A., 2013a. Back to the old man's back: reassessment of the anatomical determination of the vertebrae of the Neandertal individual of La Chapelle-aux-Saints. Ann. Paléontol. 99, 43–55.
Gómez-Olivencia, A., 2013b. The presacral spine of the La Ferassie 1 Neandertal: a revised inventory. Bull. Mém. Soc. Anthropol. Paris 25, 19–38.
Gómez-Olivencia, A., 2015. The costal skeleton of the Neandertal individual of La Chapelle-aux-Saints 1. Ann. Paléontol. 101, 127–141.
Gómez-Olivencia, A., Carretero, J.M., Arsuaga, J.L., Rodríguez-García, L., García-González, R., Martínez, I., 2007. Metric and morphological study of the upper cervical spine from the Sima de los Huesos site (Sierra de Atapuerca, Burgos, Spain). J. Hum. Evol. 53, 6–25.
Gómez-Olivencia, A., Eaves-Johnson, K.L., Franciscus, R.G., Carretero, J.M., Arsuaga, J.L., 2009. Kebara 2: new insights regarding the most complete Neandertal thorax. J. Hum. Evol. 57, 75–90.
Gómez-Olivencia, A., Carretero, J.M., Lorenzo, C., Arsuaga, J.L., Bermúdez de Castro, J., Carbonell, E., 2010. The costal skeleton of *Homo antecessor*: preliminary results. J. Hum. Evol. 59, 620–640.
Gómez-Olivencia, A., Been, E., Arsuaga, J.L., Stock, J.T., 2013a. The Neandertal vertebral column 1: The cervical spine. J. Hum. Evol. 64, 608–630.
Gómez-Olivencia, A., Couture-Veschambre, C., Madelaine, S., Maureille, B., 2013b. The vertebral column of the Regourdou 1 Neandertal. J. Hum. Evol. 64, 582–607.
Gorjanović-Kramberger, K., 1906. Der Diluviale Mensch von Krapina in Kroatien: Ein Beitrag zur Paläoanthropologie. C. W. Kreidel's Verlag, Wiesbaden.
Grabowski, M., Hatala, K.G., Jungers, W.L., Richmond, B.G., 2015. Body mass estimates of hominin fossils and the evolution of human body size. J. Hum. Evol. 85, 75–93.
Graves, R.R., Lupo, A.C., McCarthy, R.C., Wescott, D.J., Cunningham, D.L., 2010. Just how strapping was KNM-WT 15000? J. Hum. Evol. 59, 542–554.

Haeusler, M., Martelli, S.A., Boeni, T., 2002. Vertebrae numbers of the early hominid lumbar spine. J. Hum. Evol. 43, 621–643.
Haeusler, M., Schiess, R., Boeni, T., 2011. New vertebral and rib material point to modern bauplan of the Nariokotome *Homo erectus* skeleton. J. Hum. Evol. 61, 575–582.
Haeusler, M., Fremondiere, P., Fornai, C., Frater, N., Mathews, S., Thollon, L., Marchal, F., 2016. Virtual reconstruction of the MH2 pelvis (*Australopithecus sediba*) and obstetrical implications. Am. J. Phys. Anthropol. 159 (S62), 165.
Haile-Selassie, Y., Latimer, B., Alene, M., Deino, A.L., Gibert, L., Melillo, S.M., Saylor, B.Z., Scott, G.R., Lovejoy, C.O., 2010. An early *Australopithecus afarensis* postcranium from Woranso-Mille, Ethiopia. Proc. Natl. Acad. Sci. USA 107, 12121–12126.
Harcourt-Smith, W.E.H., Throckmorton, Z., Congdon, K.A., Zipfel, B., Deane, A.S., Drapeau, M.S.M., Churchill, S.E., Berger, L.R., DeSilva, J.M., 2015. The foot of *Homo naledi*. Nat. Commun. 6, 8432.
Holliday, T.W., 2011. Body size, body shape, and the circumscription of the genus *Homo*. Curr. Anthropol. 53, S330–S345.
Jellema, L.M., Latimer, B., Walker, A., 1993. The rib cage. In: Walker, A., Leakey, R. (Eds.), The Nariokotome *Homo erectus* Skeleton. Harvard University Press, Cambridge, pp. 294–325.
Johanson, D.C., Lovejoy, C.O., Kimbel, W.H., White, T.D., Ward, S.C., Bush, M.E., Latimer, B.M., Coppens, Y., 1982. Morphology of the Pliocene partial hominid skeleton (A.L. 288-1) from the Hadar formation, Ethiopia. Am. J. Phys. Anthropol. 57, 403–451.
Johanson, D.C., Masao, F.T., Eck, G.G., White, T.D., Walter, R.C., Kimbel, W.H., Asfaw, B., Manega, P., Ndessokia, P., Suwa, G., 1987. New partial skeleton of *Homo habilis* from Olduvai Gorge, Tanzania. Nature 327, 205–209.
Jungers, W.L., 1984. Scaling of the hominoid locomotor skeleton with special reference to lesser apes. In: Preuschoft, H., Chivers, D.J., Brockelman, W.Y. (Eds.), The Lesser Apes: Evolutionary and Behavioral Biology. Edinburgh University Press, Edinburgh, pp. 146–169.
Kibii, J.M., Churchill, S.E., Schmid, P., Carlson, K.J., Reed, N.D., de Ruiter, D.J., Berger, L.R., 2011. A partial pelvis of *Australopithecus sediba*. Science 333, 1407–1411.
Kivell, T.L., Deane, A.S., Tocheri, M.W., Orr, C.M., Schmid, P., Hawks, J., Berger, L.R., Churchill, S.E., 2015. The hand of *Homo naledi*. Nat. Commun. 6, 8431.
Latimer, B., Lovejoy, C.O., Haile-Selassie, Y., 2016. The thoracic cage of KSD-VP-1/1. In: Haile-Selassie, Y., Su, D.F. (Eds.), The Postcranial Anatomy of *Australopithecus afarensis*. Springer, Dordrecht, Netherlands, pp. 143–153.
Leakey, R., Walker, A., Ward, C.V., Grausz, H.M., 1989. A partial skeleton of a gracile hominid from the Upper Burgi Member of the Koobi Fora Formation, East Lake Turkana, Kenya. In: Giacobini, G. (Ed.), Hominidae: Proceedings of the 2nd International Congress of Human Paleontology. Jaca Book, Milan, pp. 167–173.
Leakey, R.E.F., Walker, A.C., 1985. Further hominids from the Plio-Pleistocene of Koobi Fora, Kenya. Am. J. Phys. Anthropol. 67, 135–163.
Lordkipanidze, D., Jashashvili, T., Vekua, A., Ponce de León, M.S., Zollikofer, C.P.E., Rightmire, G.P., Pontzer, H., Ferring, R., Oms, P., Tappen, M., Bukhsianidze, M., Agusti, J., Kahlke, R., Kiladze, G., Martínez-Navarro, B., Mouskhelishvili, A., Nioradze, M., Rook, L., 2007. Postcranial evidence from early *Homo* from Dmanisi, Georgia. Nature 449, 305–310.
Lovejoy, C.O., 2005. The natural history of human gait and posture. Part 1. Spine and pelvis. Gait Posture 21, 95–112.
Lovejoy, C.O., McCollum, M.A., 2010. Spinopelvic pathways to bipedality: why no hominids ever relied on a bent-hip—bent-knee gait. Phil. Trans. R. Soc. B 365, 3289–3299.
Lovejoy, C.O., Johanson, D.C., Coppens, Y., 1982. Elements of the axial skeleton recovered from the Hadar Formation: 1974–1977 collections. Am. J. Phys. Anthropol. 57, 631–635.
Martiniano, R., Coelho, C., Ferreira, M.T., Neves, M.J., Pinhasi, R., Bradley, D.G., 2014. Genetic evidence of African slavery at the beginning of the trans-Atlantic slave trade. Sci. Rep. 4, 5994.
McCown, T.D., Keith, A., 1939. The Stone Age of Mount Carmel II. Clarendon Press, Oxford.
Meyer, M.R., 2005. Functional biology of the *Homo erectus* axial skeleton from Dmanisi, Georgia. PhD Dissertation, University of Pennsylvania.
Meyer, M.R., 2016. The cervical vertebrae of KSD-VP-1/1. In: Haile-Selassie, Y., Su, D.F. (Eds.), The Postcranial Anatomy of *Australopithecus afarensis*. Springer, Dordrecht, Netherlands, pp. 63–111.
Meyer, M.R., Haeusler, M., 2015. Spinal cord evolution in early *Homo*. J. Hum. Evol. 88, 43–53.
Meyer, M.R., Williams, S.A., Smith, M.P., Sawyer, G.J., 2015. Lucy's back: reassessment of fossils associated with the A.L. 288-1 vertebral column. J. Hum. Evol. 85, 174–180.
Mitteroecker, P., Gunz, P., 2009. Advances in geometric morphometrics. Evol. Biol. 36, 235–247.
O'Higgins, P., 2000. The study of morphological variation in the hominid fossil record: biology, landmarks and geometry. J. Anat. 197, 103–120.
O'Higgins, P., Jones, N., 1999. Morphologika. Tools for shape analysis. University College London, London, United Kingdom.
Ohman, J.C., 1986. The first rib of hominoids. Am. J. Phys. Anthropol. 70, 209–229.
Preuschoft, H., 2004. Mechanisms for the acquisition of habitual bipedality: are there biomechanical reasons for the acquisition of upright bipedal posture? J. Anat. 204, 363–384.
Robinson, J., 1972. Early hominid posture and locomotion. University of Chicago Press, Chicago.
Ruff, C., 2010. Body size and body shape in early hominins—implications of the Gona Pelvis. J. Hum. Evol. 58, 166–178.
Sanders, W.J., 1998. Comparative morphometric study of the australopithecine vertebral series Stw-H8.H41. J. Hum. Evol. 34, 249–302.
Sanders, W.J., Bodenbender, B.E., 1994. Morphometric analysis of lumbar vertebra UMP 67-28: implications for spinal function and phylogeny of the Miocene Moroto hominoid. J. Hum. Evol. 26, 203–237.
Sawyer, G.J., Maley, B., 2005. Neanderthal reconstructed. Anat. Rec. 283B, 23–31.
Schmid, P., 1983. Eine Rekonstruktion des Skelettes von A.L. 288-1 (Hadar) und deren Konsequenzen. Fol. Primatol. 40, 283–306.
Schmid, P., Churchill, S.E., Nalla, S., Weissen, E., Carlson, K.J., de Ruiter, D.J., Berger, L.R., 2013. Mosaic morphology in the thorax of *Australopithecus sediba*. Science 340, 1234598.
Schroeder, L., Scott, J.E., Garvin, H.M., Laird, M.F., Dembo, M., Radovčić, D., Berger, L.R., de Ruiter, D.J., Ackermann, R.R., 2017. Skull diversity in the *Homo* lineage and the relative position of *Homo naledi*. J. Hum. Evol. 104, 124–135.
Schultz, A.H., 1961. Vertebral column and thorax. Primatologia 4, 1–66.
Simpson, S.W., Quade, J., Levin, N.E., Butler, R., Dupont-Nivet, G., Everett, M., Semaw, S., 2008. A female *Homo erectus* pelvis from Gona, Ethiopia. Science 322, 1089–1092.
Simpson, S.W., Spurlock, L.B., Lovejoy, C.O., Latimer, B., 2010. A new reconstruction of the KNM-WT 15000 juvenile male pelvis. Am. J. Phys. Anthropol. 141, 217.
Simpson, S.W., Quade, J., Levin, N.E., Semaw, S., 2014. The female *Homo* pelvis from Gona: response to Ruff (2010). J. Hum. Evol. 68, 32–35.
Tawane, G., García-Martínez, D., Eyre, J., Bastir, M., Berger, L., Nalla, S., Williams, S.A., 2016. A hominin first rib discovered at the Sterkfontein Caves, South Africa. S. Af. J. Sci. 112, 1–7.
Thompson, N.E., Demes, B., O'Neill, M.C., Holowka, N.B., Larson, S.G., 2015. Surprising trunk rotational capabilities in chimpanzees and implications for bipedal walking proficiency in early hominins. Nat. Commun. 6, 8416.
Toussaint, M., Macho, G.A., Tobias, P.V., Partridge, T.C., Hughes, A.R., 2003. The third partial skeleton of a late Pliocene hominin (Stw 431) from Sterkfontein, South Africa. S. Af. J. Sci. 99, 215–223.
Trinkaus, E., 1983. The Shanidar Neandertals. Academic Press, New York.
VanSickle, C., Williams, S.A., Cofran, Z.D., Garcia-Martinez, D., Churchill, S.E., Berger, L.R., Hawks, J. Pelvic remains of *Homo naledi*, from Dinaledi, South Africa. J. Hum. Evol., Submitted for publication.
Ward, C.V., 1993. Torso morphology and locomotion in *Proconsul nyanzae*. Am. J. Phys. Anthropol. 92, 291–328.
Ward, C.V., Kimbel, W.H., Harmon, E.H., Johanson, D.C., 2012. New postcranial fossils of *Australopithecus afarensis* from Hadar, Ethiopia. J. Hum. Evol. 63, 1–51.
Wasterlain, S.N., Neves, M.J., Ferreira, M.T., 2016. Dental Modifications in a Skeletal Sample of Enslaved Africans Found at Lagos (Portugal). Int. J. Osteoarchaeol. 26, 621–632.
Williams, S.A., 2011. Evolution of the Hominoid Vertebral Column. Ph.D. Dissertation, University of Illinois, Urbana-Champaign.
Williams, S.A., 2012a. Modern or distinct axial bauplan in early hominins? Comments on Haeusler et al. (2011). J. Hum. Evol. 63, 552–556.
Williams, S.A., 2012b. Placement of the diaphragmatic vertebra in catarrhines: implications for the evolution of dorsostability in hominoids and bipedalism in hominins. Am. J. Phys. Anthropol. 148, 111–122.
Williams, S.A., Russo, G.A., 2015. Evolution of the hominoid vertebral column: the long and the short of it. Evol. Anthropol. 24, 15–32.
Williams, S.A., Ostrofsky, K.R., Frater, N., Churchill, S.E., Schmid, P., Berger, L.R., 2013. The vertebral column of *Australopithecus sediba*. Science 340, 1232996.
Williams, S.A., Middleton, E.R., Villamil, C.I., Shattuck, M.R., 2016. Vertebral numbers and human evolution. Yearb. Phys. Anthropol. 159, S19–S36.

Supplementary Online Material

Scott A. Williams, Daniel García-Martínez, Markus Bastir, Marc R. Meyer, Shahed Nalla, John Hawks, Peter Schmid, Steven E. Churchill, Lee R. Berger.

1 Figure: S1

2 Tables: S1–S2

Figure S1. U.W. 101-524 in situ in the Dinaledi Chamber. It was found alongside the 10th and 11th thoracic vertebrae (U.W. 101-855 and -1733, respectively) in near articulation.

Table S1. Complete inventory of Dinaledi hominin postcranial axial material.

Diagnosable vertebrae

U.W. 101-651	Atlas (C1) neural arch fragment (right)
U.W. 101-331	Atlas (C1) neural arch fragment (midline)
U.W. 101-1279 & U.W. 101-489	Axis (C2) vertebral body
U.W. 101-1692	Axis (C2) vertebral body fragment—immature odontoid process
U.W. 101-732	Axis (C2) neural arch fragment (indet. side)
U.W. 101-174	Cervical neural arch fragment (midline, mostly left)
U.W. 101-1673	Cervical neural arch fragment—immature articular facets (right)
U.W. 101-081	Lower cervical/upper thoracic spinous process
U.W. 101-1599	Lower cervical or upper thoracic neural arch fragment (left)
U.W. 101-581	Upper thoracic isolated spinous process
U.W. 101-1614	Upper thoracic neural arch (midline; mostly left)
U.W. 101-581	Upper thoracic isolated spinous process
U.W. 101-1493	Upper thoracic neural arch fragment—immature
U.W. 101-663	Middle thoracic neural arch (midline; mostly right)
U.W. 101-015	Middle thoracic neural arch (midline; mostly left)
U.W. 101-575A	Middle thoracic neural arch (midline; mostly left)
U.W. 101-1669	Middle thoracic isolated spinous process
U.W. 101-515	Middle to lower thoracic vertebral body
U.W. 101-855	Tenth thoracic vertebra (T10)
U.W. 101-1733	Eleventh thoracic vertebra (T11)
U.W. 101-465	Lower thoracic vertebral body
U.W. 101-1124	Lower thoracic isolated spinous process
U.W. 101-1302	Thoracic neural arch fragment (left)
U.W. 101-656	Thoracic isolated superior articular facet
U.W. 101-439	Thoracic neural arch fragment—immature

U.W. 101-1054	Lower thoracic/upper lumbar isolated spinous process
U.W. 101-478	Lower lumbar vertebra
U.W. 101-984	Lumbar vertebral body
U.W. 101-1338	Lumbar vertebral body fragment
U.W. 101-1337	Lumbar neural arch (midline, mostly right)
U.W. 101-765	Lumbar isolated lumbar transverse process (left)

Indeterminate vertebrae

U.W. 101-872	Vertebral isolated superior articular facet
U.W. 101-1601	Vertebral isolated articular facet
U.W. 101-1711	Vertebral body fragment
U.W. 101-362	Neural arch fragment
U.W. 101-615	Neural arch fragment
U.W. 101-619	Neural arch fragment
U.W. 101-673	Neural arch fragment
U.W. 101-685	Neural arch fragment
U.W. 101-1307	Neural arch fragment
U.W. 101-1382	Neural arch fragments
U.W. 101-1383	Neural arch fragments
U.W. 101-994	Left superior articular facet and lamina and spinous process
U.W. 101-847	Possible vertebral body fragment
U.W. 101-407	Possible neural arch fragment
U.W. 101-681	Possible neural arch fragment
U.W. 101-1144	Possible neural arch fragment
U.W. 101-1604	Possible neural arch fragment
U.W. 101-323	Possible neural arch fragments
U.W. 101-1615	Possible neural arch fragments
U.W. 101-025	Possible vertebra fragment
U.W. 101-592	Possible vertebra fragment

U.W. 101-620	Possible vertebra fragment
U.W. 101-1621	Possible vertebra fragment
U.W. 101-1699	Possible vertebra fragment
U.W. 101-1003	Possible vertebra fragment
U.W. 101-1079	Possible vertebra fragments
U.W. 101-1397	Possible vertebra fragments

Diagnosable ribs

U.W. 101-083	Left 1st rib
U.W. 101-621	Left 1st rib
U.W. 101-385	Right 2nd rib
U.W.101-1291	2nd rib shaft fragment (left)
U.W.101-1009/979	3rd-6th rib shaft fragment (right)
U.W.101-351/464/953	6th-9th rib shaft fragment with posterior angle (right)
U.W. 101-524	Left 11th rib
U.W. 101-1119	Left 12th rib

Additional rib fragments

U.W.101-1280	3rd-4th rib partial shaft with posterior angle (left)
U.W.101-1090	3rd-4th rib shaft fragment with partial neck (left)
U.W.101-1596	3rd-4th rib shaft fragment (right)
U.W.101-1125	4th-6th rib shaft fragment (right)
U.W.101-840	4th-6th rib shaft fragment with posterior angle (left)
U.W.101-748	4th-6th rib shaft with posterior angle and costal groove (left)
U.W.101-839	4th-6th rib shaft fragment
U.W.101-1670	4th-6th rib shaft fragment with costal groove (left)
U.W.101-657	6th-9th rib shaft fragment (right)
U.W.101-079	6th-9th rib shaft fragment (right)
U.W.101-479	6th-9th rib shaft fragment (right)
U.W.101-456	6th-9th rib shaft fragment (left)

U.W.101-951	6^{th}-9^{th} rib shaft fragment with costal groove (right)
U.W.101-514	6^{th}-9^{th} rib shaft fragment with costal groove (right)
U.W.101-797	6^{th}-9^{th} rib shaft fragment with costal groove (left)
U.W.101-1360	6^{th}-9^{th} rib shaft fragment
U.W.101-745	6^{th}-9^{th} rib shaft fragment with costal groove (right)
U.W.101-995	6^{th}-9^{th} rib shaft fragment with costal groove (left)
U.W.101-1569	6^{th}-9^{th} rib shaft fragment with costal groove (left)
U.W.101-1344	6^{th}-9^{th} rib shaft fragment with costal groove (left)
U.W.-101-927	6^{th}-9^{th} rib shaft fragment with costal groove (left)
U.W.101-1080	7^{th} rib shaft fragment with costal groove (left)
U.W.101-1109	7^{th}-8^{th} rib shaft fragment with costal groove (right)
U.W.101-509	7^{th}-8^{th} rib shaft fragment with costal groove (left)
U.W.101-978	8^{th}-10^{th} rib shaft fragment with costal groove (right)
U.W.101-669	8^{th}-10^{th} rib shaft fragment with costal groove (right)
U.W.101-024	8^{th}-10^{th} rib fragment (right)
U.W.101-764	10^{th}-12^{th} rib head (left)
U.W.101-1613	10^{th} rib shaft fragment with costal groove (left)
U.W.101-629	10^{th}-12^{th} rib shaft fragment (right)
U.W.101-1394	10^{th}-12^{th} rib shaft fragment (right)
U.W.101-578	10^{th}-12^{th} rib shaft fragment with costal groove (right)
U.W.101-431	10^{th}-12^{th} rib shaft fragment
U.W.101-1059	10^{th}-12^{th} rib shaft fragment (left)
U.W.101-392 (left)	11^{th}-12^{th} rib shaft with posterior angle and costal groove
U.W.-101-1668	Unknown rib shaft fragment with costal groove (right)
U.W.101-919	Unknown rib fragment with costal groove
U.W.101-034	Unknown rib shaft fragment (left)

U.W.101-158	Unknown rib shaft fragment
U.W.101-1411	Unknown rib shaft fragment
U.W.101-535	Unknown rib fragment
U.W.101-1472	Unknown rib fragment
U.W.101-437	Unknown rib fragment
U.W.101-273	Unknown rib fragment
U.W.101-1586	Unknown rib fragment
U.W.101-1502	Unknown rib fragment

Table S2. Minimum number of elements (MNE) and minimum number of individuals (MNI) from diagnostic material.*

	MNE		MNI	
	Adult	Immat.	Adult	Immat.
C1	2		2	
C2	1	1	1	1
C[a]	1	1	1	1
C/T[b]	1		1	
T[a]	9	2	1	1
T10	1		1	
T11	1		1	
T/L[c]	1		1	
L[a]	3		1	
Rib1	2		2	
Rib2	2		1	
Ribm[d]	2		1	
Rib11	1		1	
Rib12	1		1	

*In addition to two adult left ribs, two immature individuals present different ages; thus, there are a minimum of four individuals represented in the Dinaledi vertebral and costal sample.
[a]General cervical (C), thoracic (T), or lumbar (L) vertebra
[b]Lower thoracic or upper thoracic vertebra
[c]Lower thoracic or upper lumbar vertebra
[d]Middle (3rd-9th) rib

Garcia-Martinez et al.

3D Assessment of Rib Curvatures in KNM-WT 15000

KNM-WT 15000 (Walker and Leakey 1993) is a juvenile specimen of African *H. erectus* from West Turkana (Kenya) dated around 1.47 Ma (McDougall et al. 2012). It preserves one of the most complete ribcages in the hominin fossil record and is crucial for understanding the evolution of the hominin thorax and body shape. KNM-WT 15000 has been described as the earliest evidence for a tall, narrow modern human body shape (Jellema et al. 1993; Ruff 1991). However, based on its pelvis and long bone morphology, a heavy and wide body configuration, similar to Lower and Midpleistocene *Homo*, has been proposed (Arsuaga et al. 1999; Gómez-Olivencia et al. 2009, 2010; Graves et al. 2010; Holliday 2012; Ruff 2010). Here we re-assess the evidence provided by the ribs of KNM-WT 15000 using 3D geometric morphometrics. Using 17 (semi)landmarks, we quantified the shape of eight ribs of KNM-WT 15000 (CT-based 3D reconstructions of AG, AY&AZ, AQ, CB, AP, AL, AM, AO) and of two ribs of Mid-Pleistocene hominins from Gran Dolina TD-6 (high quality casts of ATD6-39, ATD6-89+206). We used principal components analyses to compare these fossils with mean rib shapes of adults and sub-adults of *P. troglodytes* and modern humans from Europe and Africa (N=408). A plot of PC2 against PC1 shows variation related to serial rib position and ontogeny. PC3 reflects species-related variation with chimpanzees showing negative scores and modern humans more positive scores. Fossil *Homo* ribs fall close to modern humans at the upper-central thorax level but strongly differ from humans and chimpanzees at the lower thorax with highly positive scores representing greater axial rib curvature. Although thorax shape results from rib and vertebral morphology (Bastir et al. 2014), greater axial rib curvatures are compatible with increased lower thorax width. Because these features are similar in Lower and Mid-Pleistocene *Homo*, a wider lower thorax could be the primitive condition in *Homo*.

Dentro del **objetivo específico 5c** "**Contribuciones al conocimiento de la caja torácica Neandertal y sus implicaciones funcionales y evolutivas**" se han publicado 2 artículos y otros 2 se encuentran actualmente aceptados:

García-Martínez, D., Barash, A., Recheis, W., Utrilla, C., Torres-Sánchez, I., García-Rio, F., 2014. On the chest size of Kebara 2. Journal of Human Evolution 70, 69-72.

DOI: 10.1016/j.jhevol.2014.02.003

Bastir, M., **García-Martínez, D.**, Estalrrich, A., García-Tabernero, A., Huguet, R., Ríos, L., Barash, A., Recheis, W., de la Rasilla, M., Rosas, A., 2015. The relevance of the first ribs of the El Sidrón site (Asturias, Spain) for the understanding of the Neanderthal thorax. Journal of Human Evolution 80, 64-73.

DOI: 10.1016/j.jhevol.2014.10.008

García-Martínez, D., Bastir, M., Huguet, R., Estalrrich, A., García-Tabernero, A., Ríos, L., Cunha, E., de la Rasilla, M., Rosas, A., en prensa. The costal remains of the El Sidrón Neandertal site (Asturias, northern Spain) and its importance for understanding the Neandertal thorax morphology. Journal of Human Evolution.

Bastir, M., **García-Martínez, D.**, Ríos, L., Higuero, A., Barash, A., Martelli, S., García-Tabernero, A., Estalrrich, A., Huguet, R., de la Rasilla, M., Rosas, A., aceptado. 3D morphometrics of thoracic vertebrae in Neandertals: fossil evidence from El Sidrón (Asturias, Northern Spain). Journal of Human Evolution.

Journal of Human Evolution 70 (2014) 69–72

Contents lists available at ScienceDirect

Journal of Human Evolution

journal homepage: www.elsevier.com/locate/jhevol

News and views

On the chest size of Kebara 2

Daniel García-Martínez [a], Alon Barash [b], Wolfgang Recheis [c], Cristina Utrilla [d], Isabel Torres Sánchez [d], Francisco García Río [d], Markus Bastir [a,*]

[a] Paleoanthropology Group, Museo Nacional de Ciencias Naturales (MNCN-CSIC), J.G. Abascal 6, 28006 Madrid, Spain
[b] Faculty of Medicine, Galilee Bar Ilan University, Zefat, Israel
[c] Department of Radiology, Medizinische Universität Innsbruck, Austria
[d] Hospital Universitario La Paz, Biomedical Research Institute (IdiPAZ), Madrid, Spain

ARTICLE INFO

Article history:
Received 10 October 2013
Accepted 6 February 2014
Available online 6 March 2014

Keywords:
Skeletal thorax
Rib
Morphometrics
Respiratory system
Evolution
Paleophysiology

Introduction

Chest size is important for reconstructing Neandertal paleobiology. The large size of the Neandertal skeletal thorax has been interpreted in relation to cold adaptation, increased body mass, specific body shape and increased activity levels (Franciscus and Churchill, 2002; Churchill, 2006; Gómez-Olivencia et al., 2009). Large Neandertal chests should also be expected because chest and lung sizes are correlated developmentally (Thurlbeck, 1982; Bastir et al., 2013a), because lung size scales isometrically with body mass across mammals (Stahl, 1967), and because body mass was larger in Neandertals than in modern humans (Ruff et al., 1997; Froehle and Churchill, 2009).

The notion of large chests has recently been reinforced by Gómez-Olivencia et al. (2009), who measured the ribs of the Kebara 2 Neandertal male using arc lengths. Their study suggested that the upper ribs of Kebara 2 are within the range of modern humans, and middle (ribs 4, 5, 7) and lower (ribs 8, 10) thoracic ribs exceed the range of modern human variation. Consequently, this predicts that total thorax size (the sum of the sizes of each of the ribs) should be larger in Kebara than in modern humans.

* Corresponding author.
E-mail address: mbastir@mncn.csic.es (M. Bastir).

However, Gómez-Olivencia et al. (2009) also identified a problem in the original reconstruction of the 6th and 7th ribs of Kebara due to a misidentification of fragments fitted together by Arensburg (1991), who stated that the ribs of "Kebara man are quite similar in metric and morphological respects to those of ribs in present human populations" (Arensburg, 1991: 142). Nevertheless, misidentifications such as those identified by Gómez Olivencia et al. (2009) could affect size assessments.

Bastir et al. (2012) measured the reconstruction of the Kebara rib cage (Sawyer and Maley, 2005) using 3D geometric morphometrics and no evidence for such enlarged chest size was found, supporting Arensburg's (1991) opinion. Thus, the size of one of the best preserved Neandertal male thoracic skeletons is currently unclear.

Recent advances in virtual morphological methods and geometric morphometrics can be used to clarify this situation. First, standard measurements of rib morphology, such as chords and arcs can be improved using 3D landmarks and geometric morphometrics because 3D coordinates of landmarks at rib heads, sternal extremities and rib-shafts quantify all features of rib morphology together (García-Martínez et al., 2012, 2013; Bastir et al., 2013b). This method provides a size measurement (centroid size, Zelditch et al., 2004) along the extent of the entire rib from the head to its sternal extremities. Second, once scanned by computed tomography (CT) or surface scanners, virtual morphological reconstructions can be carried out and measured on the computer screen, without modifying the original precious fossils or historical reconstructions.

The aim of this study was to carry out a new virtual reconstruction of lower thoracic elements of Kebara 2 and to compare the new reconstruction with the original (Arensburg, 1991), testing several hypotheses on differences in rib and chest size between the Kebara 2 Neandertal and modern humans in light of Neandertal paleobiology and paleophysiology.

Material and methods

We measured 20 landmarks and semilandmarks on the head, sternal extremities and outer curvature of the rib-shaft of the first ten ribs (Bastir et al., 2013a) on 3D reconstructions of CT-scanned original fossils of Kebara 2 using the most complete of right or

left ribs (rib1 left (l), rib2 right (r), rib3 l, rib4 r, rib5 r, rib6 l, rib7 l, rib8 l, rib9 l, rib10 r).

Isolated 1st to 10th ribs ($N = 200$) of the left hemithorax were also measured on 3D reconstructions obtained from CT-scans of 20 skeletally normal European adult males from the University Hospital La Paz, Madrid (Spain) and the Medical University of Innsbruck (Austria). The CT-data from Austria ($N = 5$) were obtained from subjects that were scanned previously for medical reasons unrelated to this study, but who showed no statistically significant alteration when compared with known healthy adults (Bastir et al., 2013a). The CT-data from the University Hospital La Paz in Madrid (IdiPAZ) were obtained from 15 healthy volunteers serving as the control group of a research project separate from the present study. Consent was given to use these CT-data for investigation, and data were anonymized in order to comply with the requisites of local ethics committees and the Helsinki declaration (Goodyear et al., 2007).

Following the standard geometric morphometrics protocol (Mitteroecker and Gunz, 2009; Bastir et al., 2013a), landmarks of isolated ribs were registered by Procrustes superimposition and semilandmarks were slid iteratively along their curves so as to minimize the bending energy between each specimen and the Procrustes average. Missing data were estimated conservatively using the densely sampled rib semilandmarks and thin-plate spline interpolation of the modern human mean onto the corresponding Neandertal structure (Gunz et al., 2009; Bastir et al., 2011). This was necessary in some cases because only a few heads of the Kebara ribs were complete. Centroid size was calculated from these landmark configurations.

Virtual morphological methods were used to reconstruct the 7th rib following the revision by Gómez-Olivencia et al. (2009). Accordingly, we removed part of the rib-shaft fragment of rib 6 and added it to the rib-head fragment of rib 7 (García-Martínez, 2014). Centroid size was also calculated for the new reconstruction and compared with the original and reference sample.

Average, individual, and cumulative rib sizes were calculated for the full thorax (ribs 1–10), for the upper thorax (ribs 1–5) and the lower thorax (ribs 6–10) (Bastir et al., 2013a). To contextualize these size assessments further with overall body size, thorax size was standardized as the percentage of stature that was available for 15 modern humans (mean = 173.50 cm; standard deviation = 4.66) and for Kebara 2 (166 cm; Churchill, 2006).

We used a Kolmogorov–Smirnov (K–S) test to address normality and both Mann–Whitney and "one sample *t*-tests" (Sokal and Rohlf, 1998: 227–229) for comparisons of the reference population with the original and new data for the Kebara 2 ribs, testing the following null hypotheses:

H1) Average sizes of the 1st to 10th ribs of the Kebara Neandertal are not larger than the corresponding average of modern humans.
H2) Average sizes of each of the 1st to 10th ribs of modern humans are not smaller than those of Kebara.
H3) Average cumulative sizes of the upper (ribs 1–5) and lower thorax (ribs 6–10) are not larger in Kebara than in modern humans.
H4) Total thorax size of Kebara (sum of all rib sizes) is not larger than in modern humans.

Results

Fig. 1 shows the virtual reconstruction of the fragments of the 6th and 7th rib. (H1) The sizes of the 210 ribs were not normally distributed (K–S; $p = 0.000$). A Mann–Whitney test showed that the average rib size of modern humans (mean = 342.70, standard deviation = 97.95) was not statistically different ($p = 0.4$) from the Kebara rib size mean (original = 351.29, new = 443.67). (H2) Individual rib sizes were normally distributed and the results of the mean comparisons are listed in Table 1. Ribs 1 and 2 are significantly smaller in Kebara, and rib 3 of Kebara was smaller at $p < 0.06$. However, while in the original reconstruction ribs 5 to 7 in Kebara were not larger, in the new reconstruction rib 7 is larger. The ribs of the lower thorax (ribs 8–10) are all larger in Kebara. (H3) Table 2 shows that the upper thorax of Kebara is small, close to the lower limit of the 95% confidence interval, but not statistically smaller than modern humans. The lower thorax is statistically larger in both reconstructions (Table 2). (H4) The full thorax in the new reconstruction (3512.88 mm) is significantly larger than in modern humans (3427.87 mm). The original (3436.68 mm) does not differ from the modern human mean. Relative to stature, the lower and total thorax sizes are larger in Kebara, but not the upper thorax.

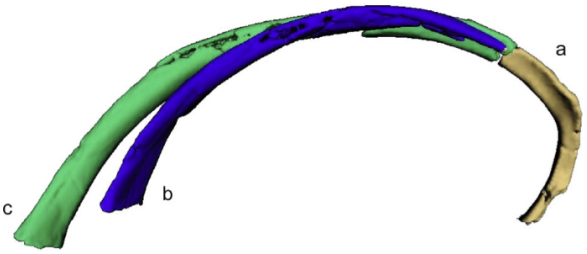

Figure 1. Virtual models of ribs 6 and 7 in the original and new reconstructions. Vertebral fragment (a) was fitted to rib number 6 (b) (Arensburg, 1991) but has been associated by Gómez-Olivencia et al. (2009) to the 7th rib (c). The new reconstruction of the 7th rib now is considerably larger than the previous reconstruction, contributing to an increased lower thorax in Kebara 2.

Discussion

Although many researchers have speculated on enlarged and capacious rib cages in Neandertals (Gorjanovic Kramberger, 1906; McCown and Keith, 1939; Ruff et al., 1997; Franciscus and Churchill, 2002; Sawyer and Maley, 2005; Gómez-Olivencia et al., 2009), uncertainties still exist. This is because traditional morphometrics of the Kebara ribs suggest a larger thorax (Gómez-Olivencia et al., 2009), while Bastir et al. (2012) found a lack of evidence for larger size in the Kebara thorax reconstructed by Sawyer and Maley (2005), which is also consistent with the original assessment of Arensburg (1991).

Table 1
Rib centroid sizes of the new Kebara reconstructions, modern human means, confidence intervals, one sample *t*-tests and *p*-values.

Rib	Kebara	Modern humans	Modern humans 95%	*p*	*t*
rib 1	135.88	163.03	158.38–167.68	<0.01	12.23
rib 2	236.73	260.15	253.19–267.12	<0.01	7.04
rib 3	316.93	323.44	316.49–330.42	0.06	1.96
rib 4	395.06	366.27	357.82–374.72	<0.01	−7.13
rib 5	395.09	393.24	382.88–403.60	0.71	−0.37
rib 6	420.72 (397.50)	406.17	395.84–416.50	<0.01 (0.17)	−2.95 (−1.49)
rib 7	453.22 (400.20)	412.57	403.49–421.64	<0.01 (0.01)	−9.37 (2.89)
rib 8	426.52	399.22	391.86–406.58	<0.01	−7.76
rib 9	381.95	372.26	365.95–378.58	<0.01	−3.21
rib 10	350.79	331.06	324.39–337.72	<0.01	−6.20

Values (data, statistics) given in parentheses are from the original reconstruction and differ from the new reconstruction.

Table 2
Rib centroid sizes of the new Kebara reconstructions, modern human means, confidence intervals, one sample *t*-tests and *p*-values.

	Kebara (new)	Modern humans	95% C.I:	*t*	*p*
Total thorax	3512.88 (3436.68)	3427.87	3361.20–3493.60	−2.701 (−0.293)	0.014 (0.773 ns)
Upper thorax	1479.69	1506.15	1471.50–1540.80	1.6	0.126 ns
Lower thorax	2033.20 (1957.00)	1921.27	1885.90–1956.60	−6.623 (−2.114)	<0.0001 (0.048)
Rel. tot. thorax	2116.19 (2070.30)	1987.21	1937.00–2037.40	−4.763 (−3.552)	0.0003 (0.003)
Rel. up. thorax	891.38	869.88	844.51–895.27	−1.816	0.09 ns
Rel. low. thorax	1224.82 (1178.92)	1127.34	1097.30–1157.40	−6.963 (−3.684)	<0.0001 (0.002)

Values (data, statistics) given in parentheses are from the original reconstruction and differ from the new reconstruction. Relative sizes are calculated as follows [(absolute thorax size/stature)*100].
ns: not significant.

When incorporating the new rib reconstructions (Fig. 1) into cumulative rib size (Table 2), the original total thorax size of Kebara increases to give rise to a significantly larger rib cage (Table 2, Fig. 2). This explains the findings of Bastir et al. (2012) who measured the thorax model of Sawyer and Maley (2005), which was built using the original rib material.

After virtually refitting the fragments of the 6th and 7th rib, a significant size increase of the lower thorax is observed (Franciscus and Churchill, 2002; Sawyer and Maley, 2005; Gómez-Olivencia et al., 2009). Also, in Arensburg's (1991) reconstruction, the 8th rib is the absolute largest, instead of the 7th as in modern humans (Table 1, Fig. 2). This difference could imply a qualitatively different thorax (bauplan) in Neandertals, which, however, disappears in the new reconstruction (Fig. 2), suggesting that the upper and lower thorax in Kebara and modern humans differ in a quantitative rather than qualitative way. Independent upper and lower thorax evolution can relate to development. A recent study has shown that the upper thorax grows differently than the lower thorax (Bastir et al., 2013a). Also, the upper part is related to thoracic breathing and upper limb movement, while the lower part seems more related to diaphragmatic breathing, body posture and locomotion (Openshaw et al., 1984; Bastir et al., 2013a). This fits also with mosaic evolutionary change in the upper and lower thorax in australopiths (Schmid et al., 2013).

The larger sizes of the lower Neandertal ribs have been observed in previous studies (McCown and Keith, 1939; Franciscus and Churchill, 2002; Sawyer and Maley, 2005; Gómez-Olivencia et al., 2009) and related to the greater diaphragmatic contribution to respiration in Neandertals. During inspiration the lower parts of the lungs, close to the diaphragm, are the most expansive areas (Bellemare et al., 2003; Ward, 2005) and in Kebara, therefore, greater expansion than in modern humans is likely.

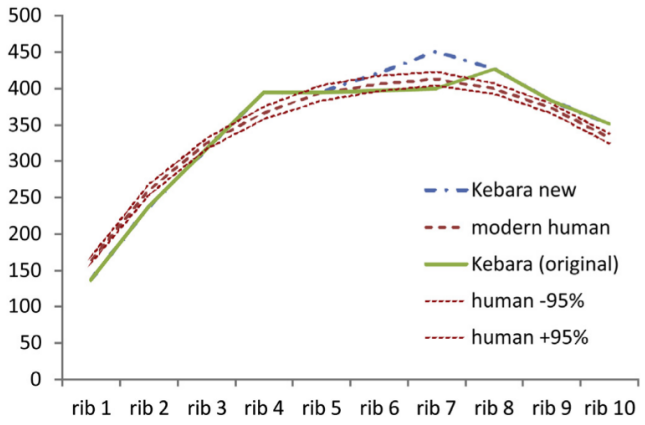

Figure 2. Curves connecting the mean centroid sizes (*y*-axis) of rib 1 to rib 10 (*x*-axis) of modern humans and both Kebara reconstructions. Modern human means are connected by bold dashed line. The thin dashed lines delimit the upper and lower 95% confidence intervals. The original reconstructions of Kebara 2 ribs are shown by a bold continuous line, the new reconstruction by bold dashed dotted line. Note the smaller sizes of the upper ribs and the larger lower ribs in the Neandertal specimen, suggesting a smaller upper and a larger lower thorax. Note also that in the old reconstruction, rib 8 is the largest while in the new reconstruction rib 7 is the largest as in the modern human reference.

These differences relate to body shape, climatic adaptations or enhanced physical activity and energetics (Franciscus and Churchill, 2002; Gómez-Olivencia et al., 2009; Weaver, 2009). However, because all of these factors can be associated with similar morphological adaptations, our explanations are hampered by morphological 'equifinality' identified previously by Churchill (2006) and caused by the bauplan of a high-energy consuming hominin organism (Bastir, 2008).

After standardizing upper, lower and full thorax sizes to stature (Table 2), all values increase due to the lower stature in Neandertals (Churchill, 2006). Table 2 shows that total thorax size in the original reconstruction was not larger than in modern humans, while in the new reconstruction both relative and absolute thorax sizes are larger. Standardization to body mass could give different results because body mass is higher in Neandertals than in modern humans, reflecting differences in body shape *and* body size (Churchill, 2006). Thus, different variables give different standardization results and one should be guided by the biology of the research question. While body mass is interesting in bio-energetics, comparisons with industrial populations is problematic for reasons such as obesity. Lean body mass can be calculated in industrial populations but not as easily in fossil humans (Steegmann et al., 2002). More research is necessary.

Alternatively, cleverly designed experimental research might allow us to disentangle some factors of body shape, function and evolution, and is currently underway (Utrilla et al., 2014). So far, our findings are further evidence for morpho-functional regionalization of the rib cage and that the lower thorax is particularly important for reconstructing the Neandertal respiratory system.

Acknowledgments

We thank Ofer-Bar Yosef, Bernard Vandermeersch, Baruch Arensburg, and Israel Hershkovitz for permission to use CT-data of the orginal Kebara fossils, and Rafael Coronado Santos, Ángela de Pinto, and Ana María Pérez Álvarez (Spanish Staff of Siemens Healthcare AG Inc, Erlangen, Germany) for assistance with the Syngo inSpace 4D Lung Parenchyma Analysis module. We thank Asier Gómez Olivencia, Trenton Holliday, Margit Berner and Luis María Carascál for discussion, one anonymous reviewer and the associate editor for helpful comments on a previous version. This research was funded by the Spanish Ministry of Economy and Competitiveness (CGL2012-37279, MINECO), the Leakey Foundation, and PI10/02089 (Fondo de Investigación Sanitaria) Ministry of Health, Spain.

References

Arensburg, B., 1991. The vertebral column, thoracic cage, and hyoid bone, Le Squelette Mousterien de Kebara 2. CNRS, Paris, pp. 113–146.

Bastir, M., 2008. A systems-model for the morphological analysis of integration and modularity in human craniofacial evolution. J. Anthropol. Sci. 86, 37–58.

Bastir, M., Rosas, A., Gunz, P., Pena-Melian, A., Manzi, G., Harvati, K., Kruszynski, R., Stringer, C., Hublin, J.-J., 2011. Evolution of the base of the brain in highly encephalized human species. Nat. Commun. 2, 588.

Bastir, M., García-Martínez, D., Coquerelle, M., Barash, A., Recheis, W., 2012. Systems-approaches to skeletal variation in paleoanthropology: the human thorax in: PESHE. ESHE, European Society for the study of human evolution, Bordeaux, p. 14.

Bastir, M., García Martínez, D., Recheis, W., Barash, A., Coquerelle, M., Rios, L., Peña-Melián, Á., García Río, F., O'Higgins, P., 2013a. Differential growth and development of the upper and lower human thorax. PLoS ONE 8, e75128.

Bastir, M., García-Martínez, D., Recheis, W., Barash, A., Coquerelle, M., Rios, L., Peña, A., O'Higgins, P., 2013b. 3D analysis of human ribcage ontogeny. Am. J. Phys. Anthropol. S56, 75.

Bellemare, F., Jeanneret, A., Couture, J., 2003. Sex differences in thoracic dimensions and configuration. Am. J. Respir. Crit. Car. Med. 168, 305–312.

Churchill, S.E., 2006. Bioenergetic perspectives on Neanderthal thermoregulatory and activity budgets. In: Harvati, K., Harrison, T. (Eds.), Neanderthals Revisited: New Approaches and Perspectives. Springer Verlag, New York, pp. 113–156.

Franciscus, R.G., Churchill, S.E., 2002. The costal skeleton of Shanidar 3 and a reappraisal of Neandertal thoracic morphology. J. Hum. Evol. 42, 303–356.

Froehle, A., Churchill, S.E., 2009. Energetic competition between Neandertals and anatomically modern humans. Paleoanthropology 2009, 96–116.

García-Martínez, D., 2014. The form, function and evolution of the hominin thorax. Doctoral Dissertation, Museo Nacional de Ciencias Naturales (CSIC), Autónoma University, Madrid, Spain (in preparation).

García-Martínez, D., Recheis, W., Bastir, M., 2012. The whole and its parts: 3D geometric morphometrics of human thorax evolution. Encuentro de Jóvenes Investigadores en Paleontología Valencia.

García-Martínez, D., Bastir, M., Recheis, W., Barash, A., 2013. Two different barrels for two different primates: 3D geometric morphometrics of sliding semilandmarks of the Hominoidea superfamily thorax. Sociedad Española de Antropología Física, Bilbao, p. 39.

Gómez-Olivencia, A., Eaves-Johnson, K.L., Franciscus, R.G., Carretero, J.M., Arsuaga, J.L., 2009. Kebara 2: new insights regarding the most complete Neandertal thorax. J. Hum. Evol. 57, 75–90.

Goodyear, M.D.E., Krleza-Jeric, K., Lemmens, T., 2007. The Declaration of Helsinki. Brit. Med. J. 335, 624–625.

Gorjanovic Kramberger, K., 1906. Der diluviale Mensch von Krapina in Kroatien. C. W. Kreidel's Verlag, Wiesbaden.

Gunz, P., Mitteroecker, P., Neubauer, S., Weber, G.W., Bookstein, F.L., 2009. Principles for the virtual reconstruction of hominin crania. J. Hum. Evol. 57, 48–62.

McCown, T., Keith, A., 1939. The Stone Age of Mount Carmel II: The Fossil Human Remains from the Levalloiso-Mousterian. Clarendon Press, Oxford.

Mitteroecker, P., Gunz, P., 2009. Advances in geometric morphometrics. Evol. Biol. 36, 235–247.

Openshaw, P., Edwards, S., Helms, P., 1984. Changes in rib cage geometry during childhood. Thorax 39, 624–627.

Ruff, C.B., Trinkaus, E., Holliday, T.W., 1997. Body mass and encephalization in Pleistocene *Homo*. Nature 387, 173–176.

Sawyer, G.J., Maley, B., 2005. Neanderthal reconstructed. Anat. Rec. 283B, 23–31.

Schmid, P., Churchill, S.E., Nalla, S., Weissen, E., Carlson, K.J., de Ruiter, D.J., Berger, L.R., 2013. Mosaic morphology in the thorax of *Australopithecus sediba*. Science 340, 6129.

Sokal, R.R., Rohlf, F.J., 1998. Biometry, third ed. W. H. Freeman and Company, New York.

Stahl, W.R., 1967. Scaling of respiratory variables in mammals. J. Appl. Physiol. 22, 453–460.

Steegmann, A.J., Cerny, F., Holliday, T., 2002. Neandertal cold adaptation: physiological and energetic factors. Am. J. Hum. Biol. 14, 566–583.

Thurlbeck, W.M., 1982. Postnatal human lung growth. Thorax 37, 564–571.

Utrilla, C., Fernandez-Velilla, M., Casitas, R.G., Martinez Ceron, I., García-Río, F., Torres-Sanchez, M.I., 2014. Correlation between lung volumes obtained by quantitative thoracic CT and pulmonary function tests. In: So, E. (Ed.), Radiology. European Society of Radiology, Vienna. http://dx.doi.org/10.1594/ecr2014/C-1625.

Ward, J., 2005. Physiology of breathing I. Surgery 23, 419–424.

Weaver, T.D., 2009. The meaning of Neandertal skeletal morphology. Proc. Natl. Acad. Sci. 106, 16028–16033.

Zelditch, M.L., Swiderski, D.L., Sheets, H.D., Fink, W.L., 2004. Geometric Morphometrics for Biologists: A Primer. Elsevier Academic Press, San Diego.

Journal of Human Evolution 80 (2015) 64–73

Contents lists available at ScienceDirect

Journal of Human Evolution

journal homepage: www.elsevier.com/locate/jhevol

The relevance of the first ribs of the El Sidrón site (Asturias, Spain) for the understanding of the Neandertal thorax

Markus Bastir [a, *], Daniel García-Martínez [a], Almudena Estalrrich [a], Antonio García-Tabernero [a], Rosa Huguet [a, b, c, d], Luis Ríos [a, e], Alon Barash [f], Wolfgang Recheis [g], Marco de la Rasilla [h], Antonio Rosas [a]

[a] Paleoanthropology Group, Museo Nacional de Ciencias Naturales (CSIC), J. G. Abascal 2, 28006, Madrid, Spain
[b] Institut Català de Paleoecologia Humana i Evolució Social (IPHES), C/ Marcel.lí Domingo s/n e Campus Sescelades URV (Edifici W3), 43007 Tarragona, Spain
[c] Àrea de Prehistòria, Universitat Rovira i Virgili (URV), Avinguda de Catalunya 35, 43002 Tarragona, Spain
[d] Unidad asociada al CSIC, Departamento de Paleobiología, Museo Nacional de Ciencias Naturales, Calle José Gutierrez Abascal, 2. 28006 Madrid, Spain
[e] Sociedad de Ciencias Aranzadi-Aranzadi Zientzia Elkartea, Alto de Zorroaga Bidea, 11, 20014, Donostia, Gipuzkoa, Spain
[f] Faculty of Medicine in the Galilee, Bar Ilan University, Henrietta Szold, 8, P.O.B 1589, 1311502, Zefat, Israel
[g] Department of Radiology, Medical University Innsbruck, Anichstrasse 35, 6020 Innsbruck, Austria
[h] Department of History, University of Oviedo, Campus del Milán, C/ Teniente Alfonso Martínez s/n, 33011, Oviedo, Spain

ARTICLE INFO

Article history:
Received 18 March 2014
Accepted 17 October 2014
Available online 3 January 2015

Keywords:
Costal skeleton
Body shape
Integration
Semilandmarks
Homo neanderthalensis

ABSTRACT

Reconstructing the morphology of the Neanderthal rib cage not only provides information about the general evolution of human body shape but also aids understanding of functional anatomy and energetics. Despite this paleobiological importance there is still debate about the nature and extent of variations in the size and shape of the Neandertal thorax. The El Sidrón Neandertals can be used to contribute to this debate, providing new costal remains ranging from fully preserved and undistorted ribs to highly fragmented elements. Six first ribs are particularly well preserved and offer the opportunity to analyze thorax morphology in Neandertals. The aims of this paper are to present this new material, to compare the ontogenetic trajectories of the first ribs between Neandertals and modern humans, and, using geometric morphometrics, to test the hypothesis of morphological integration between the first rib and overall thorax morphology. The first ribs of the El Sidrón adult Neandertals are smaller in centroid size and tend to be less curved when compared with those of modern humans, but are similar to Kebara 2. Our results further show that the straightening of the first ribs is significantly correlated with a straightening of the ribs of the upper thorax ($R = 0.66$; $p < 0.0001$) in modern humans, suggesting modularity in the upper and lower thorax units as reported in other hominins. It also supports the hypothesis that the upper thorax of Neandertals differs in shape from modern humans with more anteriorly projecting upper ribs during inspiration. These differences could have biomechanical consequences and account for stronger muscle attachments in Neandertals. Different upper thorax shape would also imply a different spatial arrangement of the shoulder girdle and articulation with the humerus (torsion) and its connection to the upper thorax. Future research should address these inferences in the context of Neandertal overall body morphology.

Introduction

Hypotheses about the paleobiological significance of Neandertal thorax morphology have referred to different factors ranging from cold adaptations, energetics and activity levels, and increased body mass (Franciscus and Churchill, 2002; Churchill, 2006) to questions related to the evolution of overall body shape (Jellema et al., 1993; Ruff, 2002, 2010; Gómez-Olivencia et al., 2009; García-Martínez et al., 2012; Bastir et al., 2013a,b). Despite its importance, the extent of differences in the size and shape of the Neandertal thorax is still not entirely clear (Franciscus and Churchill, 2002; Churchill, 2006; Gómez-Olivencia et al., 2009). The question of size and shape

* Corresponding author.
E-mail address: mbastir@mncn.csic.es (M. Bastir).

http://dx.doi.org/10.1016/j.jhevol.2014.10.008
0047-2484/

differences is also important in the light of recent evidence that supports a division of the thorax into an upper and a lower part for functional, developmental and evolutionary reasons in different hominin species (Arensburg, 1991; Schmid et al., 2013; Bastir et al., 2013b, in press). While the upper part (ribs 1–5) has been related to thoracic breathing and to upper limb locomotion, the lower part (ribs 6–12) reflects features related to diaphragmatic breathing, posture and body shape as well as sub-thoracic organ content (Bastir et al., 2013b).

In a pioneering quantitative analysis of isolated ribs of the Shanidar 3 Neandertal, Franciscus and Churchill (2002) suggested that the lower Neandertal thorax is larger in volume with more rounded cross sections of the lower ribs than in modern humans. Other researchers have suggested that the ribs of the lower thorax in Kebara 2 are relatively large (Gómez-Olivencia et al., 2009; García Martínez et al., 2014a). This evidence, together with a complete reconstruction of a Neandertal skeleton (Sawyer and Maley, 2005) suggests a wider lower thorax in Neandertals than in modern humans.

The morphology of the upper thorax in Neandertals is considerably less well known. Sizes of the upper ribs of Kebara 2 seem to be all within or at the lower end of the range of modern humans (Gómez-Olivencia et al., 2009; García Martínez et al., 2014a). However, there is also evidence suggesting that the shape might be different. Karl Gorjanović-Kramberger (1906) described the first ribs of the Krapina Neandertals as particularly straight, much less curved than those of modern humans. Straightness of the first ribs in other Neandertals has also been observed in subsequent work (McCown and Keith, 1939; Franciscus and Churchill, 2002; Gómez-Olivencia et al., 2009). Based on his observations of the first ribs, Gorjanović-Kramberger (1906) further speculated that the entire rib cage of the Krapina Neandertals probably projected more anteriorly than in modern humans ("wodurch auch der Brustkorb mehr vorgewölbt war"; Gorjanović-Kramberger, 1906: 212). Thus, by predicting that the morphology of the first rib is significantly correlated to the shape of the remaining thorax, Gorjanović-Kramberger (1906) proposed an important hypothesis that is relevant to the previously mentioned studies on general thorax morphology and evolution (Franciscus and Churchill, 2002; Gómez-Olivencia et al., 2009).

Anatomically, Gorjanović-Kramberger's (1906) hypothesis is related to the fact that the upper ribs of the thorax share an intimate relation with the respiratory system and are mutually connected by the intercostal muscles and the costo-sternal cartilages to form the chest wall (De Troyer et al., 2005). These soft-tissue connections and the need for coordinated function during lung ventilation (Franciscus and Churchill, 2002; West, 2012) probably account for the integration of the superior ribs into a morpho-functional upper thoracic unit that has been reported in different hominin species (Schmid et al., 2013; Bastir et al., 2013b). These anatomical and morphological observations justify the assumption of rib covariation patterns in modern humans and Neandertals. However, the hypothesis of Gorjanović-Kramberger (1906) has not yet been tested. The scantiness of upper thorax elements (for example, first ribs) in the Neandertal fossil record as well as the difficulty in properly quantifying the curved morphology of the outer rib circumference have thus far hampered a thorough analysis of this important problem.

The El Sidrón Neandertal site in Asturias, northern Spain (Fortea et al., 2003; Rosas et al., 2006, 2012), which to date has produced the largest sample of Neandertal fossils in the Iberian Peninsula, also provides a significant contribution to the fossil record of thoracic elements. In addition, geometric morphometrics of 3D landmarks can be used for rigorous quantification of rib curvature, which is a key factor of overall thoracic morphology and variation (García-Martínez et al., 2012, 2013; Bastir et al., 2013b). When combining geometric morphometrics and partial least squares (PLS) analysis, it is also possible to quantify and visualize shape covariation of two different anatomical systems (Rohlf and Corti, 2000; Bastir et al., 2005), such as the first rib and the remaining thorax. Thus, the aim of the present study is to describe and analyze a set of first ribs of the El Sidrón Neandertals within the framework of Gorjanović-Kramberger's (1906) hypothesis that the morphology of the first rib morphology is significantly related to the shape of the remaining skeletal thorax.

Material and methods

The fossil site of El Sidrón (Asturias, Spain) has produced a considerable sample of thoracic elements, ranging from fully preserved and undistorted ribs to highly fragmented elements. Six first ribs SD-417, SD-1225, SD-1699 + SD-1685 (two fragments fitted together, termed SD-1699+ onwards), SD-1767, SD-2148, SD-2172, are particularly well preserved (Fig. 1; Table 1). The ribs, like most of the fossils from the El Sidrón site (Rosas et al., 2006; Bastir et al., 2010) were covered to a variable degree with calcite concretions as a result of being embedded in the sedimentary matrix (Rosas et al., 2006, 2011). Prior to analyses, these concretions were mechanically removed to facilitate the best possible observation of surface details of the bones for anatomical description (Fernández Cascón et al., 2010).

Once the concretions had been removed, morphological descriptions and linear measurements (Tables 2 and 3) were undertaken for the original El Sidrón rib fossils. The comparative sample included linear measurements of high quality casts of earlier *Homo* [KNM-WT 15000 (African *Homo erectus* or *Homo ergaster*), ATD6-108, *Homo antecessor*] and 3D reconstructions of CT scans of the first ribs of Kebara 2 (Arensburg, 1991) and of La Ferrassie VI, a Neandertal child of approximately three to five years of age (Heim, 1982; Tompkins and Trinkaus, 1987). These data, and data taken from the literature, were compared with measurements on 3D reconstructions of CT scans of a growth series of isolated first ribs of 27 modern humans ranging from newborns to adults of both sexes, including infants (0–3 years), children (<7 years), juveniles (<10 years), adolescents (<15 years) and adults (>16 years) (Bastir et al., 2013b). This data set was also used to study covariation between the first ribs and other ribs that articulated with the spine in order to quantify thorax shape covariation.

Linear measurements

Rib arcs (Gómez-Olivencia et al., 2009), cords and shaft diameters (Franciscus and Churchill, 2002; Gómez-Olivencia et al., 2009, 2010) were measured on the original fossils and on the comparative fossil sample with standard anthropometric instruments following the definitions listed in Table 2. Each measurement was calculated from the average of three measurements in order to reduce intra-observer error (Franciscus and Churchill, 2002; Gómez-Olivencia et al., 2009, 2010). These are presented in Table 3. In order to evaluate the symmetry pattern in antimeric ribs we calculated the following index: size difference between antimeres divided by the smaller antimere size multiplied by 100, following Trinkaus (1984) and Franciscus and Churchill (2002). The results are presented in Table 4.

Ontogenetic state assessment

Maturation state of the first ribs was evaluated using the scoring system proposed by Ríos and Cardoso (2009) based on the epiphyseal fusion of the articular tubercle of the rib

Figure 1. Cranial views of Neandertals from El Sidrón compared with modern humans. Juvenile (a, d) and adult (e, j) modern humans are shown to illustrate the greater curvature than that of Neandertals (b) SD-2148, c) D-2172, f) SD-1767, g) SD-417, h) SD-1225, i) SD-1699+. Dashed outlines mark the original limit of the bones. Circled labels indicate modern human first ribs for comparison. Note that not all concretions could be removed during restoration and thus cover different fossils to a variable degree.

(preserved in most cases in our sample). According to this protocol, three ranges of maturation can be differentiated: 1 – no fusion; 2 – partial fusion; 3 – complete fusion, but it should be noted that the maturation rate of Neandertal epiphyseal fusion could differ from that of modern humans. When the articular tubercle of the rib was missing, an ontogenetic assessment was carried out through comparisons with centroid size and mid-shaft maximum diameter (see Fig. 2).

Table 1
Inventory of the first ribs of the El Sidrón site and its position in Fig. 1.

Specimen	Side	Ontogenetic assessment	Head	Neck	Articular tubercle	Shaft	Sternal end	Figure label
SD-2148	Right	Juvenile 1	No	Half	Yes	Yes	Yes	1b
SD-2172	Left	Juvenile 1	No	No	No	Yes	Yes	1c
SD-1767	Left	Large adolescent or small adult (female?)	No	No	Half	Yes	Yes	1f
SD-417	Left	Juvenile 2	No	No	No	Half	No	1g
SD-1225	Right	Juvenile 2	No	Half	Yes	Yes	Half	1h
SD-1699+	Right	Young adult	No	No	Yes	Yes	Half	1i

Table 2
Measurement definitions based on previous work (Franciscus and Churchill, 2002; Gómez-Olivencia et al., 2009, 2010).

Variable	Name	Description
TVC	Tuberculo-ventral chord	Straight line distance between the dorsal-most margin of the articular tubercle to the ventral-most point of the sternal end of the rib.
TVA	Tuberculo-ventral arc	Straight line distance between the dorsal-most margin of the articular tubercle to the ventral-most point of the sternal end of the rib.
THD	Tubercle horizontal diameter	Maximum diameter from the internal surface of the rib to the further extent of the articular tubercle.
MMxD	Mid-shaft maximum diameter	Measured at the midshaft, maximum diameter from the internal to external surface, at the groove for the subclavian artery.
MMnD	Mid-shaft minimum diameter	Measured at the midshaft, minimum diameter from the internal to external surface, at the groove for the subclavian artery.
SEMxD	Sternal end maximum diameter	Measured at the sternal end. Maximum diameter, approximately horizontal.
SEMnD	Sternal end minimum diameter	Measured at the sternal end. Minimum diameter, approximately vertical.

Table 3
Linear measurements (mm).

	SD-2148 1R	SD-2172 1L	SD-1225 1L	SD-417 1R	SD-1767 1R	SD-1699+ 1L	K2 1R	K2 1L	Amud 1 1L	Krapina 117.2 1R	Krapina 117.3 1R	Krapina 118.2 1R	Krapina 118.4 1L	Krapina 117.1 1L	KNM-WT 15000 1R	KNM-WT 15000 1L	ATD6-108 1R
TVC	55.84	–	(75.16)	–	79.05	(83.00)	85.7	82.7							(81.0)	(80.5)	(90.0)
TVA	70.10	–	(104.50)	–	105.00	(115.0)	99.0	(96.0)							(116.0)	(115.0)	(107.0)
THD	11.18	–	13.76	–	16.95	15.35	19.8	19.4		17.1	(16.5)	15.2		15.4	14.8	14.6	17.9
MMxD	9.95	9.25	11.31	10.90	16.05	17.90	(20.7)	20.5	>19.0	14.0	13.8	13.2	15.6		19.0	17.1	15.4
MMnD	3.57	3.35	4.27	4.25	4.55	5.75	3.3	3.5	4.2	3.5	4.3	4.0	3.4		3.0	2.8	3.3
SEMnD	4.78	4.75	4.43	–	6.15	5.95	8.4	9.3	8.9						5.1	5.2	5.9
SEMxD	11.97	11.05	(15.17)	–	19.00	(17.30)	19.8	17.8							20.5	20.5	–

Estimated data in parentheses.
Measurements from Amud 1 and Krapina were taken from Gómez-Olivencia et al. (2009, 2010).

Table 4
Asymmetric percentage calculated in possible antimeres.

Variable	SD-2148/ SD-2172	SD-1225/ SD-417	SD-1767/ SD-1699	Kebara 2 L/R	KNM-WT 15.000 L/R
TVC	–	–	4.99	3.62	0.62
TVA	–	–	9.52	3.12	0.87
THD	–	–	10.42	2.06	1.37
MMxD	7.56	3.76	11.52	0.97	11.11
MMnD	6.57	0.47	26.37	6.06	7.14
SEMnD	0.63	–	3.36	10.71	1.96
SEMxD	8.32	–	(9.82)	11.24	0.00
Asymmetry average	5.77	2.11	10.85	5.39	3.30

Morphological analysis

A detailed description of surface morphology, such as the marks of the scalene and serratus muscle attachments and the subclavian artery, as well as preservation status was carried out in the costal elements SD-417, SD-1225, SD-1699+, SD-1767, SD-2148, SD-2172, based on the principal anatomical features of this rib (Spalteholz, 1970; Aiello and Dean, 1990; Gómez-Olivencia et al., 2009, 2010; White et al., 2011).

Geometric morphometric analyses

Data from 3D landmarks at the tubercle and angle, as well as the internal and external sternal extremities, and 13 semilandmarks along the shaft (García-Martínez et al., 2012, 2013; Bastir et al., 2013b) were taken for comparative analyses employing the software Viewbox 4.0 (dHAL software, Kifissia, Greece; www.dhal.com; Polychronis et al., 2013). Semilandmarks were slid to the generalized Procrustes analysis (GPA) average to minimize bending energy between each specimen and the GPA-consensus. Missing data were few and estimated using the thin-plate spline approach available for 3D semilandmark techniques (Gunz et al., 2009; Bastir et al., 2011, 2013b) using Viewbox 4.0.

Size was measured as centroid size and shape as Procrustes shape coordinates (O'Higgins, 2000). For comparative purposes, descriptive statistics were calculated for ontogenetic age groups defined previously following the categories proposed by Bogin (1999) and plotted together with the fossil data. Because of the small samples of the ontogenetic age groups, normality of size could not be assumed and the modern human sample was analyzed by non-parametric Kruskal–Wallis analysis of variance (ANOVA) by rank (StatSoft, 1999).

Shape data were analyzed in two ways. First, a principal components analysis (PCA) in Procrustes form space was performed in the EVAN Toolkit (ET) software (EVAN Society, 2010) to explore shape variation and allometric growth trajectories (Mitteroecker et al., 2004; Bastir et al., 2007). Second, to assess non-growth dependent shape covariation, data were corrected for ontogenetic growth allometry by multivariate regression of shape on centroid size (CS). Non-allometric residual shape variation of the first rib was correlated with that of the remaining ribs 2–10 of the 27 thoraces in modern humans by a PLS analysis (Rohlf and Corti, 2000; Bastir et al., 2005). These analyses were carried out in MorphoJ (Klingenberg, 2011) and visualized in ET software (EVAN Society, 2010). Block 1 consisted of the shape data of the first ribs, and block 2 of the remaining thorax shape (ribs 2–10). The PLS analysis was carried out using separate Procrustes registrations for the two blocks. The PLS analysis was undertaken to test the hypothesis of Gorjanović-Kramberger (1906), which predicts that straightness of the first rib is associated with straightness of the remaining ribs of the thorax.

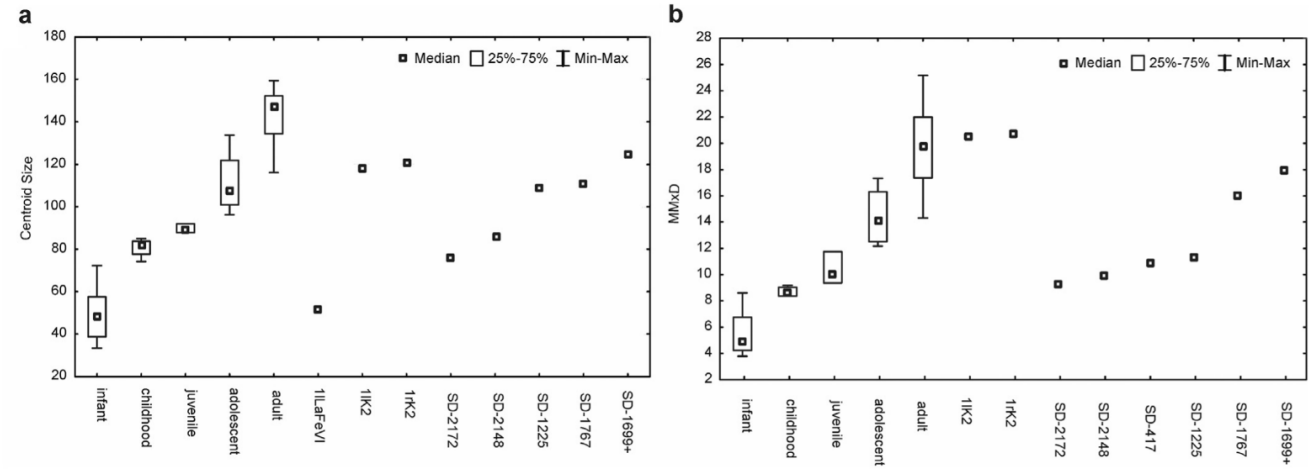

Figure 2. Comparative size analysis of the first ribs. Data show the median, second and third quartiles, minima and maxima of the modern human age groups. a) Centroid size, note that adult (large) Neandertal first ribs tend to be at the lower margin of the modern human range. b) Mid-shaft maximum diameter (MMxD).

Results

Anatomical descriptions

SD-2148 (Fig. 1b) is a first rib of the right side that preserves half of the neck, the articular tubercle and the shaft of the rib including the complete sternal end. The groove of the subclavian artery, the anterior scalene tubercle, the insertion of the medium scalene and the insertion of the serratus anterior are slightly marked in this individual. Regarding ontogenetic stage, SD-2148 does not preserve the rib head, but the epiphysis of the articular tubercle is not fused in this individual (stage 1), which suggests a maximum age of 18 years at the time of death (Ríos and Cardoso, 2009). Centroid size is at the upper childhood-lower juvenile range, and mid-shaft maximum diameter (MMxD) at the lower juvenile range (Fig. 2).

SD-2172 (Fig. 1c) is a first rib of the left side. It preserves the shaft of the rib from half of the insertion of the medium scalene and serratus anterior muscles to the sternal end and lacks the costal tubercle, the neck and head of the rib. The groove of the subclavian artery and the anterior scalene tubercle are very slightly marked. In this rib, the ontogenetic state cannot be assessed at the epiphyseal fusion of the head nor at the articular tubercle because these parts are not preserved. Centroid size is at the lower childhood range, and MMxD at the lower juvenile range (Fig. 2).

Overall morphology, MMxD, mid-shaft minimum diameter (MMnD), and sternal end minimum and maximum diameter (SEMnD and SEMxD, respectively) of SD-2148 and SD-2172 are very similar in both elements and very different from the rest of the ribs in the sample. This fact, together with a low symmetric percentage (5.77) (Table 4), suggests that these ribs are probably antimeres belonging to one individual (probably Juvenile 1 following Rosas et al., 2012).

SD-1225 (Fig. 1h) is a first rib of the left side that preserves the rib shaft from half of the neck to the sternal extremity. The groove of the subclavian artery presents a smoother surface and is clearly identifiable, as are the insertions of the anterior and medium scalene muscles and the serratus anterior. The epiphyseal surface of the articular tubercle is not fused (stage 1), suggesting a maximum age of 18 years at the time of death (Ríos and Cardoso, 2009). Centroid size is close to the median of the adolescent sample, while MMxD is in the upper juvenile range (Fig. 2).

SD-417 (Fig. 1g) is a fragment (43 mm) of the medial part of the rib shaft of a right rib. The groove of the subclavian artery is preserved, the anterior scalene tubercle is eroded and the insertion of the medium scalene muscle is marked only at its distal half. The features of this rib do not allow any direct association to ontogenetic stage, but the linear measurements (MMxD and MMnD) (Fig. 2) and the low asymmetry obtained in comparison with SD-1225 (2.11) (Table 4), suggest that SD-417 and SD-1225 are antimeres belonging to the same individual (probably Juvenile 2, according to Rosas et al., 2013).

SD-1767 (Fig. 1f) is a first rib of the right side that preserves the shaft from the distal part of the articular tubercle to the sternal end. The fossil has lost the neck and the head of the rib and the upper surface of the vertebral extreme is eroded. Thus, neither the proximal part of the articular tubercle nor the serratus anterior muscle insertion can be observed. The subclavian groove is present and the anterior scalene tubercle is very marked. The insertion mark of the medium scalene muscle is missing at its vertebral part due to the aforementioned taphonomic damage. As in SD-2172, epiphyseal fusion could not be assessed. Centroid size is at the lower adult range and MMxD is within the main adolescent range (Fig. 2). Thus, this specimen belongs either to a smaller adult (female?) or a larger adolescent.

SD-1699+ (Fig. 1i) is a first rib from the left side, which lacks the rib neck, the head of the rib and a fragment of the interior border of the rib shaft at the sternal end. The rib presents small cracks (4 mm) along the axis of the shaft, which, however, do not alter its morphology. One such fracture is located at the upper part, at the vertebral extreme above the insertion of the serratus anterior and the other fracture is situated at the lower border, near the anterior scalene tubercle. The insertions of the anterior and medium scalene muscle are very prominent. The groove of the subclavian artery is present. The articular tubercle is well preserved and the epiphysis is not fused with the metaphysis (state 1), suggesting a maximum age of 18 years at the time of death (Ríos and Cardoso, 2009). Centroid size is at the lower adult range (close to Kebara 2), MMxD within the third quartile of the adult range. This specimen likely belongs to a young adult (Fig. 2). However, assuming that SD-1767 (Fig. 1f) and SD-1699+ (Fig. 1i) are both adults, it is unlikely that they belong to the same individual for two reasons: the symmetric value is the highest of our sample (10.85) and there are seven adult individuals represented in the site (Rosas et al., 2012).

Linear measurements

The results of the linear measurements of the individuals of our sample are listed in Table 3. The comparative data from Amud 1 and Krapina were taken from Gómez-Olivencia et al. (2009, 2010). The

values of tuberculo-ventral cord (TVC), tuberculo-ventral arc (TVA), and tuberculo-horizontal diameter (THD) could not be measured in the ribs SD-2172 and SD-417. The THD and also MMXD values of the El Sidrón fossils are lower, more similar to Krapina than to Kebara 2 or Amud 1 (Table 3). Likewise, the SEMnD and SEMxD could not be assessed in SD-417. The values SEMxD, TVA and TVC were estimated in the ribs SD-1225 and SD-1699+ (Table 1).

Geometric morphometric analysis

There were significant ontogenetic increases in centroid size across the age classes [Kruskal Wallis ANOVA, H (4, $N = 28$) = 24.99, $p = 0.0001$]. Fig. 2 shows distributions (median, second and third quartiles, minima and maxima) of the modern human age groups in comparison with the Neandertal fossils. La Ferrassie VI plots within the modern human infant range, SD-2172 (CS = 76.0) within the range of the child sample and SD-2148 (CS = 85.6) slightly above and below the juvenile percentiles. The remaining fossils are above the median of the modern human adolescents and below the adults. The Kebara 2 ribs are close in size to the minimum of the adult modern humans, but inside the 75% of modern adolescents. SD1699+ (CS = 124.6) is the largest of the Neandertal sample.

Fig. 3 shows the results of the comparative ontogenetic analysis in Procrustes form space. Principal component 1 (96.9% of total variance) displays common growth variation with the small and younger individuals plotting towards the negative scores and the larger and adult individuals towards the positive PC1 scores (Fig. 3a). Along PC2 (1.47% of total variance), all Neandertals plot at the positive scores but a certain overlap with modern humans can be seen. General growth allometry is shown along PC1 (Fig. 3b). Larger specimens in later developmental classes decrease in outer rib curvature, indicating that growth allometry modifies rib curvature. Shapes associated with PC2 (Fig. 3c) are important because they quantitatively and visually confirm a trend towards a straight shaft in Neandertal first ribs compared with a curved outline in modern humans. The adult and/or largest Neandertals plot at the lower range of the adult modern humans, reflecting smaller centroid sizes than in modern humans.

The PLS analysis reveals highly statistically significant correlations between the first ribs and the remaining rib cage with different morphological patterns. The pattern associated with PLS1, $r = 0.79$; $p < 0.0001$, 79% of covariation) reflects covariation related to upwards and downwards inclination of the lateral part of the rib shaft relative to the vertebral end. However, while this is an important part of covariance, it is not relevant to Gorjanović-Kramberger's (1906) hypothesis addressed here that the straightness of the first rib is indicative of the straightness of the remaining rib cage. The pattern associated with PLS2, nevertheless, is very relevant ($r = 0.66$; $p < 0.0001$; 13.7% of covariation) as it reflects shape correlations between the first ribs and the remaining rib cage related to straightening, such as indicated by Gorjanović-Kramberger (1906). This is shown in Fig. 4, indicating that

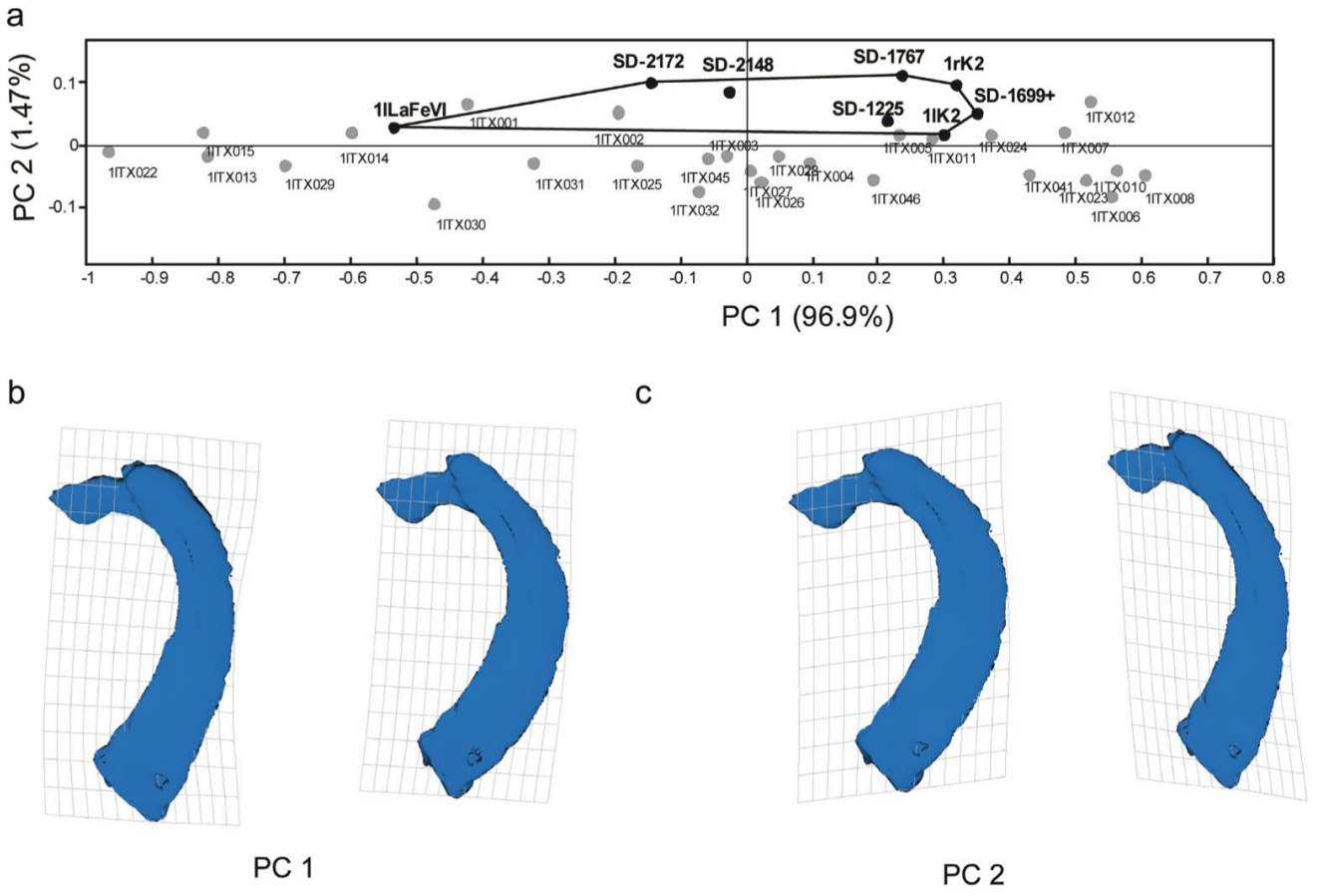

Figure 3. Form space growth trajectories. a) Distributions along PC1 and PC2 axes. Neandertal labels: 1lLaFEVI: first left rib of La Ferrassie VI; 1lK2: first left rib of Kebara 2, 1rK2: first right rib of Kebara 2; and El Sidrón (SD) first ribs (see Table 1), b) shape changes related to growth allometry along negative (left) and positive (right) PC1 scores, note again the relatively smaller sizes of adult/larger Neandertals compared with adult modern humans along PC1. c) Shapes associated to negative (left) and positive (right) PC2 scores contrasting modern humans and Neandertals.

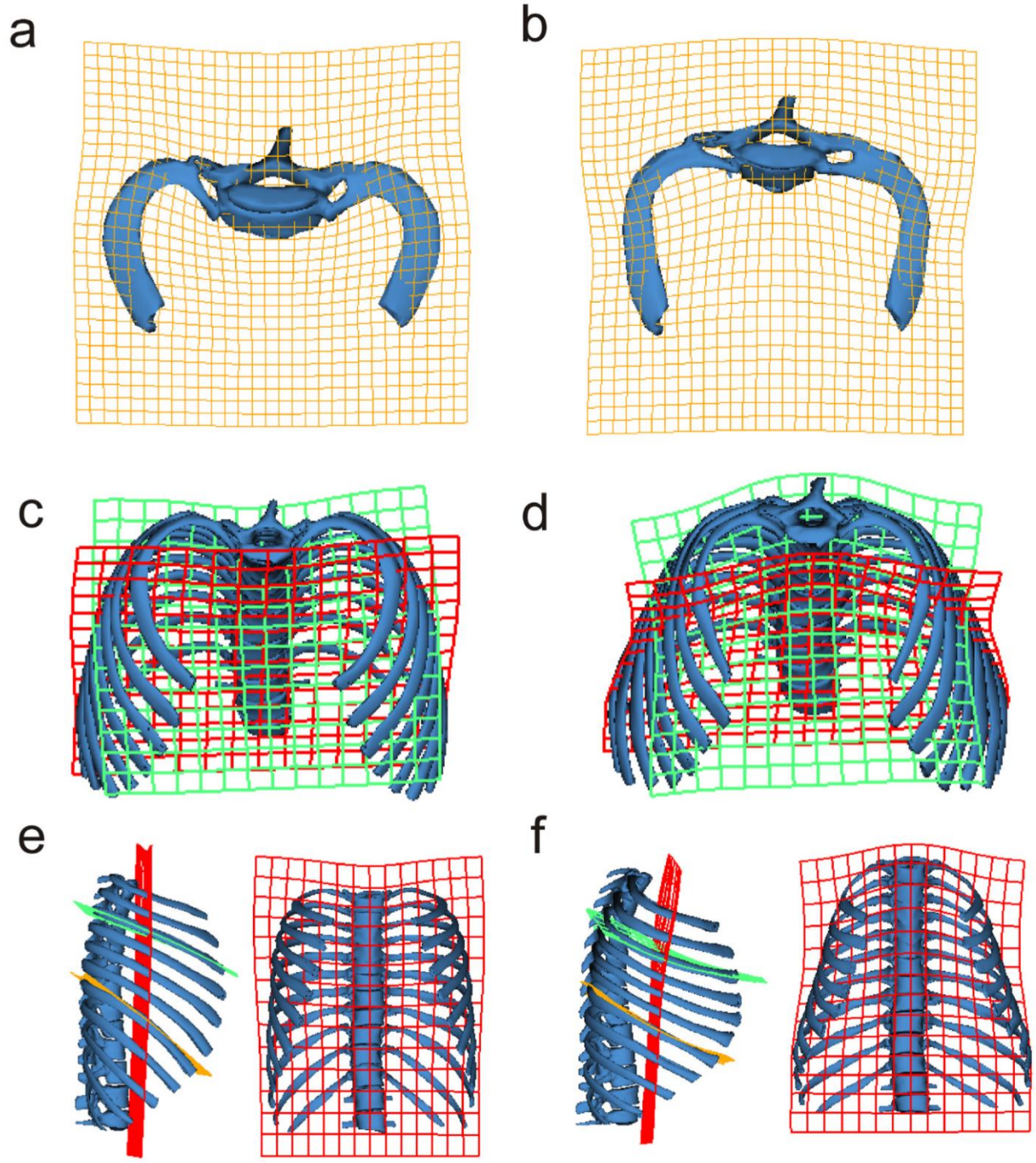

Figure 4. 2-block partial least squares (PLS) analysis of first ribs (block 1) and the remaining ribs of the thorax in anatomical connection (block 2) in modern humans. Curved first ribs (a) are correlated with thorax shapes (c) and (e) showing also curved (rounded) outlines in the upper thorax and a narrowing at the lower thorax. Straight first ribs (b) are correlated with thorax shapes (d) and (f) reflecting straighter ribs in the upper thorax (ribs 2–5) and a widening at the lower thorax (ribs 6–10). The 3D model in antero-superior view (c) shows how the curved ribs produce the widening of the upper thorax and a narrowing of the lower thorax (c). The 3D model in (d) in antero-superior view shows that the straightened ribs are accompanied by a relative narrowing and elongation of the upper thorax and a widening in the lower thorax (c). Note that shape covariation between the first rib and the remaining thorax is more pronounced in the upper than in the lower thorax. The thin-plate spline (TPS) grids illustrate the shape transformation of mean shape (rectangular and undeformed TPS grid) into negative (curved first ribs) and positive (straight first ribs) loadings along the PLS 2 scores. TPS-grids in first ribs (a,b) are located in the axial plane. TPS-grids in (c,d) are located in the coronal plane (red), and the axial (green) plane, through upper thorax (ribs 4). The TPS grids in (e,f) show right lateral views and frontal views. Lateral view in (e) shows how curved ribs are related to antero-posteriorly short (shallow) rib cages and illustrate medio-lateral expansion at the upper thorax. Lateral view in (f) show how rib straightening is related to antero-posteriorly long (deep) rib cages, with a medio-lateral expansion at the lower thorax. (For interpretation of the references to color in this figure legend, the reader is referred to the web version of this article.)

straightened first ribs are accompanied by a similar straightening (and lowering) of the remaining ribs of the upper thorax (Appendix A, Supplementary Online Material (SOM) 1). In addition, Fig. 4c,d shows that this straightening is more pronounced in the upper thorax, that is, from ribs 2 to rib 5, while in the lower ribs there is also a medio-lateral widening and an elevation of the sternal end of the shaft (Fig. 4e,f; SOM 1). In sum, these effects produce an increase in depth, which could support part of the hypothesis of Gorjanović-Kramberger (1906).

Discussion

The aims of this paper were to present new costal fossils of the El Sidrón Neandertals, to compare the ontogenetic trajectories of the first ribs between Neandertals and modern humans, and to test, using geometric morphometrics, Gorjanović-Kramberger's (1906) hypothesis that straightness of the first rib is correlated with straightness of the remaining thorax.

Individual and ontogenetic identifications were carried out combining epiphyseal fusion status, and the distributions of centroid size and mid-shaft maximum diameter. The analysis of centroid size suggests consistently lower values in Neandertals when compared with the corresponding age groups in the modern human reference population. Mid-shaft maximum diameters seem to reflect overall additional ontogenetic growth changes well. These criteria for ontogenetic assessment lead us to suggest that SD-2148 and SD-2172 belong to the individual Juvenile 1, SD-1225 and SD-417 to Juvenile 2, SD-1767 either to a larger adolescent or a smaller adult (maybe female) and 1699+ to a young adult (Rosas et al., 2012, 2013).

The first ribs of the El Sidrón Neandertals show strong muscle markings and a decreased outer curvature, particularly in the distal part of the shaft. Such features have been observed previously in other Neandertals (Gorjanović-Kramberger, 1906; McCown and Keith, 1939; Arensburg, 1991; Franciscus and Churchill, 2002; Gómez-Olivencia et al., 2009). However, this morphological pattern has not yet been quantified geometrically. The specific morphology of the first rib is not only evident from Fig. 1 but also from the quantitative analysis (Figs. 2 and 3; Table 3).

Shape, as inferred from the relationship of TVC and TVA, suggests that Kebara 2 is similar to the adult El Sidrón ribs such as SD-1699+ or also SD-1767. The form space analysis (Fig. 3) also reflects these relations. The second principal component in the comparative ontogenetic analysis clearly demonstrates the straight shaft profile in the first ribs of Neandertals proposed earlier, although those data also indicate some overlap (Gorjanović-Kramberger, 1906; McCown and Keith, 1939; Arensburg, 1991; Franciscus and Churchill, 2002). Such a pattern of straightness, although not as marked, has also been suggested on the basis of linear measurement in ATD6-108, *H. antecessor* (Gómez-Olivencia et al., 2010). In addition, overlap of straight and curved first ribs has been noted in fossils from Krapina (Franciscus and Churchill, 2002).

Comparative Neandertal data about the ribs exist for immature individuals (Heim, 1982; Madre-Dupouy, 1992) but costal ontogenetic series of Neandertal individuals belonging to the same population are not yet available. Thus, the data from the El Sidrón site presented here will provide a reference for immature to adult Neandertals onwards. Clearly, ontogenetic growth changes are not only displayed in the rib outline, which is particularly indicative of overall thorax shape. The rib shaft diameters also increase during ontogeny (Fig. 2). However, the outline data of the first rib further points towards reduced proportions in the upper thorax of Neandertals compared with adult modern humans (see Figs. 2 and 3, and also García Martínez et al., 2014a).

In fact, smaller overall upper rib size (measured as the centroid size at the external curvature) seems to be associated with larger articulations at the heads of the upper ribs compared with lower ones (García Martínez et al., 2014b) and could fit with the increased height of the upper vertebrae (Gómez-Olivencia et al., 2013). It may reflect their shared development (Aoyama et al., 2005) and also common function in the costo-vertebral joints (De Troyer et al., 2005).

Less curved and smaller first ribs, together with greater lower thorax capacities (Franciscus and Churchill, 2002; Gómez-Olivencia et al., 2009; García Martínez et al., 2014a) necessarily imply differences in the shape of the overall rib cage configuration. This could also be inferred from our PLS analysis of morphological covariation between the first ribs and the remaining rib cage (ribs in anatomical connection) in the modern human sample. As suggested by Gorjanović-Kramberger (1906), increased anterior projection of the first ribs, due to their decreased curvature, would accompany a similar anterior projection of the remaining ribs. Extending this argument, one would expect that, if the first ribs are different and their shapes correlated with the rest of the ribs, the entire thorax would be different in Neandertals. This can be assumed because the ribs are connected anatomically by the intercostal soft-tissue matrix, which constrains independent rib shape variation and provides a coordinated muscle action and chest wall movement during respiratory ventilation (De Troyer et al., 2005; West, 2012). Also, the fact that the upper ribs connect directly with the sternum may contribute to coordinated (integrated) and distinctive rib shape variation within the upper thorax, which has been reported for different human species (Schmid et al., 2013; Bastir et al., 2013b).

The PLS analysis (Fig. 4, SOM 1) in modern humans demonstrates a strong correlation between the first rib and the remaining rib cage. These results show two related aspects: 1) the first rib is correlated with the shape of the remaining thorax, and 2) the straightness of the first ribs is correlated mostly with straightness of the ribs of the upper thorax (Fig. 4) and less so within the lower rib cage. These different patterns may be another hint towards morpho-functional differentiation of upper and lower regions of the human thorax (Bastir et al., 2013b, in press).

If for the previously anatomical and morphological reasons (De Troyer et al., 2005; West, 2012; Schmid et al., 2013; Bastir et al., 2013b), a comparable covariation of upper ribs is assumed in modern humans and Neandertals, then rib straightening sensu Gorjanović-Kramberger (1906) would be much more pronounced in the upper thorax than the lower. In fact, straightening of the ribs in the upper thorax is reported by McCown and Keith (1939) for Tabún C1 (rib 2) and by Franciscus and Churchill (2002) comparing Tabún C1 and La Chapelle aux Saints (rib 2, but see Gómez-Olivencia et al., 2009), and also Shanidar rib 6 (Franciscus and Churchill, 2002), at the limit towards the lower thorax.

In the lower thorax of the modern human sample, only slight straightening together with other features can be observed (Fig. 4e,f, SOM 1). Anterior projection is still there but this is produced by an upwards flexion of the sternal extremes for which all segments of the ribs are in the same axial plane. Thus, the upper and lower parts of the rib cage show different morphological covariation patterns with the first ribs.

A separation of the entire rib cage into upper and lower thoracic units also makes sense from a growth perspective. We have shown elsewhere that diverging growth trajectories of the upper and lower thorax likely reflect a different integration of these body parts within the entire skeletal system and body plan (Bastir, 2008; Bastir et al., 2013b). The upper thorax relates to respiration (in thoracic mode) and upper limb function, while the lower thorax relates more to diaphragmatic respiration, sub-thoracic organ

content and locomotion. Furthermore, morpho-functional regionalization of the rib cage into upper and lower parts also emerges from 3D-analysis of the variation of thoracic vertebrae (Bastir et al., in press), but more research is necessary in this direction.

A smaller upper thorax may reflect a developmental trade-off between the needs of the respiratory apparatus and its relation to the shoulder girdle, the upper limbs and their muscles. Differences in humeral morphology of Neandertals and modern humans may be one feature of this different arrangement (Carretero et al., 1997; Rosas et al., submitted). Theoretically, a straighter shape of the first rib could affect the leverage of the scalene muscles and relate to differences in robustness of the insertion marks in modern humans and Neandertals. In turn, a larger lower thorax might relate to climatic adaptations, body-mass related energetics and/or retention of the archaic body plan (Franciscus and Churchill, 2002; Carretero et al., 2004; Churchill, 2006; Gómez-Olivencia et al., 2009). In any case, from a functional point of view, a wider lower thorax likely reflects an increased diaphragmatic contribution to respiration. Future studies on the lower ribs of a larger comparative sample will shed more light on the biological significance and evolution of this important part of the human axial skeleton and trunk.

Acknowledgments

We thank the El Sidrón excavation team, Antoine Balzeau, Alain Froment, Philippe Mennecier, Ofer-Bar Yosef, Bernard Vandermeersch, Baruch Arensburg, and Israel Hershkovitz. We also thank Asier Gómez-Olivencia for discussion and constructive comments on an earlier draft of this manuscript. This project is funded by the Leakey Foundation, and by the Spanish Ministry of Economy and Competitivity: CGL2012-37279 (MB), and CGL2012-36682 (AR). El Sidrón fieldwork is supported by Consejería de Cultura del Principado de Asturias, Grant sponsor: Convenio Universidad de Oviedo-CSIC, Grant number: 060501040023.

Appendix A. Supplementary material

Supplementary material related to this article can be found online at http://dx.doi.org/10.1016/j.jhevol.2014.10.008.

References

Aiello, L., Dean, C., 1990. An Introduction to Human Evolutionary Anatomy. Academic Press Harcourt Brace & Company, London.
Aoyama, H., Mizutani-Koseki, S., Koseki, H., 2005. Three developmental compartments involved in rib formation. Int. J. Dev. Biol. 49, 325–333.
Arensburg, B., 1991. The vertebral column, thoracic cage and hyoid bone. In: Bar Yosef, O., Vandermeersch, B. (Eds.), Le squelette Mousterien de Kebara 2. CNRS, Paris, pp. 125–146.
Bastir, M., 2008. A systems-model for the morphological analysis of integration and modularity in human craniofacial evolution. J. Anthropol. Sci. 86, 37–58.
Bastir, M., Rosas, A., Sheets, D.H., 2005. The morphological integration of the hominoid skull: A Partial Least Squares and PC analysis with morphogenetic implications for European Mid-Pleistocene mandibles. In: Slice, D. (Ed.), Modern Morphometrics in Physical Anthropology. Kluwer Academic/Plenum Publishers, New York, pp. 265–284.
Bastir, M., O'Higgins, P., Rosas, A., 2007. Facial ontogeny in Neandertals and modern humans. Proc. R. Soc. B 274, 1125–1132.
Bastir, M., Rosas, A., Tabernero, A.G., Peña-Melián, A., Estalrrich, A., de la Rasilla, M., Fortea, J., 2010. Comparative morphology and morphometric assessment of the Neandertal occipital remains from the El Sidrón site (Asturias, Spain: years 2000–2008). J. Hum. Evol. 58, 68–78.
Bastir, M., Rosas, A., Gunz, P., Pena-Melian, A., Manzi, G., Harvati, K., Kruszynski, R., Stringer, C., Hublin, J.-J., 2011. Evolution of the base of the brain in highly encephalized human species. Nat. Commun. 2, 588.
Bastir, M., García-Martínez, D., García Tabernero, A., Huguet, R., Barash, A., Recheis, W., de la Rasilla, M., 2013a. A preliminary assessment of the thoracic remains of the El Sidrón Neandertal (Asturias, Spain). In: PESHE (Ed.), 3rd Annual Meeting of the European Society for the Study of Human Evolution, Vienna, p. 38.
Bastir, M., García Martínez, D., Recheis, W., Barash, A., Coquerelle, M., Rios, L., Peña-Melián, Á., García Río, F., O'Higgins, P., 2013b. Differential Growth and Development of the Upper and Lower Human Thorax. PLoS One 8, e75128.
Bastir, M., Higuero, A., Ríos, L., García Martínez, D., 2014. Three-dimensional analysis of sexual dimorphism in human thoracic vertebrae: Implications for the respiratory system and spine morphology. Am. J. Phys. Anthropol. http://dx.doi.org/10.1002/ajpa.22604.
Bogin, B., 1999. Patterns of Human Growth, Second edition. Cambridge University Press, Cambridge.
Carretero, J.M., Lorenzo, C., Arsuaga, J.L., 1997. Clavicles, scapulae and humeri from the Sima de los Huesos site (Sierra de Atapuerca, Spain). J. Hum. Evol. 33, 357–408.
Carretero, J.M., Arsuaga, J.-L., Martinez, I., Quam, R.M., Lorenzo, C., Gracia, A., Ortega, A.I., 2004. Los humanos de la Sima de los Huesos (Sierra de Atapuerca) y la evolucion del cuerpo en el genero *Homo*. In: Baquedano, E. (Ed.), Homenaje a Emiliano Aguirre. Museo Arqueologico Regional, Alcala de Henares, pp. 120–136.
Churchill, S.E., 2006. Bioenergetic perspectives on Neandertal thermoregulatory and activity budgets. In: Harvati, K., Harrison, T. (Eds.), Neandertals Revisited. Springer Verlag, New York, pp. 113–156.
De Troyer, A., Kirkwood, P.A., Wilson, T.A., 2005. Respiratory action of the intercostal muscles. Physiol. Rev. 85, 717–756.
EVAN Society, 2010. ET, Toolkit for Geometric Morphometric Analysis.
Fernández Cascón, B., Estalrrich, A., García-Tabernero, A., García-Vargas, S., Huguet, R., Bastir, M., Santamaría, D., de la Rasilla, M., Fortea, J., 2010. Preparation of the Neandertal remains from the El Sidrón cave (Asturias, Spain). Paleontologia i Evolució 4, 175–182.
Fortea, J., de la Rasilla, M., Martínez, E., Sánchez-Moral, S., Cañaveras, J.C., Cuezva, S., Rosas, A., Soler, V., Julià, R., Torres, T. de, Ortiz, J.E., Castro, J., Badal, E., Altuna, J., Alonso, J., 2003. La Cueva de El Sidrón (Borines, Piloña, Asturias): primeros resultados. Estud. Geol. 59, 159–179.
Franciscus, R.G., Churchill, S.E., 2002. The costal skeleton of Shanidar 3 and a reappraisal of Neandertal thoracic morphology. J. Hum. Evol. 42, 303–356.
García-Martínez, D., Recheis, W., Bastir, M., 2012. The whole and its parts: 3D geometric morphometrics of human thorax evolution. Encuentro de Jovenes Investigadores en Paleontología, Valencia.
García-Martínez, D., Bastir, M., Recheis, W., Barash, A., 2013. Two different barrels for two different primates: 3D geometric morphometrics of sliding semilandmarks of the Hominoidea superfamily thorax. Sociedad Española de Antropología Física, Bilbao, p. 39.
García Martínez, D., Barash, A., Recheis, W., Utrilla, C., Torres Sanchez, I., Garcia Rio, F., Bastir, M., 2014a. On the chest size of Kebara 2. J. Hum. Evol. 70, 69–72.
García Martínez, D., Bastir, M., Estalrrich, A., García Tabernero, A., Huguet, R., Cunha, E., de la Rasilla, M., Rosas, A., 2014b. Preliminary study of the head-neck complex of Neanderthal ribs from the El Sidrón site (Asturias, Spain). In: PESHE (Ed.). Society for the Study of Human Evolution, Florence, p. 76.
Gómez-Olivencia, A., Eaves-Johnson, K.L., Franciscus, R.G., Carretero, J.M., Arsuaga, J.L., 2009. Kebara 2: new insights regarding the most complete Neandertal thorax. J. Hum. Evol. 57, 75–90.
Gómez-Olivencia, A., Carretero, J.M., Lorenzo, C., Arsuaga, J.L., Bermúdez de Castro, J.M., Carbonell, E., 2010. The costal skeleton of *Homo antecessor*: preliminary results. J. Hum. Evol. 59, 620–640.
Gómez-Olivencia, A., Couture-Veschambre, C., Madelaine, S., Maureille, B., 2013. The vertebral column of the Regourdou 1 Neandertal. J. Hum. Evol. 64, 582–607.
Gorjanović-Kramberger, K., 1906. Der diluviale Mensch von Krapina in Kroatien. C. W. Kreidel's Verlag, Wiesbaden.
Gunz, P., Mitteroecker, P., Neubauer, S., Weber, G.W., Bookstein, F.L., 2009. Principles for the virtual reconstruction of hominin crania. J. Hum. Evol. 57, 48–62.
Heim, J.L., 1982. Les Enfants Néandertaliens de La Ferrassie. Masson et Fondation singer Polignac, Paris.
Jellema, L.M., Latimer, B., Walker, A., 1993. The rib cage. In: The Nariokotome *Homo erectus* Skeleton. Harvard University Press, Cambridge, pp. 294–325.
Klingenberg, C.P., 2011. MorphoJ: an integrated software package for geometric morphometrics. Mol. Ecol. Res. 11, 353–357.
Madre-Dupouy, M., 1992. L'enfant du Roc de Marsal. Etude analytique et comparative. Cah. Paléoanthropol. 296.
McCown, T., Keith, A., 1939. The Stone Age of Mount Carmel II: The Fossil Human Remains from the Levalloiso-Mousterian. Clarendon Press, Oxford.
Mitteroecker, P., Gunz, P., Bernhard, M., Schaefer, K., Bookstein, F.L., 2004. Comparison of cranial ontogenetic trajectories among great apes and humans. J. Hum. Evol. 46, 679–698.
O'Higgins, P., 2000. The study of morphological variation in the hominid fossil record: biology, landmarks and geometry. J. Anat. 197, 103–120.
Polychronis, G., Christou, P., Mavragani, M., Halazonetis, D.J., 2013. Geometric morphometric 3D shape analysis and covariation of human mandibular and maxillary first molars. Am. J. Phys. Anthropol. 152, 186–196.
Ríos, L., Cardoso, H.F.V., 2009. Age estimation from stages of union of the vertebral epiphyses of the ribs. Am. J. Phys. Anthropol. 140, 265–274.
Rohlf, F.J., Corti, M., 2000. The use of two-block partial least-squares to study covariation in shape. Syst. Zool. 49, 740–753.
Rosas, A., Martinez-Maza, C., Bastir, M., Garcia-Tabernero, A., Lalueza-Fox, C., Huguet, R., Ortiz, J.E., Julia, R., Soler, V., Torres, T.d., Martinez, E., Cañaveras, J.C., Sanchez-Moral, S., Cuezva, S., Lariol, J., Santamaria, D., de la Rasilla, M., Fortea, J., 2006. Paleobiology and comparative morphology of a late Neandertal sample from El Sidrón, Asturias, Spain. Proc. Natl. Acad. Sci. 103, 19266–19271.

Rosas, A., Estalrrich, A., García-Vargas, S., García-Tabernero, A., Bastir, M., Huguet, R., Peña-Melián, A., 2011. Los fósiles neandertales de la Cueva de El Sidrón. In: de la Rasilla, M., Rosas, A., Cañaveras, J.C., Lalueza-Fox (Eds.), Una investigación interdisciplinar de un grupo neandertal, Excavaciones arqueológicas de Asturias. Monografías I. Gobierno del Principado de Asturias, Oviedo, pp. 81–116.

Rosas, A., Estalrrich, A., García-Tabernero, A., Bastir, M., García-Vargas, S., Sánchez-Meseguer, A., Huguet, R., Lalueza-Fox, C., Peña-Melián, Á., Kranioti, E.F., Santamaría, D., de la Rasilla, M., Fortea, J., 2012. The Neandertals from El Sidrón (Asturias, Spain). Updating of a new sample, Les Néandertaliens d'El Sidrón (Asturies, Espagne). Actualisation d'un nouvel échantillon. L'Anthropologie 116, 57–76.

Rosas, A., Estalrrich, A., García-Vargas, S., García-Tabernero, A., Huguet, R., Lalueza-Fox, C., de la Rasilla, M., 2013. Identification of Neandertal individuals in fragmentary fossil assemblages by means of tooth associations: The case of El Sidrón (Asturias, Spain). C. R. Palevol 12, 279–291.

Rosas, A., Perez-Criado, L., Bastir, M., Estalrrich, A., Huguet, R., García-Tabernero, Pastor, F.A., de la Rasilla, M., 2014. A geometric morphometrics comparative analysis of the Neandertal humeri (epiphyses-fused) from the El Sidron cave site (Asturias, Spain). J. Hum. Evol. (in revision).

Ruff, C., 2002. Variation in human body size and shape. A. Rev. Anthropol. 31, 211–232.

Ruff, C., 2010. Body size and body shape in early hominins – implications of the Gona Pelvis. J. Hum. Evol. 58, 166–178.

Sawyer, G.J., Maley, B., 2005. Neandertal reconstructed. Anat. Rec. 283B, 23–31.

Schmid, P., Churchill, S.E., Nalla, S., Weissen, E., Carlson, K.J., de Ruiter, D.J., Berger, L.R., 2013. Mosaic morphology in the thorax of *Australopithecus sediba*. Science 340.

StatSoft, I., 1999. STATISTICA for Windows, 99 edition. StatSoft, Tulsa, OK 74104.

Spalteholz, W., 1970. Atlas de Anatomía Humana, Fifth edition. Labor S.A., Barcelona.

Tompkins, R.L., Trinkaus, E., 1987. La Ferrassie 6 and the development of Neandertal pubic morphology. Am. J. Phys. Anthropol. 73, 233–239.

Trinkaus, E., 1984. Neandertal pubic morphology and gestation length. Curr. Anthropol. 25, 509–514.

West, J.B., 2012. Respiratory Physiology: The Essentials, Ninth edition. Wolters Kluwer, Lippincott Williams & Williams, Philadelphia.

White, T.D., Black, M.T., Folkens, P.A., 2011. Human Osteology, Third edition. Academic Press, New York.

Journal of Human Evolution xxx (2017) 1–15

Contents lists available at ScienceDirect

Journal of Human Evolution

journal homepage: www.elsevier.com/locate/jhevol

Three-dimensional morphometrics of thoracic vertebrae in Neandertals and the fossil evidence from El Sidrón (Asturias, Northern Spain)

Markus Bastir [a, *, 1], Daniel García Martínez [a, 1], Luis Rios [a], Antonio Higuero [b], Alon Barash [c], Sandra Martelli [d], Antonio García Tabernero [a], Almudena Estalrrich [a], Rosa Huguet [a, e], Marco de la Rasilla [f], Antonio Rosas [a]

[a] Paleoanthropology Group, Museo Nacional de Ciencias Naturales (CSIC), J. G. Abascal 2, 28006, Madrid, Spain
[b] Universidad de Cantabria, Instituto Internacional de Investigaciones Prehistóricas de Cantabria (IIIPC), Avda. de los Castros, s/n, E-39005, Santander, Cantabria, Spain
[c] Faculty of Medicine Galilee, Bar Ilan University, Henrietta Szold, 8 P.O.B 1589, 1311502, Zefat, Israel
[d] Department Of Cell And Developmental Biology, University College London, WC1E 6BT, London, United Kingdom
[e] Institut Català de Paleoecologia Humana i Evolució Social (IPHES), Zona Educacional 4 – Campus Sescelades URV (Edifici W3), 43007, Tarragona, Spain
[f] Department of History, University of Oviedo, Campus del Milán C/ Teniente Alfonso Martínez s/n, E-33011, Oviedo, Spain

ARTICLE INFO

Article history:
Received 19 March 2015
Accepted 14 March 2017
Available online xxx

Keywords:
Thoracic spine
Axial skeleton
Neandertals
Respiratory apparatus
Geometric morphometrics

ABSTRACT

Well-preserved thoracic vertebrae of Neandertals are rare. However, such fossils are important as their three-dimensional (3D) spatial configuration can contribute to the understanding of the size and shape of the thoracic spine and the entire thorax. This is because the vertebral body and transverse processes provide the articulation and attachment sites for the ribs. Dorsal orientation of the transverse processes relative to the vertebral body also rotates the attached ribs in a way that could affect thorax width. Previous research indicates possible evidence for greater dorsal orientation of the transverse processes and small vertebral body heights in Neandertals, but their 3D vertebral structure has not yet been addressed. Here we present 15 new vertebral remains from the El Sidrón Neandertals (Asturias, Northern Spain) and used 3D geometric morphometrics to address the above issues by comparing two particularly well-preserved El Sidrón remains (SD-1619, SD-1641) with thoracic vertebrae from other Neandertals and a sample of anatomically modern humans. Centroid sizes of El Sidrón vertebrae are within the human range. Neandertals have larger T1 and probably also T2. The El Sidrón vertebrae are similar in 3D shape to those of other Neandertals, which differ from *Homo sapiens* particularly in central-lower regions (T6–T10) of the thoracic spine. Differences include more dorsally and cranially oriented transverse processes, less caudally oriented spinous processes, and vertebral bodies that are anteroposteriorly and craniocaudally short. The results fit with current reconstructions of Neandertal thorax morphology.

1. Introduction

Recent research on fossil ribs has provided solid evidence for capacious dimensions of the Neandertal thorax (Franciscus and Churchill, 2002; Gómez-Olivencia et al., 2009; García-Martínez et al., 2014a, in revision; Bastir et al., 2015a). A recent three-dimensional (3D) assessment of rib size in Kebara 2 has shown that the ribs close to the diaphragm (ribs at levels 6–9) are larger than in modern humans, which is valid both absolutely as well as relative to body size (e.g., estimates of stature, García-Martínez et al., 2014a). Also, Neandertal rib shape differs from that of modern humans in a way that contributes to larger thorax capacity. Several researchers have observed an elongated midshaft of the ribs and also reduced torsion, suggesting a deep and wide chest in Neandertals (Franciscus and Churchill, 2002; Gómez-Olivencia et al., 2009; Bastir et al., 2012, 2015a; García-Martínez et al., in revision).

The large chest is a characteristic feature of the short and wide shape of the stocky Neandertal body (Sawyer and Maley, 2005).

* Corresponding author.
E-mail address: mbastir@mncn.csic.es (M. Bastir).
[1] These authors contributed equally to this manuscript.

http://dx.doi.org/10.1016/j.jhevol.2017.03.008
0047-2484/

Estimated average stature in Neandertals is low (165.9 cm) relative to their body mass estimates, which are comparatively high (72 kg) and associated with an estimated daily energy expenditure that is almost twice as high as in anatomically modern humans adapted to cold environments (Neandertal males: 5500 kcal d^{-1}; Inuit males: just below 3000 kcal d^{-1}; Churchill, 2014). In relation to this, the large thorax of Neandertals has been associated functionally with elevated oxygen consumption (Steegmann et al., 2002; Churchill, 2006, 2014; Bastir, 2008).

In this sense, the large Neandertal thorax is the postcranial part of an overall large respiratory system, which is also reflected by the dimensions of their nasal and pharyngeal airways (Franciscus, 1999; Rosas et al., 2006; Bastir, 2008, in press; Bastir and Rosas, 2011, 2013, 2016). Thus, the craniofacial and postcranial parts together reflect the functional anatomy of a respiratory apparatus expected for a high-energy consuming and heavy-bodied hominin (Rosas et al., 2006a; Bastir, 2008; Churchill, 2014). However, hypotheses on the size and shape of the Neandertal chest (i.e., thorax capacity) cannot be addressed on the basis of rib morphology alone. This is because the rib cage is an anatomical complex, composed by ribs that are dorsally connected with the thoracic vertebrae at the costo-vertebral and -transverse joints, and ventrally with the sternum by the costosternal cartilages. Consequently, the size and shape of the thorax as well as its capacity depend on the size and shape of the ribs (Franciscus and Churchill, 2002; Gómez-Olivencia et al., 2009; García-Martínez et al., 2014a; Bastir et al., 2015a), the sternum (Gómez-Olivencia et al., 2012), and on the morphology of the thoracic vertebrae (Bastir et al., 2015b).

It has been suggested that greater dorsal orientation of the transverse processes together with proximal rib curvature increase the invagination of the thoracic spine within the ribcage in relation to evolutionary changes in locomotor function in early hominins (Jellema et al., 1993; Latimer and Ward, 1993; Ward et al., 2012). However, transverse process orientation could also be important for respiratory function. In *Homo sapiens*, the thoracic capacity of males is greater than in females, both absolutely and relative to stature (Silbernagl and Despopoulos, 1991; Bellemare et al., 2003, 2006; García-Martínez et al., 2016a). It has been shown recently that the larger male thoracic capacity can be related to a greater dorsal orientation of the transverse processes of their thoracic vertebrae, particularly the lower ones (T6–T9; Bastir et al., 2014). A more dorsal orientation of the rib attachment at the transverse processes rotates a given pair of ribs into a position that increases the medio-lateral diameters of the rib cage (Jellema et al., 1993; Latimer and Ward, 1993; Ward et al., 2012; Bastir et al., 2014), and when combined with longer ribs, greater dorsal orientation of the transverse process also increases the capacity of the thorax. Small angular variations could thus have large effects on thorax morphology. This geometric effect, together with the fact that Neandertal ribs are longer, particularly in the middle and lower thorax (Franciscus and Churchill, 2002; Gómez-Olivencia et al., 2009; García-Martínez et al., 2014a), allows us to establish the hypothesis that the greater thorax capacity in Neandertals is not only the result of rib elongation (Franciscus and Churchill, 2002; Gómez-Olivencia et al., 2009; García-Martínez et al., 2014a), but also of a greater dorsal orientation of the rib attachments at the transverse processes of thoracic vertebrae (Bastir et al., 2015b).

Arensburg (1991) and Been et al. (2010, their Fig. 3) already show illustrations and data suggesting strongly dorsally oriented transverse processes in thoracic vertebrae of the Kebara 2 Neandertal. Similar features can be observed in illustrations of other recent descriptions of thoracic vertebrae in Neandertals of Regourdou 1, La Chapelle-aux-Saints 1, or La Ferrassie 1 (Gómez-Olivencia et al., 2013a; Gómez-Olivencia, 2013a,b). These studies suggested further subtle and variable differences, such as greater laminae heights in the first and second thoracic vertebrae in La Ferrassie 1, shorter spinous processes in La Ferrassie 1 and Kebara 2 (Gómez-Olivencia, 2013a), and smaller median heights in some vertebral bodies (T7, T10, T11) of Regourdou 1 (Gómez-Olivencia et al., 2013a). Interestingly, median vertebral body height of T7 is similarly low in La-Chapelle-aux-Saints 1 and Kebara 2, and outside the minimum of the human reference sample as reported by Gómez-Olivencia et al. (2013a, their Table 5).

On the basis of this previous work, it has been proposed that "the overall vertebral size of the modern comparative samples are similar to that of the Neandertal male sample and that the differences found in only some of the variables suggest true morphological difference" (Gómez-Olivencia et al., 2013a:603). There is thus reason to expect differences between anatomically modern humans and Neandertals in their 3D vertebral architecture, that is, shape but not in size. However, 3D variation in thoracic vertebrae of other Neandertals has yet only been addressed in a preliminary way (Bastir et al., 2015b).

The Neandertal site from El Sidrón (Asturias, Northern Spain) dated to 49 ka (Rosas et al., 2006b, 2012) can potentially contribute to these questions. Over the past years, 15 fossil thoracic vertebral elements (Figs. 1 and 2) have been recovered at this site. These remains provide information that is relevant in the context outlined above, and some of these fossils (SD-1619, SD-1641, and Fig. 1) are complete enough to include them in comparative 3D geometric morphometric (3D-GM) analysis.

There are two aims to this study. First, we present and describe thoracic fossil remains of the El Sidrón Neandertal site. Second, a 3D-GM analysis is carried out addressing the hypothesis that the orientation of the transverse processes and vertebral body heights are involved in overall differences of 3D shape in Neandertal thoracic vertebrae when compared with modern humans.

2. Material and methods

The thoracic vertebral fossils from the El Sidrón site (Asturias, Spain) constitute a sample that ranges from fairly well preserved and undistorted vertebrae (Fig. 1) to more fragmented elements (Fig. 2). Following previous work on the Neandertal spine (Gómez-Olivencia et al., 2013a; Gómez-Olivencia, 2013a,b), the anatomical determination of the El Sidrón thoracic vertebrae relied on comparisons with complete modern human thoracic spines. Specifically, determination was based on observations of changes in shape, orientation, and size of different vertebral structures (e.g., transverse processes, articular facets, and demifacets) along the spine. We also followed previously used terminology for descriptions and anatomical determination of the Neandertal spine (Gómez-Olivencia et al., 2013a; Gómez-Olivencia, 2013a,b).

The first step in the determination process was to divide the vertebral remains into four groups based on degree of completeness: almost complete vertebrae (including parts of the arches, processes, and body of the same element), fragments including transverse process, fragments including laminae, and fragments of vertebral body. Each group was described separately.

The metric description followed measurements used and described by Gómez-Olivencia et al. (2013a). The age at death was only estimated through assessment of the degree of maturation of the thoracic vertebral epiphyses, following data for modern humans provided by Cardoso and Ríos (2011).

For the 3D-GM analysis, the comparative human data were obtained from 239 vertebrae from complete vertebral columns of 24 identified individuals (12 males and 12 females, one female lacked a third thoracic vertebra), ranging in age from 20 to 42 years. The bones belong to the identified skeletal collection curated at the School of Legal Medicine, Universidad Complutense de Madrid. The

Please cite this article in press as: Bastir, M., et al., Three-dimensional morphometrics of thoracic vertebrae in Neandertals and the fossil evidence from El Sidrón (Asturias, Northern Spain), Journal of Human Evolution (2017), http://dx.doi.org/10.1016/j.jhevol.2017.03.008

Figure 1. The two most complete thoracic vertebrae from El Sidrón. On the left, cranial (top) and lateral left (bottom) views of SD-1619 are presented. In this vertebra, identified as T6–T7, the dorsal orientation of the transverse processes, together with the sagittal orientation of the facets for the rib tubercle, can be observed (see text for discussion of these features). On the right, cranial (top) and lateral right (bottom) views of SD-1641 are presented. In this vertebra, identified as T3–T4, there is lack of fusion of the epiphyses of the transverse processes, but a sagittal orientation of the immature surfaces on the tip of the transverse processes can be observed (especially on the right side). Scale bar equals 10 mm.

completeness and preservation of the skeletons from this collection is excellent and only the youngest skeletons were selected for study in order to avoid vertebral degenerative joint disease. Cases with other pathological conditions affecting the spine were also excluded. Only the first 10 thoracic vertebrae were selected for comparative study (Jellema et al., 1993; Latimer and Ward, 1993), as well as in order to collect the same landmarks in all vertebrae, including those located at the transverse costal facets, the presence of which at T11 and T12 is highly variable (Ríos and Cardoso, 2009; Cardoso and Ríos, 2011).

2.1. Landmark measurements

Forty-six 3D landmarks were measured per vertebra with a Microscribe G2 digitizer following the definitions of Bastir et al. (2014) that are depicted in Figure 3. Despite the excellent quality and preservation state of this osteological collection, a few landmarks were missing and estimated using multivariate regression methods as described in Bastir et al. (2014).

Measurements of the Neandertal vertebrae sample were obtained from 3D reconstructions of computed tomography (CT) scans of the original fossils. Medical CT-scans of the Kebara 2 male Neandertal were produced at the Sackler Faculty of Medicine of Tel Aviv University (General Electric, Discovery CT750 HD, 120 kV, 1.25 mm slice thickness, 1 mm overlap) and that of La Chapelle-aux-Saints 1 and La Ferrassie 1 were provided by the Muséum National d'Histoire Naturelle (Paris; Philips iCT128; 120 kV; 0.625 mm slice thickness). Three-dimensional landmarks of the El Sidrón SD-1619 and SD-1641 vertebrae (Fig. 1) were measured on virtual models obtained by high-resolution surface scans. While Kebara 2, La Chapelle-aux-Saints 1, and La Ferrassie 1 individuals are assumed to be males (Arensburg, 1991; Gómez-Olivencia, 2013a,b), the El Sidrón vertebrae were not assigned to a given sex.

Viewbox 4.0 software (http://www.dhal.com) was used to digitize 3D landmarks on virtual models of the Neandertal thoracic vertebrae. The modern human reference sample was measured on real bones and the associated intra-observer error is reported in Bastir et al. (2014). The fossil samples were measured using virtual 3D models obtained from CT and surface scans. Landmarks measurements on real bone and 3D models based on clinical CT scans are comparable in geometric morphometrics as shown previously (Rosas et al., 2016). The comparability of landmark measurements taken on real bones and on 3D models obtained from surface scans was assessed here by producing a surface scan of one of the modern human vertebrae (T8 of individual Acc-62) that was physically digitized using a Microscribe G2 digitizer in Bastir et al. (2014) and by re-measuring the same 3D landmarks repeatedly on the virtual model of this bone.

Although nine out of 12 thoracic vertebrae are preserved in La Chapelle-aux-Saints 1 (Gómez-Olivencia, 2013b) only at levels T1, T2, and T8–T10, the overall geometry was considered complete enough, preserving parts of the body, neural arches, and processes, allowing for reasonable reconstructions of missing landmarks and 3D-GM analysis (see Supplementary Online Material [SOM] Table S1). Also in La Ferrassie 1, only vertebrae of the cranial part of the thoracic spine (T1–T3) could be analyzed by 3D-GM despite preserving remains from T1–T4, T12, and five elements between T5 and T9 (Gómez-Olivencia, 2013a). Thus, most fossils required estimation of some missing landmarks except T7 and T9 of Kebara 2, which provided all structures for landmark measurements. The

Please cite this article in press as: Bastir, M., et al., Three-dimensional morphometrics of thoracic vertebrae in Neandertals and the fossil evidence from El Sidrón (Asturias, Northern Spain), Journal of Human Evolution (2017), http://dx.doi.org/10.1016/j.jhevol.2017.03.008

Figure 2. Vertebral fragments from El Sidrón; see Tables 1 and 2 for vertebral number identification. Top: Fragments with transverse process. The five fragments correspond to the right side and are presented in cranial view, ordered from T1 (SD-719) on the left to T5–T7 (SD-1050b) on the right. The dorsal orientation of the transverse processes and the sagittal orientation of the transverse costal facets can be observed. Middle: Fragments including lamina. The five fragments are presented in ventral view, ordered from T1 (SD-1446) on the left to T8–T9 (SD-1657) on the right. Bottom: Fragments of vertebral body. The three fragments are presented in two views, cranial and lateral right, ordered from T1 (SD-1932) on the left to T2–T4 (SD-1679) on the right. Scale bar equals 10 mm.

missing structures and landmarks of the fossil vertebrae and the methods of their estimations are listed in SOM Table S1. Following Gunz et al. (2009), we first exploited the symmetry of the object to estimate missing symmetric structures when one of the antimeres was preserved (transverse processes, demifacets, articular processes, or parts of the vertebral body). Specifically, we used reflected relabeling in order to estimate these missing symmetric structures by data of the same specimen (Mardia et al., 2000; Gunz et al., 2009). Reflected relabeling required all vertebrae of the entire sample to be symmetrized. For the estimation of unilateral missing landmarks at the mid-sagittal plane (e.g., spinous process and landmarks at the mid-sagittal plane of the vertebral body), we used a reference-based approach (Gunz et al., 2009). Thin plate spline (TPS) interpolations were applied to estimate missing landmarks with the most similar Neandertal vertebra (of the same level of another individual) as a source whenever possible. In absence of conspecific specimens from the same level, we used the mean shape of the corresponding modern human vertebral level as a source for the TPS estimation. This leads to statistically conservative reconstructions when compared with anatomically modern human data.

To address potential uncertainty in the positional assignment on the basis of morphological criteria of SD-1619 (T6 or T7) and SD-1641 (T3 or T4), these vertebrae were reconstructed twice. In the first reconstruction the fossils were reconstructed as if they belonged to level 3 for SD-1641 (labeled SD-1641-T3) and to level 6 for SD-1619 (labeled SD-1619-T6). In a second set of reconstructions we assumed level 4 for SD-1641 (labeled SD-1641-T4) and level 7 for SD-1619 (labeled SD-1619-T7; SOM Table S1).

2.2. Statistical analyses

Shape data were extracted as shape coordinates after generalized Procrustes registration and size was obtained as centroid size, the square root of the summed squared distances between the landmarks and their centroid (O'Higgins, 2000; Zelditch et al., 2012). Intra-observer error was tested by repeated landmark measurements on virtual models in a principal components analysis (PCA) and further analyzed by comparisons of Procrustes distances among these repeated measurements.

The Neandertal centroid sizes were compared with the 95% confidence intervals of the modern human males and of females separately. Shape data were analyzed first by a PCA of levels T3–T4 for comparisons with SD-1641-T3 and SD-1641-T4 and of levels T6–T7 for analysis of SD-1619-T6 and of SD-1619-T7. Then a PCA was performed on all levels between T3 and T7 to investigate the El Sidrón vertebrae with respect to changes in seriality. All PCAs were also subjected to regression analysis to statistically address the amount of variance explained by seriality (1000 permutations). Both quantitative reconstructions (SD-1619-T6 and SD-1619-T7; SD-1641-T3 and SD-1641-T4) were included simultaneously in all analyses.

Please cite this article in press as: Bastir, M., et al., Three-dimensional morphometrics of thoracic vertebrae in Neandertals and the fossil evidence from El Sidrón (Asturias, Northern Spain), Journal of Human Evolution (2017), http://dx.doi.org/10.1016/j.jhevol.2017.03.008

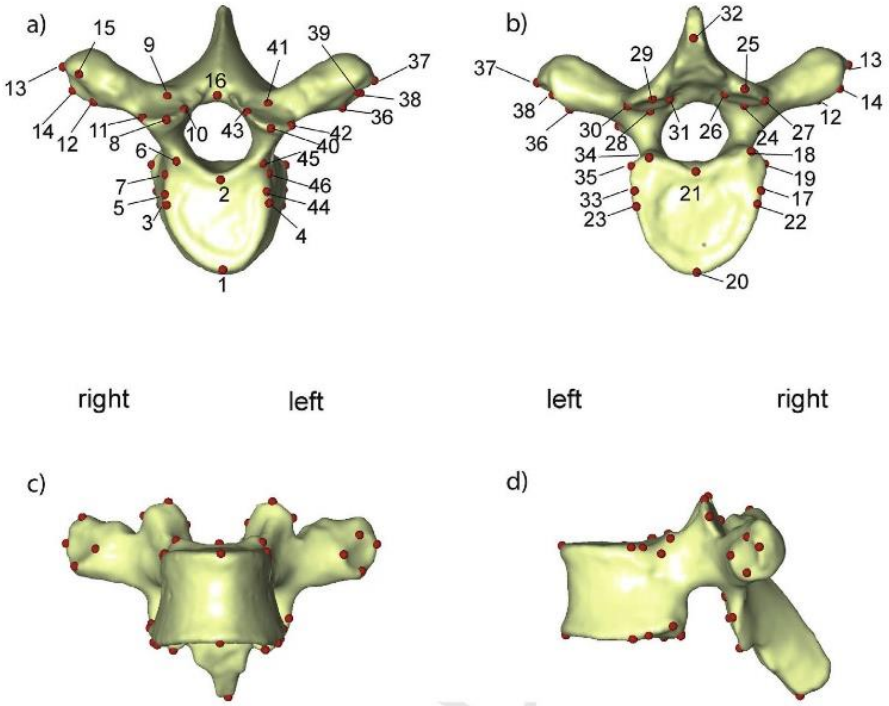

Figure 3. Thoracic vertebra and 3D landmarks as per Bastir et al. (2014). a) Cranial view, b) caudal view, c) frontal view, and d) left lateral view.

Finally, we used permutation tests ($N = 1000$) to assess mean shape differences between thoracic levels T1 and T10 in Neandertals and in modern human males. Mean shape differences were quantified as Procrustes distances, defined as the square root of the summed square interlandmark distances after Procrustes registration (O'Higgins, 2000; Zelditch et al., 2012), at each vertebral level from T1 to T10. All shape analyses were carried out in MorphoJ-software (Klingenberg, 2011). EVAN Toolkit software (EVAN-Society, 2010) was used for 3D visualizations.

3. Results

3.1. Descriptive morphology and comparative analysis of the thoracic vertebral remains of El Sidrón

The 15 thoracic vertebral specimens from El Sidrón represent 10 different vertebrae. This number was estimated by considering those specimens with preservation of overlapping regions from the right transverse process, pedicle, and dorsolateral corner of the body (SD-022, SD-719, SD-1050b, SD-1228, SD-1619, SD-1641, SD-1657, SD-1679, SD-1697, SD-1932). The estimation of the number of individuals represented by these vertebrae was based on the maturation state of the epiphyseal rings from the vertebral bodies and of the epiphyses from the tip of the transverse processes (Cardoso and Ríos, 2011). Complete fusion of the epiphyses from the transverse process was observed in five cases (SD-719, SD-1228, SD-022, SD-1050b, SD-1619), while absence of that epiphysis was observed in two cases (SD-1641, SD-1697), an incompatible maturation state within a single spine resulting in a minimum number of two individuals. Almost complete vertebrae are shown in Figure 1. Fragments including transverse process, fragments including lamina, and fragments of vertebral body are depicted in Figure 2. A metric study of the two most complete vertebrae (SD-1619, SD-1679) and of the rest of the vertebral fragments is presented in Tables 1 and 2, alongside age-at-death estimations based on thoracic epiphyses.

3.2. Vertebrae preserving body, neural arches, and processes

3.2.1. SD-1619 (Fig. 1) Almost complete vertebra, with postmortem absence of the upper left articular facet, the spinous process, and the caudal third of both lower articular facets. Both transverse processes are horizontal (their longitudinal axes are located in the transverse plane) and their cranial edges are located below the caudal edges of the upper right articular facets. The cranio-caudal diameter of both transverse processes is similar along their lengths. The outline of the cranial edges of both laminae presents a U shape with a horizontal plateau at the midline. In the vertebral body, both cranial demifacets are almost completely separated from the cranial body surface and are located on the lateral surface of the pedicles. Their shape is dorso-ventrally elongated. Both lower costal demifacets are almost completely separated from the caudal body surface. The vertebral body and endplate surfaces are intermediate in size, considering size variation within a modern human thoracic spine from T1 to T12. In cranial view, on the left side of the body, a clear aortic impression is present. Comparison of these features with modern human spines suggests an identification of this vertebra as T6–T7. The epiphyses from the transverse and spinous processes are completely fused, but the cranial and caudal epiphyseal rings are in active fusion. The cranial vertebral endplate presents a semicircular defect in its dorsal third.

3.2.2. SD-1641 (Fig. 1) Almost complete vertebra, with postmortem absence of the ventral half of the vertebral body and the tip of the spinous process. Both transverse processes are cranially oriented (especially the right one), with their cranial edges above the caudal edges of the upper articular facets. The cranio-caudal diameter of both transverse processes is larger at the lateral extreme than at the base. The outline of the cranial edges of both laminae presents a U shape. Both superior demifacets are lateral extensions of the cranial body surface and do not reach the pedicles in their most dorsal projection. Both inferior demifacets

Table 1
Raw dimensions (in mm) from the two most complete vertebrae from El Sidrón, following the measurements described by Gómez-Olivencia et al. (2013a).[a]

Measurement	SD-1619	SD-1641
Identification	T6–T7	T3–T4
Age estimation (years)	14–27	≤17
Maximum transverse diameter (MaxTrDi)	58.53	55.99
Superior transverse diameter (SupTrDi)	27.52	31.19
Inferior transverse diameter (ITrDi)	32.14	30.79
Canal dorsoventral diameter (M10)	14.96	14.41
Canal transverse diameter (M11)	14.86	14.31
Body ventral craniocaudal diameter (M1)	20.88	–
Body dorsal craniocaudal diameter (M2)	21.91	17.66
Body median craniocaudal diameter (M3)	18.39	(15.29)
Body superior dorsoventral diameter (M4)	25.36	–
Body inferior dorsoventral diameter (M5)	26.69	–
Body superior transverse diameter (M7)	29.57	–
Body inferior transverse diameter (M8)	32.53	(29.5)
Pedicle craniocaudal diameter (PedCrCdDi)	11.25/11.04	11.03/11.37
Pedicle transverse diameter (PedTrDi)	5.80/6.79	6.26/5.89
Articular pillar bi-articular diameter (BiArtDi)	–/–	31.25/30.25
Transverse process maximum length (TrPrMaxLe)	29.25/30.74	26.28/25.74
Upper articular facet sagittal diameter (UFaSgDi)	13.97/–	11.05/–
Upper articular facet transverse diameter (UFaTrDi)	8.12/–	10.63/10.45
Lower articular facet sagittal diameter (LwFaTrDi)	–/–	9.1/10.14
Lower articular facet transverse diameter (LwFaTrDi)	9.26/9.78	10.45/11.18
Laminae craniocaudal diameter (LamCrCdDi)	–/–	18.19/17.22
Laminae thickness (LamTh)	7.3/7.27	6.4/6.59

[a] For age estimation, the degree of fusion of the vertebral epiphyses from Cardoso and Ríos (2011) was used. Note that SD-1641 is an immature vertebra lacking fusion of cranial and caudal epiphyseal rings, and the epiphyses of both transverse processes. In comparison with values from fully mature vertebrae, measurements from these vertebrae (especially those including the body and transverse processes) can be considered an underestimation of their respective adult values. Values between parentheses are estimates. Cells that contain two entries are for the right and left sides (right/left). M = Martin number.

Table 2
Raw dimensions (in mm) from the vertebral fragments from El Sidrón, following the measurements described by Gómez-Olivencia et al. (2013a).[a]

Measurement	SD-1428	SD-1932	SD-719	SD-2222	SD-1446	SD-456	SD-1228	SD-1679	SD-1697	SD-022	SD-147	SD-1050b	SD-1657
Identification	T1	T1	T1	T1–T2	T1–T2	T1–T4	T2–T3	T2–T4	T3–T4	T4–T6	T4–T9	T5–T7	T8–T9
Age (years)	≥18	14–21	≥17	≤21	–	–	≥15	15–24	≤17	≥15	–	14–27	–
M1	–	–	–	–	–	–	–	18.37[b]	–	–	–	–	–
M3	–	–	–	–	–	–	–	16.49	–	–	–	–	–
PedCrCdDi	–/–	–/–	–/–	–/–	–/–	–/–	–/–	11.22/–	–	11.94/–	–/–	11.8/–	14.73/–
PedTrDi	–/–	–/–	–/–	–/–	–/–	–/–	–/–	7/–	6.5/–	7.07/–	–/–	6.6/–	7.6/–
BiArtDi	–/–	–/–	–/–	–/29.97	–/–	–/–	–/–	–/–	32.94/–	–/–	–/–	–/–	38.13/–
TrPrMaxLe	–/–	–/–	–/–	–/–	–/–	–/–	26.63/–	–/–	26.82/–	30.72/–	–/–	(31.8)/–	–/–
UFaSgDi	–/–	–/–	–/–	–/13	–/–	–/–	–/–	–/–	13.9/–	12.78/–	–/–	11.85/–	13.27/–
UFaTrDi	–/–	–/–	–/–	–/14	–/–	–/–	–/–	(9.34)/–	12.81/–	11.19/–	–/–	10.47/–	9.33/–
LwFaTrDi	–/–	–/–	11.41/–	–/13.83	–/14.19	–/–	11.18/–	–/–	12.39/–	–/–	–/–	–/–	13.28/–
LwFaTrDi	–/–	–/–	11.84/–	–/13.46	–/15.17	–/–	10.59/–	–/–	12.27/–	–/–	–/–	–/–	12.08/–
LamCrCdDi	–/–	–/–	–/–	–/–	18.63	17.69	18.9	–/–	17.23	–/–	–/–	–/–	19.63
LamTh	–/–	–/–	7.05	–/–	6.72	5.69	5.56	–/–	5.83/5.71	–/–	–/–	–/–	5.86

[a] For age estimation, information from Cardoso and Ríos (2011) was used. Values between parentheses are estimates. Cells that contain two entries are for the right and left sides (right/left).
[b] The caudal epiphyseal ring presents active fusion, while the cranial epiphyseal ring is absent. Abbreviations defined in Table 1.

are cranio-lateral extensions of the caudal body surface. Comparison of these features with modern human spines suggests an identification of this vertebra as T3–T4. There is absence of fusion of the epiphyses from the transverse processes and cranial and caudal epiphyseal rings.

3.3. Fragments including transverse process

3.3.1. SD-719 (Fig. 2) Fragment consisting of the caudal part of the root and complete dorsal half of the spinous process, the right lamina with the lower articular facet, and most of the right transverse process. The transverse process is cranially oriented, as can be observed by the obtuse angle formed by its caudal edge and the lateral edge of the lamina (higher than in SD-1228). The lower articular facet is horizontally elongated. The spinous process projects horizontally with very limited caudal projection. There is almost no caudal extension of the lamina beyond the caudal edge of the lower articular facet. Comparison of these features with modern human spines suggests an identification of this vertebra as T1. The epiphyses of the right transverse process and the spinous process are completely fused.

3.3.2. SD-1228 (Fig. 2) Fragment consisting of the base of the spinous process, the right lamina and complete lower articular facet, caudal portion of the upper articular facet, right transverse process, and the base of the right pedicle. The transverse process is cranially oriented and above the caudal edge of the upper articular facet. The transverse process is projected more ventrally in comparison, for instance, with SD-1619. The cranio-caudal diameter of the transverse process is larger in the lateral extreme than at its

Please cite this article in press as: Bastir, M., et al., Three-dimensional morphometrics of thoracic vertebrae in Neandertals and the fossil evidence from El Sidrón (Asturias, Northern Spain), Journal of Human Evolution (2017), http://dx.doi.org/10.1016/j.jhevol.2017.03.008

base. The outline of the cranial edge of the left lamina presents a U shape. Comparison of these features with modern human spines suggests an identification of this vertebra as T2–T3. The epiphysis of the right transverse process is completely fused.

3.3.3. SD-1697 (Fig. 2) Fragment consisting of the right transverse process, right lamina, right upper and lower articular facets, dorsal half of the right pedicle, root of the spinous process, and medial portion of the left lamina. The transverse process is horizontal and its cranial edge is above the caudal edge of the upper articular facet. The cranio-caudal diameter of the transverse process is larger at the lateral extreme than at the base. The outline of the cranial edges of both laminae presents a U shape, with a horizontal plateau at the midline. Comparison of these features with modern human spines suggests an identification of this vertebra as T3–T4. There is lack of fusion of the epiphysis of the right transverse process.

3.3.4. SD-022 (Fig. 2) Fragment consisting of a complete right transverse process, right upper articular facet, most of the right pedicle, and the right dorso-lateral corner of the cranial vertebral body surface. The transverse process is cranially oriented, with its cranial edge above the caudal edge of the upper articular facet. The cranio-caudal diameter of the transverse process is larger at the extreme than at the base. The upper articular facet is horizontally elongated. The upper demifacet is a lateral extension of the cranial vertebral body surface with a clear dorsal projection, positioning the demifacet in the pedicle. Comparison of these features with modern human spines suggests an identification of this vertebra as T4–T6. The epiphysis of the right transverse process is completely fused, while the fragment of cranial epiphyseal ring is scored as active fusion/recent fusion.

3.3.5. SD-1050b (Fig. 2) Fragment consisting of an almost complete right transverse process, right upper articular facet, most of the right pedicle, and the right dorso-lateral corner of the cranial vertebral body surface. The orientation of the transverse process cannot be precisely described, but a horizontal projection above the level of the caudal edge of the upper articular facet is suggested. The cranio-caudal diameter of the transverse process is similar along its length. The upper demifacet is a lateral extension of the cranial vertebral body surface with a clear dorsal projection, positioning the demifacet in the pedicle. Comparison of these features with modern human spines suggests an identification of this vertebra as T5–T7. The epiphysis of the right transverse process is completely fused, while the fragment of epiphyseal ring is in active fusion. The dorso-ventral diameter or thickness of the transverse process is clearly smaller in comparison with the dimensions of the transverse processes of the other vertebrae from El Sidrón.

3.4. Fragments including lamina

3.4.1. SD-1446 (Fig. 2) Fragment consisting of the lateral part of the left lamina and the left lower articular facet. The preserved cranial edge of the lamina indicates a clear U shape outline. The shape of the articular facet is horizontally elongated with triangular shape. Comparison of these features with modern human spines suggests an identification of this vertebra as T1–T2, possibly T1.

3.4.2. SD-2222 (Fig. 2) Fragment consisting of the upper and lower left articular facets, the base of both the left lamina and pedicle, and the ventral half of the left transverse process. The cranial edge of the transverse process contacts the upper articular facet in its cranial third. The shape of both preserved upper and lower articular facets is horizontally elongated with triangular shape. Comparison of these features with modern human spines suggests an identification of this vertebra as T1–T2, possibly T1. The costal facet of the left transverse process is partially preserved.

3.4.3. SD-456 (Fig. 2) Fragment consisting of the root of the spinous process and the right lamina, with the medial third of the lower articular facet. The spinous process is horizontally oriented, with limited caudal extension of the lamina beyond the caudal border of the lower articular facet. Comparison of these features with modern human spines suggests a position of this fragment within the upper third of the thoracic spine (T1–T4).

3.4.4. SD-147 (Fig. 2) Fragment consisting of the left upper articular facet and most of the left pedicle. The cranial edge of the transverse process is inserted below the caudal edge of the upper articular facet. The preserved portion of the left upper demifacet is located on the lateral surface of the pedicle. Comparison of these features with modern human spines suggests a position of this fragment as middle thoracic, T4–T9.

3.4.5. SD-1657 (Fig. 2) Partially preserved neural arch consisting of the medial part of the left lamina, root of the spinous process, complete right lamina with upper and lower articular facets, base of the right transverse process, and part of the right pedicle. At its base, the cranial edge of the right transverse process is located below the caudal-most edge of the upper articular facet, suggesting a horizontal orientation of the transverse process. The transverse process is projected more dorsally in comparison, for instance, with SD-1619. The outline of the cranial edges of both laminae presents a V shape. The upper demifacet connects with the cranial vertebral body surface but it is located dorsally, on the lateral surface of the pedicle, and its shape is cranio-caudally elongated. Comparison of these features with modern human spines suggests an identification of this vertebra as T8–T9.

3.5. Fragments of vertebral body

3.5.1. SD-1932 (Fig. 2) Fragment consisting of the right dorso-caudal corner of the vertebral body with the base of the right pedicle. The lower demifacet is completely preserved and it is separated from the caudal vertebral body surface. Only the caudal half of the upper demifacet is preserved, but it can be said that it is well developed on the lateral surface of the body. There is a short distance between the edges of both demifacets (6.8 mm). Comparison of these features with modern human spines suggests an identification of this vertebra as T1. The cranial epiphyseal ring preserved at the dorso-caudal corner of the vertebral body is fused (postmortem breakage allows observing a sharply defined vertebral body border and empty space between the epiphyseal ring and the vertebral body surface).

3.5.2. SD-1428 (Fig. 2) Fragment consisting of the right ventro-lateral third of the vertebral body, with the ventral half of the upper right demifacet. At least the ventral half of the demifacet is located in the lateral surface of the vertebral body and its cranial border is slightly below the level of the cranial vertebral body surface. The vertebral body seems to present a transverse elongated shape. Comparison of these features with modern human spines suggests an identification of this vertebra as T1. The preserved fragments of the cranial and caudal epiphyseal rings are fused.

3.5.3. SD-1679 (Fig. 2) Fragment consisting of complete right pedicle, partial upper right articular facet, and ventral and right halves of the vertebral body. The preserved upper demifacet is a lateral extension of the cranial vertebral body surface, and the main feature is an almost vertical wall shared by both the body surface and the demifacet that creates a well-defined step just ventral to the proper pedicle. Comparison of these features with modern

Please cite this article in press as: Bastir, M., et al., Three-dimensional morphometrics of thoracic vertebrae in Neandertals and the fossil evidence from El Sidrón (Asturias, Northern Spain), Journal of Human Evolution (2017), http://dx.doi.org/10.1016/j.jhevol.2017.03.008

human spines suggests an identification of this vertebra as T2–T4. The caudal epiphyseal ring is in active fusion, while the cranial epiphyseal ring is absent, possibly postmortem.

3.6. Centroid size analysis

Centroid size of the El Sidrón and other Neandertals is shown in Table 3, while Table 4 shows the 95% range of modern human males and females. Figure 4 plots these data together for visual comparisons of the fossil and recent samples. In the first two thoracic segments, Neandertal vertebrae are mostly outside the 95% range of modern human males (except T2 of Kebara 2). T3 of Kebara 2 falls at the upper size limit of the modern male sample. The first thoracic vertebra in all Neandertals is particularly large compared with the human reference sample. At more caudal levels, centroid size is comparable to that of human males with La Chapelle-aux-Saints 1 being outside the human male range at T9 and T10. The El Sidrón vertebrae are within the male ranges of the modern human sample. SD-1641-T4 is smaller than modern males at this level. The modern human females are all considerably smaller than the males and the Neandertals.

3.7. Shape analysis: intra-observer error

Shape variation related to repeated measurement on the virtual model measured as Procrustes distance (PD) was very low (average PD = 0.009) and the largest difference due to measurement error between the data obtained from the real bone and from its virtual model was 0.048, which was almost 50% smaller than the smallest distance between two different real vertebrae (PD = 0.092). In correspondence with these small Procrustes distances, in a PCA (not shown) the virtual models plotted very closely to its physical counterpart indicating that different methods of landmark measurement produce very similar results. These results demonstrate quantitatively that methodological error is acceptable.

3.8. Shape analysis of the El Sidrón vertebrae

Figure 5a shows the principal components analysis of levels T3 and T4 to assess both reconstructions of SD-1641-T3 and SD-1641-T4 in a comparative context. Principal component (PC) 1 accounts for 19.9% of total variance, PC2 for 12.7%. The scatterplot indicates that the El Sidrón SD-1641-T3 reconstruction is close to the modern human T4 range and the SD-1641-T4 plots outside the corresponding modern human range. Also, La Ferrassie T3 is within the human T4 distribution and T3 of Kebara 2 at the limit of modern human T3 scores along PC1 and in the center of the human T4 range. Regression analysis of PC1 on serial position indicates that 28.2% of total variance is significantly ($p < 0.001$) related to seriality (no significant signal along PC2, $p < 0.09$, 5.75%). This PCA illustrates that the Neandertal vertebrae tend to plot one level inferiorly to the shape of the corresponding human level. Their shape differences follow the serial pattern. The warps associated with PC1 show relatively longer bodies, more dorsally and cranially oriented transverse processes, and slightly longer spinous processes towards positive PC1 scores.

Figure 5b shows the PCA of levels T6 and T7 to assess both reconstructions of SD-1619-T6 and SD-1619-T7 in a comparative context. Principal component 1 accounts for 21.7% of total variance, PC2 for 12.5%. In this analysis there is no statistical signal of seriality at all (regression of PC1 on serial position: 1.6% of total variance, $p < 0.38$; PC2: 0.01% of total variance, $p < 0.92$). Both reconstructions of El Sidrón and both Kebara 2 vertebrae fall outside the human PC1 range. Morphologically, PC1 shows relatively shorter (both antero-posteriorly and cranio-caudally) and medio-laterally wider vertebral bodies, more dorsally and more cranially oriented transverse processes, and more horizontally (less caudally) oriented spinous processes towards positive scores. At level T6–T7, interspecific differences are not associated with serial variation (Fig. 5b).

Figure 6 shows a similar picture but visualizing more directly the interaction between seriality and non-serial interspecific features between levels T3 and T7. Principal component 1 accounts for 24.1% of total variance, PC2 for 14.7% (Fig. 6a). Principal component 1 polarizes serial levels, with T3 plotting towards negative PC1 scores and T7 towards positive PC1 scores (95% confidence intervals of seriality are shown in SOM Fig. S1). Regression analysis reveals that serial shape change accounts for 67.46% of total variance

Table 3
Centroid sizes of Neandertal vertebrae.[a]

Level	El Sidrón	Kebara 2	La Chapelle-aux-Saints 1	La Ferrassie 1
T1		173.53	174.07	168.46
T2		158.26	166.33	165.27
T3	148.36[b]	154.48		150.61
T4	145.18[c]	154.53		
T5		155.74		
T6	158.88[d]	158.88		
T7	159.17[e]	163.68		
T8		162.29	162.56	
T9		165.00	183.20	
T10		167.52	179.07	

[a] Underlined values indicate Neandertal centroid sizes outside the range of the human male reference sample (shown in Table 4).
[b] SD-1641 estimated as T3.
[c] SD-1641 estimated as T4.
[d] SD-1619 estimated as T6.
[e] SD-1619 estimated as T7.

Table 4
Mean centroid sizes and 95% confidence intervals of modern human male and female vertebrae.

Level	Male mean	95%−	95%+	Female mean	95%−	95%+
T1	160.77	157.38	164.15	146.49	143.90	149.09
T2	155.50	152.12	158.89	140.58	137.99	143.18
T3	150.97	147.58	154.36	135.74	133.03	138.45
T4	150.36	146.97	153.74	136.53	133.94	139.13
T5	153.05	149.66	156.43	138.58	135.99	141.18
T6	157.49	154.11	160.88	142.43	139.84	145.03
T7	159.51	156.13	162.90	143.85	141.26	146.45
T8	161.22	157.84	164.61	145.15	142.55	147.74
T9	162.33	158.94	165.71	146.11	143.52	148.71
T10	165.35	161.96	168.74	150.16	147.56	152.75

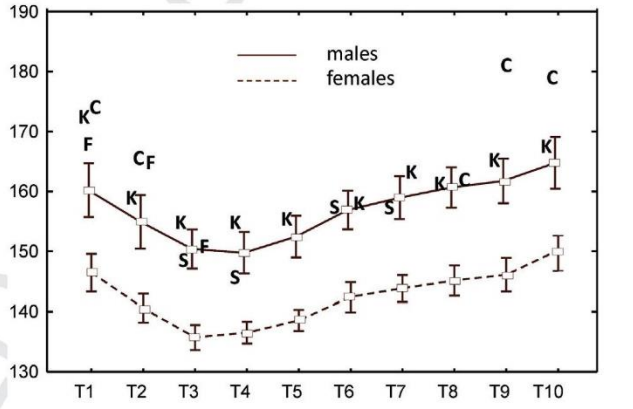

Figure 4. Centroid size comparisons. X-axis shows different vertebral levels from T1 to T10; y-axis shows means and 95% confidence intervals of vertebrae of modern human males (solid lines) and females (dashed lines) and Neandertals. K = Kebara 2, C = La-Chapelle-aux-Saints 1, F = La Ferrassie 1, S = El Sidrón (SD-1641 in comparison of T3, T4; SD-1619, in comparison of T6, T7).

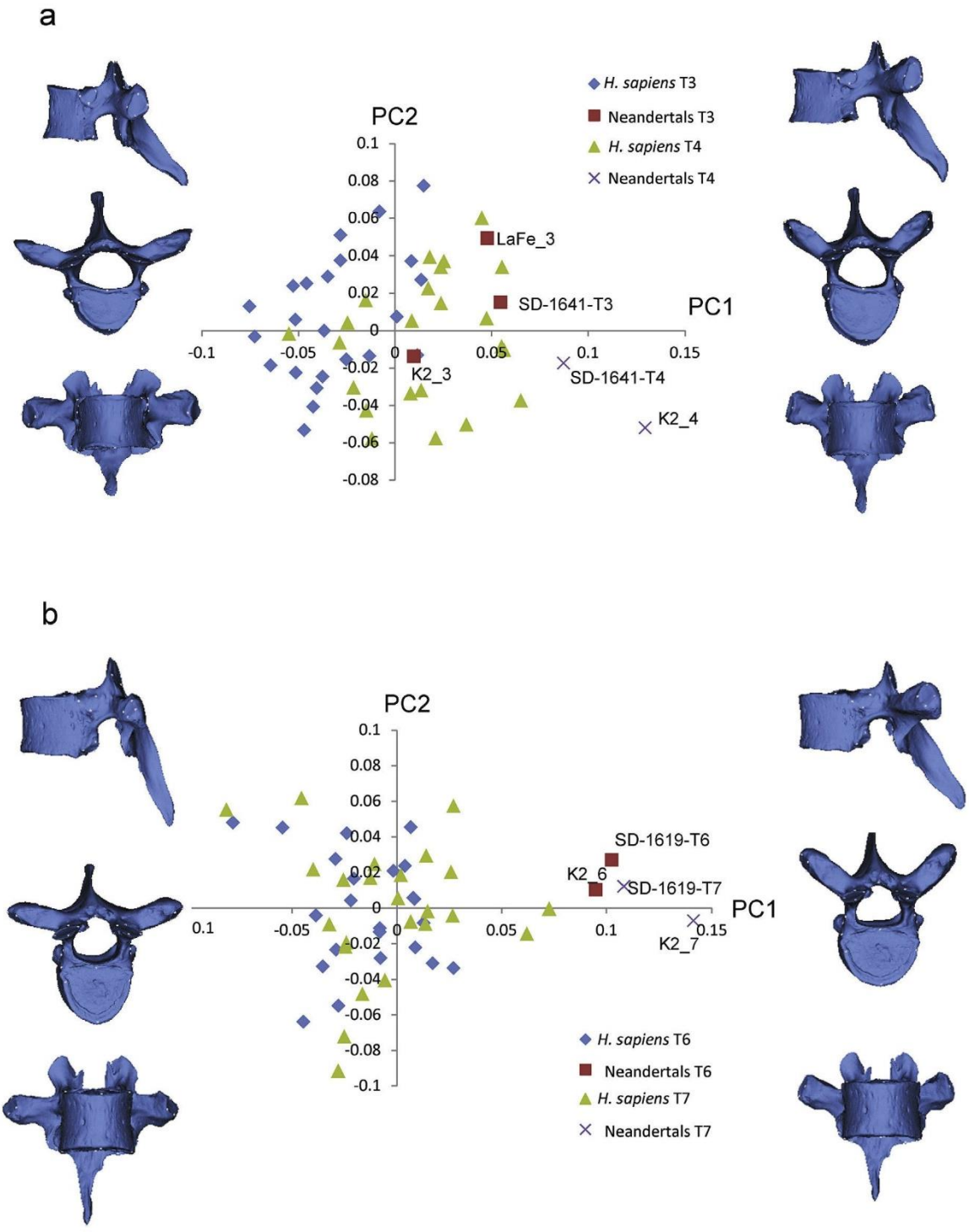

Figure 5. Principal components analyses of El Sidrón reconstructions. a) Comparisons of SD-1641-T3 and SD-1641-T4. The scatterplot of PC1 (19.9% total variance) and PC2 (12.7% total variance) illustrates shape distributions of T3 and T4 along PC1 and relations to other Neandertal vertebrae and *Homo sapiens*. LaFe_3 = T3 of La Ferrassie 1, K2_3 = T3 of Kebara 2, K2_4 = T4 of Kebara 2. Note that the Neandertal vertebrae belonging to level T3 fall within the human T4 range and the Neandertal T4 vertebrae fall outside the human T4 range. Three-dimensional models show associated shapes. b) Comparisons of El Sidrón SD-1619-T6 and SD-1619-T7. The scatterplot of PC1 (21.7% total variance) and PC2 (12.5% total variance) illustrates shape distributions of T6 and T7 along PC1 and relations to other Neandertals and *H. sapiens* K2_6 = T6 of Kebara 2, K2_7 = T7 of Kebara 2. There is no statistical signal of shape variation related to serial position in these PCs. The Neandertals fall outside the modern human ranges of T6 and T7, which overlap to a great extent. 3D models show shapes associated to PC1. The scale factor of 3D warps in both PCA visualizations is the magnitude of the shape change as a Procrustes distance corresponding to Procrustes distances of −0.1 and +0.1 along PC1.

Please cite this article in press as: Bastir, M., et al., Three-dimensional morphometrics of thoracic vertebrae in Neandertals and the fossil evidence from El Sidrón (Asturias, Northern Spain), Journal of Human Evolution (2017), http://dx.doi.org/10.1016/j.jhevol.2017.03.008

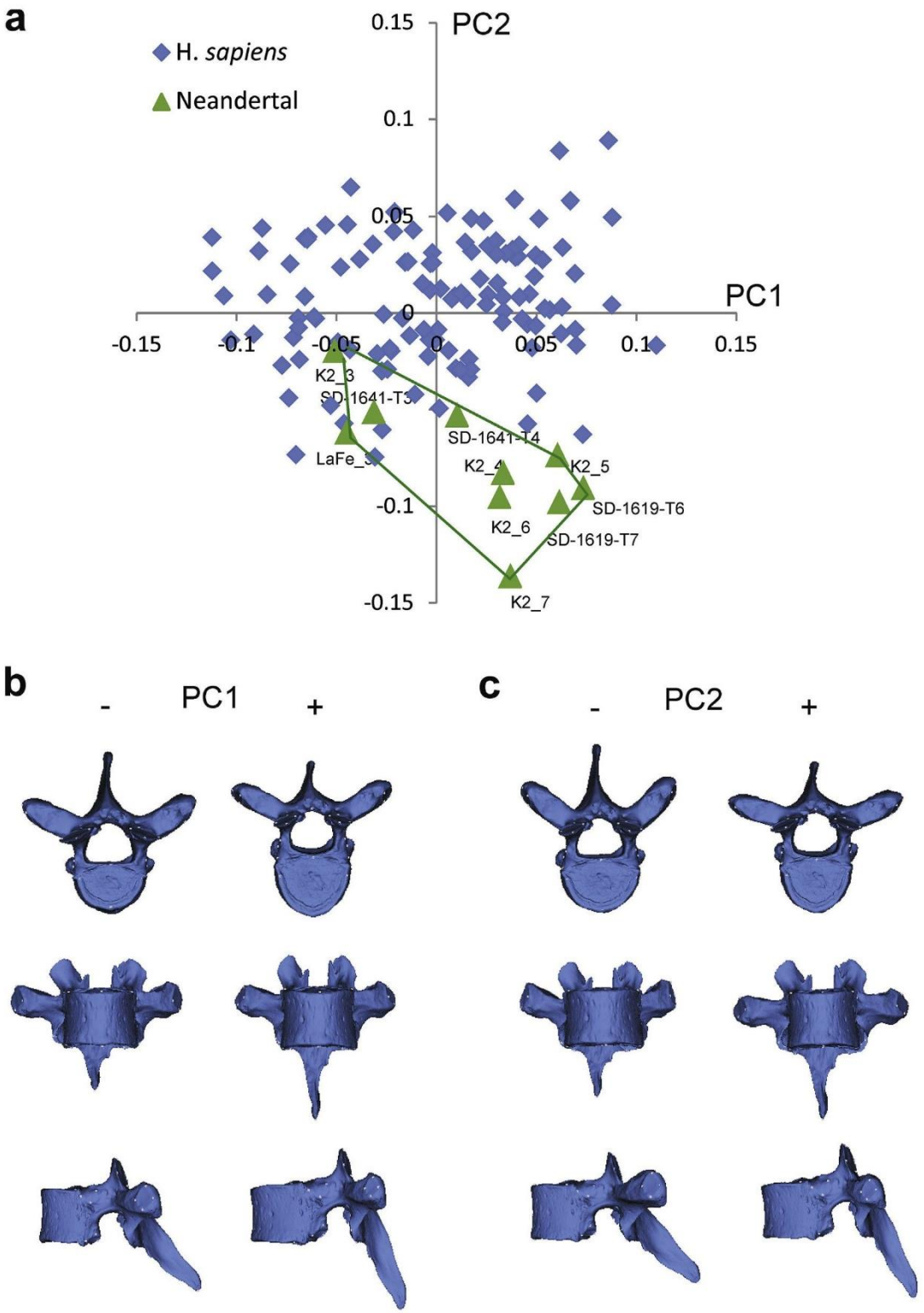

Figure 6. Principal components analysis of the thoracic spine between levels T3–T7. (a) The scatterplot of PC1 (24.1% total variance) and PC2 (14.7% total variance) illustrates diverging trajectories of serial shape change in modern humans and Neandertals. Polygon marks the Neandertal range. Principal component 1 carries a strong serial signal (indicated by regression analysis, see also SOM Fig. S1). Principal component 2 shows interspecific trends that increase towards positive PC1 scores. Shape changes associated with PC1 (b) and PC2 (c) are depicted in (b) and (c). Serial shape changes along PC1 include increase in vertebral body length, increasingly caudally oriented spinous processes and transverse processes that become slightly shorter, and slightly more dorsally oriented and cranially oriented transverse costal facets. Interspecific shape changes along PC2 include transverse processes that are markedly more dorsally and cranially oriented, with more cranially facing and slightly larger transverse costal facets, slightly less caudally oriented spinous processes and relatively shorter vertebral bodies with very slightly decreased central body height towards negative PC2 scores, a range that is occupied by Neandertals.

Please cite this article in press as: Bastir, M., et al., Three-dimensional morphometrics of thoracic vertebrae in Neandertals and the fossil evidence from El Sidrón (Asturias, Northern Spain), Journal of Human Evolution (2017), http://dx.doi.org/10.1016/j.jhevol.2017.03.008

($p < 0.0001$) of PC1. No serial signal is detected along PC2 (0.83% of total variance, $p < 0.31$). On PC2, there is overlap between both species within more cranial vertebral levels and differences towards more caudal thoracic levels. Thus non-serial species-specific differences increase caudally.

Morphological features of serial shape change of the thoracic vertebrae are shown in Figure 6b. The relative antero-posterior length of the vertebral body increases from T3 approaching T7 and the spinous processes change from a more horizontal orientation to more caudal one. Cranio-caudally the transverse processes get relatively shorter and very slightly more dorsally oriented. The transverse costal facets are oriented laterally towards more superior levels of the thoracic spine and slightly more cranially at inferior levels of the spine (Fig. 6b). Non-serial species-specific differences show up more clearly towards negative PC2 scores and caudal levels of the thoracic spine (i.e., positive PC1 scores) as a greater dorsal orientation of the transverse processes, relatively larger transverse costal facets, and more horizontally aligned spinal processes (Fig. 6c). The diverging serial trajectories in Figure 6a indicate also that patterns of serial shape change may differ in modern humans and Neandertals.

3.9. Differences in mean shape of thoracic levels 1–10 between Neandertals and modern human males

Mean shape comparisons (Table 5, Fig. 7) show interspecific differences in standardized anatomic views at each level. Table 5 further indicates an increase of shape differences towards more caudal vertebral levels of the thoracic spine. All shape differences (except at T5) are statistically significant at least at $p < 0.05$ (Table 5).

At T1, Neandertals show more sagittally oriented transverse costal facets, a relatively longer spinous process, and a relatively shorter (antero-posteriorly) vertebral body. The central part of the body is slightly higher in modern humans. At the T2 of Neandertals, both the spinous process and the body (antero-posteriorly) are relatively longer. From T3–T4 onwards, the transverse processes are oriented slightly cranially and they also become progressively more dorsally oriented. Also, the relative size of the transverse costal facets is larger than in modern humans. Central vertebral body heights are relatively reduced between T7 and T10 and the shape of these vertebral bodies, particularly between T8–T10, displays a more oval outline that is relatively wider than long when compared with the modern human means. Spinous processes between T6 and T10 are more horizontally oriented in Neandertals than in modern human males.

4. Discussion

This study presents new thoracic vertebral remains of the El Sidrón Neandertal site and uses geometric morphometric methods to compare the 3D spatial architecture of some of these vertebrae with those of other Neandertals and with a sample of anatomically modern humans. Recent comparative work has indicated growing evidence for differences in the morphological structure of the Neandertal vertebral column, not only in the morphology of cervical (Gómez-Olivencia et al., 2013b) and lumbar regions (Been et al., 2010), but also in thoracic vertebrae (Gómez-Olivencia et al., 2013a; Gómez-Olivencia, 2013a,b; Bastir et al., 2015b; Been et al., 2017a). For example, linear measurements could indicate greater cranio-caudal diameters of the laminae in upper thoracic vertebrae of La Ferrassie 1 (Gómez-Olivencia, 2013a) and slightly shorter spinous process lengths in mid and lower thoracic vertebrae in La Ferrassie 1 and Kebara 2 (Gómez-Olivencia, 2013a). However, such features were not observed in La Chapelle-aux-Saints 1 (Gómez-Olivencia, 2013b). In addition, slightly smaller vertebral body heights were found in some vertebrae of Regourdou 1 (T3, T7, T11) but not in other vertebrae of this individual, although at T7 the vertebral body heights are also small in Kebara 2 and La-Chapelle-aux-Saints 1 (Gómez-Olivencia et al., 2013a).

No clear general idea emerges from these previous comparisons, and also the linear measurements from the El Sidrón vertebrae do not contribute much to clarify this situation. Tables 1 and 2 show that measurements of specimens from the El Sidrón site are all within the ranges of other Neandertals, but also overlap with modern humans, as already shown by Gómez-Olivencia et al. (2013a) for the majority of measurements of their Neandertal sample. However, a classic metric comparative assessment with vertebrae from other Neandertals and from modern humans is beyond our objective; rather, metric data from El Sidrón are presented here to increase the available Neandertal vertebral record.

This situation gets a bit clearer when analyzing size and shape data obtained by the 3D landmark data collected here. In terms of centroid size, Table 3 shows that in most Neandertals (except Kebara 2) the upper thoracic vertebrae within T1–T2 are larger. Clearly, all first thoracic vertebrae are outside the modern human male range (). This could reflect developmental effects between thoracic and adjacent cervical segments (McIntyre et al., 2007), because in Neandertals cervical vertebrae have been shown recently to be "mediolaterally wider and dorsoventrally longer" (Gómez-Olivencia et al., 2013b:608). Such differences should translate into greater overall centroid sizes of Neandertal vertebrae in the cervico-thoracic transition, although cervical vertebrae still need to be investigated with 3D-GM.

At the cranial part of the thoracic spine (T1, T2) there may be reason to reject the hypothesis of similar sizes, whereas between T3 and T8 the Neandertal centroid sizes are within the human male range and thus in agreement with previous hypotheses of similar sizes (Gómez-Olivencia et al., 2013a). Also, in more caudal thoracic vertebrae, i.e., between T9 and T10, Kebara is close to the upper 95% confidence interval and within the distribution of modern males (K2; Fig. 4). Only La-Chapelle-aux-Saints 1 plots outside. However, taphonomic and pathological alterations may influence these results, as noted already by Gómez-Olivencia (2013:21b), although Q3 the "amount of pathological lesions in the thoracic spine" of La-Chapelle-aux-Saints 1 may be lower than previously assumed.

In terms of centroid size, we find evidence that upper thoracic vertebrae (T1–T2; might be larger in Neandertals than in anatomically modern humans), while in more central and caudal Q4 regions the hypothesis of similar overall sizes is supported. However, caution is necessary until more fossils and wider geographic ranges of *H. sapiens* are analyzed. With respect to the El Sidrón fossils, the analysis of centroid size (Fig. 4) supports an assignment of SD-1619 to a young (and not so large) adult and of SD-1641 to an adolescent individual. All reconstructions of vertebrae of El Sidrón are within the human range of centroid size. Interestingly, while

Table 5
Mean shape differences between modern human and Neandertal male vertebrae in Procrustes distance (Pd; *p*-values calculated from 1000 permutations).

Level	Pd	*p*-value	*n*
T1	0.124	0.002	3
T2	0.094	0.011	3
T3	0.106	<0.001	3
T4	0.123	0.006	2
T5	0.131	0.090	1
T6	0.126	0.010	2
T7	0.141	0.010	2
T8	0.134	<0.001	2
T9	0.145	0.004	2
T10	0.175	0.005	2

Please cite this article in press as: Bastir, M., et al., Three-dimensional morphometrics of thoracic vertebrae in Neandertals and the fossil evidence from El Sidrón (Asturias, Northern Spain), Journal of Human Evolution (2017), http://dx.doi.org/10.1016/j.jhevol.2017.03.008

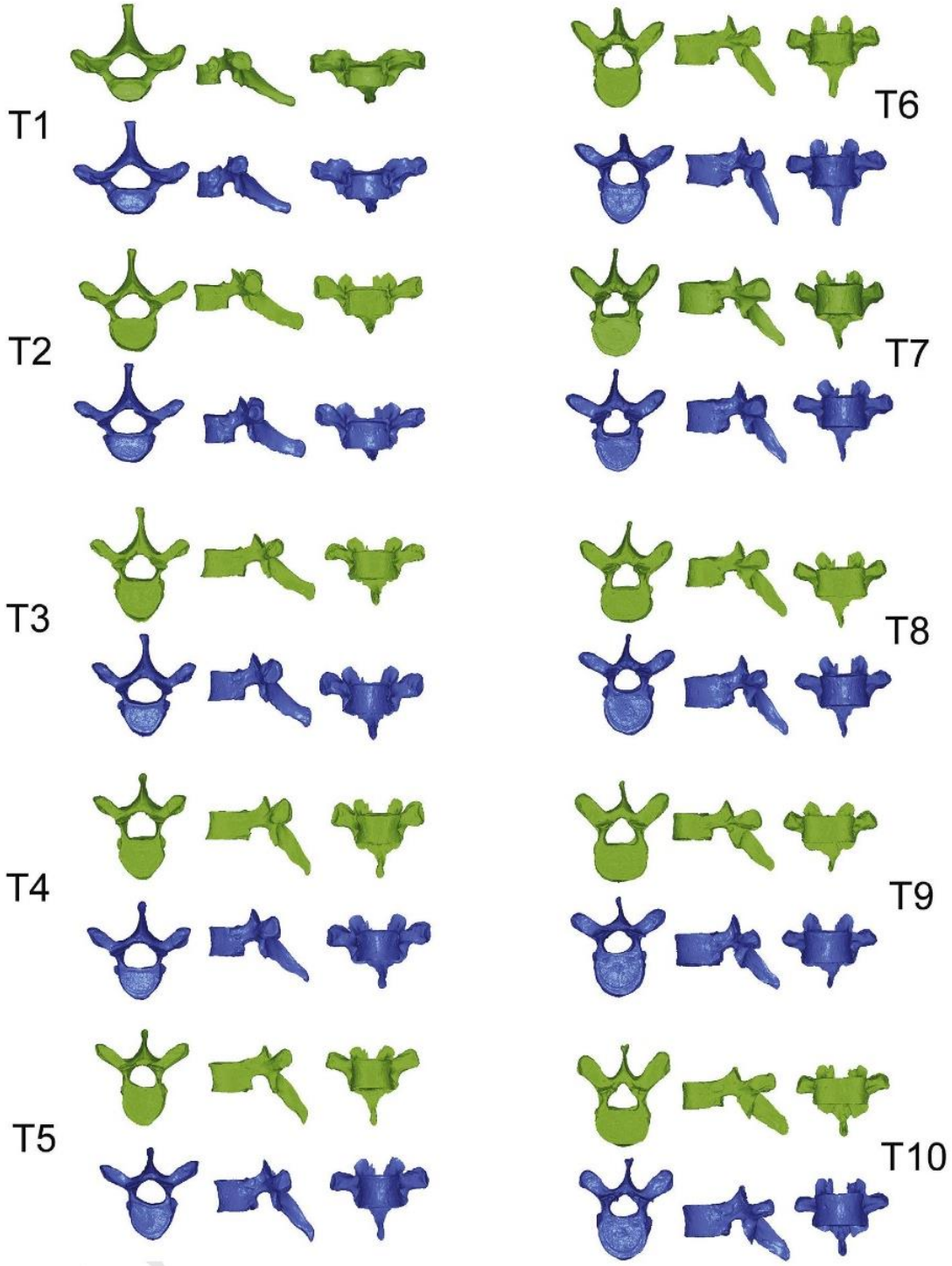

Figure 7. Mean shape differences at each vertebral level between the modern human males (blue) and the Neandertal (green) samples in standardized anatomical views. Note that the Neandertal sample sizes varied among the different levels. At T5, Neandertal shape is from one individual only (Kebara 2), while between levels T1 and T3 mean shapes are composed of three individuals and between T6 and T10 of two individuals. (For interpretation of the references to color in this figure legend, the reader is referred to the web version of this article.)

vertebral body height SD-1619 (18.39 mm) is within the modern human range of a published T7 sample (18.71 mm mean, ranging from 16.8 to 20.7 mm; Gómez-Olivencia et al., 2013a, their Table 5), two other thoracic vertebrae from El Sidrón, SD-1641 (estimate: 15.29 mm) and SD-1679 (16.49 mm), are below and more similar to Regourdou 1, Kebara 2, and La Chapelle-aux-Saints 1 (Gómez-Olivencia et al., 2013a). This supports suggestions of these authors that low vertebral body height might be a Neandertal specific feature (Gómez-Olivencia et al., 2013a). Lateral views of the mean shapes in Figure 7 also indicate variable, but reduced, relative vertebral body heights between T6 and T10 and support their suggestions. The data on vertebral body height from the El Sidrón

Please cite this article in press as: Bastir, M., et al., Three-dimensional morphometrics of thoracic vertebrae in Neandertals and the fossil evidence from El Sidrón (Asturias, Northern Spain), Journal of Human Evolution (2017), http://dx.doi.org/10.1016/j.jhevol.2017.03.008

fossils, together with the geometric morphometric analyses presented here, also statistically support a recent virtual reconstruction of the lumbar and thoracic part of the Kebara 2 spine (Been et al., 2017a), which is considerably shorter in vertical height, at least in comparison with a modern human individual.

In a more general morphological framework, the current study addressed the hypothesis that the enlarged thorax of Neandertals is not only the result of larger ribs (Franciscus and Churchill, 2002; Gómez-Olivencia et al., 2009; García-Martínez et al., 2014a; Bastir et al., 2015a), but also of a more dorsal orientation of the transverse processes of the thoracic vertebrae (Bastir et al., 2015b). A similar kind of influence of vertebral shape on rib cage morphology has been proposed in *Australopithecus* (Ward et al., 2012) and *Homo ergaster/erectus* (Jellema et al., 1993; Latimer and Ward, 1993), and more recently also identified as a geometric feature of modern human sexual dimorphism (Bastir et al., 2014; García-Martínez et al., 2016a). Shape data of both El Sidrón (SD-1641-T3, -T4; SD-1619-T6, -T7) vertebral reconstructions available for 3D analysis (Figs. 5 and 6), together with the morphological descriptions of the more fragmentary El Sidrón thoracic sample described above and shown in Figure 2, shed more light on this issue. Our results clearly suggest that Neandertal thoracic vertebrae, including specimens SD-1619 and SD-1641 (Figs. 1, 5, 6), but also SD-719, SD-1050b, and SD-1657 (Fig. 2) from the El Sidrón sample, are characterized by strongly posteriorly oriented transverse processes. This is particularly evident in the geometric morphometric comparisons with the modern human reference sample and fits with images of T10 of Regourdou 1 (Gómez-Olivencia et al., 2013a) and T12 of Kebara 2 (Been et al., 2010), and images presented in Gómez-Olivencia (2013a,b) as well as images presented by Arensburg (1991).

Clearly, dorsal orientation is also a feature of seriality that increases cranio-caudally, as shown in Figures 5 and 6 and previously in other studies (Jellema et al., 1993; Latimer and Ward, 1993; Ward et al., 2012; Bastir et al., 2014), and could potentially contribute to confusing serial and interspecific differences. However, in our analyses, serial variation has been quantitatively controlled for (Figs. 5 and 6) and is a priori absent in the mean shape comparisons (Table 5, Fig. 7), assuming correct serial assignments in the fossils. Thus, we propose that difference in transverse process orientation between Neandertals and the modern human reference sample likely reflects true species differences. These species-specific differences may have a serial developmental genetic signal in more cranial levels T3–T5 (McIntyre et al., 2007), and may involve features less related to seriality in central-lower parts of the thoracic spine. Although more research is necessary in this respect, differences in transverse process orientation may add to the reduced vertebral body heights shown already in other studies (Gómez-Olivencia et al., 2013a; Been et al., 2017a).

All mean shape analyses indicate statistically significant differences (except T5) in the sum of their geometric features, not only regarding the orientation of the transverse processes. Figure 7 shows also slightly greater relative antero-posterior vertebral body lengths in Neandertals along levels T2–T7. Gómez-Olivencia et al. (2013a) found greater dorso-ventral length at the body of T2 in Regourdou 1. On the other hand, between levels T8 and T10 these lengths become relatively shorter again in Neandertals (Fig. 7), which contribute to differences in general vertebral shape (Table 5).

Also, the relative sizes of the transverse costal facets seem to differ between Neandertals and humans (Fig. 6c). These features are compatible either with greater rib size in Neandertals in general (Franciscus and Churchill, 2002; Gómez-Olivencia et al., 2009; García-Martínez et al., 2014a) or with particularly larger articular rib tubercles (Franciscus and Churchill, 2002). García-Martínez et al. (2014b, 2016b, in revision) have observed greater articular tubercles in the El Sidrón costal skeleton and discussed this in a biomechanical context. Furthermore, the more sagittal and slightly cranial orientation of the transverse costal facets (Figs. 1, 2, 6c) might indicate subtle biomechanical differences in breathing kinematics in Neandertals. Sagittal–cranial orientation of these facets facilitate vertical and oblique gliding movements, allowing for greater medio-lateral expansions (Bastir et al., 2017), particularly in combination with longer ribs possibly in response to greater diaphragmatic action on central and lower parts of the thorax (T7–T10; Franciscus and Churchill, 2002; Gómez-Olivencia et al., 2009; García-Martínez et al., 2014a; Bastir et al., 2015a). All these aspects are compatible with bio-energetic arguments related to greater muscle and body mass estimates in Neandertals.

The more horizontally oriented spinous processes could indicate a thicker layer of epaxial muscles, particularly those of the transverso-spinalis and longissimus group in Neandertals, and possibly differences in muscle morphology and biomechanics. A similar feature was observed in the spinous processes of KNM-WT 15.000, where Jellema et al. (1993) discussed these differences in terms of muscle morphology and biomechanical changes. "More horizontally oriented spinous processes have the effect of deepening the vertebral gutter," which "would also increase the moment arm of the associated musculature" (Jellema et al., 1993:286–287). Again, thicker muscle layers would fit with greater estimated body and muscle mass and the associated bio-energetic aspects (Churchill, 2014).

The less caudal orientation of the spinous processes in the thoracic vertebrae fits with findings reported by Gómez-Olivencia et al. (2013b), who observed longer and more horizontally oriented spinous processes in cervical vertebrae. These authors discussed spinous process length and orientation in relation to biomechanics of cranial posture and cranial morphology. Occipital morphology differs considerably between Neandertals and modern humans (Bastir et al., 2010) and parts of these differences relate to the head-neck muscles. It seems therefore that a common axial muscular factor links the orientations of the spinous processes of lower cervical vertebrae and thoracic vertebrae with specific functional implications in the cervical areas, associated with head-neck relations, and in the thoracic areas, associated with postural stability.

Similar to Jellema et al. (1993) and Ward et al. (2012), spinous process orientation was linked with biomechanical implications in lumbar vertebrae with respect to spine leverage (Been et al., 2010) because greater horizontal projection increases the moment arms of erector spinae muscles attaching to them. These authors suggest further that greater horizontal orientation implies less "imbrication" and thus greater mobility. Interestingly, Been et al. (2010, 2017a) also find a more cranial orientation of the transverse processes of lumbar vertebrae in Neandertals similar to the cranial orientation of the transverse processes of the thoracic vertebrae (Fig. 7). This coincidence might suggest systemic effects of erector spinae musculature between thoracic and lumbar segments similar to the shared horizontal orientations of the spinous processes in lower cervical (Gómez-Olivencia et al., 2013b) and thoracic vertebrae.

From a structural point of view, the greater dorsal orientation of transverse processes at the thoracic spine may indicate its greater overall invagination within the ribcage. Similar propositions were made in the context of early hominins, although in the context of changing features in locomotor evolution (Jellema et al., 1993; Latimer and Ward, 1993; Ward et al., 2012). Morphologically, these arguments would also apply to Neandertals, possibly in relation to posture. A more anterior position of the thoracic part of the spine within the ribcage should be accompanied by corresponding adjustments of lumbar parts of the Neandertal spino-pelvic alignment (Been et al., 2014, in press). Positional variations

Please cite this article in press as: Bastir, M., et al., Three-dimensional morphometrics of thoracic vertebrae in Neandertals and the fossil evidence from El Sidrón (Asturias, Northern Spain), Journal of Human Evolution (2017), http://dx.doi.org/10.1016/j.jhevol.2017.03.008

of the spine affect the demands on the global muscles to provide postural stability (Wagner et al., 2012) and the altered spinous processes of the thoracic vertebrae contribute to this stability as mentioned above. It has been proposed that the sacrum of Neandertals is more vertically oriented within the pelvis and possibly located more anteriorly (Been et al., 2014, 2017a, in press). These differences in position may influence indirectly the position of the thoracic part of the spine within the ribcage, and thus contribute to increased invagination and different spine biomechanics. These factors likely account for the covariation between the orientations of the transverse and spinous processes reported here. Future studies should address these questions in the context of the entire spine and cannot be addressed using the data from the current study.

While the present study provides findings important for understanding Neandertal thorax form and function, caution is also necessary because of several limitations. One limitation relates to the modern human reference sample. Because intraspecific variation in 3D thoracic vertebral shape of *H. sapiens* is not well known, the hypothesis that reported differences in vertebral structure are taxonomically relevant will need further comparison with heterogeneous comparative samples. Gómez-Olivencia et al. (2013a:596) propose that "Neandertals are significantly different in having small ventral and median heights of the vertebral body", specifically at T11. This implies taxonomic differences. Because differences in vertebral body heights are also present in other thoracic levels and accompanied by differences in overall body morphology and the orientations of transverse and spinous processes, potential taxonomic relevance of the shape differences can be assumed.

A further important limitation is the very small sample and fragmentary nature of thoracic vertebrae. We excluded badly preserved vertebrae of La Ferrassie 1 and La-Chapelle-aux-Saints 1, following detailed descriptions of Gómez-Olivencia (2013a,b), but pathology, taphonomy, and uncertainty in serial assignments could influence aspects of shape variations interpreted here. Most fossils required at least some landmark estimations and reconstructions (SOM Table S1). Because Kebara 2 is one of the most complete individuals, using these data for reference-based reconstructions (Gunz et al., 2009) might bias our interpretations by disregarding Neandertal intraspecific variability. Ideally, less fragmented or less deformed thoracic vertebrae should be analyzed. Fortunately, some of the new thoracic vertebral fossils from the El Sidrón site provide further evidence for potential Neandertal features, including a more dorsal orientation of the transverse processes, a sagittal orientation of larger transverse costal facets (SD-1619, SD-1641, Fig. 1; SD-1657, Fig. 2), and reduced body height at T7 in two out of three fossils.

Future studies should expand the comparative samples both at intraspecific adult and subadult levels to enhance our understanding of geographic, ontogenetic, and interspecific variation of thoracic vertebral structure. This will produce a better idea of the taxonomic relevance of the 3D morphological characteristics of the thoracic vertebrae in human evolution.

Uncited references

Q8 Bastir et al., 2013; Gómez-Olivencia, 2015.

Acknowledgments

We thank the El Sidrón excavation team and appreciate discussions on previous versions of this manuscript with Ella Been and Asier Gómez-Olivencia. This research is funded by CGL2012-37279, CGL2012-36682, and CGL2015-63648-P (Ministerio de Economía y Q5 Competitividad, Spain) and by The Leakey Foundation. José Antonio Sánchez Sánchez, Bernardo Perea Pérez, and David Antonio Cáceres Monllor kindly provided access to the skeletal collections at the Faculty of Medicine, Universidad Complutense de Madrid. Pedro Osborne Márquez (Virtual Morphology Lab, MNCN-CSIC) assisted with surface scanning. Antoine Balzeau, Alain Froment, Philippe Mennecier, Ofer-Bar Yosef, Bernard Vandermeersch, Baruch Arensburg, and Israel Hershkovitz provided access to CT data.

Supplementary Online Material

Supplementary online material related to this article can be found at http://dx.doi.org/10.1016/j.jhevol.2017.03.008.

References

Arensburg, B., 1991. The vertebral column, thoracic cage, and hyoid bone. In: Bar Yosef, O., Vandermeerch, B. (Eds.), Le Squelette Mousterien de Kebara 2. CNRS, Paris, pp. 113–146.
Bastir, M., 2008. A systems-model for the morphological analysis of integration and modularity in human craniofacial evolution. J. Anthropol. Sci. 86, 37–58.
Bastir, M., 2017. Back to Basics: Morphological Analysis in Paleoanthropology. Biological Theory (in press). Q6
Bastir, M., Rosas, A., 2011. Nasal form and function in Midpleistocene human facial evolution. A first approach. Am. J. Phys. Anthropol. 144, 83.
Bastir, M., Rosas, A., 2013. Cranial airways and the integration between the inner and outer facial skeleton in humans. Am. J. Phys. Anthropol. 152, 287–293.
Bastir, M., Rosas, A., 2016. Cranial base topology and basic trends in the facial evolution of *Homo*. J. Hum. Evol. 91, 26–35.
Bastir, M., Rosas, A., Tabernero, A.G., Peña-Melián, A., Estalrrich, A., de la Rasilla, M., Fortea, J., 2010. Comparative morphology and morphometric assessment of the Neandertal occipital remains from the El Sidrón site (Asturias, Spain: years 2000–2008). J. Hum. Evol. 58, 68–78.
Bastir, M., García-Martínez, D., Coquerelle, M., Barash, A., Recheis, W., 2012. Systems-approaches to skeletal variation in paleoanthropology: the human thorax. In: Proceedings of the European Society for the Study of Human Evolution (PESHE 1), Bordeaux, p. 14.
Bastir, M., García Martínez, D., Recheis, W., Barash, A., Coquerelle, M., Rios, L., Peña-Melián, Á., García Río, F., O'Higgins, P., 2013. Differential growth and development of the upper and lower human thorax. PLoS One 8, e75128.
Bastir, M., Higuero, A., Ríos, L., García Martínez, D., 2014. Three-dimensional analysis of sexual dimorphism in human thoracic vertebrae: implications for the respiratory system and spine morphology. Am. J. Phys. Anthropol. 155, 513–521.
Bastir, M., García-Martínez, D., Estalrrich, A., Tabernero, A.G., Huguet, R., Ríos, L., Barash, A., Recheis, W., Rasilla, M.d.l., Rosas, A., 2015a. The relevance of the first ribs of the El Sidrón site (Asturias, Spain) for the understanding of the Neanderthal thorax. J. Hum. Evol. 80, 64–73.
Bastir, M., García-Martínez, D., Barash, A., 2015b. The 3D structure of thoracic vertebrae and their significance for size and shape of the ribcage in Neandertals. In: Proceedings of the European Society for the Study of Human Evolution (PESHE 4), London, p. 42.
Bastir, M., García-Martínez, D., Torres-Tamayo, N., Sanchis-Gimeno, J.A., O'Higgins, P., Utrilla, C., Torres Sánchez, I., García Río, F., 2017. In vivo 3D analysis of thoracic kinematics: changes in size and shape during breathing and their implications for respiratory function in recent humans and fossil hominins. Anat. Rec. 300, 255–264.
Been, E., Peleg, S., Marom, A., Barash, 2010. Morphology and function of the lumbar spine of the Kebara 2 Neandertal. Am. J. Phys. Anthropol. 142, 549–557. Q7
Been, E., Bastir, M., Barash, A., 2014. Spino-pelvic alignment. In: Proceedings of the European Society for the Study of Human Evolution (PESHE 3), Florence, p. 58.
Been, E., Gómez-Olivencia, A., Kramer, P.A., Barash, A., 2017a. 3D Reconstruction of the spinal posture in the Kebara 2 Neanderthal. In: Marom, A., Hovers, E. (Eds.), Human Paleontology and Prehistory. Springer Verlag, New York University, pp. 239–251.
Been, E., Gómez- Olivencia, A., Shefi, S., Soudack, M., Bastir, M., Barash, A., 2017b. The evolution of spinopelvic alignment in hominins. Anat. Rec. (in press).
Bellemare, F., Jeanneret, A., Couture, J., 2003. Sex differences in thoracic dimensions and configuration. Am. J. Resp. Crit. Care Med. 168, 305–312.
Bellemare, F., Fuamba, T., Bourgeault, A., 2006. Sexual dimorphism of human ribs. Resp. Physiol. Neurobiol. 150, 233–239.
Cardoso, H., Ríos, L., 2011. Age estimation from stages of union of epiphyseal union in the presacral vertebrae. Am. J. Phys. Anthropol. 144, 238–247.
Churchill, S.E., 2006. Bioenergetic perspectives on Neanderthal thermoregulatory and activity budgets. In: Harvati, K., Harrison, T. (Eds.), Neanderthals revisited. Springer Verlag, New York, pp. 113–156.
Churchill, S.E., 2014. Thin on the Ground: Neandertal Biology, Archeology and Ecology. Wiley Blackwell, Ames, Chichester, Oxford.
EVAN-Society, 2010. ET, Toolkit for geometric morphometric analysis.
Franciscus, R.G., 1999. Neandertal nasal structures and upper respiratory tract "specialization". Proc. Natl. Acad. Sci. 96, 1805–1809.

Please cite this article in press as: Bastir, M., et al., Three-dimensional morphometrics of thoracic vertebrae in Neandertals and the fossil evidence from El Sidrón (Asturias, Northern Spain), Journal of Human Evolution (2017), http://dx.doi.org/10.1016/j.jhevol.2017.03.008

Franciscus, R.G., Churchill, S.E., 2002. The costal skeleton of Shanidar 3 and a reappraisal of Neandertal thoracic morphology. J. Hum. Evol. 42, 303–356.
García-Martínez, D., Barash, A., Recheis, W., Utrilla, C., Torres Sánchez, I., García Río, F., Bastir, M., 2014a. On the chest size of Kebara 2. J. Hum. Evol. 70, 69–72.
García-Martínez, D., Bastir, M., Estalrrich, A., García Tabernero, A., Huguet, R., Cunha, E., de la Rasilla, M., Rosas, A., 2014b. Preliminary study of the head-neck complex of Neanderthal ribs from the El Sidrón site (Asturias, Spain). In: Proceedings of the European Society for the Study of Human Evolution (PESHE 3), Florence, p. 76.
García-Martínez, D., Torres-Tamayo, N., Torres-Sanchez, I., García-Río, F., Bastir, M., 2016a. Morphological and functional implications of sexual dimorphism in the human skeletal thorax. Am. J. Phys. Anthropol. 161, 467–477.
García-Martínez, D., Bastir, M., Huguet, R., Estalrrich, A., García-Tabernero, A., Cunha, E., de la Rasilla, M., Rosas, A., 2016b. Positional rib assessment of the adult costal remains of the El Sidrón Neanderthal site (49000 y/o, Asturias, northern Spain). In: Proceedings of the European Society for the Study of Human Evolution (PESHE 5), Madrid, p. 104.
García-Martínez, D., Bastir, M., Huguet, R., Estalrrich, A., García-Tabernero, A., Luis Río, Eugenia Cunha, Marco de la Rasilla, Rosas, A., in revision. The costal remains of the El Sidrón Neanderthal site (Asturias, northern Spain) and its importance for understanding the Neanderthal thorax morphology. J. Hum. Evol.
Gómez-Olivencia, A., 2013b. Back to the old man's back: reassessment of the anatomical determination of the vertebrae of the Neandertal individual of La Chapelle-aux-Saints. Ann. Paléontol. 99, 43–65.
Gómez-Olivencia, A., 2013a. The presacral spine of the La Ferrassie 1 Neandertal: a revised inventory. Bull. Mém. Soc. Anthropol. 1–20.
Gómez-Olivencia, A., 2015. The costal skeleton of the Neandertal individual of La Chapelle-aux-Saints 1. Ann. Paléontol. 101, 127–141.
Gómez-Olivencia, A., Eaves-Johnson, K.L., Franciscus, R.G., Carretero, J.M., Arsuaga, J.L., 2009. Kebara 2: new insights regarding the most complete Neandertal thorax. J. Hum. Evol. 57, 75–90.
Gómez-Olivencia, A., Franciscus, R.G., Couture-Veschambre, C., Maureille, B., Arsuaga, J.L., 2012. The mesosternum of the Regourdou 1 Neandertal revisited. J. Hum. Evol. 62, 511–519.
Gómez-Olivencia, A., Been, E., Arsuaga, J.L., Stock, J.T., 2013b. The Neandertal vertebral column 1: The cervical spine. J. Hum. Evol. 64, 608–630.
Gómez-Olivencia, A., Couture-Veschambre, C., Madelaine, S., Maureille, B., 2013a. The vertebral column of the Regourdou 1 Neandertal. J. Hum. Evol. 64, 582–607.
Gunz, P., Mitteroecker, P., Neubauer, S., Weber, G.W., Bookstein, F.L., 2009. Principles for the virtual reconstruction of hominin crania. J. Hum. Evol. 57, 48–62.
Jellema, L.M., Latimer, B., Walker, A., 1993. The rib cage. The Nariokotome *Homo erectus* Skeleton. Harvard University Press, Cambridge, pp. 294–325.
Klingenberg, C.P., 2011. MorphoJ: an integrated software package for geometric morphometrics. Mol. Ecol. Res. 11, 353–357.
Latimer, B., Ward, C.V., 1993. The thoracic and lumbar vertebrae. The Nariokotome *Homo erectus* Skeleton. Harvard University Press, Cambridge, pp. 266–293.
Mardia, K.V., Bookstein, F.L., Moreton, I.J., 2000. Statistical assessment of bilateral symmetry of shapes. Biometrika 87, 285–300.
McIntyre, D.C., Rakshit, S., Yallowitz, A.R., Loken, L., Jeannotte, L., Capecchi, M.R., Wellik, D.M., 2007. Hox patterning of the vertebrate rib cage. Development 134, 2981–2989.
O'Higgins, P., 2000. The study of morphological variation in the hominid fossil record: biology, landmarks and geometry. J. Anat. 197, 103–120.
Ríos, L., Cardoso, H., 2009. Age estimation from stages of union of the vertebral epiphyses of the ribs. Am. J. Phys. Anthropol. 140, 265–274.
Rosas, A., Bastir, M., Martínez-Maza, C., García-Tabernero, A., Lalueza-Fox, C., 2006a. Inquiries into Neanderthal cranio-facial development and evolution: 'accretion' vs 'organismic' models. In: Harrison, T., Harvati, K. (Eds.), Neanderthals Revisited. Springer Verlag, New York, pp. 38–69.
Rosas, A., Martínez-Maza, C., Bastir, M., García-Tabernero, A., Lalueza-Fox, C., Huguet, R., Ortiz, J.E., Julia, R., Soler, V., Torres, T.d., Martínez, E., Cañaveras, J.C., Sanchez-Moral, S., Cuezva, S., Lariol, J., Santamaria, D., de la Rasilla, M., Fortea, J., 2006b. Paleobiology and comparative morphology of a late Neandertal sample from El Sidrón, Asturias, Spain. Proc. Natl. Acad. Sci. USA 103, 19266–19271.
Rosas, A., Estalrrich, A., García-Tabernero, A., Bastir, M., García-Vargas, S., Sánchez-Meseguer, A., Huguet, R., Lalueza-Fox, C., Peña-Melián, Á., Kranioti, E.F., Santamaría, D., De la Rasilla, M., Fortea, J., 2012. The Neandertals from El Sidrón (Asturias, Spain). Updating of a new sample, Les Néandertaliens d'El Sidrón (Asturies, Espagne). Actualisation d'un nouvel échantillon. L'Anthropologie 116, 57–76.
Rosas, A., Rodriguez-Perez, F.J., Bastir, M., Estalrrich, A., Huguet, R., García-Tabernero, A., Pastor, J.F., de la Rasilla, M., 2016. Adult Neandertal clavicles from the El Sidrón site (Asturias, Spain) in the context of *Homo* pectoral girdle evolution. J. Hum. Evol. 95, 55–67.
Sawyer, G.J., Maley, B., 2005. Neanderthal reconstructed. Anat. Rec. 283B, 23–31.
Silbernagl, S., Despopoulos, A., 1991. Taschenatlas der Physiologie. Georg Thieme Deuscher Taschenbuch-Verlag, Stuttgart.
Steegmann, A.J., Cerny, F., Holliday, T., 2002. Neandertal cold adaptation: physiological and energetic factors. Am. J. Hum. Bio. 14, 566–583.
Wagner, H., Liebetrau, A., Schinowski, D., Wulf, T., de Lussanet, M., 2012. Spinal lordosis optimizes the requirements for a stable erect posture. Theoret. Biol. Med. Mod. 9, 13.
Ward, C., Kimbel, W., Harmon, E., Johanson, D., 2012. New postcranial fossils of *Australopithecus afarensis* from Hadar, Ethiopia (1990–2007). J. Hum. Evol. 63, 1–51.
Zelditch, M.L., Swiderski, D.L., Sheets, H.D., Fink, W.L., 2012. Geometric Morphometrics for Biologists: A Primer, 2nd edition. Elsevier Academic Press, San Diego.

Please cite this article in press as: Bastir, M., et al., Three-dimensional morphometrics of thoracic vertebrae in Neandertals and the fossil evidence from El Sidrón (Asturias, Northern Spain), Journal of Human Evolution (2017), http://dx.doi.org/10.1016/j.jhevol.2017.03.008

Aceptación de artículo García-Martínez et al., titulado “The costal remains of the El Sidrón Neanderthal site (Asturias, northern Spain) and its importance for understanding the Neanderthal thorax morphology”.

Ref.: Submission HUMEV-E-16-00500R2
The costal remains of the El Sidrón Neandertal site (Asturias, northern Spain) and its importance for understanding the Neandertal thorax morphology.
Journal of Human Evolution

Dear Daniel

Thank you for your revised manuscript. I am happy that you have addressed the reviewer queries, and so am informally accepting the mansucript. I have sent it to our copy editor and will be back in touch with the copy edits for your attention and approval as soon as I can. Please note that this may not be until April, as I will be away from Friday for two weeks with no access to my editorial inbox, and our copy editor may not be able to return the manuscript to me in sufficient time before I go.

With kind regards,

Sarah

Sarah Elton
Editor

****
For further assistance, please visit our customer support site at http://help.elsevier.com/app/answers/list/p/7923. Here you can search for solutions on a range of topics, find answers to frequently asked questions and learn more about EES via interactive tutorials. You will also find our 24/7 support contact details should you need any further assistance from one of our customer support representatives.

The costal remains of the El Sidrón Neanderthal site (Asturias, northern Spain) and its importance for understanding Neanderthal thorax morphology.

Daniel García-Martínez[a,b]*, Markus Bastir[a], Rosa Huguet[c, d, a], Almudena Estalrrich[a], Antonio García-Tabernero[a], Luis Ríos[a], Eugenia Cunha[e], Marco de la Rasilla[f] y Antonio Rosas[a]

[a] Paleoanthropology Group, Museo Nacional de Ciencias Naturales (CSIC), J. G. Abascal 2, 28006, Madrid, Spain.

[b] Biology Department, Faculty of Sciences, Universidad Autónoma De Madrid. Darwin 2, Madrid 28049, Spain.

[c] Institut Catalá de Paleoecologia Humana i Evolució Social (IPHES), C/ Marcellí Domingo s/n e Campus escelades URV (Edifici W3), 43007 Tarragona, Spain.

[d] Area de Prehistoria, Universitat Rovira i Virgili (URV), Avinguda de Catalunya 35, 43002 Tarragona, Spain.

[e] Departamento de Ciências da Vida (Centro de Ecologia Funcional), Universidade de Coimbra, Calçada Martim de Freitas 3000-456, Coimbra, Portugal.

[f] Departmento de Historia, University of Oviedo, Campus del Milán, C/ Teniente Alfonso Martínez s/n, 33011, Oviedo, Spain.

***Corresponding author:** Daniel García-Martínez.

Paleoanthropology group, Museo Nacional de Ciencias Naturales, 28006 Madrid, Spain.

+34.91.566.89.86; dan.garcia@mncn.csic.es

Keywords: rib cage, evolution, ribs, geometric morphometrics, virtual reconstruction, fossils.

Abstract

The study of the Neanderthal thorax has drawn the attention of the scientific community for more than a century. There is an agreement about the more capacious thorax in Neanderthals compared to modern humans. Nonetheless, whether this was caused by a medio-lateral or an antero-posterior expansion of the thorax is still debated and it is key to understanding breathing biomechanics and body shape in Neanderthals. The fragile nature of ribs, the metameric structure of the thorax and difficulties in morphological quantification all contribute to the uncertainty regarding precise aspects of Neanderthal thoracic shape. The El Sidrón site has yielded costal remains ranging from the upper to the lower thorax, as well as several proximal rib ends (frequently missing in the Neanderthal record), which could shed light on this issue. We compared the El Sidrón costal elements with ribs from current modern humans as well as with fossil modern humans and other Neanderthals through traditional morphometric methods and 3D geometric morphometrics, combined with missing data estimation and virtual reconstruction (at the 1st, 5th and 11th levels). Our results show that Neanderthals present larger rib heads and articular tubercles than their modern human counterparts. Overall size results show that Neanderthal 1st ribs are smaller than in modern humans, whereas 5th and 11th ribs are considerably larger. When we articulated mean ribs (size and shape) with their corresponding vertebral elements, we observed that the Neanderthal thorax presents a medio-lateral expansion at every level, especially at T5 and T11 levels, compared to modern humans. Therefore, in light of the evidence from the El Sidrón costal remains, we hypothesize that the volumetric expansion of the Neanderthal thorax proposed by previous authors would be mainly produced by a medio-lateral expansion of the thorax.

Resumen

El estudio del tórax Neandertal ha atraído el interés de la comunidad científica por más de un siglo. Existe acuerdo acerca de la mayor capacidad torácica en Neandertales en comparación con humanos modernos. Sin embargo, si esto es causado por una expansión antero-posterior o medio-lateral del tórax es debatido a día de hoy y es clave para el entendimiento de la biomecánica respiratoria y la morfología corporal en Neandertales. La frágil naturaleza de las costillas y las dificultades en la cuantificación morfológica contribuyen a la incertidumbre en referencia a aspectos de la morfología torácica Neandertal. El yacimiento de El Sidrón ha proporcionado elementos costales que comprenden desde el tórax superior hasta el inferior, así como diferentes restos costales proximales (frecuentemente ausentes en el registro fósil Neandertal), los cuales pueden arrojar luz sobre esta incertidumbre. Nosotros comparamos las costillas de El Sidrón con costillas de humanos modernos actuales, así como con humanos modernos fósiles y otros Neandertales, a través de técnicas de MG 3D , combinadas con técnicas de estimación de datos perdidos y de reconstrucción virtual (en las costillas 1, 5 y 11). Nuestros resultados muestran que los Neandertales presentan cabezas costales y tubérculos articulares más grandes que humanos modernos. Con referencia al tamaño global de las costillas, las 1ª costillas Neandertales son más pequeñas que las de humanos modernos, mientras que las 5ª y 11ª son considerablemente más grandes. Cuando articulamos costillas medias (forma y tamaño) con sus correspondientes elementos vertebrales, nosotros observamos que el tórax Neandertal presenta una expansión medio-lateral en los diferentes niveles estudiados con respecto a humanos modernos, aunque esto es más evidente a nivel de T5 y T11. Por lo tanto, nosotros hipotetizamos que la expansión volumétrica Neandertal propuesta por autores previos, debería ser fundamentalmente producida por una expansión medio-lateral del tórax.

Introduction

The morphology of the rib cage is highly informative for the interpretation of biological aspects of extinct hominin species. Beyond internal organ protection, thoracic morphology is directly tied to respiratory dynamics. Expansion of the lungs during breathing and consequent oxygen intake into the organism is caused by the action of the intercostal muscles, the diaphragm and other accessory muscles (Spalteholz, 1970; De Troyer et al., 2005). Therefore, oxygen availability, basal metabolic rate (BMR) and physical activity are also dependent on various aspects of rib cage morphology (Franciscus and Churchill, 2002; Churchill, 2006; Froehle and Churchill, 2009; Gómez-Olivencia et al., 2009; García-Martínez et al., 2014, 2016a; Bastir et al., 2017).

Additionally, the rib cage contributes to the configuration of gross trunk shape in hominins due to its morphological integration with the pelvic system in the caudal part (Jellema et al., 1993; Bastir et al., 2014a) and with the upper limb in the cranial part (Churchill, 1994; Bastir et al., 2013; Schmid et al., 2013). Specifically, wide trunks consisting of a wide lower thorax linked to a wide pelvis have been proposed to be the characteristic bauplan of several fossil hominin species such as Neanderthals (Franciscus and Churchill, 2002; Gómez-Olivencia et al., 2009; García-Martínez et al., 2014; Bastir et al., 2015a), Middle Pleistocene hominins (Arsuaga et al., 1999; Carretero et al., 2004), *Homo erectus* (Arsuaga et al., 1999; Carretero et al., 2004; Graves et al., 2010; Holliday, 2012; García-Martínez et al., 2016b; but see Walker and Leakey, 1993) and even the recently discovered species of *Homo naledi* (Berger et al., 2015; Van Sickle et al., in review; Williams et al., 2017). Finally, some authors have proposed that other factors such as gut size or function could also potentially account for morphological differences in the lower part of the rib cage (Aiello and Weeler, 1995; Ben-Dor et al., 2016).

However, despite the importance of rib cage anatomy, it must be noted that traditionally, morphological variation in the thorax has received much less attention than other cranial and postcranial elements (Gómez-Olivencia et al., 2009). Therefore, aspects such as inter-specific thoracic variation in fossil hominin species and its paleo-biological implications are still not clear. This is mainly caused by several factors: 1) the fragile nature of thoracic elements (ribs and vertebrae) means that they usually appear broken or taphonomically distorted in the fossil record of hominins; 2) the metameric structure of the rib cage and the fact that not every part (ribs and vertebrae) of the whole (thorax) is usually found in the fossil record means that in most cases thorax morphology has been inferred from a couple of elements, usually distorted and isolated from their anatomical context; and 3) the quantification of the complex 3D curvature of the costal elements by linear measurements such as chords, angles or diameters potentially complicates the interpretation of fossil thorax morphology.

Historic perspective on the study of the Neanderthal ribcage

The first studies of fossil hominin thoracic morphology were carried out at the end of the 19th and early 20th century on the Neanderthal ribs from the Feldhofer Grotte (Fuhlrott, 1859), Krapina (Gorjanović-Kramberger, 1906), La Chapelle-aux-Saints (Boule, 1911-1913) and Tabun 1 (McCown and Keith, 1939). Although Fuhlrott (1859) and Boule (1911-1913) provided mainly inventories of those costal remains, Gorjanović-Kramberger (1906) and McCown and Keith (1939) carried out metric analyses drawing attention to interesting features of the ribs such as their marked robustness, their rounded cross section or the straightness of the 1st ribs. These morphological features were linked by McCown and Keith (1939) to a greater respiratory capacity in Neanderthals compared to modern humans. Later, at the end of the 20th century, the monographs of the Shanidar Neanderthals (Trinkaus, 1983), La Ferrassie (Heim, 1976) and Kebara 2 individual

(Arensburg, 1991; Bar-Yosef et al., 1991) also addressed the study of the ribs of these specimens. The study carried out by Heim (1976) was mainly a summary of the remains of La Ferrassie individuals and did not find any differences between La Ferrassie costal morphology and that of modern humans. Trinkaus (1983) concluded that the ribs of Shanidar 3 were thicker and more robust than in modern humans, but the incompleteness of the remains did not allow for an overall idea of their thoracic configuration. Arensburg (1991) concluded that the morphology of the Kebara 2 Neanderthal rib cage did not differ from the thoraces of modern populations.

It is important to note that even though some of the previously cited studies carried out metric analyses on the fossils, the comparative samples (if there were any) were always very small, so differences between Neanderthals and modern humans were assessed without any statistics. The break with previous methods of study happened at the end of the 20th century with the publication of the monograph on the *H. ergaster* or *H. erectus* KNM-WT 15000 (Walker and Leakey, 1993). This was the first complete and detailed comparative study carried out on thoracic fossils (ribs and vertebrae) using statistical analyses and large comparative samples (Jellema et al., 1993; Latimer and Ward, 1993). These authors pointed out that the modern human rib cage morphology arose with the emergence of *Homo erectus*, with features such as the volumetric expansion of the upper rib cage, the invagination of the spine and the declination of the ribs. However, other authors have recently questioned the modernity of the KNM-WT 15000 rib cage (García-Martínez et al., 2016b).

In the decades that followed, authors used similar methods (traditional measurements such as arcs, chords or angles) to publish very complete and detailed comparative studies of Neanderthal ribs. This greatly improved the understanding of

Neanderthal rib cage morphology (Franciscus and Churchill, 2002; Weinstein, 2008; Gómez-Olivencia et al., 2009; Gómez-Olivencia, 2015).

Franciscus and Churchill (2002) carried out an exhaustive and comprehensive metric analysis on the Shanidar 3 Neanderthal ribs, comparing them with a wide range of Neanderthals (from Western European to Levantine individuals) as well as with early and modern European *H. sapie*ns. Based on the upper ribs analysis, they observed that the Neanderthal upper thorax (although variable) could be more antero-posteriorly expanded than in modern humans. They stated that this feature was more evident in Western European Neanderthals than in the Levantine ones. These observations are consistent with the straightness of the 1st ribs observed in the Krapina sample by Gorjanović-Kramberger (1906) or the straightness in the 2nd rib of Tabun 1 observed by McCown and Keith (1939), which would be consistent with the elongated clavicles observed by other authors (Churchill, 1994; Rosas et al., 2016). However, a later reassessment of La Chapelle-aux-Saints 2nd rib by Gómez-Olivencia et al. (2009) challenged this idea, since they proposed that 2nd rib of La Chapelle-aux-Saints was less straight than previously thought.

Finally, Franciscus and Churchill (2002) concluded that although there is some degree of variation in the Neanderthal thorax (perhaps caused by factors such as sexual dimorphism and possibly eco-geographical variation), their rib cages were more voluminous (mainly at the caudal part). They hypothesized a greater vital capacity for them compared to modern populations. They stated that the larger volume of the Neanderthal thorax was produced by a medio-lateral expansion of the lower thorax in Tabun 1, by a medio-lateral and an antero-posterior expansion of the thorax in Kebara 2 and by an antero-posterior expansion of the overall thorax in Shanidar 3. The larger inspiratory volume of Neanderthals is consistent with their larger nasal cavities (Bastir and Rosas, 2016), which could be linked to a higher oxygen demand due to greater

physical activity compared to modern humans (Churchill, 2006; Froehle and Churchill, 2009). However, other explanations such as cold adaptation and/or genetic drift as causal mechanisms for generating this thorax morphology were not excluded by Franciscus and Churchill (2002).

The results of Franciscus and Churchill (2002) were later confirmed by Weinstein (2008), who measured Shanidar 3 and Tabun 1 ribs and compared them to Andean populations, which are known to present enlarged thoraces in response to a higher oxygen demand because of their hypoxic living conditions. She observed that both Neanderthals' rib cages were slightly larger than their Andean counterparts, concluding that the large Neanderthal thorax may reflect an adaptation to both a high oxygen intake and high activity levels. Subsequently, Gómez-Olivencia et al. (2009) carried out a very detailed analysis of the Kebara 2 Neanderthal ribs in comparison to populations inhabiting moderate and cold climates. They found size differences in the central (4, 5 and 7) and lower ribs (8 and 10) of Kebara 2. As these are larger than comparative ribs of modern humans, they inferred a large thorax capacity for this individual. It is important to mention that ribs 6 and 9 were not complete, so the lack of differences in those ribs could be attributed to this. However, they could not definitively conclude whether these differences were caused by a medio-lateral expansion of the thorax, an antero-posterior expansion, or both. Clarifying this issue would contribute not only to the understanding of the breathing kinematics in Neanderthals (which is dependent on thorax shape), but also to the understanding of their body shape.

Although the previous research has laid the groundwork for better understanding differences between thorax morphology in Neanderthals and modern humans, and while it has greatly improved our knowledge of its paleo-biological implications, several issues should be noted. First, linear measurements (chords, arcs, angles) do not accurately

quantify the complex three-dimensional morphology of ribs. Also, missing costal ends are very difficult to estimate using such methods. For example, Shanidar 3 does not preserve any of the distal or proximal ends of the ribs in connection with the rib shaft, as noticed by Trinkaus (1983). Therefore, the estimation of the rib ends and the evaluation of the overall curvature of the rib present a serious challenge in some cases.

Secondly, inferences about thorax morphology based solely on rib size and shape, regardless of its anatomical connection with the thoracic vertebrae, might lead to misinterpretations of antero-posterior or medio-lateral expansion of the thorax. It has recently been observed that a different orientation of the transverse processes of the thoracic vertebrae could significantly alter the thorax widening (Bastir et al., 2014b, 2015a; 2017, in review; García-Martínez et al., 2016c). Therefore, the same rib morphology could produce a different thoracic configuration depending on the degree of dorsal orientation of the transverse processes of the thoracic vertebra. This fact makes evident the need to combine the knowledge of both ribs and vertebrae in order to make inferences about features such as the antero-posterior or the medio-lateral expansion of the thorax, which are emergent features of the anatomical composite that can hardly be inferred from individual elements.

Recent perspectives on the study of the Neanderthal ribcage

Methodological advances such as the development of Virtual Anthropology (Recheis et al., 1999; Weber et al., 2015) and improvements of 3D quantification of sliding semilandmarks methods have allowed for a more accurate quantification both of the thorax and individual ribs, even when the record is fragmentary (Bastir et al., 2013, 2015a; García-Martínez et al., 2014, 2016b, c; Shi et al., 2014; Weber at al., 2014; Williams et al., 2017). Virtual reconstruction and virtual estimation of missing elements or distorted parts has allowed for analyses of fossils previously regarded as uninformative

or for the re-analyses of fossils that were previously reconstructed wrongly (Zollikofer et al., 2005; Gunz et al., 2009; Bastir et al., 2010; García-Martínez et al., 2014; Gómez-Olivencia et al., 2015). Indeed, one of the most complete studies about the Neanderthal thorax (Gómez-Olivencia et al., 2009: 87) stated the following years ago: "The application of virtual reconstruction techniques may in the near future improve our understanding of the Neandertal thorax".

Regarding semilandmarks methods, García-Martínez et al. (2014) quantified the size of individual ribs of the Kebara 2 Neanderthal from 1st to 10th using 3D geometric morphometrics techniques. In this study we carried out a virtual reconstruction of the 6th and 7th ribs from the left side following the reassessment made by Gómez-Olivencia et al. (2009). We found that, in accordance with previous research using traditional morphometrics, the ribs belonging to the lower thorax (from 7th onwards) presented larger centroid size than their corresponding ribs in modern humans. Therefore, since these are the ribs functionally linked to diaphragmatic action, we hypothesized a greater diaphragmatic contribution to Neanderthal breathing than that found in modern humans. This was consistent with previous research (Franciscus and Churchill, 2002; Weinstein, 2008; Gómez-Olivencia et al., 2009) and with the hypothesis of a high oxygen demand because of high levels of physical activity (Churchill, 2006; Rosas et al., 2006; Bastir, 2008; Froehle and Churchill, 2009; Bastir and Rosas, 2016).

Later, Bastir et al. (2015a) studied the 1st ribs sample of the El Sidrón site from an ontogenetic point of view in a comparative framework with modern humans, finding divergent ontogenetic trajectories for the 1st rib ontogeny of both species. These ontogenetic differences explained why adult Neanderthal 1st ribs presented, on average, less curvature in cranial view than their modern human counterparts. Additionally, Bastir et al. (2015a) tested the hypothesis of Gorjanović-Kramberger (1906) that straighter 1st

ribs in Neanderthals should be correlated with antero-posterior projection of their entire ribcage. Bastir and collaborators (2015a) found that the straightness of the 1st rib was correlated with the anterior projection of the upper thorax but with a lateral expansion of the lower thorax in the comparative modern human thoraces sample (ribs and vertebrae in anatomical articulation). Because of this correlation, along with the evidence of straighter ribs in Neanderthals, their data supported Gorjanović-Kramberger's hypothesis (1906) only with respect to the upper thorax, because the lower rib cage could be more medio-laterally expanded than in modern humans. It is important to note that years earlier, Sawyer and Maley (2005) created a physical reconstruction of a Neanderthal rib cage (mainly based on the ribs and vertebrae from Kebara 2) which also predicted a medio-lateral expansion of the lower thorax for this Neanderthal. Even though some "artistic license" was used for that reconstruction (Sawyer and Maley, 2005: 26), the morphology of that rib cage is consistent with the hypothetic model proposed by Bastir et al. (2015a), and both studies are the only ones that considered both ribs and vertebrae in order to infer Neanderthal thorax morphology.

The El Sidrón site

El Sidrón site is a karstic cave located in Asturias in northern Spain, in the "Surco Oviedo-Infiesto" -a band of Mesozoic and Cenozoic sediments limited to the north and south by Paleozoic reliefs (Fortea et al., 2003; Rosas et al., 2006). Archaeological excavations in the cave were conducted from 2000 to 2014. They uncovered 415 lithic tools (Santamaría et al., 2010), 51 macro-mammal remains (Rosas et al., 2011), and more than 2500 Neanderthal bone fragments (Rosas et al., 2013) all from the same archaeological unit (Unit III; Cañaveras et al., 2011), representing the most complete Neanderthal sample of the Iberian Peninsula (Rosas et al., 2006, 2012, 2015). These remains were found in a secondary position; the original deposit, worn out by erosion, is

thought to have been either on the surface or in an upper karst level (Fortea et al., 2003). Several dating methodologies applied to the Neanderthal bones and teeth give a consistent date of around 49,000 BP (de Torres et al., 2010; Wood et al., 2013), with environmental conditions similar to those of the present (Fortea et al., 2003; Badal-García, 2011; Rosas et al., 2011; Sanchíz and Martín, 2011).

All of the Neanderthal skeletal regions have been preserved, and several regions (e.g., thorax, arms, feet and hand bones) were recovered in anatomical articulation (Rosas et al., 2006, 2013). A total of 13 Neanderthal individuals have been identified from El Sidrón (Rosas et al., 2013, 2015), including 7 adults (4 females, 3 males), three adolescents (1 female, 2 males), 2 juveniles (1 male, 1 for which sex determination is still in progress), and one infant (whose sex is indeterminate).

Aims of this study

The main aim of this study is to describe and analyze in a comparative context the costal material from the El Sidrón site. It is important to note that in this study we did an in-depth analysis of all the costal material except the one that could belong to juveniles 1 and 2 (according to Rosas et al., 2013). Since previous studies have been based mainly on the costal morphology of four Neanderthal individuals (Kebara 2, Shanidar 3, La Chapelle-aux-Saints and Tabun 1), the El Sidrón material can shed light on Neanderthal thorax morphology by addressing the following issues:

Regarding the proximal part of the rib, articular tubercles have been observed as larger and more heavily remodeled than in modern humans (Franciscus and Churchill, 2002; Gómez-Olivencia, 2015). However, the rib head in Neanderthals has never been studied in a comparative context because of the aforementioned fossil record biases. Because of the good preservation of several rib heads in the El Sidrón sample, we aim to lay the groundwork on this matter. Since there is a lack of evidence about differences

between rib heads of both species, we test the hypothesis **(H1)** that predicts that Neanderthals and modern humans present the same dimensions at the proximal rib end.

Additionally, there is a consensus about the more capacious rib cage in Neanderthals. However, it is still unknown if this expansion is produced by changes in the antero-posterior, the medio-lateral dimensions, or both together. Since ribs from the upper, middle and lower thorax are preserved in the El Sidrón sample, we aim to clarify this debate in the light of Sawyer and Maley's (2005) hypothetic reconstruction and findings made by Bastir et al. (2015a) testing the hypothesis **(H2)** that predicts that the Neanderthal thorax morphology is more antero-posteriorly expanded in the upper thorax and more medio-laterally expanded in the lower thorax than in modern humans.

Material and Methods

The El Sidrón costal remains

The site has yielded a large number of costal remains, ranging from remains of the 1st ribs to the 12th ribs (García-Martínez et al., 2016d). Although the costal sample is fragmentary, every part of the rib anatomy is represented: head, neck, rib shaft and distal end. Importantly, the costal sample includes several well preserved proximal ends (head and articular tubercle) that are rare and scarce in the Neanderthal fossil record. Articular tubercles are preserved in several Neanderthals but, regarding the rib head, only Kebara 2 presents two partially complete rib heads from true ribs and four almost complete ones from floating ribs. Moreover, the most complete studies on this fossil individual (Franciscus and Churchill, 2002; Gómez-Olivencia et al., 2009; García-Martínez et al., 2014) do not address the study of this anatomic costal area. The rib heads from the El Sidrón site could help to improve the knowledge about this important anatomical region in Neanderthals.

The Neanderthal costal remains of the El Sidrón site are temporarily housed at the Department of Paleobiology of the Museo Nacional de Ciencias Naturales (MNCN-CSIC) in Madrid, Spain. The most informative costal remains addressed in this study are shown in Figures 1-3 and general parameters such as number of individual specimens (NISP), minimum number of elements (MNE) and minimum number of individuals (MNI) are shown in Table 1. A complete list of specimens addressed in-depth in this study is included in Table S1.

Comparative sample for traditional measurements

We compared the El Sidrón original ribs with adult ribs belonging to European modern humans (Spain, N=120 ribs; Portugal, N=120 ribs; Austria, N=48 ribs; 12 males and 12 females in total). Individual ribs from the Spanish and Austrian populations were segmented from CT scans of healthy subjects throughout semiautomatic methods in Mimics software (http://www.materialise.com/en/medical/software/mimics) in order to get measurable 3D models of individual ribs. The data were obtained from hospital subjects that were scanned previously as a healthy control group in order to compare with pathological individuals belonging to a different research project at the Hospital Universitario La Paz (Madrid, Spain) and Medizinischen Universität Innsbruck (Innsbruck, Austria). Individual ribs from the Portuguese population (21st century Identified Skeletal Collection, housed at the Laboratory of Forensic Anthropology, University Of Coimbra, Portugal; Ferreira et al., 2014) were scanned through a Next Engine HD 3D laser scanner in 'wide mode' (with a resolution 0.38 mm and an accuracy of 6 points per mm). In none of the cases could any pathologies affecting skeletal thorax form be identified. Detailed information on the comparative sample can be found in Table S2.

Comparative sample for geometric morphometrics

Since only 1st, 5th and 11th ribs from the El Sidrón site were measured by 3D geometric morphometrics, we only used the corresponding ribs of the modern human comparative sample mentioned above (See table S2). Additionally, different HD surface 3D models of fossils belonging to these levels were studied for geometric morphometrics analyses (Table S2). We compared the El Sidrón 1st ribs with two 1st ribs from the Krapina site (117.2 and 118.2; Gorjanović-Kramberger, 1906) as well as the two 1st ribs from Kebara 2 (Arensburg, 1991). Additionally, we included several fossil *Homo sapiens* in the comparative sample: the 1st rib from the Mladeč site (Trinkaus et al., 2006), the 1st rib from the Cueva de la Paloma site (Hernández-Pacheco, 1923), the 1st rib from the Oetrange site (Meiklejohn et al., 2014) and the two 1st ribs from a 19 years old female *H. sapiens* named "La Femme de Tigermoyen". This individual was discovered at the d´Arlit region (Nigeria) by Henri Lothe in 1974 and dated in 5,420 BP. It is housed at the MNHN (Paris, France) and it has never been properly published to the date. Regarding the 5th and 11th ribs, we compared the ones from the El Sidrón site with their corresponding ribs from the Kebara 2 Neanderthal (Arensburg, 1991; Gómez-Olivencia et al., 2009).

Position and side assessment of the costal remains

The side of the remains was assessed using anatomical features such as the costal groove or the rib axis orientation. For diagnosis of the anatomical position, we used morphological features together with specific diagnostic features for assessing remains belonging to atypical ribs (1st, 2nd, 11th and 12th). These features include the presence of specific muscle insertions for the 1st and 2nd ribs (scalene and serratus insertions), the absence of the articular tubercle for the 11th and 12th ribs and the presence of a single facet at the rib head on the 1st, 11th and 12th ribs. Even though these features are "standard" (Spalteholz, 1970), it is important to mention that some variation could be

found in those traits, such as the presence of a double facet at the rib head (Ohman, 1986; Tawane et al., 2016) or the lack of the articular tubercle in the 10th rib (such as in the case of Kebara 2 individual; see Gómez-Olivencia et al., 2009). For the typical ribs (from 3rd to 10th) we used comparative anatomy to evaluate a possible positional range for ribs when the proximal end (and thus the rib head) was missing. For evaluating remains of unknown position where the rib head was preserved (five specimens in the sample), we explored changes in the rib head shape along the costal sequence by calculating an index of rib head height by rib head width in ribs from 1st to 10th in our comparative sample. Head height was measured by the head cranio-caudal diameter (HCCD) following definition of Gómez-Olivencia et al. (2010) and head width (HW) is defined in this study as the maximum length of the articular surface of the rib head perpendicular to the cranio-caudal axis (coinciding with the length of the inter-articular crest, when applicable). Once the index was calculated, we measured Neanderthal rib heads of known anatomical position (assessed at the excavation) in order to validate the modern human index as a proxy for positioning Neanderthal ribs: the 1st and 2nd from Kebara 2 and an 8th from the El Sidrón (in anatomical connection within a partial thorax). The 3rd rib from the El Sidrón site was evaluated because of its anatomy. Measurements on the modern humans, as well as in Kebara 2 rib heads, were taken on 3D virtual models using Artec v11 software (www.artec3d.com), whereas the measurements on the El Sidrón sample were taken on original specimens by standard anthropometric instruments.

Morphological descriptions, metrics and qualitative analyses of the more diagnostic remains

A full morphological description, seriation, qualitative observations, state of preservation as well as standard measurements (following Franciscus and Churchill, 2002 and Gómez-Olivencia et al., 2010) and assessment of developmental age (following Ríos

and Cardoso, 2009) was conducted on the best preserved and most informative specimens from the El Sidrón collection addressed here (N=18; see results). Fragments preserving information about anatomical position but lacking diagnostic morphology are listed with approximate identification and preservation in Table S1. In the best preserved proximal rib remains, apart from the aforementioned measurements at the rib head (HCCD and HW), other measurements at the articular tubercle (ATH and ATW, following Franciscus and Churchill, 2002) and at the neck (TNL, following Gómez-Olivencia et al., 2010) were also carried out. Measurements of La Chapelle-aux-Saints 1 were taken from Gómez-Olivencia (2015), the ones of Kebara 2 and Shanidar 3 were taken on 3D models using Artec v11 software. The last fossil 3D data was obtained from surface scanner and CT-scanner of the original remains, respectively. Measurements in the fossils were compared with the ones of modern humans throughout 95% confidence intervals for the mean (Sokal and Rohlf, 1973: 140) in SPSS software (SPSS Inc., 1995).

Virtual reconstruction methods

Because of the preservation of some remains, virtual reconstruction of a 5th and an 11th rib from the El Sidrón sample was needed in order to recreate hypothetic morphologies for those ribs. We created parsimonious hypothetic anatomical composites using virtual techniques such as mirror imaging, fusing or smoothing, etc. (similar to the methods used by Gómez-Olivencia et al., 2015). The final 3D models allowed us to measure variables that were previously not possible to measure in individual remains, such as the TVC, TVA and TID2 (for the 5th rib) and the HVC and HVA (for the 11th rib). These linear measurements provide an overall idea of the curvature in cranial view of the rib (Gómez-Olivencia et al., 2009, 2010). Additionally, these virtual reconstructions were analyzed through 3D geometric morphometric techniques.

3D geometric morphometrics of individual ribs

3D geometric morphometrics were carried out at different thoracic levels, according to the best preserved elements from the El Sidrón sample. Consequently, we analyzed the thorax at the 1st, 5th and 11th thoracic levels.

1st ribs

In the 1st rib sample (total N=35; see material) we measured 55 3D landmarks and semi-landmarks in Viewbox4 software (www.dhal.com) in order to quantify rib head morphology, 3D rib curvature, shaft height and shaft thickness for geometric morphometric analyses (Fig. S1). Missing data estimation was carried out also in Viewbox 4 software (www.dhal.com) through Thin Plate Spline and following bending energy approach (Gunz, 2005; Gunz et al., 2009). When missing data needed to be estimated at the proximal or distal ends of the *H. sapiens* ribs (both early and modern) the mean coordinates of their respective sample were used as a reference for estimating missing landmarks. For the missing landmarks at the proximal ends of Neanderthal 1st ribs (SD-1767; SD-1699+SD-1685; Krapina 117.2; Krapina 118.2), we used the Kebara 2 1st rib as a reference to estimate these missing points. When missing landmarks were at the distal end of 1st ribs (SD-1699+SD-1685; Krapina 117.2; Krapina 118.2) we used the average coordinates of the 1st ribs of the Neanderthals preserving this region (SD-1767; both antimeres of Kebara 2) as a reference for estimating missing points.

Because of uncertainty in their locations along a rib, semi-landmarks were slid along their corresponding curves relative to the fixed landmarks to minimize bending energy. Firstly, this was done between each specimen and the template (first specimen). Then, semi-landmarks were slid a second time along their curves so as to minimize bending energy between each specimen and the sample average (Gunz et al., 2005, 2009;

Mitteroecker and Gunz, 2009). This sliding procedure adjusts their relative locations along the curve.

5th ribs

In the 5th rib sample (total N=27, see material), we measured 61 3D landmarks and semi-landmarks in Viewbox4 software (www.dhal.com) in order to quantify rib head morphology, 3D rib curvature, shaft height and shaft thickness for geometric morphometric analyses (Fig. S2). No missing data estimation was needed in the virtual reconstruction of the El Sidrón 5th rib and we used the average coordinates of SD virtual reconstruction as a reference for estimating missing points at the missing ends of the Kebara 2 ribs. This estimation was made using Viewbox 4 software (www.dhal.com) through Thin Plate Spline and following a bending energy approach (Gunz et al., 2005, 2009; Mitteroecker and Gunz, 2009). We followed the same sliding protocol as in the case of the 1st ribs.

11th ribs

In the 11th rib sample (total N=27), we measured 44 3D landmarks and semi-landmarks in Viewbox4 software (www.dhal.com) in order to quantify rib head morphology, 3D rib curvature, shaft height and shaft thickness for geometric morphometric analyses (Fig. S3). No missing data estimation was needed in the virtual reconstruction of the El Sidrón site 11th rib and we used the coordinates of SD virtual reconstruction for estimating missing points at the rib heads of the Kebara 2 11th left (rib head taphonomically damaged) and right ribs (rib head wrongly glued to the rib shaft; Asier Gómez-Olivencia, personal communication). This estimation was also carried out in Viewbox 4 software following the same protocol as with the 1st and 5^{th} ribs (Gunz et al., 2005, 2009; Mitteroecker and Gunz, 2009).

Geometric morphometrics analyses

Shape data were obtained by Generalized Procrustes Analysis (GPA). Size was quantified as centroid size (i.e. the square root of the summed squared distances of each landmark to the centroid; O'Higgins, 2000; Mitteroecker and Gunz, 2009) and 95% confidence intervals for the mean were used to compare and explore the size relations between the El Sidrón ribs and the rest of the sample in SPSS software (SPSS Inc., 1995). Shape data were subjected to Principal Components Analysis (PCA) to reduce the dimensionality of data and to visualize the main axes of variation (O'Higgins, 2000) using MorphoJ software (Klingenberg, 2011). Shapes associated with variations along PC axes were visualized as warps of the sample mean shape into shapes corresponding to the observed maximum and minimum ranges of PC scores for the 1st and 11th ribs, where differences between Neanderthals and the rest of the sample could be observed. This was done using the EVAN Toolkit (ET-software) version 1.71 (http://www.evan3 society.org/). Moreover, in order to reaffirm differences in shape between both species at the 1st, 5th and 11th costal levels, mean shapes analyses were carried out in MorphoJ software (Klingenberg et al., 2011). Differences were assessed through Procrustes distance between means and a permutation test (N=10,000) for testing equal group means. Group means were also warped and shown using EVAN Toolkit when differences were statistically significant.

Results

Position and side assessment of the costal remains

Assessment of anatomical position and side was possible in 94 costal remains. Because of the preservation of some remains, a precise side and position assessment was not possible in 82 of them. The analyses of atypical ribs allowed for determination of five

1st rib remains (two from the left side and three from the right side), three 2nd rib remains (all of them from the left side), seven 11th rib remains (four from the left side and three from the right side) and six 12th rib remains (three from each side). Additionally, 16 remains were attributed to a range from 2nd to 4th ribs (eight from each side), 35 remains to a range from 4th to 8th ribs (20 from the left side and 15 from the right side) and 22 remains to a range from 8th to 12th ribs (11 from the left side and 10 from the right side). Results of HCCD/HW index, displayed in Figure 4, show an increase of this value along the costal sequence from the 1st (index around 1) to the 10th (index between 2 and 2.5). This indicates that upper ribs present similar dimensions of HCCD and HW (more square-shaped rib heads) whereas lower ribs present larger HCCD compared to HW (taller and narrower rib heads).

Additionally, as can be observed in Figure 4, Neanderthal ribs of known position fall within their correspondent modern human ranges. This indicates that the modern human index calculated in this study is useful for anatomically assessing Neanderthal rib heads of unknown anatomical position. Following this method, SDR-161+ was evaluated as 4th rib, SD-695a and SD-448 as 5th ribs and SD-666 and SD-788 as 6th or 7th ribs.

Morphological descriptions, metrics and qualitative analysis of the more diagnostic remains

Because of the preservation of the remains, morphological descriptions, metrics and qualitative analyses were carried out in 18 costal elements (24 remains), ranging from the upper (1st ribs) to the lower thorax (12th ribs).

True ribs

- SD-1767 and SD-1699+ (Fig. 1): These are 1st ribs from the left and right side respectively. A full morphological description and metric comparison of these elements can be found in Bastir et al. (2015a).
- SD-1534 (Fig. 1): This is a proximal part of a 1st rib from the right side. It is flattened in its cranio-caudal direction and preserves the articular tubercle and the area adjacent to it. It also preserves part of the rib neck but lacks the rib shaft almost entirely. Measurements available in this element can be found in Table 2.
- SD-695b (Fig. 1): This is a proximal part of a 2nd rib from the left side that preserves part of the neck, the articular and non-articular tubercles and part of the rib shaft, including the posterior angle and part of the insertion of the posterior scalene muscle. This insertion is considerably marked, being more marked than in every other adult Neanderthal 2nd rib known (Fig. S4). The epiphysis at the articular tubercle is completely fused so a minimum age of 11 or 14 years old (depending on the sex) is estimated for this individual. Measurements available in this element can be found in Table 2.
- SDR-159 (Fig. 1): This is a distal fragment of a left 2nd rib, preserved from the distal part of the serratus anterior muscle insertion (which is not very pronounced) to the distal end, which is complete and not damaged. The shaft is cranio-caudally flattened and presents a lack of curvature in cranial view, similar to the one proposed for Tabun 1 by McCown and Keith (1939) and much straighter than both antimeres of the Kebara 2 individual. Although SD-695b and SDR-159 do not refit together, we cannot exclude that both remains belong to the same element because both belong to the left side and there is no anatomical overlap between them. Measurements available in this element can be found in Table 2.

- SDR-026+SDR-166 (SDR-026+ onwards; Fig. 2): This is a proximal-medium part of a 3rd rib from the left side of the rib cage. It is preserved from the rib head to beyond the costal angle, reaching almost the midshaft. The insertions for the intercostal muscles are pronounced, both at the costal groove and at the superior border of the rib. The posterior angle is not fully apparent as it is eroded, but the articular tubercle and the rib head are complete and not taphonomically damaged in this individual. The epiphysis at the articular tubercle is completely fused, so a minimum age of 11 to 14 years old (depending on the sex) is estimated for this individual. Measurements available in this element can be found in Table 2.
- SDR-161+SDR-196+SDR-192 (SDR-161+ onwards; Fig. 2): This is a proximal part of a 4th rib from the left side of the thorax. It is well preserved from the rib head to the costal tubercle. This element comes from the refitting of three fragments, but some parts of the shaft and behind the articular tubercle are missing. The epiphysis at the articular tubercle is completely fused but the one at the rib head is not fused, so an age range of 14 to 21 years old (depending on the sex) is estimated for this individual. Measurements available in this element can be found in Table 2.
- SD-695a (Fig. 2): This is a proximal part of a 5th rib from the right side, preserved from the rib head to beyond the articular tubercle. The rib head and the articular and non-articular tubercles are well preserved, although the head has slight erosion in the superior part. The epiphysis at the articular rib head is completely fused, so a minimum age of 18 years old is estimated for this individual. Measurements available in this element can be found in Table 2.
- SD-448 (Fig. 2): This is a proximal part of a 5th rib from the left side which is preserved from the rib head to the articular tubercle. The superior part of the rib

head is missing but the articular tubercle is well preserved. The epiphysis at the rib head is in active fusion, so an age range of 15 to 22 years old (depending on the sex) is estimated for this individual. Measurements available for this element can be found in Table 2.

- SD-1450 (Fig. 1): This is a medial-distal part of what is probably a 5th rib, which is preserved from the posterior angle almost to the almost the distal end. It is one of the most complete rib shafts from the central thorax of the El Sidrón costal sample. The posterior angle, which is complete and well preserved, is very pronounced (as observed in Kebara 2 Neanderthal; Fig. S5) so a strong *latissimus dorsae* muscle could be inferred for this rib. Both proximal and distal ends are missing in this remain. Measurements available for this element can be found in Table 2.
- SD-666 (Fig. 2): This is a proximal part of a 6th or 7th rib from the right side of the thorax. It is preserved from the rib head to beyond the articular tubercle. The rib head and the articular and non-articular tubercles are well preserved in this remain, although the head presents erosion in the superior part. The epiphysis at the rib head is in active fusion, so an age range from 15 to 22 years old (depending on the sex) is estimated for this individual. Measurements available in this element can be found in Table 2.
- SD-788 (Fig. 2): This is a proximal part of a 6th-7th rib from the right side. It is preserved from the rib head to the articular tubercle. The rib head and the articular tubercle are well preserved in this remain, although the head presents erosion in the inferior part The epiphysis at the rib head is in active fusion, so an age range from 15 to 22 years old (depending on the sex) is estimated for this individual. Measurements available for this element can be found in Table 2.

False ribs

- SD-2001+SD-1834+SD-1771 (2001+ onwards; Fig. 1): This is a rib shaft probably belonging to a 9th or 10th rib from the right side. It presents a superior-inferior expansion of the rib shaft at the midshaft, which is characteristic of 9th and 10th ribs. It preserves from the posterior angle to beyond the midshaft. The shaft at the inferior part of the posterior angle is eroded. The element is composed of three fragments. Measurements available for this element can be found in Table 2.

Floating ribs

- SD-2187 (Fig. 1): This is a partially complete 11th rib shaft from the left side, which only lacks the very proximal and distal parts. It is one of the most complete rib shafts from the lower thorax of the El Sidrón costal sample. Measurements available for this element can be found in Table 2.
- SDR-131 (Fig. 1): This is a proximal part of an 11th rib of the right side of the thorax, which preserves the rib head (complete) and part of the proximal shaft. The rib head presents a single facet. Measurements available for this element are shown in Table 2.
- SD-695c: This is a rib head of an 11th rib from the left side. It clearly presents a single facet. The epiphysis at the rib head is in active fusion, so an age range from 15 to 23 years old (depending on the sex) is estimated for this individual. Measurements available for this element can be found in Table 2.
- SD-573c: This is a rib head of a 12th rib from the right side. It only has a single facet and the epiphysis at the rib head is in active fusion, so an age range from 15

to 21 years old (depending on the sex) is estimated for this individual. Measurements available for this element can be found in Table 2.

- SD-653a: This is a rib head of a 12th rib from the left side. It only has a single facet and the epiphysis at the rib head is in active fusion, so an age range from 15 to 21 years old (depending on the sex) is estimated for this individual. Measurements available for this element can be found in Table 2.
- SD-56: This is a proximal-medial part of a 12th rib which present the insertion of the diaphragm in the cranial part (Fig. S6). This insertion is very similar to the ones observed on the 12th ribs of Kebara 2 or Shanidar 3 (Fig. S6).

Regarding traditional measurements, 95% confidence interval for the mean of measurements taken in the modern human sample with measurements carried out in the El Sidrón and the comparative fossil sample at the articular tubercle (ATH, ATW), rib head (HCCD, HW) and rib neck (TNL) are displayed in Tables S4-S9. Results of Neanderthal rib heads show that these are larger in the cranio-caudal (HCCD) and medio-lateral (HW) dimension in the El Sidrón ribs at almost every level and within the modern human range for the Kebara 2 rib heads belonging to non-floating ribs. Kebara 2 floating ribs are larger than in modern humans (except for the HW of the 11th left rib). Our results on articular tubercles show that articular tubercle height (ATH) is close to the modern human range in the upper ribs but is remarkably larger in the lower ribs, both in Kebara 2 and El Sidrón Neanderthals (Table S5). Articular tubercle width (ATW) is more variable in Neanderthals but we also observed that this measurement at the lower thorax is (overall) larger in Neanderthals (Table S7). Regarding tubercle neck length, we observed that these measurements in Neanderthals felt within the modern human ranges (Table S9).

Our results show that, although Neanderthal head index is comparable to that of modern humans, there are remarkable differences in some individual measurements (HCCD, HW, ATH and ATW) between both groups. This allows us to reject **H1,** which predicts that "Neanderthals and modern humans present the same dimensions at the proximal rib end." However, we specify that differences in head measurements are more pronounced in the lower than at the upper thorax.

Virtual reconstructions

Virtual reconstruction was carried out when the rib shaft was almost complete but the proximal and distal ends were missing. This was necessary for reconstructing SD-1450 (5th rib from the right side) and SD-2187 (11th rib from the left side). For reconstruction of the SD-1450 proximal part, we used the proximal shaft SD-965a as a proxy, which is assessed as a 5th rib. In order to align them, we superimposed SD-1450 and SD-695a to the 5th right rib of Kebara. We used the tubercle-angle distance of the Kebara 2 5th rib to set the distance between SD-1450 and SD-695a. Once the proximal part was correctly aligned, we superimposed at the posterior angle SD-1450 and the 5th right rib of Kebara 2 in order to estimate the missing part of the distal end of SD-1450 (we estimated that 98.9 mm were lacking). Then, we cut off the necessary part from the Kebara 2 rib and fused it virtually to SD-1450+SD-695a in order to create a virtual reconstruction of a complete 5th rib from the El Sidrón sample, whose anatomy was consistent with the anatomy of 5th ribs (Figure 5a). For reconstruction of the proximal part of SD-2187, we used the mirror image of SDR-131, a very complete proximal end of an 11th rib from the El Sidrón. Mirror imaging was necessary in SDR-131, since both elements were from different sides. In order to align them, we used the 11th left rib of Kebara 2 to superimpose SD-2187 and the mirror image of SDR-131, to estimate its relative position. In order to confirm the alignment, we applied the rib head-posterior

angle distance of the Kebara 2 11th right rib to set the distance between SD-2187 and SDR-131. Once the proximal part was correctly aligned, we superimposed at the posterior angle SD-2187+SDR-131 (mirror image) and the mirror image of the 11th right rib of Kebara 2 (the distal end of which was complete) in order to estimate the missing part of the distal end of SD-2187 (we estimated that 53.3 mm were lacking). Then, we cut off the necessary part from the Kebara 2 rib and we fused it virtually to SD-2187+SDR-131 (mirror image) in order to create a virtual reconstruction of a 11th rib from the El Sidrón, whose anatomy was consistent with the anatomy of 11th ribs (Figure 5b).

The virtually reconstructed ribs allowed us to measure their values of TVA (329.50 mm.), TVC (226.85 mm) and TID2 (46.23) for the 5th rib, as well as HVA (249.62 mm) and HVC (180.74 mm) for the 11th one (Table S3). According to our results, Kebara 2 and the reconstructed ribs from the El Sidrón site presented values that are outside of the modern human 95% confidence interval for the mean of modern human in every value, except for the TID2 of the Kebara 2 right rib, which was close to the upper part of the confidence interval for modern human males. It should be noted that the larger values observed in the El Sidrón virtually reconstructed ribs and in the Kebara 2 11th right rib must be considered carefully since the estimation methods could introduce some error.

3D geometric morphometrics of individual ribs

1st ribs

Size was quantified as centroid size (CS). Results of the 95% confidence interval for the mean show that males of modern humans are larger than females (Fig. 6a). Early modern human ribs were highly variably in CS, ranging from the small right rib of the Nigerian individual called “La Femme de Tigermoyen” (168.36) to the large 1st rib from

Cueva de la Paloma site (205.66). All of these individuals are below the confidence interval of both males and females (Fig. 6a). Regarding Neanderthal 1st ribs, their centroid size distribution was less dispersed than in the case of modern human fossils, ranging from SD-1767 (202.81) to the Krapina 117.2 (222.18). Neanderthal 1st ribs are located below the modern range for males, even the ones from Kebara 2 that are known as belonging to a male individual. Krapina 117.2 is the only exception to this, but it is located within the lowest part of the confidence interval of modern males (Fig. 6a). Every Neanderthal 1st rib is located around the confidence interval of modern females.

Regarding shape, PC1-PC2 projection (which explains 61.67% of the variability of the sample) shows that Neanderthal 1st ribs are more polarized towards the negative values of PC1 than their modern human counterparts, while fossil *H. sapiens* fall within the center of the distribution of modern humans (Fig. 7a). We can observe in the associated warps that positive values of PC1 are characterized by 1st ribs presenting a stronger curvature in cranial view than the ones at the negative values. Additionally, different orientations of both proximal and distal ends are explained by this PC. At the proximal end, positive values present a more closed angle between the neck and the proximal part of the shaft, whereas negative values present a more opened angle between the neck and the proximal shaft. A more medial orientation of the distal end is observed in the warps associated to the positive scores PC1, whereas the other pole of the axis is characterized by a more lateral orientation of the distal end (Fig. 7a).

Results of mean comparisons (Table 3) show statistical differences ($p<0.01$) between the Neanderthal group and modern humans, both fossil and current. The largest Procrustes distance (0.09) is found between Neanderthals and current modern humans. Warps associated with means are shown in Figure 8a, and indicate that the differences between Neanderthals and modern human groups are the same as observed in the warps

associated with PC1: less curvature in cranial view, more opened angle at the tubercle between the neck and the proximal shaft, and a more lateral orientation of the distal end is found in Neanderthals than in modern humans.

5th ribs

Results of the error bar graph (95% confidence interval for the mean) show that 5th ribs of modern human males are larger than female ones (Fig. 6b). Additionally, the Kebara 2 left rib is located within the highest part of the interval for modern males but the Kebara 2 right rib and the reconstructed 5th rib from El Sidrón are above this range (Fig. 6b).

Regarding shape, Neanderthal 5th ribs were not polarized in any PC, overlapping with modern humans in every PC projection. This lack of differences is also confirmed by results of mean comparisons (Table 4), because no statistical differences between the groups could be found.

11th ribs

Results of the error bar graph (95% confidence interval for the mean) show that males are larger than females in the modern human sample (Fig. 6c). Neanderthal CS distribution of 11^{th} ribs ranged from the 11th left rib of Kebara 2 (462.36) to the reconstructed 11th rib of the El Sidrón site (469.18). Every Neanderthal 11th rib is located clearly above the modern human range (Fig. 6c).

Regarding shape, PC1-PC2 projection (which explains 81.81% of the variability of the sample) shows that Neanderthal 11th ribs are more polarized towards the negative values of PC1 than those of their modern human counterparts (Fig. 7b). As it can be observed in the associated warps, negative values of PC1 characterize 11th ribs presenting a stronger curvature in cranial view than the 11th ribs located at the positive values.

Additionally, the relative head-posterior angle distance is shorter in the negative values of the PC1 and, therefore, the posterior angle-distal end distance is relatively larger in the ribs at the negative values than in the ones at the positive values (Fig. 7b).

Results of mean comparisons show that there are statistically significant differences between the groups studied (Table 5). Warps associated with means are observed in Figure 8b. The same differences observed in the PC1 scores warps are observed in the means: stronger curvature in cranial view and a shorter relative head-posterior angle distance is observed in Neanderthals than in modern humans.

Discussion

The El Sidrón site has provided costal remains ranging from 1st to 12th ribs and including several proximal ends (rib head, neck and articular tubercle) that could enhance our understanding of the Neanderthal thorax morphology. The aim of this paper was to present the material through descriptive, qualitative and comparative methods, but costal remains that can be clearly attributed to subadults are not addressed in this study. Therefore, we tested the hypothesis **(H1)** which predicts that Neanderthals and modern humans present the same dimensions at the proximal rib end, and the hypothesis **(H2)** which predicts that Neanderthal thorax morphology is more antero-posteriorly expanded in the upper thorax and more medio-laterally expanded in the lower thorax than in modern humans.

Position assessment of the rib heads from the El Sidrón sample and its implications

The proximal ends of ribs are important for rib kinematics because this is the part that articulates with the adjacent vertebra/e, where a significant portion of the costal movements take place (Spalteholtz, 1970; De Troyer et al., 2005). However, only a few Neanderthal proximal rib ends have been preserved in the fossil record and the ones that

have been preserved have never been measured in a comparative context. The El Sidrón site has yielded several well preserved proximal ends that could help to improve our knowledge of this important part of the rib anatomy. Since the position of some of these rib heads was difficult to assess through anatomy, we have created and validated a method using information of HCCD and HW to assess, for the first time, the position of Neanderthal rib heads of unknown position as shown in Figure 4.

Seriation of ribs has been traditionally carried out using qualitative methods that deal with morphological variation along the rib sequence in features such as the degree of torsion, curvature, etc. (Mann, 1993; Dudar, 1993). These methods are useful when the entire rib sequence is preserved, but they are constrained when assessing the fragmentary or commingled costal remains that are found in the archaeological or fossil record. Other methods based on quantitative analyses have been used extensively to study traditional measurements of the proximal segment of the rib (Hoppa and Saunders, 1998; Owers and Pastor, 2004; Cirillo and Henneberg, 2005), yielding positive results. However, none of them have ever combined HCCD and HW to look for costal position assessment as we do in this study. It is important to mention that we define HW here as the maximum length of the articular surface of the rib head perpendicular to the cranio-caudal axis (coinciding with the length of the inter-articular crest, when it applies), but Cirillo and Henneberg (2005) measured HW as the "Distance between the most lateral aspects of the rib head when the articular facet of the rib head and articular facet of the tubercle are aligned in a straight line (180°) on a surface situated on a horizontal plane" (Cirillo and Henneberg, 2005: 185). Although the two ways of measuring HW are similar, we think that ours is more straightforward since measuring the inter-articular crest of the rib head is based on an anatomical feature and not in geometric constructions. We use this method in ribs 1-

10, since specific features of the 11th and 12th ribs such as the presence of a single facet at the head or the absence of the articular tubercle are diagnostic enough.

Costal anatomy and relevant features of the ribs from the El Sidrón site

Morphological and qualitative analyses on the El Sidrón costal remains show salient features at different thoracic levels.

Upper thorax

The morphology of 1st ribs SD-1699+ and SD-1767, as described in Bastir et al. (2015a) and observed in Figures 7a and 8a, show that these ribs present less curvature in cranial view than in modern humans. Also, insertion of the anterior serratus and scalene muscles are pronounced on these ribs. The morphology of the neck could not be observed either in SD-1699+ and SD-1767 or in SD-1534, since their proximal part is missing. Regarding 2nd ribs, SD-695b (a proximal shaft) shows an extremely pronounced insertion of the posterior scalene muscle. Indeed, this insertion is more pronounced than in any other known Neanderthal 2nd rib (Fig. S4) known. SDR-159 (a distal shaft preserving the distal end) shows a low degree of curvature in cranial view (Fig. 1). The curvature in cranial view is controversial in 2nd ribs. McCown and Keith (1939) described the 2nd rib of Tabun 1 as presenting a low degree of curvature in cranial view, but Franciscus and Churchill (2002) brought into question the morphology of this rib since its proximal part is missing and the overall morphology could be uncertain. Second ribs from Kebara 2 are described as curved by Franciscus and Churchill (2002) and Gómez-Olivencia et al. (2009). However, it must be noted that the left 2nd rib is incomplete and heavily reconstructed and the right one presents some degree of reconstruction in the middle of the shaft, which could alter the degree of curvature in cranial view and, thus, its interpretation (Daniel García-Martínez, personal observation).

Our observations of antero-posteriorly straight ribs in the upper thorax of the Neanderthals (as observed in both the 1st and 2nd ribs) are consistent with those of previous authors (Gorjanović-Kramberger, 1906; McCown and Keith, 1939; Bastir et al., 2015a). Other complete Western European Neanderthal upper ribs, such as the ones from the Regourdou site (Maureille et al., 2015) or the Sima de Las Palomas site (Walker et al., 2011) will be helpful in confirming our results.

Central thorax

Only one specimen of what is probably a 5th rib of the central thorax, SD-1450, bears enough diagnostic features to be informative. The degree of curvature in cranial view is difficult to assess since both proximal and distal ends are missing. The insertion of the *iliocostalis* at the posterior angle is very pronounced, as it is in other Neanderthal 5th ribs such as the Kebara 2 right rib (Fig. S5).

Lower thorax

Several remains belonging to 11th and 12th ribs are preserved in the El Sidrón costal sample. Although its 12th rib record is based mainly on fragmentary remains (several rib heads and proximal shafts), the SD-2187 11th rib is preserved enough to evaluate some features of its morphology, as aforementioned. Additionally, the proximal part of a 12th rib (SD-56), although short, presents a strongly pronounced insertion for the diaphragm as other do Neanderthals (Fig. S6).

Furthermore, as has been observed in the results, articular tubercles of ribs belonging to the lower thorax are taller in Neanderthals than in modern humans (Table S7). It is important to recall that larger tubercles in the lower thorax were previously reported by Franciscus and Churchill (2002: 350). They observed that this larger size of Neanderthal tubercles could be caused by in-vivo remodeling due to a more frequent or

greater degree of joint excursion during breathing. However, since the Neanderthal individuals addressed in Franciscus and Churchill (2002) were mainly old adults (Heim, 1976; Trinkaus, 1983; Bar-Yosef et al., 1991) and results in documented collections show that age is an important factor for articulation remodeling (Cardoso and Henderson, 2010; Cardoso et al., 2016), it is still unknown if large articular tubercles were acquired during the lifetime of the individuals due to the remodeling process of age, or if they were inherently large.

The costal evidence of the El Sidrón site shed light on this question since the proximal remains SD-666 and SD-788 (assessed here as 6th or 7th ribs) belong to young adults (epiphysis of the head in active fusion, see results above and Figure 2), do not present remodeling of the articular tubercle, and do present values of ATH and ATW larger than those of modern humans (Figure S7). Therefore, our results suggest that the larger (or at least taller) articular tubercles could be a feature of Neanderthal lower ribs. Larger tubercles, together with larger rib heads, could contribute to strong breathing kinematics at the lower thorax, perhaps caused by an intense diaphragmatic action, as described in previous studies (Franciscus and Churchill, 2002; Gómez-Olivencia et al., 2009; García-Martínez et al., 2014; Bastir et al., 2015a). The bony changes evidenced in older Neanderthals could be the result of both the aging process and the greater biomechanical stress imposed by a larger ribcage. Furthermore, these changes would probably not be observed in young adult Neanderthals, since the bone elements of the ribcage would have been adjusted to greater biomechanical demand throughout the growth period. This adjustment would have happened at least since the time of the development of the Neanderthal rib cage differential size, shape and physiology (in comparison with modern humans), a fact that could occur early in ontogeny.

V*irtual reconstruction methods, geometric morphometrics analyses of individual ribs and its importance for understanding Neanderthal thorax morphology*

Virtual reconstruction has been observed to be an efficient method for reconstructing different parts of the skeleton including the ribs and thorax (Zollikofer et al., 2005; Gunz et al., 2009; Bastir et al., 2010; García-Martínez et al., 2014; Gómez-Olivencia et al., 2015). Here we applied these methods to reconstruct and measure a fairly complete 5th and 11th Neanderthal rib shafts that only lacked both ends. These techniques, combined with missing data estimation through TPS in the 1st ribs, allowed us to evaluate the morphology of the El Sidrón ribs at the 1st, 5th and 11th levels. In order to explore the interaction between ribs shape and thorax shape in those levels, we articulated mean ribs obtained from the results of this study with their corresponding vertebrae for Neanderthals and modern humans (see Figure 9). As those vertebral models, we used the vertebrae from Kebara 2 for articulating mean Neanderthal ribs and a modern human from the Santarém Collection (Coimbra, Portugal) for articulating mean modern human ribs. However, these results should be analyzed with caution, because the Neanderthal sample size is small for the 5th and 11th ribs.

<u>1st ribs</u>

Our results show that Neanderthal 1st ribs are smaller than those found in modern males and their distribution is close to the size range of modern females. Additionally, as observed in the results of the PCA and mean comparisons, Neanderthal 1st ribs present less curvature in cranial view than found in modern humans. This is caused by differential features at both ends, since Neanderthal 1st ribs present a more opened angle at the proximal end and a more lateral orientation at the distal end compared to modern humans. These features would produce straighter ribs in Neanderthals than in modern humans, which is consistent with a more antero-posterior expansion of the upper thorax. However,

when mean (size and shape) Neanderthal and modern human 1st ribs are articulated with their corresponding vertebrae (T1), respectively, Neanderthal upper thoraces appear relatively more medio-laterally expanded than in modern humans. This is because the transverse processes of the T1 vertebra of Neanderthals are more dorsally oriented than in modern humans´ T1 (Bastir et al., 2015b, in review; Fig. 9a, b). Therefore, the orientation of the transverse processes, coupled with the more opened angle at the proximal end and the more lateral orientation of the distal end, would generate a wider thoracic aperture in cranial view at T1 level, which would also leave a wide space for the manubrium. There are a few studies on the Neanderthal manubrium (Vallois and Félice, 1976; Pap et al., 1995), but they do not provide information about inter-specific differences. However, recent studies on the Neanderthal mesosternum from Regourdou (Gómez-Olivencia et al., 2012) proposed a larger mesosternum than in modern humans, a fact that Demonet (1905) linked to a large vital capacity based on living humans. However, since sternum morphology and its relation with the upper thorax are not the focus of our study, all these issues should be addressed in future research.

Additionally, Churchill (1994) proposed a correlation between the clavicle and the 1st rib, concluding that the elongation of Neanderthal clavicles would be linked to ribs with less curvature in cranial view and, thus, an antero-posterior expansion of the rib cage. Even though there could be a correlation between 1st rib and clavicle morphology, our results show that less curvature in cranial view of the 1st rib would produce a different thoracic configuration depending on the orientation of the transverse process of the adjacent vertebra (Bastir et al., 2015b, in review).

5th ribs

A large size of the Neanderthal 5th rib has also been found in previous research (Gómez-Olivencia et al., 2009), which proposed a volumetric expansion in this area.

When mean (size and shape) Neanderthal and male modern human 5th ribs are articulated with their corresponding vertebral levels (T4-T5), respectively, we observe that the Neanderthal thorax at this level would be more medio-laterally expanded but also more antero-posteriorly projected (Figs. 9a, c). Therefore, a more volumetric expansion in this area is expected for Neanderthals, according to previous findings by Gómez-Olivencia et al. (2009). However, when studied in isolation, the 5th rib shape does not differ between species according to our results (Table 4), but when taking into account the articulation with the vertebrae, the differences become apparent.

11th ribs

Linear measurements of HVC and HVA show that the El Sidrón reconstructed rib presents a considerably larger HVA and HVC compared to our modern human sample. These results are also supported by the 3D analyses on centroid size distribution. However, it has been observed on a different comparative sample (Gómez-Olivencia et al., 2009) that 11th ribs of Neanderthals could be similar in size to modern humans, which could be produced by differences in sample composition.

Moreover, Neanderthal 11th ribs present more curvature in cranial view than their modern human counterparts according to our results. It is important to note that other Lower Pleistocene hominins (such as the ones from Gran Dolina TD6 or the *H. ergaster* KNM-WT 15000) have also hypothesized to present a stronger curvature in cranial view in some lower ribs (Jellema et al., 1993; García-Martínez et al., 2016b). This greater curvature, producing an expansion of the lower thorax, could be a character inherited and shared with Lower Pleistocene hominins. Additionally, 11th Neanderthal ribs according to our results, present a relatively shorter head-posterior angle distance but, in absolute size, this distance has been proposed to be larger in Neanderthals than in modern humans (Franciscus and Churchill, 2002; Gómez-Olivencia et al., 2009).

Finally, when mean (size and shape) Neanderthal and male modern human 11th ribs are articulated with their corresponding vertebrae, respectively, we observe that the Neanderthal thorax at this level is notably more medio-laterally expanded than in modern humans (Fig. 9a, d). Therefore, a more volumetric expansion in this area is expected for Neanderthals compared to modern humans at the T11 level, which is consistent with results obtained by authors at other lower levels, such as the 8th and the 10th (Franciscus and Churchill, 2002; Gómez-Olivencia et al., 2009; García-Martínez et al., 2014).

Limitations of this study

First of all, it is important to note that the assumptions of correlation between ribs and thorax morphology, both taken from Bastir et al. (2015a) and emerging from this study, are based on modern human samples. This could be a constraint, because when using modern humans as a basis for assuming patterns of correlation in Neanderthals, we have to take into account that the patterns of correlation of the two species could be different.

Additionally, because of limitations of the El Sidrón costal sample, here we address the thorax morphology only at three different levels: 1st, 5th and 11th. Even though, as observed in figure 9, the three levels together outline the overall morphology of the Neanderthal rib cage, it should be noted that some rib levels are lacking in this study. Central thorax levels, such as the 6th or the 7th, have been hypothesized to be very informative of thorax shape and breathing kinematics (Franciscus and Churchill, 2002; Gómez-Olivencia et al., 2009; García-Martínez et al., 2014), so they should be studied in the future to complement and confirm the results obtained here, if and when enough fossil record becomes available.

Finally, this study shows that it is crucial to study ribs and vertebrae together in order to accurately interpret the morphological information obtained from individual elements. However, we do not mean to discredit studies of individual bones. Studying both ribs and vertebrae together is usually not possible due to bias in the fossil record. In these cases, the study of individual elements could also be informative of thorax morphology, as observed by previous research (Jellema et al., 1993; Franciscus and Churchill, 2002; Gómez-Olivencia et al., 2009, 2010; Schmid et al., 2013; Bastir et al., 2015a; Latimer et al., 2016; Williams et al., 2017).

Conclusions

The El Sidrón site has yielded costal remains ranging from the 1st to 12th ribs and comprising every part of rib anatomy. Rib head remains are especially relevant in this site since there is an overall lack of this part of the rib in the Neanderthal fossil record. We developed and validated a method based on head diameters (HCCD and HW) for assessing position of Neanderthal rib heads out of their anatomical context. Additionally, the El Sidrón costal sample comprises remains from the 1st, 5th and 11th levels that could be informative of the Neanderthal thorax morphology. Although not complete, missing data estimation and virtual reconstruction methods were applied in order to study those remains. Our results support previous findings of the lack of curvature in cranial view in the 1st rib of Neanderthals or the larger costal size of the 5th Neanderthal ribs. However, we also expand the knowledge of 11th ribs, showing that these ribs in Neanderthals are remarkably larger and more curved than in modern humans. These results are important since Neanderthal floating ribs are sometimes not studied because they are usually taphonomically less well preserved.

Previous studies have studied thoracic morphology based only on ribs, but it is important to note that ribs and vertebrae have to be considered together in order to

understand thoracic morphology (Bastir et al., 2015b, in review). Virtual reconstruction is crucial in this regard (García-Martínez et al., 2014; Gómez-Olivencia et al., 2015). However, the bias in the fossil record regarding the axial skeleton usually makes this task challenging. For the first time, we combined the knowledge of both Neanderthal ribs and vertebrae in articulation. Our results based on the El Sidrón and Kebara 1st, 5th and 11th ribs allow us to hypothesize that the Neanderthal thorax was more medio-laterally expanded relatively in the cranial part, more medio-laterally and antero-posteriorly expanded in the central part and remarkably more medio-laterally expanded in the caudal part. This evidence allows us to accept only partially **H2**, which predicts that the Neanderthal thorax morphology is more antero-posteriorly expanded in the upper thorax and more medio-laterally expanded in the lower thorax than in modern humans. Our results show that the Neanderthal lower thorax is clearly more medio-laterally expanded than in modern humans, but the upper thorax is not more antero-posteriorly expanded. Although evidence from individual 1st rib means suggests an antero-posterior expansion, the articulation with the transverse processes of their corresponding vertebrae (which are more posteriorly oriented in Neanderthals) indicate that their rib cages were probably relatively more medio-laterally expanded than in modern humans (Fig. 9). It is important to note that Bastir et al. (2015a) used patterns of covariation of modern human rib cages in articulation in order to hypothesize about Neanderthal morphology. However, the orientation of the transverse processes in thoracic vertebrae of Neanderthals differ from that of modern humans, which could explain the differences of the present findings from the model proposed by Bastir et al. (2015a).

The Neanderthal rib cage, according to the evidence of the El Sidrón site, would be more volumetrically expanded than in modern humans due to a slight antero-posterior expansion of the central thorax, coupled with a medio-lateral expansion of the upper,

central and caudal thorax. This would be caused not only by differences in size and shape of the ribs, but also by a different orientation of the transverse processes of the adjacent vertebra/e (according to Bastir et al., 2015b; in review). This thoracic morphology would be consistent with a higher level of diaphragmatic action and greater oxygen intake in Neanderthals than in modern humans, which is linked to a higher energetic demand and BMR (Franciscus and Churchill, 2002; Churchill, 2006; Weinstein et al., 2008; Froehle and Churchill, 2009; Gómez-Olivencia et al., 2009; García-Martínez et al., 2014; Bastir et al., 2015a; Gómez-Olivencia, 2015). This greater diaphragmatic action would also be supported by costal evidence such as the insertion of the diaphragm on the 12th ribs or the larger articular tubercles at diaphragmatic ribs, which, according the evidence of the El Sidrón, would be inherently larger. However, we do not exclude that other factors could cause the differences observed in the Neanderthal thorax, such as cold adaptation or a plesiomorphic condition similar to previous members of the genus *Homo*. However, this should be tested in future studies.

Acknowledgments

We acknowledge the Paleoanthropology group of MNCN-CSIC for support and especially Francisco Javier Rodriguez Pérez, Ana Isabel Ferrando Espinar and Laura Pérez Criado for fruitful discussions. We acknowledge the El Sidrón fieldwork team and we also acknowledge Davorka Radovčić for kindly providing access to the Krapina collection. We also acknowledge the work of the associate editor as well as the reviewers, who helped improving this manuscript with fruitful comments. This study was funded by The Leakey Foundation, the Ministerio de Economía y Competitividad of Spain (CGL2012-36682, CGL2015-63648-P and CGL2012-37279) and the Convenio Principado de Asturias-Universidad de Oviedo (CN-09-084). MB and DGM were funded

by the European Commission's Research Infrastructure Action via the Synthesys Projects (AT-TAF-4616 for MB and DK-TAF-3494 and BE-TAF-5639 for DGM).

References

Aiello, L.C., Wheeler, P., 1995. The expensive-tissue hypothesis: the brain and the digestive system in human and primate evolution. Current Anthropology 36, 199-221.

Arensburg, B., 1991. The vertebral column, thoracic cage and hyoid bone. In: BarYosef, O., Vandermeersch, B. (Eds.), Le squelette mousteérien de Kebara 2. Éditions du CNRS, Paris, pp. 113–147.

Arsuaga, J.L., Lorenzo, C., Carretero, J.-M., Gracia, A., Martínez, I., García, N., de Castro, J.-M.B., Carbonell, E., 1999. A complete human pelvis from the Middle Pleistocene of Spain. Nature 399, 255-258.

Badal, E., 2011. La materia vegetal carbonizada, La cueva de El Sidrón (Borines, Piloña, Asturias): investigación interdisciplinar de un grupo Neanderthal. Gobierno del Principado de Asturias, pp. 157-158.

Bar-Yosef, O., Vandermeersch, B. (Eds.), 1991. Le squelette moustérien de Kebara 2. Éditions du CNRS, Paris.

Bastir, M., 2008. A systems-model for the morphological analysis of integration and modularity in human craniofacial evolution. Journal of Anthropological Sciences 86, 37-58.

Bastir, M., Rosas, A., Tabernero, A.G., Peña-Melián, A., Estalrrich, A., de la Rasilla, M., Fortea, J., 2010. Comparative morphology and morphometric assessment of the Neanderthal occipital remains from the El Sidrón site (Asturias, Spain: years 2000–2008). Journal of Human Evolution 58, 68-78.

Bastir, M., García Martínez, D., Recheis, W., Barash, A., Coquerelle, M., Ríos, L., Peña-Melián, Á. García Río, F., O'Higgins, P., 2013. Differential growth and development of the upper and lower human thorax. PLoS ONE 8, e75128.

Bastir, M., García-Martínez, D., Barash, A., Been, E., Torres, I., García-Río, F., 2014a. Thorax kinematics and the reconstruction of body models in hominin evolution. In: Proceedings of the ESHE, Florence. p 35.

Bastir, M., Higuero, A., Ríos, L., García Martínez, D., 2014b. Three-dimensional analysis of sexual dimorphism in human thoracic vertebrae: Implications for the respiratory system and spine morphology. American Journal of Physical Anthropology 155, 513-521.

Bastir, M., García-Martínez, D., Estalrrich, A., García-Tabernero, A., Huguet, R., Ríos, L., Barash, A., Recheis, W., de la Rasilla, M., Rosas, A., 2015a. The relevance of the first ribs of the El Sidrón site (Asturias, Spain) for the understanding of the Neandertal thorax. Journal of Human Evolution 80, 64-73.

Bastir, M., García-Martínez, D., Barash, A., 2015b. The 3D structure of thoracic vertebrae and their significance for size and shape of the ribcage in Neanderthals. In: Proceedings of the ESHE, London. p 42.

Bastir, M., Rosas, A., 2016. Cranial base topology and basic trends in the facial evolution of *Homo*. Journal of Human Evolution 91:26-35.

Bastir, M., García-Martínez, D., Torres-Tamayo, N., Sanchis-Gimeno, J. A., O'Higgins, P., Utrilla, C., Torres Sánchez, I. and García Río, F., (2017). In Vivo 3D Analysis of Thoracic Kinematics: Changes in Size and Shape During Breathing and Their Implications for Respiratory Function in Recent Humans and Fossil Hominins. Anat. Rec., 300: 255–264. doi:10.1002/ar.23503

Bastir, M., García-Martínez, D., Ríos, L., Higuero, A., Barash, A., Martelli, S., García-Tabernero, A., Estalrrich, A., Huguet, R., de la Rasilla, M., Rosas A., in review. 3D morphometrics of thoracic vertebrae in Neanderthals: fossil evidence from El Sidrón (Asturias, Northern Spain). Journal of Human Evolution.

Ben-Dor, M., Gopher, A., Barkai, R., 2016. Neandertals' large lower thorax may represent adaptation to high protein diet. American Journal of Physical Anthropology 160: 367–378. doi:10.1002/ajpa.22981

Berger, L.R., Hawks, J., de Ruiter, D.J., Churchill, S.E., Schmid, P., Delezene, L.K., Kivell, T.L., Garvin, H.M., Williams, S.A., DeSilva, J.M., Skinner, M.M., Musiba, C.M., Cameron, N., Holliday, T.W., Harcourt-Smith, W., Ackermann, R.R., Bastir, M., Bogin, B., Bolter, D., Brophy, J., Cofran, Z.D., Congdon, K.A., Deane, A.S., Dembo, M., Drapeau, M., Elliott, M.C., Feuerriegel, E.M., García-Martínez, D., Green, D.J., Gurtov, A., Irish, J.D., Kruger, A., Laird, M.F., Marchi, D., Meyer, M.R., Nalla, S., Negash, E.W., Orr, C.M., Radovčić, D., Schroeder, L., Scott, J.E., Throckmorton, Z., Tocheri, M.W., VanSickle, C., Walker, C.S., Wei, P., Zipfel, B., 2015. *Homo naledi*, a new species of the genus *Homo* from the Dinaledi Chamber, South Africa. eLife 4.

Boule, M., 1911–1913. L'homme fossile de la Chapelle aux Saints. Annales de Paléontologie 6, 111–172; 7, 21–56, 85–192; 8, 1–70.

Cañaveras, J.C., Moral, S.S., Lario, J., Robleño, S.C., Fernández-Cortés, A., Cervera, M.C.M., 2011. El modelo de relleno, o cómo llegaron los restos a la Galería del Osario, La Cueva de El Sidrón (Borines, Piloña, Asturias): investigación interdisciplinar de un grupo Neandertal. Gobierno del Principado de Asturias, pp. 43-64.

Cardoso, F.A., Henderson, C., 2010. Enthesopathy formation in the humerus: Data from known age-at-death and known occupation skeletal collections. American Journal of Physical Anthropology 141, 550-560.

Cardoso, F.A., Assis, S., Henderson, C., 2016. Exploring poverty: skeletal biology and documentary evidence in 19th–20th century Portugal. Annals of human biology 43, 102-106.

Carretero, J.M., Merino, C.L., Quam, R.M., Martínez, I., Arsuaga, J.L., 2004. Los humanos de la Sima de los Huesos (Sierra de Atapuerca) y la evolución del cuerpo en el género *Homo*. Miscelánea en homenaje a Emiliano Aguirre. Museo Arqueológico Regional, pp. 120-135.

Churchill, S., 1994. Medial clavicular length and upper thoracic shape in Neanderthals and Europeans early modern humans. American Journal of Physical Anthropology S18, 67-68.

Churchill, S.E., 2006. Bioenergetic perspectives on Neanderthal thermoregulatory and activity budgets, Neanderthals revisited: New approaches and perspectives. Springer, pp. 113-133.

Cirillo, J., Henneberg, M., 2012. Sequencing human ribs into anatomical order by quantitative multivariate methods. HOMO-Journal of Comparative Human Biology 63, 182-201.

De Torres, T., Ortiz, J., Grün, R., Eggins, S., Valladas, H., Mercier, N., Tisnérat-Laborde, N., Juliá, R., Soler, V., Martínez, E., 2010. Dating of the hominoid (*Homo neanderthalensis*) remains accumulation from el Sidrón cave (Piloña, Asturias, North Spain): an example of a multi-methodological approach to the dating of upper Pleistocene sites. Archaeometry 52, 680-705.

De Troyer, A., Kirkwood, P.A., Wilson, T.A., 2005. Respiratory action of the intercostal muscles. Physiological Reviews 85, 717-756.

Demonet, E., 1905. Recherches sur la capacité vitale absolue et relative suivant le sexe et suivant certaines dimensions du corps. Bull. Mém. Soc. Anthropol. Paris 6, 5-100.

Dudar, J.C., 1993. Identification of rib number and assessment of intercostal variation at the sternal rib end. Journal of Forensic Science 38, 788-797.

Ferreira, M.T., Vicente, R., Navega, D., Gonçalves, D., Curate, F., Cunha, E., 2014. A new forensic collection housed at the University of Coimbra, Portugal: The 21st century identified skeletal collection. Forensic science international, 245, 202-e1.

Fortea, J., De la Rasilla, M., Martínez, E., Sánchez-MoraI, S., Cañaveras, J., Cuezva, S., Rosas, A., Soler, V., Julià, R., De Torres, T., 2003. La Cueva de El Sidrón (Borines, Piloña, Asturias): Primeros resultados. Estud. Geol., 59, pp. 159–179

Franciscus, R.G., Churchill, S.E., 2002. The costal skeleton of Shanidar 3 and a reappraisal of Neandertal thoracic morphology. Journal of Human Evolution 42, 303-356.

Froehle, A.W., Churchill, S.E., 2009. Energetic competition between Neandertals and anatomically modern humans. PaleoAnthropology 96:116.

Fuhlrott, C., 1859. Menschliche Ueberreste aus einen Felsengrotte des Dusselthals. Verhandlungen des Nat. Verein des Preus. Rheinl. Und Westfalens, 16e jrg., Bonn.

García-Martínez, D., Barash, A., Recheis, W., Utrilla, C., Torres Sánchez, I., García Río, F., Bastir, M., 2014. On the chest size of Kebara 2. Journal of Human Evolution 70, 69-72.

García-Martínez, D., Torres-Tamayo, N., Torres-Sanchez, I., García-Río, F. and Bastir, M., 2016a. Morphological and functional implications of sexual dimorphism in the human skeletal thorax. American Journal of Physical Anthropology 161: 467–477. doi:10.1002/ajpa.23051

García-Martinez, D., Spoor, F., Bastir, M., 2016b. 3D assessment of rib curvatures in KNM-WT 15000. Abstracts of the Paleoanthropology Society 2016 Meeting; PaleoAnthropology 2016:A13.

García-Martínez, D., Recheis, W., Bastir, M., 2016c. Ontogeny of 3D rib curvature and its importance for the understanding of human thorax development. American Journal of Physical Anthropology 159, 423-431.

García-Martínez, D., Bastir, M., Huguet, R., Estalrrich, A., García-Tabernero, A., Cunha, E., de la Rasilla, M., Rosas, A., 2016d. Positional rib assessment of the adult costal remains of the El Sidrón Neanderthal site (49000 y/o, Asturias, northern Spain). In: Proceedings of the ESHE, Madrid. p 104.

Gómez-Olivencia, A., 2015. The costal skeleton of the Neandertal individual of La Chapelle-aux-Saints 1, Annales de Paléontologie 101, 127-141.

Gómez-Olivencia, A., Eaves-Johnson, K.L., Franciscus, R.G., Carretero, J.M., Arsuaga, J.L., 2009. Kebara 2: new insights regarding the most complete Neandertal thorax. Journal of Human Evolution 57, 75-90.

Gómez-Olivencia, A., Carretero, J.M., Lorenzo, C., Arsuaga, J.L., Bermúdez de Castro, J.M., Carbonell, E., 2010. The costal skeleton of *Homo antecessor*: preliminary results. Journal of Human Evolution 59, 620-640.

Gómez-Olivencia, A., Franciscus, R.G., Couture-Veschambre, C., Maureille, B., Arsuaga, J.L., 2012. The mesosternum of the Regourdou 1 Neanderthal revisited. Journal of Human Evolution 62, 511-519.

Gómez-Olivencia, A., Barash, A., Arlegi, M., García-Martínez, D., Kramer, PA., Bastir, M., Been, E., 2015. 3D virtual reconstruction of the Kebara 2 thorax. In: Proceedings of the ESHE, London. p 100.

Gorjanović-Kramberger, D., 1906. Der diluviale Mensch von Krapina in Kroatien: ein Beitrag zur Paläoanthropologie. CW Kreidel.

Graves, R.R., Lupo, A.C., McCarthy, R.C., Wescott, D.J., Cunningham, D.L., 2010. Just how strapping was KNM-WT 15000? Journal of Human Evolution 59, 542-554.

Gunz, P., Mitteroecker, P., Bookstein, F.L., 2005. Semilandmarks in three dimensions. In: Slice, D. (Ed.), Modern Morphometrics in Physical Anthropology. Kluwer Academic/Plenum Publishers, New York, pp. 73-98.

Gunz, P., Mitteroecker, P., Neubauer, S., Weber, G.W., Bookstein, F.L., 2009. Principles for the virtual reconstruction of hominin crania. Journal of Human Evolution 57, 48-62.

Heim, J.L., 1976. Les hommes fossiles de la Ferrassie. Masson. Paris

Hernández-Pacheco, E., 1923. La vida de nuestros antecesores paleolíticos según los resultados de las excavaciones en la caverna de la Paloma: Asturias. Comisión de Investigaciones Paleontológicas y Prehistóricas, Junta para Ampliación de Estudios e Investigaciones Científicas, 31, 38 pp.

Holliday, T.W., 2012. Body size, body shape, and the circumscription of the genus *Homo*. Current Anthropology 53, S330-S345.

Hoppa, R., Saunders, S., 1998., Two quantitative methods for rib seriation in human skeletal remains. Journal of Forensic Science 43, 174-177.

Jellema, L.M., Latimer, B., Walker, A., 1993. The rib cage. The Nariokotome *Homo erectus* Skeleton. Harvard University Press, Cambridge, MA, 294-325.

Kendall, D., 1977. The diffusion of shape, Advances in Applied Probability 9, 428–430.

Klingenberg, C.P., 2011. MorphoJ: an integrated software package for geometric morphometrics. Molecular Ecology Resources 11, 353-357.

Latimer, B., Ward, C.V., 1993. The thoracic and lumbar vertebrae, The Nariokotome *Homo erectus* Skeleton. Harvard University Press, Cambridge, pp. 266-293.

Mann, R.W., 1993. A method for siding and sequencing human ribs. Journal of Forensic Science 38, 151-155.

Martiniano, R., Coelho, C., Ferreira, M.T., Neves, M.J., Pinhasi, R., Bradley D.G., 2014. Genetic evidence of African slavery at the beginning of the trans-Atlantic slave trade. Scientific Reports 4: 5994. DOI: 10.1038/srep05994.

Maureille, B., Gómez-Olivencia, A., Couture-Veschambre, C., Madelaine, S., Holliday, T., 2015. Nouveaux restes humains provenant du gisement de Regourdou (Montignac-sur-Vézère, Dordogne, France). PALEO. Revue d'archéologie préhistorique, 117-138.

McCown, T.D., Keith, S.A., 1939. The Stone Age of Mount Carmel: The Fossil Human Remains from the Levallosiso-Mousterian. Clarendon Press, Oxford.

Mitteroecker, P., Gunz, P., 2009. Advances in geometric morphometrics. Evolutionary Biology 36, 235-247.

O'Higgins, P., 2000. The study of morphological variation in the hominid fossil record: biology, landmarks and geometry. Journal of Anatomy 197, 103-120.

Ohman, J.C., 1986. The first rib of hominoids. American Journal of Physical Anthropology 70, 209-229.

Owers, S.K., Pastor, R.F., 2005. Analysis of quantitative methods for rib seriation using the Spitalfields documented skeletal collection. American Journal of Physical Anthropology 127, 210-218.

Pap, I., Tillier, A., Arensburg, B., Chech, M., 1996. The Subalyuk Neanderthal remains (Hungary): a re-examination. Annales historico naturales-musei nationalis hungarici. Hungarian Natural History Museum, pp. 233-270.

Radovčić, J., 1988. The Krapina hominids: An illustrated catalog of skeletal collection. Mladost. Zagreb: Mladost Publishers.

Recheis, W., Weber, G.W., Schäfer, K., Knapp, R., Seidler, H., zur Nedden, D., 1999. Virtual reality and Anthropology. European Journal of Radiology 31, 88-96.

Ríos, L., Cardoso, H.F., 2009. Age estimation from stages of union of the vertebral epiphyses of the ribs. American Journal of Physical Anthropology 140, 265-274.

Rosas, A., Bastir, M., Martínez-Maza, C., García-Tabernero, A., Lalueza-Fox, C., 2006. Inquiries into Neanderthal cranio-facial development and evolution: 'accretion' vs 'organismic' models. In: Harrison, T., Harvati, K. (Eds.), Neanderthals Revisited. Springer Verlag, New York University, pp. 38-69.

Rosas, A., Estalrrich, A., García-Tabernero, A., Bastir, M., García-Vargas, S., Sánchez-Meseguer, A., Huguet, R., Lalueza-Fox, C., Peña-Melián, Á. Kranioti, E.F., 2012. Les Néandertaliens d'El Sidrón (Asturies, Espagne). Actualisation d'un nouvel échantillon. L'Anthropologie 116, 57-76.

Rosas, A., Estalrrich, A., García-Vargas, S., García-Tabernero, A., Huguet, R., Lalueza-Fox, C., de la Rasilla, M., 2013. Identification of Neanderthal individuals in fragmentary fossil assemblages by means of tooth associations: the case of El Sidrón (Asturias, Spain). Comptes Rendus Palevol 12, 279-291.

Rosas, A., Huguet, R., Estalrrich, A., García-Vargas, S., García-Tabernero, A., Bastir, M., Peña-Melián, Á., 2011. Fauna de macromamíferos en la Galería del Osario. M. de la Rasilla, A. Rosas, J.C. Cañaveras, C. Lalueza-Fox (Eds.), La Cueva de El Sidrón (Borines, Piloña, Asturias). Una investigación interdisciplinar de un grupo Neandertal. Excavaciones arqueológicas de Asturias. Monografías I. Gobierno del Principado de Asturias, Oviedo (2011), pp. 147–148

Rosas, A., Martínez-Maza, C., Bastir, M., García-Tabernero, A., Lalueza-Fox, C., Huguet, R., Ortiz, J.E., Julià, R., Soler, V., de Torres, T., 2006. Paleobiology and comparative morphology of a late Neanderthal sample from El Sidrón, Asturias, Spain. Proceedings of the National Academy of Sciences 103, 19266-19271.

Rosas, A., Rodriguez-Perez, F.J., Bastir, M., Estalrrich, A., Huguet, R., García-Tabernero, A., Pastor, J.F., de la Rasilla, M., 2016. Adult Neanderthal clavicles from the El Sidrón site (Asturias, Spain) in the context of *Homo* pectoral girdle evolution. Journal of Human Evolution 95, 55-67.

Sanchiz, B., Blanco, C.M., 2011. La herpetofauna del yacimiento de El Sidrón, La cueva de El Sidrón (Borines, Piloña, Asturias): investigación interdisciplinar de un grupo Neandertal. Gobierno del Principado de Asturias, pp. 155-156.

Santamaría, D., Fortea, J., De la Rasilla, M., Martinez, L., Martinez, E., Cañaveras, J.C., Sánchez-Moral, Rosas, A., Estalrrich, A., García-Tabernero, A., 2010. The technological and typological behaviour of a Neanderthal group from El Sidrón cave (Asturias, Spain). Oxford Journal of Archaeology 29, 119-148.

Sawyer, G., Maley, B., 2005. Neanderthal reconstructed. The Anatomical Record Part B: The New Anatomist 283, 23-31.

Schmid, P., Churchill, S.E., Nalla, S., Weissen, E., Carlson, K.J., de Ruiter, D.J., Berger, L.R., 2013. Mosaic Morphology in the Thorax of *Australopithecus sediba*. Science 340, 1234598-2.

Sokal, R.R., Rohlf, F.J., 1973. Introduction of Biostatistics. San Francisco: W. H. Freeman

Spalteholz, W., 1970. Atlas de Anatomía Humana. Ed. Labor, S.A. Barcelona. 5ª ed.

SPSS Inc., 1995. Statistical package for the social sciences. SPSS Inc., Chicago, Illinois.

Tawane, G., García-Martínez, D., Eyre, J., Bastir, M., Berger, L.R., Schmid, P., Nalla, S., Williams, S.A., 2016. A hominin first rib discovered at the Sterkfontein Caves, South Africa. South African Journal of Science 112, (5/6) 1-7.

Trinkaus, E., Smith, F.H., Stockton, T.C., Shackelford, L.L., 2006. The human postcranial remains from Mladeč. In: Teschler-Nicola, M. (Ed.), Early Modern Humans

at the Moravian Gate. The Mladeč Caves and Their Remains. Springer, Vienna, pp. 385-445.

Vallois, H., de Félice, S., 1976. Neanderthal sternum from Regourdou. Complementary note. Anthropologischer Anzeiger; Bericht über die biologisch-anthropologische Literatur 35, 229.

Van Sickle, C., Williams, S.A., Garcia-Martinez, D., Cofran, Z.D., Churchill, S.E., Hawks, J., Berger, L.R., In review. The pelvis of *Homo naledi*. Journal of Human Evolution.

Walker, A., Leakey, R.E., 1993. The Nariokotome *Homo erectus* skeleton. Cambridge: Harvard University Press.

Walker, M.J., Ortega, J., López, M.V., Parmová, K., Trinkaus, E., 2011. Neanderthal postcranial remains from the Sima de las Palomas Del Cabezo Gordo, Murcia, southeastern Spain. American Journal of Physical Anthropology 144, 505-515.

Weber, G.W., 2015. Virtual anthropology American Journal of Physical Anthropology 156, 22-42.

Williams, S.A., García-Martínez, D., Bastir, M., Nalla, S., Meyer, M.R., Schmid, P., Churchill, S.E., Berger. L.R., 2017. The axial skeleton of *Homo naledi*. Journal of Human Evolution. http://dx.doi.org/10.1016/j.jhevol.2016.11.003

Zollikofer, C.P., de León, M.S.P., Lieberman, D.E., Guy, F., Pilbeam, D., Likius, A., Mackaye, H.T., Vignaud, P., Brunet, M., 2005. Virtual cranial reconstruction of *Sahelanthropus tchadensis*. Nature 434, 755-759.

Table 1: Number of individual specimens (NISP), minimum number of elements (MNE) and minimum number of individuals (MNI) calculations for the *El Sidrón costal sample*.

	NISP				MNE			MNI	
AD	SubAD	Indet	Total	AD	SubAD	Total	AD	SubAD	Total
94	92	82	268	45	40	85	4	4	8

Table 2: measurements available (in mm.), side and position assessment in the more diagnostic costal fossils of the El Sidrón sample addressed in this study. Each measurement shown represents the average of three repetitions in order to reduce intra-observer error. Measurements were made following descriptions provided by Franciscus and Churchill (2002) and Gómez-Olivencia et al. (2010). Measurements showing * aside are estimated.

	Level	Side	HCCD	HW	TNL	NMnCCD	NTh	ATH	ATW	TID2	DSMxD	DSMnD	SMxD	SMnD	MMxD	MMnD	SEMxD	SEMnD
SD-1534	1	R	-	-	-	6.2	-	5.17	7.23	-	-	-	-	-	-	-	-	-
SD-695b	2	L	-	-	-	-	8.59	4.63	7.55	23.64	14.36	8.36	15.25	8.6	11.96	12.67	-	-
SDR-159	2	L	-	-	-	-	-	-	-	-	-	-	-	-	-	6.6	11.38	8.02
SDR-26+	3	L	14.52	12.77	33.85	9.86*	6.36	6.4	7.15	47.51*	9.94	8.92	13.41*	9.13	-	-	-	-
SDR-161+	4	L	13.28	10.23	33.64	12.69	5.87	7.26*	6.56	-	-	-	-	-	-	-	-	-
SD-1450	5	R	-	-	-	-	-	-	-	-	-	-	22.37	9.06	14.98	6.31	-	-
SD-695a	5	R	15.24	11.5	36.73	12.29	6.61	6.35	9.09	-	11.37	9.94	-	-	-	-	-	-
SD-448	5	L	13.99*	9.96*	35.13	10.53	5.91	7.2	7.28	-	-	-	-	-	-	-	-	-
SD-2187	11	L	-	-	-	-	-	-	-	-	8.72	8.99	12.97	9.64	14.72	7.13	-	-
SDR-131	11	R	13.93	8.47														
SD-653a	12	L	14.41	9.36*	-	-	-	-	-	-	-	-	-	-	-	-	-	-
SD-695c	11	L	14.26*	9.43	-	-	-	-	-	-	-	-	-	-	-	-	-	-
SD-573c	12	R	14.38	8.72*	-	-	-	-	-	-	-	-	-	-	-	-	-	-
SD-788	6-7	R	17.66*	10.36 *	33.31 *	13.89	8.13	10.46	9.75	-	-	-	-	-	-	-	-	-
SD-666	6-7	R	15.08*	8.96*	30.09	14.36	5.58	12.45	10.68	-	11.43	9.73	-	-	-	-	-	-
SD-2001+	9-10	R	-		-	-	-	-	-	-	8.36	7.53	13.3	9.43	17.23	6.88	-	-

Table 3: Results of mean comparisons between the different groups of 1st ribs studied. Mean Procrustes distance and p-value, respectively, are shown between each group. Statistically significant values are shown in bold letters.

1st rib	Fossil modern human	Current modern human	Neanderthal
Fossil modern human	0	0.03; 0.72	**0.08; <0.01**
Current modern human	0.03; 0.72	0	**0.09; <0.01**
Neanderthal	**0.08; <0.01**	**0.09; <0.01**	**0**

Table 4: Results of mean comparisons between the different groups of 5th ribs studied. Mean Procrustes distance and p-value, respectively, are shown between each group. Statistically significant values are shown in bold letters

5th rib	Current modern human	Neanderthal
Current modern human	0	0.04; 0.25
Neanderthal	0.04; 0.25	0

Table 5: Results of mean comparisons between the different groups of 11th ribs studied. Mean Procrustes distance and p-value, respectively, are shown between each group. Statistically significant values are shown in bold letters

11th rib	Current modern human	Neanderthal
Current modern human	0	**0.14; <0.01**
Neanderthal	**0.14; <0.01**	**0**

Figure 1: The most diagnostic ribs studied in the El Sidrón costal sample. Ribs are shown in cranial view.

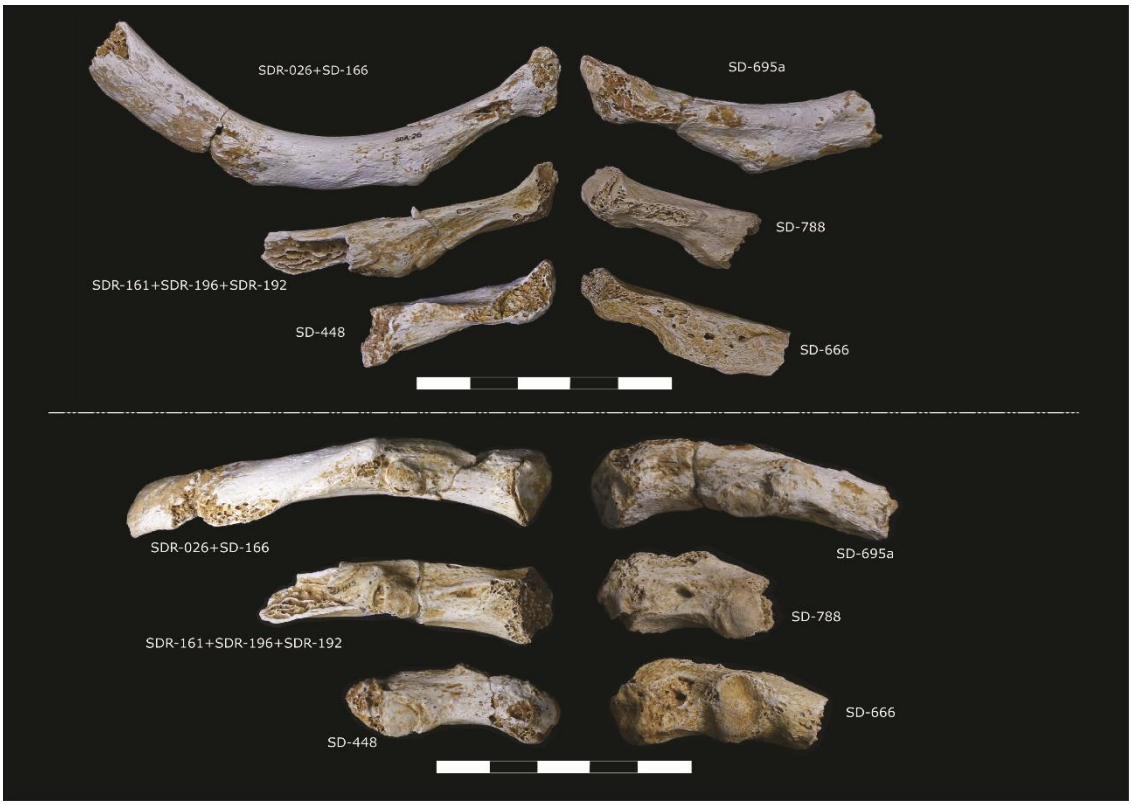

Figure 2: The most diagnostic proximal rib remains studied in the El Sidrón costal sample. Ribs are shown in cranial view in the top of the figure and in external view in the bottom of the figure.

Figure 3: The most diagnostic proximal ends of floating ribs in the El Sidrón costal sample. A detail of the articular facet in external view is shown.

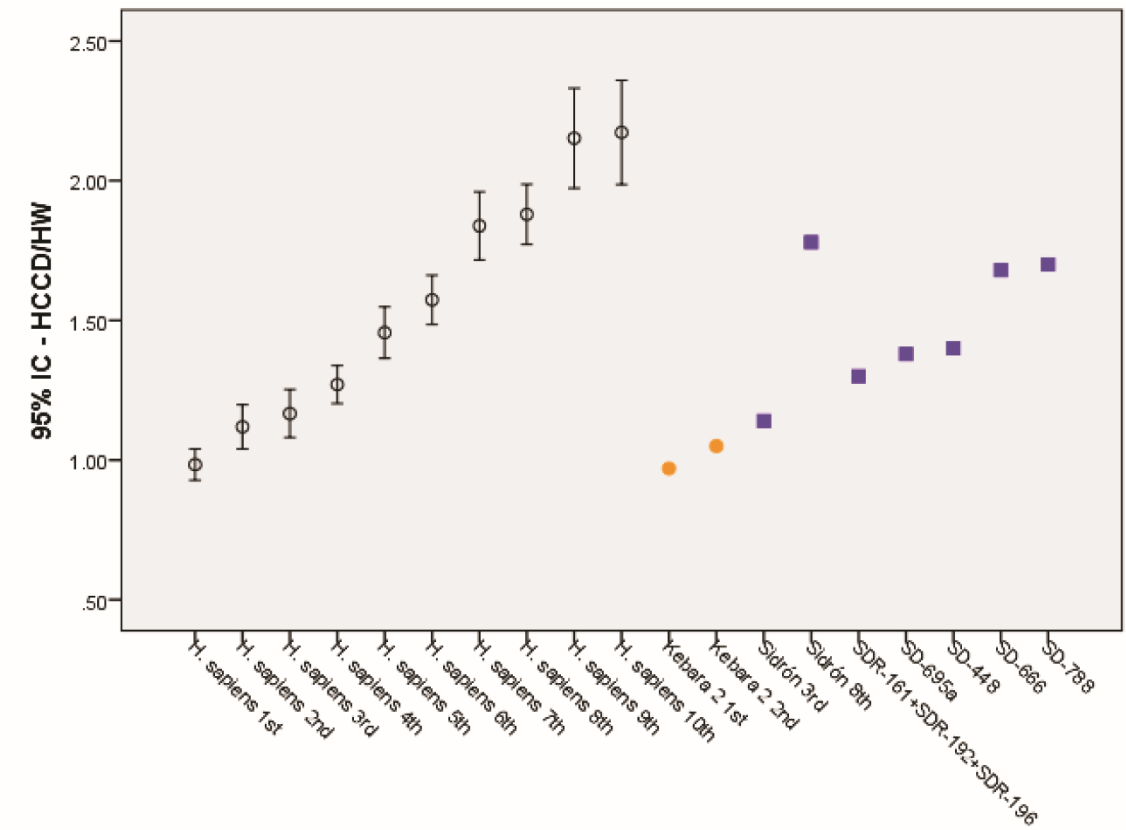

Figure 4: HCCD/HW index with 95% confidence interval for the mean of modern human ribs from 1st to 10th. Kebara 2 (orange circles) and El Sidrón (blue squares) are shown. Neanderthal proximal ends of known position (Kebara 2, 1st; Kebara 2, 2nd; El Sidrón, 3rd; El Sidrón, 8th) fall into the confidence interval of their modern human counterparts. Head cranio-caudal diameter (HCCD) follows definition of Gómez-Olivencia et al. (2010) and head width (HW) is defined in this study as the maximum length of the articular surface of the rib head perpendicular to the cranio-caudal axis (coinciding with the length of the inter-articular crest, when applicable).

Figure 5: Virtual reconstruction of the 5th (a) and 11th (b) ribs from the El Sidrón site. The 5th rib was reconstructed based on SD-695a, SD-1450 and the distal end of the Kebara 2 5th rib. The 11th rib was reconstructed based on SD-2187, SDR-131 (mirror image) and the distal end of the Kebara 2 11th rib.

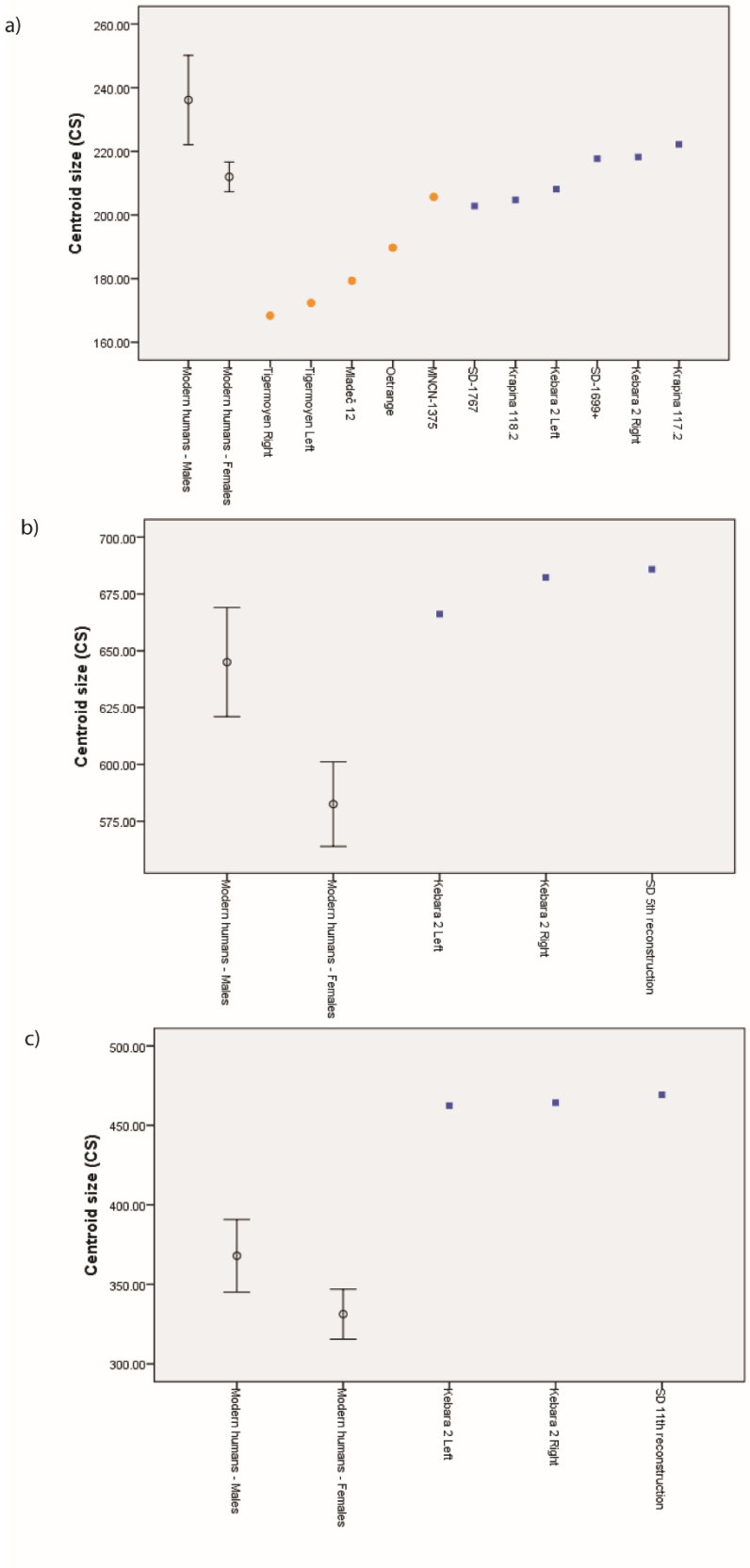

Figure 6: Centroid size (CS) distribution with 95% confidence interval for the mean of modern human 1st (a), 5th (b) and 11th (c) ribs separated by sex. Early modern humans (orange circles) and Neanderthals (blue squares) are compared to them.

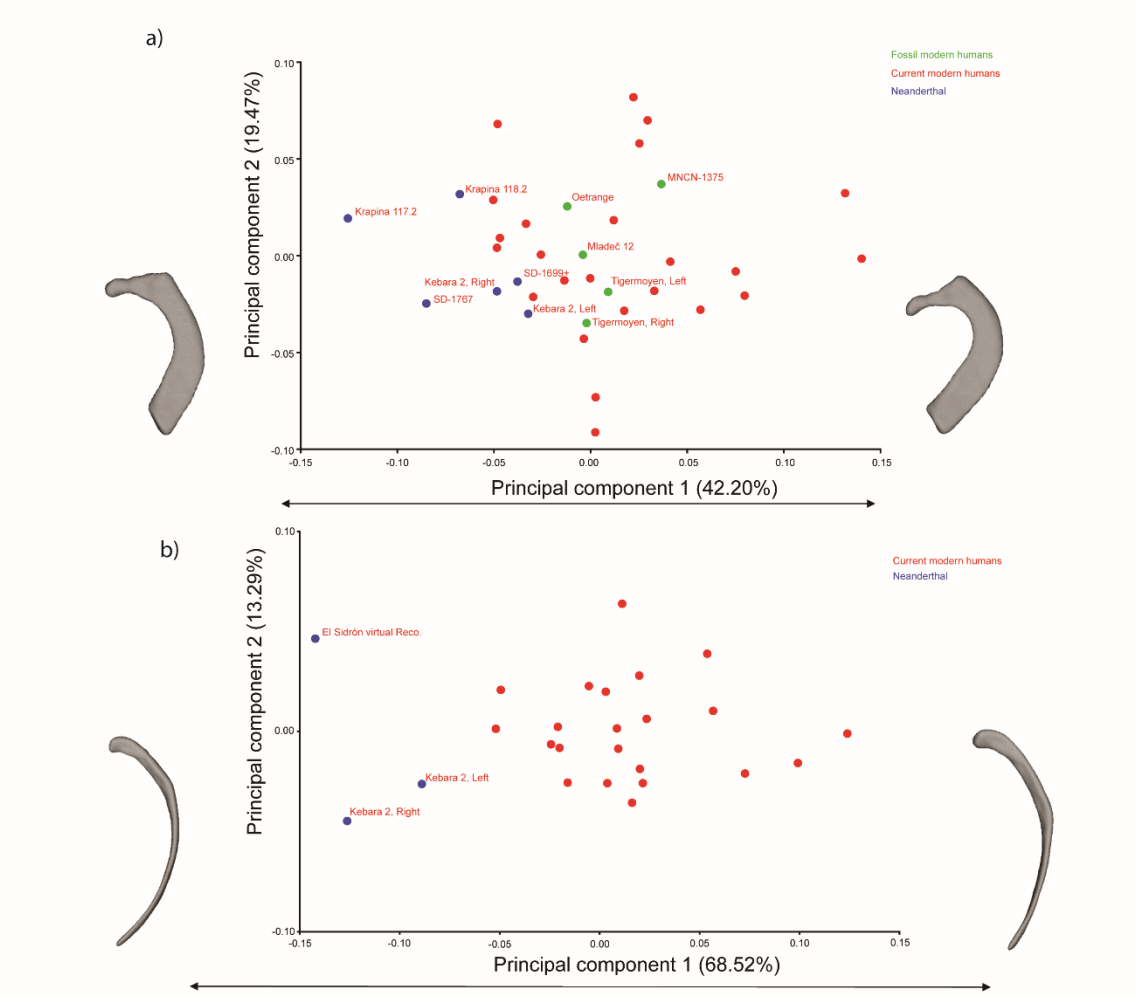

Figure 7: PC-shape analysis of 1st (a) and 11th (b) ribs. Scatterplot of PC 1 and PC 2 (see percentage of total variance explained in parenthesis in each axis), and warped 3D models of PC-scores of 1st and 11th ribs in cranial view. For 1st ribs note that Neanderthal specimens (blue) are located in the negative values of the axis, whereas early modern humans (green) are located in the centre of the current modern humans distribution. For 11th ribs note that Neanderthal specimens (blue) are located in the negative values of the axis.

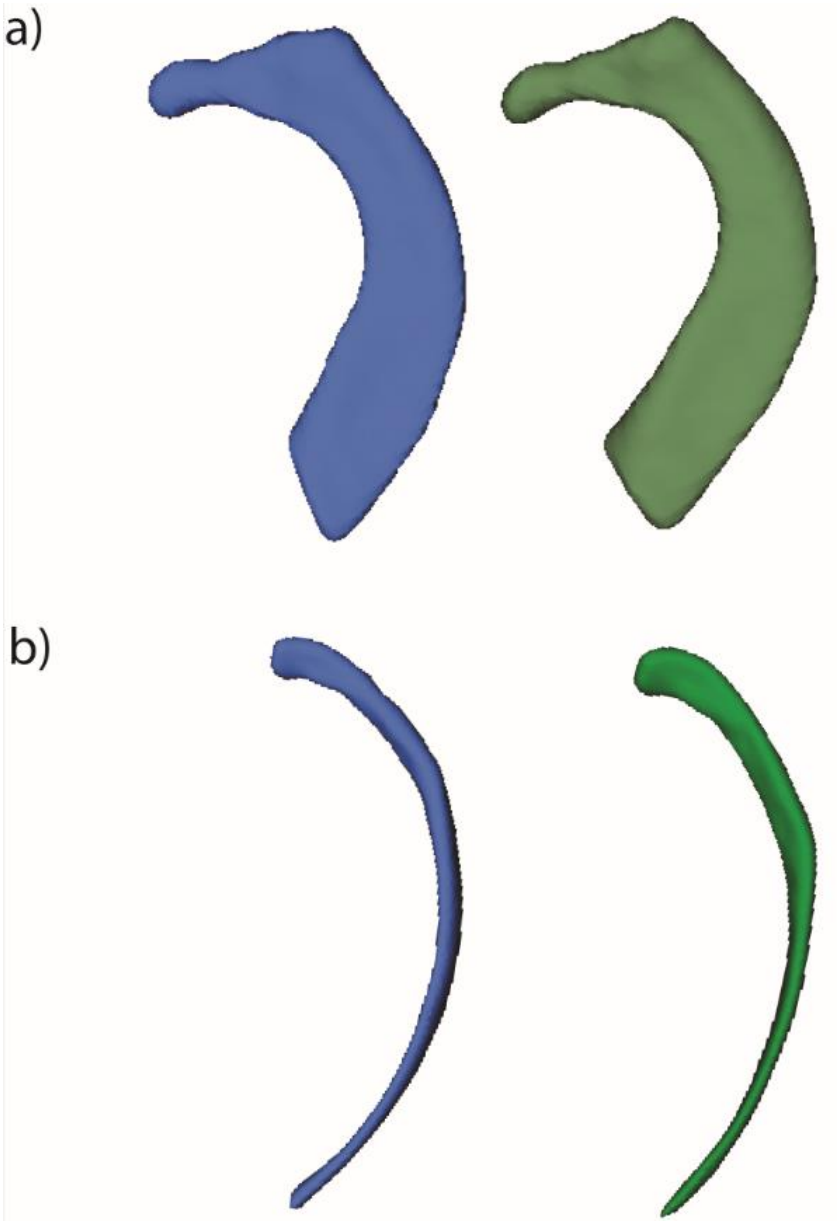

Figure 8: Mean shapes of 1st (a) and 11th ribs (b) of Neanderthals (blue, left) and current European modern humans (green, right).

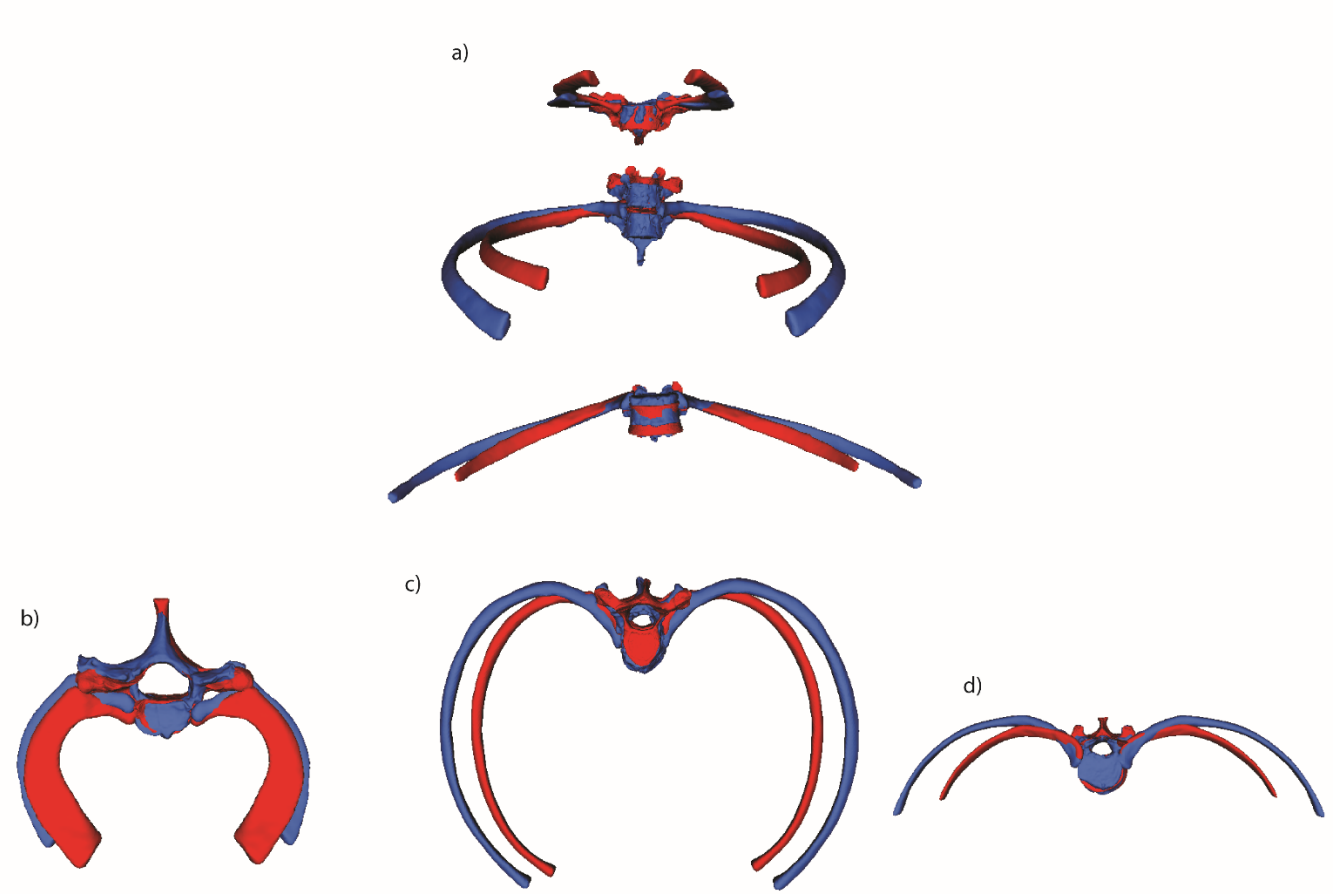

Figure 9: Mean 1st, 5th and 11th ribs (size and shape) of Neanderthals (blue) and European modern humans (red) obtained from our results in articulation with their corresponding vertebral levels. As those vertebral models, we used the vertebrae from Kebara 2 for articulating mean Neanderthal ribs and a modern human from the Santarém Collection (Coimbra, Portugal) for articulating mean modern human ribs. A frontal view of the whole hypothetic model (a) as well as a cranial view of each level studied (1st – b; 5th – c; 11th – d) are shown. The most remarkable features are the slight medio lateral expansion of the thorax at T1 level and the remarkably medio-lateral expansion of the rib cage at T5 and T11 levels).

Supplementary Online Material

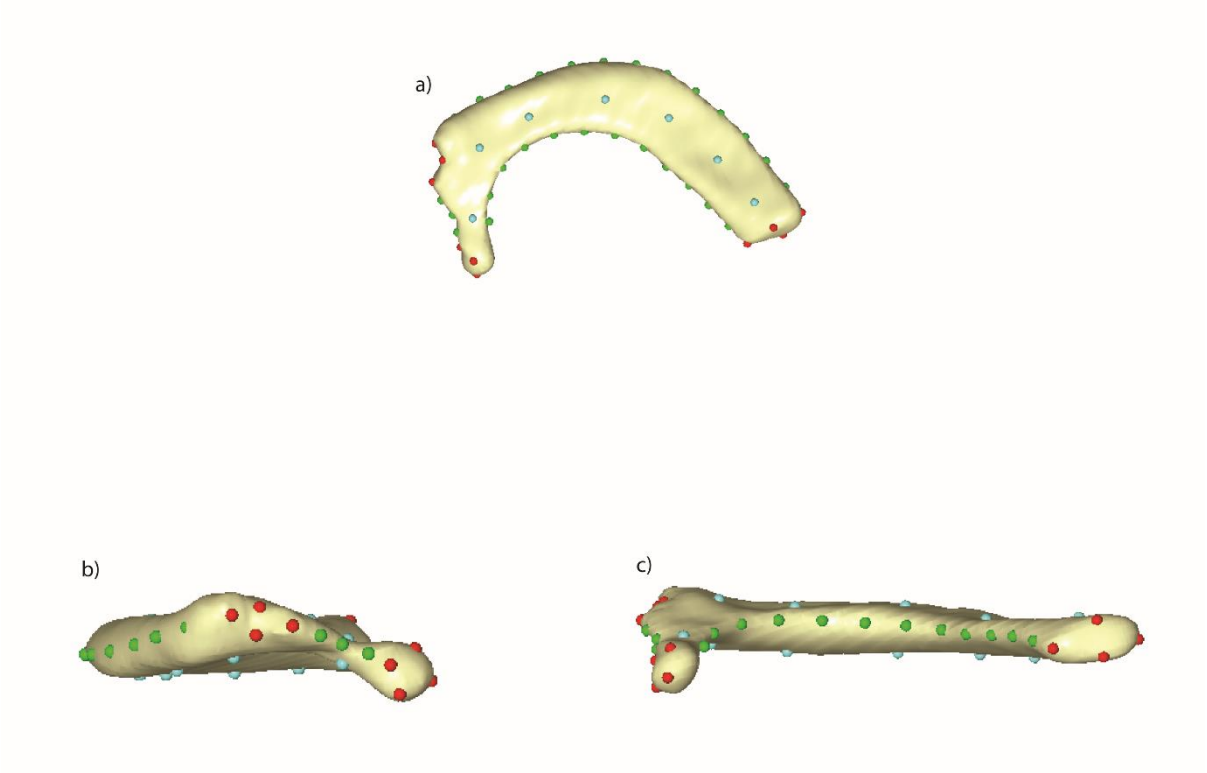

Figure S1: Four landmarks were measured at the cranial-, caudal-, medial- and lateral-most points of the rib head, four landmarks were measured at the cranial-, caudal-, medial- and lateral-most points of the articular tubercle and four landmarks were measured at the internal-, external-, superior- and inferior-most points of the sternal end. In order to better quantify rib curvature and shaft height we used the following semilandmark quantification: Exterior costal border – three equidistant curve semilandmarks were located along the midline of the shaft between the lateral-most point of the rib head and the medial-most point of the articular tubercle; 13 equidistant curve-semilandmarks were located following the external costal border from the lateral-most point of the articular tubercle to the external-most point of the distal end. Interior costal border – 13 equidistant curve-semilandmarks located following the internal costal border from the medial-most point of the rib head facet to the internal-most point of the distal end. Superior surface – seven surface semi-landmarks were equidistantly located at the superior surface of the rib shaft following the midline of it from the superior-most point of the rib head to the superior-most point of the distal end. Inferior surface – seven surface semi-landmarks were equidistantly located at the inferior surface of the rib shaft following the midline of it from the inferior-most point of the rib head to the inferior-most point of the distal end. Each 1st rib was thus described by 55 3D landmarks.

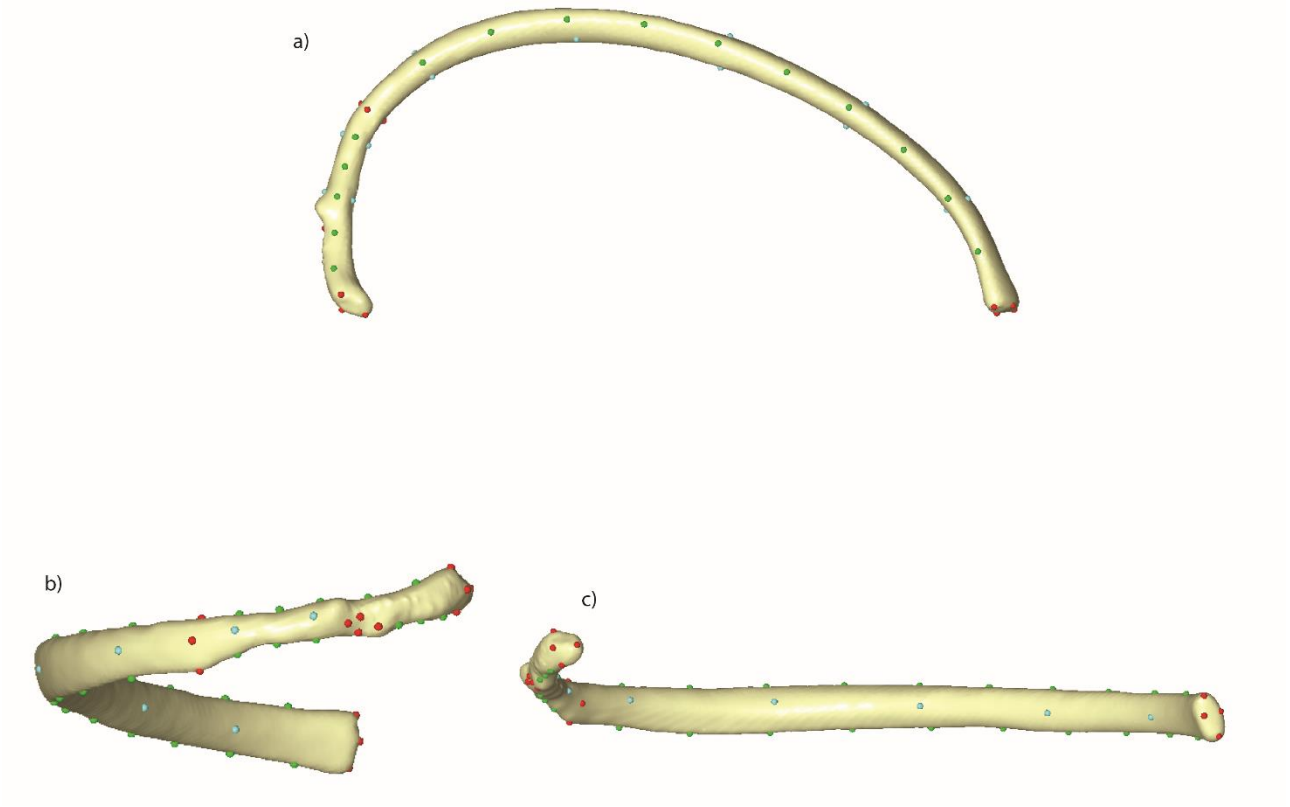

Figure S2: In order to quantify 5th rib morphology, four landmarks were measured at the cranial-, caudal-, medial- and lateral-most points of the rib head and four landmarks were measured at the cranial-, caudal-, medial- and lateral-most points of the articular tubercle. Other four landmarks were place at the posterior angle, two of them were located in the cranio-caudal dimension at the caudal- and cranial-most point at the maximum distance following the shaft maximum diameter at angle (SMXD; Franciscus and Churchill, 2002) and the other two were located in the medio-lateral dimension at the medial- and lateral-most point at the maximum distance following the shaft minimum diameter at angle (SMND; Franciscus and Churchill, 2002). Other four landmarks internal-, external-, superior- and inferior-most points of the sternal end. In order to better quantify rib curvature and shaft height we used the following semilandmark approach: Lower costal border - three equidistant curve semi-landmarks were located between the inferior-most point of the rib head and the medial-most point of the articular tubercle; three equidistant curve semi-landmarks were located between the lateral-most point of the articular tubercle and the caudal-most point of the posterior angle cross section; 10 equidistant curve semi-landmarks were located between caudal-most point of the posterior angle cross section and the caudal-most point of distal end. Upper costal border – five equidistant curve semi-landmarks were located between the superior-most point of the rib head and the cranial-most point of the posterior angle cross section. 10 equidistant curve semi-landmarks were located between cranial-most point of the posterior angle cross section and the cranial-most point of distal end. External surface – two surface semi-landmarks were equidistantly located at the external surface of the rib shaft following the midline of it from the lateral-most point of the rib head to the lateral-most point of the posterior angle cross section; five surface semi-landmarks were equidistantly located at the external surface of the rib shaft following the midline of it from the lateral-most point of the posterior angle cross section to the lateral-most point of the distal end. Internal surface – two surface semi-landmarks were equidistantly located at the internal surface of the rib shaft following the midline of it from the medial-most point of the rib head to the medial-most point of the posterior angle cross section; five surface semi-landmarks were equidistantly located at the internal surface of the rib shaft following the midline of it from the medial-most point of the posterior angle cross section to the medial-most point of the distal end. Each 5th rib was thus described by 61 3D landmarks.

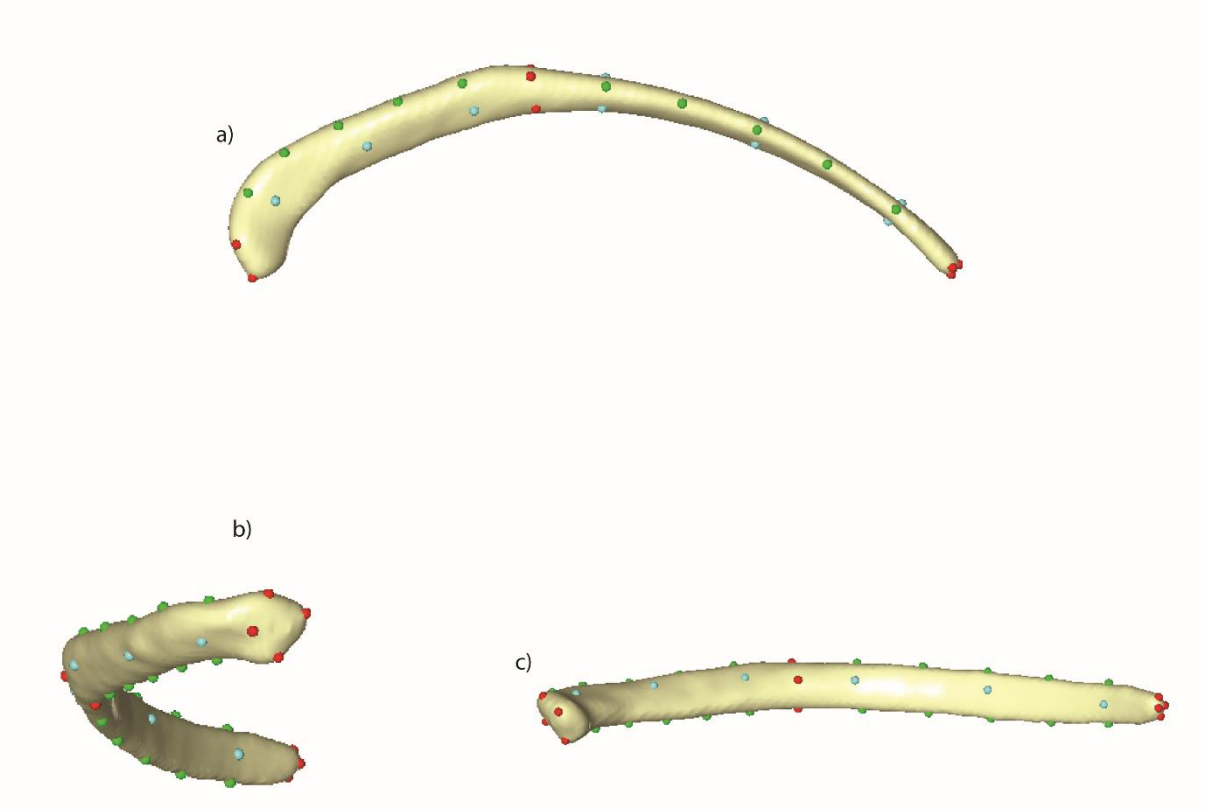

Figure S3: Four landmarks were measured at the cranial-, caudal-, medial- and lateral-most points of the rib head. Four landmarks were place at the posterior angle, two of them were located in the cranio-caudal dimension at the caudal- and cranial-most point at the maximum distance following the shaft maximum diameter at angle (SMXD; Franciscus and Churchill, 2002) and the other two were located in the medio-lateral dimension at the medial- and lateral-most point at the maximum distance following the shaft minimum diameter at angle (Franciscus and Churchill, 2002). Other four landmarks internal-, external-, superior- and inferior-most points of the sternal end. In order to better quantify rib curvature and shaft height we used the following semilandmark approach: Lower costal border - five equidistant curve semi-landmarks were located between the inferior-most point of the rib head and the caudal-most point of the posterior angle cross section; five equidistant curve semi-landmarks were located between caudal-most point of the posterior angle cross section and the caudal-most point of distal end. Upper costal border – five equidistant curve semi-landmarks were located between the superior-most point of the rib head and the cranial-most point of the posterior angle cross section. Five equidistant curve semi-landmarks were located between cranial-most point of the posterior angle cross section and the cranial-most point of distal end. External surface – Three surface semi-landmarks were equidistantly located at the external surface of the rib shaft following the midline of it from the lateral-most point of the rib head to the lateral-most point of the posterior angle cross section; three surface semi-landmarks were equidistantly located at the external surface of the rib shaft following the midline of it from the lateral-most point of the posterior angle cross section to the lateral-most point of the distal end. Internal surface – three surface semi-landmarks were equidistantly located at the internal surface of the rib shaft following the midline of it from the medial-most point of the rib head to the medial-most point of the posterior angle cross section; three surface semi-landmarks were equidistantly located at the internal surface of the rib shaft following the midline of it from the medial-most point of the posterior angle cross section to the medial-most point of the distal end. Each 11h rib was thus described by 44 3D landmarks.

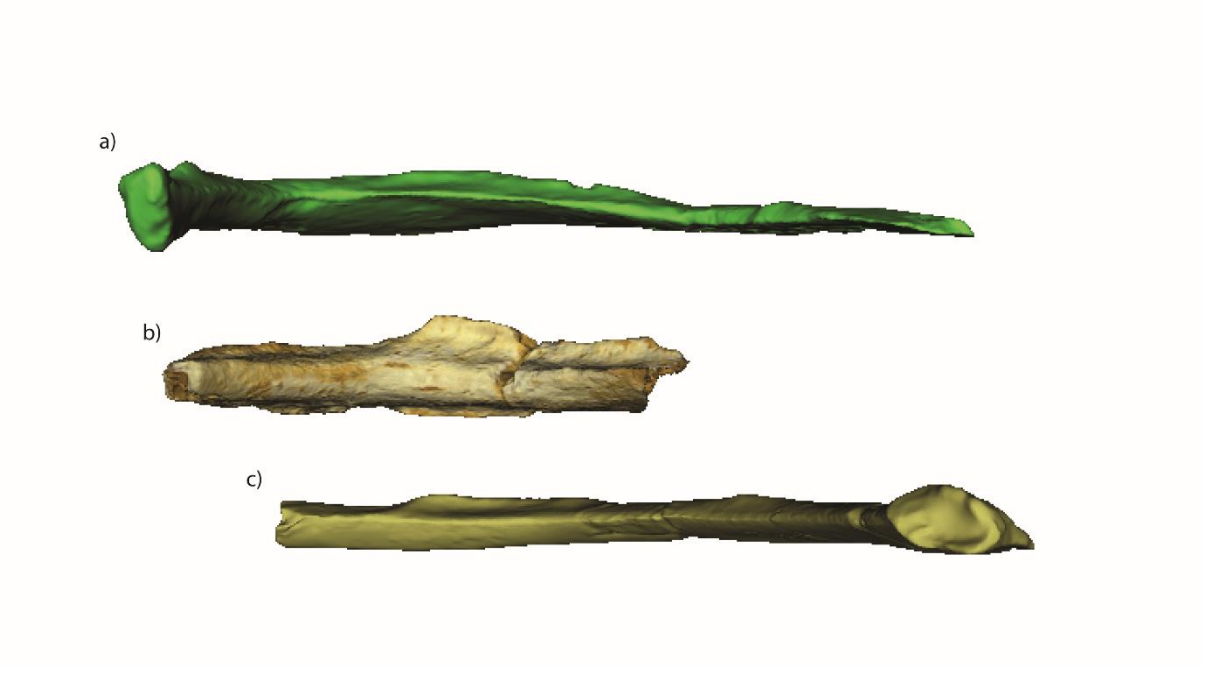

Figure S4: Lateral-internal view of Neandertal 2nd ribs, where the height of the impression of the scalene muscle insertion can be observed in a) Kebara 2, b) El Sidrón SDR-695b and c) Tabun 1. The ribs are shown from left (proximal) to right (distal) and they are aligned at the insertion of the scalene muscle.

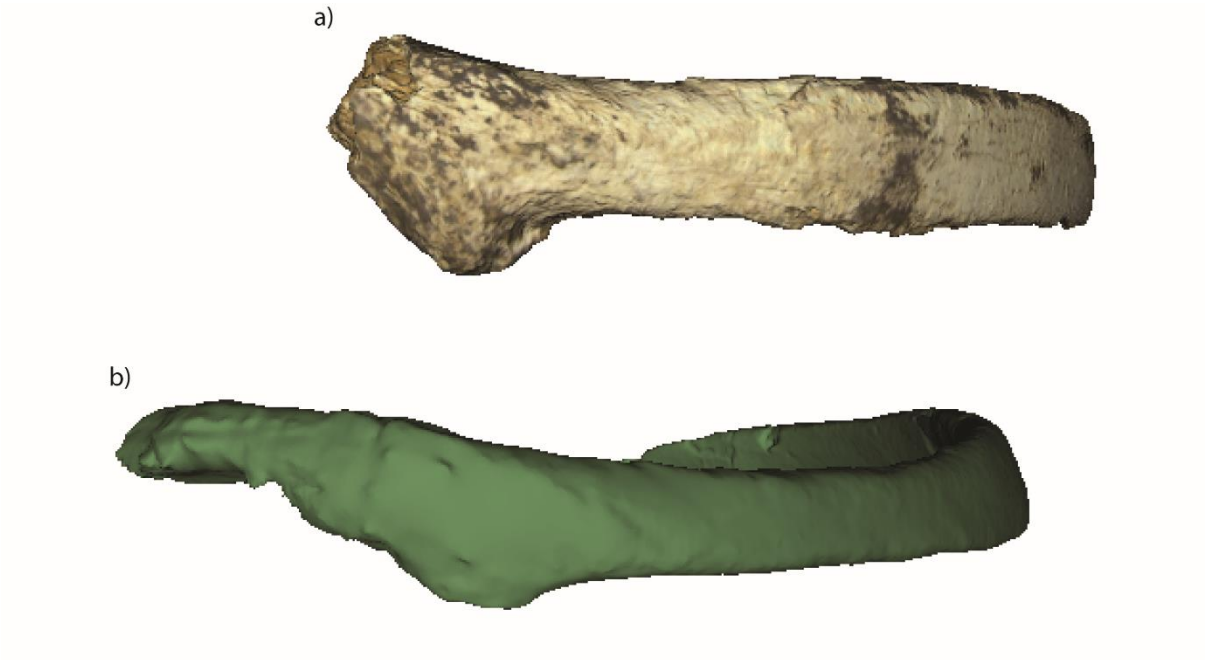

Figure S5: Lateral-external view of Neandertal 5th ribs, where the height of the impression of the *latissimus dorsae* insertion can be observed in a) El Sidrón SD-1450 and b) Kebara 2. The ribs are shown from left (proximal) to right (distal) and they are aligned at the insertion of the iliocostalis muscle.

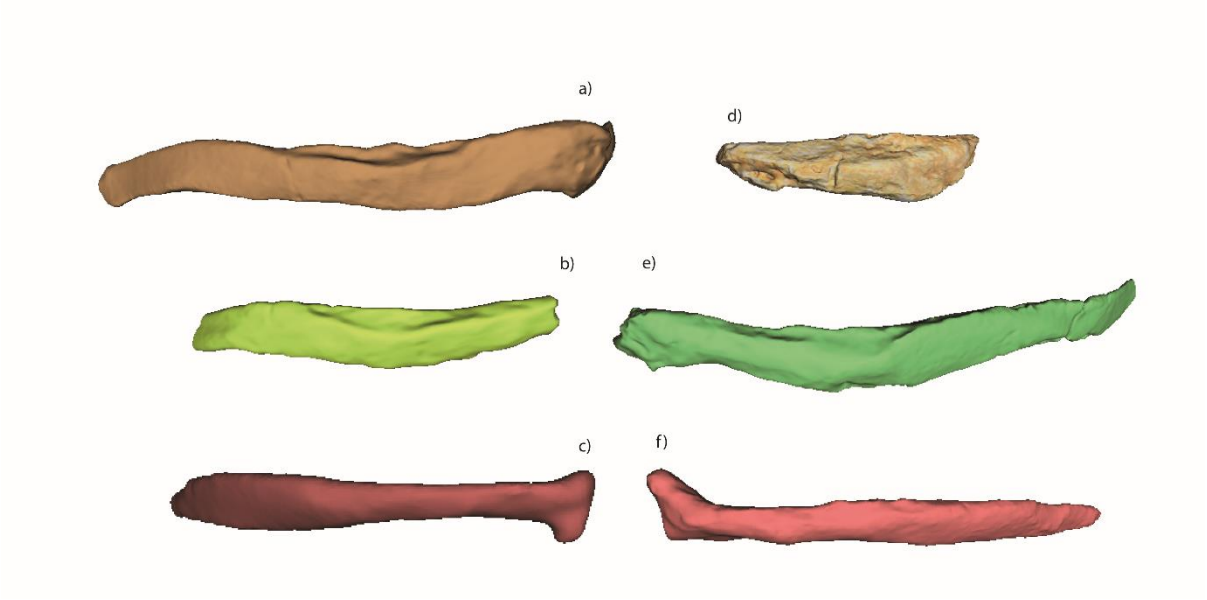

Figure S6: external-cranial view of Neandertal 12h ribs, where the impression of the diaphragm insertion can be observed in a) Kebara 2 (Left), b) Shanidar 3 (Left, d) El Sidrón SD-56, e) Kebara 2 (Right) in comparison with 12th ribs of modern humans (c and f; left and right, respectively). The ribs are shown from left (distal) to right (proximal) in a-c and from left (proximal) to right (distal) in d-f. Ribs are aligned at the insertion of the diaphragm.

Table S1: Inventory of diagnostic costal material studied here, with anatomical position, side, and preserved parts. Provisional determinations since some identifications subject to change with further analyses. R = right; L = left; c = complete or largely preserved; p = partial; N/A = not applicable.

Specimen	Anatomical Position	Side	Preserved anatomical portions					
			Head	Neck	Tubercle	Posterior angle	Shaft	Distal end
SD-1699+	1	L	-	-	c	N/A	c	p
SD-1442	1	R	p	p	-	N/A	-	-
SD-1767	1	R	-	-	p	N/A	c	p
SD-1534	1	R	-	p	c	N/A	-	-
SD-695b	2	L	-	p	c	c	p	-
SDR-159	2	L	-	-	-	-	p	c
SD-695f	2	L	-	-	-	-	p	-
SD-2318	3	L	-	-	-	p	p	-
SDR-234	2-3	L	-	-	-	-	p	-
SD-1401	2-3	R	-	-	-	-	p	-
SD-709b	2-3	R	-	-	-	-	p	-
SDR-26+	3	L	c	c	c	p	p	-
SD-1703	3-4	L	-	-	c	-	-	-
SD-445	3-4	L	-	-	-	-	p	-
SD-1830	3-4	L	-	-	-	-	p	-
SD-579a	3-4	L	-	-	-	-	p	-
SD-447	3-4	R	p	p	-	-	-	-
SD-280h	3-4	R	p	c	c	-	p	-
SD-450	3-4	R	p	p	-	-	-	-
SD-706	3-4	R	-	-	-	c	p	-
SDR-202e	3-4	R	-	-	-	p	p	-
SD-229	3-4	R	-	-	-	-	p	-
SDR-161+	4	L	c	c	c	-	p	-
SDR-164	4-5	L	-	-	c	-	-	-
SD-1450	5	R	-	-	-	c	c	-
SD-695a	5	R	c	c	c	-	p	-
SD-448	5	L	p	c	c	-	-	-
SD-690a	5-7	R	-	p	c	-	-	-
SD-354g	5-7	R	-	-	-	c	-	-
SD-788	6-7	R	p	c	c	-	-	-
SD-666	6-7	R	c	c	c	-	-	-
SD-2111	4-8	L	-	-	-	c	p	-
SD-1038a	4-8	L	-	-	-	c	p	-
SDR-033	4-8	L	-	-	-	-	-	c
SD-1731	4-8	L	-	-	-	p	p	-
SDR-030	4-8	L	-	-	-	-	p	-
SDR-028	4-8	L	-	-	-	p	p	-
SD-2003	4-8	L	-	-	-	-	p	-
SD-234	4-8	L	-	-	-	p	p	-

SD-2025	4-8	L	-	-	-	-	p	-
SDR-165+SDR-220	4-8	L	-	-	-	-	p	-
SD-1763	4-8	L	-	-	-	-	p	-
SD-443	4-8	L	-	-	-	-	p	-
SD-1424	4-8	L	-	-	-	-	p	-
SD-765	4-8	L	-	-	-	-	p	-
SD-709a	4-8	L	-	-	-	-	p	-
SD-1036	4-8	R	-	-	-	-	p	-
SD-721+SD-771	4-8	R	-	-	-	c	p	-
SDR-027	4-8	R	-	-	-	-	p	-
SDR-162	4-8	R	-	-	-	-	p	-
SD-1423	4-8	R	-	-	-	-	p	-
SDR-163	4-8	R	-	-	-	-	p	-
SD-1593	4-8	R	-	-	-	-	p	-
SD-1507	8-9	R	-	c	c	-	-	-
SDR-029+SD-628	8-9	R	-	-	-	-	p	-
SD-2001+	9-10	R	-	-	-	p	p	-
SD-1613+SD-1636	8-10	L	-	-	-	c	p	-
SD-307	8-10	L	-	c	c	-	-	-
SDR-190	8-12	L	-	-	-	-	p	c
SD-1307b	8-12	L	-	-	-	p	p	-
SD-1506	8-12	L	-	-	-	-	p	-
SD-1928+SD-1826	8-12	L	-	-	-	-	p	-
SDR-217	8-12	L	-	-	-	-	p	-
SD-1895	8-12	L	p	-	-	-	p	-
SDR-031	8-12	R	-	-	-	-	p	-
SDR-219	8-12	R	-	-	-	p	p	-
SDR-214	8-12	R	-	-	-	-	p	-
SD-2187	11	L	-	p	N/A	c	c	-
SD-1303b	11	L	p	p	N/A	-	-	-
SD-350	11	L	-	-	-	-	p	-
SD-280g	11	L	-	-	-	-	p	-
SD-695c	11	L	c	p	N/A	-	-	-
SD-131	11	R	c	c	N/A	-	-	-
SD-2012	11	R	p	p	N/A	c	p	-
SD-1508	11	R	-	-	-	-	p	-
SD-1331	12	L	-	-	-	-	p	-
SD-653a	12	L	c	p	N/A	-	-	-
SD-573c	12	R	c	p	N/A	-	-	-
SD-56	12	R	-	-	-	-	p	-
SD-1038b	12	R	-	-	-	-	p	-
SD-774	10-11	L	-	-	-	p	p	-
SD-1532	11-12	R	-	p	N/A	-	p	-
SDR-204	11-12	R	-	-	-	-	p	-

Table S2: Comparative material of modern humans used in this study. Note that ribs 1-12 of each individual were used for traditional measurements but only ribs 1, 5 and 11 were used for 3D GM.

Id	Population	Sex	Data collection method
UC71	Portugal	Male	Laser scanner
UC62	Portugal	Male	Laser scanner
UC63	Portugal	Male	Laser scanner
UC58	Portugal	Male	Laser scanner
UC34	Portugal	Male	Laser scanner
UC2	Portugal	Female	Laser scanner
UC38	Portugal	Female	Laser scanner
UC8	Portugal	Female	Laser scanner
UC3	Portugal	Female	Laser scanner
UC26	Portugal	Female	Laser scanner
Spn683814	Spain	Male	CT scanner
Spn1989386	Spain	Male	CT scanner
Spn1583242	Spain	Male	CT scanner
Spn2749218	Spain	Male	CT scanner
Spn2318866	Spain	Male	CT scanner
Spn1376099	Spain	Female	CT scanner
Spn2688253	Spain	Female	CT scanner
Spn717040	Spain	Female	CT scanner
Spn611461	Spain	Female	CT scanner
Spn1638379	Spain	Female	CT scanner
Innsmale1	Austria	Male	CT scanner
Innsmale2	Austria	Male	CT scanner
InnsFem8	Austria	Female	CT scanner
InnsFem9	Austria	Female	CT scanner

Table S3: values of tubercle-ventral chord (TVC), tubercle-ventral arch (TVA) and tubercle-iliocostal line distance 2 (TID2) measured for 5th ribs, as well as values of head-ventral chord (HVC) and head ventral arch (HVA) measured for 11th ribs. For modern humans, mean, standard deviation and 95% confidence intervals for the mean (between parentheses) are shown. Measurements were taken following descriptions provided by Gómez-Olivencia et al. (2010). Note that measurements of 11th rib of Kebara 2 have been estimated because of the aforementioned damage (see material section). Measurements are shown in mm.

	Neanderthals			**European modern humans**	
	El Sidrón reconstruction	**Kebara 2, Left**	**Kebara 2, Right**	**Males**	**Females**
	5th ribs				
TVA	**329.50**	**297.32**	**310.80**	285.95, 12.84 (277.80 – 294.11)	259.39, 11.35 (252.32 – 266.47)
TVC	**226.85**	**223.56**	**222.26**	212.49, 15.17 (202.86 – 222.13)	190.88, 12.17 (183.15 – 198.61)
TID2	**46.23**	**40.88**	39.72	37.54, 3.47 (35.33 – 39.74)	32.57, 3.54 (30.32 – 34.82)
	11th ribs				
HVA	**249.62**	**228.09**	**229.38**	169.46, 18.34 (157.80 – 181.11)	173.86, 20.44 (160.88 – 186.85)
HVC	**180.74**	**191.75**	**190.43**	142.10, 15.80 (132.07 – 152.14)	149.22, 13.51 (140.64 – 157.81)

Table S4. Mean, standard deviation (sd.) and 95% confidence interval for the mean of modern human males and females for head measurements (head cranio-caudal diameter, HCCD; head width, HW). Measurements in mm.

	HCCD				**HW**			
	Male mean, sd.	**95% CI**	**Female mean, sd.**	**95% CI**	**Male mean, sd.**	**95% CI**	**Female mean, sd.**	**95% CI**
1st	8.78, 0.88	8.33-9.24	7.12, 1.41	6.39-7.84	9.16, 1.50	8.39-9.93	7.11, 1.95	6.11-8.11
2nd	10.40, 1.97	9.39-11.42	9.25, 1.40	8.53-9.97	9.13, 1.59	8.31-9.94	8.53, 1.46	7.78-9.28
3rd	10.36, 1.53	9.57-11.15	8.63, 1.91	7.65-9.61	9.43, 2.02	8.39-10.47	7.98, 1.55	7.49-8.78
4th	11.90, 2.24	10.75-13.05	9.52, 1.45	8.77-10.27	9.57, 1.33	8.89-10.25	7.54, 1.21	6.93-8.17
5th	12.95, 1.43	12.22-13.70	11.12, 1.30	10.45-11.78	9.50, 1.86	8.55-10.45	7.76, 1.14	7.18-8.35
6th	13.77, 1.97	12.76-14.79	11.82, 1.39	11.11-12.53	9.24, 1.88	8.27-10.02	7.50, 1.12	6.92-8.08
7th	14.92, 1.94	13.92-15.92	12.66, 1.52	11.90-13,42	8.31, 1.62	7.47-9.14	7.30, 1.38	6.61-7.99
8th	14.84, 1.15	14.25-15.43	12.77, 1.86	11.78-13.76	8.14, 1.40	7.44-8.85	7.27, 1.03	6.72-7.82
9th	14.53, 1.87	13.58-15.50	12.71, 1.68	11.88-13.55	7.42, 1.70	6.55-8.30	5.97, 1.24	5.35-6.59
10th	13.60, 1.84	12.66-14.55	12.20, 1.88	11.19-13.20	6.98, 1.46	6.23-7.73	5.87, 1.56	5.04-6.70
11th	12.28, 1.09	11.59-12.97	11.34, 2.16	9.97-12.72	8.20, 1.14	7.47-8.92	6.71, 1.34	5.86-7.56
12th	10.47, 2.45	8.72-12.22	11.76, 2.06	10.35-13.11	6.73, 1.33	5.77-7.68	7.74, 1.30	6.87-8.61

Table S5. Head measurements (head cranio-caudal diameter, HCCD; head width, HW) in Neanderthal ribs. Bolded and underlined values are outside modern human ranges, both for males and females. Measurements in mm.

	HCCD			**HW**		
	El Sidrón	**Kebara 2**	**Mean**	**El Sidrón**	**Kebara 2**	**Mean**
1st		8.36 (Left)	8.36		8.63 (Left)	8.63
2nd		10.07 (Left)	10.07		9.64 (Left)	9.64
3rd	**14.52** (SDR-26+)		**14.52**	**12.77** (SDR-26+)		**12.77**
4th	**13.28** (SDR-161+)		**13.28**	10.23 (SDR-161+)		10.23
5th	**15.24** (SD-695a)		**15.24**	**11.50** (SD-695a)		**11.50**
6th	**17.66; 15.08** (SD-788; SD-666)		**16.37**	**10.36**; 8.96 (SD-788; SD-666)		9.66
7th	**17.66**; 15.08 (SD-788; SD-666)		**16.37**	**10.36**; 8.96 (SD-788; SD-666)		**9.66**
8th	**16.85** (Block)		**16.85**	**9.48** (Block)		**9.48**
9th						
10th						
11th	**13.93; 14.26** (SD-131; SD-695c)	**13.86** (Left)	**14.01**	8.47; **9.43** (SD-131; SD-695c)	8.88 (Left)	**8.93**
12th	**14.41; 14.38** (SD-653a; SD-573c)	**15.43** (Left)	**14.74**	**9.36; 9.43** (SD-131; SD-695c)	**8.93** (Left)	**9.24**

Table S6. Mean, standard deviation (sd.) and 95% confidence interval for the mean of modern human males and females for articular tubercle measurements (articular tubercle height, ATH; articular tubercle width, ATW). Measurements in mm.

	ATH				ATW			
	Male mean, sd.	**95% CI**	**Female mean, sd.**	**95% CI**	**Male mean, sd.**	**95% CI**	**Female mean, sd.**	**95% CI**
1st	6.15, 0.90	5.51-6.79	4.39, 1.15	3.57-5.20	9.81, 1.49	8.75-10.88	6.84, 1.34	5.89-7.81
2nd	5.87, 0.83	5.28-6.47	4.77, 1.01	4.01-5.49	7.62, 1.05	6.87-8.37	6.99, 1.92	5.62-8.36
3rd	6.39, 0.93	5.73-7.05	5.21, 0.97	4.52-5.90	8.10, 1.35	7.13-9.06	6.85, 0.98	6.15-7.56
4th	6.92, 1.41	5.91-7.92	6.17, 1.49	5.10-7.23	8.86, 1.65	7.68-10.04	7.02, 1.06	6.26-7.78
5th	6.87, 1.10	6.08-7.66	5.95, 1.04	5.21-6.69	8.14, 0.89	7.50-8.78	7.22, 0.96	6.54-7.91
6th	6.31, 0.68	5.82-6.79	5.62, 0.62	5.18-6.07	8.04, 1.44	7.01-9.07	7.41, 1.15	6.58-8.23
7th	6.64, 1.08	5.87-7.42	5.37, 1.02	5.37-6.75	8.38, 0.89	7.74-9.01	6.80, 1.22	5.98-7.63
8th	6.70, 1.21	5.84-7.57	5.67, 0.93	4.95-6.38	8.05, 1.21	7.19-8.92	6.91, 1.29	5.92-7.90
9th	6.74, 1.92	5.36-8.11	6.33, 1.77	5.14-7.52	7.74, 2.05	6.27-9.20	7.94, 1.76	6.76-9.12
10th	5.69, 1.89	4.34-7.04	5.72, 2.47	3.83-7.62	6.96, 2.06	5.48-8.43	6.85, 2.70	4.78-8.93

Table S7a. Articular tubercle height (ATH) in Neanderthal ribs. Bolded and underlined values are outside modern human ranges, both for males and females. Underlined and not bolded values are outside of the modern human male range but inside of the female range Measurements in mm.

	ATH				
	El Sidrón	**Kebara 2**	**La Chapelle-aux-Saints**	**Shanidar 3**	**Mean**
1st	5.17 (SD-1534)	**7.53; 7.16** (Right; Left)			6.62
2nd	4.63 (SD-695b)	6.14; 5.45 (Right; Left)			5.34
3rd	6.40 (SDR-26+)	5.67 (Left)			6.04
4th	7.26 (SDR-161+)	7.02; 6.66 (Right; Left)			6.98
5th	7.20; 6.35 (SDR-695a; 448)			**9.51** (Right)	**7.69**
6th	**10.46; 12.45** (SD-788; SD-666)				**11.46**
7th	**10.46; 12.45** (SD-788; SD-666)	5.84; 5.55 (Right; Left)	**10.60** (Right)	**9.37** (Right)	**9.05**
8th	**8.40** (Block)	7.21 (Right)	**11.10** (Right)	**8.64** (Right)	**8.78**
9th		**8.27**; 7.58 (Right; Left)	**12.90** (Right)	**10.44; 13.03** (Right; Left)	**10.44**
10th					

Table S7b. Articular tubercle width (ATW) in Neanderthal ribs. Bolded and underlined values are outside modern human ranges, both for males and females. Underlined and not bolded values are outside of the modern human male range but inside of the female range Measurements in mm.

	ATW				
	El Sidrón	**Kebara 2**	**La Chapelle-aux-Saints**	**Shanidar 3**	**Mean**
1st	7.23 (SD-1534)	**11.83; 11.65** (Right; Left)			10.25
2nd	7.55 (SD-695b)	**8.41**; 8.16 (Right; Left)			8.04
3rd	7.15 (SDR-26+)	7.50 (Right)			7.33
4th	6.56 (SDR-161+)	7.84; 8.53 (Right; Left)			7.64
5th	7.28; **9.09** (SDR-695a; 448)			8.28 (Right)	8.23
6th	**9.75; 10.68** (SD-788; SD-666)				**10.22**
7th	**9.75; 10.68** (SD-788; SD-666)	8.53; **9.89** (Right; Left)	**11.20** (Right)	**9.77** (Right)	**9.97**
8th	7.56 (Block)	8.09 (Right)	**10.30** (Right)	**9,30; 10.42** (Right; Left)	**9.13**
9th		7.90; 7.64 (Right; Left)	**10.90** (Right)	**12.77; 10.67** (Right; Left)	**9.98**
10th					

Table S8. Mean, standard deviation (sd.) and 95% confidence interval for the mean of modern human males and females for total neck length (TNL). Measurements in mm.

	TNL			
Level	**Male mean, sd.**	**95% CI**	**Female mean, sd.**	**95% CI**
1st	37.75, 2.92	33.05-38.46	30.03, 2.41	27.80-32.26
2nd	37.78, 1.48	35.41-38.15	31.36, 2.47	29.07-33.64
3rd	33.35, 2.25	31.27-35.43	31.78, 2.68	29.30-34.26
4th	34.87, 1.87	33.15-36.60	30.71, 1.78	29.13-32.43
5th	34.88, 2.44	32.62-37.14	31.82, 1.11	30.80-32.85
6th	35.49, 4.61	31.22-39.76	32.21, 2.59	29.82-34.61
7th	34.26, 3.32	31.19-37.33	32.62, 1.81	30.94-34.29
8th	33.29, 2.73	30.77-35.82	31.61, 1.61	30.12-33.09
9th	32.76, 3.78	29.26-36.26	30.52, 2.15	28.53-32.51
10th	27.57, 2.36	25.39-29.76	26.22, 3.96	22.56-29.89

Table S9. Total neck length (TNL) in Neanderthal ribs. Underlined and not bolded values are outside of the modern human male range but inside of the female range Measurements in mm.

	TNL		
Level	**El Sidrón**	**Kebara 2**	**Mean**
1st		*32.98* (Left)	*32.98*
2nd		35.59 (Right)	35.59
3rd	33.85 (SDR-26+)		33.85
4th	33.64 (SDR-161+)		33.64
5th	35.13; 36.73 (SD-695a; SD-448)		35.93
6th	33.31; *30.09* (SD-788; SD-666)		32.00
7th	33.31; *30.09* (SD-788; SD-666)		32.00
8th			
9th			
10th			

CAPÍTULO IX – DISCUSIÓN GENERAL

Se conoce poco acerca de los detalles tridimensionales de la variabilidad morfológica torácica, tanto intra-específica (ontogenia, el dimorfismo sexual y la anatomía funcional) como inter-específica (anatomía comparada y la anatomía evolutiva). El objetivo básico de esta tesis es esclarecer todos estos campos de conocimiento. Hasta ahora, sólo algunos aspectos de la biomecánica torácica habían sido estudiados en sus detalles 3D, pero con un enfoque muy aplicado al estudio de las fracturas potenciales relacionadas con accidentes de tráfico (Gayzik, 2008; Shi et al., 2014; Weaver et al., 2014). Tras esta tesis, se ha ampliado el considerablemente el conocimiento en todos los campos de la Antropología Física anteriormente mencionados, aunque ciertos aspectos todavía habrán de ser profundizados en el futuro.

Uno de los principales problemas a los que esta tesis se enfrentaba es el de la cuantificación rigurosa y precisa de la anatomía costal y torácica, la cual se caracteriza por estar definida por elementos curvos de difícil medición mediante técnicas tradicionales como cuerdas, arcos o ángulos (Jellema et al., 1993; Franciscus y Churchill, 2002; Gómez-Olivencia et al., 2009). Para solventar este problema, se ha desarrollado en esta tesis todo un protocolo metodológico que permite la cuantificación tridimensional tanto de costillas y vértebras individualizadas, como de la caja torácica en su conjunto mediante técnicas de MG 3D de *sliding semilandmarks*. En las publicaciones donde se han presentado análisis de fósiles, las técnicas de MG se han complementado con medidas tradicionales a fin de poder ser evaluables y comparables con resultados obtenidos por otros autores que no tienen acceso a dichas técnicas tridimensionales.

Capítulo 9.1 Ontogenia torácica.

Los resultados de la presente tesis doctoral (**capítulo 4**), muestran que la ontogenia de la caja torácica es altamente más compleja de lo propuesto hasta la fecha. En primer lugar, lo más destacable que se ha observado es que el tórax superior y el inferior responden a patrones de crecimiento diferenciales, ya que los vectores de crecimiento de ambos divergen significativamente en 36,4º (Bastir et al., 2013), lo cual es confirmado por la diferente pendiente de las rectas de crecimiento de las costillas del tórax superior e inferior (García-Martínez et al., 2016a). Estos hechos se reflejan en que los cambios morfológicos observados en el tórax superior e inferior son diferentes a lo largo de la ontogenia. De acuerdo a los resultados aquí presentados, la expansión medio-lateral propuesta por Openshaw et al. (1984) para la ontogenia torácica se observa únicamente a nivel relativo del tórax superior, estando la ontogenia del tórax inferior caracterizada por una reducción medio-lateral relativa (Bastir et al., 2013; Fig. 10).

Estos cambios morfológicos diferenciales en los diferentes niveles torácicos ocurren, al menos parcialmente, por cambios morfológicos en las costillas individuales. Como se observa en los resultados de García-Martínez et al. (2016a; Fig. 10), las costillas experimentan un incremento de la curvatura en vista craneal a lo largo de la ontogenia. Sin embargo, el punto de máxima curvatura costal, el cual se encuentra situado en la parte central del eje en individuos infantiles, se encuentra posicionado en dirección más dorsal en las costillas del tórax inferior en adultos. Esto no ocurre en las costillas pertenecientes al tórax superior, ya que estas presentan siempre el punto de máxima curvatura en la parte central del eje tanto en infantiles como en adultos. Este factor puede estar relacionado con el aumento de la lordosis de la parte inferior del tórax que ha sido observado a lo largo de la ontogenia humana (Openshaw et al., 1984; Bastir et al., 2013).

Es importante señalar también que el incremento de la declinación costal observado a lo largo de la ontogenia (Openshaw et al., 1984; Bastir et al., 2013), no es únicamente debido a una rotación mecánica en dirección caudal de las costillas (como se propone explícitamente en Gray, 1918), sino que hay cambios en la propia morfología costal, como es el aumento en la torsión, que pueden contribuir a esa declinación costal (García-Martínez et al., 2016a). Además, las costillas que presentan una mayor torsión costal, estarían en principio asociadas a un modo de respiración basado en la utilización de los músculos intercostales; mientras que las costillas con poca torsión, estarían vinculadas a una respiración más diafragmática (De Troyer et al., 2005). Esto es debido a que las costillas con más torsión (o declinadas) tendrían un mayor rango de movimiento en dirección cráneo-caudal que las costillas con poca torsión (o poco declinadas), por lo que la elevación de las mismas a través de los músculos intercostales durante la inspiración sería más eficiente. Los individuos con costillas con poca torsión o declinadas (como los infantiles), al no tener una elevada acción de los músculos intercostales, habrán de compensar esto con una elevada acción diafragmática (De Troyer et al., 2005; García-Martínez et al., 2016a).

Adicionalmente, aunque observamos que los mayores cambios en la configuración torácica son adquiridos en torno a la edad de 2-3 años (acorde a Openshaw et al., 1984), también hay que señalar que de esa edad en adelante ocurren también cambios significativos en forma y tamaño de la caja torácica (Bastir et al., 2013). De este modo, se observa un aumento considerable de su altura relativa, así como un gran aumento en su tamaño, lo cual puede ser debido al aumento del tamaño corporal también observado por otros autores (Baume et al. 1983).

Los cambios morfológicos observados en la ontogenia del tórax (los cuales hacen que la caja torácica pase de una configuración con una morfología más piramidal a una morfología más prismática) pueden ser debidos a factores tales como el cambio en la postura corporal, la

organización espacial de los órganos internos, cambios hormonales, así como a factores más puramente alométricos o isométricos debidos al incremento de tamaño corporal (Openshaw et al., 1984; Bastir et al, 2013; García-Martínez et al., 2016a).

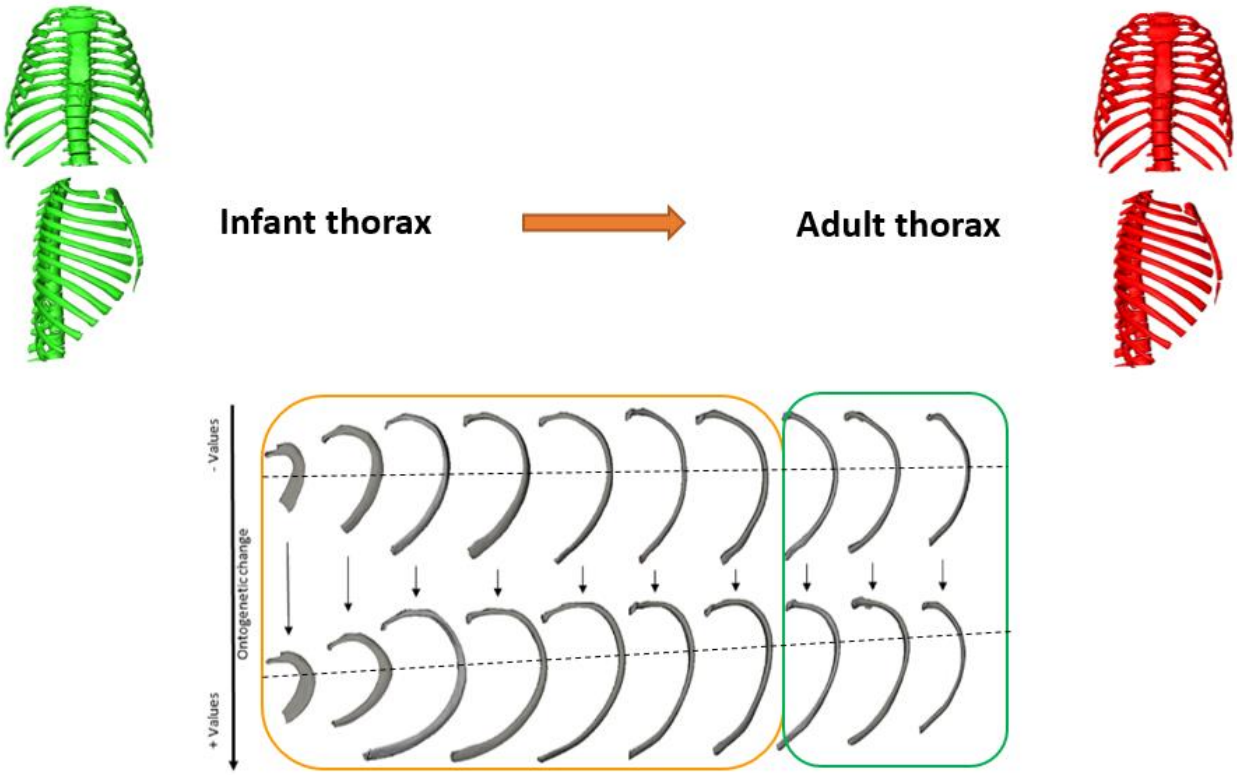

Figura 10: Cambio morfológico observado en la ontogenia de la caja torácica completa (parte superior) y de las costillas individuales (parte inferior). En la imagen inferior se observa que el cambio morfológico que ocurre en las costillas superiores (costillas 1-7; cuadro naranja) es diferente del que ocurre en las inferiores (costillas 8-10; cuadro verde).

Capítulo 9.2 Dimorfismo sexual.

El dimorfismo sexual en el sistema respiratorio torácico, ha sido considerablemente menos estudiado que el del sistema respiratorio cráneo-facial. Respecto a este último, ha sido observado que los individuos masculinos presentan tamaños mayores que los individuos femeninos a nivel absoluto y relativo, lo cual ha sido estudiado tanto en tejido blando como en tejido duro (Rosas y Bastir, 2002; Hall, 2005; Bulygina et al., 2006; Bastir et al., 2011; Holton et al., 2014). Esto ha sido vinculado a diferencias en la composición corporal y la bioenergética de ambos sexos, ya que los individuos masculinos poseen una mayor demanda de oxígeno que los femeninos, además de un mayor porcentaje de masa magra y un menor porcentaje de masa

grasa que los femeninos, respectivamente (Bitar et al., 1999; Hall, 2005; Wells, 2007; Froehle y Churchill, 2009).

Debido a que existe una conexión morfo-funcional hipotética entre la parte esquelética cráneo-facial (cavidad nasal y vías aéreas superiores) y la parte esquelética post-craneal (caja torácica y pulmones) (Bastir, 2008, en prensa), la gran entrada de aire a través de la vía cráneo-facial que ha sido propuesta para los individuos masculinos (Bastir et al., 2011), debería verse reflejada en una gran capacidad torácica en los mismos.

Trabajos previos utilizando medidas tradicionales han observado que la caja torácica femenina se caracteriza por un menor tamaño (de acorde a lo esperado), costillas más declinadas y una menor anchura relativa de la caja torácica respecto de individuos masculinos (Bellemare et al., 2003, 2006). Sin embargo, los detalles tridimensionales de estas diferencias y la posibilidad de una influencia alométrica (cambios en forma debidos a cambios en tamaño) sobre las mismas nunca habían sido estudiados hasta la fecha.

Los resultados de la presente tesis doctoral en este aspecto (**capítulo 5**), muestran que los individuos masculinos presentan una caja torácica un 12.4% mayor de media que los individuos femeninos en un estado cinemático neutral (calculado como la forma media entre inspiración y espiración). Adicionalmente, los individuos masculinos tienen un incremento del tamaño en el ciclo expiración-inspiración un 33% mayor que las mujeres (García-Martínez et al., 2016b). Estos datos, estarían de acuerdo con la mayor capacidad respiratoria en la parte cráneo-facial de individuos masculinos frente a femeninos observada por autores previos (Rosas y Bastir, 2002; Hall, 2005; Bulygina et al., 2006; Bastir et al., 2011; Holton et al., 2014).

Respecto a la forma, los datos aquí presentados están de acuerdo con lo propuesto por autores previos (Bellemare et al., 2003), ya que observamos que los tórax masculinos son relativamente más bajos y anchos que los femeninos, pero en esta tesis doctoral (**capítulo 5**)

se especifica que esta última característica se hace más evidente en el tórax inferior que en el superior. Adicionalmente, los resultados obtenidos en esta tesis doctoral confirman que las costillas femeninas están más declinadas que las masculinas y que el esternón se localiza en una posición más alta en los individuos femeninos que en los masculinos (de acuerdo con Bellemare et al., 2003). También se ha mostrado que la menor altura relativa del tórax masculino es debida únicamente a factores alométricos, pero otros factores como la mayor declinación de las costillas femeninas o la mayor anchura relativa del tórax masculino perduran aún eliminando el factor alométrico (García-Martínez et al., 2016b).

Ha sido demostrado por otros autores que las variaciones en la configuración toraco-abdominal tienen implicaciones en el modo de respiración del individuo (Goldman et al., 1978; Grassino et al., 1978; Pinet, 2004). De este modo, ha sido observado que la biomecánica de la pared abdominal refleja ampliamente la cinemática diafragmática, mientras que la mecánica de los músculos intercostales estaría bien reflejada en la pared torácica (Goldman et al., 1978; Grassino et al., 1978; Pinet, 2004). Por lo tanto, las diferencias morfológicas observadas en esta tesis doctoral, pueden ser hipotéticamente debidas a diferencias en patrones de respiración, ya que la mayor anchura en la parte inferior del tórax (como observado en los individuos masculinos frente a los femeninos), podría estar vinculada a una actividad diafragmática más potente (De Troyer et al., 2005).

Es importante señalar que Bellemare et al. (2003) vincularon hipotéticamente la mayor declinación de las costillas a una mayor eficiencia respiratoria. Aunque esto puede ser cierto, es probable que la menor eficiencia de los músculos intercostales masculinos se vea compensada por una actividad diafragmática mayor. El hecho de que se ha observado en el **capítulo 5** que los individuos masculinos expanden un 33% más la caja torácica que los femeninos durante la inspiración, revela que los individuos masculinos no presentan menos eficacia respiratoria que los femeninos (si se entiende la eficacia respiratoria como la capacidad

para expandir el tórax e introducir aire en los pulmones). Esto vendría apoyado por algunos estudios acerca de la mecánica ventilatoria de la pared toraco-abdominal que han mostrado que, al menos durante ciertos experimentos, los individuos masculinos tienen un modo de respiración más abdominal (relacionado con la acción diafragmática) que las mujeres (relacionado con la acción de los intercostales), las cuales presentan un modo de respiración más torácico (Verschakelen y Demedts, 1995; Ragnarsdottir y Kristinsdottir, 2006; Kaneko y Horie, 2012).

Adicionalmente, se ha propuesto que los tórax femeninos podrían también estar adaptados para acomodar una expansión volumétrica durante el embarazo (Bellemare et al., 2003). Por lo tanto, la longitud cráneo-caudal relativamente mayor observada en las mujeres podría estar involucrada en el alojamiento de los órganos reproductivos internos, así como el alojamiento de un potencial feto durante el embarazo. Finalmente, los resultados aquí expuestos también han mostrado que las diferencias morfológicas observadas en el tórax completo, pueden ser parcialmente debidas a diferencias en la configuración morfológica tridimensional de las vértebras torácicas (Bastir et al., 2014b; Fig. 11). Esto es así porque en la presente tesis doctoral se ha observado que los procesos transversos de las vértebras del tórax inferior en individuos masculinos tienen una orientación más posterior que en el caso de los individuos femeninos (Bastir et al., 2014b; Fig. 11). Esta mayor posteriorización de los procesos transversos produciría una rotación hacia posterior de las costillas articuladas con esas vértebras, lo cual podría estar relacionado con la mayor expansión del tórax inferior anteriormente mencionada (García-Martínez et al., 2016b), contribuyendo de este modo a la mayor capacidad torácica masculina.

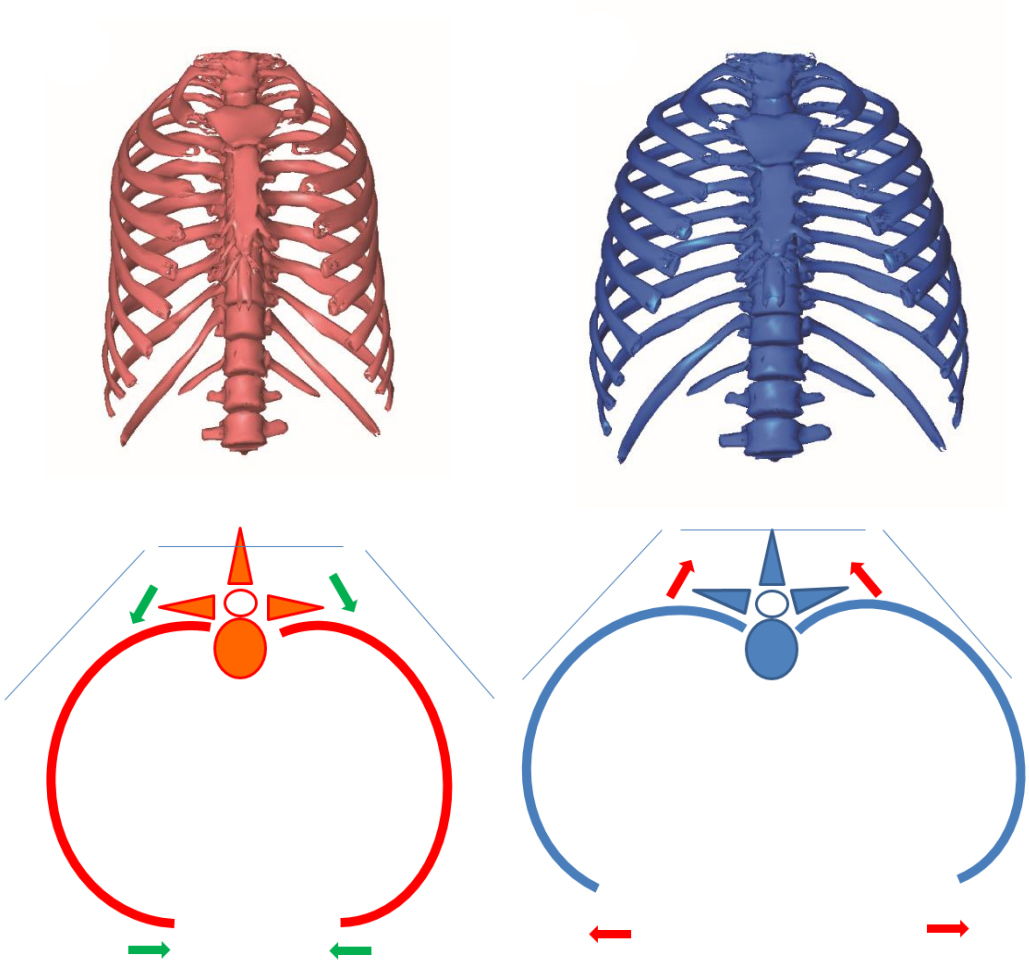

Figura 11: Dimorfismo sexual observado en la caja torácica (parte superior) e ilustración de cómo el cambio morfológico en las *partes* (orientación de los procesos transversos de las vértebras torácicas) puede influir en la forma del *todo* al que pertenece (tórax).

Capítulo 9.3 Anatomía funcional.

Han sido descritos dos patrones fundamentales de movimiento diferentes dentro de la caja torácica: el descrito como *pump handle-like* en las costillas superiores (movimiento en dirección cráneo-caudal y producido por la acción de los músculos intercostales) y el descrito como *bucket handle-like* en las costillas inferiores (movimiento en dirección medio-lateral y producido por la acción del diafragma) (Williams y Warwick, 1980; Shipman et al., 1985; Aiello y Dean, 1999; Franciscus y Churchill, 2002; West, 2012; Beyer et al., 2014). En el **capítulo 6,** se han explorado los cambios geométricos que ocurren en la caja torácica durante la respiración en este marco fundamentalmente dicotómico de clasificación dinemática. Del

mismo modo, también se han estudiado las implicaciones funcionales de los cambios de forma y tamaño durante la respiración en las diferentes regiones torácicas.

En primer lugar, los resultados del **capítulo 6** muestran que la caja torácica inferior y superior presentan vectores cinemáticos diferentes y, por lo tanto, diferente modo de movimiento respiratorio en *shape space* (divergencia de 36,6 º), lo cual estaría de acuerdo con autores previos (Williams y Warwick, 1980; Shipman et al., 1985; Aiello y Dean, 1999; Franciscus y Churchill, 2002; West, 2012; Beyer et al., 2014). Adicionalmente, aquí se muestra que las costillas más superiores probablemente poseen una cinemática ligeramente diferente al resto del tórax, lo cual no había sido observado hasta la fecha (Bastir et al., 2017). Esto puede ser debido a la presencia de músculos accesorios en las costillas superiores, como pueden ser los escalenos o los serratos, así como a la morfología plana tan peculiar que tienen dichas costillas (Gray, 1918; Spalteholtz, 1970).

En este punto es importante señalar que también se ha encontrado apoyo para la separación del tórax superior e inferior en unidades morfo-funcionales en la ontogenia de la caja torácica, donde se ha observado un vector ontogenético divergente entre el tórax superior e inferior (Bastir et al., 2013; García-Martínez et al., 2016a; **capítulo 4**). Adicionalmente, en anatomía musculo-esquelética también se ha observado que, debido a que el diafragma sólo inserta en las costillas 7-12, estas pueden presentar una mecánica diferente de la que presentan las costillas no diafragmáticas (Ward et al., 1992; Kenyon et al., 1997). Finalmente, en la anatomía evolutiva (Schmid et al., 2013; Bastir et al., 2015) también se ha hablado de que el tórax superior e inferior pueden haber evolucionado en diferentes *tempos* a lo largo de la evolución humana, debido a la evolución bajo presiones selectivas diferenciales y a la integración de las diferentes partes del tórax, con otros sistemas. De este modo, la evolución de la caja torácica superior estaría vinculada a la evolución del miembro superior y de la cintura escapular, mientras que el tórax inferior estaría vinculado a la evolución del sistema pélvico.

Esto daría una vez más apoyo a la presencia de diferentes módulos en la caja torácica, como ha sido propuesto en el **capítulo 4** (Bastir et al.; 2013).

A pesar de esta separación clara, se observa que utilizar los términos *bucket-* o *pump-handle like* para diferenciar el modo de respiración del tórax superior y el inferior, puede ser una sobre-simplificación del cambio morfológico real del tórax (Bastir et al., 2017). Aunque el movimiento *bucket-handle like* es más observable en el tórax inferior y el *pump-handle like* se observa más en el superior, los datos presentados en el **capítulo 6** muestran que tanto en el tórax superior como en el inferior se dan ambos movimientos, en dirección medio-lateral y en dirección cráneo-caudal, aunque en diferentes grados. Para apoyar a esta conclusión, observamos que los vectores cinemáticos de los niveles costales estudiados por pares son de pequeño tamaño y no hay ningún "salto" claro entre el ángulo de las diferentes parejas de vectores (Bastir et al., 2017).

Finalmente, cabe señalar que los resultados aquí presentados también han mostrado que los cambios de forma en el tórax superior producen un menor diferencial de tamaño durante la inspiración que los cambios morfológicos en el tórax inferior, donde pequeños cambios de forma producen grandes diferencias en tamaño (Bastir et al., 2017). Esto no sólo tiene una importancia puramente funcional, sino que esta información puede ser extendida al dimorfismo sexual, donde ha sido observado también en la presente tesis doctoral que los individuos masculinos presentan un tórax inferior más medio-lateralmente expandido que los individuos femeninos (García-Martínez et al., 2016b). De manera relevante con lo anteriormente comentado, ha sido observado también en esta tesis que los individuos masculinos producen un 33% más de cambio en tamaño durante la inspiración que los femeninos, lo cual puede ser debido a estas diferencias morfológicas en el tórax inferior (García-Martínez et al., 2016b; **capítulo 5**).

Capítulo 9.4 Anatomía comparada.

Respecto a la anatomía comparada de la caja torácica humana, el conocimiento actual viene fundamentado por las bases sobre anatomía propuestas por el primatólogo Adolf Schultz (1930; 1961). En sus trabajos, él proponía una dicotomía nominal para describir la caja torácica de los grandes simios, incluyendo humanos. De este modo, los géneros *Pan*, *Pongo* y *Gorilla* estarían caracterizados por una caja torácica *funnel-shaped* o en forma de embudo invertido, mientras que los géneros *Homo* e *Hylobates* estarían caracterizados por una caja torácica *barrel-shaped* o en forma de barril (véase introducción). La morfología de los primeros, estaría caracterizada por una caja torácica superior proporcionalmente estrecha y una caja torácica inferior proporcionalmente expandida en dirección medio-lateral. El patrón opuesto se encontraría en los individuos que presentaban un tórax en forma de barril, con una caja torácica superior proporcionalmente expandida en dirección medio-lateral, y un tórax inferior proporcionalmente más estrecho (Schultz, 1961). Se ha hipotetizado, que estas diferencias morfológicas vendrían fundamentalmente causadas por el diferente medio de locomoción de las diferentes especies (Schultz, 1961). Por una parte, los individuos que presentan hipotéticamente un tórax *funnel-shaped*, tienen un medio de locomoción terrestre sobre cuatro extremidades, con utilización del medio arbóreo para la locomoción suspensoria bimanual, aunque con variaciones entre las diferentes especies (Schultz, 1961; Hunt et al., 1996; Schmid et al., 2013). Este tipo de locomoción habría producido una reorganización de la cintura pélvica y escapular, así como de la caja torácica (*funnel-shaped*). Por otra parte, los individuos hipotéticamente caracterizados como *barrel-shaped* presentan un medio de locomoción muy diferente, ya que *Homo sapiens* presenta una locomoción bípeda, mientras que *Hylobates* presenta una locomoción arbórea conocida como braquiación (Schultz, 1961; Hunt et al., 1996; Holliday, 2012). Sin embargo, ha sido propuesto que la similitud morfológica entre ambos puede ser debido a un fenómeno de convergencia evolutiva ya que, tanto la bipedestación como

la braquiación, son medios de locomoción que hacen que el cuerpo del organismo se desplace en posición vertical durante la locomoción (Holliday, 2012; García-Martínez et al., 2013a).

En la presente tesis doctoral (**capítulo 7**), se contrastan las afinidades morfológicas anteriormente mencionadas tanto en la caja torácica en las costillas 1-7 (aproximación del tórax superior), como en las costillas 1-11 (aproximación de la caja torácica completa). Los resultados del **capítulo 7** muestran que, analizando el tórax superior, las diferencias entre los hipotéticos tórax *funnel*- and *barrel-shaped* no son claras. De hecho, cuando se analiza el tórax superior, los individuos *Homo* se agrupan en nuestros análisis junto con *Gorilla* y *Pongo*, mientras que los Hilobátidos se agrupan junto con *Pan*. Esto hace evidente que los efectos de tamaño pueden estar parcialmente detrás de la morfología del tórax superior, ya que la polarización se hace en base al tamaño de los individuos. De este modo, los individuos de gran tamaño son caracterizados por cajas torácicas superiores proporcionalmente expandidas en dirección medio-lateral debido a la gran curvatura de las costillas en vista craneal y la invaginación de la columna a niveles del tórax superior-medio, si bien es cierto que esta invaginación se hace más evidente en el género *Homo* (Bastir et al., en revisión).

Cuando realizamos análisis del tórax en las costillas 1-11, las evidencias dicotómicas se hacen más evidentes. Por lo tanto, información de ambas partes del tórax (superior e inferior) es necesaria para la asignación del patrón morfológico torácico de un individuo. Sin embargo, de manera relevante, la dicotomía que muestran los análisis de Bastir et al. (en revisión; **capítulo 7**) no es la misma que la dicotomía propuesta por Schultz (1961; Fig. 12), ya que los individuos del género *Pongo* son más similares a *Homo* e Hilobátidos que a *Pan* y *Gorilla*. Esta diferencia morfológica puede ser debida en parte a la diferencia en el número de segmentos torácicos, ya que *Pongo* comparte el mismo número de segmentos con *Homo* (N=12), mientras que *Pan* lo hace con *Gorilla* (Schultz, 1961; Aiello y Dean, 1991; Williams, 2012; Williams et al., 2016). Sin embargo, el rechazo a esta hipótesis se encuentra en que la

caja torácica de Hilobátidos, que presenta el mismo número de segmentos que *Gorilla* y *Pan* (N=13), es más similar a *Homo* según los resultados mostrados en el **capítulo 7**.

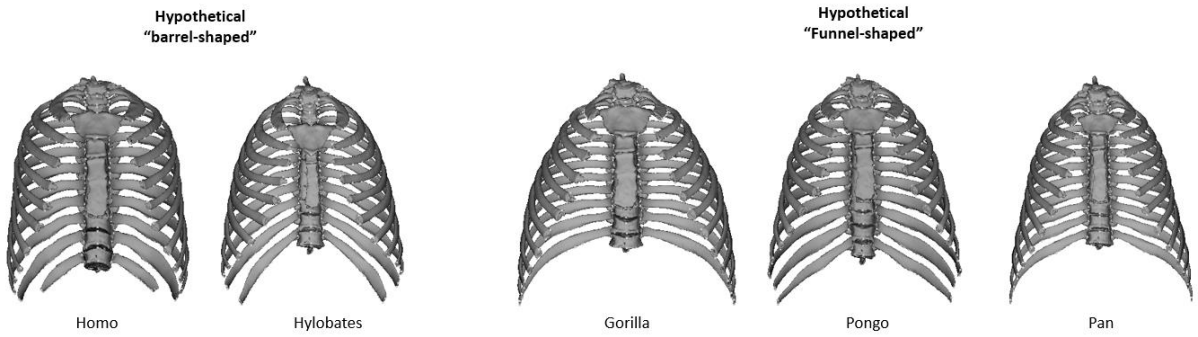

Figura 12: Forma media de las cajas torácicas de las especies del clado *Hominoidea* (según los resultados de Bastir et al., en revisión). Como se observa, hay diferencias considerables en morfología de las hipotéticas cajas torácicas *funnel-shaped* y *barrel-shaped*.

La diferencia en la clasificación propuesta por Schultz y los resultados observados en esta tesis, se basan en que la primera clasificación está basada en los contornos de las cajas torácicas en vista frontal, sin atender al detalle anatómico de los elementos que la componen. La caja torácica es un complejo anatómico cuya geometría se produce por la interacción de costillas y vértebras mediante la articulación costo-vertebral (Gray, 1918; Spalteholtz, 1970). Por lo tanto, la cuantificación tridimensional rigurosa de sus elementos (como se ha realizado en este trabajo), será más apta para el estudio de la morfología torácica que lo propuesto por autores previos. De hecho, una morfología torácica cuya morfología en vista frontal es de barril, puede ser producida por varias combinaciones de morfologías torácicas y vertebrales. Para discernir más claramente este asunto, en el futuro será necesario el estudio detallado de los elementos individuales que componen la caja torácica.

Aunque la nomenclatura dicotómica fue útil para describir a *grosso modo* las diferencias encontradas en la morfología torácica de diferentes primates, a día de hoy suponen un grave obstáculo a la hora de comprender y avanzar en el estudio de las diferencias tridimensionales detalladas de la caja torácica en diferentes primates. Esto es así porque esta propuesta dicotómica, ha estado muy arraigada durante más de medio siglo en el conocimiento

científico (Schultz, 1930, 1961), llegando a ser poco cuestionada por ningún autor hasta la fecha. El único trabajo que ha parcialmente tratado de contrastar las hipótesis de Schultz (Kagaya et al., 2008) presentaba la limitación de que no utilizaban esqueletos articulados anatómicamente, sino que era una articulación artificial. Adicionalmente, para entender el origen evolutivo de dichas afinidades o diferencias morfológicas, será necesario el estudio de los fósiles torácicos como los del género *Proconsul* (en la base del clado *Hominoidea*; Ward, 1993) o los del género *Pierolapithecus* (en la base del clado *Hominidae*; Moyà-Solà et al., 2004).

Capítulo 9.5 Anatomía evolutiva.

Si la variabilidad morfológica tridimensional de la caja torácica ha sido poco conocida en las diferentes vertientes de la Antropología Física anteriormente discutidas, el des-conocimiento de la anatomía evolutiva ha sido el máximo exponente en este sentido. Esto se debe, entre otros factores, a la mala preservación y escasez de los fósiles de esqueleto axial (costillas y vértebras) comparado con otros elementos esqueléticos.

Adicionalmente, la evolución de la forma del tórax ha sido, de manera lógica, estudiada en un marco de anatomía comparada con otros primates, fundamentalmente hominoideos (Jellema et al., 1993; Latimer and Ward, 1993; Schmid et al., 2013; **capítulo 8**). Sin embargo, el escaso conocimiento anteriormente comentado en la anatomía tridimensional detallada de la morfología torácica de hominoideos, ha hecho que el marco comparado en el cual se intentaba comprender la anatomía evolutiva haya sido confuso. Esto es así porque los términos *barrel-shaped* o *funnel-shaped*, que han demostrado ser poco claros en referencia al detalle tridimensional (**capítulo 7**), han sido utilizados tradicionalmente para definir la caja torácica de algunas especies homininas como *Australopithecus*, sin dejar lugar a la aparición de morfología intermedias o transicionales entre diferentes formas hipotéticas.

El escenario empezó a cambiar cuando Schmid et al. (2013) propusieron una evolución en mosaico para la caja torácica de *Australopithecus sediba*, proponiendo que el tórax de esta especie no se adaptaba estrictamente a una morfología de embudo o de barril, sino que su caja torácica sería proporcionalmente estrecha en la parte superior (como en los tórax *funnel-shaped*) pero más estrecha que en grandes simios en la parte inferior (similar a los tórax *barrel-shaped*). Más tarde, otra hipótesis propuesta por Latimer et al. (2016) apoyaba las formas torácicas transicionales en base a los restos torácicos del *Australopithecus afarensis* KSD-VP 1/1. En ese trabajo, Latimer et al. (2016) propusieron que la morfología torácica de *Australopithecus afarensis* podría ser abovedada en su parte superior (similar a *Homo sapiens*) pero también amplia en su parte inferior (similar a los grandes simios). Para describir esta morfología torácica utilizaron el concepto tórax *bell-shaped*, el cual había sido propuesto en 2005 para la caja torácica Neandertal por Sawyer y Maley. El uso del mismo término para ambos genera aún más confusión en el entendimiento de la morfología torácica, ya que en el tórax *bell-shaped* propuesto por Sawyer y Maley (2005) contendría una caja torácica superior más expandida que en *Homo sapiens*, mientras que según la definición de tórax *bell-shaped* de Latimer et al. (2016), la caja torácica superior sería expandida, similar a *Homo sapiens*. Respecto al tórax inferior, tanto Latimer et al. (2016) como Sawyer and Maley (2005) coincidían en que la caja torácica inferior de un tórax *bell-shaped* sería más medio-lateralmente expandida que en *Homo sapiens*.

Los resultados presentados en esta tesis doctoral pueden esclarecer algunos aspectos de esta confusión (**Capítulo 8**). En primer lugar, respecto al tórax superior de *Australopithecus*, se ha observado en el **capítulo 8a** (Tawane et al., 2016) que la morfología de la parte proximal de la primera costilla de diferentes especies del género *Australopithecus* (*africanus*, *sediba* y *afarensis*) respondía a una morfología más tipo *Homo* que tipo grandes simios. Adicionalmente, sobre la morfología costal de *Australopithecus sediba* (Bastir et al. 2016;

capítulo 8a), hemos observado que la primera costilla de esta especie presentaba ciertas similitudes morfológicas con *Homo* que, en combinación con la orientación de los procesos transversos de la vértebra T1, daría como resultado una caja torácica superior proporcionalmente más expandida que en grandes simios. Esto puso en evidencia una vez más la necesidad de incluir la información de costilla y vértebras en conjunto para poder estudiar la morfología torácica (Bastir et al., 2016).

Aunque la morfología del tórax inferior de *Australopithecus* no ha sido podido ser estudiada en detalle en la presente tesis doctoral, la opción más parsimoniosa de acuerdo a la bibliografía actual parece la de que la caja torácica inferior sería ancha (según Latimer et al., 2016; Fig. 13), lo cual iría en consonancia con una pelvis también más medio-lateralmente expandida en *Australopithecus* que en *Homo sapiens* (Schmid et al., 1991; Latimer et al., 2016; Haeusler et al., 2016). Sin embargo, en esta tesis doctoral se aboga por no utilizar términos como *bell-shaped* o *funnel-shaped* para describir la morfología torácica ya que se ha visto que introducen confusión y no son capaces de describir la morfología tridimensional torácica detallada.

Respecto a la caja torácica de los primeros miembros del género *Homo*, sólo está disponible información precisa sobre la anatomía torácica del fósil de *Homo ergaster* KNM-WT 15000 (Latimer y Ward, 1993; Jellema et al., 1993). Desgraciadamente, no hay material costal asociado a *Homo habilis* u *Homo rudolfsensis* y el material costal del yacimiento georgiano de Dmanisi, atribuido a *Homo georgicus*, no ha sido publicado con la suficiente profundidad como para extraer conclusiones claras (Lordkipanidze et al., 2007). Respecto al fósil KNM-WT 15000, un estudio detallado sobre la anatomía torácica en base a medidas lineales como cuerdas, arcos y ángulos (Jellema et al., 1993), propuso que la morfología costal y torácica de este individuo era plenamente moderna, similar a *Homo sapiens*. Adicionalmente, según estos autores, esta morfología torácica (hipotéticamente moderna) estaría en consonancia

con una morfología pélvica también estrecha (hipotéticamente moderna), según Ruff y Walker (1993).

Sin embargo, el estudio tridimensional llevados a cabo en la presente tesis doctoral usando técnicas de MG 3D, acerca de la morfología torácica de este individuo (García-Martínez et al., 2016c; **capítulo 8b**), ha concluido que aunque el tórax superior era similar al tórax moderno, las costillas pertenecientes al tórax inferior presentarían una mayor curvatura en vista craneal que las costillas de *Homo sapiens*. Es importante señalar que aunque Jellema et al. (1993: 309-310), también observaron este factor en KNM-WT 15000, no hicieron ninguna conclusión o inferencia al respecto. Sin embargo, en esta tesis doctoral se propone que esta morfología de las costillas inferiores, podría ir ligada a una caja torácica inferior más expandida que en *Homo sapiens* (Fig. 13) y, quizá, con una potencia diafragmática mayor. Adicionalmente, estudios acerca de la morfología pélvica de este individuo llevados a cabo por otros investigadores usando técnicas de cuantificación tridimensional (Haeusler et al., 2016) apuntan también a que las primeras reconstrucciones de la cintura pélvica de este individuo podían ser erróneas y que probablemente la pelvis era más ancha de lo propuesto hasta la fecha, lo cual había sido propuesto previamente a través de medidas tradicionales por Arsuaga et al. (1999).

Otra especie del género *Homo*, la especie *Homo naledi*, presenta material torácico el cual se presenta por primera vez en esta tesis doctoral (Williams et al., 2017; **capítulo 8b**). Aunque el material está muy fragmentado, nos ha permitido hacer inferencias sobre la morfología torácica de esta especie. En primer lugar, cabe señalar el tamaño tan pequeño de los restos torácicos de *Homo naledi*, los cuales se encuentran entre los más reducidos de todo el registro fósil torácico homínido presente hasta la fecha. Adicionalmente, una vértebra torácica T11 asociada a una costilla 11, nos han permitido observar que las costillas del tórax inferior de esta especie estaban muy declinadas y que presentaban poca torsión costal en la

parte proximal del eje. Estos factores en el tórax inferior (al menos en primates actuales) son asociados con cajas torácicas inferiores medio-lateralmente expandidas, lo cual propusimos para la especie *Homo naledi* (Fig. 13). Esto iría en consonancia con una morfología pélvica también ancha, denominada platipeloide, según la nomenclatura de Delprete (2017), que ha sido propuesta por VanSickle et al. (en revisión) para la especie *Homo naledi*. La morfología del tórax superior de esta especie es más incierta ya que los restos pertenecientes a esta parte de la caja torácica se encuentran peor preservados.

Sin embargo, al no tener cronología para esta especie, su morfología torácica es difícil de evaluar en términos evolutivos. Si esta especie tuviese una cronología antigua, como las afinidades craneales indican (Thackeray, 2015; Dembo et al., 2016), podría ser representativa de la morfología torácica de las primeras especies del género *Homo*, indicando que estas aún estaban caracterizadas por una caja torácica inferior medio-lateralmente expandida, quizá similar a *Australopithecus* (plesiomorfía). En el hipotético caso de que *Homo naledi* fuese un relicto evolutivo, entendido como una especie de aparición antigua pero que perduró hasta hace recientemente con sólo ligeros cambios morfológicos (similar a lo que podría haber ocurrido con la especie *Homo floresiensis*), esto no tendría automáticamente que excluir la posibilidad de que los primeros miembros del género *Homo* no tuvieran una morfología torácica como la vista en *Homo naledi*. De hecho, podría sugerir que la morfología torácica de los primeros *Homo* era como la observada en la especie *Homo naledi*, y esta, al igual que otras partes arcaicas observadas como el cráneo (Laird et al., 2017; Schroeder et al., 2016), se habría mantenido sin cambios desde su aparición. Con respecto a los aspectos funcionales, la expansión inferior de la caja torácica podría estar ligada tanto a una alta actividad diafragmática como a albergar un aparato digestivo de gran tamaño para procesar una dieta rica en recursos vegetales (Aiello y Wheeller, 2005; Williams et al., 2017).

La información de la morfología torácica de otras especies homininas intermedias entre estas especies previamente mencionadas y los últimos representantes de linajes humanos (humanos anatómicamente modernos y Neandertales) es escasa. Específicamente, la información de la anatomía costal de *Homo antecessor* no ha permitido (con las técnicas tradicionales empleadas) hacer distinciones entre la morfología torácica de esta especie y de humanos modernos (Gómez-Olivencia et al., 2010). Sin embargo, recientes estudios presentados también en esta tesis doctoral, reforzarían lo observado previamente para Nariokotome (García-Martínez et al., 2016c; **capítulo 8b**): una caja torácica superior similar a la humana actual, pero con la parte inferior más ancha que estos (Fig. 13), lo cual sería debido a una curvatura en vista craneal de las costillas inferiores más pronunciada que en *Homo sapiens*. Estudios futuros han de centrarse en contrastar estas hipótesis, teniendo también en cuenta la morfología vertebral.

Finalmente, con respecto a los Neandertales (**capítulo 8c**), la presente tesis doctoral ha presentado el material vertebral y costal del yacimiento asturiano de El Sidrón, cuyo detallado estudio tridimensional mediante técnicas de MG 3D ha permitido ampliar considerablemente el conocimiento sobre la anatomía torácica de estos homininos (Bastir et al., en prensa; García-Martínez et al., aceptado).

La caja torácica Neandertal ha sido estudiada durante más de un siglo (Gorjanović-Kramberger, 1906; Boule, 1911-1913; McCown y Keith, 1939; Arensburg, 1991, Franciscus y Churchill, 2002; Gómez-Olivencia et al., 2009; Gómez-Olivencia, 2015), habiendo acuerdo en la comunidad científica de que la caja torácica de estos era más voluminosa que la de humanos modernos, pero sin poder concretar si este mayor tamaño era producido por diferencias en las dimensiones medio-laterales, antero-posteriores o ambas (Gómez-Olivencia et al., 2009). Nuestros resultados sobre las vértebras torácicas del yacimiento de El Sidrón (Bastir et al., en prensa; **capítulo 8c**) han mostrado que las vértebras torácicas inferiores de los Neandertales

tenían los procesos transversos más posteriorizados que en *Homo sapiens*. Es importante señalar, dado que se ha observado por otros autores que este factor entra dentro de la variabilidad humana tanto en *Australopithecus* como en *Homo ergaster* (Latimer and Ward, 1993; Ward, 2012), que es posible que la extrema orientación posterior de los procesos transversos de las vértebras torácicas de los Neandertales sea un factor autapomórfico, o exclusivo de esta especie.

Adicionalmente, los resultados obtenidos en los análisis de las costillas de El Sidrón (García-Martínez et al., aceptado; **capítulo 8c**) muestran que las costillas del tórax superior son más pequeñas en los Neandertales que en *Homo sapiens*, mientras que las del tórax medio e inferior son considerablemente más grandes (Fig. 13). Esto también ha sido observado en otro trabajo aquí presentado sobre el tórax del Neandertal de Kebara 2 (García-Martínez et al., 2014; **capítulo 8c**). También es importante señalar que se han observado diferencias en costillas Neandertales, no sólo en lo referente al tamaño, sino también en lo referente a la forma. Dichas diferencias se han observado en base a las costillas de El Sidrón, ya que las primeras costillas de los Neandertales presentarían menos curvatura en vista craneal que *Homo sapiens* mientras que las del tórax inferior estarían más curvadas (García-Martínez et al., aceptado). Cuando articulamos costillas y vértebras medias de Neandertales y humanos modernos, observamos una expansión medio-lateral de la caja torácica Neandertal a todos los niveles (siendo más evidente en la parte caudal). Esta morfología se aproximaría a la morfología propuesta por Sawyer y Maley (2005), y a la propuesta por Bastir et al. (2015), la cual también es parte de la presente tesis doctoral (**capítulo 8c**; Fig. 13).

Aunque como se ha observado en capítulos anteriores (**capítulos 4-6**), una caja torácica medio-lateralmente expandida en la parte inferior suele ir ligada a una gran potencia diafragmática, los cual sería plausible para los Neandertales. Esto es así debido a que ha sido propuesto que los Neandertales tenían un gasto energético diario mucho mayor que *Homo*

sapiens (Churchill, 2006; Froehle y Churchill, 2009), por lo que una gran entrada de aire en el organismo sería probablemente necesaria para esta especie. Esta hipótesis vendría también apoyada por el hecho de que los Neandertales tenían una cavidad nasal también más grande que la de humanos modernos (Bastir y Rosas, 2016). Po lo tanto, la hipótesis de una caja torácica amplia en la parte inferior, ligada a una gran actividad diafragmática y a un gran gasto energético es la opción más parsimoniosa para la morfología torácica propuesta para esta especie en la presente tesis doctoral.

Adicionalmente, otros factores como la posibilidad de una adaptación a climas fríos o una morfología plesiomórfica (similar a *Homo ergaster* e incluso *Australopithecus*) no pueden ser descartados completamente. Para comprobar la hipótesis de la plesiomorfía sería necesario un estudio tridimensional riguroso de costillas y vértebras de especies homininas previas junto con Neandertales.

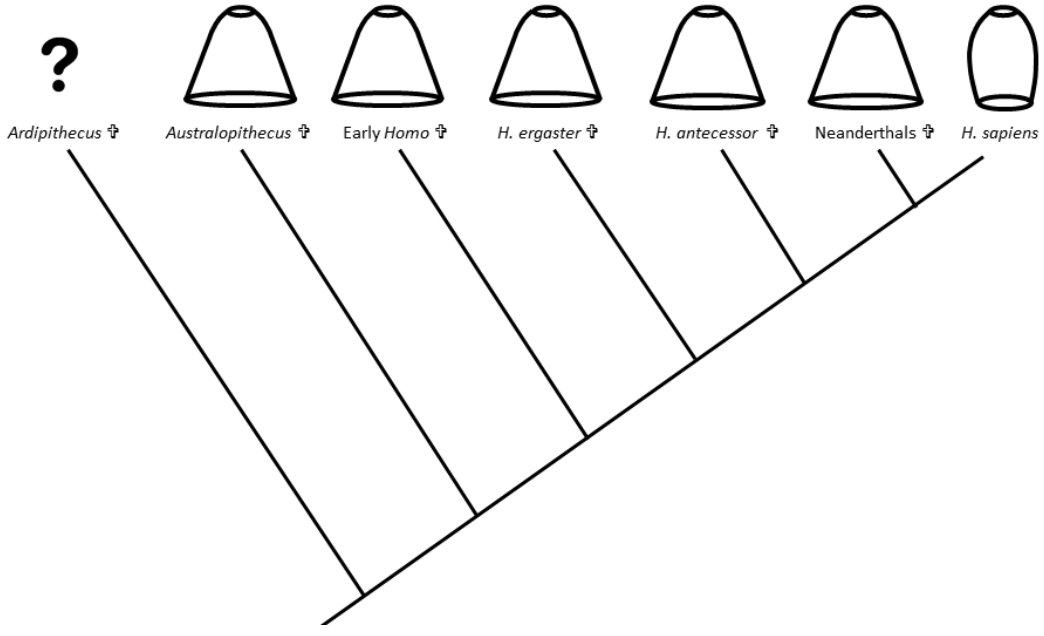

.

Figura 13: Esquema filogenético del clado de la Subtribu *Hominini* basado en Dembo et al. (2016), donde se representan géneros o especies de homininos, así como su hipotética morfología torácica según los resultados obtenidos en la presente tesis doctoral. Nótese que únicamente se representan aquellos de los que se tiene conocimiento de su tórax y *Homo georgicus* se excluye debido a la falta de resultados concluyentes sobre sus restos costales. La caja torácica representada como "*early Homo*" está basada en la especie *Homo naledi*. Aunque no se tiene cronología para esta especie, estudios realizados con análisis bayesianos han mostrado que se podría encontrar en la base de *Homo ergaster* y *Homo antecessor*. El símbolo ✞ significa que son géneros o especies extintas.

Capítulo 9.6 Perspectivas de futuro.

Este trabajo abre la puerta a un gran abanico de posibilidades en cuanto al estudio de la caja torácica en los diferentes campos de la Antropología Física. En esta tesis se ha profundizado en aspectos básicos de la variabilidad morfológica torácica, que no habían sido debidamente cuantificados hasta la fecha mediante técnicas tridimensionales. Respecto a la ontogenia, se ha llevado a cabo un estudio de los cambios morfológicos durante el desarrollo, tanto en la caja torácica completa, como en las costillas individuales. Sin embargo, la ontogenia detallada de las vértebras torácicas, y de cómo el cambio en ellas contribuye a generar la forma torácica adulta, es un campo no cubierto por esta tesis que ha de ser estudiado en el futuro. Adicionalmente, se ha llevado a cabo en este trabajo un estudio pormenorizado del dimorfismo sexual torácico, pero estudiar la ontogenia de la caja torácica teniendo en cuenta el factor sexo, será crucial para entender el origen de las diferencias observadas en adultos.

También se ha realizado en este trabajo un estudio sobre cambios morfológicos *in vivo* que ocurren en la caja torácica durante los ciclos respiratorios, observando que los cambios morfológicos en la caja torácica inferior, son más significativos de cara a ampliar la capacidad respiratoria, que los cambios morfológicos en la caja torácica superior. Sin embargo, en el futuro es necesario realizar un estudio pormenorizado de los elementos torácicos aislados (costillas y vértebras), para poder observar que morfologías costales y vertebrales son las que contribuyen a producir una mayor capacidad respiratoria. Esto también será de gran relevancia para el estudio e interpretación de fósiles torácicos de homininos no humanos.

Adicionalmente, aquí hemos encontrado que la clasificación tradicional de las cajas torácicas como *barrel-* y *funnel-shaped* (Schultz, 1961), no es completamente compatible con lo propuesto cuando se analiza el detalle tridimensional. Este estudio, no sólo amplia el conocimiento actual sobre la variabilidad morfológica del tórax de los miembros del clado

Hominoidea, sino que da pie a un gran abanico de posibilidades: dimorfismo sexual, ontogenia o incluso el estudio de la caja torácica de otros primates no hominoideos (lo que Schultz llamaba *monkeys*). También será importante incluir en las bases de datos actuales, fósiles costales de los primeros hominoideos, como los de *Pierolapithecus catalaunicus*, a fin de contrastar si su caja torácica era como la que se observa en hominoideos actuales.

Finalmente, con respecto a la variabilidad morfológica observada en especies extintas, la presente tesis doctoral ha profundizado en la morfología torácica de diferentes especies homininas de los géneros *Australopithecus* y *Homo*. Respecto al tórax de *Australopithecus*, los trabajos aquí presentados han permitido concluir que la hipótesis más parsimoniosa es la de que su caja torácica fuese similar a *Homo sapiens* en la parte superior, pero más medio-lateralmente expandida en la parte inferior, lo cual estaría a favor de la hipótesis de evolución en mosaico para la caja torácica. Sin embargo, para poder confirmar definitivamente estas hipótesis, futuros estudios habrán de estudiar la morfología costal y vertebral de *Australopithecus* en un marco comparado amplio. Otros pasos, habrán de ir encaminados al estudio de la ontogenia torácica de *Australopithecus* ya que, por fortuna, se conservan individuos inmaduros de *Australopithecus sediba*, los cuales podrán ser cruciales para comprender la ontogenia de estos homininos. Los datos aquí obtenidos apuntan a que algunos miembros arcaicos del género *Homo* podrían también presentar una morfología torácica similar a la de los *Australopithecus*, moderna en la parte superior, pero arcaica en la inferior. A estas conclusiones se ha llegado en esta tesis a partir de los fósiles de *Homo naledi*, *Homo ergaster* y *Homo antecessor*. Ya que los fósiles del *Homo ergaster* KNM-WT 15000 y algunos de *Homo antecessor* representan individuos inmaduros, este hecho supone una excelente oportunidad para intentar hacer estimaciones de la morfología adulta de estos miembros del género *Homo*. Finalmente, es esta tesis se ha profundizado en el estudio de la caja torácica Neandertal, llegándose a la conclusión de que esta podría ser medio-lateralmente más expandida que en

Homo sapiens, lo cual sería más evidente en la caja torácica inferior, ligado posiblemente a una gran capacidad diafragmática. Ya que en algunos individuos Neandertales, ha sido inferido el sexo (Kebara 2, La Chapelle-aux-Saints, La Ferrassie, Shanidar 3, Tabun 1), estudios de dimorfismo sexual también pueden ser llevados a cabo en esta especie. Adicionalmente, el registro fósil de los Neandertales, destaca en comparación con el de otras especies fósiles, por la gran cantidad relativa de individuos inmaduros hallados. De este modo, el estudio de los individuos inmaduros de yacimientos como El Sidrón, La Ferrassie, Roc de Marsal, Le Mostieur o Mezmaiskaya, podrá contribuir al entendimiento de la ontogenia torácica Neandertal en un marco evolución y desarrollo (*EVO-DEVO*).

CAPÍTULO X – CONCLUSIONES

Esta tesis ha estudiado, por vez primera, la variabilidad torácica tridimensional en todas sus vertientes, desde la variabilidad intra-específica (ontogenia, dimorfismo sexual y anatomía funcional en *Homo sapiens*) hasta la variabilidad inter-específica (anatomía comparada de primates y variabilidad fósil en especies como *Australopithecus afarensis*, *Australopithecus sediba*, *Homo ergaster*, *Homo naledi*, *Homo antecessor* y Neandertales). De la presente tesis doctoral se obtienen dos conclusiones generales, así como varias conclusiones específicas, asociadas a los diferentes objetivos propuestos.

Las conclusiones generales que emanan de esta tesis doctoral son:

1. La variabilidad torácica es mucho más compleja de lo propuesto hasta la fecha cuando se estudian sus detalles tridimensionales, tanto del *todo* torácico como a sus *partes* individuales, las costillas y las vértebras. Esto evidencia la necesidad de llevar a cabo estudios en tres dimensiones cuando, como en el caso de caja torácica, los elementos esqueléticos a estudiar estén fundamentalmente compuestos por curvas. Adicionalmente, es importante remarcar que conocer no sólo la morfología de las *partes*, sino conocer cómo las partes articulan, será imprescindible para tener una visión completa del *todo* torácico. De esta manera, cuando se articulan las *partes*, se pueden conocer en ocasiones morfologías emergentes del *todo* al que pertenecen, que serían difícilmente entendibles a través de las *partes* aisladas.
2. La terminología propuesta hasta la fecha para definir la morfología torácica como *barrel-*, *funnel-*, *hyperbarrel-*, *dome-* o *bell-shaped*, aunque es útil para generar una idea global de la morfología hipotética de la caja torácica del individuo, es

realmente una simplificación excesiva que no describe los detalles anatómicos tridimensionales reales del *todo* torácico. Tal es así, que términos como *barrel-* o *funnel-shaped* han sido utilizados para definir la caja torácica de homínidos cuyos detalles tridimensionales, distan mucho de asociarse bajo un mismo nombre. Otro ejemplo de la confusión que generan estos términos, sería el uso del término "tórax *bell-shaped*", el cual ha sido utilizado de diferentes modos para definir diferencias entre especies homininas (véase discusión). Por ello, desde la presente tesis doctoral se aboga por evitar el uso de estos términos genéricos y utilizar descripciones más detalladas y específicos que describan la morfología tridimensional. Un ejemplo de esto sería el uso de descripciones tales como "la caja torácica inferior de este individuo es medio-lateralmente expandida debido a la orientación más posterior de los procesos transversos y a una mayor curvatura en vista craneal del eje de la costilla".

Las conclusiones específicas que emanan de la presente tesis doctoral son:

1. La ontogenia de la caja torácica está marcada por una expansión medio-lateral relativa de la parte superior y una reducción en la amplitud medio-lateral relativa de la parte inferior desde infantiles a adultos, ligado a una posible naturaleza modular de la caja torácica. Aunque los mayores cambios en forma se dan en torno a los 2-3 años de edad, se siguen dando cambios en tamaño y parcialmente en forma hasta la edad adulta. Estos cambios son en parte debidos a un incremento de la curvatura en vista craneal de la costilla, así como de la torsión de la misma.

2. El dimorfismo sexual de la caja torácica, se ve reflejado en una mayor amplitud medio-lateral relativa de la caja torácica (más visible en el tórax inferior), una menor altura relativa y unas costillas más horizontalmente dispuestas en individuos

masculinos que en femeninos. Aunque la alometría puede explicar factores como la menor altura relativa de la caja torácica masculina, otros factores como la disposición de las costillas o la amplitud relativa, no pueden ser explicados por la alometría. Factores bioenergéticos, de composición corporal o incluso la interacción morfo-funcional de la caja torácica con otros sistemas como el reproductivo, pueden estar detrás de las diferencias observadas.

3. Las partes pulmonar y diagramática de la caja torácica presentan diferencias notables en cuanto a la cinemática respiratoria. Aunque el grado de deformación es similar en ambas partes, el modo en que se deforman difiere ampliamente. Esto puede ser debido a limitaciones en el movimiento producidas por la unión directa con el esternón en las costillas pertenecientes al tórax superior (lo cual no presentan las costillas del tórax inferior). Además, para una misma cantidad de deformación morfológica, la parte diafragmática del tórax presenta mayores cambios en tamaño en referencia al tórax superior, por lo que pequeños cambios en la forma del tórax inferior, tendrán más repercusiones funcionales que cuando los cambios son producidos en el tórax superior.

4. La anatomía comparada del tórax de primates *Hominoidea* es realmente más compleja que la clásica dicotomía *funnel-* vs. *barrel-shaped* propuesta tradicionalmente y basada en la nomenclatura de Schultz (1961). Cuando se tiene en cuenta el estudio del tórax de las costillas 1-7, las similitudes morfológicas distan mucho de lo propuesto por Schultz, ya que *Homo* se asocia junto con *Gorilla* y *Pongo*, mientras que *Pan* se asocia con *Hylobates*. Cuando estudiamos el tórax hasta la costilla 11, las similitudes se acercan más a lo propuesto por Schultz, pero

con la peculiaridad de que *Pongo* se asocia con *Homo* e *Hylobates*, y no con *Pan* y *Gorilla*, como se propuso previamente en los trabajos de Schultz (1961).

5. Los análisis realizados hasta la fecha sobre la morfología costal tridimensional de *Australopithecus* apuntan a que la caja torácica superior de esta especie presentaba una morfología similar a *Homo sapiens*, mientras que su caja torácica inferior sería más medio-lateralmente expandida que en estos. Esta morfología torácica ancha en la parte inferior, estaría en consonancia con una pelvis también ancha, lo cual sería coherente con la integración morfo-funcional entre el tórax inferior y la pelvis propuesta por otros autores (Jellema et al., 1993; Schmid et al., 2013; Bastir et al., 2014a). La morfología torácica amplia en la parte inferior podría responder al hecho de poseer un gran sistema digestivo o la preservación de un patrón arcaico hipotéticamente similar a hominoideos del Mioceno como *Pierolapithecus*. Los primeros miembros del género *Homo*, como *Homo habilis* u *Homo rudolfensis*, no presentan material costal que pueda ser analizado. Recientes estudios sobre la morfología costal tridimensional de *Homo* del Pleistoceno Inferior (*Homo ergaster* y *Homo antecessor*) apuntan a que sus costillas superiores eran similares a *Homo sapiens*, mientras que las costillas inferiores presentaban una mayor curvatura en vista craneal, por lo que presentarían una expansión torácica en esta parte con respecto a *Homo sapiens*. La especie *Homo naledi* presenta también un tórax ancho en la parte inferior, pero al no conocer su datación, las inferencias evolutivas sobre esta morfología se han de realizadas con cautela. Finalmente, nuestros estudios han demostrado que los Neandertales también presentaban una caja torácica inferior más medio-lateralmente expandida que en *Homo sapiens*, aunque también presentan esta expansión (menos evidente) a otros los niveles torácicos. La

morfología del tórax inferior puede responder a requerimientos energéticos elevados, aunque una morfología plesiomórfíca o una posible adaptación a climas fríos o no pueden ser completamente descartados.

CHAPTER X – CONCLUSIONS

This dissertation has studied, for the first time, the 3D variability of the rib cage in topics such as intra-specific variability (ontogeny, sexual dimorphism and functional anatomy) and inter-specific variability (comparative anatomy and fossil variation in species such *Australopithecus afarensis*, *Australopithecus sediba*, *Homo ergaster*, *Homo naledi*, *Homo antecessor* and Neanderthals). Two general conclusions, as well as several more specific conclusions, can be drawn from this dissertation.

The general conclusions of the present dissertation are as follows:

1. Thoracic variability is far more complex than previously proposed when taking into account the three-dimensional details of the thoracic *whole* and its individual *parts*, ribs and vertebrae. Therefore, when the elements under research are elements of curved nature such as in the case of the thorax, the ribs and the vertebrae, three dimensional studies are clearly needed. Additionally, it is important to note that not only the morphology of the *parts* (the ribs and the vertebrae), but also the way in which these *parts* articulate, is important for understanding the morphology of the *whole* (the thorax).

2. Even though terms such as barrel-, funnel-, hyperbarrel-, dome- or bell-shaped, are useful for giving an overall idea of the hypothetic thoracic morphology, they are very limited for defining the 3D details of the rib cage and its elements. These terms have been used to group the rib cage morphology of primates whose 3D details

show that they should not be grouped under the same category. Additionally, another example of the confusion caused by those terms in the case of the term "bell-shaped", which has been used in different ways to define similarities and differences between different primate species. Therefore, in this dissertation, I aim to avoid those general terms and replace them with terms that describe the actual morphology of the 3D rib cage. Descriptions such as "this individual presents a medio-lateral expansion of the lower rib cage caused by the more posterior orientation of the transverse processes of the lower thoracic vertebrae and also by a more curved lower ribs in cranial view" could better describe thoracic morphology.

The specific conclusions that can be drawn from this dissertation are as follows:

1. The rib cage ontogeny is characterized by a relative medio-lateral expansion in the lower rib cage and a relative medio-lateral narrowing of the lower thorax from infants to adults, linked to a possible modular nature of the rib cage. Even though the largest changes in shape occur before the age of 2-3 years, other changes in size and also in shape occurring until adulthood. The shape changes are, at least in part, due to an increasing of the curvature in cranial view as well as in rib torsion.

2. Sexual dimorphism in the rib cage shows that the male rib cages are wider than female rib cages, which is more evident at the caudal part. Male rib cages are also relatively shorter and have more horizontally oriented ribs than female rib cages. Even though allometry could account for some of these changes, such as relatively short male rib cage, other factors such as the medio-lateral expansion or the orientation of the ribs, cannot be explained by allometry. Bioenergetics, body composition or even other

factors such as the morphological interaction of the rib cage with other systems such as the reproductive system, could also account for the differences observed.

3. Regarding kinematics, there are important differences in the pulmonary and the diaphragmatic parts of the rib cage. Even though the degree of deformation is similar in both parts, the type of deformation is very different. This could be caused by constraints of the upper ribs due to their direct link with the sternum through the costal cartilage. Additionally, it is important to note that, for the same morphological deformation, the diaphragmatic rib cage presents a larger size increase than the lower one. Therefore, small changes in the diaphragmatic rib cage would have more functional implications than changes in the upper one.

4. Comparative anatomy of the hominoid thorax is highly more complex than the dichotomy barrel- vs. funnel-shaped classically proposed by Schultz (1961) and accepted by the scientific community. When we study the morphology of the thorax from ribs 1-7 we find that the morphological similarities are far from Schultz's proposal, since *Homo* is close Gorilla and Pongo, whereas *Pan* is close to *Hylobates*. When we studied the rib cage from ribs 1-11, the similarities became closer to Schultz's proposal, but there are still some differences, since *Pongo* is closer to *Homo* and *Hylobates* than it is to *Pan* and *Gorilla*.

5. The analyses carried out to date suggest that the morphology of the upper thorax in *Australopithecus*, is similar to the morphology of *Homo sapiens*, whereas the lower rib cage is more medio-laterally expanded. This could be linked to differences in body shape, since the pelvis girdle of *Australopithecus* has also been proposed as broad. This

body shape, which could be inherited from Miocene apes such as *Pierolapithecus*. The first members of the genus *Homo*, such as *Homo habilis* and *Homo rudolfensis*, do not present thoracic material that can be used to make inferences of their thoracic morphology. Lower Pleistocene hominins (*Homo ergaster* and *Homo antecessor*) could be characterized by an expanded upper thorax similar to modern humans, and by lower ribs presenting a stronger curvature in cranial view than modern humans. This could produce differences in the lower rib cage morphology compared to *Homo sapiens*. *Homo naledi* also presented an expanded lower thorax, but since there is no date for this species, evolutionary inferences cannot be made. Finally, our results have demonstrated that the Neanderthals also presented a more expanded thorax than in *Homo sapiens*, which is more evident at the caudal part. This morphology of the lower rib cage could be a plesiomorphy inherited from *Homo ergaster* and *Homo antecessor* (or even from *Australopithecus*), but it could also be caused by climatic adaptations to cold environments or an adaptation to high energetic requirements, which is one of the most parsimonious explanations.

CAPÍTULO XI – BIBLIOGRAFÍA

Aiello, L., Dean, C., 1990. An introduction to human evolutionary anatomy. Academic Press Harcourt Brace & Company, London.

Aiello, A., Wheeler, P., 1995. The expensive tissue hypothesis: the brain and digestive system in human and primate evolution. Current Anthropology 36, 199-221.

Ankel, F., 1967. Morphologie von Wirbelsäule und Brustkorb. Primatologia 4, 1-120.

Antón, S.C., Snodgrass, J.J., 2012. Origins and evolution of genus *Homo*: New Perspectives. Current Anthropology 53, S479-S496.

Arensburg, B., 1991. The vertebral column, thoracic cage, and hyoid bone, Le Squelette Mousterien de Kebara 2. CNRS, Paris 113-146.

Arsuaga, J.L., Lorenzo, C., Carretero, J.M., Gracia, A., Martínez, I., García, N., Bermúdez De Castro, J.M., Carbonell, E., 1999. A complete human pelvis from the middle pleistocene of Spain. Nature 399, 255-258.

Azzaroli, A., Boccaletti, M., Delson, E., Moratti, G., Torre, D., 1986. Chronological and paleogeographical background to the study of *Oreopithecus bambolii*. Journal of Human Evolution 15, 533-540.

Basmajian, J.V., 1975. Grant's Method of Anatomy, 9th edition. Baltimore: The Williams and Wilkins Company.

Bastir, M., 2008. A systems-model for the morphological analysis of integration and modularity in human craniofacial evolution. Journal of Anthropological Sciences 86, 37-58.

Bastir, M., Rosas, A., 2016. Cranial base topology and basic trends in the facial evolution of *Homo*. Journal of Human Evolution 91, 26-35.

Bastir, M., Godoy, P., Rosas, A., 2011. Common features of sexual dimorphism in the cranial airways of different human populations. American Journal of Physical Anthropology 146(3), 414-422.

Bastir, M., Martínez, D.G., Recheis, W., Barash, A., Coquerelle, M., Rios, L., Peña-Melián., Á, García-Río, F., O'Higgins, P., 2013. Differential growth and development of the upper and lower human thorax. PloS One 8(9), e75128.

Bastir, M., García-Martínez, D., Barash, A., Been, E., Torres, I., García Río, F., 2014a. Thorax kinematics and the reconstruction of body models in hominin evolution. Proceedings of the European Society for the Study of Human Evolution (ESHE), Florence, p. 35.

Bastir, M., Higuero, A., Ríos, L., García-Martínez, D., 2014b. Three-dimensional analysis of sexual dimorphism in human thoracic vertebrae: implications for the respiratory system and spine morphology. American Journal of Physical Anthropology 155(4), 513-521.

Bastir, M., García-Martínez, D., Estalrrich, A., García-Tabernero, A., Huguet, R., Ríos, L., Barash, A., Recheis, W., de la Rasilla, M., Rosas, A., 2015. The relevance of the first ribs of the El Sidrón site (Asturias, Spain) for the understanding of the Neandertal thorax. Journal of Human Evolution 80, 64-73.

Bastir, M., García-Martínez, D., Williams, S. A., Nalla, S., Eyre, J., Oishi, M., Ogihara, N., Churchill, S.E., Hawks, J., Berger, L.R., Schmid, P., 2016. Preliminary findings of 3D

analyses of the costal remains of *Australopithecus sediba*. Abstracts of the Paleoanthropology Society 2016 Meeting; Paleoanthropology 2016: A3.

Bastir, M., García-Martínez, D., Torres-Tamayo, N., Sanchis-Gimeno, J.A., O'Higgins, P., Utrilla, C., Torres Sánchez, I., García Río, F., 2017. In vivo 3D analysis of thoracic kinematics: changes in size and shape during breathing and their implications for respiratory function in recent humans and fossil hominins. The Anatomical Record 300, 255-264.

Bastir, M., García-Martínez, D., Ríos, L., Higuero, A., Barash, A., Martelli, S., García-Tabernero, A., Estalrrich, A., Huguet, R., de la Rasilla, M., Rosas, A., en prensa. 3D morphometrics of thoracic vertebrae in Neandertals: fossil evidence from El Sidrón (Asturias, Northern Spain). Journal of Human Evolution.

Bastir, M., en prensa. The morphological, functional and structural integration of the upper airways in Neanderthals: nasal cavity, pharynx, larynx, in: Maddux, S., Cowgill, L. (Eds.), Neandertal Skeletal Anatomy. Cambridge University Press.

Bateson, W., 1894. Materials for the Study of Variation, pp. 102–128. London: MacMillan.

Baume, R.M., Buschang, P.H., Weinstein, S., 1983. Stature, head height, and growth of the vertical face. American Journal of Orthodontics 83(6), 477-484.

Bellemare, F., Jeanneret, A., Couture, J., 2003. Sex differences in thoracic dimensions and configuration. American Journal of Respiratory and Critical Care Medicine 168, 305-312.

Bellemare, F., Fuamba, T., Bourgeault, A., 2006. Sexual dimorphism of human ribs. Respiratory Physiology and Neurobiology 150 233-239.

Benazzi, S., Kullmer, O., Schulz, D., Gruppioni, G., Weber, G.W., 2013. Individual tooth macrowear pattern guides the reconstruction of Sts 52 (A. africanus) dental arches. American Journal of Physical Anthropology 150, 324-329.

Ben-Dor, M., Gopher, A., Barkai, R., 2016. Neandertals' large lower thorax may represent adaptation to high protein diet. American Journal of Physical Anthropology 160, 367-378.

Berger, L.R., Churchill, S.E., De Klerk, B., Quinn, R.L., 2008. Small-bodied humans from Palau, Micronesia. PLoS One 3, e1780.

Berger, L.R., de Ruiter, D.J., Churchill, S.E., Schmid, P., Carlson, K.J., Dirks, P.H.G.M., Kibii, J.M., 2010. *Australopithecus sediba*: A new species of *Homo*-Like Australopith from South Africa. Science 328, 195-204.

Berger, L.R., Hawks, J., de Ruiter, D.J., Churchill, S.E., Schmid, P., Delezene, L.K., Kivell, T.L., Garvin, H.M., Williams, S.A., DeSilva, J.M., Skinner, M.M., Musiba, C.M., Cameron, N., Holliday, T.W., Harcourt-Smith, W., Ackermann, R.R., Bastir, M., Bogin, B., Bolter, D., Brophy, J., Cofran, Z.D., Congdon, K.A., Deane, A.S., Dembo, M., Drapeau, M., Elliott, M.C., Feuerriegel, E.M., Garcia-Martinez, D., Green, D.J., Gurtov, A., Irish, J.D., Kruger, A., Laird, M.F., Marchi, D., Meyer, M.R., Nalla, S., Negash, E.W., Orr, C.M., Radovcic, D., Schroeder, L., Scott, J.E., Throckmorton, Z., Tocheri, M.W., VanSickle, C., Walker, C.S., Wei, P., Zipfel, B., 2015. *Homo naledi*, a new species of the genus *Homo* from the Dinaledi Chamber, South Africa. eLife 4, e09560.

Bermúdez de Castro, J.M., Arsuaga, J.L., Carbonell, E., Rosas, A., Martınez, I., Mosquera, M., 1997. A hominid from the Lower Pleistocene of Atapuerca, Spain: possible ancestor to Neandertals and modern humans. Science 276, 1392-1395.

Beyer, B., Sholukha, V., Dugailly, P.M., Rooze, M., Moiseev, F., Feipel, V., Van Sint Jan, S., 2014. In vivo thorax 3D modelling from costovertebral joint complex kinematics. Clinical Biomechanics 29, 434-438.

Bitar, A., Fellmann, N., Vernet, J., Coudert, J., Vermorel, M., 1999. Variations and determinants of energy expenditure as measured by whole-body indirect calorimetry during puberty and adolescence. The American Journal of Clinical Nutrition 69(6), 1209-1216.

Bolliger, S.A., Ross, S., Thali, M.J., Hostettler, B., Menkveld-Gfeller, U., 2012. Scenes from the past: initial investigation of early Jurassic vertebrate fossils with multidetector CT. Radiographics 32, 1533–1559.

Bookstein, F.L., 1991. Morphometric tools for landmark data: geometry and biology. [Orange Book]. Cambridge, NY: Cambridge University Press.

Bookstein, F.L., 1997. Morphometric tools for landmark data: geometry and biology. Cambridge, NY: Cambridge University Press.

Bookstein, F.L., Streissguth, A.P., Sampson, P.D., Connor, P.D., Barr, H.M., 2002. Corpus callosum shape and neuropsychological deficits in adult males with heavy fetal alcohol exposure. Neuroimage 15(1), 233-251.

Bots, J., Wijnaendts, L.C., Delen, S., Van Dongen, S., Heikinheimo, K., Galis, F., 2011. Analysis of cervical ribs in a series of human fetuses. Journal of Anatomy 219, 403-409.

Boule, M., 1911–1913. L'homme fossile de la Chapelle-aux-Saints. Annales de Paléontologie 6, 111-172; 7, 21-56, 85-192; 8, 1-70.

Brant, W.E., Helms, C.A., 2012. Fundamentals of diagnostic radiology. Lippincott Williams & Wilkins.

Bulygina, E., Mitteroecker, P., Aiello, L., 2006. Ontogeny of facial dimorphism and patterns of individual development within one human population. American Journal of Physical Anthropology 131(3), 432-443.

Burghardt, A. J., Link, T. M., Majumdar, S., 2011. High-resolution computed tomography for clinical imaging of bone microarchitecture. Clinical Orthopaedics and Related Research 469(8), 2179-2193.

Bushberg, J.T., Seibert, J.A., Leidholdt Jr, E.M., Boone, J.M., 2012. X-ray production, x-ray tubes, and x-ray generators. The Essential Physics of Medical Imaging, 3rd ed. (Lippincott Williams & Wilkins, Philadelphia, PA, 2011), 171-206.

Campillo, D., Subirà, E., 2004. Antropología física para arqueólogos. Editorial Ariel, Barcelona.

Carbonell, E., De Castro, J.B., Arsuaga, J., Allue, E., Bastir, M., Benito, A., Cacères, I., Canals, T., Díez, J., van der Made, J., 2005. An early Pleistocene hominin mandible from Atapuerca-TD6, Spain. Proceedings of the National Academy of Sciences of the United States of America 102, 5674-5678.

Carlson, B.M., 1994. Human Embryology and Developmental Biology. St. Louis: Mosby-Year Book.

Carlson, K.J., Grine, F.E., Pearson, O.M., 2007. Robusticity and sexual dimorphism in the postcranium of modern hunter-gatherers from Australia. American Journal of Physical Anthropology 134, 9-23.

Carretero, J.M., Lorenzo, C., Arsuaga, J.L., 1999. Axial and appendicular skeleton of *Homo antecessor*. Journal of Human Evolution 37, 459-499.

Chila, A., 2010. Foundations of Osteopathic Medicine, 3 ed. Lippincott Williams & Wilkins, Philadelphia.

Churchill, S.E., 2006. Bioenergetic perspectives on Neanderthal thermoregulatory and activity budgets. In Neanderthals revisited: new approaches and perspectives (pp. 113-133). Springer Netherlands.

Conroy, G.C., Vannier, M.W., 1984. Noninvasive three-dimensional computer imaging of matrix-filled fossil skulls by high-resolution computed tomography. Science 226(4673), 456-458.

De Troyer, A., Kirkwood, P.A., Wilson, T.A., 2005. Respiratory Action of the Intercostal Muscles. Physiological Reviews 85, 717-756.

Delprete, H., 2017. Pelvic inlet shape is not as dimorphic as previously suggested. The Anatomical Record 300, 706-715.

Dembo, M., Matzke, N.J., Mooers, A.Ø., Collard, M., 2015. Bayesian analysis of a morphological supermatrix sheds light on controversial fossil hominin relationships. Proceedings of the Royal Society B, 20150943.

Dembo, M., Radovčić, D., Garvin, H.M., Laird, M.F., Schroeder, L., Scott, J.E., Brophy, J., Ackermann, R.R., Musiba, C.M., de Ruiter, D.J., 2016. The evolutionary relationships and age of *Homo naledi*: An assessment using dated Bayesian phylogenetic methods. Journal of Human Evolution 97, 17-26.

Dirks, P.H., Kibii, J.M., Kuhn, B.F., Steininger, C., Churchill, S.E., Kramers, J.D., Pickering, R., Farber, D.L., Mériaux, A.S., Herries, A.I., 2010. Geological setting and age of *Australopithecus sediba* from southern Africa. Science 328, 205-208.

Dirks, P.H., Berger, L.R., Roberts, E.M., Kramers, J.D., Hawks, J., Randolph-Quinney, P.S., Elliott, M., Musiba, C.M., Churchill, S.E., de Ruiter, D.J., Schmid, P., Backwell, L.R., Belyanin, G.A., Boshoff, P., Hunter, K.L., Feuerriegel, E.M., Gurtov, A., Harrison, J.d.G., Hunter, R., Kruger, A., Morris, H., Makhubela, T.V., Peixotto, B., Tucker, S., 2015. Geological and taphonomic context for the new hominin species *Homo naledi* from the Dinaledi Chamber, South Africa. eLife 4, e09561.

Drake, R., Vogl, A.W., Mitchell, A.W., 2009. Gray's anatomy for students. Elsevier Health Sciences.

Edelman, R.R., Warach, S., 1993. Magnetic resonance imaging. New England Journal of Medicine 328, 708-716.

Ferring, R., Oms, O., Agustí, J., Berna, F., Nioradze, M., Shelia, T., Tappen, M., Vekua, A., Zhvania, D., Lordkipanidze, D., 2011. Earliest human occupations at Dmanisi (Georgian Caucasus) dated to 1.85–1.78 Ma. Proceedings of the National Academy of Sciences 108, 10432-10436.

Feuerriegel, E.M., Green, D.J., Walker, C.S., Schmid, P., Hawks, J., Berger, L.R., Churchill, S.E., 2017. The upper limb of *Homo naledi*. Journal of Human Evolution 104, 155-173.

Fleagle, J.G., Simons, E.L., 1982. The humerus of *Aegyptopithecus zeuxis*: a primitive anthropoid. American Journal of Physical Anthropology 59(2), 175-193.

Foley, W.J., Whitehouse, W.M., 1969. Supernumerary Thoracic Ribs 1. Radiology 93, 1333-1334.

Franciscus, R.G., Churchill, S.E., 2002. The costal skeleton of Shanidar 3 and a reappraisal of Neandertal thoracic morphology. Journal of Human Evolution 42, 303-356.

Froehle, A.W., Churchill, S.E., 2009. Energetic competition between Neandertals and anatomically modern humans. PaleoAnthropology 2009, 96-116.

Fuhlrott, C., 1859. Mensliche Ueberreste aus einer Felsengrotte des Düsselthals. Verhandlungen des Naturhistorischen Vereines 60, 131–153.

Gabunia, L., Vekua, A., Lordkipanidze, D., III, C.C.S., Ferring, R., Justus, A., Nioradze, M., Tvalchrelizde, M., Antón, S.C., Bosinsky, G., Jöris, O., Lumley, M.-A.d., Majsuradze, G., Mouhkelishvili, A., 2000. Earliest Pleistocene Hominid Cranial Remains from Dmanisi, Republic of Georgia: Taxonomy, Geological Setting, and Age. Science 288, 1019-1025.

García-Martínez, D., Bastir, M., Recheis, W., Barash, A., 2013a. Two different barrels for two different primates: 3D geometric morphometrics of sliding semilandmarks of the *Hominoidea* superfamily thorax, Proceedings of Sociedad Española de Antropología Física, Bilbao 2013, p. 39.

García-Martínez, D., 2013b. 3D geometric morphometrics of the rib cage of the Homo ergaster KNM-WT 15000 and their possible evolutionary implications: an application of sliding semi-landmarks on virtual anthropology to the morphology of the ribs. Trabajo Fin de Master (TFM). Universidad Autónoma de Madrid-Museo Nacional de Ciencias Naturales (CSIC).

García-Martínez, D., Barash, A., Recheis, W., Utrilla, C., Torres Sánchez, I., García Río, F., Bastir, M., 2014. On the chest size of Kebara 2. Journal of Human Evolution 70, 69-72.

García-Martínez, D., Recheis, W., Bastir, M., 2016a. Ontogeny of 3D rib curvature and its importance for the understanding of human thorax development. American Journal of Physical Anthropology 159(3), 423-431.

García-Martínez, D., Torres- Tamayo, N., Torres- Sánchez, I., García- Río, F., Bastir, M., 2016b. Morphological and functional implications of sexual dimorphism in the human skeletal thorax. American Journal of Physical Anthropology 161(3), 467-477.

García-Martínez, D., Spoor, F., Bastir, M., 2016c. 3D Assessment of rib curvatures in KNM-WT 15000. Abstracts of the Paleoanthropology Society 2016; Paleoanthropology Meeting 2016: A13.

García-Martínez, D., Bastir, M., Huguet, R., Estalrrich, A., García-Tabernero, A., Ríos, L., Cunha, E., de la Rasilla, M., Rosas, A., aceptado. The costal remains of the El Sidrón Neandertal site (Asturias, northern Spain) and its importance for understanding the Neandertal thorax morphology. Journal of Human Evolution.

Gayzik, F.S., Mao, M.Y., Danelson, K.A., Slice, D.E., Stitzel, J.D., 2008. Quantification of age-related shape change of the human rib cage through geometric morphometrics. Journal of biomechanics 41(7), 1545-1554.

Goldman, M., Grassino, A., Mead, J., Sears, T., 1978. Mechanics of the human diaphragm during voluntary contraction: dynamics. Journal of Applied Physiology 44, 840-848.

Gómez, C., Özbudak, E.M., Wunderlich, J., Baumann, D., Lewis, J., Pourquié, O., 2008. Control of segment number in vertebrate embryos. Nature 454, 335-339.

Gómez-Olivencia, A., Eaves-Johnson, K.L., Franciscus, R.G., Carretero, J.M., Arsuaga, J.L., 2009. Kebara 2: new insights regarding the most complete Neandertal thorax. Journal of Human Evolution 57, 75-90.

Gómez-Olivencia, A., Carretero, J.M., Lorenzo, C., Arsuaga, J.L., Bermúdez de Castro, J.M., Carbonell, E., 2010. The costal skeleton of *Homo antecessor*: preliminary results. Journal of Human Evolution 59, 620-640.

Gómez-Olivencia, A., 2015. The costal skeleton of the Neandertal individual of La Chapelle-aux-Saints 1. Annales de Paléontologie 101, 127-141.

Goodman, M., Porter, C.A., Czelusniak, J., Page, S.L., Schneider, H., Shoshani, J., Gunnell, G., Groves, C.P., 1998. Toward a Phylogenetic Classification of Primates Based on DNA Evidence Complemented by Fossil Evidence. Molecular Phylogenetics and Evolution 9, 585-598.

Goodyear, M., Krleza-Jeric, K., Lemmens, T., 2007. The declaration of Helsinki.

Gorjanović-Kramberger, D., 1902. Der paleolithische Mensch und seine Zeitgenossen aus dem Dilivium von Krapina in Kroatien, II. MAGW 31, 189-216.

Gorjanović-Kramberger, K., 1906. Der diluviale Mensch von Krapina in Kroatien. C. W. Kreidel's Verlag, Wiesbaden.

Grassino, A., Goldman, M., Mead, J., Sears, T., 1978. Mechanics of the human diaphragm during voluntary contraction: statics. Journal of Applied Physiology 44, 829-839.

Gray, H., 1918. Anatomy of the human body. Lea & Febiger, Philadelphia.

Green, W.D.K., 1996. The thin-plate spline and images with curving features. In: Mardia KV, Gill CA, Dryden IL, editors. Image fusion and shape variability. Leeds: University of Leeds Press, pp 79-87.

Gunz, P., Mitteroecker, P., Bookstein, F.L., 2005. Semilandmarks in three dimensions, in: Slice, D. (Ed.), Modern Morphometrics in Physical Anthropology, New York, pp. 73-98.

Gunz, P., Mitteroecker, P., Neubauer, S., Weber, G.W., Bookstein, F.L., 2009. Principles for the virtual reconstruction of hominin crania. Journal of Human Evolution 57, 48-62.

Gunz, P., Mitteroecker, P., 2013. Semilandmarks: a method for quantifying curves and surfaces. Hystrix, the Italian Journal of Mammalogy 24(1), 103-109.

Haeusler, M., Martelli, S.A., Boeni, T., 2002. Vertebrae numbers of the early hominid lumbar spine. Journal of Human Evolution 43, 621-643.

Haeusler, M., Fremondiere, P., Fornai, C., Frater, N., Mathews, S., Thollon, L., Marchal, F., 2016. Virtual reconstruction of the MH2 pelvis (*Australopithecus sediba*) and obstetrical implications. American Journal of Physical Anthropology 159(S62), 165.

Haile-Selassie, Y., Latimer, B.M., Alene, M., Deino, A.L., Gibert, L., Melillo, S.M., Saylor, B.Z., Scott, G.R., Lovejoy, C.O., 2010. An early *Australopithecus afarensis* postcranium from Woranso-Mille, Ethiopia. Proceedings of the National Academy of Sciences 107, 12121-12126.

Hall, R.L., 2005. Energetics of nose and mouth breathing, body size, body composition, and nose volume in young adult males and females. American Journal of Human Biology 17(3), 321-330.

Heim, J.L., 1976. Les Hommes fossiles de la Ferrassie. I. Le gisement. Les squelettes adultes (crâne et squelette du tronc). Masson, Paris.

Heligman, D., Sullivan, R.C., Millar, E.A., 1987. Sacral ribs: A case report. Orthopedics 10, 1439-1442.

Herries, A.I., Pickering, R., Adams, J.W., Curnoe, D., Warr, G., Latham, A.G., Shaw, J., 2013. A multi-disciplinary perspective on the age of *Australopithecus* in southern Africa, The paleobiology of *Australopithecus*. Springer, pp. 21-40.

Holton, N.E., Yokley, T.R., Froehle, A.W., Southard, T.E., 2014. Ontogenetic scaling of the human nose in a longitudinal sample: implications for genus *Homo* facial evolution. American Journal of Physical Anthropology 153(1), 52-60.

Holliday, T.W., 2012. Locomotor convergence and other homoplasies: the *Homo* and *Hylobates* example, in: Proceedings of the European Society for the study of human evolution (ESHE), Bordeaux, p. 14.

Holliday, T.W., 2012. Body Size, Body Shape, and the Circumscription of the genus *Homo*. Current Anthropology 53, S330-S345.

Hunt, K.D., Cant, J.G., Gebo, D.L., Rose, M.D., Walker, S.E., Youlatos, D., 1996. Standardized descriptions of primate locomotor and postural modes. Primates 37(4), 363-387.

Jellema, L.M., Latimer, B., Walker, A., 1993. The rib cage, The Nariokotome *Homo erectus* Skeleton. Harvard University Press, Cambridge, pp. 294-325.

Jenkins, F.A., 1970. Anatomy and function of expanded ribs in certain edentates and primates. Journal of Mammalogy 51, 288-301.

Johanson, D.C., Lovejoy, C.O., Kimbel, W.H., White, T.D., Ward, S.C., Bush, M.E., Latimer, B.M., Coppens, Y., 1982. Morphology of the Pliocene partial hominid skeleton (A.L. 288-1) from the Hadar formation, Ethiopia. American Journal of Physical Anthropology 57, 403-451.

Kagaya, M., Ogihara, N., Nakatsukasa, M., 2008. Morphological study of the anthropoid thoracic cage: scaling of thoracic width and an analysis of rib curvature. Primates 49, 89-99.

Kaneko, H., Horie, J., 2012. Breathing movements of the chest and abdominal wall in healthy subjects. Respiratory Care 57(9), 1442-1451.

Kay, R.F., Fleagle, J.G., Simons, E.L., 1981. A revision of the Oligocene apes of the Fayum Province, Egypt. American Journal of Physical Anthropology 55(3), 293-322.

Kenyon, C., Cala, S., Yan, S., Aliverti, A., Scano, G., Duranti, R., Pedotti, A., Macklem, P.T., 1997. Rib cage mechanics during quiet breathing and exercise in humans. Journal of Applied Physiology 83, 1242-1255.

Kibii, J.M., Churchill, S.E., Schmid, P., Carlson, K.J., Reed, N.D., de Ruiter, D.J., Berger, L.R., 2011. A Partial Pelvis of *Australopithecus sediba*. Science 333, 1407-1411.

Kimbel, W.H., Delezene, L.K., 2009. "Lucy" redux: A review of research on *Australopithecus afarensis*. American Journal of Physical Anthropology 140, 2-48.

King, W., 1864. The Reputed Fossil Man of the Neanderthal. Quarterly Journal of Science 1, 88-97.

Kranioti, E.F., Bastir, M., Sánchez-Meseguer, A., Rosas, A., 2009. A geometric-morphometric study of the Cretan humerus for sex identification. Forensic Science International 189, 111-118.

Kuhl, F.P., Giardina, C.R., 1982. Elliptic Fourier features of a closed contour. Comput Graphics Image Process 18, 236-258.

Laird, M.F., Schroeder, L., Garvin, H.M., Scott, J.E., Dembo, M., Radovčić, D., Musiba, C.M., Ackermann, R.R., Schmid, P., Hawks, J., Berger, L.R., de Ruiter, D.J., 2017. The skull of *Homo naledi*. Journal of Human Evolution 104, 100-123.

Larson, S.G., 2007. Evolutionary transformation of the hominin shoulder. Evolutionary Anthropology: Issues, News, and Reviews 16, 172-187.

Larson, S.G., 2015. Humeral torsion and throwing proficiency in early human evolution. Journal of Human Evolution 85, 198-205.

Latimer, B., Ward, C.V., 1993. The thoracic and lumbar vertebrae. The Nariokotome Homo erectus skeleton. Cambridge, MA: Harvard University Press. p, 266-293.

Latimer, B.M., Lovejoy, C.O., Spurlock, L., Haile-Selassie, Y., 2016. The thoracic cage of KSD-VP-1/1, The Postcranial Anatomy of *Australopithecus afarensis*. Springer, pp. 143-153.

Lele, S.R., Richtsmeier, J.T., 1991. Euclidean distance matrix analysis: a coordinate free approach for comparing biological shapes using landmark data. American Journal of Physical Anthropology 86, 415-427.

Lordkipanidze, D., Jashashvili, T., Vekua, A., de León, M.S.P., Zollikofer, C.P., Rightmire, G.P., Pontzer, H., Ferring, R., Oms, O., Tappen, M., 2007. Postcranial evidence from early *Homo* from Dmanisi, Georgia. Nature 449, 305-310.

Lovejoy, C.O., 2005. The natural history of human gait and posture. Gait & Posture 21, 95-112.

Lovejoy, C.O., McCollum, M.A., 2010. Spinopelvic pathways to bipedality: why no hominids ever relied on a bent-hip–bent-knee gait. Philosophical Transactions of the Royal Society of London B: Biological Sciences 365, 3289-3299.

Lynnerup, N., 2003. The Greenland mummies. In: Lynnerup N, Andreasen C, Berglund J, editors. Mummies in a new millennium. In: Proceedings of the 4th World Congress on Mummy Studies, September 4–10, 2001, Nuuk, Greenland. Copenhagen: Danish Polar Center. pp. 17–19.

Magee, D.J., 2014. Orthopedic Physical Assessment, 6th ed. Saunders Elsevier.

Mallo, M., Wellik, D.M., Deschamps, J., 2010. Hox genes and regional patterning of the vertebrate body plan. Developmental Biology 344, 7-15.

McDougall, I., Brown, F.H., Vasconcelos, P.M., Cohen, B.E., Thiede, D.S., Buchanan, M.J., 2012. New single crystal 40Ar/39Ar ages improve time scale for deposition of the Omo Group, Omo–Turkana Basin, East Africa. Journal of the Geological Society 169, 213-226.

McCown, T., Keith, A., 1939. The Stone Age of Mount Carmel II: The Fossil Human Remains from the Levalloiso-Mousterian. Clarendon Press, Oxford.

Moyà-Solà, S., Kohler, M., Alba, D.M., Casanovas-Vilar, I., Galindo, J., 2004. *Pierolapithecus catalaunicus*, a new Middle Miocene great ape from Spain. Science 306, 1339-1344.

Nalla, S., 2013. The morphology of the upper thorax of *Australopithecus sediba* within the context of selected hominoids. University of the Witwatersrand.

Neubauer, S., Gunz, P., Mitteroecker, P., Weber, G.W., 2004. Three-dimensional digital imaging of the partial *Australopithecus africanus* endocranium MLD 37/38. Journal of the Canadian Association of Radiology 55, 271-278.

O'Higgins, P., Cobb, S. N., Fitton, L. C., Gröning, F., Phillips, R., Liu, J., Fagan, M. J., 2011. Combining geometric morphometrics and functional simulation: an emerging toolkit for virtual functional analyses. Journal of Anatomy 218(1), 3-15.

Openshaw, P., Edwards, S., Helms, P., 1984. Changes in rib cage geometry during childhood. Thorax 39, 624–627.

Pais, J., Levine, A., Pais, S., 1978. Coccygeal ribs: development and appearance in two cases. American Journal of Roentgenology 131, 164-166.

Partridge, T., Granger, D., Caffee, M., Clarke, R., 2003. Lower Pliocene hominid remains from Sterkfontein. Science 300, 607-612.

Pérez, S.I., Bernal, V., Gonzalez, P., 2006. Differences between sliding semilandmarks methods: implications for shape analyses of human populations. Journal of Anatomy 208, 769-784.

Pinet, C., 2004. Propriétés mécaniques et fonctionnelles de la cage thoracique. Revue des Maladies Respiratoires 21, 652-655.

Ponce de León, M.S., Golovanova, L., Doronichev, V., Romanova, G., Akazawa, T., Kondo, O., Ishida, H., Zollikofer C.P., 2008. Neanderthal brain size at birth provides insights into the evolution of human life history. Proceedings of the National Academy of Sciences 105, 13764–13768.

Pourquié, O., Tam, P.P., 2001. A nomenclature for prospective somites and phases of cyclic gene expression in the presomitic mesoderm. Developmental Cell 1, 619-620.

Ragnarsdóttir, M., Kristinsdottir, E.K., 2006. Breathing movements and breathing patterns among healthy men and women 20-69 years of age. Respiration 73(1), 48-54.

Reno, P.L., Meindl, R.S., McCollum, M.A., Lovejoy, C.O., 2003. Sexual dimorphism in Australopithecus afarensis was similar to that of modern humans. Proceedings of the National Academy of Sciences 100, 9404-9409.

Ritman, E.L., 2004. Micro-computed tomography-current status and developments. Annual Review of Biomedical Engineering 6, 185-208.

Roach, N.T., Richmond, B.G., 2015. Clavicle length, throwing performance and the reconstruction of the *Homo erectus* shoulder. Journal of Human Evolution 80, 107-113.

Robinson, J.T., 1972. Early hominid posture and locomotion. University of Chicago Press.

Rodríguez-Pérez, F.J., Rosas, A., García-Martínez, D., Bastir, M., García-Tabernero, A., Estalrrich, A., Huguet, R., Pastor, J.A., en revisión. A 3D form comparative analysis of the Neandertal glenoid fossa in the context of the genus *Homo*. Quaternary International.

Rohlf, F.J., Slice, D., 1990. Extensions of the Procrustes method for the optimal superimposition of landmarks. Systematic Biology 39(1), 40-59.

Röntgen, W.C., 1895. Über eine neue Art von Strahlen Vorläufige Mitteilung Sitzungsbericht der Würzburger Physik. Hof- u.Univers.-Buch-uKunsthandlung. pp 1–10.

Rosas, A., Bastir, M., 2002. Thin- plate spline analysis of allometry and sexual dimorphism in the human craniofacial complex. American Journal of Physical Anthropology 117(3), 236-245.

Rosas, A., Pérez-Criado, L., Bastir, M., Estalrrich, A., Huguet, R., García-Tabernero, A., Pastor, J.F., De la Rasilla, M., 2015. A geometric morphometrics comparative analysis of Neandertal humeri (epiphyses-fused) from the El Sidrón cave site (Asturias, Spain). Journal of Human Evolution 82, 51-66.

Rosas, A., Rodríguez-Pérez, F.J., Bastir, M., Estalrrich, A., Huguet, R., García-Tabernero, A., Pastor, J.F., de la Rasilla, M., 2016. Adult Neandertal clavicles from the El Sidrón site (Asturias, Spain) in the context of *Homo* pectoral girdle evolution. Journal of Human Evolution 95, 55-67.

Ruff, C., Walker, A., 1993. Body size and body shape, in: Walker, A., Leakey, R. (Eds.), The Nariokotome *Homo erectus* Skeleton. Cambridge: Harvard University Press, pp. 234-265.

Sampson, P.D., Bookstein, F.L., Sheehan, F.H., Bolson, E.L., 1996. Eigenshape analysis of left ventricular outlines from contrast ventriculograms. In Advances in morphometrics. Springer US. (pp. 211-233

Sánchez, S., Ahlberg, P. E., Trinajstic, K. M., Mirone, A., Tafforeau, P., 2012. Three-dimensional synchrotron virtual paleohistology: a new insight into the world of fossil bone microstructures. Microscopy and Microanalysis 18(5), 1095-1105.

Sawyer, G.J., Maley, B., 2005. Neanderthal reconstructed. The Anatomical Record Part B: The New Anatomist 283B, 23-31.

Schmid, P., 1983. Eine Rekonstruktion des Skelettes von A.L. 288-1 (Hadar) und deren Konsequenzen. Folia Primatolika 40, 283-306.

Schmid, P., 1991. The trunk of the australopithecines, in: Coppens, Y., Senut, B. (Eds.), Origine(s) de la Bipédie chez les Hominidés. Anatole, France: Éditions du Centre National de la Recherche Scientifique, pp. 225-234.

Schmid, P., Churchill, S.E., Nalla, S., Weissen, E., Carlson, K.J., de Ruiter, D.J., Berger, L.R., 2013. Mosaic morphology in the thorax of *Australopithecus sediba*. Science 340, 1234598.

Schroeder, L., Scott, J.E., Garvin, H.M., Laird, M.F., Dembo, M., Radovčić, D., Berger, L.R., de Ruiter, D.J., Ackermann, R.R., 2017. Skull diversity in the *Homo* lineage and the relative position of *Homo naledi*. Journal of Human Evolution 104, 124-135.

Schultz, A.H., 1930. The skeleton of the trunk and limbs of higher primates. Human Biology 2, 303-438.

Schultz, A.H., 1961. Vertebral column and thorax, in: Hofer, H., Schultz, A.H., Starck, D. (Eds.), Primatologia, Handbuch der Primatenkunde. Karger, Basel (Schweiz), New York, pp. 1-66.

Seidler, H., Bernhard, W., Teschler-Nicola, M., Platzer, W., zur Nedden, D., Henn, R., Oberhauser, A., Sjovold, T., 1992. Some anthropological aspects of the prehistoric Tyrolean Ice Man. Science 258, 455-457.

Seidler, H., Falk, D., Stringer, C., Wilfing, H., Müller, G.B., zur Nedden, D., Weber, G.W., Reicheis, W., Arsuaga, J.L., 1997. A comparative study of stereolithographically modelled skulls of Petralona and Broken Hill: implications for future studies of middle Pleistocene hominid evolution. Journal of Human Evolution 33(6), 691-703.

Sheets, H.D., Kim, K., Mitchell, C.E., 2004. A combined landmark and outline-based approach to ontogenetic shape change in the Ordovician trilobite *Triarthrus becki*. In Morphometrics. Springer Berlin Heidelberg. pp. 67-82.

Shi, X., Cao, L., Reed, M.P., Rupp, J.D., Hoff, C.N., Hu, J., 2014. A statistical human rib cage geometry model accounting for variations by age, sex, stature and body mass index. Journal of Biomechanics 47, 2277-2285.

Shipman, P., Walker, A., Bichell, D., 1985. The Human Skeleton. Cambridge: Harvard University Press.

Silverthorn, D.U., Ober, W.C., Garrison, C.W., Silverthorn, A.C., Johnson, B.R., 2009. Human physiology: an integrated approach. Pearson/Benjamin Cummings San Francisco, CA, USA.

Skinner, M.M., Wood, B.A., Boesch, C., Olejniczak, A.J., Rosas, A., Smith, T.M., Hublin, J.-J., 2008. Dental trait expression at the enamel-dentine junction of lower molars in extant and fossil hominoids. Journal of Human Evolution 54, 173-186.

Spalteholz, W., 1970. Atlas de Anatomía Humana, 5 ed. Labor S.A., Barcelona.

Spoor, F., Wood, B., Zonneveld, F., 1994. Implications of early hominid labyrinthine morphology for evolution of human bipedal locomotion. Nature 369, 645-648.

Spoor, F., Jeffery, N., Zonneveld, F., 2000. Using diagnostic radiology in human evolutionary studies. Journal of Anatomy 197(1), 61-76.

Thackeray, F.J., 2015. Estimating the age and affinities of *Homo naledi*. South African Journal of Science 111(11-12), 1-2.

Tawane, G., García-Martínez, D., Eyre, J., Bastir, M., Berger, L., Schmid, P., Nalla, S., Williams, S.A., 2016. A hominin first rib discovered at the Sterkfontein Caves, South Africa. South African Journal of Science 112(5-6), 1-7.

Toussaint, M., Macho, G.A., Tobias, P.V., Partridge, T.C., Hughes, A.R., 2003. The third partial skeleton of a late Pliocene hominin (Stw 431) from Sterkfontein, South Africa. South African Journal of Science, 99(5-6), 215-223.

Trinkaus, E., 1983. The Shanidar Neandertals. Academic, New York.

VanSickle, C., Cofran, Z.D., García-Martínez, D., Williams, S.A., Churchill, S.E., Berger, L.R., Hawks, J., en revisión. Pelvic remains of *Homo naledi*, from Dinaledi, South Africa. Journal of Human Evolution.

Verschakelen, J.A., Demedts, M.G., 1995. Normal thoracoabdominal motions. Influence of sex, age, posture, and breath size. American Journal of Respiratory and Critical Care Medicine 151(2), 399-405.

Waldeyer, A., Mayet, A., 1987. Anatomie des Menschen, 15th edition ed. de Gruyter.

West J.B., 2012. Respiratory physiology, the essentials, 9th ed. Philadelphia: Wolters Kluwer.

Walker, A., Leakey, R., 1993. The Nariokotome *Homo erectus* skeleton, in: Walker, A., Leakey, R. (Eds.). Harvard University Press, Cambridge.

Ward, C.V., 1993. Torso morphology and locomotion in *Proconsul nyanzae*. American Journal of Physical Anthropology 92, 291-328.

Ward, M.E., Ward, J.W., Macklem, P.T., 1992. Analysis of human chest wall motion using a two-compartment rib cage model. Journal of Applied Physiology 72, 1338-1347.

Ward, C., Kimbel, W., Harmon, E., Johanson, D., 2012. New postcranial fossils of *Australopithecus afarensis* from Hadar, Ethiopia (1990–2007). Journal of Human Evolution 63, 1-51.

Weber, G.W., Bookstein, F.L., 2011. Virtual anthropology: a guide to a new interdisciplinary field. Springer.

Weber, G.W., Gunz, P., Mitteroecker, P., Thackeray, F., Bookstein, F.L., 2003. Skull reference models (SRM) and the ontogeny of *A. africanus*. American Journal of Physical Anthropology 120(S36), 221–222.

Weaver, A.A., Schoell, S.L., Stitzel, J.D., 2014. Morphometric analysis of variation in the ribs with age and sex. Journal of Anatomy 225, 246-261.

Weber, G. W., Recheis, W., Scholze, T., Seidler, H., 1998. Virtual anthropology (VA): methodological aspects of linear and volume measurements--first results. Collegium Antropologicum 22(2), 575-584.

Weber, G.W., 2015. Virtual anthropology. American Journal of Physical Anthropology 156(S59), 22-42.

Weinstein, K., 2008. Thoracic morphology in Near Eastern Neandertals and early modern humans compared with recent modern humans from high and low altitudes. Journal of Human Evolution 54, 287-295.

Wells, J.C., 2007. Sexual dimorphism of body composition. Best practice & research Clinical endocrinology & metabolism 21(3), 415-430.

West JB. 2012. Respiratory physiology, the essentials, 9th ed. Philadelphia: Wolters Kluwer.

White, T.D., Black, M.T., Folkens, P.A., 2011. Human Osteology, 3rd ed. Academic Press.

Williams, P.L. y Warwick, R., 1980. Gray's Anatomy, 36th Brit. edn. Philadelphia: W. B. Saunders.

Williams, S.A., 2012. Variation in anthropoid vertebral formulae: implications for homology and homoplasy in hominoid evolution. Journal of Experimental Zoology Part B: Molecular and Developmental Evolution 318, 134-147.

Williams, S.A., Middleton, E.R., Villamil, C.I., Shattuck, M.R., 2016. Vertebral numbers and human evolution. American Journal of Physical Anthropology 159, S19-S36.

Williams, S.A., García-Martínez, D., Bastir, M., Meyer, M.R., Nalla, S., Hawks, J., Schmid, P., Churchill, S.E., Berger, L.R., 2017. The vertebrae and ribs of *Homo naledi*. Journal of Human Evolution 104, 136-154.

Wind, J., 1984. Computerized X- ray tomography of fossil hominid skulls. American Journal of Physical Anthropology 63(3), 265-282.

Wood, B., K Boyle, E., 2016. Hominin taxic diversity: Fact or fantasy? American Journal of Physical Anthropology 159, S37-S78.

Zelditch, M.L., Swiderski, D.L., Sheets, H.D., 2012. Geometric morphometrics for biologists: a primer. Academic Press.

Zollikofer, C.P., Ponce de León, M.S., Martin, R.D., Stucki, P., 1995. Neanderthal computer skulls. Nature 375(6529), 283-285.

Zollikofer, C.P., Ponce de León M.S., 2005. Virtual reconstruction: a primer in computerassisted paleontology and biomedicine. Wiley-Interscience, Hoboken, N.J.

Zollikofer, C.P., Ponce de León, M.S., 2005. Virtual reconstruction: a primer in computer-assisted paleontology and biomedicine. Wiley-Interscience.